Stem Cells International

Mesenchymal Stem Cells and Regenerative Medicine 2021

Lead Guest Editor: Huseyin Sumer
Guest Editors: Sangho Roh and Jun Liu

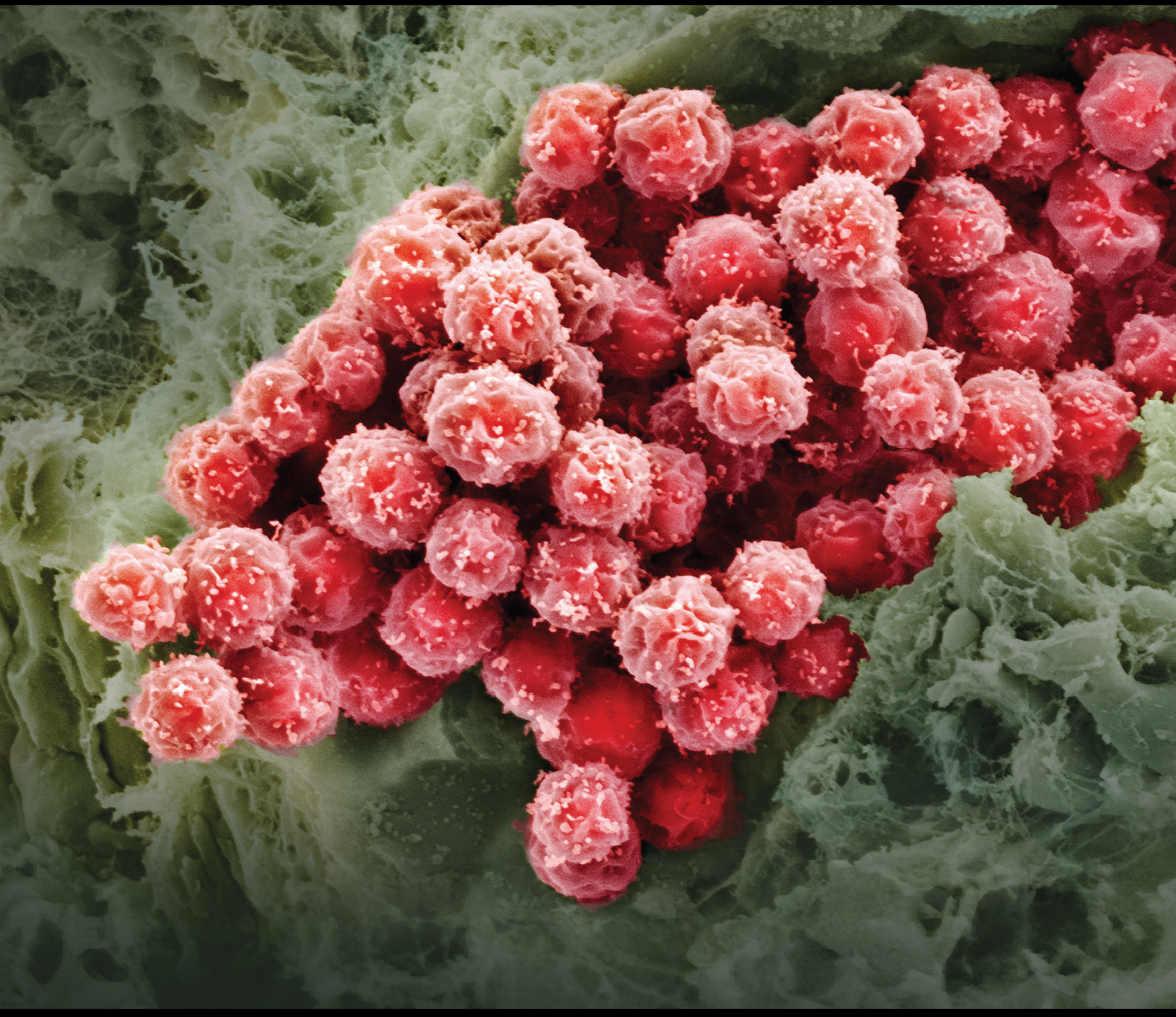

Mesenchymal Stem Cells and Regenerative Medicine 2021

Stem Cells International

Mesenchymal Stem Cells and Regenerative Medicine 2021

Lead Guest Editor: Huseyin Sumer
Guest Editors: Sangho Roh and Jun Liu

Contents

Hindawi
Stem Cells International
Volume 2022, Article ID 9589600, 8 pages
https://doi.org/10.1155/2022/9589600

Review Article

Alloreactivity of Allogeneic Mesenchymal Stem/Stromal Cells and Other Cellular Therapies: A Concise Review

Kiran Shah,[1,2] **Nirali Shah**,[1] **Fatameh Ghassemi**,[1] **Carolyn Ly**,[1] **Teena George**,[1] **Carla Lutz**,[1] **and Huseyin Sumer**[2]

[1]*Magellan Stem Cells P/L, Box Hill, Victoria, Australia*
[2]*Department of Chemistry and Biotechnology, School of Science, Computing and Engineering Technologies, Swinburne University of Technology, Hawthorn, Victoria, Australia*

Correspondence should be addressed to Kiran Shah; kshah@australianstemcells.com.au
and Huseyin Sumer; hsumer@swin.edu.au

Received 16 September 2021; Revised 8 November 2021; Accepted 23 February 2022; Published 9 March 2022

Academic Editor: Zhaoji Pan

Cellular therapies, deemed live medicine, have brought a wave of new generation biological therapies to treat previously untreatable diseases such as cancers and degenerative diseases like osteoarthritis. These cellular therapies have gained significant recognition in clinical research. The area has been further strengthened with the approval of Chimeric Antigen Receptor added on T cells (CAR-T) therapies by the regulatory authorities USA's Food and Drugs Administration (FDA), European Medical Agency (EMA), the Australian Therapeutic Goods Administration (TGA), and in many countries in 2017 to treat hematological cancers. Another milestone was achieved when allogeneic Mesenchymal Stem Cell- (MSC-) based therapy was approved by the EMA to treat Chrohn's disease in 2018. Allogeneic donor-derived MSC therapies in particular hold great promise and real hope because of their 'off-the shelf' availability and accessibility for patients in need of urgent treatment. So far, thousands of clinical trials have explored the safety and efficacy of both autologous and allogeneic cell therapies, deeming them safe, however with varying degrees of efficacy. In the current pandemic, clinical trials have begun in many parts of the world to treat severe cases of COVID with MSCs. However, the risk of tissue rejection and the development of undesirable effects due to alloreactivity of allogeneic cells are currently not adequately addressed. Therefore, this warrants careful investigation and detailed reporting of such events by clinical researchers. This review aims at discussing the current landscape of approved allogeneic MSCs along with a few other cellular therapies. We explore any possible reactivity reported to inform the readers of any safety concern and on the efficacy of such therapies.

1. Introduction

In the current pandemic, both autologous and allogeneic MSCs have been explored in several registered clinical trials around the world to treat the severe cases of COVID-19, e.g., pneumonia and acute respiratory distress syndrome (ARDS). In such a dynamic and evolving situation dealing with a novel virus globally, a recent review describes the swift and precise targeting the COVID-19-related illness with auto/allogeneic MSC trials which demonstrates the huge therapeutic potential of MSCs in the treatment of viral infection, inflammation, and immune diseases [1]. Furthermore, the importance of stem cell therapies is highlighted by a search on the http://Clinicaltrils.gov, with the search terms: "cell therapy", "stem cells", "active" and "recruiting by invitation", and "interventional" resulted in 9,949 phase I to phase III studies currently registered. These studies are investigating 25 conditions under category for over recruiting (http://Clininicaltrials.gov, accessed 08 Feb2021; https://clinicaltrials.gov/ct2/results?term = cell+therapy+OR + stem +cells&recrs = a&recrs = f&recrs = d&age_v = &gndr = &type = Intr&rslt = &Search = Apply). There are over 530 clinical trials focusing on the allogeneic stem cell therapy and have several different types of stem cells being used, e.g., hematopoietic stem cells (HSCs: CD34/NK), MSCs, and

CAR-T cells and 629 clinical trials with autologous cell sources. Figure 1 shows the distribution of the cell types currently listed on ClinicalTrials.gov.

In recent times, cell therapies have had unprecedented progress, exploring a wide range of adult stem cells other than hematopoietic stem cell transplantation (HSCT) for treatment of a number of disease through the use of MSCs, Natural Killer Cells (NK Cells), skin cells, T cells, and more. With this enormous progress, a milestone was achieved with the approval of one of the first cell therapies to treat Graft Versus Host Disease (GvHD) in Canada and New Zealand in 2015 followed by EMA and a recent approval of CAR-T therapy, Kymriah by FDA in 2018 [2, 3]. The regulatory approvals highlight that these cellular therapies hold great promises to address current unmet medical needs including potential treatment and cure of several deadly and life-threatening diseases. Consequently, cellular therapies have gained significant clinical advances with several thousands of clinical trials registered in the ClinicalTrials.gov database. These include both autologous and allogeneic cell therapies treatment modalities, each with its own set of advantages and disadvantages. Due to the multipotent therapeutic properties of MSCs, in the current pandemic, over a dozen clinical trials are underway for the treatment of COVID-19. This review will explore the current cellular types in the clinical trials with special focus on the most common cell types. We discuss the risks and benefits of autologous versus allogeneic and list the current approved cell therapy available to patients.

Over five decades ago, a ground-breaking bone marrow transplant in a sibling with a close histocompatible match was performed and heralded a new era of treating complex medical conditions. Thus, a brand-new field of therapy was uncovered and termed stem cell therapy. To date, allogeneic bone marrow transplantation (BMT) is a treatment option for a range of hematologic diseases including acute myeloid leukaemia. HSCT derived from donor bone marrow has been an established therapeutic method for over 5 decades. The curative action of HSCT is due to immune-mediated graft-versus-leukaemia effects of the donor T cells contained in the graft. However, donor T cells are also the cause of Graft-vs-Host disease (GVHD). As GVHD is a major complication arising from allogeneic HSCT, research into the prevention of GVHD has provided a unique opportunity to understand the mechanisms of alloreactivity. One such mechanism that causes severe GVHD is the production of antirecipient helper (Inerleukin-2-producing) T lymphocyte precursors (HTLp). These precursors amplify the immune response as shown by a positive correlation between patients with high HTLp and the development of GVHD [4]. These findings are supported by an earlier study where depletion of T cells from donor bone-marrow allografts prior to transplantation prevented the development of GVHD [5].

2. Autologous versus Allogeneic Stem Cell Therapies

There are number of advantages of using autologous (self-derived) cellular treatment including the following: (i) the autologous cell therapy poses a low risk of tissue rejection, (ii) less chance of getting foreign infections, and (iii) lower risk of acquiring an unwanted immune response. However, this modality is costly, time consuming, and in some cases may not be efficacious, especially in chronically ill patients with potentially compromised cell quality or inability to donate tissue due to potential surgery risk. Furthermore, the self-derived tissue may also contain underlying genetic factors that are the cause of the disease. Allogeneic (donor-derived) cell therapy also has some issues including (i) the suitability for a diverse population, (ii) chance of carrying foreign antigens that could illicit unwanted immune response, and (iii) tissue rejection. However, if these limitations are overcome with careful health screening of donors; then, allogeneic cell therapy presents many added advantages over the autologous therapy. These include the following: it is less expensive, 'off the shelf' and therefore immediately available, and well-characterised allogeneic donor cell lines with potentially increased efficacy. However, the issue with developing allogeneic reactivity in the long term remains the main concern for the allogeneic cell therapy and warrants better long-term follow-up and reporting in clinical trials.

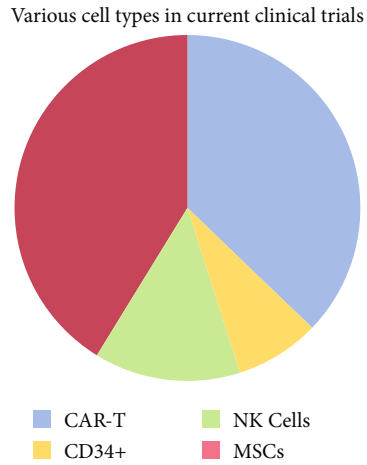

Figure 1: Current Clinical trials on exploring various types of stem cell or cell therapies registered on ClinicalTrials.gov.

In this review, given the perceived risks discussed above with allogeneic antigens in the recipients and possible tissue rejection, we reviewed the scientific literature for evidence of alloreactivity and rejection and summarise the current status of alloreactivity and allogenic MSC cell therapies.

3. Allogeneic Stem Cell Therapy and the Role of Major Histocompatibility Complex (MHC)

The MHC group of genes determines and regulates the unique molecular constituents of specific antigens and their interaction with the various immune cells. Therefore, the molecular recognition of foreign cells originates at the genetic level and the peptides on the MHC molecules contribute to allorecognition. Of the three types of MHC gene family subgroups, classes I and II are directly involved in the antigen presentation process. Class MHC class III are structurally and functionally less well defined and the gene cluster contains signalling molecules such as TNF-alpha

and heat shock protein. Classes I and II therefore orchestrate the allogeneic reactivity in the recipients' immune cells [6]. In cellular transplantations, the recipient's T cells act as major coordinator for specific immunity, facilitated by the antigen-binding site of class I and II molecules, targeting allogeneic donor's epitopes or the MHC complexes. The molecular basis for this interaction, termed alloreactivity, occurs in three different ways; first, the heterogeneous structural differences in the stimulator and the responder MHC types in allorecognition; second, alloreactive T cells may not be adequately recognised by the responder cells when closely related; and third, alloresponse may be directed against the residues on the allogeneic MHC molecules itself [6].

Many other immune cells, e.g., macrophages, B-cells, and Natural Killer (NK) cells are primed to illicit strong reactive immune responses when nonself cells or tissues are introduced. This can then trigger undesirable tissue rejection and cause severe morbidity in the recipient. These cells express high levels of class I and II MHC complexes. For this reason, several preventative measures are employed before allogeneic cell or tissue transplantation. One of many measures is cytotoxic cross-match, and together with Allomap Molecular Expression testing and ABO-compatibility, to help predict the success of transplantation [6]. With modern advances in cellular biology, many innovative and noble approaches are employed in various clinical trials to develop successful allogeneic cell therapies such as CAR-T cell therapy, CRISPR- and iPSC-derived cells, and other naturally immune-evading stem cells such as MSCs. We explore the alloreactivity of these different cell types in the sections below.

4. Types of Allogenic Stem Cell Therapies in Clinical Trials

4.1. Mesenchymal Stem Cells (MSCs). MSCs are one of the most studied therapeutic cell types; they are adult stem cells and derived from a number of connective tissues such as the bone marrow, adipose tissue, umbilical cord, placenta, and dental pulp. With the regulatory approval of the use of allogeneic MSCs for acute GvHD, the field has gained a renewed confidence in the therapeutical benefits of these multipotent cells [7]. These cells are widely known as being immune-privileged due to the lack of MHC II molecule expression and a very low level of MHC I [8, 9]. Additionally, potent stimulatory molecules such as CD86, CD40, or CD40L are not detectable in MSCs and therefore not recognised by alloreactive T cells. As a result these cells do not get rejected by the host [9]. Importantly, MSCs are now widely described as strong immunomodulators that have been shown to have antiproliferative effects on several immune cells including T cells, B-cells, and NK cells [10–12]. The underlying mechanisms of T cell inhibition by MSCs are facilitated by several key molecules including the enzymes Indoleamine 2,3 dioxygenase (IDO), Prostaglandin E2 (PGE2), Human Leukocyte Antigen -G (HLA-G), Nitric Oxide, Insulin Growth factors (IGF) binding proteins, and secreted exosome cargo [8, 13]. Depletion of tryptophan by an enzyme IDO produced by MSCs seems to have immune suppressive effects on the T cells [14]. Another molecule responsible for immune suppression is PGE2 which has been shown to convert preinflammatory T helper cells that secrete interferon gamma into T helper cells to produce anti-inflammatory cytokines IL-4 [15].

Le Blanc and coworkers first used allogeneic MSCs clinically to treat acute GVHD [16]. This landmark case study inspired researchers to apply allogeneic MSC in different clinical trials. Based on systematic analysis of MSCs clinical trials that Kabat and coworkers [17] have published last year, there is a dramatic increase in the number of newly registered clinical trials using MSCs as most recently reported in April in 2021 [1]. An outcome result of allogeneic canine MSCs treatment for lame dogs showed good efficacy and without any adverse reaction of the allogenic MSCs [18]. There are a few animal studies which have shown adverse response upon administration of allogeneic MSCs [19–21]; however, allorejection-dependent symptoms have not been reported in humans [22]. The safety of allogeneic MSC therapy and lack of serious adverse effects or toxicity have been consistently demonstrated in clinical trials, despite this, the secretion of alloantibodies has been reported in some studies [23, 24]. Furthermore, efficacy of allogeneic therapies is correlated with different factors such as cell dose, dose frequency, administration route, and source of MSC. The first and most widely used source of MSCs is derived from the bone marrow. Allogeneic MSC recipients did not display significant donor-specific antibodies with only 3.7% alloreactivity in the allogeneic group [25], while MSC therapy in both allogeneic- and autologous cell-treated groups were safe. However, in this study there was limited clinical improvement in both groups [25]. Although no serious adverse effects were seen after one month, long-term adverse effect incidence after 6 month and rehospitalization after one year in 20 million cell dose group were 2-fold higher than that of 100 million dose group. The authors attribute this anomaly to the complex disease environment and suggest that an even higher dose may be required to overcome the initial cell death and hypoxia after transplantation [25]. The study demonstrated no clinical alloreactivity in patients and both doses were considered safe and well-tolerated, while only the higher dose displayed efficacy on reduction of infarct size and improving cardiac function [25]. Similarly, in a study where a dose comparison was made of allogenic mesenchymal precursor cells (MPC) in patients with heart failure, it was demonstrated that the higher dose (150 million cells per patient) produced the greatest improvement in cardiac structure and function [23]. Results also showed that 11% of the MPC-treated patients developed donor-specific anti-HLA class I antibodies but no serious adverse events were attributed to MPC treatment [23]. Mismatched patients in the treatment groups may have been a factor as well as the requirement to administer a high cell dose [26]. To overcome these obstacles, encapsulation of allogeneic MSCs before their transplantation has been proposed which prolongs their survival and subsequently ensures long-term efficacy of the allogeneic cell therapies [27]. Activating MSCs with proinflammatory cytokines such as interferon gamma (IFN-g) and/or tissue necrosis factor-alpha (TNF-a) has also been recommended by the ISCT MSC committee to further

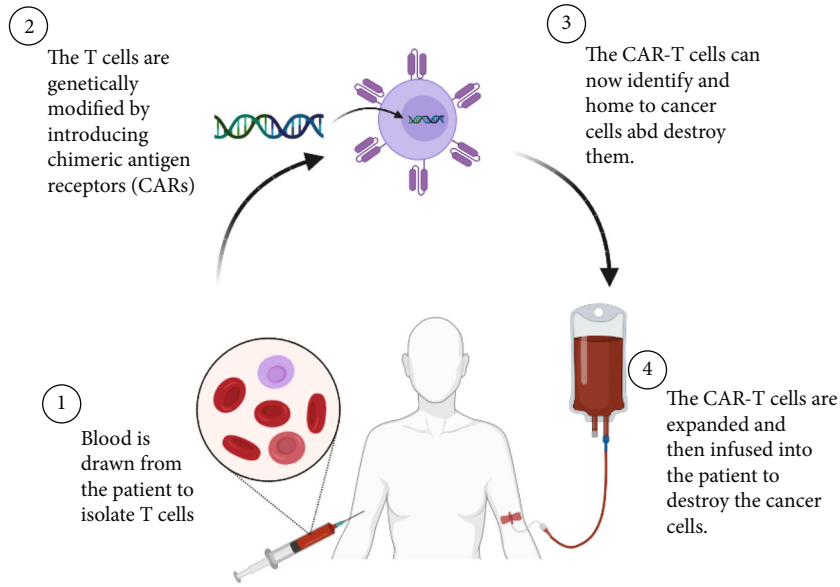

Figure 2: CAR-T cell therapy overview. The patients' T cells are isolated and genetically modified with a chimeric antigen receptors (CARs) that can home to cancer cells when infused back into the patients' blood stream.

enhance the effectiveness of these cells [20]. Allogeneic cell therapies also have added advantages over autologous cells due to the limitations of obtaining adequate tissue from already diseased patients with chronic conditions and possibly compromised efficacy in cells from such tissues. Currently, there are over a dozen clinical studies aimed at developing better delivery systems in various cell therapies such as heart conditions or degenerative disc disease using injectable hydrogels in combination with MSCs providing a better treatment model [28–30]. With a wide array of untreatable conditions being targeted by these promising off-the-shelf MSC therapies, continued and careful long-term monitoring of the implanted cells in the recipients still needs to be carried out even though allogenic MSC therapies have been shown to be safe. In particular, we would like to draw attention to new cohorts of patients with new illnesses being treated with MSCs to have close diligent clinical follow-up to assure patients of continued safety and efficacy.

4.2. CAR-T Cell Therapy. CAR-T cell therapy is one the most novel immunotherapies of the 21st century, it is used for cancer treatment and has been explored in many clinical trials globally. The process of Chimeric Antigen Receptor (CAR) is an engineered T cell receptor with the ability to recognise a predefined target antigen. It is genetically introduce to the patients' T cells which helps to activate cytotoxicity against the target cells, i.e., malignant cells. It has been described as an antitumour weapon, which acts directly in the immune system (Figure 2). A milestone was achieved recently when Kymriah and Yescarta received approval from the regulatory authorities FDA, EMA, and TGA to use CAR-T cell for commercial therapies in eligible patients [2, 3].

Furthermore, Adoptive Cell Transfer (ACT) therapy is an immunotherapy that separates immunocompetent cells in cancer patients and transfers them back in the patients after expansion or functional identification in vitro. The adoptive cells kill tumour cells directly or stimulate the body's own immune response. There are 'four-generations' of CAR-T cells that have been used in ACT therapy [31]. The first generation includes Single Chain Fragment Variable (ScFV) as the target recognition and CD34 signalling chain as the intracellular domain. The second generation encompasses a costimulatory domain such as 4-1BB (CD137) or CD28 as the secondary signal producer, in addition to properties of the first generation. Applying both costimulatory domain including CD28 and 4-1BB led to the construction of the 3rd generation. The fourth generation, also named as T cells Redirected for antigen-Unrestricted Cytokine-initiated Killing (TRUCK T cells) or armed CAR-T cells. To increase efficiency and potency, various functional elements such as interleukin genes are inserted into fourth generation CAR construction [32].

As discussed above, autologous therapies are more expensive and time-consuming, allogeneic donor-derived CAR-T provides an advantage over the autologous approach. Healthy donors with distinct HLA types generate 'off-the-shelf' CAR-T cell banks that can and be matched with the recipient HLA alleles for precision medicine and therefore avoid the risk or incidence of allograft rejection [33]. In our observations of the registered 829 clinical trials currently registered for of CAR-T cells on Clinical Trials.gov, 53 of these have completed phase I/II trials and 13 of these completed trials have results published on the website with mixed results. These early results warrant further follow-up and continued monitoring of the long-term safety of these procedures. While the data from the remaining ongoing CAR-T cell trials will be of great interest to immunotherapy researchers and cancer patients alike.

4.3. CD34 Positive Cells. The ability to select CD34+ cells from mobilized peripheral blood makes it feasible to expand these purified cells in cytokine-supported cultures for clinical

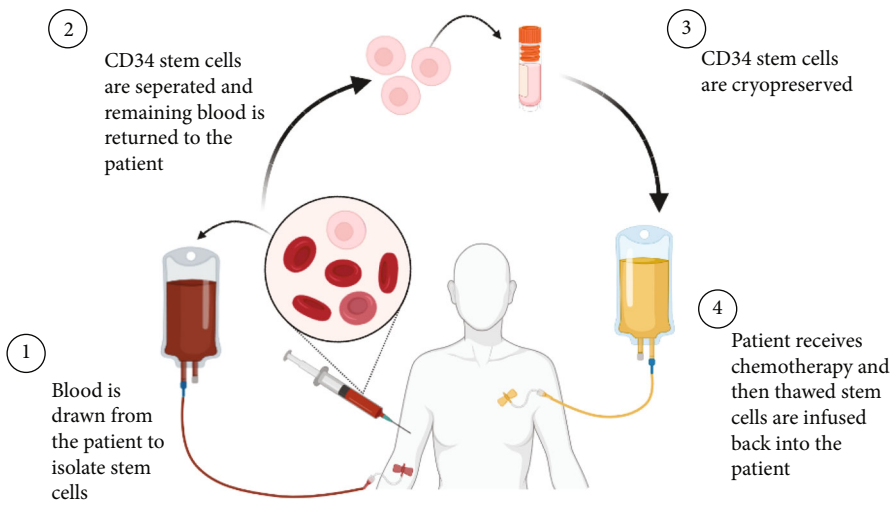

Figure 3: CD34 cell therapy overview. The patients' blood is drawn and CD34 positive cells are isolated and expanded in culture before cryopreservation. The CD34 cells can be infused back into the patient after they receive chemotherapy.

use. The transplantation of allogeneic Peripheral Blood Progenitor Cells (PBPC) provides complete and sustained hematopoietic and lymphopoietic engraftment (Figure 3). The positive selection of CD34+ cells from peripheral blood preparations simultaneously provides an approximately 1000-fold reduction of T cells. These purified CD34+ cells contain committed multipotent stem cells that are suitable for allogeneic transplantation [34]. Both CD34+ endothelial and cardiomyocyte progenitor cells are capable of neoangiogenesis/neovascularization and cardiac muscle regeneration, respectively, and can be easily collected in humans from the bone marrow or the peripheral blood. The experimental and physiological data support the use of CD34+ stem cells for cardiac repair [35]. For example, patients with severe diffuse coronary artery disease (CAD) receiving intracoronary transfusion of circulating-derived CD34+ cells directly without enrichment for endothelial progenitor cells (EPCs) were divided into angiographic low- and high-score groups after a 9-month follow-up [36]. The results of cardiac MRI and 3D echocardiography demonstrated a significant improvement of the left ventricular ejection fraction (LVEF) in the high-score subjects compared to that in their low-score counterparts. Moreover, the neovascular effects were demonstrated in a phase I/II trial, where CD34+ EPCs administered to patients with refractory angina pectoris decreased the frequency of events and increased exercise tolerance as compared to the placebo-treated patients [37]. The donor's alloreactive effector T cells and the host's antigen-presenting cells (APCs), such as dendritic cells, have been shown to have an essential role in the initiation of GVHD. Depletion of effector T cells from the HSCT graft decreases the risk of GVHD but at the same time increases the relapse rate, due to insufficient graft-versus-leukaemia (GVL) effect [38]. Therefore, these treatments further warrant careful review and fine-tuning of the treatment regime, dosages, modalities, and long-term safety evaluation.

4.4. Skin Stem Cells. Cell therapy has been a breakthrough for major burn victims for permanent skin replacement using cultured autologous epidermal grafts (Figure 4). Rheinwald and Green first established the culture of keratinocytes in vitro in 1975 [39]. In the following years, further research led to the first autologous keratinocyte cell treatment for a burn patient in 1981 [40]. Allogenic keratinocyte cell therapy followed in 1983, where wound healing was observed at an unexpectedly quicker rate compared to the conventional procedure of using cadaver autografts [41]. However, as one of the limitations with allogenic cell therapy is the potential for immunological rejection from the recipients' immune system, whether these MHC class II antigens on keratinocytes can initiate an immunological response is still largely debated with some studies showing no detectable expression of these antigens on the cell surface [42], while other studies have been able to show expression of HLA-DR on keratinocytes after IFN-γ exposure [43, 44].

Keratinocytes, like all epidermal cells, have MHC class I antigens displayed on their cell surface but the human leukocyte antigen type DR (HLA-DR), a MHC class II antigen strongly associated with immune rejection, is not constitutively expressed [44]. In an early cell therapy experiment by Morhenn et al. in 1982 examining the levels of HLA-DR expression, keratinocyte cells were stained with an anti-HLA-DR antibody [42]. This examination resulted in no detectable fluorescence even after the cells were left in culture for up to 14 days. This team also discovered significantly reduced lymphocyte activation levels in a coculture experiment of keratinocytes and lymphocytes after a seven-day period, compared with freshly harvested keratinocytes. These results suggest that the antigenicity of keratinocyte cells in culture is reduced over time.

However, other studies have shown that these MHC class II antigens on keratinocytes can be activated by stimulation with the proinflammatory cytokine IFN-γ. Castillo et al. examined the immunogenicity of cultured allogenic keratinocytes by coincubating them with peripheral blood mononuclear cells and IFN-γ [45]. They found that despite MHC class II molecules being activated by up to six times greater than baseline levels, T lymphocyte activation markers were not detected in this assay [43, 45]. Similar

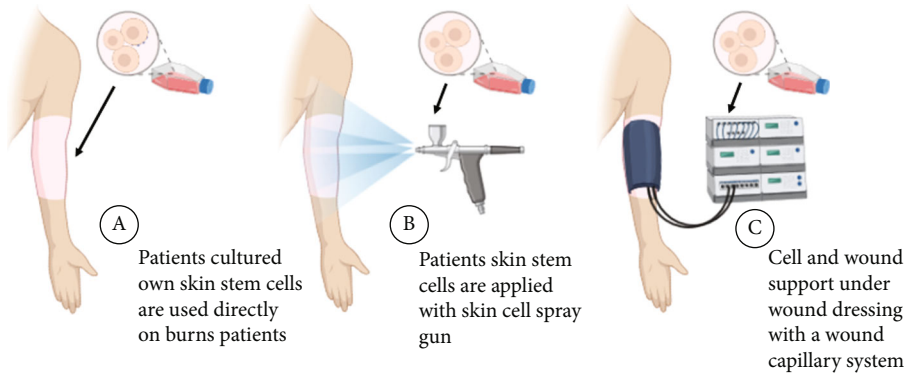

Figure 4: Skin cell therapy overview. Patients own cultured cells or allogeneic cells can be (a) used directly on the wound site, (b) applied using as an aerosol, or (c) cell replacement supported under a wound dressing with a wound capillary system.

Table 1: Current MSC-approved products for human clinical use.

Source of human tissue	Clinical condition	Trade name	Company	Approving country and year of approval
Adipose	Complex perianal fistulas in CD	ALOFISEL	TiGenix NV/Takeda	Europe (2018)
Bone Marrow	Spinal cord injury	STEMIRAC	Nipro Corp.	Japan (2018)
Bone Marrow	Critical limb ischemia	STEMPEUCEL	Stempeutics Research PVT	India (2016)
Bone Marrow	GvHD	TEMCELL HS INJ	JCR Pharmaceuticals	Japan (2015)
Bone Marrow	Amytrophic lateral sclerosis	NEURONATA-R	Corestem Inc.	South Korea (2014)
Bone Marrow	GvHD	PROCHYMAL (REMESTEMCEL-L)	Osiris Therapeutics Inc./ Mesoblast Ltd.	Canada (2012) New Zealand (2012)
Adipose	Crohn's fistula	CUPISTEM	Anterogen Co. Ltd	South Korea (2012)
Umbilical Cord	Knee articular cartilage defects	CARTISTEM	Medipost Co. Ltd.	South Korea (2012)
Bone Marrow	Acute MI	CELLGRAM-AMI	Pharmicell Co. Ltd.	South Korea (2011)
Adipose	Subcutaneous tissue defects	QUEENCELL	Anterogen Co. Ltd.	South Korea (2010)

results were also observed where IFN-γ was able to induce HLA-DR activation in keratinocytes [44]. However, key T cell activation costimulatory molecules B7-1 and B7-2 could not be detected, even with high levels of IFN-γ exposure in the coculture experiment. These results suggest that HLA-DR is not actively expressed on keratinocytes and these cells have been described as being nonprofessional antigen presenting cells with their limited immunogenicity [44].

5. Approved Allogenic Cell Therapy Treatments

With extensive clinical research in cellular therapies, there currently is a number of products that have been approved by various regulatory authorities. Currently the FDA has 19 cell therapy products approved for use in patients (https://www.fda.gov/vaccines-blood-biologics/cellular-gene-therapy-products/approved-cellular-and-gene-therapy-products).The first cell therapy product to get regulatory approval for therapeutic use was in August of 2017 for relapsed or refractory (r/r) paediatric and young-adult B-cell acute lymphoblastic leukaemia and then in May 2018 for adult r/r diffuse large B-cell lymphoma [46]. The CAR-T cell therapy trial outcome data showed significant improvement and overall response rate of 50% and in some cases it was >80% [47]. CAR-T cell therapies now represent the new standard of care for select groups of patients with B-cell lymphoma and have now been approved by the FDA, EMA, and the TGA [2].

Half a century since the discovery of the multipotency and regenerative properties of MSCs and thousands of clinical trials exploring their therapeutic benefits for several dozens of clinical indications, there are a few success stories that are emerging with successful clinical outcomes and regulatory approvals. MSC cell therapy has gained regulatory approval to address the unmet clinical needs in the areas of graft-versus-host disease, Crohn's disease, and critical limb ischemia [48]. Recently, adipose-derived MSCs were approved for the treatment of Chrohn's disease by EMA in 2018, called Alofisel [49]. The results published from this pivotal study of over 200 patients showed 56% of patients in the trial achieved lifesaving remission at 52 week post-treatment [49].

Table 1 adapted from Levy, et al. (2020) [50].

Asia is leading the way in approving and supporting these breakthrough cellular and gene therapies that have been termed Advanced Therapy Medicinal Products (ATMPs) [50]. In a 2019 report, EMA had approved fourteen ATMPS for use to address the unmet clinical need in patients and for some approved ATMPS. Some countries also support these breakthroughs but expensive therapies

through subsidies. Furthermore, there is debate throughout Europe to financially support the development and subsidise the use of these therapies in order to increase accessibility to patients in need [51, 52].

6. Conclusion

Allogeneic cell therapies are "off-the-shelf" options that provide innovative, efficacious, and safe treatment solutions for many of the untreatable diseases. Allogenic cell therapies are currently in use in many clinical trials and have also been approved for clinical use in several jurisdictions. Our review provides evidence that the alloreactivity risks of the implanted allogenic cells to the recipients are minimal and do not cause severe adverse reactions in patients. With several approved cell therapies, this heralds a new era of cell therapies for previously untreatable diseases such as Chrohn's disease and GvHD. However, many new cellular therapies that are in various stages of clinical trials and currently underway for the treatment of cancers and other degenerative medicine need close monitoring and stringent reporting of any unexpected adverse reactions along with the efficacy data. Cell therapy is an exciting emerging field and the continued reporting of the clinical outcome data is vital to help strengthen the future of this very promising modern live medicine.

Conflicts of Interest

The authors do not have any direct conflict of interest; however, they are employed by Magellan Stem Cells P/L in developing cellular therapy.

Acknowledgments

Figures were created with BioRender.com.

References

[1] W.-Z. Zhuang, Y.-H. Lin, L.-J. Su et al., "Mesenchymal stem/stromal cell-based therapy: mechanism, systemic safety and biodistribution for precision clinical applications," *Journal of Biomedical Science*, vol. 28, no. 1, 2021.

[2] A. Philippidis, *Kymriah, First CAR-T cancer immunotherapy approved by FDA*, 2017.

[3] A. Suche, O. S. Suche, K. Suche et al., "Novartis receives European Commission approval of its CAR-T cell therapy," *Kymriah®(tisagenlecleucel)*https://www.novartis.com/news/media-releases/novartis-receives-european-commission-approval-its-car-t-cell-therapy-kymriah-tisagenlecleucelhttps://novartis.gcs-web.com/Novartis-receives-European-Commission-approval-of-its-CAR-T-cell-therapy-Kymriah-tisagenlecleucel.

[4] H. Waldmann, G. Hale, G. Cividalli et al., "Elimination of graft-versus-host disease by in-vitro depletion of alloreactive lymphocytes with a monoclonal rat anti-human lymphocyte antibody (CAMPATH-1)," *The Lancet*, vol. 324, no. 8401, pp. 483–486, 1984.

[5] A. P. Schwarer, Y. Z. Jiang, A. J. Barrett et al., "Frequency of anti-recipient alloreactive helper T-cell precursors in donor blood and graft-versus-host disease after HLA-identical sibling bone-marrow transplantation," *The Lancet*, vol. 341, no. 8839, pp. 203–205, 1993.

[6] R. I. Lechler, J. Giovanna Lombardi, R. Batchelor, N. Reinsmoen, and F. H. Bach, "The molecular basis of alloreactivity," *Immunology Today*, vol. 11, pp. 83–88, 1990.

[7] R. T. Maziarz and H. M. Lazarus, "Mesenchymal stromal cells: impact on hematopoietic cell transplantation," in *Blood and Marrow Transplant Handbook*, pp. 859–870, Springer, Cham, 2021.

[8] G. Siegel, R. Schäfer, and F. Dazzi, "The immunosuppressive properties of mesenchymal stem cells," *Transplantation*, vol. 87, no. 9S, pp. S45–S49, 2009.

[9] M. F. Pittenger, A. M. Mackay, S. C. Beck et al., "Multilineage potential of adult human mesenchymal stem cells," *Science*, vol. 284, no. 5411, pp. 143–147, 1999.

[10] M. Krampera, S. Glennie, J. Dyson et al., "Bone marrow mesenchymal stem cells inhibit the response of naive and memory antigen-specific T cells to their cognate peptide," *Blood*, vol. 101, no. 9, pp. 3722–3729, 2003.

[11] P. A. Sotiropoulou, S. A. Perez, A. D. Gritzapis, C. N. Baxevanis, and M. Papamichail, "Interactions between human mesenchymal stem cells and natural killer cells," *Stem Cells*, vol. 24, no. 1, pp. 74–85, 2006.

[12] A. Corcione, F. Benvenuto, E. Ferretti et al., "Human mesenchymal stem cells modulate B-cell functions," *Blood*, vol. 107, no. 1, pp. 367–372, 2006.

[13] A. G. Zhao, K. Shah, B. Cromer, and H. Sumer, "Mesenchymal stem cell-derived extracellular vesicles and their therapeutic potential," *Stem Cells International*, vol. 2020, 10 pages, 2020.

[14] D. H. Munn, M. Zhou, J. T. Attwood et al., "Prevention of allogeneic fetal rejection by tryptophan catabolism," *Science*, vol. 281, no. 5380, pp. 1191–1193, 1998.

[15] S. Aggarwal and M. F. Pittenger, "Human mesenchymal stem cells modulate allogeneic immune cell responses," *Blood*, vol. 105, no. 4, pp. 1815–1822, 2005.

[16] L. Blanc, C. T. Katarina, K. Rosendahl, E. Zetterberg, and O. Ringdén, "HLA expression and immunologic propertiesof differentiated and undifferentiated mesenchymal stem cells," *Experimental hematology*, vol. 31, no. 10, pp. 890–896, 2003.

[17] M. Kabat, I. Bobkov, S. Kumar, and M. Grumet, "Trends in mesenchymal stem cell clinical trials 2004-2018: is efficacy optimal in a narrow dose range?," *Stem Cells Translational Medicine*, vol. 9, no. 1, pp. 17–27, 2020.

[18] K. Shah, T. Drury, I. Roic et al., "Outcome of allogeneic adult stem cell therapy in dogs suffering from osteoarthritis and other joint defects," *Stem Cells International*, vol. 2018, 7 pages, 2018.

[19] A.-J. Joswig, A. Mitchell, K. J. Cummings et al., "Repeated intra-articular injection of allogeneic mesenchymal stem cells causes an adverse response compared to autologous cells in the equine model," *Stem Cell Research & Therapy*, vol. 8, no. 1, pp. 1–11, 2017.

[20] N. Eliopoulos, J. Stagg, L. Lejeune, S. Pommey, and J. Galipeau, "Allogeneic marrow stromal cells are immune rejected by MHC class I–and class II–mismatched recipient mice," *Blood*, vol. 106, no. 13, pp. 4057–4065, 2005.

[21] L. Zangi, R. Margalit, S. Reich-Zeliger et al., "Direct imaging of immune rejection and memory induction by allogeneic mesenchymal stromal cells," *Stem Cells*, vol. 27, no. 11, pp. 2865–2874, 2009.

[22] A. K. Berglund, L. A. Fortier, D. F. Antczak, and L. V. Schnabel, "Immunoprivileged no more: measuring the immunogenicity of allogeneic adult mesenchymal stem cells," *Stem Cell Research & Therapy*, vol. 8, no. 1, pp. 1–7, 2017.

[23] E. C. Perin, K. M. Borow, G. V. Silva et al., "A phase II dose-escalation study of allogeneic mesenchymal precursor cells in patients with ischemic or nonischemic heart failure," *Circulation Research*, vol. 117, no. 6, pp. 576–584, 2015.

[24] J. M. Hare, J. E. Fishman, G. Gerstenblith et al., "Comparison of allogeneic vs autologous bone marrow–derived mesenchymal stem cells delivered by transendocardial injection in patients with ischemic cardiomyopathy," *JAMA*, vol. 308, no. 22, pp. 2369–2379, 2012.

[25] V. Florea, A. C. Rieger, D. L. DiFede et al., "Dose comparison study of allogeneic mesenchymal stem cells in patients with ischemic cardiomyopathy (the TRIDENT study)," *Circulation Research*, vol. 121, no. 11, pp. 1279–1290, 2017.

[26] L. Von Bahr, I. Batsis, G. Moll et al., "Analysis of tissues following mesenchymal stromal cell therapy in humans indicates limited long-term engraftment and no ectopic tissue formation," *Stem Cells*, vol. 30, no. 7, pp. 1575–1578, 2012.

[27] L. Gasperini, J. F. Mano, and R. L. Reis, "Natural polymers for the microencapsulation of cells," *Journal of the Royal Society Interface*, vol. 11, no. 100, p. 20140817, 2014.

[28] C. Hoeeg, A. Dolatshahi-Pirouz, and B. Follin, "Injectable hydrogels for improving cardiac cell therapy-in vivo evidence and translational challenges," *Gels*, vol. 7, no. 1, p. 7, 2021.

[29] M. E. Wechsler, V. V. Rao, A. N. Borelli, and K. S. Anseth, "Engineering the MSC secretome: a hydrogel focused approach," *Advanced Healthcare Materials*, vol. 10, no. 7, 2021.

[30] K. Shah, A. G. Zhao, and H. Sumer, "New approaches to treat osteoarthritis with mesenchymal stem cells," *Stem Cells International*, vol. 2018, 9 pages, 2018.

[31] A. K. Singh and J. P. McGuirk, "CAR T cells: continuation in a revolution of immunotherapy," *The Lancet Oncology*, vol. 21, no. 3, pp. e168–e178, 2020.

[32] R. Huang, X. Li, Y. He et al., "Recent advances in CAR-T cell engineering," *Journal of Hematology & Oncology*, vol. 13, no. 1, 2020.

[33] S. Depil, P. Duchateau, S. A. Grupp, G. Mufti, and L. Poirot, "'Off-the-shelf' allogeneic CAR T cells: development and challenges," *Nature Reviews Drug Discovery*, vol. 19, no. 3, pp. 185–199, 2020.

[34] H. Link and L. Arseniev, "CD34 positive blood cells for allogeneic progenitor and stem cell transplantation," *Leukemia & Lymphoma*, vol. 26, no. 5-6, pp. 451–465, 1997.

[35] P. Hénon, "Key success factors for regenerative medicine in acquired heart diseases," *Stem Cell Reviews and Reports*, vol. 16, no. 3, pp. 441–458, 2020.

[36] P.-H. Sung, Y.-C. Li, M. S. Lee et al., "Intracoronary injection of autologous CD34+ cells improves one-year left ventricular systolic function in patients with diffuse coronary artery disease and preserved cardiac performance—a randomized, open-label, controlled phase II clinical trial," *Journal of Clinical Medicine*, vol. 9, no. 4, p. 1043, 2020.

[37] D. W. Losordo, T. D. Henry, C. Davidson et al., "Intramyocardial, autologous CD34+ cell therapy for refractory angina," *Circulation Research*, vol. 109, no. 4, pp. 428–436, 2011.

[38] D. Wolf, M. von Lilienfeld-Toal, A. M. Wolf et al., "Novel treatment concepts for graft-versus-host disease," *Blood*, vol. 119, no. 1, pp. 16–25, 2012.

[39] J. G. Rheinwald and H. Green, "Formation of a keratinizing epithelium in culture by a cloned cell line derived from a teratoma," *Cell*, vol. 6, no. 3, pp. 317–330, 1975.

[40] H.-J. You and S.-K. Han, "Cell therapy for wound healing," *Journal of Korean Medical Science*, vol. 29, no. 3, pp. 311–319, 2014.

[41] H. Yanaga, Y. Udoh, M. Yamamoto et al., "Cryopreserved cultured epithelial allografts for pediatric deep partial dermal burns: early wound closure and suppression of scarring," *Regenerative therapy*, vol. 6, pp. 74–82, 2017.

[42] V. B. Morhenn, C. J. Benike, A. J. Cox, D. J. Charron, and E. G. Engleman, "Cultured human epidermal cells do not synthesize HLA-DR," *Journal of Investigative Dermatology*, vol. 78, no. 1, pp. 32–37, 1982.

[43] R. I. Domínguez-Castillo, E. Sánchez-Guzmán, F. Castro-Muñozledo, L. Santos-Argumedo, and W. Kuri-Harcuch, "Epidermal keratinocytes do not activate peripheral T-cells: interleukin-10 as a possible regulator," *Immunology*, vol. 125, no. 3, pp. 370–376, 2008.

[44] J. M. Centanni, J. A. Straseski, A. Wicks et al., "StrataGraft skin substitute is well-tolerated and is not acutely immunogenic in patients with traumatic wounds: results from a prospective, randomized, controlled dose escalation trial," *Annals of Surgery*, vol. 253, no. 4, pp. 672–683, 2011.

[45] J. M. Leyva-Castillo, P. Hener, H. Jiang, and M. Li, "TSLP produced by keratinocytes promotes allergen sensitization through skin and thereby triggers atopic march in mice," *Journal of Investigative Dermatology*, vol. 133, no. 1, pp. 154–163, 2013.

[46] P. Braendstrup, B. L. Levine, and M. Ruella, "The long road to the first FDA-approved gene therapy: chimeric antigen receptor T cells targeting CD19," *Cytotherapy*, vol. 22, no. 2, pp. 57–69, 2020.

[47] J. C. Chavez, C. Bachmeier, and M. A. Kharfan-Dabaja, "CAR T-cell therapy for B-cell lymphomas: clinical trial results of available products," *Therapeutic advances in hematology*, vol. 10, p. 204062071984158, 2019.

[48] K. P. Robb, J. C. Fitzgerald, F. Barry, and S. Viswanathan, "Mesenchymal stromal cell therapy: progress in manufacturing and assessments of potency," *Cytotherapy*, vol. 21, no. 3, pp. 289–306, 2019.

[49] C. Sheridan, *First off-the-shelf mesenchymal stem cell therapy nears European approval*, 2018.

[50] O. Levy, R. Kuai, E. M. Siren et al., "Shattering barriers toward clinically meaningful MSC therapies," *Advances*, vol. 6, no. 30, p. eaba6884, 2020.

[51] E. Hanna, C. Marre, and M. Toumi, "PBI59 the reimbursement status of advanced therapy medicinal products in Europe," *Value in Health*, vol. 22, p. S428, 2019.

[52] S. Walzer, M. Prada, I. Berard et al., "PBI38 innovative ATMPS: market access and reimbursement decisions in the EU5: availability or not, that is the question...," *Value in Health*, vol. 22, p. S424, 2019.

Hindawi
Stem Cells International
Volume 2022, Article ID 6450527, 13 pages
https://doi.org/10.1155/2022/6450527

Research Article

Mesenchymal Stem Cell-Derived Neuron-Like Cell Transplantation Combined with Electroacupuncture Improves Synaptic Plasticity in Rats with Intracerebral Hemorrhage via mTOR/p70S6K Signaling

Guoqiang Yang,[1,2] **Jiayi Zhu**,[3] **Guwen Zhan**,[4] **Guangbi Fan**,[3] **Li Deng**,[3] **Huajun Tang**,[3] **Xiaoqian Jiang**,[3] **Bo Chen**,[3] **and Chaoxian Yang**[3]

[1]*Research Center of Combine Traditional Chinese and Western Medicine, Affiliated Traditional Medicine Hospital, Southwest Medical University, Luzhou 646000, China*
[2]*Research Unit of Molecular Imaging Probes, Department of Radiologic Technology, Faculty of Associated Medical Sciences, Chiang Mai University, Chiang Mai 50200, Thailand*
[3]*Department of Anatomy and Histoembryology, School of Basic Medical Science, Southwest Medical University, Luzhou 646000, China*
[4]*Department of Emergency, The Fourth People's Hospital of Taizhou City, Taizhou 225300, China*

Correspondence should be addressed to Bo Chen; cb0402022@swmu.edu.cn and Chaoxian Yang; lyycx@foxmail.com

Received 8 July 2021; Revised 24 December 2021; Accepted 11 January 2022; Published 15 February 2022

Academic Editor: Sangho Roh

Previous studies have shown that the combination of mesenchymal stem cell (MSC) transplantation and electroacupuncture (EA) stimulation is a neuroprotective strategy for treating intracerebral hemorrhage (ICH). However, the underlying mechanisms by which the combined treatment promotes neuroprotection remain unclear. This study was designed to investigate the effects of the combined treatment on synaptic plasticity and elucidate their underlying mechanisms. Therefore, rat ICH models were established by injecting collagenase and heparin, and the animals were randomly divided into model control (MC), EA stimulation (EA), MSC-derived neuron-like cell transplantation (MSC-dNLCs), and MSC-dNLC transplantation combined with EA stimulation (MSC-dNLCs+EA) groups. We observed the ultrastructure of the brain and measured the brain water content (BWC) and the levels of the microtubule-associated protein 2 (MAP2), galactocerebrosidase (GALC), and glial fibrillary acidic protein (GFAP) proteins. We also measured the levels of the phosphorylated mammalian target of rapamycin (mTOR) and 70 kDa ribosomal protein S6 kinase (p70S6K) proteins, as well as the expression of synapse-related proteins. The BWC increased in rats after ICH and decreased significantly in ICH rats treated with MSC-dNLC transplantation, EA stimulation, or combined therapy. Meanwhile, after ICH, the number of blood vessels increased more evidently, but only the combined treatment reduced the number of blood vessels among rats receiving the three treatments. Moreover, the levels of MAP2, GALC, postsynaptic density 95 (PSD95), and synaptophysin (SYP) proteins, as well as the levels of the phosphorylated mTOR and p70S6k proteins, increased in the MSC-dNLCs+EA group compared with those in the MSC-dNLCs and EA groups. Compared with the MC group, GFAP expression was significantly reduced in the MSC-dNLCs, EA, and MSC-dNLCs +EA groups, but the differences among the three treatment groups were not significant. In addition, the number of synapses increased only in the MSC-dNLCs+EA group compared to the MC group. Based on these data, the combination of MSC-dNLC transplantation and EA stimulation exerts a synergistic effect on improving the consequences of ICH by relieving cerebral edema and glial scarring, promoting the survival of neurons and oligodendrocytes, and activating mTOR/p70S6K signaling to enhance synaptic plasticity.

1. Introduction

Intracerebral hemorrhage (ICH) is a crucial cause of neurological morbidity and mortality worldwide [1–3] and is estimated to affect over 1 million people worldwide each year [4]. After ICH, hematoma or edema induces oxidative stress and the inflammatory response, excitotoxicity, and reactive oxygen species (ROS) generation, which may induce the death of a large number of neuronal cells. More than 30% of ICH survivors live with severe movement dysfunction, and over 70% of these patients suffer cognitive impairment [5, 6], but few proven treatments are used in clinical practice [2, 7–9].

Mesenchymal stem cells (MSCs) are considered promising seed cells for nervous system diseases because they have the properties of weak immunogenicity, good safety, and easy cultivation [10–12]. Many studies have confirmed that MSCs improve neurological functional recovery following ICH [13–17]. However, transplanted MSCs display a limited ability to repair damaged tissue because they do not substantially increase synapse-related protein expression in the damaged brain [18, 19]. Electroacupuncture (EA) is a part of the traditional Chinese medicine field. Some studies have shown that EA improves nerve function in the brain of subjects with ICH [20–23]. Does the transplantation of MSCs combined with EA therapy exert a good therapeutic effect? Previous studies have indicated that the transplantation of MSCs combined with EA stimulation promotes axonal regeneration and functional recovery of the injured spinal cord [24, 25] and leads to a better therapeutic effect by increasing the expression of neurotrophic factors, regulating neurogenesis, and increasing the neural differentiation of transplanted cells in ischemic stroke compared with a single therapy [26, 27]. We also confirmed that the combined treatment improves neurological function in rats with ICH in a previous study [28]. However, the exact mechanism by which MSCs combined with EA improve neurological function remains to be further explored.

After ICH, the destroyed brain structure induces the destruction of the synaptic structure. Increasing synaptic plasticity and rebuilding neural functional networks are the basis of restoring neural function. Synaptic plasticity is the ability of neurons to modify their connections and is involved in brain network remodeling following brain damage [29]. Although synaptic plasticity has been widely clarified in many other diseases, including Alzheimer's disease [30] and mood disorders [31], it has rarely been studied in hemorrhagic brain injury. The mammalian target of rapamycin (mTOR) signaling pathway senses and integrates various environmental signals to regulate organismal growth and homeostasis and regulates important cellular processes, including proliferation, growth, survival, and mobility [32]. Moreover, activated mTOR increases the levels of synaptic signaling proteins and increases the number and function of new spine synapses in depressed rats [33]. mTOR promotes protein synthesis by phosphorylating two key effectors, one of which is 70 kDa ribosomal protein S6 kinase (p70S6K) [34]. To date, studies have seldom focused on changes in mTOR/p70S6K signaling related to synaptic plasticity after ICH.

In this experiment, we examined the effects of a combined treatment with MSC-derived neuron-like cells (MSC-dNLCs) and EA on the brain water content (BWC), numbers of blood vessels and synapses, expression of marker proteins of neurons, oligodendrocytes and astrocytes, synapse-associated proteins, and levels of phosphorylated mTOR and p70S6K proteins in rats with ICH. We also investigated the effect of the combined treatment on synaptic plasticity and possible mechanisms.

2. Materials and Methods

2.1. Animals. Healthy adult Sprague–Dawley rats weighing between 200 and 250 g were provided by the SPF Laboratory Animal Center of Southwest Medical University (Luzhou, Sichuan, China). All of them were housed in the same animal care facility with a standard temperature (23 ± 2°C), lighting (12/12 h light/dark cycle), and relative humidity (65 ± 5%) and free access to food and water. The procedures for the animal experiments were performed in accordance with the Guidance and Suggestions for the Care and Use of Laboratory Animals formulated by the Ministry of Science and Technology of China. The animal protocol was approved by the Animal Ethics Committee of the Animal Center of Southwest Medical University (Luzhou, Sichuan, China), and the experimental procedures were optimized to minimize the number of animals and alleviate the pain experienced by the experimental animals. The rats were randomly divided into five groups: the sham operation (SO) group, the model control (MC) group, the MSC-dNLC transplantation (MSC-dNLCs) group, the EA stimulation (EA) group, and the combined treatment with MSC-dNLC transplantation and EA stimulation (MSC-dNLCs+EA) group, which were assigned to the following five experimental procedures, respectively (Figure 1(a)).

2.2. Rat Model of Intracerebral Hemorrhage. Rats were anesthetized by intraperitoneally injecting a dose of 40 mg/kg of 1% pentobarbital sodium and fixed on a stereotaxic apparatus (in a prone position) while maintaining the anterior and posterior fontanelles at the same level. The scalp was incised sagittally approximately 10 mm; then, the anterior fontanelle was exposed after treatment with 30% H_2O_2. A burr hole (1 mm) was drilled on the right calvarial bone at a point 3 mm lateral and 0.2 mm anterior to the anterior fontanelle. A mixture containing heparin (1 μl, 2.0 U/μl) and collagenase I (2 μl, 0.125 U/μl) was drawn into a 5 μl microsyringe. The needle was fixed on the stereotaxic apparatus and inserted into the caudate nucleus (location: 6 mm depth to the hole); the location of the injection point is shown in the schematic diagrams (Figure 1(b)). Then, the mixture was slowly injected. After injection, the burr hole was sealed with bone wax, and the skin was sutured. The sham group underwent the same procedure as described above, except that the mixture was not injected.

2.3. EA Stimulation. EA stimulation was conducted as described in our previous study [20]. The rats in the MSC-dNLCs+EA and EA groups were stimulated with EA 48

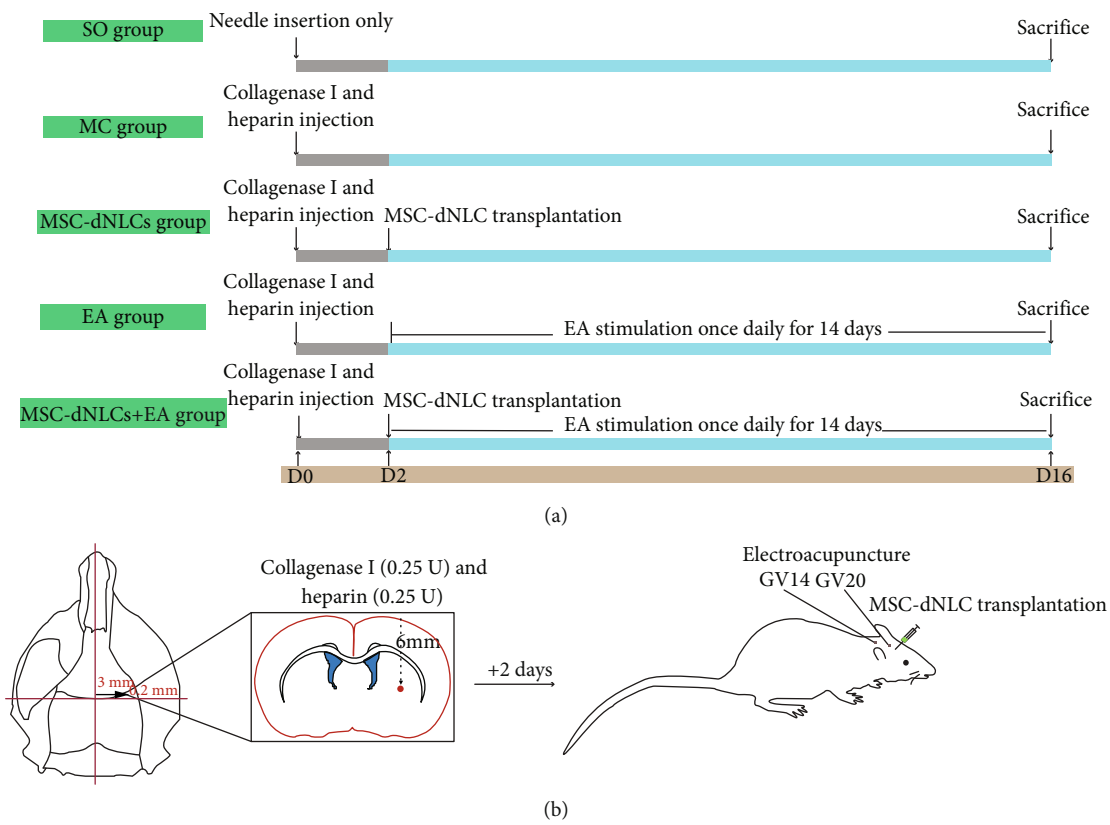

Figure 1: Conceptual illustrations of the experimental protocols. (a) Grouping and treatment strategies for experimental animals and brief timelines of the experimental procedures. (b) Schematic diagrams of the rat ICH model along with MSC-dNLC transplantation and EA stimulation.

hours after successful modeling. Two sterile acupuncture needles with diameters of 0.25 mm were inserted into the Baihui (GV20) and Dazhui (CV14) acupoints and connected to the type G-6805 EA stimulator (HM6805, China). The rats were stimulated with continuous waves at a current of 1 mA, frequency of 3 Hz, and stimulation duration of 10 min once a day. EA was performed consecutively for fourteen days until the rats were sacrificed.

2.4. Resuscitation and Culture of MSCs. Rat MSCs labeled with green fluorescent protein (GFP) (Cyagen Biosciences, China) [28] were removed from liquid nitrogen, thawed in a 37°C water bath, and then centrifuged. After centrifugation, MSCs were resuspended in alpha-minimum essential medium (α-MEM) (HyClone) supplemented with 10% fetal bovine serum (FBS, HyClone), 100 mg/ml streptomycin, and 100 U/ml penicillin and incubated in a humidified atmosphere with 5% CO_2 at 37°C. When the MSCs grew to 80% confluence, the cells were trypsinized using 0.25% trypsin and 1 mM EDTA and passaged. MSCs at passages 3-6 were used for subsequent experiments.

2.5. MSC Transplantation. Before transplantation, MSCs were induced as described in our previous study [35]. In brief, MSCs were treated with preinduction medium composed of α-MEM supplemented with 10% FBS and 1 mmol/l β-mercaptoethanol (β-ME) for 24 hours and then with neuronal induction medium composed of α-MEM supplemented with 1 mmol/l β-ME, 2% dimethylsulfoxide (DMSO), and 1 μmol/l all-trans retinoic acid (RA) (Sigma) for 6 hours. Afterward, MSC-dNLCs were collected, and the cell density was adjusted to 2.5×10^7 cells per ml. Then, an MSC-dNLC suspension (20 μl) was extracted with a microsyringe and injected into the brains (location: right of anterior fontanelle: 3 mm; anterior of anterior fontanelle: 0.2 mm; depth: 6 mm) of rats in the MSC-dNLCs+EA and the MSC-dNLCs groups at an injection rate of 2 μl/min after 48 hours when the rats were successfully modeled. Then, the needle hole was sealed with bone wax, and the skin was sutured and disinfected.

2.6. Brain Edema Examination. The BWC was measured using a previously reported method [36]. Briefly, animals were anesthetized and then decapitated. The brains were quickly removed, and the right basal ganglia were separated and weighed immediately on a precise electronic balance to determine the wet weight. After drying in an oven for 24 h at 100°C, the right basal ganglia were weighed again to measure the dry weight. The BWC was calculated as [(wet weight − dry weight)/wet weight] × 100%.

2.7. Immunohistochemistry. Rats were anesthetized by administering an intraperitoneal injection of an overdose of pentobarbital sodium and successively transcardially perfused

with 0.9% normal saline and 4% paraformaldehyde in 0.01 M phosphate-buffered saline (PBS, pH 7.4). Subsequently, the brains were removed, postfixed, and dehydrated before frozen sections were cut at a thickness of 10 μm with a freezing microtome (CM1950, Leica, Germany).

After permeabilization with 0.3% Triton X-100 in 0.01 M PBS for 30 min at room temperature (RT) and blocking with 10% goat serum, sections were immunostained with the following primary antibodies: rabbit anti-laminin (Boster, China, diluted 1 : 100), mouse anti-MAP2 (Santa Cruz, USA, diluted 1 : 200), rabbit anti-GALC (Invitrogen, USA, diluted 1 : 200), mouse anti-GFAP (Santa Cruz, USA, diluted 1 : 200), rabbit anti-mTOR (CST, USA, diluted 1 : 200), mouse anti-p70S6K (Santa Cruz, USA, diluted 1 : 200), mouse anti-PSD95 (Santa Cruz, USA, diluted 1 : 200), and mouse anti-synaptophysin (SYP) (Santa Cruz, USA, diluted 1 : 200), which were diluted with 1% BSA/PBS (w/v). The sections were incubated with the primary antibodies overnight at 4°C and then incubated with horseradish peroxidase- (HRP-) conjugated goat anti-rabbit or anti-mouse secondary antibodies (Invitrogen, USA) at RT for 1.5 h. The sections were sequentially stained with diaminobenzidine and hematoxylin. Finally, the slices were imaged using a microscope (Olympus, Japan).

2.8. Immunofluorescence Staining. Frozen sections were washed with 0.01 M PBS for 10 minutes and then treated with 0.3% Triton X-100 at RT for 20 minutes. After blocking with 10% normal goat serum at 37°C for 30 minutes, the samples were incubated with primary antibodies (MAP2, GALC, GFAP, PSD95, and SYP) overnight at 4°C under humidified conditions and then incubated with Alexa Fluor 594-conjugated goat anti-mouse/rabbit IgG (1 : 500, Invitrogen) at RT for 60 min. Finally, sections were stained with 4′,6-diamidino-2-phenylindole (DAPI) and covered with fluorescence mounting medium (Dako).

2.9. Western Blotting. After anesthetization, the animals were decapitated, and brain tissues collected from rats in different groups were homogenized in ice-cold protein extraction reagent. Then, the total protein concentration in every sample from different groups was quantified using the BCA protein assay. Equal amounts of protein (50 μg) were separated by sodium dodecyl sulfate–polyacrylamide gel electrophoresis and transferred to polyvinylidene fluoride (PVDF) membranes. Then, the membranes were incubated with primary antibodies against MAP2 (diluted 1 : 1000), GALC (diluted 1 : 1000), GFAP (diluted 1 : 1000), mTOR, p-mTOR (CST, USA, diluted 1 : 1000), p70S6K, p-p70S6K (Santa Cruz, USA, diluted 1 : 1000), PSD95 (diluted 1 : 1000), SYP (1 : 1000), and GAPDH (Abcam, United Kingdom, diluted 1 : 10000) at 4°C overnight. After incubation with HRP-conjugated goat anti-mouse/rabbit IgG (Bio-Rad, USA, diluted 1 : 2000) at RT for 2 h, the membranes were immersed in an enhanced chemiluminescence (ECL) solution (Millipore, USA) and exposed using an ImageQuant ECL Imager. The protein levels were normalized to the corresponding amount of GAPDH and analyzed using Quantity One software.

2.10. Ultrastructural Observation. Rats were anesthetized, their brains were removed, and caudoputamen samples (the peripheral hematoma zone) were dissected into 1 mm^3 pieces and fixed with 3% glutaraldehyde at 4°C. After fixation with 1% osmium tetroxide for 2 h, the pieces were dehydrated through a graded series of acetone solutions, infiltrated with propylene epoxide, and embedded in Epon 618 resin. Sections were cut at a thickness of 40 nm, mounted onto a 200-mesh copper grid, and observed with a JEM-1400 series transmission electron microscope (TEM) (Japan Electron Optics Laboratory, Japan). Digital images of the specimens were acquired using an integrated high-sensitivity complementary metal-oxide-semiconductor (CMOS) camera and analyzed by experienced electron microscopists.

2.11. Statistical Analysis. Parametric data were analyzed using GraphPad Prism 8 software and displayed as the means ± standard errors of the means (SEM). Significant differences between multiple groups were analyzed using one-way ANOVA, and $P < 0.05$ was considered statistically significant.

3. Results

3.1. Induction and Transplantation of MSCs. MSCs labeled with GFP grew in a cluster shape and presented green fluorescence under a fluorescence microscope (Figure 2(a)). After induction with neuronal induction medium, MSC-dNLCs showed changes resembling neuron-like cells (Figure 2(b)). The hemorrhagic area was still seen in the basal ganglia region in the coronal incision (Figure 2(c)). Transplanted MSC-dNLCs were observed in rats from the MSC-dNLCs and MSC-dNLCs+EA groups (Figure 2(d)).

3.2. The Combined Treatment Reduced the Number of Blood Vessels and Attenuated Brain Edema. Immunohistochemical staining for laminin was used to observe blood vessels. The number of blood vessels increased obviously in rats after ICH ($P < 0.05$), and the combined treatment significantly reduced the number of blood vessels (30.32 ± 9.71%) compared with the MC group ($P < 0.05$), but the numbers of blood vessels in the three treatment groups were not significantly different ($P > 0.05$) (Figures 3(a) and 3(c)). TEM showed that although the tissue structure around blood vessels was loose in ICH rats, the vascular structure of each group was intact (Figure 3(b)). The BWC increased significantly in rats after ICH ($P < 0.05$) but was decreased in the EA, MSC-dNLCs, and MSC-dNLCs+EA groups compared with the MC group ($P < 0.05$) (Figure 3(d)). Moreover, EA stimulation and the combined treatment reduced the BWC to a greater extent than MSC-dNLC transplantation in ICH rats (Figure 3(d)).

3.3. The Combined Treatment Increased the Levels of the MAP2 and GALC Proteins and Decreased the Level of the GFAP Protein. The expression of the MAP2 (neuron marker), GALC (oligodendrocyte marker), and GFAP (astrocyte marker) proteins was detected using immunohistochemical staining and western blotting. Figures 4(a)–4(c)

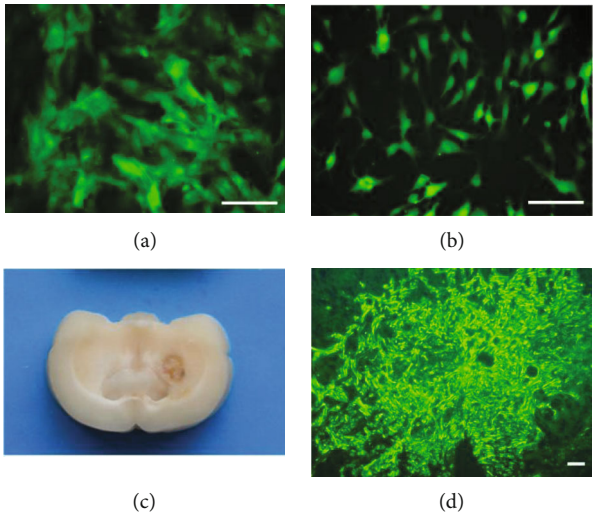

Figure 2: Induction and transplantation of MSCs. (a) Cultured MSCs labeled with GFP. Scale bar = 100 μm. (b) MSCs induced by neuronal induction medium. Scale bar = 100 μm. (c) The hemorrhagic area in the basal ganglia of the ICH model. (d) Transplanted MSC-dNLCs/GFP in the brains of ICH rats. Scale bar = 100 μm.

show the distribution of MAP2-, GALC-, and GFAP-positive cells. Immunofluorescence staining revealed that a few of the transplanted cells (GFP-positive cells) coexpressed MAP2, GALC, and GFAP in both the MSC-dNLCs and MSC-dNLCs+EA groups (Figures 4(d)–4(f)). The results of western blotting showed that the levels of the MAP2 and GALC proteins decreased, but the level of the GFAP protein was increased in rats after ICH ($P < 0.05$, Figures 4(g)–4(j)). Compared with the MC group, the expression level of the MAP2 protein was increased in the EA and MSC-dNLCs +EA groups, and the level of the GALC protein was increased in the MSC-dNLCs and MSC-dNLCs+EA groups, but the level of the GFAP protein was decreased in the EA, MSC-dNLCs, and MSC-dNLCs+EA groups ($P < 0.05$, Figures 4(g)–4(j)). Moreover, levels of the MAP2 and GALC proteins increased significantly in the MSC-dNLCs+EA group compared with the EA and MSC-dNLCs groups ($P < 0.05$, Figures 4(g)–4(i)).

3.4. The Combined Treatment Increased the Levels of Synapse-Related Proteins. Figures 5(a) and 5(b) show the distribution of PSD95 and SYP immunopositive products. In addition, the histological evaluation of transplanted MSC-dNLCs confirmed the coexpression of GFP and PSD95 or SYP in the MSC-dNLCs and MSC-dNLCs+EA groups (Figures 5(c) and 5(d)). Western blotting analyses revealed decreased levels of the PSD95 and SYP proteins in rats after ICH ($P < 0.05$, Figures 5(e)–5(g)). PSD95 expression increased in the EA, MSC-dNLCs, and MSC-dNLCs +EA groups, and SYP expression increased in the MSC-dNLCs and MSC-dNLCs+EA groups compared with the MC group ($P < 0.05$, Figures 5(e)–5(g)). Furthermore, the combined treatment obviously increased the levels of the PSD95 and SYP proteins compared with the single treatment ($P < 0.05$, Figures 5(e)–5(g)).

3.5. The Combined Treatment Increased the Number of Synapses. The synapse density was calculated to quantitatively investigate synaptic degradation, and the results showed a reduced number of synapses (per 100 μm^2) in rats after ICH ($P < 0.05$). However, a significant difference in the number of synapses was not observed among the EA, MSC-dNLCs, and MSC-dNLCs+EA groups (Figure 6). In addition, the number of synapses increased in only the MSC-dNLCs+EA group compared with that in the MC group ($P < 0.05$, Figure 6).

3.6. The Combined Treatment Activated mTOR and p70S6K. Immunohistochemical staining showed that mTOR and p70S6K proteins were expressed in all groups (Figures 7(a) and 7(b)). The western blot results showed significantly decreased levels of the phosphorylated mTOR and p70S6K proteins in rats after ICH ($P < 0.05$, Figures 7(c)–7(f)). EA stimulation increased the level of the phosphorylated mTOR protein, and MSC-dNLC transplantation increased the levels of the phosphorylated mTOR and p70S6K proteins ($P < 0.05$, Figures 7(c)–7(f)). Furthermore, compared with the MSC-dNLCs and EA groups, the levels of the phosphorylated mTOR and p70S6K proteins were obviously increased in the MSC-dNLCs+EA group ($P < 0.05$, Figures 7(c)–7(f)).

4. Discussion

The present study investigated the effect of the combination of MSC-dNLC transplantation and EA stimulation on synaptic plasticity and its molecular mechanisms in ICH rats. For this purpose, we evaluated cell survival, the number of synapses, the levels of synapse-associated proteins, and the levels of the phosphorylated mTOR and p70S6K proteins. The results suggested that the combined treatment exerts a synergistic effect on improving synaptic plasticity through mTOR/p70S6K signaling.

After ICH, brain edema occurs early, with a substantial increase of approximately 75% of its maximum volume during the first 24 hours, and then continues to develop over an extended period of days to nearly 2 weeks [2, 37, 38]. Brain

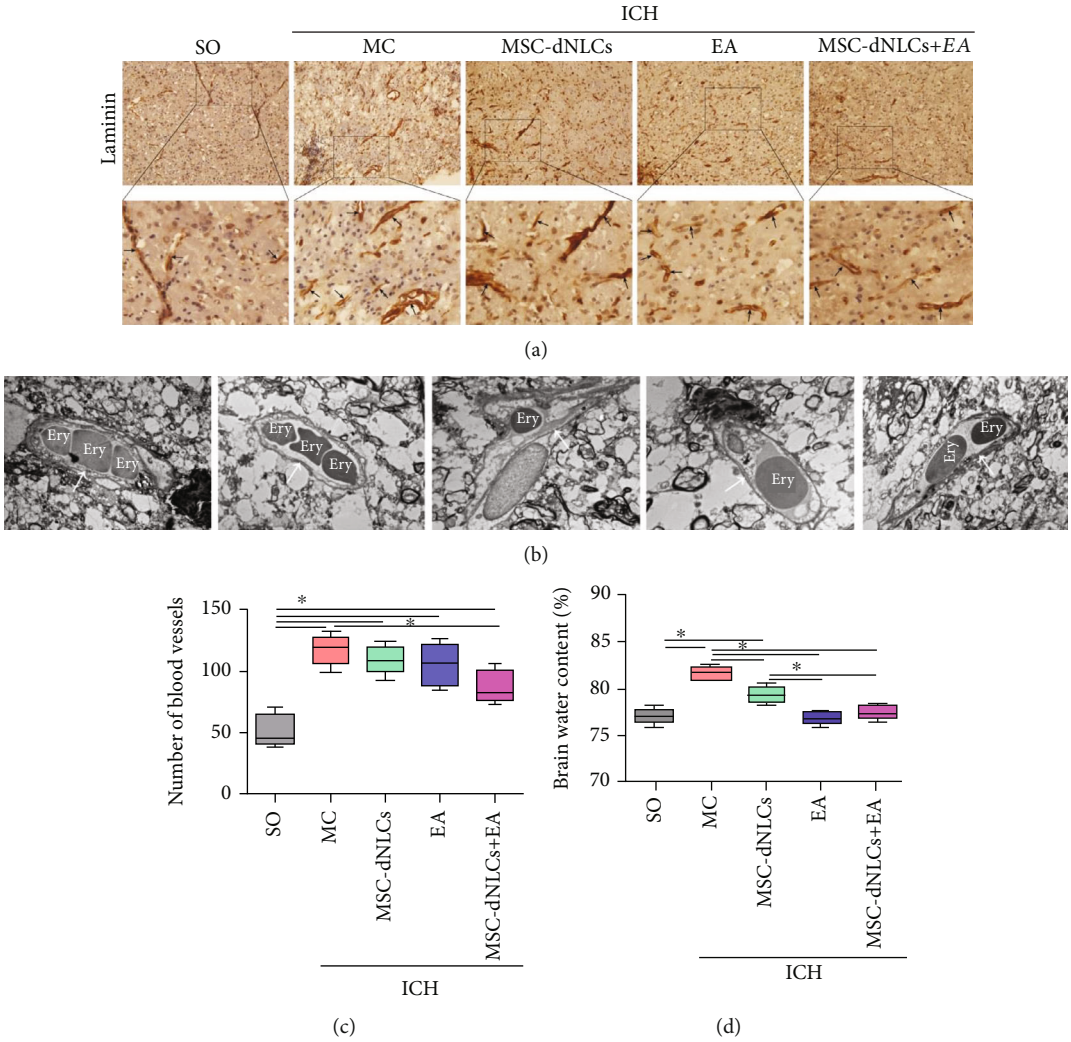

Figure 3: The combined treatment reduced the number of blood vessels and attenuated brain edema in rats with ICH. (a) Images of laminin immunohistochemistry in the ipsilateral striatum of rats. The black arrows show blood vessels. Scale bar = 100 μm. (b) Electron photomicrographs of blood vessels in the peripheral area of hemorrhagic foci. The white arrows show capillaries, and ery indicates erythrocytes. Scale bar = 5 μm. (c) The number of blood vessels in different groups ($n = 5$ rats per group; $^*P < 0.05$). (d) The brain water content of brain samples from different groups ($n = 5$ rats per group; $^*P < 0.05$).

edema is considered a radiological marker and contributes to poor outcomes in patients with ICH due to secondary injury after ICH [38–40]. In this study, our results showed that the three different treatments all reduced the BWC in ICH rats, and the BWC decreased more significantly in the MSC-dNLCs+EA group than in the MSC-dNLCs group. Thus, EA stimulation further alleviates brain edema after MSC-dNLC transplantation. Laminin, one of the primary functional components in basement membranes of blood vessels in most tissues [41–43], has been used to visualize blood vessels through immunohistochemical staining. Laminin overexpression, which is one of the consequences of vasogenic edema, may promote the migration of newly generated vessels to repair blood–brain barrier (BBB) disruption [44]. Loss of laminin aggravates BBB damage by regulating brain water homeostasis in ICH mice [45]. In this experiment, we observed an increased number of blood vessels in the MC, EA, MSC-dNLCs, and MSC-dNLCs+EA groups compared with the SO group, and the vascular structure was intact. Interestingly, the combined treatment reduced the number of blood vessels in ICH rats. The combined treatment inhibits hyperplasia of blood vessels, and a proper number of blood vessels might decrease the BWC in rats with ICH.

ICH may cause massive cell death, including glial cells and neurons [46, 47], in the brain through many mechanisms, such as inflammation [48], oxidative stress [49], and cytotoxicity [50]. Oligodendrocyte and neuron death are associated with demyelination and neurological dysfunction [51, 52]. Reactive astrogliosis, a pathological change associated with CNS injury, potentially promotes brain repair and reduces neurological impairment [53]. Reactive astrocytes exert beneficial effects by secreting neurotrophic substances that protect neurons at early stages [54]. However, excessive proliferation of reactive astrocytes leads to glial scar formation, which definitely impairs axon growth and

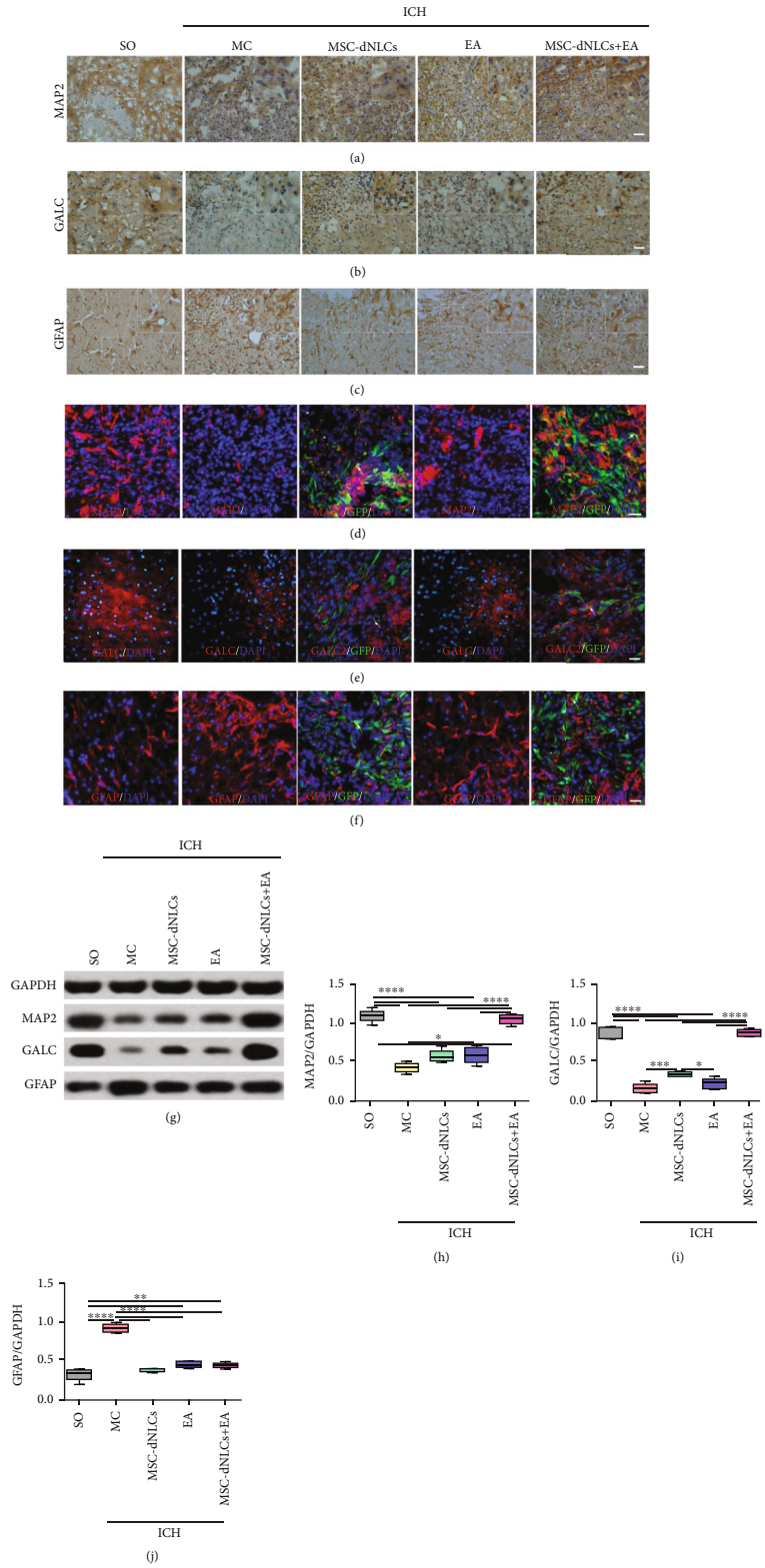

Figure 4: The expression of the MAP2, GALC, and GFAP proteins in different groups was detected using immunohistochemical staining and western blotting. (a–c) Representative images of MAP2 (a), GALC (b), and GFAP (c) immunohistochemical staining in the ipsilateral striatum of animals from different groups. Scale bar = 100 μm. (d–f) Representative images of MAP2 (d), GALC (e), and GFAP (f) immunofluorescence staining in the ipsilateral striatum of rats from different groups. Scale bar = 100 μm. (g–j) Representative results (g) and quantitative analyses (h–j) of western blotting showed the relative expression of the MAP2, GALC, and GFAP proteins in the ipsilateral striatum of rats from different groups ($n = 5$ animals per group; $^{*}P < 0.05$, $^{**}P < 0.01$, $^{***}P < 0.001$, and $^{****}P < 0.0001$).

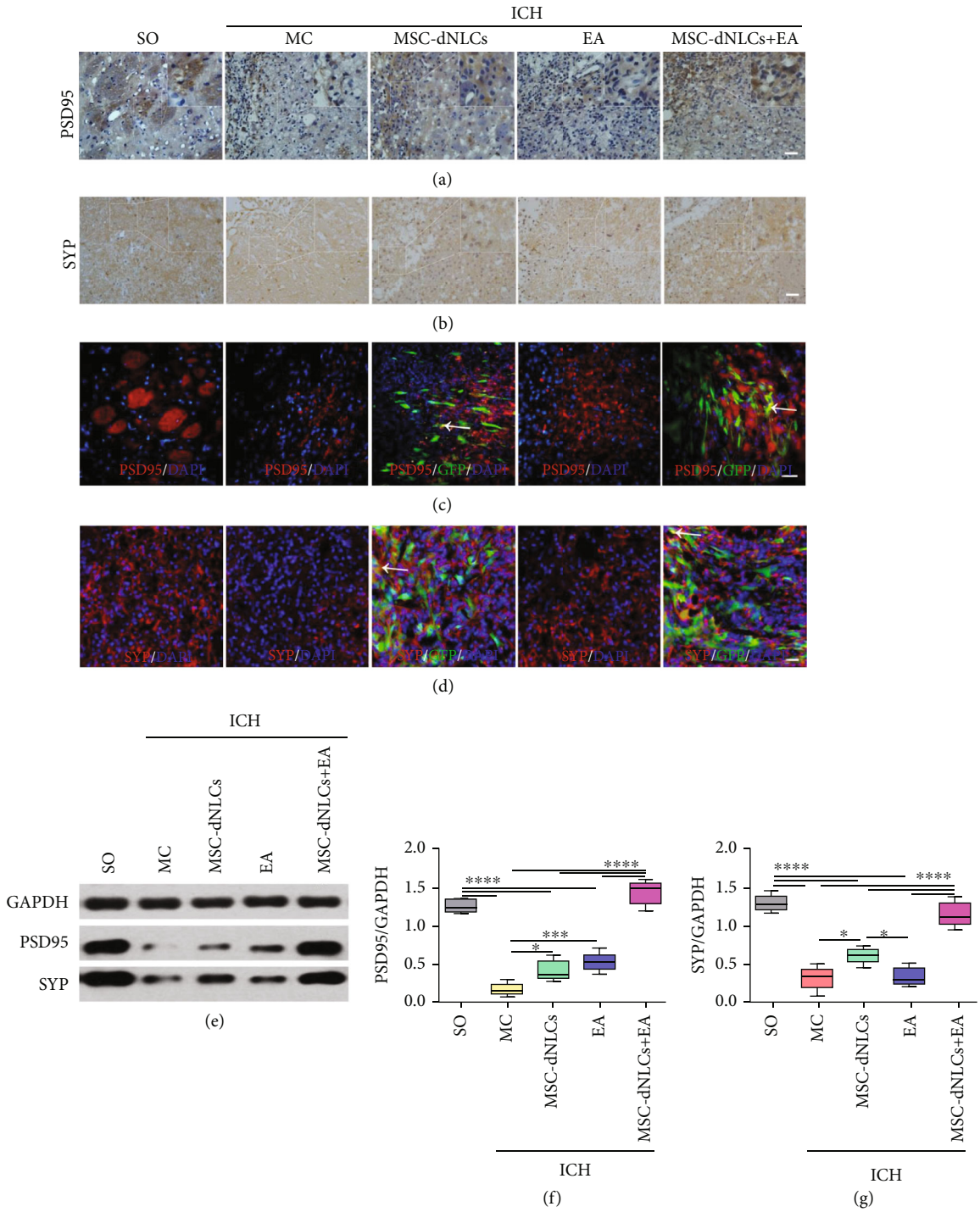

Figure 5: The expression of the PSD95 and SYP proteins in different groups. (a, b) Representative images of PSD95 (a) and SYP (b) immunohistochemical staining in the ipsilateral striatum of rats from different groups. Scale bar = PSD96. (c, d) Representative images of PSD95 (c) and SYP (d) immunofluorescence staining in the ipsilateral striatum of rats from different groups. Scale bar = 100 μm. (e–g) Representative results (e) and quantitative analyses (f, g) of western blotting showed the relative expression of the PSD95 and SYP proteins in the ipsilateral striatum of rats from different groups ($n = 5$ animals per group; $^{*}P < 0.05$, $^{***}P < 0.001$, and $^{****}P < 0.0001$).

neural network reconstruction during later periods [53, 54]. Previous studies on MSC transplantation in stroke have implied that MSCs improve neurological recovery, reduce apoptosis, inhibit scar formation, and enhance reactive astrocyte- and oligodendrocyte-related axonal remodeling [55, 56]. MSCs and EA treatment could improve the expression levels of trophic factors such as brain-derived neurotrophic factor (BDNF), neurotrophin-4 (NT4), and vascular endothelial growth factor (VEGF) in ischemic stroke, which are all very helpful for brain tissue

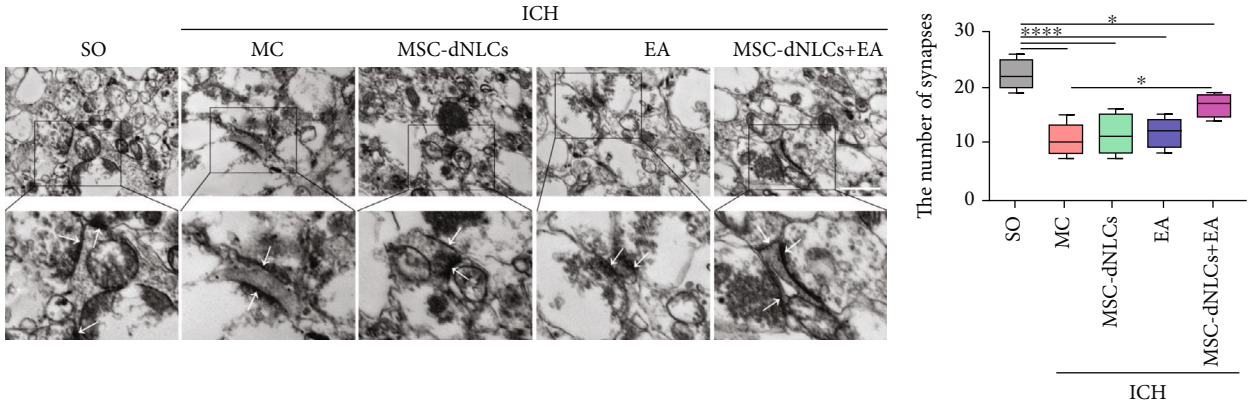

(a) (b)

Figure 6: The combined treatment increased the number of synapses in rats with ICH. (a) Electron photomicrographs of synapses in the ipsilateral striatum of brain tissues from different groups. The white arrows show synapses. Scale bar = 1 μm. (b) The number of synapses in the ipsilateral striatum (100 μm^2 area) ($n = 5$ rats per group; $^{*}P < 0.05$ and $^{****}P < 0.0001$).

regeneration [26]. MSC transplantation combination with EA treatment increased the number of neurofilament-200 positive fibers and BDA-labeled descending corticospinal tract (CST) axons in the lesion site of the injured spinal cord compared to MSC transplantation or EA treatment alone and downregulated expressions of GFAP and chondroitin sulfate proteoglycan (CSPG) proteins compared with the operated control, which inhibited axonal degeneration as well as promoted axonal regeneration [24]. In the present study, EA stimulation increased the survival of neurons, and MSC-dNLC transplantation increased the survival of oligodendrocytes, and combination of the two also inhibited the proliferation of astrocytes. Furthermore, some of the transplanted cells expressed markers of neurons and glial cells. Notably, the combined treatment exerted a synergistic effect on promoting the survival of neurons and oligodendrocytes, which helped to improve the structure of the brain tissue.

The effects of the combined treatment on synaptic plasticity in the focal area were indicated by the increased levels of synaptic structural molecules. PSD-95, a major component of glutamatergic excitatory synapses, is a scaffolding protein that modulates the synaptic localization of many adhesion molecules, channels, receptors, and signaling proteins [57, 58]. Previous studies have documented important roles for PSD95 in the formation and maintenance of synapses, and current reports have focused on PSD95 and its molecular mechanisms underlying synaptic maturation and plasticity [58, 59]. SYP has been authenticated as one of the first nerve terminal proteins [60] and performs essential functions in synaptic plasticity [61]. Some studies showed that coculture with MSCs increases the expression of synaptic density markers (such as PSD95 and SYP) in Aβ42-treated primary hippocampal neurons, and EA increases the levels of the SYP, PSD-95, and GAP-43 proteins, enhanced synaptic structural plasticity, and improved behavioral performance in rats exposed to chronic unpredictable mild stress [62, 63]. Based on our data, MSC-dNLC transplantation increased the expression of the PSD95 and SYP proteins, a few transplanted cells also expressed PSD95 and SYP proteins, and EA further increased the expression of the two proteins in ICH rats transplanted with MSC-dNLCs. Interestingly, the combination therapy also increased the number of synapses. Therefore, our results indicated that the combined therapy may contribute to improving synapse plasticity in rats with ICH.

The mTOR/p70S6K pathway is involved in stroke [32, 64]. mTOR, a serine/threonine protein kinase, is a central regulator of protein, lipid, and nucleotide synthesis, autophagy, cell survival, and proliferation [32, 34, 65]. p70S6K is one of the downstream targets of mTOR [66, 67]. The p-mTOR and p-p70S6k proteins are regarded as markers of mTOR activity [68]. However, controversy exists regarding whether mTOR activity is beneficial or detrimental to the damaged brain. Its activity increases when the injured brain is protected by some neuroprotectants, including alpha-lipoic acid, melatonin, and silibinin [64, 69, 70], suggesting that activated mTOR is beneficial for brain injury. In contrast, studies have also reported that mTOR activity is detrimental to cognitive function and that minocycline prevents cognitive deficits by inhibiting mTOR signaling, increasing the autophagy process, and increasing the expression of pre- and postsynaptic proteins (SYP and PSD95) in rats after acute ischemic stroke [71]. Our results show that MSC-dNLC transplantation increased the levels of the phosphorylated mTOR and p70S6k proteins and that EA further increased mTOR activity in ICH rats after MSC-dNLC transplantation. Some researchers have reported that EA improves learning and memory functions by upregulating the expression of mTOR in rats with vascular dementia or cerebral ischemia/reperfusion [72, 73], and MSCs affect mTOR signaling through paracrine effects or exosomes [74–76].

Recent studies have provided evidence that the neuroprotective effects of mTOR on stroke may be due to its ability to increase PSD95 and GAP-43 protein levels or promote neuronal structural stability in peri-infarct regions [77, 78]. Li et al. reported that the mTOR pathway activated by

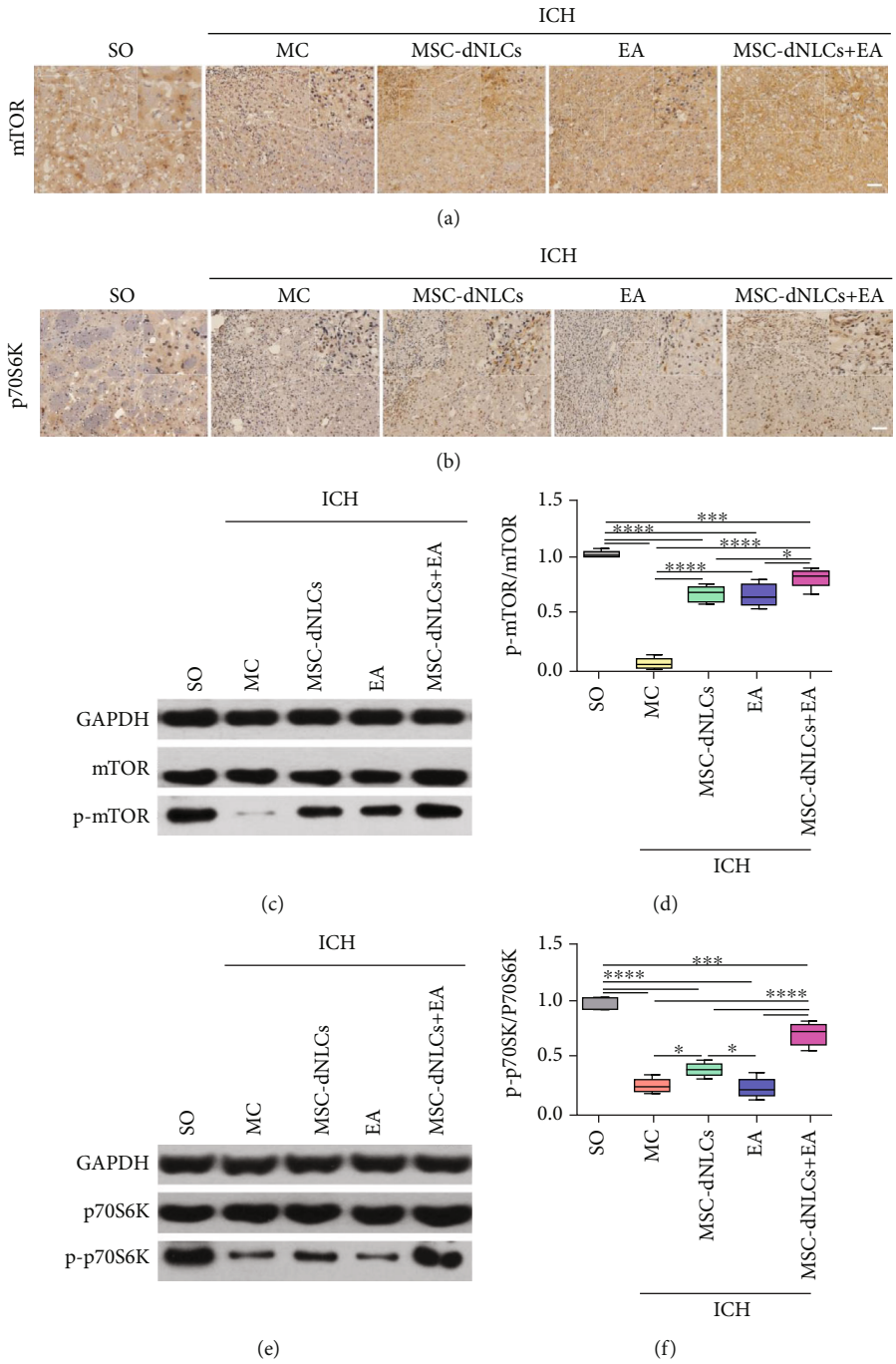

Figure 7: The levels of total and phosphorylated mTOR and p70S6K proteins in different groups. (a, b) Representative images of mTOR (a) and p70S6K (b) immunohistochemistry in the ipsilateral striatum of brain tissues from different groups. Scale bar = 100 μm. (c, d) Representative results (c) and quantitative analyses (d) of western blotting showed the level of the phosphorylated mTOR protein in different groups ($n = 5$ animals per group; $^{*}P < 0.05$, $^{***}P < 0.001$, and $^{****}P < 0.0001$). (e, f) Representative results (e) and quantitative analyses (f) of western blotting showed the level of the phosphorylated p70S6K protein in different groups ($n = 5$ animals per group; $^{*}P < 0.05$, $^{***}P < 0.001$, and $^{****}P < 0.0001$).

ketamine increases the levels of synaptic signaling proteins (synapsin I, PSD95, and GluR1) and increases the number and function of new synapses in the prefrontal cortex of rat models of depression [33]. As mentioned above, the combined therapy increased the expression of synapse-associated proteins (SYP and PSD95), and the results suggest that the protective effects of the combined therapy on mTOR may be related to its ability to increase synaptic plasticity in the hemorrhagic stroke.

The present study has some limitations. First, the observations of mTOR/p70S6K signaling and its regulation were limited to the ICH rat model. This information should be carefully considered when using the results to discuss the role of the mTOR pathway in neurological disease. Second,

we did not construct mTOR and p70S6K viruses to obtain further proof. mTOR/p70S6K signaling is an interesting target in hemorrhagic stroke that requires further investigation in subsequent research.

In summary, despite the shortcomings of this study, we provide the first evidence for the synergistic effects of a combined treatment consisting of MSC-dNLC transplantation and EA stimulation on improving synaptic plasticity, which may be associated with activated mTOR/p70S6K signaling in rats with ICH. These findings not only provide new data for the neuroprotective effect of a combined treatment consisting of MSC-dNLC transplantation and EA stimulation but also supply positive insights that will improve our understanding of the underlying molecular mechanisms and help to develop more precise therapeutic drugs and treatments for alleviating the outcomes of ICH.

Data Availability

The data that support the findings of this study are available from the corresponding author upon reasonable request.

Conflicts of Interest

The authors have no conflicts of interest to declare.

Authors' Contributions

Guoqiang Yang, Jiayi Zhu, and Guwen Zhan contributed equally to this work.

Acknowledgments

This work was supported by the Research Project of Science Foundation of Sichuan Province Educational Commission of China (12ZA077), Application Basic Research Project of Sichuan Province of China (2013JY0075), and Traditional Chinese Medicine Administration Project of Sichuan Province of China (2021MS499).

References

[1] A. L. de Oliveira Manoel, "Surgery for spontaneous intracerebral hemorrhage," *Critical Care (London, England)*, vol. 24, no. 1, pp. 45–45, 2020.

[2] Z. G. Li, M. S. Li, S. X. Shi et al., "Brain transforms natural killer cells that exacerbate brain edema after intracerebral hemorrhage," *The Journal of Experimental Medicine*, vol. 217, no. 12, p. article e20200213, 2020.

[3] M. Schrag and H. Kirshner, "Management of Intracerebral Hemorrhage:," *Journal of the American College of Cardiology*, vol. 75, no. 15, pp. 1819–1831, 2020.

[4] V. L. Feigin, C. M. Lawes, D. A. Bennett, S. L. Barker-Collo, and V. Parag, "Worldwide stroke incidence and early case fatality reported in 56 population-based studies: a systematic review," *Lancet Neurology*, vol. 8, no. 4, pp. 355–369, 2009.

[5] P. Y. Garcia, M. Roussel, J. M. Bugnicourt et al., "Cognitive impairment and dementia after intracerebral hemorrhage: a cross-sectional study of a hospital-based series," *Journal of Stroke and Cerebrovascular Diseases*, vol. 22, no. 1, pp. 80–86, 2013.

[6] L. R. Øie, M. A. Madsbu, O. Solheim et al., "Functional outcome and survival following spontaneous intracerebral hemorrhage: a retrospective population-based study," *Brain and Behavior: A Cognitive Neuroscience Perspective*, vol. 8, no. 10, article e01113, 2018.

[7] C. Cordonnier, A. Demchuk, W. Ziai, and C. S. Anderson, "Intracerebral haemorrhage: current approaches to acute management," *Lancet*, vol. 392, no. 10154, pp. 1257–1268, 2018.

[8] R. F. Keep, Y. Hua, and G. Xi, "Intracerebral haemorrhage: mechanisms of injury and therapeutic targets," *Lancet Neurology*, vol. 11, no. 8, pp. 720–731, 2012.

[9] Z. W. Shao, S. Tu, and A. W. Shao, "Pathophysiological mechanisms and potential therapeutic targets in intracerebral hemorrhage," *Frontiers in Pharmacology*, vol. 10, article 1079, 2019.

[10] G. Li, F. Yu, T. Lei et al., "Bone marrow mesenchymal stem cell therapy in ischemic stroke: mechanisms of action and treatment optimization strategies," *Neural Regeneration Research*, vol. 11, no. 6, pp. 1015–1024, 2016.

[11] D. Lo Furno, G. Mannino, and R. Giuffrida, "Functional role of mesenchymal stem cells in the treatment of chronic neurodegenerative diseases," *Journal of Cellular Physiology*, vol. 233, no. 5, pp. 3982–3999, 2018.

[12] P. H. Rosado-de-Castro, F. G. de Carvalho, G. R. de Freitas, R. Mendez-Otero, and P. M. Pimentel-Coelho, "Review of preclinical and clinical studies of bone marrow-derived cell therapies for intracerebral hemorrhage," *Stem Cells International*, vol. 2016, Article ID 4617983, 2016.

[13] P. Huang, W. D. Freeman, B. H. Edenfield, T. G. Brott, J. F. Meschia, and A. C. Zubair, "Safety and efficacy of intraventricular delivery of bone marrow-derived mesenchymal stem cells in hemorrhagic stroke model," *Scientific Reports*, vol. 9, no. 1, article 5674, 2019.

[14] S. P. Wang, Z. H. Wang, D. Y. Peng, S. M. Li, H. Wang, and X. H. Wang, "Therapeutic effect of mesenchymal stem cells in rats with intracerebral hemorrhage: reduced apoptosis and enhanced neuroprotection," *Molecular Medicine Reports*, vol. 6, no. 4, pp. 848–854, 2012.

[15] A. M. Liu, G. Lu, K. S. Tsang et al., "Umbilical cord-derived mesenchymal stem cells with forced expression of hepatocyte growth factor enhance remyelination and functional recovery in a rat intracerebral hemorrhage model," *Neurosurgery*, vol. 67, no. 2, pp. 357–366, 2010.

[16] X. J. Bao, F. Y. Liu, S. Lu et al., "Transplantation of Flk-1+ human bone marrow-derived mesenchymal stem cells promotes behavioral recovery and anti-inflammatory and angiogenesis effects in an intracerebral hemorrhage rat model," *International Journal of Molecular Medicine*, vol. 31, no. 5, pp. 1087–1096, 2013.

[17] J. Xie, B. Wang, L. Wang, F. Dong, G. Bai, and Y. Liu, "Intracerebral and intravenous transplantation represents a favorable approach for application of human umbilical cord mesenchymal stromal cells in intracerebral hemorrhage rats," *Medical Science Monitor*, vol. 22, pp. 3552–3561, 2016.

[18] A. Li, J. Y. Zhao, C. Z. Fan et al., "Delivery of exogenous proteins by mesenchymal stem cells attenuates early memory deficits in a murine model of Alzheimer's disease," *Neurobiology of Aging*, vol. 86, pp. 81–91, 2020.

[19] J. Li, S. Tian, H. Wang et al., "Protection of hUC-MSCs against neuronal complement C3a receptor-mediated NLRP3 activation in CUMS-induced mice," *Neuroscience Letters*, vol. 741, p. 135485, 2021.

[20] Y. Zhu, L. Deng, H. J. Tang et al., "Electroacupuncture improves neurobehavioral function and brain injury in rat model of intracerebral hemorrhage," *Brain Research Bulletin*, vol. 131, pp. 123–132, 2017.

[21] H. J. Zhou, T. Tang, J. H. Zhong et al., "Electroacupuncture improves recovery after hemorrhagic brain injury by inducing the expression of angiopoietin-1 and -2 in rats," *BMC Complementary and Alternative Medicine*, vol. 14, no. 1, article 127, 2014.

[22] R. Guan, Z. Li, X. Dai et al., "Electroacupuncture at GV20-GB7 regulates mitophagy to protect against neurological deficits following intracerebral hemorrhage via inhibition of apoptosis," *Molecular Medicine Reports*, vol. 24, no. 1, article 492, 2021.

[23] H. Q. Li, Y. Li, Z. X. Chen et al., "Electroacupuncture exerts neuroprotection through caveolin-1 mediated molecular pathway in intracerebral hemorrhage of rats," *Neural Plasticity*, vol. 2016, article 7308261, 2016.

[24] Y. Ding, Q. Yan, J. W. Ruan et al., "Bone marrow mesenchymal stem cells and electroacupuncture downregulate the inhibitor molecules and promote the axonal regeneration in the transected spinal cord of rats," *Cell Transplantation*, vol. 20, no. 4, pp. 475–491, 2011.

[25] Z. Liu, Y. Ding, and Y. S. Zeng, "A new combined therapeutic strategy of governor vessel electro-acupuncture and adult stem cell transplantation promotes the recovery of injured spinal cord," *Current Medicinal Chemistry*, vol. 18, no. 33, pp. 5165–5171, 2011.

[26] Y. R. Kim, S. M. Ahn, M. E. Pak et al., "Potential benefits of mesenchymal stem cells and electroacupuncture on the trophic factors associated with neurogenesis in mice with ischemic stroke," *Scientific Reports*, vol. 8, no. 1, article 2044, 2018.

[27] S. M. Ahn, Y. R. Kim, Y. I. Shin et al., "Therapeutic potential of a combination of electroacupuncture and TrkB-expressing mesenchymal stem cells for ischemic stroke," *Molecular Neurobiology*, vol. 56, no. 1, pp. 157–173, 2019.

[28] L. Deng, L. Zhou, Y. Zhu et al., "Electroacupuncture enhance therapeutic efficacy of mesenchymal stem cells transplantation in rats with intracerebral hemorrhage," *Stem Cell Reviews and Reports*, 2021.

[29] M. Stampanoni Bassi, E. Iezzi, L. Gilio, D. Centonze, and F. Buttari, "Synaptic plasticity shapes brain connectivity: implications for network topology," *International Journal of Molecular Sciences*, vol. 20, no. 24, article 6193, p. 6193, 2019.

[30] S. Peineau, K. Rabiant, O. Pierrefiche, and B. Potier, "Synaptic plasticity modulation by circulating peptides and metaplasticity: involvement in Alzheimer's disease," *Pharmacological Research*, vol. 130, pp. 385–401, 2018.

[31] E. T. Kavalali and L. M. Monteggia, "Targeting homeostatic synaptic plasticity for treatment of mood disorders," *Neuron*, vol. 106, no. 5, pp. 715–726, 2020.

[32] M. Laplante and D. M. Sabatini, "mTOR signaling in growth control and disease," *Cell*, vol. 149, no. 2, pp. 274–293, 2012.

[33] N. Li, B. Lee, R. J. Liu et al., "mTOR-dependent synapse formation underlies the rapid antidepressant effects of NMDA antagonists," *Science*, vol. 329, no. 5994, pp. 959–964, 2010.

[34] R. A. Saxton and D. M. Sabatini, "mTOR signaling in growth, metabolism, and disease," *Cell*, vol. 169, no. 2, pp. 361–371, 2017.

[35] C. Yang, L. Zhou, X. Gao et al., "Neuroprotective effects of bone marrow stem cells overexpressing glial cell line-derived neurotrophic factor on rats with intracerebral hemorrhage and neurons exposed to hypoxia/reoxygenation," *Neurosurgery*, vol. 68, no. 3, pp. 691–704, 2011.

[36] G. Q. Wang, Z. H. Li, S. J. Li et al., "Minocycline preserves the integrity and permeability of BBB by altering the activity of DKK1-Wnt signaling in ICH model," *Neuroscience*, vol. 415, pp. 135–146, 2019.

[37] A. I. Qureshi, A. D. Mendelow, and D. F. Hanley, "Intracerebral haemorrhage," *Lancet*, vol. 373, no. 9675, pp. 1632–1644, 2009.

[38] S. Urday, W. T. Kimberly, L. A. Beslow et al., "Targeting secondary injury in intracerebral haemorrhage–perihaematomal oedema," *Nature Reviews. Neurology*, vol. 11, no. 2, pp. 111–122, 2015.

[39] M. Selim and C. Norton, "Perihematomal edema: implications for intracerebral hemorrhage research and therapeutic advances," *Journal of Neuroscience Research*, vol. 98, no. 1, pp. 212–218, 2020.

[40] S. B. Murthy, S. Urday, L. A. Beslow et al., "Rate of perihaematomal oedema expansion is associated with poor clinical outcomes in intracerebral haemorrhage," *Journal of Neurology, Neurosurgery, and Psychiatry*, vol. 87, no. 11, pp. 1169–1173, 2016.

[41] J. Di Russo, M. J. Hannocks, A. L. Luik et al., "Vascular laminins in physiology and pathology," *Matrix Biology*, vol. 57-58, pp. 140–148, 2017.

[42] M. Marchand, C. Monnot, L. Muller, and S. Germain, "Extracellular matrix scaffolding in angiogenesis and capillary homeostasis," *Seminars in Cell & Developmental Biology*, vol. 89, pp. 147–156, 2019.

[43] L. F. Yousif, J. Di Russo, and L. Sorokin, "Laminin isoforms in endothelial and perivascular basement membranes," *Cell Adhesion & Migration*, vol. 7, no. 1, pp. 101–110, 2013.

[44] Y. J. Kim, J. Y. Kim, A. R. Ko, and T. C. Kang, "Over-expression of laminin correlates to recovery of vasogenic edema following status epilepticus," *Neuroscience*, vol. 275, pp. 146–161, 2014.

[45] J. Gautam, L. Xu, A. Nirwane, B. Nguyen, and Y. Yao, "Loss of mural cell-derived laminin aggravates hemorrhagic brain injury," *Journal of Neuroinflammation*, vol. 17, no. 1, p. 103, 2020.

[46] K. Matsushita, W. Meng, X. Wang et al., "Evidence for apoptosis after intercerebral hemorrhage in rat striatum," *Journal of Cerebral Blood Flow and Metabolism*, vol. 20, no. 2, pp. 396–404, 2000.

[47] W. D. Bao, X. T. Zhou, L. T. Zhou et al., "Targeting miR-124/ferroportin signaling ameliorated neuronal cell death through inhibiting apoptosis and ferroptosis in aged intracerebral hemorrhage murine model," *Aging Cell*, vol. 19, no. 11, article e13235, 2020.

[48] L. Feng, Y. Chen, R. Ding et al., "P2X7R blockade prevents NLRP3 inflammasome activation and brain injury in a rat model of intracerebral hemorrhage: involvement of peroxynitrite," *Journal of Neuroinflammation*, vol. 12, no. 1, article 190, 2015.

[49] T. Sugiyama, T. Imai, S. Nakamura et al., "A novel Nrf2 activator, RS9, attenuates secondary brain injury after intracerebral hemorrhage in sub-acute phase," *Brain Research*, vol. 1701, pp. 137–145, 2018.

[50] G. Xi, R. F. Keep, and J. T. Hoff, "Mechanisms of brain injury after intracerebral haemorrhage," *Lancet Neurology*, vol. 5, no. 1, pp. 53–63, 2006.

[51] F. Zhuo, G. Qiu, J. Xu et al., "Both endoplasmic reticulum and mitochondrial pathways are involved in oligodendrocyte apoptosis induced by capsular hemorrhage," *Molecular and Cellular Neurosciences*, vol. 72, pp. 64–71, 2016.

[52] Z. Wang, F. Zhou, Y. Dou et al., "Melatonin alleviates intracerebral hemorrhage-induced secondary brain injury in rats via suppressing apoptosis, inflammation, oxidative stress, DNA damage, and mitochondria injury," *Translational Stroke Research*, vol. 9, no. 1, pp. 74–91, 2018.

[53] M. Pekny and M. Pekna, "Astrocyte reactivity and reactive astrogliosis: costs and benefits," *Physiological Reviews*, vol. 94, no. 4, pp. 1077–1098, 2014.

[54] Y. M. Zhu, X. Gao, Y. Ni et al., "Sevoflurane postconditioning attenuates reactive astrogliosis and glial scar formation after ischemia-reperfusion brain injury," *Neuroscience*, vol. 356, pp. 125–141, 2017.

[55] Y. Li, K. McIntosh, J. Chen et al., "Allogeneic bone marrow stromal cells promote glial-axonal remodeling without immunologic sensitization after stroke in rats," *Experimental Neurology*, vol. 198, no. 2, pp. 313–325, 2006.

[56] J. Chen, Y. Li, M. Katakowski et al., "Intravenous bone marrow stromal cell therapy reduces apoptosis and promotes endogenous cell proliferation after stroke in female rat," *Journal of Neuroscience Research*, vol. 73, no. 6, pp. 778–786, 2003.

[57] E. Kim and M. Sheng, "PDZ domain proteins of synapses," *Nature Reviews. Neuroscience*, vol. 5, no. 10, pp. 771–781, 2004.

[58] J. Jeong, S. Pandey, Y. Li, J. D. Badger 2nd, W. Lu, and K. W. Roche, "PSD-95 binding dynamically regulates NLGN1 trafficking and function," *Proceedings of the National Academy of Sciences of the United States of America*, vol. 116, no. 24, pp. 12035–12044, 2019.

[59] B. Bessières, A. Travaglia, T. M. Mowery, X. Zhang, and C. M. Alberini, "Early life experiences selectively mature learning and memory abilities," *Nature Communications*, vol. 11, no. 1, article 628, 2020.

[60] G. J. Evans and M. A. Cousin, "Tyrosine phosphorylation of synaptophysin in synaptic vesicle recycling," *Biochemical Society Transactions*, vol. 33, no. 6, pp. 1350–1353, 2005.

[61] R. Janz, T. C. Sudhof, R. E. Hammer, V. Unni, S. A. Siegelbaum, and V. Y. Bolshakov, "Essential roles in synaptic plasticity for synaptogyrin I and synaptophysin I," *Neuron*, vol. 24, no. 3, pp. 687–700, 1999.

[62] L. Jiang, H. Zhang, J. Zhou et al., "Involvement of hippocampal AMPA receptors in electroacupuncture attenuating depressive-like behaviors and regulating synaptic proteins in rats subjected to chronic unpredictable mild stress," *World Neurosurgery*, vol. 139, pp. e455–e462, 2020.

[63] D. H. Kim, H. Lim, D. Lee et al., "Thrombospondin-1 secreted by human umbilical cord blood-derived mesenchymal stem cells rescues neurons from synaptic dysfunction in Alzheimer's disease model," *Scientific Reports*, vol. 8, no. 1, article aricle 354, 2018.

[64] P. O. Koh, "Melatonin prevents ischemic brain injury through activation of the mTOR/p70S6 kinase signaling pathway," *Neuroscience Letters*, vol. 444, no. 1, pp. 74–78, 2008.

[65] J. Yan, M. W. Porch, B. Court-Vazquez, M. V. L. Bennett, and R. S. Zukin, "Activation of autophagy rescues synaptic and cognitive deficits in fragile X mice," *Proceedings of the National Academy of Sciences of the United States of America*, vol. 115, no. 41, pp. e9707–e9716, 2018.

[66] Z. Zhang, L. Miao, X. Wu et al., "Carnosine inhibits the proliferation of human gastric carcinoma cells by retarding Akt/mTOR/p70S6K signaling," *Journal of Cancer*, vol. 5, no. 5, pp. 382–389, 2014.

[67] J. O. Lipton and M. Sahin, "The neurology of mTOR," *Neuron*, vol. 84, no. 2, pp. 275–291, 2014.

[68] R. Qi, X. Zhang, Y. Xie et al., "5-Aza-2′-deoxycytidine increases hypoxia tolerance-dependent autophagy in mouse neuronal cells by initiating the TSC1/mTOR pathway," *Biomedicine & Pharmacotherapy*, vol. 118, article 109219, p. 109219, 2019.

[69] X. Gao, W. Chen, J. Li et al., "The protective effect of alpha-lipoic acid against brain ischemia and reperfusion injury via mTOR signaling pathway in rats," *Neuroscience Letters*, vol. 671, pp. 108–113, 2018.

[70] M. Wang, Y. J. Li, Y. Ding et al., "Silibinin prevents autophagic cell death upon oxidative stress in cortical neurons and cerebral ischemia-reperfusion injury," *Molecular Neurobiology*, vol. 53, no. 2, pp. 932–943, 2016.

[71] S. Wang, C. Wang, L. Wang, and Z. Cai, "Minocycline inhibits mTOR signaling activation and alleviates behavioral deficits in the wistar rats with acute ischemia stroke," *CNS & Neurological Disorders Drug Targets*, vol. 19, no. 10, pp. 791–799, 2020.

[72] Y. Zhu, Y. Zeng, X. Wang, and X. Ye, "Effect of electroacupuncture on the expression of mTOR and eIF4E in hippocampus of rats with vascular dementia," *Neurological Sciences*, vol. 34, no. 7, pp. 1093–1097, 2013.

[73] H. L. Wang, F. L. Liu, R. Q. Li et al., "Electroacupuncture improves learning and memory functions in a rat cerebral ischemia/reperfusion injury model through PI3K/Akt signaling pathway activation," *Neural Regeneration Research*, vol. 16, no. 6, pp. 1011–1016, 2021.

[74] M. He, X. Shi, M. Yang, T. Yang, T. Li, and J. Chen, "Mesenchymal stem cells-derived IL-6 activates AMPK/mTOR signaling to inhibit the proliferation of reactive astrocytes induced by hypoxic-ischemic brain damage," *Experimental Neurology*, vol. 311, pp. 15–32, 2019.

[75] Z. Zheng, L. Zhang, Y. Qu et al., "Mesenchymal stem cells protect against hypoxia-ischemia brain damage by enhancing autophagy through brain derived neurotrophic factor/mammalin target of rapamycin signaling pathway," *Stem Cells*, vol. 36, no. 7, pp. 1109–1121, 2018.

[76] Y. Zhang, M. Chopp, X. S. Liu et al., "Exosomes derived from mesenchymal stromal cells promote axonal growth of cortical neurons," *Molecular Neurobiology*, vol. 54, no. 4, pp. 2659–2673, 2017.

[77] R. Xie, P. Wang, M. Cheng, R. Sapolsky, X. Ji, and H. Zhao, "Mammalian target of rapamycin cell signaling pathway contributes to the protective effects of ischemic postconditioning against stroke," *Stroke*, vol. 45, no. 9, pp. 2769–2776, 2014.

[78] P. Wang, R. Xie, M. Cheng, R. Sapolsky, X. Ji, and H. Zhao, "The mTOR cell signaling pathway is crucial to the long-term protective effects of ischemic postconditioning against stroke," *Neuroscience Letters*, vol. 676, pp. 58–65, 2018.

Hindawi
Stem Cells International
Volume 2022, Article ID 3229289, 11 pages
https://doi.org/10.1155/2022/3229289

Research Article

Small Extracellular Vesicles Derived from Human Umbilical Cord Mesenchymal Stem Cells Enhanced Proangiogenic Potential of Cardiac Fibroblasts via Angiopoietin-Like 4

Jiejie Li,[1] **Xin Xu**,[1] **Suyan Fei**,[2] **Ren Wang**,[1] **Hua Wang**,[2] **Wei Zhu**,[1] **and Yuanyuan Zhao**[1]

[1]*School of Medicine, Jiangsu University, Zhenjiang, Jiangsu, China*
[2]*The Affiliated Hospital of Jiangsu University, Zhenjiang, Jiangsu, China*

Correspondence should be addressed to Yuanyuan Zhao; 1000004441@ujs.edu.cn

Received 10 September 2021; Accepted 13 January 2022; Published 1 February 2022

Academic Editor: Huseyin Sumer

Background and Objectives. After myocardial hypoxic injury, it is important to enhance vascular formation and restore blood supply for injury repair. Previous studies have suggested that cardiac fibroblasts (CFs) play a crucial role in angiogenesis after myocardial injury. Small extracellular vesicles (sEVs) derived from human umbilical cord mesenchymal stem cells (hucMSCs) promote fibroblast-to-myofibroblast differentiation in inflammatory environment and have cardioprotective effects. It remains unknown whether sEVs regulate cardiac fibroblasts to promote angiogenesis after myocardial injury. *Methods and Results*. We isolated primary CFs from Sprague-Dawley rats (1–3 days old) and treated them with lipopolysaccharide (LPS) and LPS+sEVs. RNA sequencing analysis revealed that angiopoietin-like 4 (Angptl4) was increased in the LPS+sEVs group more than in the LPS group. After inhibition of Angptl4 expression in sEVs and CFs, cell proliferation, Transwell migration, and tube formation assays were used to detect the angiogenic activity of human umbilical vein endothelial cells. β-Catenin expression in CFs was detected by western blotting. The β-catenin inhibitor ICG001 was used to examine whether β-catenin was involved in the proangiogenic potential of CFs promoted by sEVs. sEVs enhanced the proangiogenic potential of CFs under inflammatory conditions, which was associated with β-catenin signaling. The proangiogenic potential of CFs was decreased when Angptl4 was knocked down in CFs and in hucMSCs. *Conclusions*. The sEVs regulated CFs to promote angiogenesis via Angptl4 in an inflammatory environment. This may provide a research basis for treating myocardial injury with sEVs.

1. Introduction

Acute myocardial injury has a high mortality rate. The repair mechanisms after myocardial injury include inflammation suppression, enhanced angiogenesis, reduced fibrosis, and remodeling. Angiogenesis and restoration of blood supply are crucial for inflammation clearance and injury repair [1]. Therefore, promoting angiogenesis is considered a good choice for repair of the myocardial injury. Cardiac fibroblasts (CFs) are major noncardiomyocytes and play an important role in remodeling of damaged tissues [2]. The proangiogenic potential of CFs has also been reported. Saraswati et al. isolated two different fibroblast subtypes from mouse hearts after myocardial infarction and demonstrated that FSP1+ fibroblast had a proangiogenic role [3]. The role of CFs in cardiac injury repair can shift from inflammation to angiogenesis [4, 5]. It has been proven that mesenchymal stem cells (MSCs) or exosomes promote the repair of tissue injury and angiogenesis [6, 7]. Li et al. showed that stem cell-derived small extracellular vesicles (sEVs) promoted cardiac angiogenesis by delivering miR-486-5p, which is related to fibroblastic matrix metalloprotein 19 [8]. Exosomes derived from human endothelial progenitor cells increase proliferation and angiogenesis of CFs [9]. Our previous studies have

demonstrated that exosomes derived from human umbilical cord MSCs (hucMSC-exs) had cardioprotective effects [10]. The hucMSC-exs also promote fibroblast-to-myofibroblast differentiation in the inflammatory stage and have cardioprotective effects [11]. However, whether sEVs can regulate CFs to promote angiogenesis in an inflammatory environment requires further research.

In this study, we isolated primary CFs from Sprague-Dawley (SD) rats (1–3 days old) and demonstrated that sEVs enhanced proangiogenic potential of CFs. The volcano map of differentially expressed genes (DEGs) and enrichment analysis of angiogenesis-related genes after RNA sequencing (RNA-seq) analyses of CFs showed that *Angptl4* might be a noteworthy gene. The angiopoietin-like 4 (Angptl4) is a member of the angiogenin-like protein family and is a secreted glycoprotein [12]. Therefore, we investigated the proangiogenic potential of Angptl4 in CFs in an inflammatory environment.

Several studies have demonstrated that the Wnt/β-catenin signaling pathway participated in regulating angiogenesis [13]. Angptl4 is also associated with β-catenin [14]. In this study, the role of β-catenin in the activity of CFs enhanced by sEVs was also investigated.

2. Materials and Methods

2.1. Animals. All animals' experiments were performed in accordance with the Guide for the Care and Use of Laboratory Animals and were approved by the Animal Experiment Center of Jiangsu University in Zhenjiang, Jiangsu Province, China. SD rats (1–3 days old) were used in this study.

2.2. Cell Culture. hucMSCs were isolated and cultured as described previously [15]. The umbilical cords were from the Affiliated Hospital of Jiangsu University (Jiangsu, China), and all providers gave informed consent. hucMSCs were cultured in Minimal Essential Medium Alpha (α-MEM; Gibco, Grand Island, NY, USA) with 10% fetal bovine serum (FBS; Biological Industries, Beit HaEmek, Israel) at 37°C in 5% CO_2. The primary CFs were isolated from the hearts of 1–3-day-old SD rats according to an established method [16]. Human umbilical vein endothelial cells (HUVECs) were obtained from the American Type Culture Collection (Manassas, VA, USA) and cultured in high-glucose Dulbecco's Modified Eagle's Medium (H-DMEM; Gibco) with 10% FBS at 37°C in 5% CO_2.

2.3. The sEV Extraction. When the hucMSCs reached 80% confluence in complete α-MEM, complete medium was replaced with α-MEM supplemented with 10% sEVs-depleted FBS. After 48 h, the supernatant was collected and centrifuged at $300 \times g$ for 10 min, $2{,}000 \times g$ for 20 min, and $10{,}000 \times g$ for 30 min to remove debris. The supernatant was concentrated with 100 kDa molecular weight cut-off (MWCO) ultrafiltration centrifuge tubes (Millipore, Billerica, MA, USA). The concentrated supernatant was centrifuged at $120{,}000 \times g$ for 70 min. The sedimentation at the bottom was resuspended in PBS. The mixture was centrifuged again at $120{,}000 \times g$ for 70 min, and the sediment that contained the sEVs was resuspended in PBS and stored at -80°C.

2.4. Nanoparticle Tracking Analysis (NTA). The isolated sEVs were diluted with PBS. The concentration and size distribution of sEVs were evaluated by using a Malvern Panalytical nanosight nanoparticle analyzer (Malvern, UK). The data were analyzed by using ZetaView version 8.05.12 SP1 software.

2.5. Electron Microscopy. The sEVs were mixed and 20 μL was added to the sample loading copper mesh with a diameter of 2 mm, and an excess sample was removed. The copper mesh was inverted in a 2% phosphotungstic acid drop for 5 min at room temperature for negative staining. After drying, images were obtained with a transmission electron microscope (JEOL, Tokyo, Japan).

2.6. Flow Cytometry. When the density of hucMSCs reached 90%, cells were collected and incubated with antibodies against CD34, CD19, CD45, CD90, CD29, and CD105 (eBioscience, San Diego, USA) for 30 min at 4°C, washed three times, and resuspended in 300 μL PBS. The data were immediately collected and analyzed with a flow cytometer (Becton Dickinson, Billerica, USA).

2.7. Immunofluorescence Analyses. When the density of CFs reached 70–80%, the supernatant was removed and the cells were washed three times with PBS. The cells were fixed with 4% paraformaldehyde at room temperature for 20 min and permeabilized with 0.1% Triton X-100 for 15 min. The cells were blocked with 5% bovine serum albumin (BSA) for 30 min at 37°C and incubated with primary antibodies against α-smooth muscle actin (α-SMA) (1 : 200; Boster, Birmingham, USA), vimentin (1 : 100; Cell Signaling Technology, Danvers, USA), collagen I (1 : 100; Boster), periostin (1 : 100; Proteintech, Rosemont, USA), CD31 (1 : 50; Arigo, Taiwan), and Angptl4 (1 : 100; Cell Signaling Technology) overnight at 4°C. The next day, the fluorescence-conjugated secondary antibodies (1 : 1,000; Cell Signaling Technology) were incubated with cells for 1 h at 37°C. The nuclei were counterstained with Hoechst 33342 (Sigma-Aldrich, Saint Louis, USA), and the images were viewed under a fluorescence microscope (OLYMPUS DP73, Tokyo, Japan).

2.8. Western Blotting. The proteins were isolated with RIPA lysis buffer containing protease and phosphatase inhibitors, PMSF, separated by 10–15% SDS-PAGE, and transferred to a PVDF membrane (Millipore, USA). Next, the PVDF membranes were blocked with 5% milk for 1 h and incubated overnight at 4°C with primary antibodies against CD9 (1 : 1,000; Cell Signaling Technology), TSG101 (1 : 1,000; Boster), CD81 (1 : 800; Proteintech), calnexin (1 : 1,000; Boster), α-SMA (1 : 1,000; Boster), vimentin (1 : 1,000; Cell Signaling Technology), collagen I (1 : 1,000; Boster), periostin (1 : 1,000; Proteintech), CD31 (1 : 1,000; Arigo), Angptl4 (1 : 800; Cell Signaling Technology), cyclin D1 (1 : 800; Cell Signaling Technology), β-catenin (1 : 800; Cell Signaling Technology), and GAPDH (1 : 2,000; Cell Signaling Technology). The next day, the secondary antibodies

Table 1: Primer sequences for the amplification of target genes.

Genes	Primer sequence (5′-3′)
β-Actin	Forward: 5′-TGTCACCAACTGGGACGATA-3′
	Reverse: 5′-GGGGTGTTGAAGGTCTCA-3′
Angptl4	Forward: 5′-GCAGCCTCCTAGCCTCCTCAC-3′
	Reverse: 5′-CCACGAGACTCCAGATAGCCCTAC-3′
Cyclin D1	Forward: 5′-TTGCCCTCTGCCACAGAT-3′
	Reverse: 5′-TCAGGTTCAGGCCTTGCACT-3′

(1 : 3,000; Cell Signaling Technology) were incubated with the membranes for 1 h at 37°C. The bands were visualized by enhanced chemiluminescent image analysis.

2.9. RNA-seq Analyses. The primary CFs were treated with lipopolysaccharide (LPS) (100 ng/mL) and LPS+sEVs (200 μg/mL) for 24 h. Total RNA was extracted and analyzed. All RNA sequencing data were obtained from BGI-Shenzhen (Shenzhen, China). All P values were corrected for statistical significance using the false detection rate (FDR) for multiple tests. Fold changes (absolute log 2) ≥ 1 and FDR adjusted to $P < 0.05$ were considered statistically significant.

2.10. Angptl4 siRNA Transfection. Angptl4 siRNAs were constructed by RIBOBIO (China): siRNA1: 5′-GCAGAG TTTACAGACTCAA-3′, siRNA2: 5′-GCAGCCATTCC AATCTAAA-3′, and siRNA3: 5′-GGACAATACTTCCA CTCTA-3′. When the density of cells reached 50–70%, the siRNAs or negative control (NC) RNAs were transfected into cells using Lipofectamine 2000 (Invitrogen, Carlsbad, NM, USA). After 6 h, the medium was replaced with fresh medium, and the cells were cultured for a further 48 h.

2.11. Reverse Transcription-Polymerase Chain Reaction (RT-PCR). Total RNA was extracted with the TRIzol reagent (Invitrogen). The cDNA was obtained using RT-PCR kits (CWBIO, Cambridge, MA, USA). The PCR program was conducted with UltraSYBR mix (CWBIO) on a StepOnePlus Real-Time PCR System (Applied Biosystems, Foster City, CA, USA). The mRNA expression was normalized to β-actin. All the sequences of PCR primers are listed in Table 1.

2.12. Supernatant Preparation. The primary CFs were treated with PBS (control), LPS (100 ng/mL), LPS+sEVs (200 μg/mL), or LPS+sEVs (200 μg/mL)+ICG001(10 μM) for 24 h. To further study the role of Angptl4, the primary CFs were transfected with NC-siRNA (NC-CF) or Angptl4-siRNA (si-CF) for 48 h and treated with LPS+sEVs, LPS+NC-siRNA-sEVs (LPS+NC-sEVs), and LPS+Angptl4-siRNA-sEVs (LPS+si-sEVs) for 24 h. The pretreated CFs were washed three times with PBS and changed with fresh medium for a further 24 h. All supernatants were centrifuged at $300 \times g$ for 5 min to remove debris before treating HUVECs.

2.13. Wound Healing Assay. The HUVECs were cultured in 6-well plates with serum-free H-DMEM. When the cells filled the culture wells, cell monolayers were scratched in a straight line using a sterile pipette tip. PBS was utilized to wash cell debris. The cells were treated with supernatants derived from pretreated CFs. Twelve hours later, the images were visualized with a microscope (Nikon, Tokyo, Japan). Three fields were photographed, and the migration rate was calculated by using ImageJ software.

2.14. Cell Proliferation Assay. The supernatants of pretreated CFs were collected to treat HUVECs and plated in 96-well plates (3,000 cells/well). After 24, 48, and 72 h, 10% CCK-8 reagent (Beyotime Biotechnology, Shanghai, China) was added to the wells. Two hours later, the absorbance at 450 nm was obtained by using a microplate spectrophotometer (BioTek, Winooski, VT, USA).

2.15. Transwell Migration Assay. The HUVECs were cultured with supernatant-pretreated CFs for 24 h. HUVECs were added to the upper chambers in 200 μL serum-free H-DMEM (2×10^4 cells), and 600 μL H-DMEM containing 10% FBS was added to the lower chambers. After 8 h at 37°C in 5% CO_2, the migrated cells were fixed and stained with crystal violet for 10 min. The images were visualized with a microscope (OLYMPUS DP73). Three randomly selected fields were photographed, and cells were counted by using ImageJ software.

2.16. Tube Formation Assay. The HUVECs were cultured with supernatant-pretreated CFs for 24 h. Then, 3×10^4 HUVECs/well were added to the surface of 100 μL Matrigel (Corning, NY, USA) in a 96-well plate and incubated for 6 h at 37°C. Three randomly selected fields were photographed by using an inverted microscope (Nikon). Tube formation numbers and branch points were analyzed by using ImageJ software.

2.17. Statistical Analysis. Data were given as mean ± standard deviation. Student's t-test or one-way ANOVA with the post hoc test was used to compare experimental and control groups. All data were analyzed with GraphPad Prism 8.0 software. $P < 0.05$ was considered to indicate a significant difference.

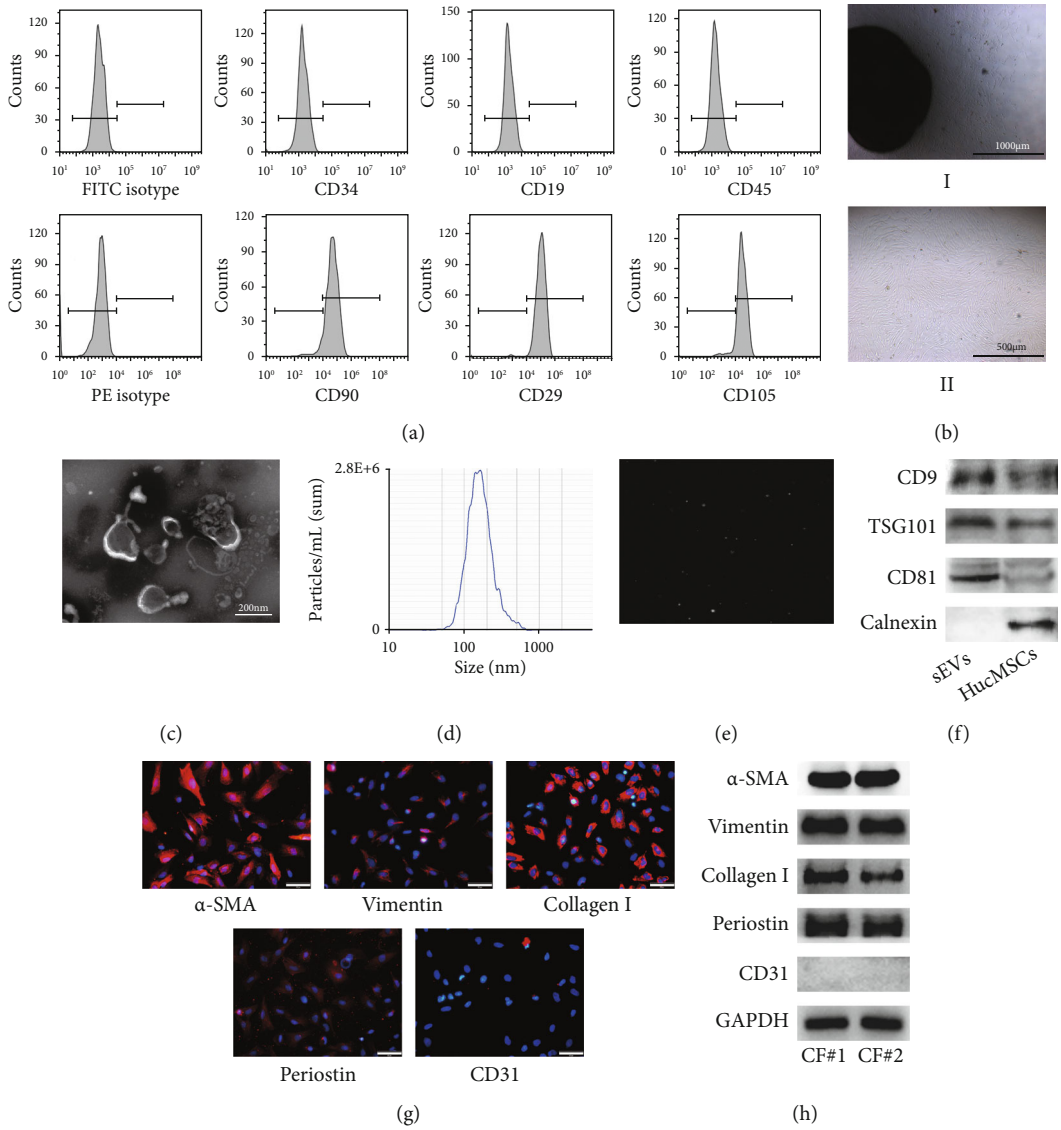

Figure 1: Characterization of hucMSCs, sEVs, and CFs. (a) The surface markers of hucMSCs measured by flow cytometry. (b) Morphology of hucMSCs. Scale bar: 1000 μm (i) and 500 μm (ii). (c) Morphology of sEVs observed by TEM. Scale bar: 200 nm. (d) Particle size distribution of sEVs measured by NTA. (e) Brownian motion image of hucMSCs. (f) Protein expression of CD9, TSG101, CD81, and calnexin in hucMSCs and sEVs. (g, h) The expression of α-SMA, vimentin, collagen I, periostin, and CD31 on primary CFs was measured by immunofluorescence (g) and western blotting (h). Scale bar: 50 μm.

3. Results

3.1. Characterization of hucMSCs, sEVs, and CFs. To identify the hucMSCs, flow cytometry was used to detect the surface antigenic profile of the cells. CD90, CD29, and CD105 were highly expressed in hucMSCs, but CD34, CD19, and CD45 were not expressed (Figure 1(a)). The morphology of hucMSCs was spindle-shaped (Figure 1(b)). Transmission electron microscopy (TEM) showed that the isolated vesicles had typical membrane structures (Figure 1(c)). NTA revealed that the size of sEVs was 50–160 nm (Figures 1(d) and 1(e)). To further identify the characterization of sEVs, we detected the expression of exosomal marker proteins by western blotting. CD9, TSG101, and CD81 were expressed in hucMSCs and sEVs, but calnexin was only expressed in hucMSCs (Figure 1(f)). We also measured the surface proteins of CFs by immunofluorescence and western blotting. α-SMA, vimentin, collagen I, and periostin were expressed in primary CFs, while CD31 was not (Figures 1(g) and 1(h)). These results provided sufficient support for subsequent experiments.

3.2. The sEVs Enhanced Proangiogenic Potential of CFs. To investigate whether sEVs regulated CFs to promote angiogenesis in inflammatory environment, we treated primary CFs with LPS or LPS+sEVs for 24 h and then collected the supernatants. HUVECs were cultured with the supernatants for 24 h. The supernatants of CFs pretreated with sEVs

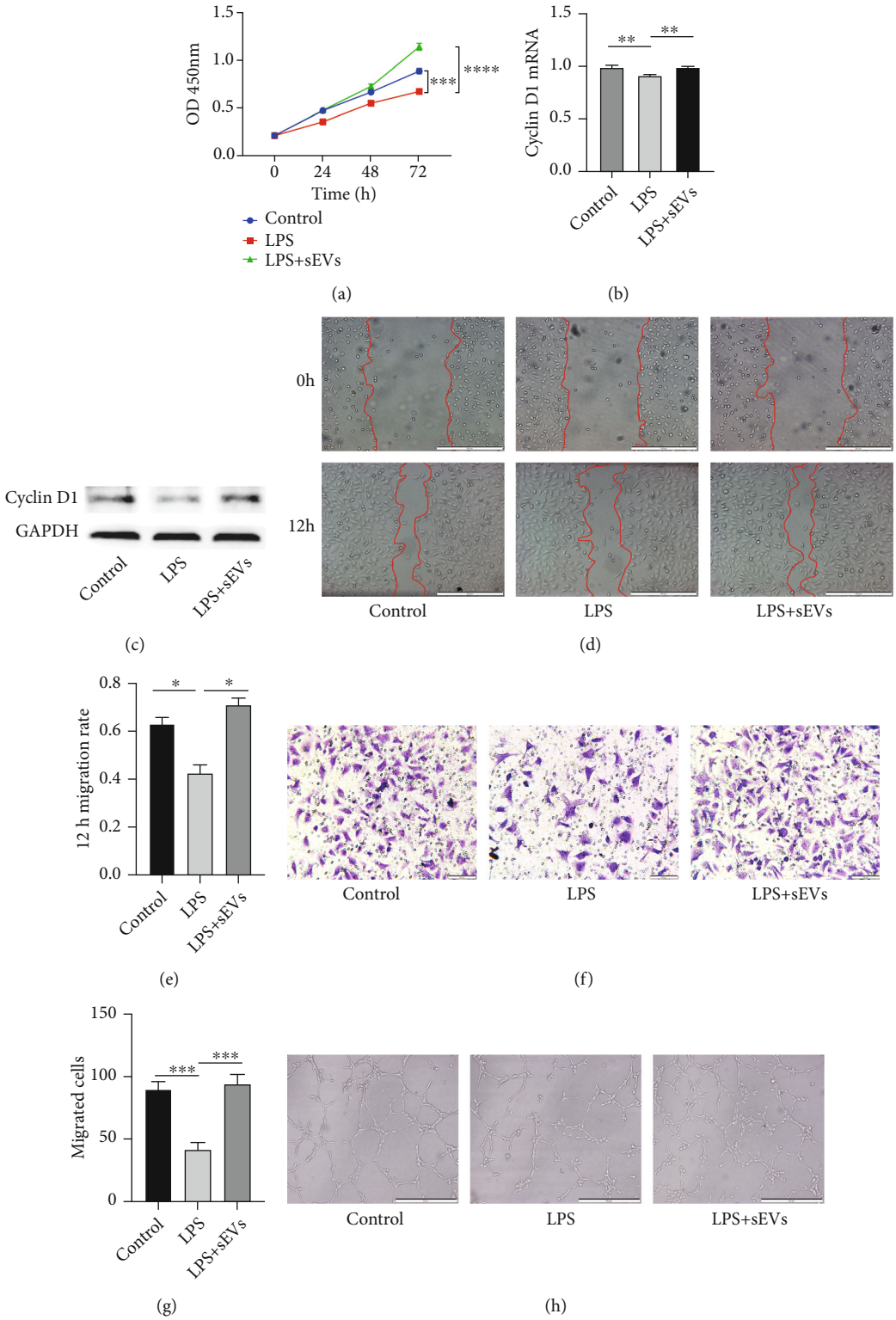

Figure 2: Continued.

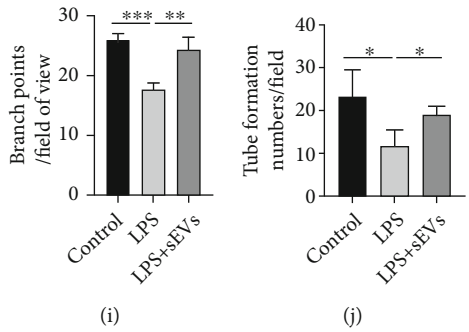

Figure 2: The sEVs enhanced proangiogenic potential of CFs. Primary CFs were treated with LPS (100 ng/mL) and LPS+sEVs (200 μg/mL) for 24 h, and supernatants were collected. HUVECs were treated with the supernatants derived from pretreated CFs. (a) Proliferation of HUVECs was detected by the CCK-8 assay. (b) The mRNA expression of cyclin D1 was measured by qRT-PCR. (c) Cyclin D1 protein expression was detected by western blotting. (d, f) Migration of HUVECs in different treatment groups was tested by the wound healing assay (d) and Transwell migration assay (f). Scale bar: 500 μm (d) and 100 μm (f). (e) Quantitative analysis of 12 h migration rate in (d). (g) Quantitative analysis of migrated cells in (f). (h–j) Tube formation ability of HUVECs was measured by the tube formation assay (h). Quantitative analysis of the total branching points (i) and tube formation numbers (j). Scale bar: 500 μm. $^{*}P < 0.05$, $^{**}P < 0.01$, $^{***}P < 0.001$, and $^{****}P < 0.0001$.

promoted proliferation of HUVECs in inflammatory environment (Figure 2(a)). Additionally, the proliferation-related protein cyclin D1 was upregulated in the LPS+sEVs group compared with the LPS group (Figures 2(b) and 2(c)). The results from wound healing and Transwell assays indicated that migration of HUVECs was increased in the LPS+sEVs group compared with the LPS group (Figures 2(d)–2(g)). The tube formation assay revealed that tube formation numbers and branch points were enhanced in the LPS+sEVs group compared with the LPS group (Figures 2(h)–2(j)).

3.3. Angptl4 Was Increased in CFs Treated with sEVs. The sEVs enhanced proangiogenic potential of CFs. To further explore the mechanism, RNA-seq analysis of CFs was performed to find the DEGs in the LPS and LPS+sEVs groups. The volcano map of DEGs and enrichment analysis of angiogenesis-related genes showed that *Angptl4* might be an important candidate gene (Figures 3(a) and 3(b)). To verify the sequencing data, qRT-PCR suggested that sEVs increased mRNA expression of Angptl4 in CF in inflammatory environment (Figure 3(c)). Additionally, the protein level of Angptl4 was also increased in the LPS+sEVs group (Figures 3(d) and 3(e)). Immunofluorescence staining showed that Angptl4 was upregulated in the LPS+sEVs group compared with the LPS group (Figures 3(f) and 3(g)).

3.4. Inhibition of Angptl4 in CFs and sEVs Resulted in Decreased Angiogenesis. Our previous studies have demonstrated that exosomes could be taken up by CFs [11, 17]. Moreover, it was shown that in Figures 3(d) and 3(f), the protein level of Angptl4 was significantly increased in the LPS+sEVs group compared with the LPS group. The expression of Angptl4 in sEVs and hucMSCs was measured. The results showed that Angptl4 was expressed in sEVs (Figure 4(a)). There are two possible mechanisms. sEVs upregulated the expression of Angptl4 in CFs, or sEVs delivered Angptl4 to CFs. Angptl4 was knocked down in hucMSCs and CFs by siRNA. Western blotting showed that siRNA3 had the best knockdown effect in hucMSCs and CFs (Figures 4(b) and 4(c)). Angptl4 was knocked down in sEVs by an Angptl4 siRNA3 (Figure 4(d)). Moreover, compared with the NC group, Angptl4 expression in CFs was significantly decreased in the LPS+si-CF+si-sEVs group (Angptl4 was knocked down in sEVs and CFs by Angptl4 siRNA3) (Figure 4(e)). Additionally, we assessed the effect of Angptl4 on angiogenesis. The results suggested that proliferation and migration of HUVECs were decreased when Angptl4 was knocked down in sEVs and CFs (Figures 4(f)–4(h)). Furthermore, as shown in Figures 4(i)–4(k), the branch points and tube formation numbers were all reduced in the LPS+si-CF+si-sEVs group. These results indicated that Angptl4 was a key molecule in regulating CFs to promote angiogenesis.

3.5. Proangiogenic Potential of CFs Enhanced by sEVs Was Associated with β-Catenin. The Wnt/β-catenin signaling pathway is involved in angiogenesis [18]. Angptl4 is also associated with β-catenin in skin dermal fibroblasts [14]. Although the interaction between Angptl4 and β-catenin has been described in other studies, the relationship in CFs has not been studied. Moreover, the regulation of Angptl4 and β-catenin in angiogenesis is unknown in CFs. Therefore, we detected β-catenin expression in CFs by western blotting. β-Catenin was increased in the LPS+sEVs group compared with the LPS group. After inhibiting Angptl4 expression in CFs and hucMSCs, expression of β-catenin was also decreased (Figure 5(a)). Therefore, Angptl4 regulated CFs to promote angiogenesis, possibly associated with β-catenin. To further elucidate the role of β-catenin in angiogenesis, CFs were treated with the β-catenin inhibitor ICG001. The most suitable inhibitor concentration was 10 μM (Figure 5(b)). Moreover, as shown in Figure 5(b), the proliferation of HUVECs was decreased after treatment with ICG001 (10 μM) compared with that in the LPS+sEVs group. The Transwell assay revealed that migration of HUVECs was also inhibited by ICG001 (Figures 5(c) and 5(d)). The tube formation

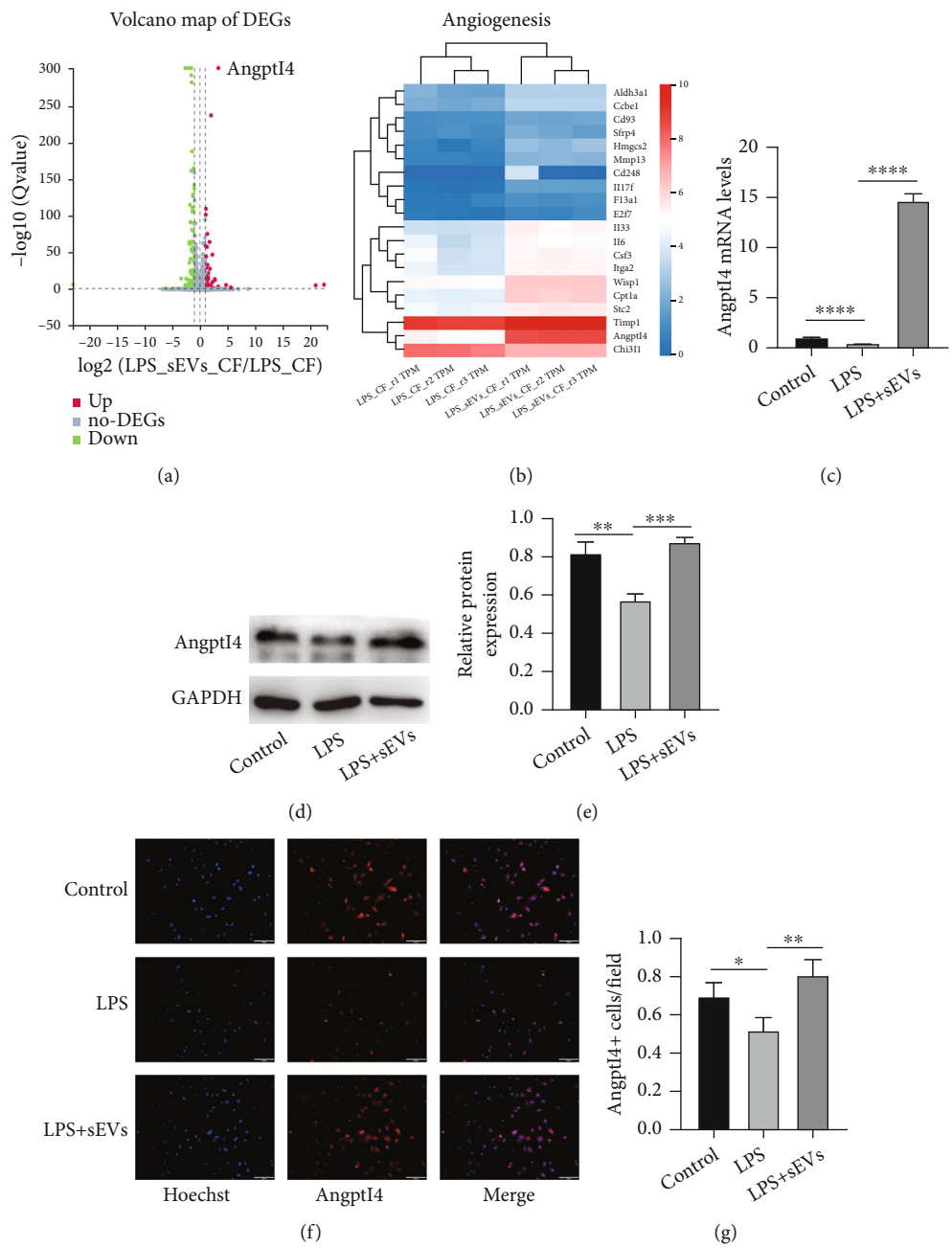

Figure 3: Angptl4 was increased in CFs treated with sEVs. Primary CFs were treated with LPS (100 ng/mL) and LPS+sEVs (200 μg/mL) for 24 h. mRNA expression of these two groups was compared via RNA-seq analysis. (a) Volcano map of DEGs. (b) Relative fold change of the top 20 angiogenesis-related genes for enrichment analysis. (c) Angptl4 mRNA expression was viewed by qRT-PCR. (d, e) Protein expression of Angptl4 was detected by western blotting. (f, g) Immunofluorescence was used to observe Angptl4 expression. Scale bar: 100 μm. $^{*}P < 0.05$, $^{**}P < 0.01$, $^{***}P < 0.001$, and $^{****}P < 0.0001$.

assay indicated that the branch points and tube formation numbers were all reduced after treatment with ICG001 (Figures 5(e)–5(g)). These results suggested that β-catenin signaling was important for proangiogenic potential of CFs enhanced by sEVs.

4. Discussion

It has been demonstrated that exosomes derived from MSCs can promote angiogenesis after myocardial infarction, thereby improving heart function [8]. In addition, CFs as major cells have proangiogenic properties in the proliferation phase after myocardial infarction [19]. In our previous work, it was revealed that exosomes promoted fibroblast-to-myofibroblast differentiation in the inflammation phase after myocardial infarction and exert cardioprotective effects. In this study, sEVs regulated CFs to promote angiogenesis in the inflammatory environment. Angptl4 is known to be associated with angiogenesis. Combined with RNA-seq data, we found that Angptl4 was increased in CFs after sEVs

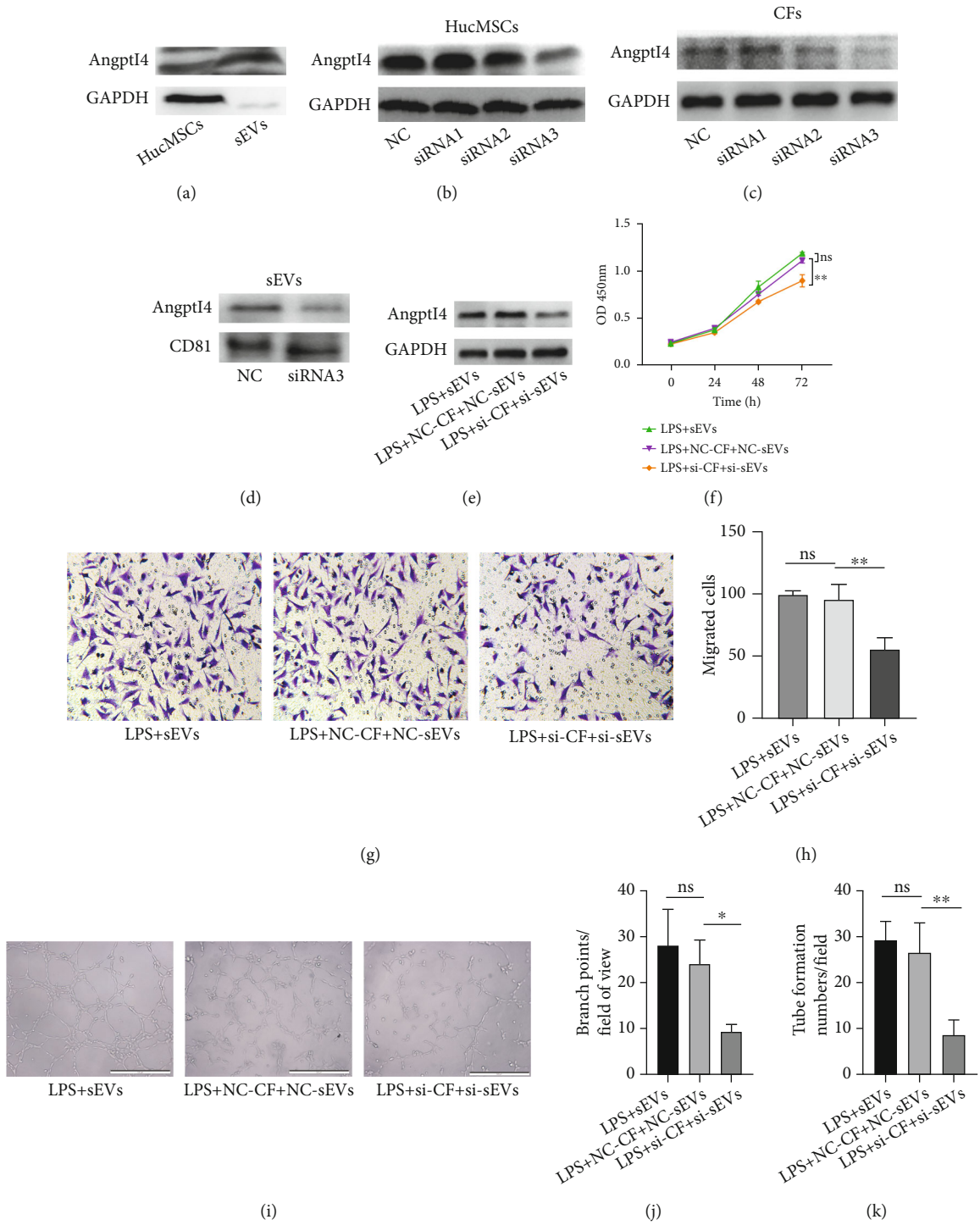

Figure 4: Inhibition of Angptl4 in primary CFs and sEVs resulted in decreased angiogenesis. (a) Angptl4 protein expression in hucMSCs and sEVs was detected by western blotting. (b, c) hucMSCs (b) and CFs (c) were transfected with Angptl4 siRNA, respectively, and expression of Angptl4 was measured by western blotting. (d) Angptl4 and CD81 expression in sEVs was observed by western blotting after transfection with siRNA. (e) Angptl4 expression in CFs was detected by western blotting after Angptl4 in CFs and in sEVs was knocked down with siRNA. (f) HUVECs were treated with the supernatants derived from pretreated CFs. The proliferation of HUVECs was measured by the CCK-8 assay. (g, h) The migration of HUVECs was detected by the Transwell migration assay (g). Scale bar: 100 μm. Quantitative analysis of the migrated cells (h). (i–k) Tube formation ability of HUVECs was measured by tube formation assay (i). Quantitative analysis of the total branching points (j) and tube formation numbers (k). Scale bar: 500 μm. $^{*}P < 0.05$ and $^{**}P < 0.01$. ns: no significant difference between two groups.

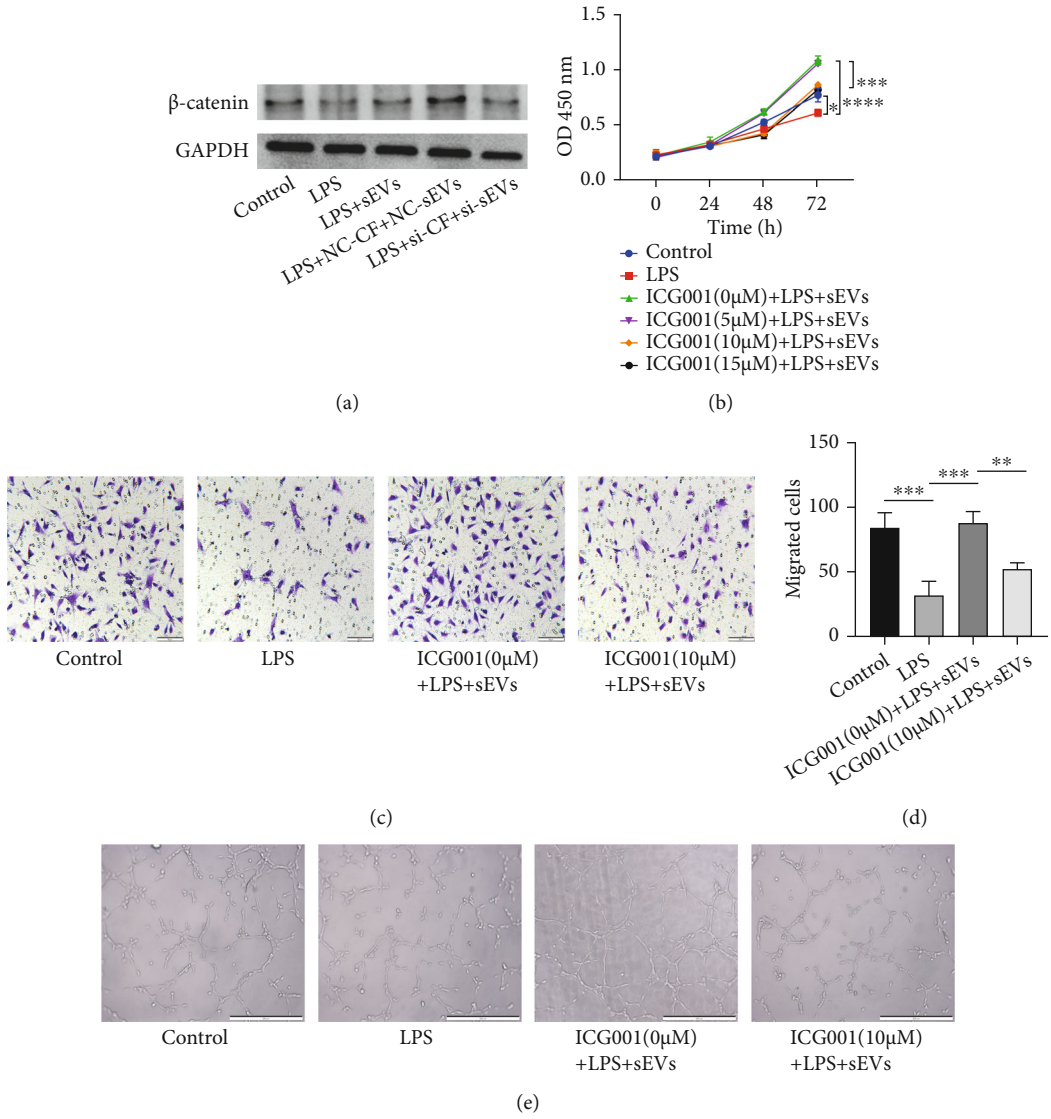

Figure 5: Continued.

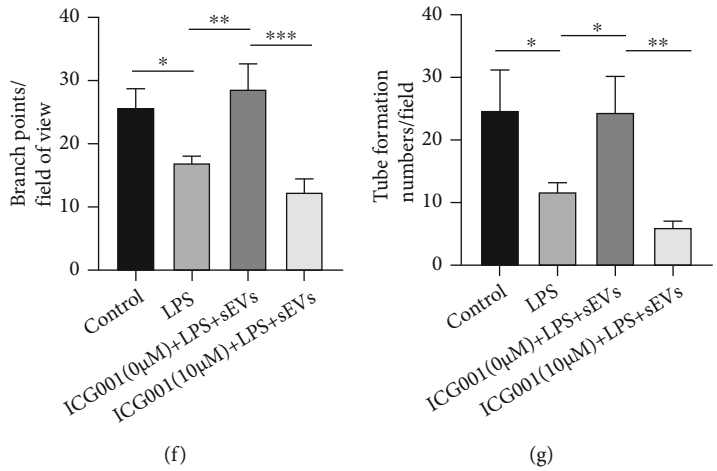

Figure 5: Proangiogenic potential of CFs enhanced by sEVs was associated with β-catenin. (a) β-Catenin expression in CFs was detected by western blotting after Angptl4 in CFs and in hucMSCs was knocked down with siRNA. (b) After using the β-catenin inhibitor ICG001 (0, 5, 10, and 15 μM), primary CFs were treated with LPS (100 ng/mL) and LPS+sEVs (200 μg/mL) for 24 h and supernatants were collected to culture HUVECs. The proliferation of HUVECs was measured by the CCK-8 assay. (c) The migration of HUVECs was measured by the Transwell migration assay. Scale bar: 100 μm. (d) Quantitative analysis of migrated cells. (e–g) Tube formation ability of HUVECs was evaluated by the tube formation assay (e). Scale bar: 500 μm. Quantitative analysis of the total branching points (f) and tube formation numbers (g). $^{*}P < 0.05$, $^{**}P < 0.01$, $^{***}P < 0.001$, and $^{****}P < 0.0001$.

treatment. Further results showed that sEVs also contained Angptl4 protein. It is possible that sEVs delivered Angptl4 to CFs or sEVs upregulated the expression of Angptl4 in CFs to promote angiogenesis. After Angptl4 was knocked down in sEVs and CFs by Angptl4 siRNA3, the angiogenic potential of CFs was decreased, which indicated that sEVs enhanced the proangiogenic potential of CFs via Angptl4. During the inflammatory stage, promoting angiogenesis may have a beneficial effect on the recovery of heart function.

It was reported that β-catenin was involved in angiogenesis [20]. Our findings suggested that expression of β-catenin in CFs was decreased after inhibiting Angptl4 expression in CFs and hucMSCs. Moreover, the proangiogenic ability of CFs enhanced by sEVs was reduced by the β-catenin transcription inhibitor ICG001. It has been shown that Angptl4 was expressed in the Spemann organizer of *Xenopus laevis* embryos and acted as a Wnt antagonist to promote notochord formation and prevent muscle differentiation [21]. Angptl4 binds to cadherin 11, releasing membrane-bound β-catenin to accelerate wound closure [14]. However, the interaction between Angptl4 and β-catenin has not been explained in studies of myocardial injury repair. The present study demonstrated that sEVs regulated CFs to promote angiogenesis via Angptl4. However, there were complex cell populations, including cardiomyocytes, fibroblasts, endothelial cells, and inflammatory cells in the inflammatory phase after myocardial infarction. The interactions among them and proangiogenic potential have been demonstrated [22]. Cardiomyocytes, macrophages, and fibroblasts secrete proteins, sEVs, or microvesicles, mediating intercellular communication after myocardial injury. Which cell type involves increased expression level of Angptl4, promoting angiogenesis and further improving heart function, has not been explored.

In recent years, sEVs therapy has become the focus in myocardial injury repair, although there are some challenges such as efficacy and yield issues. However, the advantages of sEVs are still promising. The sEVs drugs have gradually reached the clinical development stage and have become the next generation of potential drug delivery technology [23]. In this study, we found that sEVs regulated CFs to promote angiogenesis by increasing Angptl4 expression or delivering Angptl4 in an inflammatory environment. We elucidated the role of CFs in angiogenesis early after myocardial injury, which may provide a new idea for further research on the repair mechanism of myocardial injury and therapeutic applications of sEVs.

5. Conclusions

Our study demonstrated that sEVs regulated CFs to promote angiogenesis via Angptl4 in an inflammatory environment. This may provide an experimental basis for research or treatment of myocardial injury with sEVs.

Data Availability

The data used to support the findings of this study are available from the corresponding author upon request.

Conflicts of Interest

The authors confirm that they have no conflicts of interest.

Authors' Contributions

JJL performed and analyzed the experiments and wrote the manuscript. XX, SYF, and RW contributed to preparing the experimental reagents and data analysis. HW and WZ

provided the experimental materials. YYZ designed and supervised the study. All authors have read and approved the final manuscript.

Acknowledgments

This work was supported by the National Natural Science Foundation of China (grant number 81800270).

References

[1] S. Sahoo and D. W. Losordo, "Exosomes and cardiac repair after myocardial infarction," *Circulation Research*, vol. 114, no. 2, pp. 333–344, 2014.

[2] D. Fan, A. Takawale, J. Lee, and Z. Kassiri, "Cardiac fibroblasts, fibrosis and extracellular matrix remodeling in heart disease," *Fibrogenesis & Tissue Repair*, vol. 5, no. 1, p. 15, 2012.

[3] S. Saraswati, S. M. W. Marrow, L. A. Watch, and P. P. Young, "Identification of a pro-angiogenic functional role for FSP1-positive fibroblast subtype in wound healing," *Nature Communications*, vol. 10, no. 1, p. 3027, 2019.

[4] Y. Ma, R. P. Iyer, M. Jung, M. P. Czubryt, and M. L. Lindsey, "Cardiac fibroblast activation post-myocardial infarction: current knowledge gaps," *Trends in Pharmacological Sciences*, vol. 38, no. 5, pp. 448–458, 2017.

[5] A. J. Mouton, Y. Ma, O. J. Gonzalez et al., "Fibroblast polarization over the myocardial infarction time continuum shifts roles from inflammation to angiogenesis," *Basic Research in Cardiology*, vol. 114, no. 2, p. 6, 2019.

[6] X. Qi, J. Zhang, H. Yuan et al., "Exosomes secreted by human-induced pluripotent stem cell-derived mesenchymal stem cells repair critical-sized bone defects through enhanced angiogenesis and osteogenesis in osteoporotic rats," *International Journal of Biological Sciences*, vol. 12, no. 7, pp. 836–849, 2016.

[7] M. Yu, W. Liu, J. Li et al., "Exosomes derived from atorvastatin-pretreated MSC accelerate diabetic wound repair by enhancing angiogenesis via AKT/eNOS pathway," *Stem Cell Research & Therapy*, vol. 11, no. 1, p. 350, 2020.

[8] Q. Li, Y. Xu, K. Lv et al., "Small extracellular vesicles containing miR-486-5p promote angiogenesis after myocardial infarction in mice and nonhuman primates," *Science Translational Medicine*, vol. 13, no. 584, 2021.

[9] X. Ke, D. Yang, J. Liang et al., "Human endothelial progenitor cell-derived exosomes increase proliferation and angiogenesis in cardiac fibroblasts by promoting the mesenchymal-endothelial transition and reducing high mobility group box 1 protein B1 expression," *DNA and Cell Biology*, vol. 36, no. 11, pp. 1018–1028, 2017.

[10] Y. Zhao, X. Sun, W. Cao et al., "Exosomes derived from human umbilical cord mesenchymal stem cells relieve acute myocardial ischemic injury," *Stem Cells International*, vol. 2015, Article ID 761643, 2015.

[11] Y. Shi, Y. Yang, Q. Guo et al., "Exosomes derived from human umbilical cord mesenchymal stem cells promote fibroblast-to-myofibroblast differentiation in inflammatory environments and benefit cardioprotective effects," *Stem Cells and Development*, vol. 28, no. 12, pp. 799–811, 2019.

[12] L. la Paglia, A. Listì, S. Caruso et al., "Potential role of ANGPTL4 in the cross talk between metabolism and cancer through PPAR signaling pathway," *PPAR Research*, vol. 2017, Article ID 8187235, 15 pages, 2017.

[13] J. Kiewisz, T. Wasniewski, and Z. Kmiec, "Participation of WNT and β-catenin in physiological and pathological endometrial changes: association with angiogenesis," *BioMed Research International*, vol. 2015, Article ID 854056, 11 pages, 2015.

[14] Z. Teo, J. S. Chan, H. C. Chong et al., "Angiopoietin-like 4 induces a β-catenin-mediated upregulation of ID3 in fibroblasts to reduce scar collagen expression," *Scientific Reports*, vol. 7, no. 1, p. 6303, 2017.

[15] C. Qiao, W. Xu, W. Zhu et al., "Human mesenchymal stem cells isolated from the umbilical cord," *Cell Biology International*, vol. 32, no. 1, pp. 8–15, 2008.

[16] T. Thum, C. Gross, J. Fiedler et al., "MicroRNA-21 contributes to myocardial disease by stimulating MAP kinase signalling in fibroblasts," *Nature*, vol. 456, no. 7224, pp. 980–984, 2008.

[17] Q. Guo, Y. Zhao, J. Li et al., "Galectin-3 derived from HucMSC exosomes promoted myocardial fibroblast-to-myofibroblast differentiation associated withβ-catenin upregulation," *International Journal of Stem Cells*, vol. 14, no. 3, pp. 320–330, 2021.

[18] R. Daneman, D. Agalliu, L. Zhou, F. Kuhnert, C. J. Kuo, and B. A. Barres, "Wnt/beta-catenin signaling is required for CNS, but not non-CNS, angiogenesis," *Proceedings of the National Academy of Sciences of the United States of America*, vol. 106, no. 2, pp. 641–646, 2009.

[19] A. V. Shinde and N. G. Frangogiannis, "Fibroblasts in myocardial infarction: a role in inflammation and repair," *Journal of Molecular and Cellular Cardiology*, vol. 70, pp. 74–82, 2014.

[20] G. M. Birdsey, A. V. Shah, N. Dufton et al., "The endothelial transcription factor ERG promotes vascular stability and growth through Wnt/β-catenin signaling," *Developmental Cell*, vol. 32, no. 1, pp. 82–96, 2015.

[21] N. Kirsch, L. S. Chang, S. Koch et al., "Angiopoietin-like 4 is a Wnt signaling antagonist that promotes LRP6 turnover," *Developmental Cell*, vol. 43, no. 1, pp. 71–82.e6, 2017.

[22] X. Wu, M. R. Reboll, M. Korf-Klingebiel, and K. C. Wollert, "Angiogenesis after acute myocardial infarction," *Cardiovascular Research*, vol. 117, no. 5, pp. 1257–1273, 2021.

[23] M. Cully, "Exosome-based candidates move into the clinic," *Nature Reviews Drug Discovery*, vol. 20, no. 1, pp. 6-7, 2021.

Hindawi
Stem Cells International
Volume 2021, Article ID 3168428, 14 pages
https://doi.org/10.1155/2021/3168428

Research Article

Proteogenomic Analysis Reveals Proteins Involved in the First Step of Adipogenesis in Human Adipose-Derived Stem Cells

Bernardo Bonilauri,[1] **Amanda C. Camillo-Andrade**,[2] **Marlon D. M. Santos**,[2] **Juliana de S. da G. Fischer**,[2] **Paulo C. Carvalho**,[2] **and Bruno Dallagiovanna**[1]

[1]*Laboratory of Basic Biology of Stem Cells (LABCET), Carlos Chagas Institute-Fiocruz/PR, Curitiba, Paraná 81350-010, Brazil*
[2]*Laboratory for Structural and Computational Proteomics, Carlos Chagas Institute-Fiocruz/PR, Curitiba, Paraná 81350-010, Brazil*

Correspondence should be addressed to Bruno Dallagiovanna; bruno.dallagiovanna@fiocruz.br

Received 6 September 2021; Accepted 22 November 2021; Published 16 December 2021

Academic Editor: Sangho Roh

Background. Obesity is characterized as a disease that directly affects the whole-body metabolism and is associated with excess fat mass and several related comorbidities. Dynamics of adipocyte hypertrophy and hyperplasia play an important role in health and disease, especially in obesity. Human adipose-derived stem cells (hASC) represent an important source for understanding the entire adipogenic differentiation process. However, little is known about the triggering step of adipogenesis in hASC. Here, we performed a proteogenomic approach for understanding the protein abundance alterations during the initiation of the adipogenic differentiation process. *Methods*. hASC were isolated from adipose tissue of three donors and were then characterized and expanded. Cells were cultured for 24 hours in adipogenic differentiation medium followed by protein extraction. We used shotgun proteomics to compare the proteomic profile of 24 h-adipogenic, differentiated, and undifferentiated hASC. We also used our previous next-generation sequencing data (RNA-seq) of the total and polysomal mRNA fractions of hASC to study posttranscriptional regulation during the initial steps of adipogenesis. *Results*. We identified 3420 proteins out of 48,336 peptides, of which 92 proteins were exclusively identified in undifferentiated hASC and 53 proteins were exclusively found in 24 h-differentiated cells. Using a stringent criterion, we identified 33 differentially abundant proteins when comparing 24 h-differentiated and undifferentiated hASC (14 upregulated and 19 downregulated, respectively). Among the upregulated proteins, we shortlisted several adipogenesis-related proteins. A combined analysis of the proteome and the transcriptome allowed the identification of positive correlation coefficients between proteins and mRNAs. *Conclusions*. These results demonstrate a specific proteome profile related to adipogenesis at the beginning (24 hours) of the differentiation process in hASC, which advances the understanding of human adipogenesis and obesity. Adipogenic differentiation is finely regulated at the transcriptional, posttranscriptional, and posttranslational levels.

1. Introduction

Obesity is the main risk factor for several diseases such as hypertension, diabetes, insulin resistance, dyslipidemia, heart diseases, and some cancer types; it is also related to increased overall mortality [1]. Human adipose tissue is a primary regulator of metabolism and energy balance and is composed of several cell types, including adipocytes, preadipocytes, mesenchymal stem cells, fibroblasts, macrophages, and endothelial and blood cells [2, 3]. The pathophysiology of obesity is directly linked to increased adipocyte hypertrophy, adipocyte hyperplasia, or both in adipose tissue. Therefore, adipocyte size and the counterbalance between adipocyte loss and their formation through differentiation of preadipocytes are critical for human health. Therefore, adipogenesis plays a key role in the development of obesity, being the hormonal and nutritional status critical for the maintenance and development of body fat tissue [4]. Over the past two decades, adipogenesis has been extensively studied at the cellular and molecular levels, both *in vitro* and *in vivo* [4–8].

Adipose tissue is an abundant source of human adipose-derived mesenchymal stem cells (hASC), which have the ability to differentiate into adipocytes, osteoblasts, and chondrocytes [2, 9]. The adipogenic differentiation process is separated into two stages: the commitment of hASC into preadipocytes and the terminal differentiation of preadipocytes into mature adipocytes [10, 11]. Both phases are highly regulated at the transcriptional, posttranscriptional, translational, and posttranslational levels [12–14]. However, few studies have focused on molecular regulation at the earliest steps in hASC differentiation into preadipocytes [15, 16]. Thus, understanding how hASC become committed to preadipocytes and adipocyte lineages is a principal concern in the study of adipose tissue homeostasis and development.

Different techniques have been used to understand molecular changes at a global level (*e.g.*, transcriptomics and proteomics) to better understand the initial stage of adipogenesis [17–19]. In a previous study, we used ribosome profiling (Ribo-seq) to identify the translational regulation of mRNAs after 72 hours of hASC adipogenesis. We observed a significant reduction in cell size and migration, in addition to a reduction in protein synthesis after induction [20]. Similarly, we used total fraction and polysome profiling followed by RNA-seq to show the downregulation of cell cycle- and proliferation-related genes after 24 hours of induction [21]. Using these distinct high-throughput sequencing techniques of different cell fractions (i.e., bulk RNA-seq and polysomal and ribosome-associated mRNAs) may reflect a better understanding of the posttranscriptional and translational regulation of RNAs during cell differentiation, making possible a further comparison of gene expression at the RNA level with proteomics data (i.e., protein level). However, as far as we know, only one study discloses proteomic results from the early stages of human adipogenesis, focusing only on the expression of transcription factors [22, 23].

With this as a motivation, we performed a proteogenomic analysis of the early steps of adipogenesis (24 hours) in hASC. Our findings include the identification of proteins regulated at the beginning of the adipogenic differentiation process in hASC. This gene expression regulation is exerted at multiple levels, showing that human adipogenesis is a complex process and that combined strategies must be used for a better understanding.

2. Material and Methods

2.1. Ethical Statement. Tissue collection and cell isolation were performed after donors provided informed consent in accordance with guidelines for research involving human subjects and with the approval of the Ethics Committee of the Oswaldo Cruz Foundation, Brazil (approval number CAAE: 48374715.8.0000.5248). Human adipose-derived stem cells (hASC) were obtained from adipose tissue from lipoaspirate samples from three female donors (biological replicates) with a mean (±SD) age of 38 ± 12.75 and BMI of 27.06 ± 1.88 (Table 1). We randomly selected the donors since no differences in morphology, immunophenotype characteristics, proliferative rates, and differentiation potential between hASC isolated from young and old subjects were demonstrated [24].

Table 1: Subjects characteristics.

Subjects	Donor 1	Donor 2	Donor 3	Mean ± SD
Age	46	20	48	38 ± 12.75
Gender	F	F	F	F
Weight (kg)	74.5	75	90	79.8 ± 7.19
Height (cm)	166	174	175	171 ± 4.02
BMI	27.04	24.77	29.39	27.06 ± 1.88

2.2. Isolation, Cell Culture, and Characterization. Cell isolation was performed as previously described [25]. Briefly, 200 mL of adipose tissue was washed with phosphate-buffered saline (PBS) (Gibco, Invitrogen), after which digestion was carried out using 1 mg/mL type I collagenase (Gibco) for 30 min at 37°C, 5% CO_2 under constant shaking. Next, the cell suspension was treated with hemolysis buffer and filtered through a 100 μm a 40 μm mesh filter (BD Biosciences). Finally, the cells obtained were washed and plated at a density of 1×10^5 cells/cm^2 in T75 culture flasks in DMEM supplemented with 10% FBS, penicillin (100 units/mL), and streptomycin (100 μg/mL) in humid incubator at 37°C and 5% CO_2. The culture medium was changed twice a week, and all experiments were performed with cell cultures at passages four to six. For adipogenic induction, hASC were cultured for 24 hours in hMSC Adipogenic Differentiation Medium (hMSC Adipogenic Differentiation, BulletKit, Lonza). Cell characterization was performed according to the minimal criteria established by the International Society of Cellular Therapy [26], being the flow cytometry analysis conducted as previously described [27] (Supplementary Figure S1).

2.3. Sample Preparation and Quantification. Proteins were extracted with RapiGest™ detergent at a concentration of 0.1%. Protein concentrations were quantified using the fluorimetric assay on the Qubit platform (Invitrogen), following the manufacturer's instructions. One hundred micrograms of protein from each sample was reduced with dithiothreitol (DTT) (final concentration of 10 mM) for 30 minutes at 60°C. After incubation at room temperature, the samples were alkylated with iodoacetamide (final concentration of 30 mM) for 25 minutes at room temperature at dark and finally digested with trypsin in the proportion of 1/50 (E/S) for 20 hours.

The enzymatic reaction was interrupted by adding trifluoroacetic (0.4% *v*/*v* final). Peptides were successively quantified using the fluorometric test on Qubit 2.0® (Invitrogen) according to the manufacturer's recommendations. Each sample was desalted and concentrated using Stage-Tips (STop and Go-Extraction TIPs) according to Rappsilber and colleagues [28].

2.4. Mass Spectrometry Analysis. The peptide mixture was suspended in 0.1% formic acid and analyzed as follows. An UltiMate 3000 Basic Automated System (Thermo Fisher®)

was set up and connected online with a Fusion Lumos Orbitrap mass spectrometer (Thermo Fisher®). The peptide mixture was chromatographically separated on a column (15 cm in length with an internal diameter of 75 μm) packed in-house with ReproSil-Pur C18-AQ 3 μm resin (Dr. Maisch GmbH HPLC) with a flow rate of 250 nL/min of 5% to 50% ACN in 0.1% formic acid on a 140 min gradient. The Fusion Lumos Orbitrap was placed in data-dependent acquisition (DDA) mode to automatically turn between full-scan MS and MS/MS acquisition with 40 s dynamic exclusion. Survey scans (200–1500 m/z) were acquired in the Orbitrap system with a resolution of 120,000 at m/z 200. The most intense ions captured in a 2 s cycle time were chosen, excluding those which were unassigned or had a 1+ charge state. The selected ions were then isolated in sequence and fragmented using HCD (higher-energy collisional dissociation) with a normalized collision energy of 30. The fragment ions were analyzed with a resolution of 15,000 at 200 m/z. The general mass spectrometric conditions were as follows: 2.5 kV spray voltage, no sheath or auxiliary gas flow, heated capillary temperature of 250°C, predictive automatic gain control (AGC) enabled, and an S-lens RF level of 40%. Mass spectrometer scan functions and nLC solvent gradients were regulated using the Xcalibur 4.1 data system (Thermo Fisher®).

2.5. Peptide Spectrum Matching (PSM). Data analysis was performed with the PatternLab for Proteomics 5 software, which is freely available at http://www.patternlabforproteomics.org. Data analysis was performed according to the software's protocol [29]. Briefly, the sequences from *Homo sapiens* were downloaded on December 17, 2020, from the Swiss-Prot database, and a target decoy database was generated to include a reversed version of each sequence plus those from 104 common mass spectrometry contaminants. The Comet 2019.01 rev. 5 search engine was used to identify the mass spectra [30]. The search parameters considered were: fully and semitryptic peptide candidates with masses between 550 and 5500 da, up to two missed cleavages, 40 ppm for precursor mass, and bins of 0.02 m/z for MS/MS. The modifications were carbamidomethylation of cysteine as fixed and oxidation of methionine as a variable.

2.6. Validation of PSMs. The validity of the PSMs was assessed using Search Engine Processor (SEPro) [31]. First, the identifications were grouped by charge state (2+ and ≥3+) and then by tryptic status, resulting in four distinct subgroups. For each group, the XCorr, DeltaCN, DeltaPPM, and Peak Match values were used to generate a Bayesian discriminator. Next, the identifications were sorted in nondecreasing order according to the discriminator score. Finally, the cutoff score accepted a false discovery rate (FDR) of 1% at the peptide level based on the number of decoys [32]. This process was independently performed on each data subset, resulting in an FDR independent of the charge state or tryptic status. Moreover, a minimum sequence length of six amino acid residues was imposed, as was and a protein score greater than two were imposed. Lastly, identifications deviating by more than 10 ppm from the theoretical mass were discarded. This last filter decreased the rate of FDRs, now at the protein level, to less than 1% of all search results [33].

2.7. Proteomic Data Analysis. Our experimental design considered three biological replicates for each biological condition (*i.e.*, adipogenic induction (ADI) and undifferentiated cells (CT)), with two technical replicates. Quantitation was performed using Extracted Ion Chromatograms (XICs) normalized according to the total ion current (Supplementary Table 1). Differentially abundant proteins were listed by using PatternLab's TFold module to compare ADI versus CT [34].

2.8. Transcriptomic Data Analysis. Our previous RNA-seq data was used to perform transcriptomic analysis [25]. Briefly, bioinformatics analyses for mapping and counting were performed with the *rsubread* package with the new human genome version (GRCh38). Parameters were set for unique mapping reads. To determine the differential expression between undifferentiated hASC (CT) and 24 h-differentiated hASC (ADI), only genes with a count of more than 1 per million in at least three conditions were considered. To identify differentially expressed genes (DEGs), we used the *edgeR* Bioconductor package [35]. DEGs were selected using a stringent analysis using a false discovery rate (FDR) threshold of ≤0.05 (5%) and $\log_2$ fold change ($\log_2$ FC) ≥ 1.5 or ≤-1.5. All statistical analyses were conducted in R.

Gene Ontology (GO) analysis of the identified proteins was performed with the Database for Annotation, Visualization, and Integrated Discovery (DAVID) [36], using a cutoff criterion of $P \leq 0.05$ for "biological processes." Predicted protein-protein interaction networks were performed with STRING [37] using default parameters, and the network was created with Cytoscape (v.3.5.0).

3. Results

3.1. Study and Sample Overview. We isolated hASC from human adipose tissue obtained after liposuction surgery of three female subjects, followed by cell characterization and expansion, as previously described [21, 27]. Afterward, hASC were induced to adipogenic differentiation by culturing with a differentiation induction medium (*i.e.*, adipogenic cocktail (ADI)) for 24 hours. Noninduced cells were cultured with control-supplemented medium (CT). Cells were harvested, and proteins were immediately extracted (see Material and Methods). Next, we performed a shotgun proteomic analysis using the Fusion Lumos Orbitrap mass spectrometer followed by bioinformatic analysis (Figure 1(a)). We used PatternLab's Clustergram module to perform unsupervised clustering of the proteomic profiles of ADI and CT samples; the results show a clear stratification between the two experimental conditions (Figure 1(b)). Finally, the assessment of the chromatographic reproducibility of technical replicates was performed using RawVegetable [38] software (Supplementary Figure S2).

3.2. Uniquely Identified Proteins in 24 h-Differentiated (ADI) versus Undifferentiated (CT) hASC. To understand the

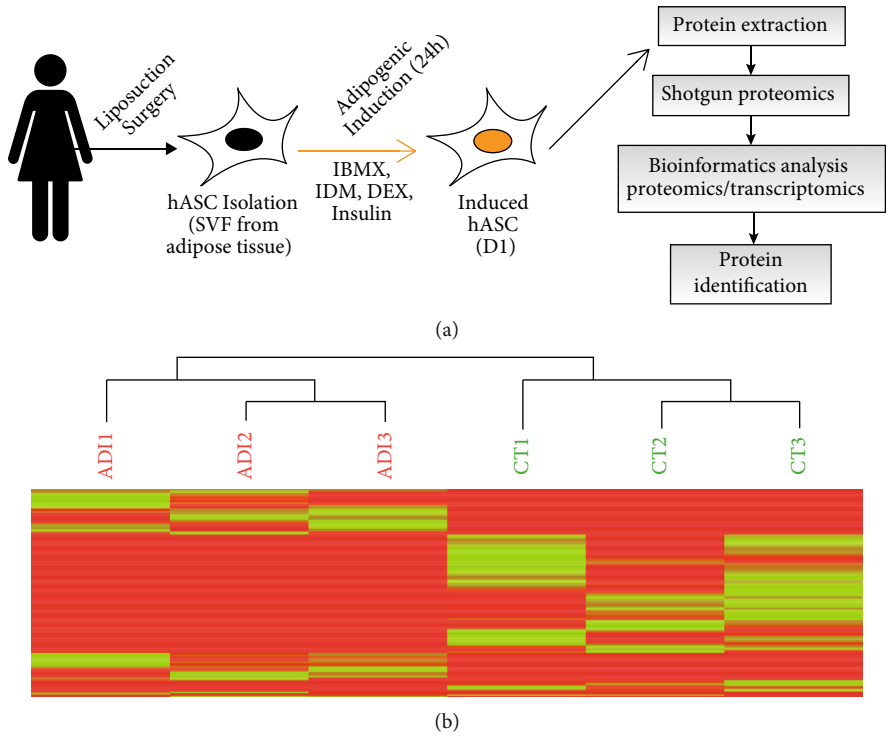

Figure 1: Triggering adipogenesis in hASC. (a) Schematic illustration of adipose tissue collection following by hASC isolation and *in vitro* adipogenic differentiation process with standard cocktail. (b) The clustergram was generated by applying hierarchical clustering to the ADI and CT proteomic profiles. The red and green indicate ADI and CT samples, respectively. Each line encodes the NIAF quantitation for a peptide; the encoding ranges from red for low-intensity NIAF quantitation to green for high-intensity NIAF quantitation.

changes in the proteome of hASC after the first day of adipogenic differentiation, we performed a shotgun proteomic approach followed by a proteomics analysis using the *PatternLab for Proteomics* protocol [10]. We were able to identify 53 exclusive proteins in two or more biological replicates in the ADI condition and 92 exclusive proteins in the CT condition, with 2322 proteins common in both conditions (Figure 2(a)). All exclusive proteins were manually curated in the scientific literature (Supplementary Table 1). Next, we performed a GO analysis of exclusive proteins from the ADI condition and found biological processes related to protein catabolism, negative regulation of sodium ion transport, ESCRT III complex, disassembly, regulation of mitotic spindle assembly, ribosomal large subunit biogenesis, and ceramide biosynthetic process (Figure 2(b)). We observed biological process pathways related to angiogenesis, mitochondrial translation, and chloride transmembrane transport for the exclusive proteins from CT condition. In addition, pathways related to cell-cell adhesion, translation initiation, and cotranslational membrane targeting were shown for common proteins (Supplementary Figure S3). Several ADI proteins have at least one report related to adipogenesis, adipocytes, or adipose tissue. This is the case of the ASAP1 protein, which regulates cytoskeletal dynamics and intracellular vesicle trafficking [39]. Another interesting example is the cochaperone FKBP5, which represses the Akt-p38 kinase pathway, inhibiting the glucocorticoid receptor-α (GRα) while also stimulating PPARγ [40–42].

We also found exclusively CT proteins with at least one report related to differentiation, mesenchymal stem cells, and adipogenesis. We highlight the cellular retinoic acid-binding protein II (CRABP2), which mediates the accessibility of retinoic acid (RA) to different receptors (RARs). Previous reports show that RA inhibits adipocyte differentiation when administered during the early steps of differentiation [43, 44].

3.3. Differentially Abundant Proteins after Adipogenic Triggering. We performed a differential analysis to visualize changes in protein abundance between ADI and CT using the PatternLab T-Fold analysis under stringent criteria (see Material and Methods). The analysis showed that 33 proteins had significantly different abundance levels between treatments, with 14 proteins upregulated and 19 downregulated after 24 hours of adipogenic differentiation (Figure 2(c), Supplementary Table 2). The upregulated proteins were related to pathways linked to the oxidation-reduction process, alpha-linolenic acid metabolic process, unsaturated fatty acid biosynthetic process, cell-cell adhesion, response to drugs, and organic cyclic compounds, cell spreading, and response to insulin (Supplementary Figure S4A). On the other hand, the downregulated proteins related to pathways involving response to amino acid stimulus, collagen catabolic process, protein heterotrimerization, positive regulation of cell migration, extracellular matrix organization, endochondral ossification, endodermal cell differentiation, iron-ion

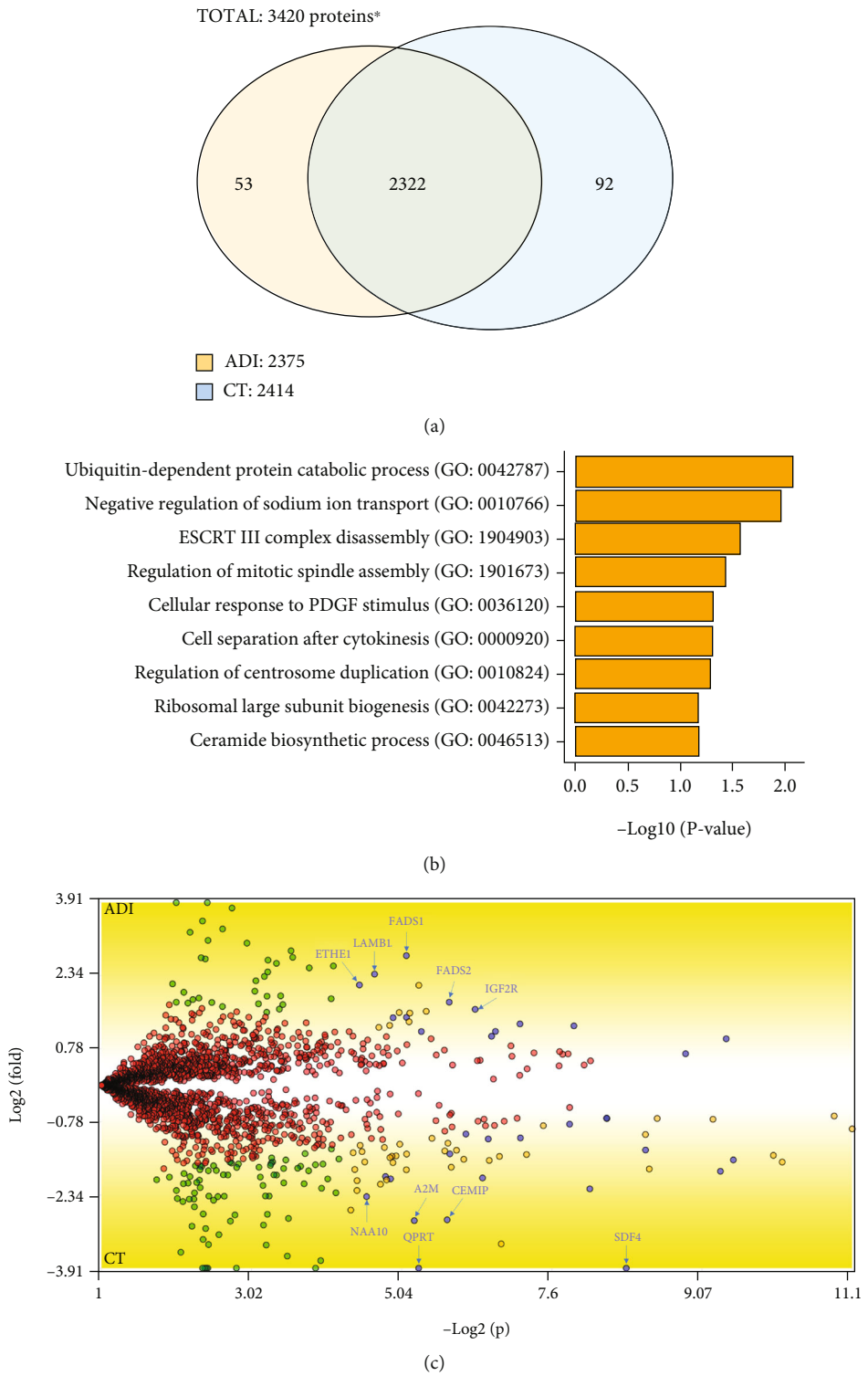

Figure 2: Proteins identified in 24 h-differentiated and undifferentiated hASC. (a) A total of 3420 proteins were identified. The Venn diagram shows that 2322 proteins are common to 24 h-differentiated (ADI) and undifferentiated hASC (CT) conditions. Cells exposed to 24 hours of adipogenic cocktail have 53 exclusive proteins. Undifferentiated hASC have 92 exclusive proteins. *The Venn diagram represents the number of proteins that satisfy a minimum of 2 replicates. (b) Gene Ontology analysis of the 53 uniquely identified proteins after adipogenic induction. Only biological processes with $P \leq 0.05$ are shown. (c) Differently abundant proteins identified in hASC exposed to 24 hours of adipogenic differentiation. Blue dots represent the 33 proteins that satisfy our stringent criteria. Red dots represent proteins with no satisfying fold change cutoff and established FDR. Green dots represent proteins that satisfy only the fold change cutoff. Orange dots represent proteins that satisfy both criteria but received very low quantitative values. The five proteins with the highest and lowest abundance are named.

homeostasis, and collagen fibril organization were identified (Supplementary Figure S4B).

3.4. Hidden Proteins Identified in Proteomics. To study protein expression regulation, we verified the presence of all identified proteins in the transcriptomics data. We found that approximately 99.13% of the identified ADI (2355 of 2375) and CT (2393 of 2414) proteins were assigned to the corresponding transcripts detected by RNA-seq in the total fraction (Figure 3(a)). Similarly, approximately 98.85% of the identified ADI (2350 of 2375) and CT (2387 of 2414) proteins were assigned to the corresponding transcripts detected by RNA-seq in the polysomal fraction (Figure 3(b)). We found 16 common proteins lacking an mRNA cognate in ADI and CT conditions across the total and polysomal fractions (Figure 3(c)). In the CT condition, only five proteins were missing from RNA-seq data across both fractions (*i.e.*, CTNNA2, OVCA2, MT-ND5, APOB, and PZP) (Figure 3(c)). Little is known about these proteins, particularly regarding their function and mechanisms in stem cells. On the other hand, in the ADI condition, only four proteins are missing from RNA-seq data across both fractions (*i.e.*, C11orf98, DCD, ATP1A2, and NDUFA7) (Figure 3(c)). Little is known about the role of these proteins in adipogenesis and stem cell biology.

Taken together, these results shed light on these hidden proteins, which are missing from the RNA-seq data, enabling new hypotheses regarding their participation in the self-renewal and differentiation processes of hASC.

3.5. Comparison of Proteomics and Transcriptomics Data. To gain more in-depth insights, we used our previous next-generation sequencing data (RNA-seq) of the total and polysomal fractions of hASC submitted to 24 hours of adipogenic differentiation to understand the different levels of gene expression regulation [25].

To understand the relationship between mRNA and protein levels, we calculated Spearman's correlation coefficient of normalized mRNA counts and normalized protein intensity of the induced (ADI) and control cells (CT) (Supplementary Table 3). First, we compared RNA-seq data from the total and polysomal fractions. We observed a high positive correlation coefficient (Figures 4(a) and 4(d)). Furthermore, a significant positive correlation between mRNA and protein was observed when comparing protein levels with mRNAs from total RNA (CT: 0.38, $P < 2.2e-16$; ADI: 0.37, $P < 2.2e-16$) and polysomal RNA fractions (CT: 0.40, $P < 2.2e-16$; ADI: 0.41, $P < 2.2e-16$). The correlation with the polysomal fraction is slightly higher for both conditions (Figure 4).

To analyze the relationship between mRNA and protein levels in greater detail, we first observed differential mRNA expression in both RNA fractions. We determined a cutoff criterion for DEGs of fold change $(\log_2) \geq 1.5$ or $\leq$-1.5 and FDR $\leq$ 5%. We identified 407 upregulated and 580 downregulated DEGs in the total RNA fraction, and 481 upregulated and 585 downregulated DEGs in the polysomal RNA fraction (Supplementary Table 4). We then examined the mRNA expression of the unique and differentially abundant proteins identified in our proteomic analysis. Figure 5(a) shows the mRNA profile of the 53 exclusive ADI proteins in the RNA-seq data. Most mRNAs in total and polysomal fractions followed the upregulation expression after adipogenic induction (Figure 5(a); orange box), including nine DEGs. However, some mRNAs appear to be downregulated (Figure 5(a); blue box), which may indicate a specific posttranscriptional regulation of these transcripts. The differentially expressed mRNA THBD (thrombomodulin), which is involved in development, adipogenesis, and lipid metabolism, is one such example. THBD mRNA was shown to change during adipogenesis, while it is significantly increased after 72 hours of adipogenic differentiation [45–47]. Here, we demonstrate the presence of the THBD protein in cells undergoing early differentiation and downregulation of THBD mRNA in the total and polysomal fractions after this step.

Figure 5(b) shows the mRNA profile of the 92 exclusive CT proteins in the RNA-seq data. As seen above, the same pattern emerges for the CT proteins, with most mRNAs in total and polysomal fraction downregulated after adipogenic induction (Figure 5(b); blue box), including seven DEGs. Meanwhile, some mRNAs appear upregulated (Figure 5(b); orange box). Curiously, the mRNA MSMO1 appears to be differentially upregulated in the total and polysomal fractions, which may indicate a distinct regulation of the transcript. In a study of adipogenesis in 3T3-L1 preadipocytes, Xin et al. used RNA-seq to demonstrate that the expression of MSMO1 was downregulated after 13 days of induction. The knockdown of MSMO1 stimulated the differentiation and upregulation of the expression of adipogenic marker genes, while MSMO1 overexpression had the opposite effect [48].

Interestingly, only seven differentially abundant proteins (five upregulated and two downregulated) are differentially expressed in transcriptomic data, both in the total and polysomal fraction, respectively (Figures 5(c) and 5(d)). With this result, we concluded that of the 14 upregulated proteins, nine (64%) cognate mRNAs did not undergo significant changes. Moreover, of the 19 downregulated proteins, 17 (89%) cognate mRNAs did not undergo significant changes in their expression, which may indicate a posttranscriptional regulation of these transcripts and turnover control of these downregulated proteins.

4. Discussion

4.1. Differentially Expressed Proteins and mRNAs. In this study, we used a proteomic approach to identify proteins that are differentially expressed at the onset of adipogenic differentiation of hASC. This approach complements previous studies using RNA-seq analysis and allowed us to find new potential early markers of differentiation. FKBP5 and ASAP1 proteins appear to be interesting differentiation-related markers.

FKBP5 is an adipocyte differentiation marker in 3T3-L1 cells, and knockdown of the protein leads to a reduction in lipid accumulation and the expression of adipogenic-related genes (including PPARγ) *in vitro* and *in vivo* [40, 42]. Dexamethasone exposure directly increases the FKBP5

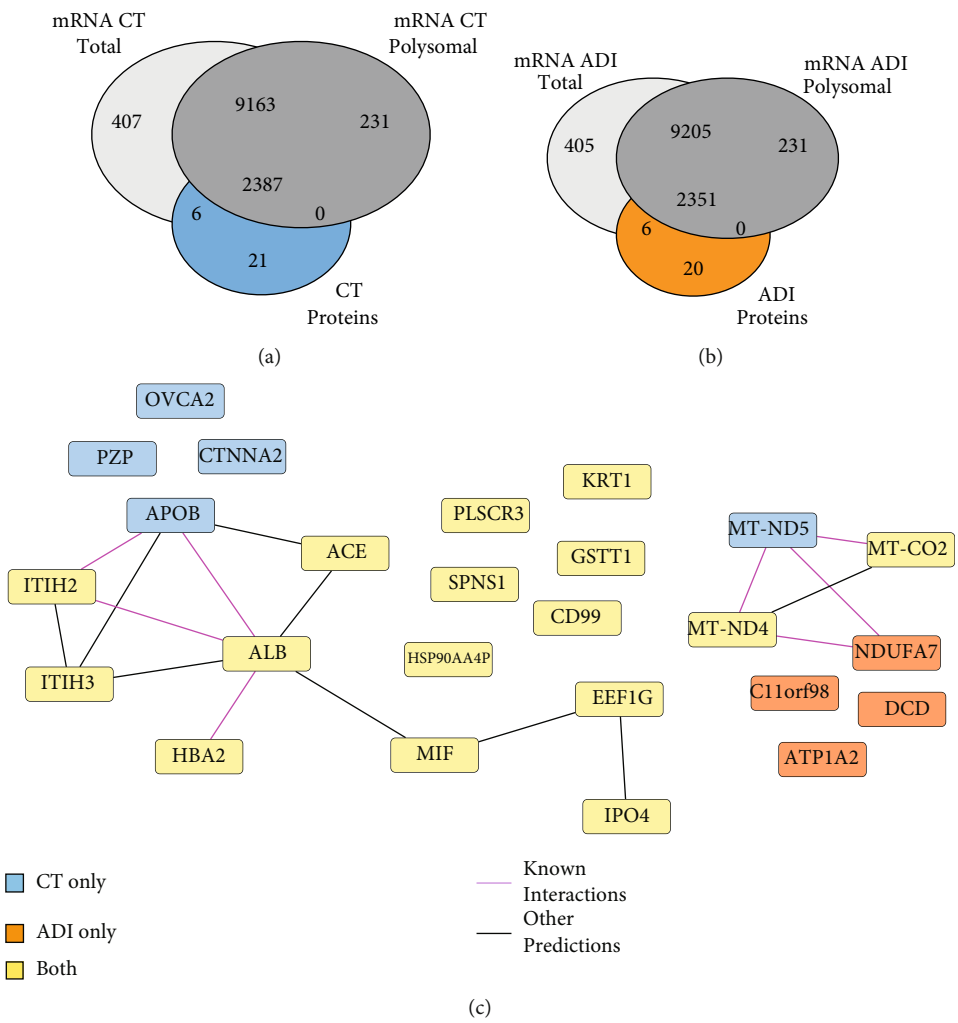

Figure 3: Unseen genes in the transcriptome are revealed by proteomics. (a) Venn diagram comparing all proteins and total mRNAs identified in the CT (left Venn diagram) and ADI (right Venn diagram) conditions. (b) Venn diagrams comparing all proteins and polysomal mRNAs identified in the CT (left Venn diagram) and ADI (right Venn diagram) conditions. Boxes show hidden proteins detected exclusively in the CT (5 proteins) and ADI (4 proteins) conditions. (c) Protein-protein interaction network demonstrating the identified hidden proteins. CT represents undifferentiated hASC, ADI represents 24 h-differentiated cells, and BOTH represents total and polysomal fractions.

gene and protein expression in human subcutaneous and omental adipose tissues [41]. Our results demonstrated the expression of FKBP5 at the very beginning of the adipogenic differentiation process in hASC, possibly regulated by dexamethasone exposure.

Another interesting protein is ASAP1, a regulator of cytoskeletal dynamics. Loss of ASAP1 causes growth retardation, delayed ossification, and reduced adipogenesis *in vivo*, suggesting an essential role for this protein in mesenchymal differentiation [39].

We also found that CRABP2 was only present in nondifferentiated cells and tightly downregulated at the beginning of differentiation. The effect of RA is related to the activation of RARs, which is mediated by CRABP2. However, when preadipocytes are exposed to three components of the adipogenic cocktail (*i.e.*, insulin, IBMX, and DEX), the expression of CRABP2 is repressed, and the RA effects are inhibited [43, 44]. We previously demonstrated the downregulated expression of the mRNA CRABP2 after 24 hours of adipogenic and osteogenic differentiation of hASC, reinforcing its importance in the maintenance of the undifferentiated state [25].

When comparing our proteomic data with previous gene expression profiles of differentiated hASC, we were not able to find the related mRNAs for a small group of proteins (Figure 3). However, a closer analysis of the proteins revealed that many of them were serum proteins, probably contaminants from the culture media (*e.g.*, ALB) (Supplementary Figure S5). This shows that, although they were thoroughly washed, the cells retained proteins from the serum present during cultivation. Another group of proteins was of mitochondrial origin (*e.g.*, MT-ND4 and MT-CO2). Most of these were coded in the mitochondrial genome and are probably the result of a bias of the RNA-seq assay.

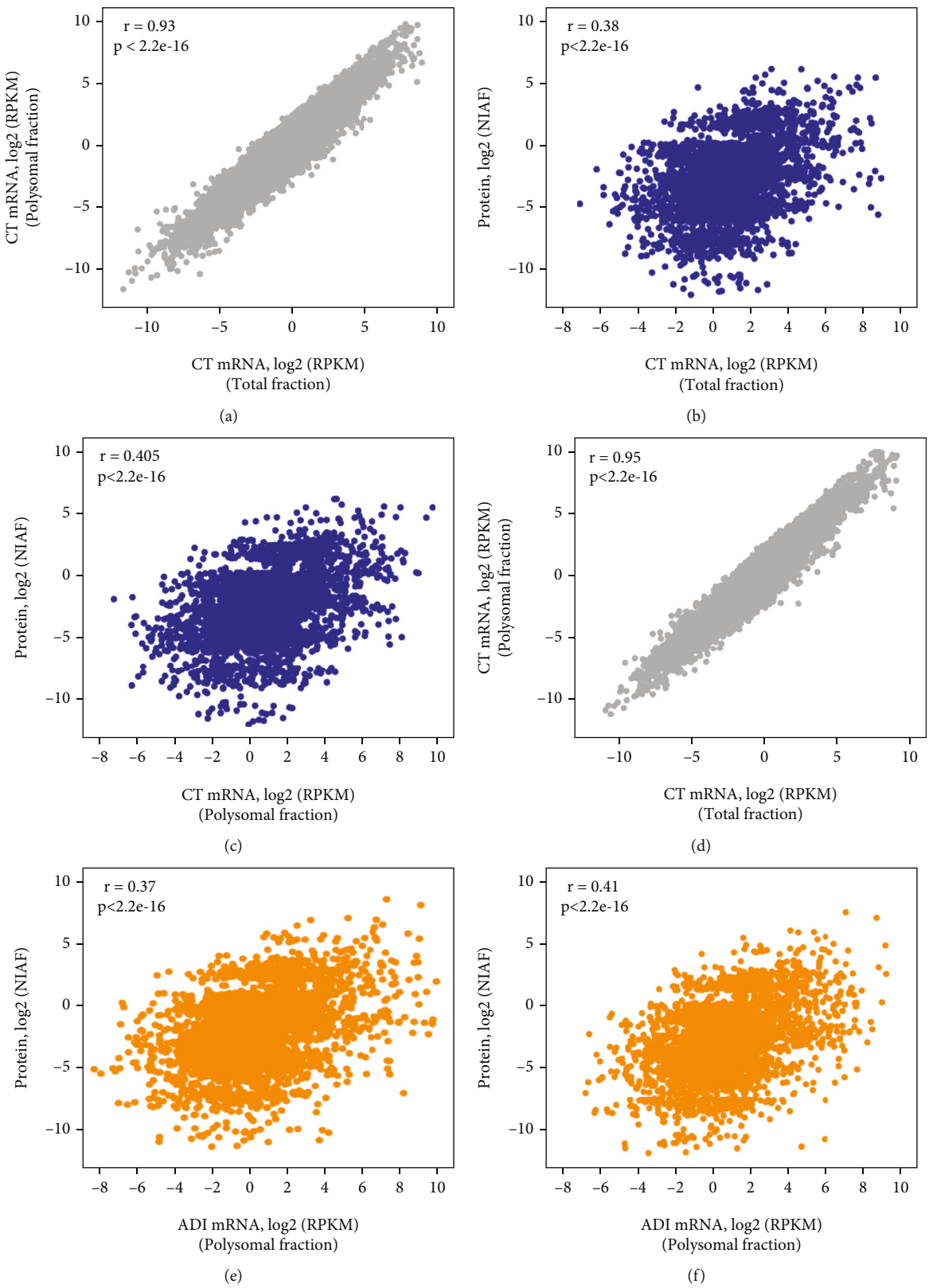

Figure 4: Relationship of identified proteins and mRNAs in control and induced hASC. (a) Correlation coefficient of CT mRNAs from the total and polysomal fractions. (b, c) Proteins versus CT mRNAs from the total and polysomal fractions, respectively. (d) Correlation coefficient of ADI mRNAs from the total and polysomal fractions. (e, f) Proteins versus ADI mRNAs from the total and polysomal fractions, respectively.

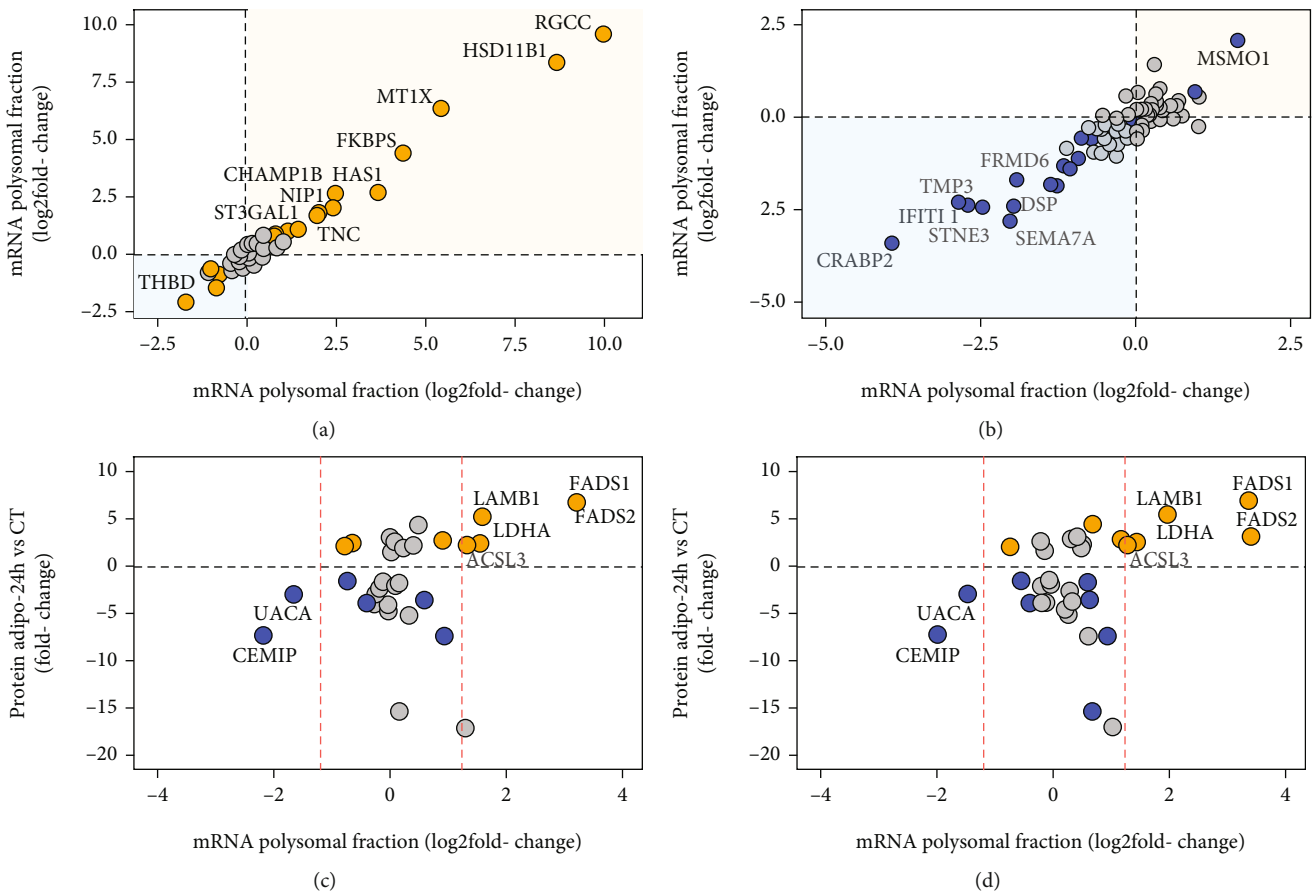

Figure 5: Gene expression regulation during the first step of human adipogenesis. (a) Scatterplot comparing RNA-seq from the total and polysomal fractions of hASC submitted to adipogenesis (24 hours), showing 53 proteins uniquely identified in 24 h-differentiated cells. (b) The same analysis with the 92 proteins uniquely identified in undifferentiated hASC. Orange and blue dots represent genes with FDR $\leq 5\%$. The named dots represent DEGs in the total and polysomal fractions. Orange and blue boxes represent adipogenesis (24 hours) and undifferentiated hASC, respectively. The differentially abundant proteins (up- and downregulated) were compared with the mRNA expression of the (c) total and (d) polysomal fraction. Orange and blue dots represent genes with FDR $\leq 5\%$ in the ADI and CT conditions, respectively. Dashed red lines represent the cutoff criteria for fold change in the RNA-seq data.

We identified proteins with differential abundance after 24 hours of adipogenic differentiation. The mRNAs corresponding to the most upregulated proteins were also differentially expressed in the total and polysomal fractions. We highlight Δ-5 Fatty Acid Desaturase (FADS1) and Δ-6 Fatty Acid Desaturase (FADS2), proteins that regulate the biosynthesis of polyunsaturated fatty acids (PUFA). Altered desaturase activity is an important issue in adipose tissue, body weight, and glucose uptake. FADS1 and FADS2 are expressed in adipocytes and have a functional pathway that can be regulated by PUFA. Thus, both eicosapentaenoic acid (EPA) and arachidonic acid (AA) reduced the expression of FADS1 and FADS2, while alpha-linoleic acid (ALA) and linoleic acid (LA) did not [49]. Genetic polymorphisms in FADS genes are associated with changes in fatty acid metabolism (*e.g.*, concentration), as well as overweight, obesity, metabolic syndrome, and cognition functions [50–53]. Furthermore, knockout- (KO-) Fads2 mice develop obesity resistance and impaired lipogenesis [54]. We previously demonstrated the expression of FADS2 mRNA in total and polysomal fractions after 24 hours of adipogenesis in hASC [25], while its expression at the protein level is demonstrated in this study. Similarly, the ACSL3 protein is a member of the long-chain acyl-CoA synthetase family, which plays an important role in fatty acid metabolism. The protein is located in the endoplasmic reticulum (ER), from where it is effectively translocated to lipid droplets when lipid synthesis is stimulated. Its overexpression promotes an increase in the triglyceride content of lipid droplets. Therefore, ACSL3 plays a key role in adipocyte differentiation [55, 56].

Another interesting protein is the laminin subunit beta 1 (LAMB1), which has functions related to the extracellular matrix (ECM). Recently, high levels of LAMB1 were observed in visceral adipose tissue and during *in vitro* adipogenesis. Obesity alters the gene expression profile of ECM genes in adipose tissue (LAMB1 was upregulated in visceral and subcutaneous adipose tissue) [57–60]. The lactate dehydrogenase A protein (LDHA) catalyzes the conversion of pyruvate to lactate in the glycolytic metabolism. Although insulin stimulates glycolysis, the lactate production of adipocytes not only depends on glucose availability and uptake but is also maintained during insulin resistance. This

indicates that lactate production is an important aspect of adipocyte and adipose tissue metabolism [61]. Here, we demonstrate the early expression of LDHA in adipogenic differentiation, though the mechanism and influence of this protein during the differentiation process remain unknown.

4.2. Posttranscriptional Regulation of Differential Abundant Proteins. We are interested in studying the posttranscriptional regulation of the hASC differentiation process. To do so, we used different global approaches to determine the gene expression profile in the transcriptome, translatome, and proteome on the first day of adipogenic differentiation. We found a strong correlation between the transcriptome and the translatome, corroborating our group's previous findings [14]. We have observed that regulation of mRNA abundance is predominant at the initial steps of adipogenesis, with translational regulation increasing on the last days of differentiation [14, 20, 21]. A positive correlation was also observed between mRNA and protein expression data. Despite the positive correlation between mRNAs and proteins, the differences may be related to the different half-lives of the proteins and/or mRNAs, translational rates, protein modifications, and other posttranslational mechanisms [62, 63].

Of the 33 identified proteins with differential abundance, 26 (78%) did not have differential expression of their cognate mRNAs in the total and polysomal fractions (Figures 5(c) and 5(d)). These proteins may be undergoing strong posttranscriptional, translational, and/or posttranslational regulation. As mentioned above, there is no differential expression of their cognate mRNAs of the nine upregulated proteins. Some of these proteins are related to lipid metabolism or the adipogenic process.

For example, type 2 insulin-like growth factor receptor (IGF2R) is a protein (also called the cation-independent mannose-6-phosphate receptor) that modulates the tissue and circulating levels of IGF2 by internalization and targeting lysosomes for degradation. Insulin exposure increases the steady-state number of IGF2R, in addition to increasing the ligation, internalization, and degradation of IGF2 [64, 65]. These findings are curious due to the high levels of IGF2 expression in obese individuals with type 2 diabetes mellitus and because high doses of IGF2 increase *in vitro* differentiation and lipid accumulation [66, 67]. Furthermore, Igf2r-KO directly reduced brown adipogenesis and brown adipocyte survival [68]. To date, the exact mechanism of action of IGF2R in the adipogenic differentiation process and adipose tissue has been unknown. In this study, we demonstrated the expression of IGF2R at the protein level in differentiating cells since the receptor may have been directly induced by insulin exposure and may play a role in the control of lipid accumulation at the very beginning of hASC differentiation.

Another protein that was shown to be upregulated and which responds to insulin is eukaryotic translational initiation factor 6 (EIF6). This protein regulates the translation of specific mRNAs through the control of 60S availability [69]. Recently, it was shown that eIF6 controls glycolysis and fatty acid synthesis, in addition to influencing the translational activation of adipogenic transcription factors (*e.g.*, C/EBPβ and ATF4) and lipogenic enzymes in the adipogenic process of MSC [70].

The focal adhesion fermitin family member 2 protein (FERMT2), also known as Kindlin-2 protein, is expressed in multiple cell types (including MSC) and plays a critical role during early embryogenesis since global protein deletion results in peri-implantation lethality in mice. FERMT2 appears to have essential functions in the chondrogenesis, osteogenesis, and adipogenesis of MSC [71]. Recently, it was demonstrated that the expression of FERMT2 in hMSC undergoing osteogenic differentiation was markedly increased. However, protein levels were reduced during adipogenesis (after 14 days). The knockdown of FERMT2 in hMSC results in cells spontaneously differentiating into adipocytes and PPARγ and aP2 expression increasing significantly [72, 73]. Despite that, transgenic mice with the deletion of FERMT2 in adipocytes possess severe lipodystrophy with drastically reduced adipose tissue mass. Protein loss suppressed adipocyte gene expression and differentiation [74]. In this study, we show only the differential abundance of the FERMT2 protein (not cognate mRNA expression) in early adipogenesis of hASC. This may indicate a transient expression throughout the differentiation process, and new studies should be conducted to better understand the gene's expression dynamics.

Emerin protein (EMD) is anchored in the inner nuclear membrane. It binds and regulates the nuclear accumulation of the β-catenin protein (Wnt signaling) [75]. In mouse preadipocytes undergoing adipogenesis, β-catenin was downregulated at the protein level and was accompanied by a significant upregulation of emerin (mRNA and protein level). Emerin controls the redistribution of β-catenin from the nucleus to the cytoplasm, facilitating its degradation and consequently allowing the adipogenic program [76]. Despite this, it has been shown that after 10 days of adipogenic differentiation, a fraction of adipocytes (approximately 70%) lacked emerin and other proteins related to nuclear lamina [77]. Our results, therefore, indicate that emerin may play a role in β-catenin regulation at the very beginning of adipogenesis in hASC, being subsequently regulated throughout the differentiation process.

Fibroblast growth factor (FGF) signaling is another important pathway that controls stem cells [78]. For example, FGF2 has the ability to inhibit the adipogenic process. The lysyl oxidase protein (LOX) catalyzes the cross-linking of lysine residues in elastin and collagen, fortifying the extracellular matrix. It partially enhances the adipogenesis of preadipocytes through the inhibition of FGF2 receptor signaling (including downregulation of AKT and ERK1/2) [79]. Interestingly, the TGF- β/SMAD signaling pathway plays a critical role in adipocyte commitment of MSCs as well. Both BMP4 and BMP2 activated the expression and phosphorylation of SMAD1/5/8 to form a complex with SMAD4. This complex is translocated to the nucleus to regulate LOX during adipocyte commitment [80, 81]. Here, we identified the expression of SMAD4 in 24 h-differentiated cells (Supplementary Table 1) and found that LOX was differentially abundant at the protein level in these induced cells (Supplementary Table 2). The remaining identified

proteins (ATP1A1, ETHE1, PACSIN2, and BUB3) may play important roles in mitochondrial metabolism, lipid metabolism, vesicular traffic, cell migration, and cell cycle regulation [82–85].

On the other hand, we identified 17 downregulated proteins with no differential expression of their cognate mRNAs. These proteins may be undergoing extreme proteolytic activity since their abundance is critical for starting adipogenesis in hASC. Some of these proteins exhibit antiadipogenic activity, suppressing the differentiation process. This is the case of alpha-2-macroglobulin (A2M), a protease inhibitor protein. Accumulation of the A2M protein in murine preadipocytes inhibits adipogenesis, while the depletion of intracellular A2M increases lipid accumulation and adipocyte-gene marker expression [86]. Curiously, adult bovine serum does not support adipogenic differentiation in a similar manner to fetal bovine serum since the A2M concentration is 3.5 times higher [87].

Finally, the two most downregulated proteins identified here (QPRT and SDF4) have no known relationship with adipogenesis. Quinolinate phosphoribosyl transferase protein (QPRT) catabolizes quinolinic acid to nicotinic acid mononucleotide for de novo NAD synthesis (kynurenine pathway). It has been shown that both L-kynurenine and L-tryptophan significantly increase the stemness and migration of hBMSC, in addition to suppressing adipogenesis [88–90]. The rapid degradation of QPRT may thus be necessary for the loss of self-renewal capacity in hASC and triggering adipogenesis. The stromal cell-derived factor 4 protein (SDF-4), also called Cab45, is a Ca^{2+}-binding protein involved in cell migration and proliferation through regulation of the cytosolic calcium level. Ca^{2+} plays an important role in different stages of hMSC differentiation and proliferation [91]. For example, hASC exposed to Ca^{2+} significantly reduced adipogenic differentiation and triglyceride content [92]. The SDF-4 downregulation we observed may therefore exert control on hASC proliferation through cytosolic Ca^{2+} regulation.

Taken together, these results represent novel information on the regulation of gene expression at the beginning of the adipogenic differentiation process in hASC. The processes that regulate mRNA transcription and translation and protein degradation are thus critical for human adipogenesis.

5. Conclusion

In conclusion, we have demonstrated that the initial step of the adipogenic differentiation process is highly controlled at the transcriptional, posttranscriptional, and posttranslational levels. We were able to identify proteins with potentially important roles in adipocyte commitment at the very beginning of differentiation. These results may contribute to a better understanding of human adipogenesis and the development of obesity.

Data Availability

The raw proteomic data used to support the findings of this study have been deposited in the PRIDE database under the accession number PXD026299. The raw RNA-seq data were downloaded from the ArrayExpress repository under the accession number E-MTAB-6298. The analyzed datasets used to support the findings of this study are included within the article.

Conflicts of Interest

The authors declare that they have no competing interests.

Authors' Contributions

B.B. contributed to the analysis and interpretation of the data, drafting, writing, and revision of the manuscript. A.C.CA, M.D.M.S., and P.C.C. performed proteomics analysis. B.B., M.D.M.S., and J.S.G.F. performed all experimental assays. B.D. contributed to the conception, design, and revision of the manuscript. All authors revised and approved the final version of the manuscript.

Acknowledgments

This study was supported by Fiocruz and CNPq PROEP/ICC grant no. 442353/2019-7. PCC and BD received fellowships from CNPq.

Supplementary Materials

Figure S1: human adipose-derived stem cell (hASC) characterization. Figure S2: sample chromatographies. Figure S3: Gene Ontology (GO) analysis of identified proteins in the proteomics assay. Figure S4: Gene Ontology (GO) analysis of differentially abundant proteins identified in the proteomic assay. Figure S5: mass spectrometer spectrum of identified hidden proteins in CT, ADI, and in both conditions. Table S1: proteins identified in the proteomic analysis of undifferentiated and induced hASC. Table S2: differentially abundant proteins during the first 24 hours of adipogenesis. Table S3: expression quantification of identified proteins and peptides. Table S4: differentially expressed genes in the total and polysomal RNA-seq during the first 24 hours of adipogenesis. *(Supplementary Materials)*

References

[1] M. Desai, M. Beall, and M. G. Ross, "Developmental origins of obesity: programmed adipogenesis," *Current Diabetes Reports*, vol. 13, no. 1, pp. 27–33, 2013.

[2] F. Ruiz-Ojeda, A. Rupérez, C. Gomez-Llorente, A. Gil, and C. Aguilera, "Cell models and their application for studying adipogenic differentiation in relation to obesity: a review," *IJMS*, vol. 17, no. 7, p. 1040, 2016.

[3] S. Gesta, Y.-H. Tseng, and C. R. Kahn, "Developmental origin of fat: tracking obesity to its source," *Cell*, vol. 131, no. 2, pp. 242–256, 2007.

[4] B. M. Spiegelman and J. S. Flier, "Adipogenesis and obesity: rounding out the big picture," *Cell*, vol. 87, no. 3, pp. 377–389, 1996.

[5] G. Hotamisligil, N. Shargill, and B. Spiegelman, "Adipose expression of tumor necrosis Factor-α: direct role in obesity-

linked insulin resistance," *Science*, vol. 259, no. 5091, pp. 87–91, 1993.

[6] K. L. Spalding, E. Arner, P. O. Westermark et al., "Dynamics of fat cell turnover in humans," *Nature*, vol. 453, no. 7196, pp. 783–787, 2008.

[7] A. Sorisky, A. S. D. Molgat, and A. Gagnon, "Macrophage-induced adipose tissue dysfunction and the preadipocyte: should I stay (and differentiate) or should I go?," *Advances in Nutrition*, vol. 4, no. 1, pp. 67–75, 2013.

[8] Z. Wu, P. Puigserver, U. Andersson et al., "Mechanisms controlling mitochondrial biogenesis and respiration through the thermogenic coactivator PGC-1," *Cell*, vol. 98, no. 1, pp. 115–124, 1999.

[9] A. W. Robert, B. H. Marcon, B. Dallagiovanna, and P. Shigunov, "Adipogenesis, osteogenesis, and chondrogenesis of human mesenchymal stem/stromal cells: a comparative transcriptome approach," *Frontiers in Cell and Development Biology*, vol. 8, p. 561, 2020.

[10] E. D. Rosen and O. A. MacDougald, "Adipocyte differentiation from the inside out," *Nature Reviews Molecular Cell Biology*, vol. 7, no. 12, pp. 885–896, 2006.

[11] A. G. Cristancho and M. A. Lazar, "Forming functional fat: a growing understanding of adipocyte differentiation," *Nature Reviews Molecular Cell Biology*, vol. 12, no. 11, pp. 722–734, 2011.

[12] R. Siersbaek, R. Nielsen, S. John et al., "Extensive chromatin remodelling and establishment of transcription factor 'hotspots' during early adipogenesis," *The EMBO Journal*, vol. 30, no. 8, pp. 1459–1472, 2011.

[13] Y.-J. Hu, H. Belaghzal, W.-Y. Hsiao et al., "Transcriptional and post-transcriptional control of adipocyte differentiation by Jumonji domain-containing protein 6," *Nucleic Acids Research*, vol. 43, no. 16, pp. 7790–7804, 2015.

[14] L. Spangenberg, P. Shigunov, A. P. R. Abud et al., "Polysome profiling shows extensive posttranscriptional regulation during human adipocyte stem cell differentiation into adipocytes," *Stem Cell Research*, vol. 11, no. 2, pp. 902–912, 2013.

[15] T. Song, Y. Yang, S. Jiang, and J. Peng, "Novel insights into adipogenesis from the perspective of transcriptional and RNA N6-methyladenosine-mediated post-transcriptional regulation," *Advancement of Science*, vol. 7, no. 21, article 2001563, 2020.

[16] L. S. Carnevalli, K. Masuda, F. Frigerio et al., "S6K1 plays a critical role in early adipocyte differentiation," *Developmental Cell*, vol. 18, no. 5, pp. 763–774, 2010.

[17] C. Chiellini, O. Cochet, L. Negroni et al., "Characterization of human mesenchymal stem cell secretome at early steps of adipocyte and osteoblast differentiation," *BMC Molecular Biology*, vol. 9, no. 1, p. 26, 2008.

[18] H. Molina, Y. Yang, T. Ruch et al., "Temporal profiling of the adipocyte proteome during differentiation using a five-Plex SILAC based strategy," *Journal of Proteome Research*, vol. 8, no. 1, pp. 48–58, 2009.

[19] J. Zhong, S. A. Krawczyk, R. Chaerkady et al., "Temporal profiling of the secretome during adipogenesis in humans," *Journal of Proteome Research*, vol. 9, no. 10, pp. 5228–5238, 2010.

[20] B. H. Marcon, F. B. Holetz, G. Eastman et al., "Downregulation of the protein synthesis machinery is a major regulatory event during early adipogenic differentiation of human adipose-derived stromal cells," *Stem Cell Research*, vol. 25, pp. 191–201, 2017.

[21] B. H. Marcon, P. Shigunov, L. Spangenberg et al., "Cell cycle genes are downregulated after adipogenic triggering in human adipose tissue-derived stem cells by regulation of mRNA abundance," *Scientific Reports*, vol. 9, no. 1, p. 5611, 2019.

[22] S. Li, T. Xue, F. He et al., "A time-resolved proteomic analysis of transcription factors regulating adipogenesis of human adipose derived stem cells," *Biochemical and Biophysical Research Communications*, vol. 511, no. 4, pp. 855–861, 2019.

[23] E. Kim, W. Kim, K.-J. Oh, B. Han, S. Lee, and K. H. Bae, "Recent advances in proteomic studies of adipose tissues and adipocytes," *IJMS*, vol. 16, no. 3, pp. 4581–4599, 2015.

[24] C. D. Horinouchi, M. J. Barisón, A. W. Robert, C. Kuligovski, A. M. Aguiar, and B. Dallagiovanna, "Influence of donor age on the differentiation and division capacity of human adipose-derived stem cells," *World Journal of Stem Cells*, vol. 12, no. 12, pp. 1640–1651, 2020.

[25] B. H. Marcon, L. Spangenberg, B. Bonilauri et al., "Data describing the experimental design and quality control of RNA-Seq of human adipose-derived stem cells undergoing early adipogenesis and osteogenesis," *Data in Brief*, vol. 28, article 105053, 2020.

[26] M. Dominici, K. le Blanc, I. Mueller et al., "Minimal criteria for defining multipotent mesenchymal stromal cells. The International Society for Cellular Therapy position statement," *Cytotherapy*, vol. 8, no. 4, pp. 315–317, 2006.

[27] A. W. Robert, A. B. B. Angulski, L. Spangenberg et al., "Gene expression analysis of human adipose tissue-derived stem cells during the initial steps of in vitro_ osteogenesis," *Scientific Reports*, vol. 8, no. 1, p. 4739, 2018.

[28] J. Rappsilber, Y. Ishihama, and M. Mann, "Stop and go extraction tips for matrix-assisted laser desorption/ionization, nanoelectrospray, and LC/MS sample pretreatment in proteomics," *Analytical Chemistry*, vol. 75, no. 3, pp. 663–670, 2003.

[29] P. C. Carvalho, D. B. Lima, F. V. Leprevost et al., "Integrated analysis of shotgun proteomic data with PatternLab for proteomics 4.0," *Nature Protocols*, vol. 11, no. 1, pp. 102–117, 2016.

[30] J. K. Eng, M. R. Hoopmann, T. A. Jahan, J. D. Egertson, W. S. Noble, and M. J. MacCoss, "A Deeper Look into Comet—Implementation and Features," *Journal of the American Society for Mass Spectrometry*, vol. 26, no. 11, pp. 1865–1874, 2015.

[31] P. C. Carvalho, J. S. G. Fischer, T. Xu et al., "Search engine processor: filtering and organizing peptide spectrum matches," *Proteomics*, vol. 12, no. 7, pp. 944–949, 2012.

[32] R. Barboza, D. Cociorva, T. Xu et al., "Can the false-discovery rate be misleading?," *Proteomics*, vol. 11, no. 20, pp. 4105–4108, 2011.

[33] J. R. Yates 3rd, S. K. R. Park, C. M. Delahunty et al., "Toward objective evaluation of proteomic algorithms," *Nature Methods*, vol. 9, no. 5, pp. 455-456, 2012.

[34] P. C. Carvalho, J. R. Yates 3rd, and V. C. Barbosa, "Improving the TFold test for differential shotgun proteomics," *Bioinformatics*, vol. 28, no. 12, pp. 1652–1654, 2012.

[35] M. D. Robinson, D. J. McCarthy, and G. K. Smyth, "edgeR: a Bioconductor package for differential expression analysis of digital gene expression data," *Bioinformatics*, vol. 26, no. 1, pp. 139-140, 2010.

[36] D. W. Huang, B. T. Sherman, and R. A. Lempicki, "Systematic and integrative analysis of large gene lists using DAVID bioinformatics resources," *Nature Protocols*, vol. 4, no. 1, pp. 44–57, 2009.

[37] D. Szklarczyk, A. L. Gable, D. Lyon et al., "STRING v11: protein–protein association networks with increased coverage, supporting functional discovery in genome-wide experimental

datasets," *Nucleic Acids Research*, vol. 47, no. D1, pp. D607–D613, 2019.

[38] L. U. Kurt, M. A. Clasen, M. D. M. Santos et al., "RawVegetable - A data assessment tool for proteomics and cross-linking mass spectrometry experiments," *Journal of Proteomics*, vol. 225, article 103864, 2020.

[39] C. Schreiber, S. Saraswati, S. Harkins et al., "Loss of ASAP1 in mice impairs adipogenic and osteogenic differentiation of mesenchymal progenitor cells through dysregulation of FAK/Src and AKT signaling," *PLoS Genetics*, vol. 15, no. 6, article e1008216, 2019.

[40] L. A. Stechschulte, T. D. Hinds, S. S. Khuder, W. Shou, S. M. Najjar, and E. R. Sanchez, "FKBP51 controls cellular adipogenesis through p38 kinase-mediated phosphorylation of GRα and PPARγ," *Molecular Endocrinology*, vol. 28, no. 8, pp. 1265–1275, 2014.

[41] M. J. Pereira, J. Palming, M. K. Svensson et al., "FKBP5 expression in human adipose tissue increases following dexamethasone exposure and is associated with insulin resistance," *Metabolism*, vol. 63, no. 9, pp. 1198–1208, 2014.

[42] L. A. Stechschulte, B. Qiu, M. Warrier et al., "FKBP51 null mice are resistant to diet-induced obesity and the PPARγ agonist rosiglitazone," *Endocrinology*, vol. 157, no. 10, pp. 3888–3900, 2016.

[43] D. C. Berry, H. Soltanian, and N. Noy, "Repression of Cellular Retinoic Acid-binding Protein II during Adipocyte Differentiation," *Journal of Biological Chemistry*, vol. 285, no. 20, pp. 15324–15332, 2010.

[44] E. J. Schwarz, M. J. Reginato, D. Shao, S. L. Krakow, and M. A. Lazar, "Retinoic acid blocks adipogenesis by inhibiting C/EBP-beta-mediated transcription," *Molecular and Cellular Biology*, vol. 17, no. 3, pp. 1552–1561, 1997.

[45] D. A. Dumesic, J. D. Phan, K. L. Leung et al., "Adipose insulin resistance in normal-weight women with polycystic ovary syndrome," *The Journal of Clinical Endocrinology & Metabolism*, vol. 104, no. 6, pp. 2171–2183, 2019.

[46] S. Singh, Y. S. Rajput, A. K. Barui, R. Sharma, and S. Grover, "Expression of developmental genes in brown fat cells grown in vitro is linked with lipid accumulation," *In Vitro CellDevBiol-Animal*, vol. 51, no. 10, pp. 1003–1011, 2015.

[47] D. M. Mutch, C. Rouault, M. Keophiphath, D. Lacasa, and K. Clément, "Using gene expression to predict the secretome of differentiating human preadipocytes," *International Journal of Obesity*, vol. 33, no. 3, pp. 354–363, 2009.

[48] Y. Xin, C. Li, Y. Guo, R. Xiao, H. Zhang, and G. Zhou, "RNA-Seq analysis reveals a negative role ofMSMO1with a synergizedNSDHLexpression during adipogenesis of 3T3-L1," *Bioscience, Biotechnology, and Biochemistry*, vol. 83, no. 4, pp. 641–652, 2019.

[49] J. C. Ralston, S. Matravadia, N. Gaudio, G. P. Holloway, and D. M. Mutch, "Polyunsaturated fatty acid regulation of adipocyte FADS1 and FADS2 expression and function," *Obesity*, vol. 23, no. 4, pp. 725–728, 2015.

[50] B. Koletzko, E. Reischl, C. Tanjung et al., "FADS1andFADS2Polymorphisms modulate fatty acid metabolism and dietary impact on health," *Annual Review of Nutrition*, vol. 39, no. 1, pp. 21–44, 2019.

[51] S. Park, D. S. Kim, and S. Kang, "Carrying minor allele of FADS1 and haplotype of FADS1 and FADS2 increased the risk of metabolic syndrome and moderate but not low fat diets lowered the risk in two Korean cohorts," *European Journal of Nutrition*, vol. 58, no. 2, pp. 831–842, 2019.

[52] A. Muzsik, J. Bajerska, H. H. Jeleń, J. Walkowiak, P. Krzyżanowska-Jankowska, and A. Chmurzynska, "FADS1 and FADS2 polymorphism are associated with changes in fatty acid concentrations after calorie-restricted Central European and Mediterranean diets," *Menopause*, vol. 26, no. 12, pp. 1415–1424, 2019.

[53] Z. He, R. Zhang, F. Jiang et al., "FADS1-FADS2 genetic polymorphisms are associated with fatty acid metabolism through changes in DNA methylation and gene expression," *Clinical Epigenetics*, vol. 10, no. 1, p. 113, 2018.

[54] W. Stoffel, I. Hammels, B. Jenke et al., "Obesity resistance and deregulation of lipogenesis in Δ6-fatty acid desaturase (FADS 2) deficiency," *EMBO Reports*, vol. 15, no. 1, pp. 110–120, 2014.

[55] Y. Lv, Y. Cao, Y. Gao et al., "Effect ofACSL3Expression levels on preadipocyte differentiation in Chinese red steppe cattle," *DNA and Cell Biology*, vol. 38, no. 9, pp. 945–954, 2019.

[56] M. Poppelreuther, B. Rudolph, C. Du et al., "The N-terminal region of acyl-CoA synthetase 3 is essential for both the localization on lipid droplets and the function in fatty acid uptake," *Journal of Lipid Research*, vol. 53, no. 5, pp. 888–900, 2012.

[57] C. Henegar, J. Tordjman, V. Achard et al., "Adipose tissue transcriptomic signature highlights the pathological relevance of extracellular matrix in human obesity," *Genome Biology*, vol. 9, no. 1, article R14, 2008.

[58] S. Mori, S. Kiuchi, A. Ouchi, T. Hase, and T. Murase, "Characteristic expression of extracellular matrix in subcutaneous adipose tissue development and adipogenesis; comparison with visceral adipose tissue," *International Journal of Biological Sciences*, vol. 10, no. 8, pp. 825–833, 2014.

[59] C. Strieder-Barboza, N. A. Baker, C. G. Flesher et al., "Depot-specific adipocyte-extracellular matrix metabolic crosstalk in murine obesity," *Adipocytes*, vol. 9, no. 1, pp. 189–196, 2020.

[60] L. Mor-Yossef Moldovan, M. Lustig, A. Naftaly et al., "Cell shape alteration during adipogenesis is associated with coordinated matrix cues," *Journal of Cellular Physiology*, vol. 234, no. 4, pp. 3850–3863, 2019.

[61] J. R. Krycer, L.-E. Quek, D. Francis et al., "Lactate production is a prioritized feature of adipocyte metabolism," *Journal of Biological Chemistry*, vol. 295, no. 1, pp. 83–98, 2020.

[62] Y. Liu, A. Beyer, and R. Aebersold, "On the dependency of cellular protein levels on mRNA abundance," *Cell*, vol. 165, no. 3, pp. 535–550, 2016.

[63] B. Dallagiovanna, I. T. Pereira, A. C. Origa-Alves, P. Shigunov, H. Naya, and L. Spangenberg, "lncRNAs are associated with polysomes during adipose-derived stem cell differentiation," *Gene*, vol. 610, pp. 103–111, 2017.

[64] Y. Oka, L. M. Rozek, and M. P. Czech, "Direct demonstration of rapid insulin-like growth factor II Receptor internalization and recycling in rat adipocytes. Insulin stimulates 125I-insulin-like growth factor II degradation by modulating the IGF-II receptor recycling process.," *The Journal of Biological Chemistry*, vol. 260, no. 16, pp. 9435–9442, 1985.

[65] J. Brown, E. Y. Jones, and B. E. Forbes, "Keeping IGF-II under control: Lessons from the IGF-II-IGF2R crystal structure," *Trends in Biochemical Sciences*, vol. 34, no. 12, pp. 612–619, 2009.

[66] L. Xuan, J. Ma, M. Yu et al., "Insulin-like growth factor 2 promotes adipocyte proliferation, differentiation and lipid deposition in obese type 2 diabetes," *Journal of Translational Science*, vol. 6, no. 5, 2020.

[67] M. N. Alfares, C. M. Perks, J. P. Hamilton-Shield, and J. M. P. Holly, "Insulin-like growth factor-II in adipocyte regulation: depot-specific actions suggest a potential role limiting excess visceral adiposity," *American Journal of Physiology-Endocrinology and Metabolism*, vol. 315, no. 6, pp. E1098–E1107, 2018.

[68] M. Hashimoto, T. Kusudo, T. Takeuchi, N. Kataoka, T. Mukai, and H. Yamashita, "CREG1 stimulates brown adipocyte formation and ameliorates diet-induced obesity in mice," *The FASEB Journal*, vol. 33, no. 7, pp. 8069–8082, 2019.

[69] M. Ceci, C. Gaviraghi, C. Gorrini et al., "Release of eIF6 ($p27^{BBP}$) from the 60S subunit allows 80S ribosome assembly," *Nature*, vol. 426, no. 6966, pp. 579–584, 2003.

[70] D. Brina, A. Miluzio, S. Ricciardi et al., "eIF6 coordinates insulin sensitivity and lipid metabolism by coupling translation to transcription," *Nature Communications*, vol. 6, no. 1, p. 8261, 2015.

[71] C. Wu, H. Jiao, Y. Lai et al., "Kindlin-2 controls TGF-β signalling and Sox9 expression to regulate chondrogenesis," *Nature Communications*, vol. 6, no. 1, p. 7531, 2015.

[72] H. Cao, Q. Yan, D. Wang et al., "Focal adhesion protein Kindlin-2 regulates bone homeostasis in mice," *Bone Research*, vol. 8, no. 1, p. 2, 2020.

[73] L. Guo, T. Cai, K. Chen et al., "Kindlin-2 regulates mesenchymal stem cell differentiation through control of YAP1/TAZ," *Journal of Cell Biology*, vol. 217, no. 4, pp. 1431–1451, 2018.

[74] H. Gao, Y. Guo, Q. Yan et al., "Lipoatrophy and metabolic disturbance in mice with adipose-specific deletion of kindlin-2," *JCI Insight*, vol. 4, no. 13, article e128405, 2019.

[75] E. Markiewicz, K. Tilgner, N. Barker et al., "The inner nuclear membrane protein Emerin regulates β-catenin activity by restricting its accumulation in the nucleus," *The EMBO Journal*, vol. 25, no. 14, pp. 3275–3285, 2006.

[76] K. Tilgner, K. Wojciechowicz, C. Jahoda, C. Hutchison, and E. Markiewicz, "Dynamic complexes of A-type lamins and emerin influence adipogenic capacity of the cell via nucleocytoplasmic distribution of β-catenin," *Journal of Cell Science*, vol. 122, no. 3, pp. 401–413, 2009.

[77] V. L. R. M. Verstraeten, J. Renes, F. C. S. Ramaekers et al., "Reorganization of the nuclear lamina and cytoskeleton in adipogenesis," *Histochemistry and Cell Biology*, vol. 135, no. 3, pp. 251–261, 2011.

[78] M. Mossahebi-Mohammadi, M. Quan, J.-S. Zhang, and X. Li, "FGF signaling pathway: a key regulator of stem cell pluripotency," *Frontiers in Cell and Development Biology*, vol. 8, p. 79, 2020.

[79] J. D. Griner, C. J. Rogers, M.-J. Zhu, and M. du, "Lysyl oxidase propeptide promotes adipogenesis through inhibition of FGF-2 signaling," *Adipocytes*, vol. 6, no. 1, pp. 12–19, 2017.

[80] H. Huang, T.-J. Song, X. Li et al., "BMP signaling pathway is required for commitment of C3H10T1/2 pluripotent stem cells to the adipocyte lineage," *Proceedings of the National Academy of Sciences*, vol. 106, no. 31, pp. 12670–12675, 2009.

[81] S.-N. Li and J.-F. Wu, "TGF-β/SMAD signaling regulation of mesenchymal stem cells in adipocyte commitment," *Stem Cell Research & Therapy*, vol. 11, no. 1, p. 41, 2020.

[82] T. M. Hildebrandt, I. di Meo, M. Zeviani, C. Viscomi, and H. P. Braun, "Proteome adaptations in Ethe1-deficient mice indicate a role in lipid catabolism and cytoskeleton organization via post-translational protein modifications," *Bioscience Reports*, vol. 33, no. 4, article e00052, 2013.

[83] J. Adachi, C. Kumar, Y. Zhang, and M. Mann, "In-depth Analysis of the Adipocyte Proteome by Mass Spectrometry and Bioinformatics," *Molecular & Cellular Proteomics*, vol. 6, no. 7, pp. 1257–1273, 2007.

[84] H. Meng, L. Tian, J. Zhou et al., "PACSIN 2 represses cellular migration through direct association with cyclin D1 but not its alternate splice form cyclin D1b," *Cell Cycle*, vol. 10, no. 1, pp. 73–81, 2011.

[85] J. Lee, C. G. Lee, K.-W. Lee, and C. W. Lee, "Cross-talk between BubR1 expression and the commitment to differentiate in adipose-derived mesenchymal stem cells," *Experimental & Molecular Medicine*, vol. 41, no. 12, p. 873, 2009.

[86] K.-L. Choi, Y. Wang, C. A. Tse, K. S. L. Lam, G. J. S. Cooper, and A. Xu, "Proteomic analysis of adipocyte differentiation: evidence that α2 macroglobulin is involved in the adipose conversion of 3T3 L1 preadipocytes," *Proteomics*, vol. 4, no. 6, pp. 1840–1848, 2004.

[87] J. Park, J. Park, S.-S. Nahm, I. Choi, and J. Kim, "Identification of anti-adipogenic proteins in adult bovine serum suppressing 3T3-L1 preadipocyte differentiation," *BMB Reports*, vol. 46, no. 12, pp. 582–587, 2013.

[88] H. Pham, M. Ono, E. Hara et al., "Tryptophan and kynurenine enhances the stemness and osteogenic differentiation of bone marrow-derived mesenchymal stromal cells in vitro and in vivo," *Materials*, vol. 14, no. 1, p. 208, 2021.

[89] Z. Wang, Y. Gao, C. Zhang et al., "Quinolinate phosphoribosyltransferase is an antiviral host factor against hepatitis C virus infection," *Scientific Reports*, vol. 7, no. 1, p. 5876, 2017.

[90] M. Pokusa, N. Hlavacova, A. Csanova, M. Franklin, S. Zorad, and D. Jezova, "Adipogenesis and aldosterone: a study in lean tryptophan-depleted rats," *General Physiology and Biophysics*, vol. 35, no. 3, pp. 379–386, 2016.

[91] W. Gong, T. Martin, A. Sanders, A. Jiang, P. Sun, and W. Jiang, "Location, function and role of stromal cell-derived factors and possible implications in cancer (review)," *International Journal of Molecular Medicine*, vol. 47, no. 2, pp. 435–443, 2020.

[92] F. Goudarzi, A. Mohammadalipour, I. Khodadadi et al., "The role of calcium in differentiation of human adipose-derived stem cells to adipocytes," *Molecular Biotechnology*, vol. 60, no. 4, pp. 279–289, 2018.

Hindawi
Stem Cells International
Volume 2021, Article ID 2612480, 18 pages
https://doi.org/10.1155/2021/2612480

Research Article

Cytological Effects of Serum Isolated from Polytraumatized Patients on Human Bone Marrow-Derived Mesenchymal Stem Cells

Yazhou Long, Katrin Bundkirchen, Pascal Gräff, Christian Krettek, Sandra Noack, and Claudia Neunaber

Trauma Department, Hannover Medical School, 30625 Hannover, Germany

Correspondence should be addressed to Claudia Neunaber; neunaber.claudia@mh-hannover.de

Received 29 August 2021; Accepted 3 November 2021; Published 28 November 2021

Academic Editor: Jun Liu

Due to their immunomodulatory and regenerative capacity, human bone marrow-derived mesenchymal stem cells (hBMSCs) are promising in the treatment of patients suffering from polytrauma. However, few studies look at the effects of sera from polytraumatized patients on hBMSCs. The aim of this study was to explore changes in hBMSC properties in response to serum from polytrauma patients taken at different time points after the trauma incident. For this, sera from 84 patients with polytrauma (collected between 2010 and 2020 in our department) were used. In order to test the differential influence on hBMSC, sera from the 1st (D1), 5th (D5), and 10th day (D10) after polytrauma were pooled, respectively. As a control, sera from three healthy donors (HS), matched with respect to age and gender to the polytrauma group, were collected. Furthermore, hBMSCs from four healthy donors were used in the experiments. The pooled sera of HS, D1, D5, and D10 were analyzed by multicytokine array for pro-/anti-inflammatory cytokines. Furthermore, the influence of the different sera on hBMSCs with respect to cell proliferation, colony forming unit-fibroblast (CFU-F) assay, cell viability, cytotoxicity, cell migration, and osteogenic and chondrogenic differentiation was analyzed. The results showed that D5 serum significantly reduced hBMSC cell proliferation capacity compared with HS and increased the proportion of dead cells compared with D1. However, the frequency of CFU-F was not reduced in polytrauma groups compared with HS, as well as the other parameters. The serological effect of polytrauma on hBMSCs was related to the time after trauma. It is disadvantageous to use BMSCs in polytraumatized patients at least until the fifth day after polytrauma as obvious cytological changes could be found at that time point. However, it is promising to use hBMSCs to treat polytrauma after five days, combined with the concept of "Damage Control Orthopedics" (DCO).

1. Introduction

Polytrauma is not a mere addition of multiple injuries; instead, it has significant effects on the entire body function and changes in pathophysiology. People affected by this kind of injury often suffer from serious disabilities and, in extreme cases, lose their lives. Therefore, polytrauma is a leading cause of death and disability worldwide [1, 2]. A classification for polytrauma is important for proper and accurate benchmarking of care and results [3]. The most widely accepted classification system for polytrauma is the Injury Severity Score (ISS). For its calculation, first, the Abbreviated Injury Scale (AIS), which classifies each injury by body region on a 6-point scale, is used. Next, the ISS is derived from the AIS by calculating the sum of the squares of the AIS scores of the three most severely injured body regions [4, 5]. The internationally accepted criterion for serious polytrauma is an ISS ≥ 16 [6, 7]. The new "Berlin definition" states that polytrauma is defined by an AIS ≥ 3 for two or more different body regions and one or more additional variables from five physiologic parameters [8].

Polytrauma induces serious multisite damage and can even result in multiple organ dysfunction syndrome (MODS) and sepsis [8, 9]. The nature of polytraumatic

inflammatory response is the body's physiological immune response to damage and microorganisms [10–12]. Trauma triggers the production of different inflammatory mediators and associated peptides. Tumor necrosis factor-α (TNF-α), interleukin- (IL-) 1, IL-6, IL-8, and IL-10 can be secreted from monocytes/macrophages [12, 13]. Inflammatory cascade activation plays a major role in the development of immune dysfunction and MODS following polytrauma [14].

Mesenchymal stem cells (MSCs) are defined as nonhematopoietic multipotent stromal stem cells which are characterized by their ability for self-renewal and to differentiate into adipocytes (fat), osteoblasts (bone), and chondrocytes (cartilage) [15]. Human bone marrow-derived mesenchymal stem cells (hBMSCs), as one of the most studied cells in bone and cartilage tissue engineering, show good osteogenic and cartilage potential [16]. MSCs possess immunomodulatory properties that can be activated by signalling molecules such as interferon gamma (IFN-γ), TNF-α, and IL-1α/β [17, 18]. Distinctive chemokines induce MSC migration to the site of injury, for instance, stromal cell-derived factor 1 α (SDF-1α) [19].

As a defect of bone and cartilage is often a common complication after trauma [20], MSCs, which can be induced to differentiate into osteoblasts and chondrocytes *in vitro*, are promising cells to treat these defects [21–23]. Therefore, a promising solution is called the MSC-based bone regeneration [24], where polymer scaffolds seeded with MSCs are used to induce differentiation of MSCs into osteoblasts *in vivo*. Experimental studies have shown that good results have already been achieved [24–26]. Chondrocytes can be obtained by culturing MSCs in a special differentiation medium using classic pellet culture methods [27], and cartilage can also be generated with the help of tissue engineering techniques using 3D cell scaffolds (e.g., hydrogels [28] and electrospun scaffolds [29]) *in vitro*.

Improving the treatment of polytrauma and strengthening posttraumatic care are a difficult challenge for the world. The rationale for using MSCs in polytrauma patients is their anti-inflammatory immune regulation and tissue regeneration capacity [30]. However, it is known that the complex changes of serum cytokines after polytrauma [31] exert a complex impact on the characteristics and properties of MSCs [30, 32]. Therefore, the effects of inflammatory mediators on MSCs present in the blood of multiple trauma patients at different times after trauma should be further investigated. So far, there have been only a few studies on this topic [30, 33]; due to our knowledge, no studies using large number of serum samples exist in which the influence of sera from different time points posttrauma was investigated on MSC properties. Therefore, the aim of this study was to find out whether serum from different days after polytrauma (D1, D5, and D10) has a negative influence on cell survival and the ability of hBMSCs to migrate, proliferate, and differentiate. In this study, it was hypothesized that higher cytokine levels in D1 and D5 sera may lead to reduced proliferation of hBMSCs, which can lead to a decrease of CFU-F colonies and an obvious migration of hBMSCs compared with HS and D10 sera. In addition, it was postulated that osteogenic and/or chondrogenic differentiation may be significantly inhibited due to the high cytokine levels of D1 or D5 sera.

2. Materials and Methods

2.1. Source of Serum and Cells. The serum of polytrauma patients (ISS ≥ 16) was obtained from the Polytrauma Serum Bank of the Trauma Department of Hannover Medical School (year: 2010-2020). The study protocol and sample donation were approved by the local ethical review committee (Hannover Medical School No. 4980). 84 patients with polytrauma (median of ISS = 34, interquartile range: 27-43.5) were used as donors, and the sera from the 1st day, 5th day, and 10th day after trauma were pooled to ensure sufficient amounts. As control, three healthy donor sera were matched and pooled (HS) according to the age and gender ratio of patients with polytrauma. For the experiments, four healthy hBMSC donors were chosen from our cell bank of human bone marrow-derived mesenchymal stem cells. hBMSC donation protocol and sample donation were approved by the local ethical review committee (Hannover Medical School No. 2562). BMSC selection was based on the following criteria: no history of smoking, alcohol, allergies, tumors, and routine medication. Written informed consent was obtained from all donors prior to inclusion into the studies, and it was ensured that the study protocol and process of sample donation for the studies complied with the Declaration of Helsinki. In Table 1, the age distribution, gender, and ISS score of polytraumatized patients (PT), healthy serum donors (HS), and hBMSC donors can be seen.

2.2. Multicytokine Array. Semiquantitative detection of multicytokines was performed by Tebu-bio (Paris, France) using the Human Cytokine Antibody Array Kit (Ref: AAH-CYT-G5-8, RayBio®) [34] with pooled serum as duplicate from HS, D1, D5, and D10. The change of cytokine concentration is shown as heat map which was first calculated by normalized fluorescence intensity (NFI) and then normalized by standard score (Z-score) and analyzed by fold change relative to healthy serum (FCRH).

2.3. Cell Culture and Passaging. Stored hBMSCs were thawed and cultured with hBMSC normal growth medium, which contained 10% fetal calf serum (FCS, #S0615, Biocell), 1% penicillin/streptomycin (#A2212, Biochrom), 2.5% hydroxyethyl piperazineethanesulfonic (HEPES, #L1613, Biochrom), 86.5% Dulbecco's modified Eagle medium (DMEM, #FG0415, Bio-cell), and 100 ng/μl human-fibroblast growth factor-2 (h-FGF-2, #100-18B, PeproTech) in cell culture flasks at 37°C and 5% CO_2. Upon reaching a confluency of 80-90%, cells were harvested by using 0.05% Trypsin/EDTA (0.5%/0.2% w/v, #L1825, Biochrom) solution and counted by flow cytometry (Attune NxT, Thermo Fisher Scientific, USA). In order to ensure that there were enough cells for the experiments, the cells were expanded and all experiments were performed using hBMSCs in passage 3 (P_3).

Table 1: List of donors.

Parameters	PT patients	HS volunteers	hBMSC donors	p value
Age (Y)	45 (29.5-55)	39 (31.5-53)	43 (41.5-56.25)	0.69
Gender (M/F)	56/28	2/1	3/1	0.94
ISS score	34 (27-43.5)	n/a	n/a	

Note: parameters are given as median (interquartile range) as the data are nonparametric, which was tested by the Shapiro-Wilk test. The age (in years, Y) and gender (male/female, M/F) were compared by the Kruskal-Wallis test and showed no statistical differences ($p > 0.05$).

2.4. Colony Forming Unit-Fibroblast (CFU-F) Assay. 250 cells were seeded in 6-well plates using media corresponding to each group (10% HS/D1/D5/D10). Total medium change with corresponding media was performed on day 3 and day 7 after seeding. The CFU-F assay was stopped on day 10 by fixating the cells with 2 ml cold methanol and staining with 1% aqueous crystal violet at room temperature for 30 minutes before performing macroscopically visible colony counting. The results are shown as percentage of the number of colonies per 250 cells seeded.

2.5. Cell Proliferation Experiments and Live and Dead Assay. 30,000 cells were seeded in each well of a six-well plate and incubated with corresponding media for each group (10% HS/D1/D5/D10) for 72 hours at 37°C and 5% CO_2. After that, the cells were detached with 0.05% Trypsin/EDTA and stained with Fixable Viability Dye eFluor™ 450 (#650863, Thermo Fisher Scientific) and evaluated by flow cytometry (Attune NxT Flow Cytometer; Thermo Fisher Scientific, USA). The total cell number and percentage of dead cells in each well were calculated by the Invitrogen™ Attune™ NxT Software (Attune; Thermo Fisher Scientific, USA) at the same time.

2.6. WST Assay. To assess cell viability/proliferation and cytotoxicity, a WST assay was performed. WST-1 (#5015944001, Roche) is a tetrazolium salt which forms formazan in the presence of metabolically active cells. 100 μl hBMSC suspension (8000 cells) was added to each well in a 96-well plate, and each experimental group was tested in three replicates. After incubation for 24 hours at 37°C and 5% CO_2 with the corresponding media, 10 μl WST-1 reagent was added to each well. After 30 minutes, 1 hour, 2 hours, and 4 hours, the absorbance at 450 nm of each well was measured using an Epoch reader (Epoch, USA) and analyzed by Gen 5™ software (BioTek, Winooski, VT, USA), to quantify the cell activity. The absorbance at 630 nm was measured for correction of unspecific background absorption.

2.7. Transwell Experiments. 600 μl of cell culture medium containing 10% human serum from one of the serum groups (HS, D1, D5, and D10) was added into each well of a 24-well plate (#662160, CellStar) with three duplicates for each serum group. Then, 1×10^5 cells were resuspended in 100 μl serum-free media and pipetted to the upper chamber of each tissue culture insert (TC, 24-well plate, pore 8 μm, Sarstedt, Germany). These TC inserts were then placed into the wells containing the 10% human serum as lower well. After cultivation at 37°C and 5% CO_2 for 12 hours, the medium from all upper and lower chambers was discarded. 600 μl 0.05% Trypsin/EDTA solution was pipetted to the lower well of each TC insert, respectively, and for liquid balance purposes, 100 μl 0.05% Trypsin/EDTA solution was pipetted to the upper chamber. After 8 minutes of incubation at 37°C and 5% CO_2, the cells that migrated to the lower well were counted separately. The percentage of cells that had migrated from the upper to the lower chamber was calculated with the following formula:

$$\text{Migration}[\%] = \frac{\text{Number of migrated cells}}{1 \times 10^5 \text{ cells}} \times 100\%. \quad (1)$$

2.8. Scratch Assay. 30,000 cells from each group, which were pretreated for one passage with the corresponding sera (HS, D1, D5, and D10), were resuspended in 70 μl serum-free medium. *ibidi* inserts (#81176, ibidi, Germany) were placed in a 6-well plate, and the cell suspension was added to corresponding *ibidi* inserts. The plates were transferred into an incubator at 37°C and 5% CO_2 for 6-8 hours until the seeded cells formed a monolayer. Then, the *ibidi* inserts were removed from the 6-well plates and 2 ml of serum-free media was added to each well after the cells and media had been rinsed with PBS. After this, a defined scratch in the middle of the cells was visible after the removal of the inserts. Pictures of each *scratch* were taken at 0, 4, 8, and 24 hours under an optical microscope (CKX41 Olympus, Tokyo, Japan) with a magnification of 40x. Photoshop software (version 21.0.2, Adobe Company, USA) was used to merge the images, and the scale of the crop area size was set to 2000 pixels × 8000 pixels with a picture resolution of 72 ppi. Microsoft PowerPoint Software (version 16.37, Microsoft® Office 365 for MAC, Microsoft Corporation, Washington, USA) was used to define and scribe the boundary of cell migration and color the region free of migrated cells in the gap. Afterwards, the images were analyzed by a self-written tool from a member of the laboratory relying on the OpenCV library version 4.1.0 [35] for image processing. The nonmigrated proportion was shown by the percentage of black pixels, and 100% nonmigrated region was obtained at the initial 0 hour. Then, the cell migration area ratio at each time point was obtained from the decreased proportion of the area of interest.

2.9. Osteogenic Differentiation. 15×10^4 cells were resuspended in 2 ml 10% FCS normal growth media per well in 6-well plates. After cultivation in an incubator at 37°C and 5% CO_2 for 24 hours, the media were changed to osteogenic differentiation media consisting of DMEM (#FG0415, Biocell), which contained 10% serum (HS, D1, D5, D10, or FCS) and was supplemented with 20 mM HEPES (#L1613,

Biochrom), 1% penicillin/streptomycin (#A2212, Biochrom), 100 nM dexamethasone (#D4902, Sigma), 50 μM ascorbate-2-phosphate (#A8960, Sigma), and 3 mM di-Natriumhydrogenphosphat-Dihydrat (#106508, Merck). The osteogenic differentiation should be performed over 28 days with medium change every seven days and was stopped by fixing the cells with 4% formalin solution. Staining was performed with 0.5% alizarin red solution (pH = 4.5) protected from light for 10 minutes at room temperature.

Pictures at 40x magnification were taken along the central axis of the wells using a CKX41 Olympus microscope. The images were analyzed by a self-written tool from a member of the laboratory relying on the OpenCV library version 4.1.0 [35]. The calcium deposit proportion was calculated from the percentage of nonblack pixels.

For a second measurement to evaluate the osteogenesis, the stained cells were incubated in 10% cetylpyridinium chloride solution (#8400080025, Sigma-Aldrich) adjusted to a pH of 7 at room temperature for six hours until all red color had completely dissolved. The relative content of alizarin red was then measured by determining its light absorbance at 600 nm using an Epoch reader (Gene 5, BioTek, Winooski, VT, USA).

2.10. Chondrogenic Differentiation. For each group, 2.5×10^5 cells were resuspended in 2 ml of normal growth media containing 10% FCS in a 15 ml falcon tube (#188271, CellStar) and centrifuged for 10 minutes at $200 \times g$ and room temperature to form a pellet. With the lid slightly open to allow air circulation, the cell pellet was cultured in an incubator at 37°C and 5% CO_2 for 24 hours, and then, the medium was replaced by group-specific chondrogenic differentiation medium of DMEM (#FG0435, Bio-cell), which contained 10% serum (HS, D1, D5, D10, FCS, and serum-free) and was supplemented with 20 mM HEPES (#L1613, Biochrom), 1% penicillin/streptomycin (#A2212, Biochrom), 100 nM dexamethasone (#D4902, Sigma), 170 μM ascorbate-2-phosphate (#A8960, Sigma), 1 mM Natriumpyruvat (#L0473, Biochrom), 350 μM proline (#1713.1, Roth), 10 μl/ml insulin (#I0516, Sigma), and 1 μl/ml TGF-beta-3 (#100-36E, PeproTech). A medium change was performed every seven days for planned 28 days. Stopping the experiment was performed by fixation of the cells with 4% formalin. After fixation, the chondrogenic pellets were embedded in Tissue-Tek® O.C.T.™ Compound and wrapped in aluminum foil. The samples were frozen by placing the foil in liquid nitrogen. Afterwards, the pellets were stored at -20°C until further use.

The chondrogenic pellets were cut to slices with a thickness of 5 μm using a microtome cryostat (Microm HM 500 OM, Leica) and placed on microscope slides (SuperFrost Plus, Thermo Scientific). The slides were stained by 0.1% safranin O solution for 15 minutes at room temperature and were embedded with Vitro-Clud® (R. Langenbrinck GmbH) after drying.

Pictures of chondrogenesis were taken using a microscope (BX41 Olympus) at 40x magnification. The pictures were analyzed by a self-written tool from a member of the laboratory relying on the OpenCV library version 4.1.0 [35]. The proportion of the histological specimen containing glycosaminoglycans was calculated from the percentage of nonblack pixels.

2.11. Data Analysis and Statistics. Statistical data analysis was performed by using the SPSS Statistics® program (Version 26, IBM SPSS Statistics Corp., New York, NY), while figures were created using Prism 8 software (Version 8.4.0 for Mac OS, GraphPad Company, Santiago) and a heat map was created by Morpheus (Cambridge, Massachusetts, USA) [36]. First, the Shapiro-Wilk test was used to determine whether each set of data met the normal distribution, where a p value greater than 0.05 was indicative of normal distribution. The normally distributed data were analyzed by one-way ANOVA and the Tukey test, and the nonparametric data were analyzed by the Kruskal-Wallis test with Bonferroni correction. Descriptive p values or adjusted p values less than or equal to 0.05 were considered statistically significant.

3. Results

3.1. Multicytokine Array. Since the levels of cytokines were measured twice in pooled serum samples, the results reflect the overall difference, and no statistical analysis was performed. Only the cytokines related to this experiment are shown in the main manuscript. Compared with the healthy serum, the red-colored cytokines showed an increase after trauma whereas the blue-colored cytokines were decreased (Figure 1(a)).

3.1.1. Pro- and Anti-Inflammatory Cytokines. The level of the proinflammatory factors IL-6 (Figure 1(b)) and IL-8 (Figure 1(c)) as well as the level of the anti-inflammatory cytokine IL-10 (Figure 1(d)) showed a four times fold short-term increase on the first day after polytrauma compared to HS and decreased to two or three times higher when compared to D5 and D10. Five and ten days after the trauma incident, the level of IL-6, IL-8, and IL-10 had declined to the same level that was found in the HS group.

3.1.2. Bone Metabolism. The level of osteopontin (Figure 1(e)) gradually increased over the first ten days after polytrauma compared to the HS group. Osteoprotegerin (Figure 1(f)) increased on the first day after trauma and decreased on D5 and D10 back to serum concentration which was also seen in the HS group. Tissue inhibitor of metallopeptidase-1 (TIMP-1, Figure 1(g)) concentration was increased in the first ten days after trauma. The serum concentration of fibroblast growth factor 9 (FGF-9, Figure 1(h)) decreased directly after trauma, and the concentration remains lower over the first 10 days compared to the HS group.

3.1.3. Chondrogenesis. Among the factors that promote chondrogenic differentiation of hBMSCs, the levels of the transforming growth factor-beta (TGF-β) family members TGF-β1 (Figure 1(i)) and TGF-β2 (Figure 1(j)) decreased since D1 after trauma until D10 compared to the HS group. TGF-b3 (Figure 1(k)) level continued to decrease until D5; afterwards, at D10, it reached the same serum concentration as the HS group.

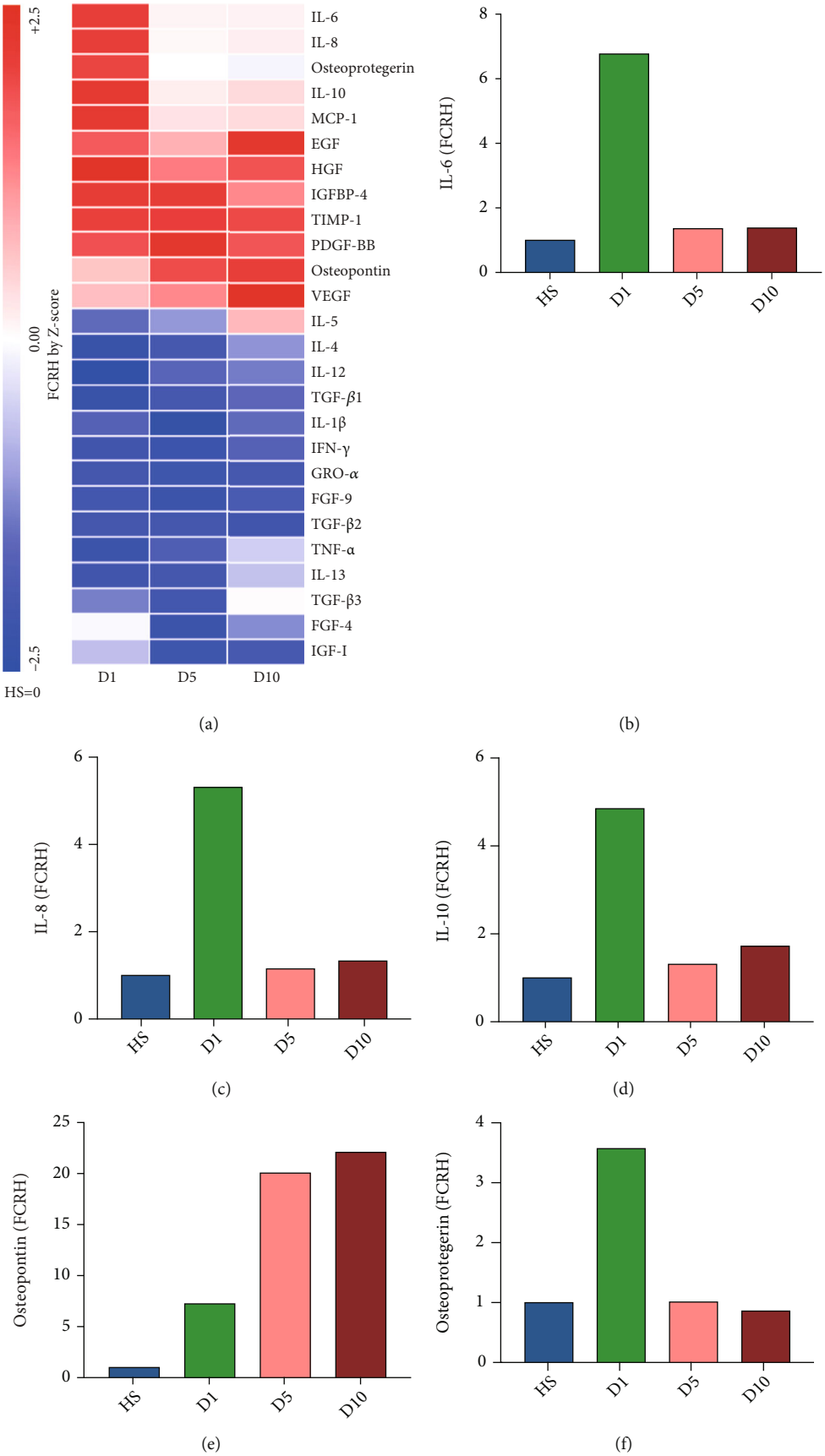

Figure 1: Continued.

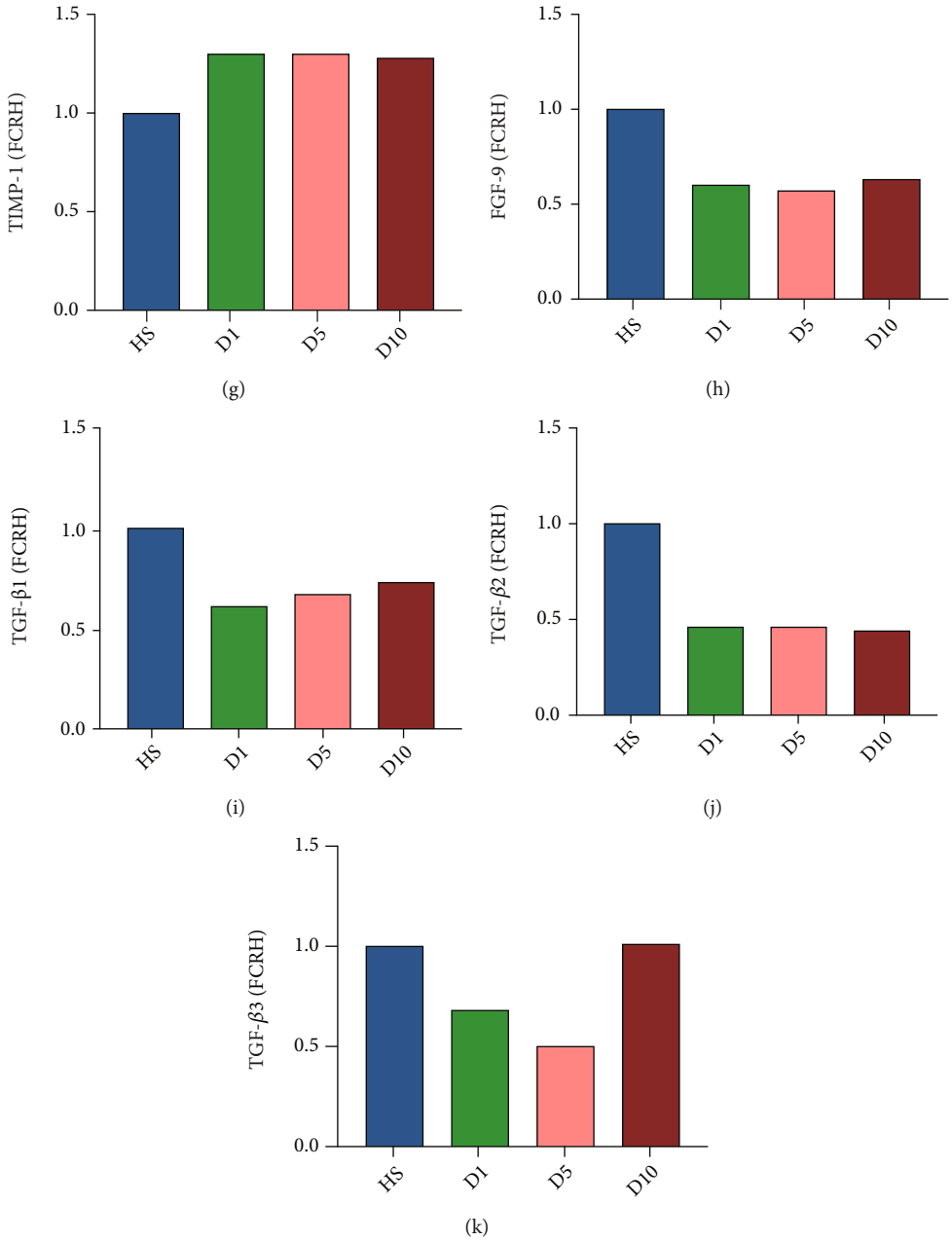

Figure 1: Results of the multicytokine array. (a) Heat map depicting the changes in cytokine levels in pooled serum from patients at day 1 (D1), day 5 (D5), and day 10 (D10) after polytrauma relative to cytokine levels in serum from healthy controls. The data are normalized by Z-score (HS = 0) and analyzed by fold change relative to healthy serum (FCRH). A Z-score of 0 is represented by white color, a Z-score of 2.5 by red color, and a Z-score of -2.5 by blue color. Z-scores in between these values are depicted by less saturated colors of the same color palette. Cluster analysis was performed, and the cytokines were ordered accordingly. Some cytokines have an acute peak on the first day after trauma, and some cytokines peak on the 5th or 10th day after trauma, but compared to HS, more than half of the cytokine levels decreased after trauma. The proinflammatory cytokines (b) interleukin- (IL-) 6 and (c) IL-8 as well as the anti-inflammatory cytokine (d) IL-10 were approximately four times higher at D1 in comparison to HS and two or three times higher when compared to D5 and D10. (e) Osteopontin was increased in the serum from all time points postpolytrauma as compared to serum from healthy donors. The increase in D1, D5, and D10 relative to HS was from six to twenty times. (f) Osteoprotegerin was higher only one day after polytrauma in comparison to HS with a fold change for about three times. (g) Tissue inhibitor of metalloproteinase (TIMP-1) was increased at all time points after polytrauma in comparison to serum from healthy controls. (h) Fibroblast growth factor 9 (FGF-9) was decreased in the polytrauma sera as compared to the HS.(i–k) Transforming growth factor-beta 1 (TGF-β1), TGF-β2, and TGF-β3 were all decreased in polytrauma serum at D1 and D5 as compared to healthy serum ($n = 1$, pooled samples out of 84 donors).

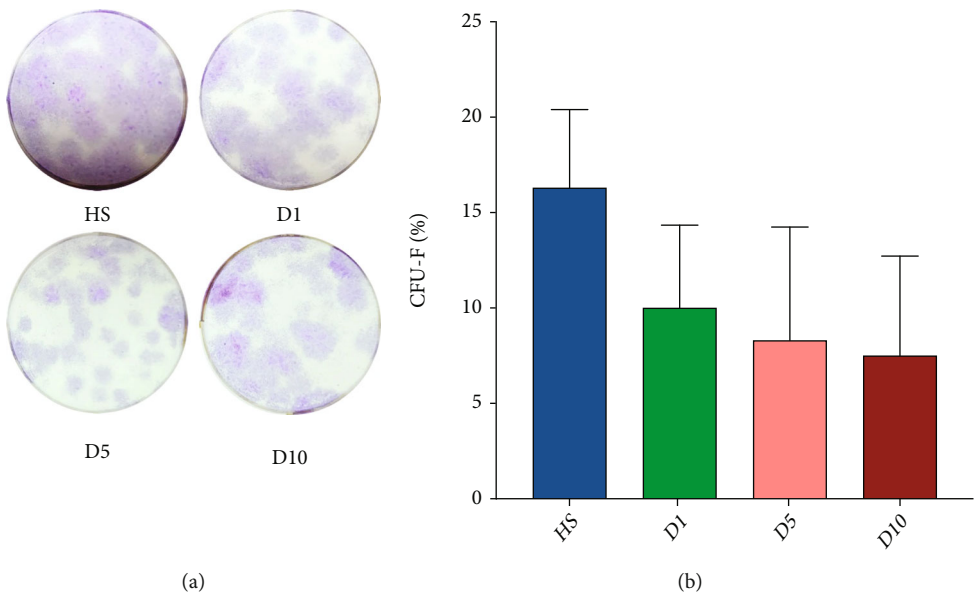

Figure 2: Colony forming unit-fibroblast assay (CFU-F assay). (a) Representative images of CFU-F assays from HS, D1, D5, and D10. (b) Results of the CFU-F assays obtained by seeding 250 cells/well. Calculation was performed using the following formula: CFU-F% = colonies/250 × 100%. The colony forming ability of polytrauma groups (D1, D5, and D10) had no significant difference when compared to the HS group ($n = 4$).

3.1.4. Growth Factors. Serum concentration of epidermal growth factor (EGF, Figure S1-a) was four times higher at D1, two times at D5, and five time higher at D10 after polytrauma compared to the HS group. Concentration level of hepatocyte growth factor (HGF) was more than eight times higher one day after polytrauma compared to the HS group, five times higher on day five, and seven times higher on day ten (Figure S1-b). Concentration level of fibroblast growth factor 4 (FGF-4) was decreased after polytrauma compared to HS (Figure S1-c). Insulin-like growth factor-binding protein 4 (IGFBP-4) was more than two times higher on D1 and D5 after polytrauma compared to the HS group but had a downward trend at D10 which is still higher than HS (Figure S1-d).

3.1.5. Migration. Among the factors that can promote chemotactic migration of MSCs, the serum concentration of insulin-like growth factor 1 (IGF-1, Figure S1-e) and growth-regulated oncogene-alpha (GRO-α, Figure S1-f) decreased after polytrauma as compared to the HS group. In contrast, the concentration of monocyte chemoattractant protein 1 (MCP-1, Figure S1-g) was increased in the serum of patients with polytrauma on D1 after the incidence. The serum level of vascular endothelial growth factor (VEGF) showed a one- to twofold increase from D1 to D10 compared to HS (Figure S1-h). The serum concentration of platelet-derived growth factor-BB (PDGF-BB) was increased in all groups after polytrauma compared to HS (Figure S1-i).

3.2. Colony Forming Unit-Fibroblast Assay. Representative images of the CFU-F assay from HS, D1, D5, and D10 are shown in Figure 2(a). The data were normally distributed and met the criteria for homogeneity of variance, and one-way ANOVA and the Tukey test were used for statistical analysis. Counting of the colonies demonstrated no significantly reduced colony forming ability at D1 (10.00 ± 4.35%), D5 (8.30 ± 5.95%), and D10 (7.50 ± 5.22%) compared to the HS group (16.30 ± 4.10%, $p > 0.05$). Also, no significant differences were found between the polytrauma groups D1, D5, and D10 (Figure 2(b)). However, the blue staining area of colonies in polytrauma groups (D1, D5, and D10) was less than HS in visual (Figure 2(a)).

3.3. Cell Counting and Viability Measurement. After 72 hours of cell proliferation, hBMSCs were stained with Fixable Viability Dye eFluor™ 450 and total cell count as well as the proportion of dead cells was measured. The experimental data were nonparametric distributed, and the Kruskal-Wallis test with the Bonferroni correction was used for statistical analysis. Total cell number in the D5 group (132,071.67 ± 25,770.13 cells) was significantly reduced compared to that in the HS group (224,842.50 ± 56,999.37 cells; $p \leq 0.01$, Figure 3(a)). No significant differences of the total cell number were observed between D1 (180,436.67 ± 47,868.25 cells, $p > 0.05$) and D10 (183,839.17 ± 73,674.91 cells, $p > 0.05$) compared to the HS group. Furthermore, the D5 group (6.56 ± 2.71%) had a significantly higher cell death ratio compared to D1 (3.37 ± 1.27%; $p \leq 0.05$) (Figure 3(b)). In summary, the D5 group shows an obvious proliferation inhibition compared to HS as well as a higher ratio of dead cells compared to D1.

3.4. WST Assay. 24 hours after cell seeding, the cell viability and proliferation capacity were tested by WST assay after an incubation period of 30 minutes, 1 hour, 2 hours, and 4

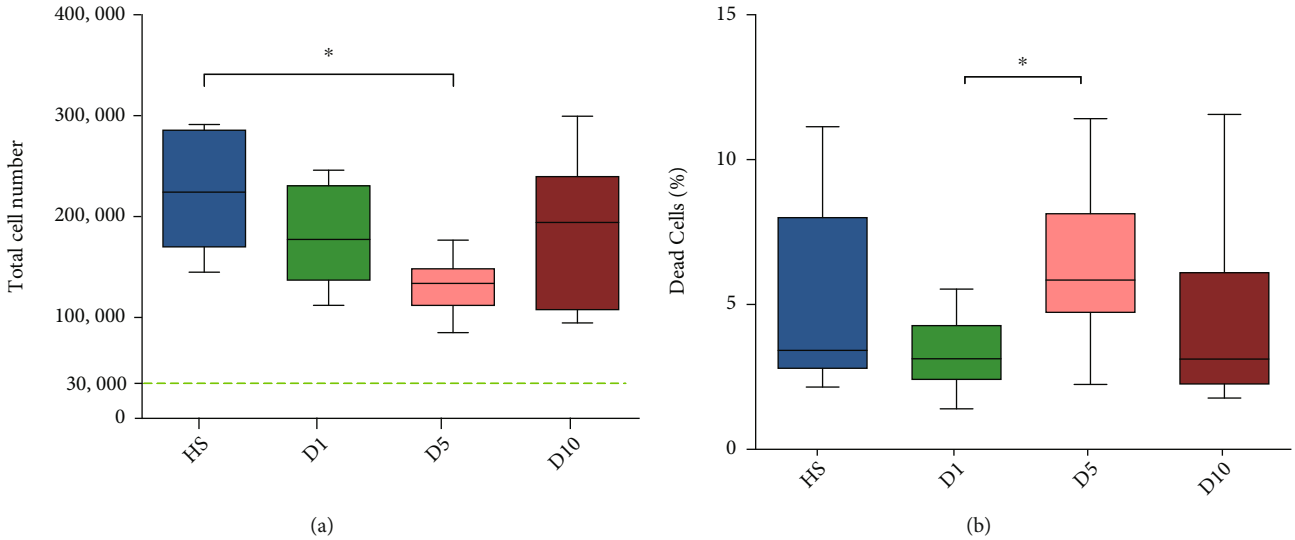

Figure 3: Evaluation of the proliferation capacity and viability of stem cells after cultivation in medium containing different sera (HS, D1, D5, or D10) for 72 hours. (a) Proliferation of hBMSCs treated with HS, D1, D5, or D10 serum. The green, dotted line shows the number of seeded cells (30,000 cells). Addition of serum from D5 to the culture medium resulted in a significantly lower proliferation of hBMSCs after 72 hours compared to HS. (b) Amount of dead cells after treatment with HS, D1, D5, or D10 serum. The D5 group demonstrated a significantly increased ratio of dead cells in comparison to D1. $^{*}p \leq 0.05$ ($n = 4$; $N = 3$).

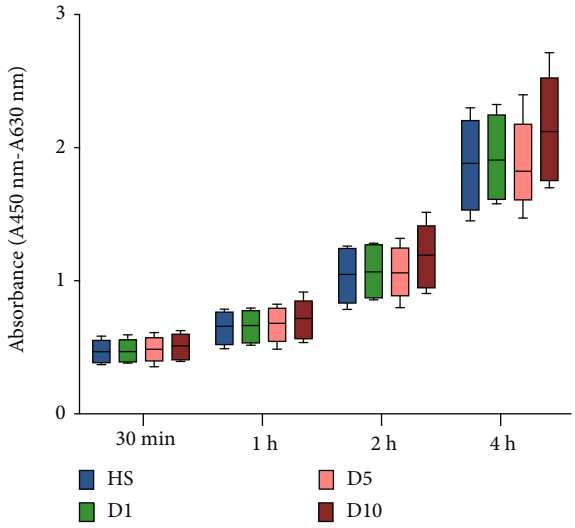

Figure 4: WST assay. Results were observed after cultivation of cells for 24 hours in medium containing different sera (HS, D1, D5, or D10 serum). No significant differences were observed between any of the groups at any of the time points analyzed (30 minutes, 1 hour, 2 hours, and 4 hours) ($n = 4$; $N = 3$).

hours (Figure 4). The experimental data were nonparametric distributed, and the Kruskal-Wallis test with the Bonferroni correction was used for statistical analysis. No significant differences in WST assay were observed among the groups at the observation point of 30 minutes (HS: 0.47 ± 0.09, D1: 0.47 ± 0.09, D5: 0.49 ± 0.10, D10: 0.51 ± 0.10, $p > 0.05$), 1 hour (HS: 0.65 ± 0.13, D1: 0.66 ± 0.12, D5: 0.67 ± 0.13, D10: 0.71 ± 0.15, $p > 0.05$), 2 hours (HS: 1.04 ± 0.21, D1: 1.07 ± 0.20, D5: 1.06 ± 0.19, D10: 1.19 ± 0.25, $p > 0.05$), and 4 hours (HS: 1.87 ± 0.36, D1: 1.93 ± 0.33, D5: 1.88 ± 0.31, D10: 2.14 ± 0.40, $p > 0.05$).

3.5. Migration Ability of hBMSCs

3.5.1. Scratch Assay. An example of the repopulation of the scratch with hBMSCs over different time points of the assay is shown in Figure 5(a), where the black-colored area demarks the area devoid of cells. The data were normally distributed and met the criteria for homogeneity of variance, and one-way ANOVA and Tukey test were used for statistical analysis. No significant difference was observed in the scratch assay at the different time points (4 h, $p > 0.05$; 8 h, $p > 0.05$; 24 h, $p > 0.05$) between any of the serum groups (Figure 5(b)).

3.5.2. Transwell Migration Assay. The transwell migration assay data were nonparametric distributed, and the Kruskal-Wallis test with the Bonferroni correction was used for statistical analysis. Cell culture media containing the different sera from patients on D1 ($60.04 \pm 9.36\%$), D5 ($60.17 \pm 12.14\%$), and D10 ($66.73 \pm 7.36\%$) after polytrauma had no differential effect on the migration behavior of the hBMSCs in comparison to culture medium containing serum from healthy donors ($67.18 \pm 10.18\%$) and neither among groups ($p > 0.05$) (Figure 5(c)).

3.6. Osteogenic Differentiation. The addition of fetal calf serum (FCS) served as a positive control for the groups HS, D1, D5, or D10 for the osteogenic differentiation assay. As preliminary experiments showed that the cells detached in the presence of human serum after 21 days (data not shown), the osteogenic differentiation was stopped at day 14 instead of day 28. The experimental data were nonparametric distributed, and the Kruskal-Wallis test with the Bonferroni correction was used for statistical analysis.

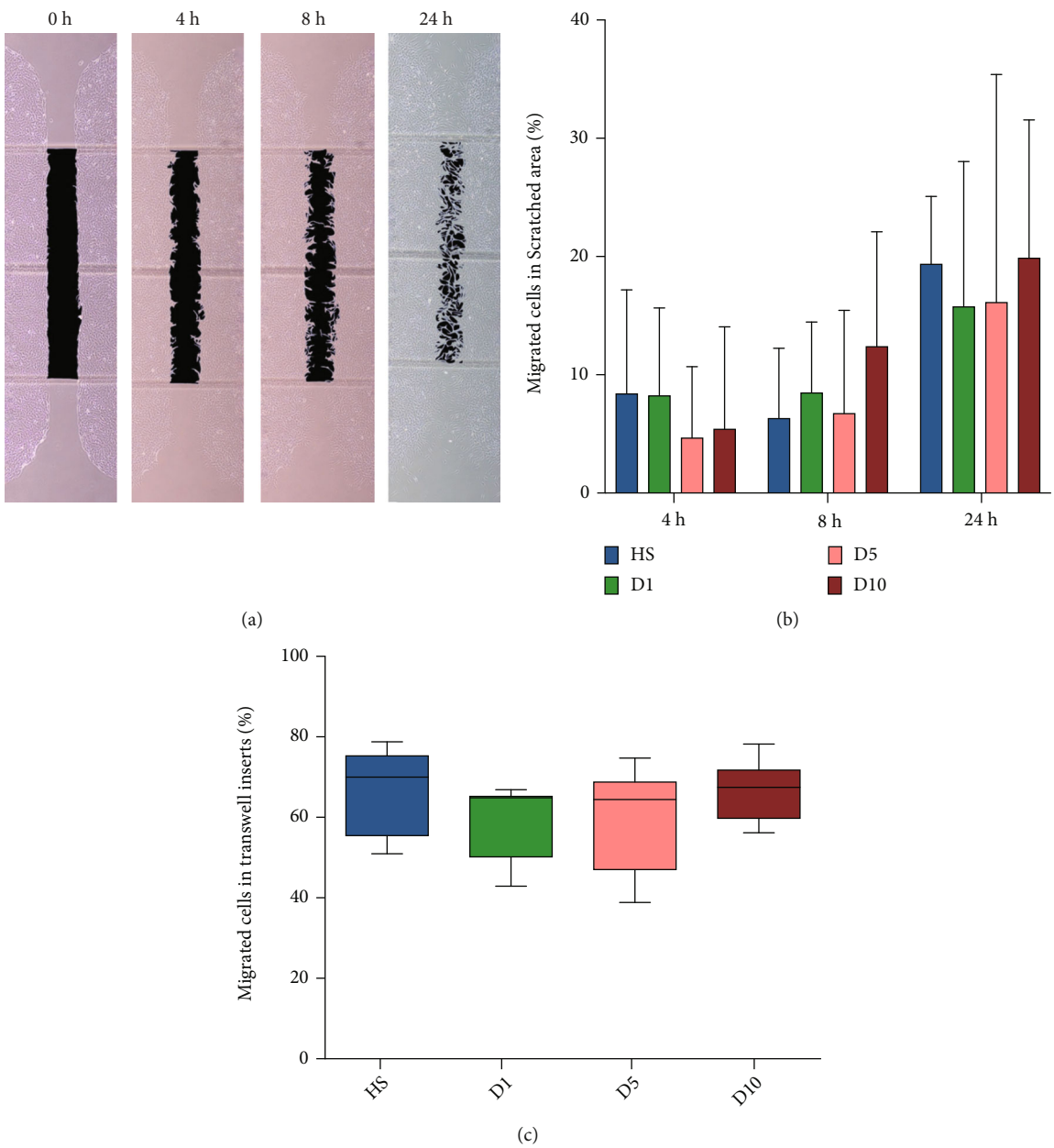

Figure 5: Scratch and transwell migration assay indicating the hBMSC repopulation ability. (a) Representative pictures of the migration and repopulation ability of hBMSCs over 24 hours treated with HS, D1, D5, and D10 sera in a scratch assay. The black area represents the scratched area. As time goes by, the injured area is gradually reduced and dispersed along with the migration of cells. (b) After 4, 8, and 24 hours, no significant increase in migration of the D1, D5, and D10 groups was found compared to the HS group ($n = 4$; $N = 2$). (c) In transwell migration assay, no significant differences in the ratio of migration were observed between the HS, D1, D5, and D10 groups 12 hours after seeding ($n = 4$; $N = 3$).

The result of the osteogenic differentiation was first quantified by image analysis stained with alizarin red (Figure 6(a)). Standardized analysis of the pictures showed that group D1 ($64.35 \pm 4.95\%$, $p \leq 0.01$) had a higher osteogenic differentiation ability compared to the FCS group ($7.52 \pm 3.49\%$), with exception of HS ($57.20 \pm 16.43\%$, $p > 0.05$), D5 ($46.74 \pm 8.59\%$, $p > 0.05$), and D10 ($55.87 \pm 12.94\%$, $p > 0.05$). However, no significant difference was found between the D5 group compared to any of the other serum groups ($p > 0.05$) (Figure 6(b)).

Analysis of the alizarin red staining quantified by extraction and measurement of absorption at 600 nm revealed significant elevated levels of calcium deposits in all groups containing human serum except serum from D5 (HS: 2.44 ± 0.27, $p \leq 0.01$; D1: 2.62 ± 0.46, $p \leq 0.01$; D5: 2.17 ± 0.54, $p > 0.05$; D10: 2.53 ± 0.35, $p \leq 0.01$) compared to the FCS group (1.30 ± 0.38, Figure 6(b)). No statistically significant difference between the osteogenic differentiations of hBMSCs cultured with human serum from polytrauma patients or with human serum from healthy controls was found ($p > 0.05$, Figure 6(c)).

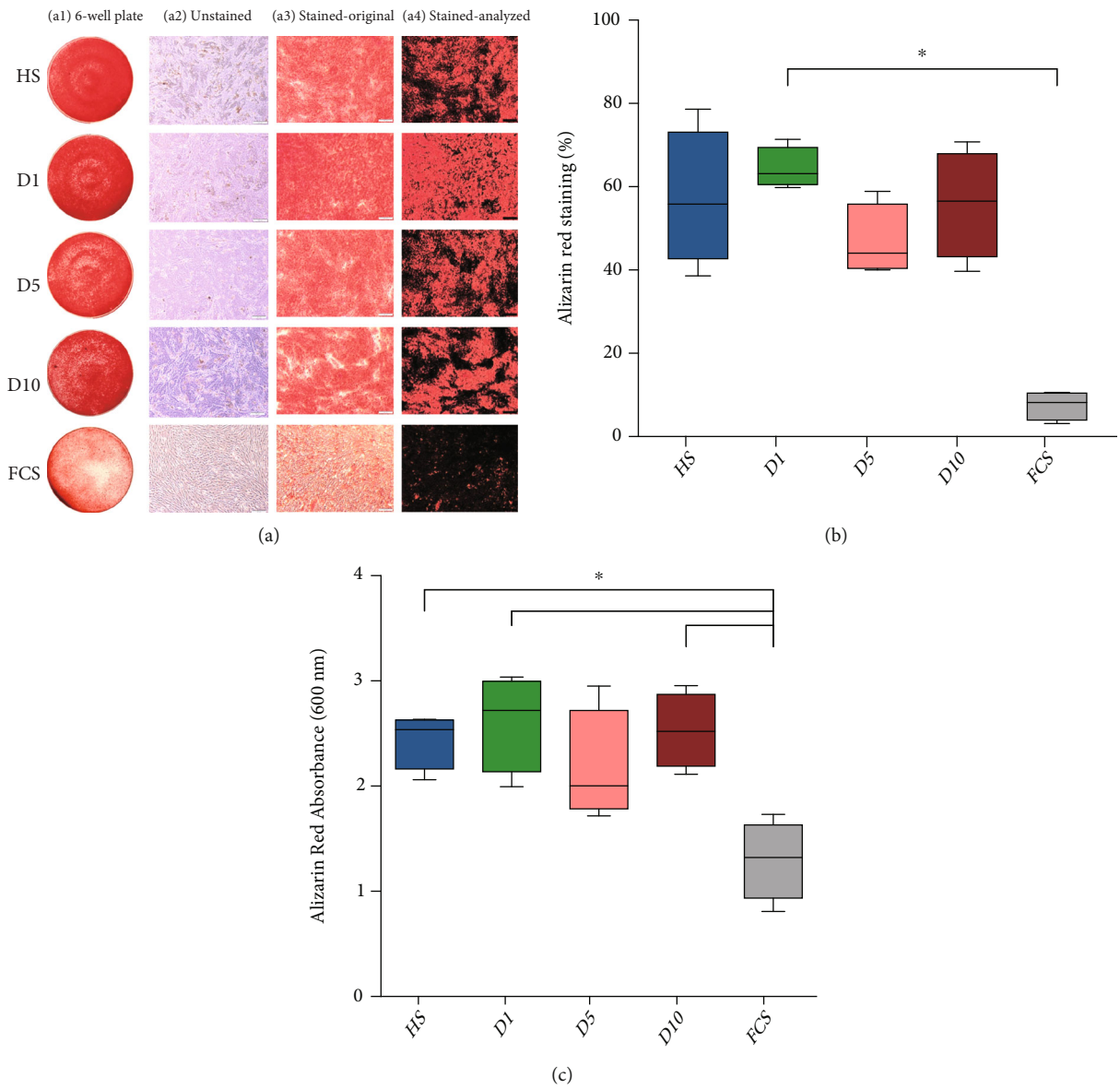

Figure 6: Osteogenic differentiation potential. (a) Alizarin red staining showed calcium deposits as red staining after culturing hBMSCs in osteogenic differentiation medium containing 10% serum from HS, D1, D5, D10, or FCS for 14 days. (a1) Macroscopic image of alizarin red staining. (a2) Cells prior to alizarin red staining at 40x magnification. (a3) Images showing the hBMSCs at a 40x magnification after staining with alizarin red. (a4) Analysis of alizarin red staining of calcium deposits using a tool based on OpenCV library (version 4.1.0). Areas without staining were color isolated as black areas. The pixel ratio of the area of interest (nonblack area) in comparison to the black area was obtained. In the groups containing human serum (HS, D1, D5, and D10), a larger area of the 6-well was positive for alizarin red staining than in the FCS group ($n = 4$). (b) Quantitative analysis of the amount of alizarin red staining quantified using a software tool to compare the relative areas positive for staining. D1 showed significantly more area of alizarin red staining when compared to the FCS group. $^{*}p \leq 0.05$ ($n = 4$). (c) Analysis of alizarin red staining indicative of osteogenic differentiation with higher concentrations of calcium deposition after 14 days of culture. HS, D1, and D10 showed significantly higher absorbance as compared to the FCS group. $^{*}p \leq 0.05$ ($n = 4$).

3.7. Chondrogenic Differentiation. Chondrogenic differentiation with serum-free medium served as positive control in this experiment. The experimental data were nonparametric distributed, and the Kruskal-Wallis test with the Bonferroni correction was used for statistical analysis. All serum groups showed comparable levels of glycosaminoglycans in the extracellular matrix (Figure 7(a)). In the healthy serum group (19.38 ± 11.86%), as well as in D1 (14.61 ± 10.31%), D5 (19.36 ± 10.67%), and D10 (14.36 ± 6.39%), no significant difference in chondrogenic differentiation was seen compared to the FCS group (20.65 ± 13.78%; Figure 7(b)). The same is true for the positive control group (40.46 ± 21.92%) which was serum-free ($p > 0.05$, Figure 7(b)).

4. Discussion

Trauma is one of today's major causes of human death and disabilities [37], and young adults are the largest

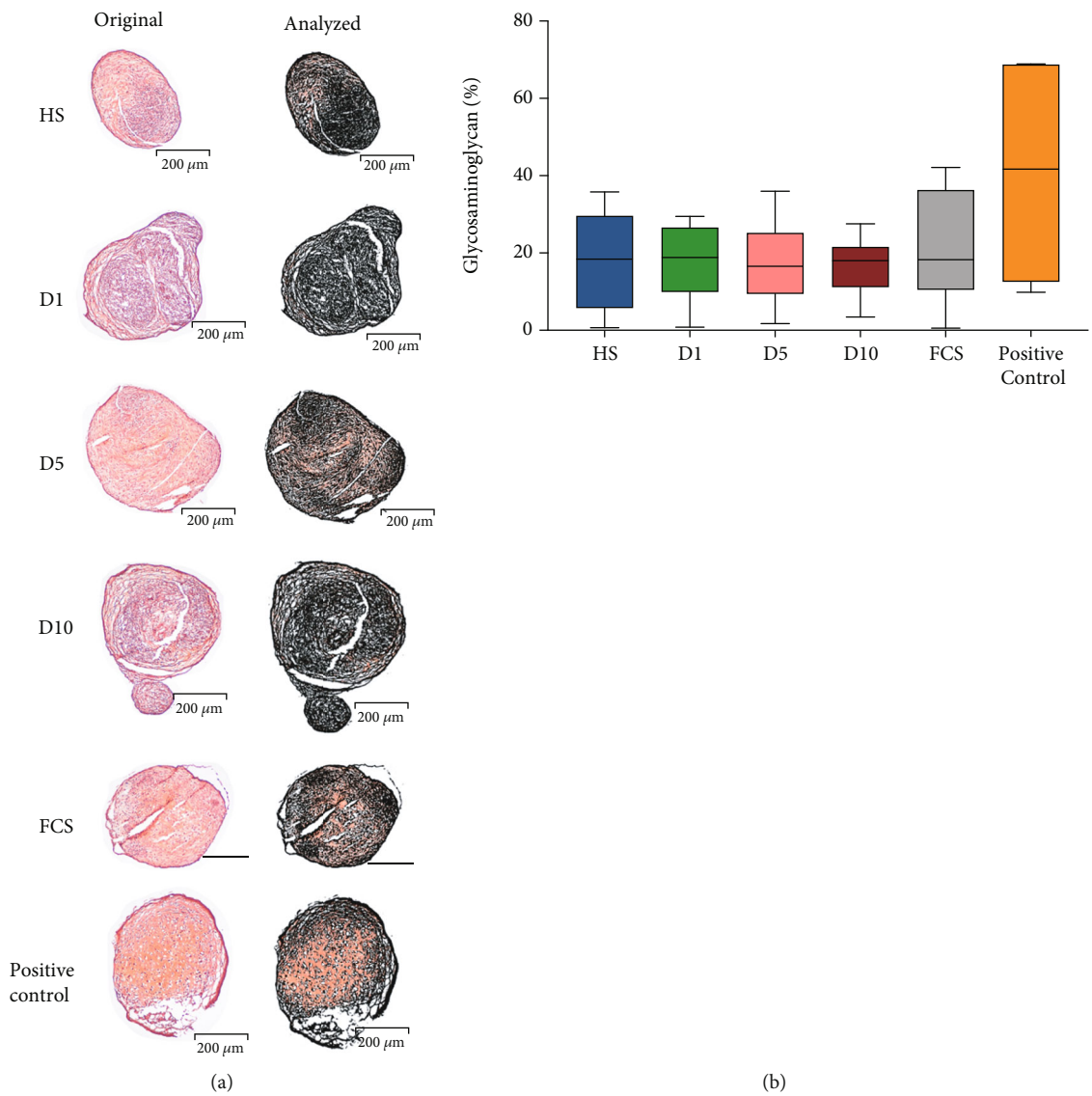

Figure 7: Chondrogenic differentiation potential. (a) Chondrogenic differentiation after 21 days of culture in chondrogenic induction medium containing either HS, D1, D5, D10 serum, FCS, or serum-free (positive control). Images were taken at a magnification of 40x. Glycosaminoglycan content is depicted in orange. Demarcation of areas not stained positively for glycosaminoglycans in black using visual analysis software (based on OpenCV library version 4.1.0). Standard parameters were used in the analysis of each image. (b) Quantitative analysis of the glycosaminoglycan content of the chondrogenic pellet showed no significant differences between different groups ($p > 0.05$, $n = 4$, $N = 2$).

demographic, correlated with social interactions and exposure to labor [38, 39], which made it a heavy burden for the society [40, 41]. As been defined in terms of a high ISS score (≥16) and described as a condition of "severely injured" or "multiple traumata," polytrauma has a high mortality rate and a high incidence of impairment.

A dysfunctional immune system caused by polytrauma often results in death from sepsis and septic shock or MODS [42–44] by breaking the balance between the systemic inflammatory response syndrome (SIRS) and the compensatory anti-inflammatory response syndrome (CARS) [43, 45, 46]. This imbalance in turn can develop into persistent inflammatory, immunosuppressed, catabolic syndrome (PICS) [47] in the late stage after trauma. Trauma triggers the production of different inflammatory mediators and associated peptides. TNF-α, IL-1, IL-6, IL-8, and IL-10 can be secreted from monocytes/macrophages [12, 13], whereby inflammatory cascade activation [10] plays a major role in the development of immune dysfunction and multiple organ dysfunction following polytrauma.

MSC can be triggered by a signal to exhibit immunomodulatory properties, and the most powerful promoters are IFN-γ, TNF-α, and IL-1β [17, 18]. Various adhesion molecules including integrins and selectins are expressed by MSC to regulate the adhesion of the cells to the target tissue's extracellular matrix (ECM) [19, 48]. It is known that MSC can be induced to differentiate into osteoblasts *in vitro* [21] and chondrocytes [22, 23] by culturing in a

special differentiation media *in vitro* using classic pellet culture methods. Therefore, the hBMSCs are promising in the treatment of patients suffering from polytrauma, but as it is known that the complex changes of serum cytokines after polytrauma [31] exert a various impact on the characteristics and properties of MSCs [30, 32], it is necessary to explore the cytological effects on hBMSCs at different time points postpolytrauma. Such a study could lead to more knowledge of whether the factor polytrauma has a negative effect on hBMSCs and at which time points hBMSCs should be used to treat polytrauma. Other studies [32, 49] used a single cytokine or stimulated cocktail including multiple factors to answer this question, but these *in vitro* cocktails cannot completely show the serological effects of polytrauma. Therefore, in our study, real serum from patients with polytrauma at D1, D5, and D10 compared to healthy serum was used.

Analysis of the serum cytokine concentration in our study showed that the proinflammatory factors IL-6 and IL-8 and the anti-inflammatory IL-10 were increased on D1 after the induction of trauma. In contrast, other proinflammatory (e.g., IL-1β, IL-12, TNF-α, and IFN-γ) and anti-inflammatory factors (e.g., IL-4, IL-5, and IL-13) were decreased after trauma induction at all time points compared to the serum from healthy controls and with concentrations that slightly recovered from D1 to D10. To sum up these findings, a sharp increase in specific cytokine concentrations was seen after acute traumatic stress as reflected by the D1 group, which decreased close to normal levels following D5 and D10 after polytrauma. In the subsequent D5 and D10 groups, proinflammatory and anti-inflammatory factors are in a relatively balanced state, as their concentrations are comparable to the HS group and showed a fluctuation trend after trauma to maintain a long-term balance which is in line with the theory of SIRS/CARS balancing, as well as the latest PICS theory [50]. A comparable study was carried out by Halbgebauer et al. [51] which conducted a cytokine analysis from seven polytrauma patients (ISS $\geq$ 32, six males and one female) four hours and one and five days posttrauma and treated the whole blood with or without lipopolysaccharide (LPS). In the results of Halbgebauer et al., the proinflammatory factors IL-12 and IFN-γ were downregulated after trauma in D1 when compared with the healthy group, and an upward trend was discovered from D1 to D10. The anti-inflammatory IL-10 was dramatically increased after trauma in D1 in comparison to the healthy group and decreased to a level which was slightly higher than the healthy group in D5, with a rising trend in D10. Upon these cytokines, the results were in line with the findings of this study. However, for IL-4, IL-5, and IL-13, Halbgebauer et al. observed an upregulation in D1 and D5 relative to the healthy group while these cytokines were downregulated in this experiment when compared with HS. Volpin et al. [52] detected the serum cytokines in 58 severe trauma patients (AIS: 3.44 ± 0.5, 35 males, 23 females) several hours after trauma compared to a healthy control group. In the results of Volpin et al., it showed that IL-4 was decreased and IL-6 and IL-8 were increased compared to healthy control as in this study, but it showed a different trend as IL-1β, IL-12, and IFN-γ were increased when compared with the healthy control, and in this study, a decreased trend was shown for these cytokines compared to HS. Differences in the results from the study by Halbgebauer et al. and Volpin et al. to this study could be explained by different patient groups (age, gender) and the severity of the trauma. At the same time, the half-life of some cytokines is relatively short. For example, TNF-α has a half-life of less than 20 minutes and IL-1 only 6 minutes [31]. Therefore, the choice of cytokine detection time point also determines the difference in cytokine changes.

In this study, the proliferation capacities of hBMSCs incubated with serum from D5 polytrauma patients were significantly reduced in comparison to cells incubated with serum from healthy controls. And when using serum from D10, however, the proliferation capacity of hBMSCs was comparable to the control. In accordance with this, the proportion of dead cells upon culture with serum from D5 was significantly higher than that of cells cultured with D1 serum. Based on the results of the cytokine analysis, it could be hypothesized that these effects might be caused by the combined action of multiple cytokines. Among the factors that promote cell proliferation and inhibit apoptosis, EGF can promote the proliferation and migration of MSCs [53, 54], short-term exposure to HGF can improve the survival rate of MSCs [55], and FGF-4 has mitotic activity and can effectively promote the proliferation of MSCs [56]. PDGF-BB can protect cells from apoptosis and is known to regulate cell proliferation [57, 58], and it also has the effect of promoting MSC osteogenic differentiation [59], while IGFBP-4 promotes senescence and apoptosis in MSCs [60]. Most of the above-mentioned factors that promote cell proliferation were significantly reduced in D5 serum, especially FGF-4, while IGFBP-4, which promotes cell senescence and apoptosis, was the highest in serum from D5. EGF and HGF might have a positive effect on proliferation and migration of hBMSCs because their concentrations were higher in serum from polytrauma patients than in the serum from healthy controls. The fact that concentrations of these cytokines were lower in D5 than D1 or D10 might explain the decreased proliferation rate and increased proportion of dead hBMSCs after culture with the respective serum. Therefore, the increase in the concentration of cytokines that can promote cell proliferation and viability is not enough to offset the effects of some cytokines that inhibit cell proliferation and promote cell apoptosis. This may also cause the decreased proliferation and viability.

Amann et al. [32] conducted an experiment where the effect of selected trauma-related factors to the effect of polytrauma serum on the inflammatory response of hBMSCs was compared. Serum from four polytrauma patients was obtained at 0, 4, 12, 24, 48, 120, and 240 hours after their admission to the clinic. The serum of five patients was used to make a medium with a 20% serum concentration to investigate the *in vitro* proliferation of human MSCs after seven days in culture. Proliferation of MSCs was decreased after treatment with serum samples from polytrauma starting after 12 hours up to 240 hours. Compared to this study, the same reduction in the proliferation ability after 72 hours of cultivation time with

serum taken at D5 (120 hours) was found. Importantly, Amann et al. determined that different mixtures of cytokines together with serum from healthy controls were not able to induce a similar effect on hBMSC properties as serum from polytrauma patients. This suggests that the effect of polytrauma serum on the proliferation, vitality, and cytotoxicity of MSCs cannot be mimicked by the influence of a single cytokine or even the combination of a few cytokines.

In the CFU-F assay of this study, the results showed that the CFU-F number was not reduced when culturing hBMSCs with polytrauma serum (D1, D5, and D10) as compared to HS. However, the blue staining area of colonies in the polytrauma groups (D1, D5, and D10) was less than that in HS (Figure 2(a)) in visual, especially in the D5 group. With reference to the results of cell proliferation experiments, on the 5th day after trauma, the total number of cells decreased and the proportion of cell death increased, but the ability of colony forming was not reduced, which might lead to less area of staining of CFU-F. The effects of cytokines differentially influencing cell proliferation, cell survival rate, and cell apoptosis are integrated and together mediate the changes in MSCs. And the reduction of factors that promote cell proliferation and the promotion of cell senescence and apoptosis may be related to this result.

The polytrauma serum has no obvious effect on the viability and cytotoxicity of MSC within 24 hours detected by WST assay. Possibly, 24-hour cultivation was not long enough to induce a reduction in cell viability, since a significant increased rate of dead cells was observed after 72 hours of cultivation by using total cell counting and live and dead assay.

Moreover, it was found in this study that there was no significant influence of the different sera on the migration properties of hBMSCs in a transwell migration assay. IGF-1, GRO, and MCP-1 can effectively promote the migration of MSCs [61, 62]. In this study, it was found that the levels of IGF-1 and GRO decreased in the sera from all polytrauma groups. However, the level of MCP-1 was found to be increased, which might result in the zero net effect of the polytrauma sera on the migration properties of hBMSCs. In difference, Hengartner et al. [49] found a promigratory effect of a polytrauma cocktail on MSCs. The method Hengartner et al. used was similar to the transwell assay in this study, and the difference was Hengartner et al. used a mixture of cytokines (cocktail). Combined with the suggestions from the study of Amann et al. [32], these differences strengthen the hypothesis of this study that a mixture of cytokines may not adequately reflect the complex influence of real polytrauma serum on MSCs.

In this study, no significant differences were found in the scratch assay between different groups and different time points. The application of serum-free medium not only ensures that all cells used in the experiment were in P_3 but also avoids the influence of cell proliferation on migration. It is known that VEGF parasecreted by MSC can promote the migration to repair vascular endothelium; both VEGF [63] and PDGF-BB [64] have the ability to migrate and repair the wounded tissue. In the results of this experiment, the ability of migration in scratch assay did not change according to the trend of cytokines. However, as the scratch assay is an *in vitro* surrogate marker for migration to repair, the actual migration-wound healing ability of hBMSCs *in vivo* may change. Therefore, further exploration *in vivo* is needed.

In vitro bone formation in this study was evaluated with alizarin red staining of calcium deposits [65] as well as with alizarin red absorbance measurement at 600 nm [66]. Comparable results were obtained with both methods, and no significant difference in osteogenic differentiation ability of hBMSCs was observed between the HS and polytrauma groups.

Interestingly, in the results of alizarin red absorbance measurement at 600 nm except for the D5 group, all groups containing human serum had a significant higher osteogenic capacity than the FCS group. Perhaps, this is related to the fact that human serum contains more proteins or growth factors [67], and the use of allogeneic human serum MSC culture has a higher beneficial influence on cell proliferation than FCS [68]. In this study, increased serum concentrations of osteopontin, osteoprotegerin, and FGF-9 as well as decreased TIMP-1 concentration were observed. Osteoprotegerin, osteopontin, and FGF-9 play a positive regulatory role in promoting osteogenic differentiation. While osteopontin can effectively promote MSC osteoblastic differentiation [69] and osteoprotegerin inhibits bone resorption [70], FGF-9 effectively increases bone differentiation [71] and is indispensable in long bone repair. In contrast to this, TIMP-1 negatively regulates osteogenic differentiation by attenuating the expression of Runx2 during bone differentiation and also inhibits cell proliferation [72]. This may explain why no negative impact of the polytrauma sera on osteogenic differentiation of hBMSCs was found.

In contrast to the results of this study, Thaweesapphithak et al. [68] conducted osteogenic differentiation experiments of human placenta and umbilical cord-derived MSCs using osteogenic differentiation medium containing human serum for four weeks and found that osteogenic differentiation was not differentially influenced by human serum in comparison to FCS. Popov et al. [73] conducted research on hBMSCs to compare osteogenic differentiation medium containing FCS and human serum, over a differentiation time of 21 days. In the study of Popov et al., human serum was only added to the differentiation medium during the first five days, because Popov et al. found in prior experiments that using human serum resulted only for five days in a better osteogenic differentiation in contrast to the continuous supplementation with human serum. Popov et al. concluded that, in comparison to FCS, the use of human serum enhanced the osteogenic differentiation ability of MSCs and the results are in line with the results obtained in this study.

Glycosaminoglycan staining by safranin O is a reliable method for the quantification of cartilage tissue [74] which was used in this study. The results showed that the chondrogenic differentiation ability of the positive control group (serum-free) was higher than that of the other experimental groups (10% serum added), although there were no significant differences between the experimental groups, indicating

that polytrauma serum from all time points had no significant effect on the chondrogenic differentiation of hBMSCs. Proteins from the TGF-β family can promote chondrogenic differentiation in MSCs [75, 76]. TGF-β1 cooperates with IGF-1 to promote MSC migration and chondrogenic differentiation [77, 78], while IL-1β [79] can inhibit chondrogenic differentiation. In the multicytokine array, polytrauma caused decreased concentrations of TGF-β1, TGF-β2, and TGF-β3, especially one day after the trauma, but this was not reflected by a negative influence of the sera on chondrogenic differentiation of hBMSCs *in vitro*. Since TGF-β3 was added to the chondrogenic differentiation medium in this experiment, the slight decline of TGF in polytrauma sera might be overruled by the general addition of TGF-β3 to the differentiation medium, thereby hiding a possible effect of this reduction.

The following limitations were present in this study. The results were obtained using hBMSCs from only four different donors. Therefore, future studies using hBMSCs from more donors should be conducted to confirm the results found here. Furthermore, pooled sera from patients with polytrauma were used to provide enough volume to perform the experiments. A disadvantage to use pooled serum is that a statistical analysis to prove the difference between groups cannot be performed. However, the most important advantage of using serum from more than 80 polytrauma patients is that individual differences with respect to cytokine changes in serum will likely be zeroed out, and it showed the real concentration change of the cytokines. Furthermore, the polytrauma pooled serum and the pooled serum from healthy donors were matched with respect to age and gender to reduce the influence of these two factors. Additionally, allogeneic serum was used on hBMSCs in this study, and this may lead to proliferation stagnation and death.

At present, many clinical trials using MSCs to treat human diseases can be found on clinicaltrials.gov [80], but the application of MSC to treat human polytrauma is still in the early stage of development. In studies concerning bones and joints, a combination of MSCs and biomaterial scaffolds has been used locally, and its effectiveness has been verified in animal experiments [24–26, 28, 29]. In this study, considering the reconstruction of surgical functions in patients with polytrauma after the basic vital signs have stabilized, the local application of MSCs is a point of interest, for instance, to add BMSC locally into the fracture gap during the final reconstruction of bones and cartilage postpolytrauma, and the influence of serology on MSCs still needs to be considered.

The central idea of the "Damage Control Orthopedics (DCO)" [81] is to implement life-saving procedures early, temporarily stabilize damaged tissues, and finally deal with fracture fixation and osteochondral treatment related to the injury. Because of the imbalance of the SIRS/CARS system, the "first hit" caused by trauma is likely to make the patient face the potential risk of deterioration after the "second hit" of the operation [82, 83]. According to reports, the definitive osteosynthesis on the second to fourth day after trauma increases the chance of MODS [84], and it is beneficial to perform the final fixation within 15 days after trauma to avoid infection of temporary external fixation [85], especially during the 5th to 10th days posttrauma which period has been defined as "window of opportunity" [86]. Based on this knowledge and the results of this study, it could be very promising to add hBMSCs locally into the fracture gap of bones and cartilage during the final reconstructive operation in the "window of opportunity" due to the "DCO" concept. However, a systemic application of MSCs after polytrauma is also conceivable in some studies. In an animal experiment of systemic application of MSCs, Tanrıverdi et al. [87] used allogeneic MSCs which significantly improved the healing ability of the liver and bone in rats after polytrauma. Furthermore, Amann et al. [88] showed that allogeneic MSCs significantly reduced injury score 24 hours after severe blunt chest trauma (TxT). However, previous studies also have shown that systemic application of MSCs, such as systemic intravenous injection, tends to accumulate in the lungs [89] or distribute in other organs, such as the liver, kidneys, long bones, and spleen, 24-48 hours after injection [90]. In addition, it is not easy to detect the donor's MSCs in the whole body after 8-10 days of injection [91]. Furthermore, a study by von Bahr et al. showed that the ability of MSCs to enter the bone marrow was very limited by intravenous injection of MSCs [92]. Therefore, a local administration of MSCs seems more promising to us than a systemic injection.

Altogether, the results indicate that hBMSCs may be useful in the treatment of fractures and cartilage defects of patients suffering from polytrauma, since the *in vitro* regenerative potential of hBMSCs is not negatively affected by cytokines present in serum one, five, or ten days after polytrauma. The best time point for the application of hBMSCs might be at least after five days of polytrauma to overcome the negative effect of polytrauma serum on hBMSCs which were seen at D5. This setup would be in line with the "DCO" concept which consisted of the provisional immobilization of long bone fractures to achieve the advantages of early treatment and minimization of complication risks, such as fat embolism, pathological inflammatory response or severe hemorrhage triggering the lethal triad, and the traumatic effects of major surgery on a patient who is already traumatized (the "second hit" effect) [93].

This study tried to mimic the effects of polytrauma on hBMSCs *in vitro*, but it must be kept in mind that the *in vivo* environment is much more complex, and the *in vitro* conditions might have different effects on the cells than *in vivo*. Therefore, although the results of this study have a certain reference value for clinical applications, further *in vivo* verification is necessary.

5. Conclusions

The composition of polytrauma serum changes over time after the trauma incident. Therefore, the effect on hBMSC biology is differentially affected by sera obtained from polytrauma patients at different time intervals after trauma. Prolonged exposure to polytrauma serum collected on D5 exerts a negative effect on hBMSCs with reduced proliferation ability and a higher cell death ratio. Polytrauma serum did not

significantly affect the colony forming ability, cells' migration, and scratch healing ability, and no significant effects on the ability to differentiate into bone and cartilage tissues were found.

Data Availability

The data used to support the findings of this study are available from the corresponding author upon request.

Disclosure

This study was part of the doctoral thesis of "Cytological effects of serum isolated from polytraumatized patients on human bone marrow-derived mesenchymal stem cells" at Hannover Medical School.

Conflicts of Interest

The authors declare to have no potential conflicts of interest.

Acknowledgments

We would like to thank Claudia Pütz and Melanie Weiß for their valuable assistance. The underlying study was financed by Hannover Medical School and Else Kröner-Fresenius-Stiftung (Grant No. 2016-A188). The research stay of Dr. Yazhou Long in Germany was supported by the China Scholarship Council (CSC) (No. 201909210006).

Supplementary Materials

Supplementary Figure S1: the level change of cytokines: growth factors (EGF, HGF, FGF-4, and IGFBP-4) and migration factors (IGF-1, GRO-α, MCP-1, VEGF, and PDGF-BB). *(Supplementary Materials)*

References

[1] J. V. Sakran, S. E. Greer, E. Werlin, and M. McCunn, "Care of the injured worldwide: trauma still the neglected disease of modern society," *Scandinavian Journal of Trauma, Resuscitation and Emergency Medicine*, vol. 20, no. 1, p. 64, 2012.

[2] D. G. F. Unfallchirurgie, "Definition of polytrauma," 2020, https://www.dgu-online.de/patienten/haeufige-diagnosen/schwerverletzte/polytrauma.html.

[3] S. Frenzel, P. Krenn, T. Heinz, and L. L. Negrin, "Does the applied polytrauma definition notably influence outcome and patient population? - a retrospective analysis," *Scandinavian Journal of Trauma, Resuscitation and Emergency Medicine*, vol. 25, no. 1, pp. 87–87, 2017.

[4] S. P. Baker and B. O'Neill, "The injury severity score: an update," *The Journal of Trauma*, vol. 16, no. 11, pp. 882–885, 1976.

[5] S. P. Baker, B. O'neill, W. Haddon JR., and W. B. Long, "The injury severity SCORE," *The Journal of Trauma*, vol. 14, no. 3, pp. 187–196, 1974.

[6] I. Marzi, T. Lustenberger, P. Störmann, K. Mörs, N. Wagner, and S. Wutzler, "Increasing overhead ressources of the trauma room," *Unfallchirurg*, vol. 122, no. 1, pp. 53–58, 2019.

[7] R. de Vries, I. H. F. Reininga, O. Pieske, R. Lefering, M. el Moumni, and K. Wendt, "Injury mechanisms, patterns and outcomes of older polytrauma patients-an analysis of the Dutch Trauma Registry," *PLoS One*, vol. 13, no. 1, article e0190587, 2018.

[8] H. C. Pape, R. Lefering, N. Butcher et al., "The definition of polytrauma revisited," *Journal of Trauma and Acute Care Surgery*, vol. 77, no. 5, pp. 780–786, 2014.

[9] V. Ciriello, S. Gudipati, P. Z. Stavrou, N. K. Kanakaris, M. C. Bellamy, and P. V. Giannoudis, "Biomarkers predicting sepsis in polytrauma patients: current evidence," *Injury*, vol. 44, no. 12, pp. 1680–1692, 2013.

[10] M. Keel and O. Trentz, "Pathophysiology of polytrauma," *Injury*, vol. 36, no. 6, pp. 691–709, 2005.

[11] G. Fabiano, A. Pezzolla, M. A. Filograna, and F. Ferrarese, "Traumatic shock–physiopathologic aspects," *Il Giornale di Chirurgia*, vol. 29, no. 1-2, pp. 51–57, 2008.

[12] A. Lenz, G. A. Franklin, and W. G. Cheadle, "Systemic inflammation after trauma," *Injury*, vol. 38, no. 12, pp. 1336–1345, 2007.

[13] P. Toft, S. K. Andersen, and E. K. Tønnesen, "The systematic inflammatory response after major trauma," *Ugeskrift for Laeger*, vol. 165, no. 7, pp. 669–672, 2003.

[14] S. D. Trancă, C. L. Petrişor, and N. Hagău, "Biomarkers in polytrauma induced systemic inflammatory response syndrome and sepsis - a narrative review," *Romanian journal of anaesthesia and intensive care*, vol. 21, no. 2, pp. 118–122, 2014.

[15] I. Ullah, R. B. Subbarao, and G. J. Rho, "Human mesenchymal stem cells - current trends and future prospective," *Bioscience Reports*, vol. 35, no. 2, 2015.

[16] K. Zha, X. Li, Z. Yang et al., "Heterogeneity of mesenchymal stem cells in cartilage regeneration: from characterization to application. npj," *Regenerative Medicine*, vol. 6, no. 1, pp. 1–5, 2021.

[17] M. Krampera, "Mesenchymal stromal cell 'licensing': a multistep process," *Leukemia*, vol. 25, no. 9, pp. 1408–1414, 2011.

[18] D. Mougiakakos, R. Jitschin, C. C. Johansson, R. Okita, R. Kiessling, and K. le Blanc, "The impact of inflammatory licensing on heme oxygenase-1-mediated induction of regulatory T cells by human mesenchymal stem cells," *Blood*, vol. 117, no. 18, pp. 4826–4835, 2011.

[19] A. Sohni and C. M. Verfaillie, "Mesenchymal stem cells migration homing and tracking," *Stem Cells International*, vol. 2013, Article ID 130763, 2013.

[20] C. Eder, K. Schmidt-Bleek, S. Geissler et al., "Mesenchymal stromal cell and bone marrow concentrate therapies for musculoskeletal indications: a concise review of current literature," *Molecular Biology Reports*, vol. 47, no. 6, pp. 4789–4814, 2020.

[21] A. J. Friedenstein, R. K. Chailakhyan, and U. V. Gerasimov, "Bone marrow osteogenic stem cells: in vitro cultivation and transplantation in diffusion chambers," *Cell and Tissue Kinetics*, vol. 20, no. 3, pp. 263–272, 1987.

[22] B. A. Ashton, T. D. Allen, C. R. Howlett, C. C. Eaglesom, A. Hattori, and M. Owen, "Formation of bone and cartilage by marrow stromal cells in diffusion chambers in vivo," *Clinical Orthopaedics and Related Research*, no. 151, pp. 294–307, 1980.

[23] J. N. Beresford, "Osteogenic stem cells and the stromal system of bone and marrow," *Clinical Orthopaedics and Related Research*, vol. 240, pp. 270–280, 1989.

[24] T. L. Arinzeh, "Mesenchymal stem cells for bone repair: preclinical studies and potential orthopedic applications," *Foot and Ankle Clinics*, vol. 10, no. 4, pp. 651–665, 2005.

[25] W. Duan, C. Chen, M. Haque, D. Hayes, and M. J. Lopez, "Polymer-mineral scaffold augments in vivo equine multipotent stromal cell osteogenesis," *Stem Cell Research & Therapy*, vol. 9, no. 1, p. 60, 2018.

[26] H. Sun, Z. Qu, Y. Guo, G. Zang, and B. Yang, "In vitro and in vivo effects of rat kidney vascular endothelial cells on osteogenesis of rat bone marrow mesenchymal stem cells growing on polylactide-glycoli acid (PLGA) scaffolds," *Biomedical Engineering Online*, vol. 6, no. 1, p. 41, 2007.

[27] H. Nejadnik, S. Diecke, O. D. Lenkov et al., "Improved approach for chondrogenic differentiation of human induced pluripotent stem cells," *Stem Cell Reviews and Reports*, vol. 11, no. 2, pp. 242–253, 2015.

[28] J. Yang, Y. S. Zhang, K. Yue, and A. Khademhosseini, "Cell-laden hydrogels for osteochondral and cartilage tissue engineering," *Acta Biomaterialia*, vol. 57, pp. 1–25, 2017.

[29] Z. Man, L. Yin, Z. Shao et al., "The effects of co-delivery of BMSC-affinity peptide and rhTGF-β1 from coaxial electrospun scaffolds on chondrogenic differentiation," *Biomaterials*, vol. 35, no. 19, pp. 5250–5260, 2014.

[30] M. Huber-Lang, R. Wiegner, L. Lampl, and R. E. Brenner, "Mesenchymal stem cells after polytrauma: actor and target," *Stem Cells International*, vol. 2016, Article ID 6289825, 10 pages, 2016.

[31] W. G. DeLong Jr. and C. T. Born, "Cytokines in patients with polytrauma," *Clinical Orthopaedics and Related Research*, vol. 422, pp. 57–65, 2004.

[32] E. Amann, A. Groß, M. T. Rojewski et al., "Inflammatory response of mesenchymal stromal cells after in vivo exposure with selected trauma-related factors and polytrauma serum," *PLoS One*, vol. 14, no. 5, article e0216862, 2019.

[33] R. Wiegner, N. E. Rudhart, E. Barth et al., "Mesenchymal stem cells in peripheral blood of severely injured patients," *European Journal of Trauma and Emergency Surgery*, vol. 44, no. 4, pp. 627–636, 2018.

[34] RayBio, "RayBio® Human Cytokine Antibody Array G-Series 5-Cat# AAH-CYT-G5-8. 2014," 2020, http://www.raybiotech.com/files/manual/Antibody-Array/AAH-CYT-G5.pdf.

[35] G. Bradski, "The OpenCV Library," *Dr. Dobb's Journal of Software Tools*, vol. 120, pp. 122–125, 2000.

[36] Morpheus2020, https://software.broadinstitute.org/morpheus.

[37] H. al-Thani, A. el-Menyar, M. Asim et al., "Evolution of the Qatar trauma system: the journey from inception to verification," *Journal of Emergencies, Trauma, and Shock*, vol. 12, no. 3, pp. 209–217, 2019.

[38] J. Wang, H. Lu, Z. Sun, and T. Wang, "Exploring factors influencing injury severity of vehicle at-fault accidents: a comparative analysis of passenger and freight vehicles," *International Journal of Environmental Research and Public Health*, vol. 17, no. 4, p. 1146, 2020.

[39] Prevention, CCfDCa, "Saving lives and protecting people from violence and injuries," 2014, https://www.cdc.gov/about/pdf/cdc-recent-accomplishments.pdf.

[40] E. F. van Beeck, L. van Roijen, and J. P. Mackenbach, "Medical costs and economic production losses due to injuries in the Netherlands," *The Journal of Trauma*, vol. 42, no. 6, pp. 1116–1123, 1997.

[41] J. L. Bastida, P. S. Aguilar, and B. D. González, "The economic costs of traffic accidents in Spain," *The Journal of Trauma*, vol. 56, no. 4, pp. 883–888, 2004, discussion 888-9.

[42] W. H. O. Geneva, "The global burden of disease," 2018, https://www.who.int/healthinfo/global_burden_disease/en/.

[43] S. Wutzler, T. Lustenberger, B. Relja, M. Lehnert, and I. Marzi, "Pathophysiologie des Polytraumas," *Chirurg*, vol. 84, no. 9, pp. 753–758, 2013.

[44] A. Wafaisade, R. Lefering, B. Bouillon et al., "Epidemiology and risk factors of sepsis after multiple trauma: an analysis of 29,829 patients from the Trauma Registry of the German Society for Trauma Surgery," *Critical Care Medicine*, vol. 39, no. 4, pp. 621–628, 2011.

[45] M. Adib-Conquy and J. M. Cavaillon, "Compensatory anti-inflammatory response syndrome," *Thrombosis and Haemostasis*, vol. 101, no. 1, pp. 36–47, 2009.

[46] R. Sturm, L. Xanthopoulos, D. Heftrig et al., "Regulatory T cells modulate CD4 proliferation after severe trauma via IL-10," *Journal of Clinical Medicine*, vol. 9, no. 4, p. 1052, 2020.

[47] J. C. Mira, S. C. Brakenridge, L. L. Moldawer, and F. A. Moore, "Persistent inflammation, immunosuppression and catabolism syndrome," *Critical Care Clinics*, vol. 33, no. 2, pp. 245–258, 2017.

[48] G. Ren, X. Zhao, L. Zhang et al., "Inflammatory cytokine-induced intercellular adhesion molecule-1 and vascular cell adhesion molecule-1 in mesenchymal stem cells are critical for immunosuppression," *Journal of Immunology*, vol. 184, no. 5, pp. 2321–2328, 2010.

[49] N.-E. Hengartner, J. Fiedler, H. Schrezenmeier, M. Huber-Lang, and R. E. Brenner, "Crucial role of IL1beta and C3a in the in vitro-response of multipotent mesenchymal stromal cells to inflammatory mediators of polytrauma," *PLoS One*, vol. 10, no. 1, article e0116772, 2015.

[50] A. M. Binkowska, G. Michalak, and R. Słotwiński, "Current views on the mechanisms of immune responses to trauma and infection," *Central-European Journal of Immunology*, vol. 40, no. 2, pp. 206–216, 2015.

[51] R. Halbgebauer, S. Kellermann, F. Schäfer et al., "Functional immune monitoring in severely injured patients-a pilot study," *Scandinavian Journal of Immunology*, vol. 91, no. 2, article e12837, 2020.

[52] G. Volpin, M. Cohen, M. Assaf, T. Meir, R. Katz, and S. Pollack, "Cytokine levels (IL-4, IL-6, IL-8 and TGFβ) as potential biomarkers of systemic inflammatory response in trauma patients," *International Orthopaedics*, vol. 38, no. 6, pp. 1303–1309, 2014.

[53] K. Tamama, V. H. Fan, L. G. Griffith, H. C. Blair, and A. Wells, "Epidermal growth factor as a candidate for ex vivo expansion of bone marrow-derived mesenchymal stem cells," *Stem Cells*, vol. 24, no. 3, pp. 686–695, 2006.

[54] C. Knight, S. James, D. Kuntin et al., "Epidermal growth factor can signal via β-catenin to control proliferation of mesenchymal stem cells independently of canonical Wnt signalling," *Cellular Signalling*, vol. 53, pp. 256–268, 2019.

[55] G. Forte, M. Minieri, P. Cossa et al., "Hepatocyte growth factor effects on mesenchymal stem cells: proliferation, migration, and differentiation," *Stem Cells*, vol. 24, no. 1, pp. 23–33, 2006.

[56] J. Farré, J. Farré, S. Roura et al., "FGF-4 increases in vitro expansion rate of human adult bone marrow-derived mesenchymal stem cells," *Growth Factors*, vol. 25, no. 2, pp. 71–76, 2007.

[57] J.-M. Zhang, F. E. Feng, Q. M. Wang et al., "Platelet-derived growth factor-BB protects mesenchymal stem cells (MSCs) derived from immune thrombocytopenia patients against apoptosis and senescence and maintains MSC-mediated immunosuppression," *Stem Cells Translational Medicine*, vol. 5, no. 12, pp. 1631–1643, 2016.

[58] D. Lennon, L. A. Solchaga, R. A. Somoza, M. D. Schluchter, S. Margevicius, and A. I. Caplan, "Human and rat bone marrow-derived mesenchymal stem cells differ in their response to fibroblast growth factor and platelet-derived growth factor," *Tissue Engineering. Part A*, vol. 24, no. 23-24, pp. 1831–1843, 2018.

[59] B. P. Hung, D. L. Hutton, K. L. Kozielski et al., "Platelet-derived growth factor BB enhances osteogenesis of adipose-derived but not bone marrow-derived mesenchymal stromal/stem cells," *Stem cells (Dayton, Ohio)*, vol. 33, no. 9, pp. 2773–2784, 2015.

[60] V. Severino, N. Alessio, A. Farina et al., "Insulin-like growth factor binding proteins 4 and 7 released by senescent cells promote premature senescence in mesenchymal stem cells," *Cell Death & Disease*, vol. 4, no. 11, pp. e911–e911, 2013.

[61] A. L. Ponte, E. Marais, N. Gallay et al., "The in vitro migration capacity of human bone marrow mesenchymal stem cells: comparison of chemokine and growth factor chemotactic activities," *Stem Cells*, vol. 25, no. 7, pp. 1737–1745, 2007.

[62] J. Bayo, A. Real, E. J. Fiore et al., "IL-8, GRO and MCP-1 produced by hepatocellular carcinoma microenvironment determine the migratory capacity of human bone marrow-derived mesenchymal stromal cells without affecting tumor aggressiveness," *Oncotarget*, vol. 8, no. 46, pp. 80235–80248, 2017.

[63] S. Barrientos, O. Stojadinovic, M. S. Golinko, H. Brem, and M. Tomic-Canic, "Perspective article: growth factors and cytokines in wound healing," *Wound Repair and Regeneration*, vol. 16, no. 5, pp. 585–601, 2008.

[64] S. G. Ball, C. A. Shuttleworth, and C. M. Kielty, "Mesenchymal stem cells and neovascularization: role of platelet-derived growth factor receptors," *Journal of Cellular and Molecular Medicine*, vol. 11, no. 5, pp. 1012–1030, 2007.

[65] H. Puchtler, S. N. Meloan, and M. S. Terry, "On the history and mechanism of alizarin and alizarin red S stains for calcium," *The Journal of Histochemistry and Cytochemistry*, vol. 17, no. 2, pp. 110–124, 1969.

[66] H. Hanna, L. M. Mir, and F. M. Andre, "In vitro osteoblastic differentiation of mesenchymal stem cells generates cell layers with distinct properties," *Stem Cell Research & Therapy*, vol. 9, no. 1, p. 203, 2018.

[67] C. Tekkatte, G. P. Gunasingh, K. M. Cherian, and K. Sankaranarayanan, ""Humanized" stem cell culture techniques: the animal serum controversy," *Stem Cells International*, vol. 2011, Article ID 504723, 14 pages, 2011.

[68] S. Thaweesapphithak, C. Tantrawatpan, P. Kheolamai, D. Tantikanlayaporn, S. Roytrakul, and S. Manochantr, "Human serum enhances the proliferative capacity and immunomodulatory property of MSCs derived from human placenta and umbilical cord," *Stem Cell Research & Therapy*, vol. 10, no. 1, pp. 79–79, 2019.

[69] M. S. Carvalho, A. A. Poundarik, J. M. S. Cabral, C. L. da Silva, and D. Vashishth, "Biomimetic matrices for rapidly forming mineralized bone tissue based on stem cell-mediated osteogenesis," *Scientific Reports*, vol. 8, no. 1, pp. 14388–14388, 2018.

[70] S. Zhou, X. Fang, H. Xin, W. Li, H. Qiu, and S. Guan, "Osteoprotegerin inhibits calcification of vascular smooth muscle cell via down regulation of the Notch1-RBP-Jκ/Msx2 signaling pathway," *PLoS One*, vol. 8, no. 7, article e68987, 2013.

[71] C. Wallner, J. Schira, J. M. Wagner et al., "Application of VEGFA and FGF-9 enhances angiogenesis, osteogenesis and bone remodeling in type 2 diabetic long bone regeneration," *PLoS One*, vol. 10, no. 3, article e0118823, 2015.

[72] T. Liang, W. Gao, L. Zhu et al., "TIMP-1 inhibits proliferation and osteogenic differentiation of hBMSCs through Wnt/β-catenin signaling," *Bioscience Reports*, vol. 39, no. 1, article BSR20181290, 2019.

[73] A. Popov, C. Scotchford, D. Grant, and V. Sottile, "Impact of serum source on human mesenchymal stem cell osteogenic differentiation in culture," *International Journal of Molecular Sciences*, vol. 20, no. 20, p. 5051, 2019.

[74] K. Király, M. Lammi, J. Arokoski et al., "Safranin O reduces loss of glycosaminoglycans from bovine articular cartilage during histological specimen preparation," *The Histochemical Journal*, vol. 28, no. 2, pp. 99–107, 1996.

[75] M. C. Goude, T. C. McDevitt, and J. S. Temenoff, "Chondroitin sulfate microparticles modulate transforming growth factor-β1-induced chondrogenesis of human mesenchymal stem cell spheroids," *Cells, Tissues, Organs*, vol. 199, no. 2-3, pp. 117–130, 2014.

[76] I. Grafe, S. Alexander, J. R. Peterson et al., "TGF-β family signaling in mesenchymal differentiation," *Cold Spring Harbor Perspectives in Biology*, vol. 10, no. 5, 2018.

[77] L. Longobardi, L. O'Rear, S. Aakula et al., "Effect of IGF-I in the chondrogenesis of bone marrow mesenchymal stem cells in the presence or absence of TGF-beta signaling," *Journal of Bone and Mineral Research*, vol. 21, no. 4, pp. 626–636, 2006.

[78] X. Fu, G. Liu, A. Halim, Y. Ju, Q. Luo, and A. G. Song, "Mesenchymal stem cell migration and tissue repair," *Cell*, vol. 8, no. 8, p. 784, 2019.

[79] T. Felka, R. Schäfer, B. Schewe, K. Benz, and W. K. Aicher, "Hypoxia reduces the inhibitory effect of IL-1β on chondrogenic differentiation of FCS-free expanded MSC," *Osteoarthritis and Cartilage*, vol. 17, no. 10, pp. 1368–1376, 2009.

[80] O. Source, *Clinical Trials*, 2021.

[81] M. B. Shapiro, D. H. Jenkins, C. William Schwab, and M. F. Rotondo, "Damage control: collective review," *The Journal of Trauma*, vol. 49, no. 5, pp. 969–978, 2000.

[82] F. Gebhard and M. Huber-Lang, "PolytraumÅ pathophysiology and management principles," *Langenbeck's Archives of Surgery*, vol. 393, pp. 825–831, 2008.

[83] P. V. Giannoudis, "Current concepts of the inflammatory response after major trauma: an update," *Injury*, vol. 34, no. 6, pp. 397–404, 2003.

[84] H. Pape, M. Stalp, M. V. Griensven, A. Weinberg, M. Dahlweit, and H. Tscherne, "Optimaler Zeitpunkt der Sekundäroperation bei polytrauma Eine Evaluation an 4314 Schwerverletzten," *Chirurg*, vol. 70, no. 11, pp. 1287–1293, 1999.

[85] P. J. Harwood, P. V. Giannoudis, C. Probst, C. Krettek, and H. C. Pape, "The risk of local infective complications after damage control procedures for femoral shaft fracture," *Journal of Orthopaedic Trauma*, vol. 20, no. 3, pp. 181–189, 2006.

[86] P. F. Stahel, C. E. Heyde, W. Wyrwich, and W. Ertel, "Aktuelle konzepte des polytraumamanagements: von ATLS zu damage control," *Der Orthopäde*, vol. 34, no. 9, pp. 823–836, 2005.

[87] A. K. Tanrıverdi, O. Polat, A. E. Elçin et al., "Mesenchymal stem cell transplantation in polytrauma: evaluation of bone

and liver healing response in an experimental rat model," *European Journal of Trauma and Emergency Surgery*, vol. 46, no. 1, pp. 53–64, 2020.

[88] E. M. Amann, M. T. Rojewski, S. Rodi et al., "Systemic recovery and therapeutic effects of transplanted allogenic and xenogenic mesenchymal stromal cells in a rat blunt chest trauma model," *Cytotherapy*, vol. 20, no. 2, pp. 218–231, 2018.

[89] U. M. Fischer, M. T. Harting, F. Jimenez et al., "Pulmonary passage is a major obstacle for intravenous stem cell delivery: the pulmonary first-pass effect," *Stem Cells and Development*, vol. 18, no. 5, pp. 683–692, 2009.

[90] J. Gao, J. E. Dennis, R. F. Muzic, M. Lundberg, and A. I. Caplan, "The dynamic in vivo distribution of bone marrow-derived mesenchymal stem cells after infusion," *Cells, Tissues, Organs*, vol. 169, no. 1, pp. 12–20, 2001.

[91] D. L. Kraitchman, M. Tatsumi, W. D. Gilson et al., "Dynamic imaging of allogeneic mesenchymal stem cells trafficking to myocardial infarction," *Circulation*, vol. 112, no. 10, pp. 1451–1461, 2005.

[92] L. von Bahr, I. Batsis, G. Moll et al., "Analysis of tissues following mesenchymal stromal cell therapy in humans indicates limited long-term engraftment and no ectopic tissue formation," *Stem Cells*, vol. 30, no. 7, pp. 1575–1578, 2012.

[93] E. Guerado, M. L. Bertrand, J. R. Cano, A. M. Cerván, and A. Galán, "Damage control orthopaedics: state of the art," *World Journal of Orthopedics*, vol. 10, no. 1, pp. 1–13, 2019.

Hindawi
Stem Cells International
Volume 2021, Article ID 5212852, 14 pages
https://doi.org/10.1155/2021/5212852

Research Article

Chemically Defined Conditions Mediate an Efficient Induction of Dental Pulp Pluripotent-Like Stem Cells into Hepatocyte-Like Cells

Carlos Gil-Recio,[1] Sheyla Montori,[1] Saddam Al Demour,[2] Mera A. Ababneh,[3] Eduard Ferrés-Padró,[4] Carles Marti,[5] Elvira Ferrés-Amat,[6] Miguel Barajas,[7] Ashraf Al Madhoun,[8] and Maher Atari[1,9]

[1]*Regenerative Medicine Research Institute, UIC Barcelona, Barcelona, Spain*
[2]*Department of Special Surgery/Division of Urology, The University of Jordan, School of Medicine, Amman, Jordan*
[3]*Department of Clinical Pharmacy, Faculty of Pharmacy, Jordan University of Science and Technology, Amman, Jordan*
[4]*Oral and Maxillofacial Surgery Department, Fundació Hospital de Nens de Barcelona, Barcelona, Spain*
[5]*Oral and Maxillofacial Surgery Department, Hospital Clinico de Barcelona, Barcelona, Spain*
[6]*Pediatric Dentistry Service, Oral and Maxillofacial Surgery Service, Hospital de Nens de Barcelona, Barcelona, Spain*
[7]*Biochemistry and Molecular Biology Department, Universidad Pública de Navarra, Pamplona, Spain*
[8]*Department of Genetics and Bioinformatics, Functional Genomic Unit, Dasman Diabetes Institute, Kuwait*
[9]*Biointelligent Technology Systems SL, Diputaccion 316, 3D, 08009 Barcelona, Spain*

Correspondence should be addressed to Ashraf Al Madhoun; ashraf.madhoun@dasmaninstitute.org and Maher Atari; matari@biointelligentsl.com

Received 15 August 2021; Revised 15 October 2021; Accepted 18 October 2021; Published 8 November 2021

Academic Editor: Jun Liu

Liver diseases are major causes of morbidity and mortality. Dental pulp pluripotent-like stem cells (DPPSCs) are of a considerable promise in tissue engineering and regenerative medicine as a new source of tissue-specific cells; therefore, this study is aimed at demonstrating their ability to generate functional hepatocyte-like cells *in vitro*. Cells were differentiated on a collagen scaffold in serum-free media supplemented with growth factors and cytokines to recapitulate liver development. At day 5, the differentiated DPPSC cells expressed the endodermal markers FOXA1 and FOXA2. Then, the cells were derived into the hepatic lineage generating hepatocyte-like cells. In addition to the associated morphological changes, the cells expressed the hepatic genes HNF6 and AFP. The terminally differentiated hepatocyte-like cells expressed the liver functional proteins albumin and CYP3A4. In this study, we report an efficient serum-free protocol to differentiate DPPSCs into functional hepatocyte-like cells. Our approach promotes the use of DPPSCs as a new source of adult stem cells for prospective use in liver regenerative medicine.

1. Introduction

The liver is the largest internal organ providing essential metabolic, exocrine, and endocrine metabolites. Hepatocytes and cholangiocytes, the bile duct epithelial cells, are parenchymal cells which comprise approximately 70% of the adult liver mass. Both cell types are derived from the embryonic definitive endoderm [1]. The liver is the main body homeostasis regulator; therefore, liver diseases cause high morbidity and mortality rates. The incidence of end-stage liver disease (ESLD) is increasing worldwide due to alcohol-induced liver disease, nonalcoholic fatty liver disease, or hepatitis [2]. Orthotopic liver transplantation (OLT) is the current optimal treatment with more than 70% of the overall 5-year survival rate for certain ESLD cases [3]. OLT obstacles include donor availability, surgical risk, high costs, and the requirement for lifelong immunosuppressors [4, 5, 6]. Alternatively, hepatocyte transplantation (HT) is a promising

procedure, less invasive, can be performed repeatedly, and mainly used to replace an inborn-deficient metabolic function [7, 8]. Yet, HT hurtles include donor availability, low cell engraftment, and longevity [9]. Therefore, the scientific community has put an effort to improve cell-based hepatocyte generation.

Dental pulp stem cells (DPSCs) are multipotent heterogeneous cell population embedded within the pulp cavity of impacted adult third molars. DPSCs were initially isolated and characterized by Gronthos et al. [10]. Subsequently, several investigators reported DPSCs' isolation, characterization, differentiation, and banking [11, 12]. In comparison with embryonic and other adult stem cells, DPSCs are obtained from disposable dental pulp after occlusion management, which is considered as a medical waste, noninvasive isolation procedure, absence of ethical constraints, and no risk of teratoma formation. Furthermore, DPSCs do not compromise their stemness, viability, proliferation, or differentiating capabilities after cryopreservation [13, 14]. Therefore, DPSCs have the potential to be a promising personalized patient-specific stem cell source for regenerative therapy. Nevertheless, a major concern is that DPSCs comprise progenitor cell populations that are marked by diverse characteristics, such as clonal heterogeneity, multilineage differentiation, self-renewal capacity, and phenotypic complexity.

In the context of cell-based hepatogenesis, DPSC-mediated hepatocyte-like generation has advanced rapidly because of the previously accumulated differentiation protocols applied for human embryonic stem cells (hESCs) and bone marrow mesenchymal cells (BM-MSCs) as prospective sources for regenerative hepatocytes [15–20]. Implementing defined, serum-free, and stepwise differentiation protocols that mimic hepatocytes' developmental stages during embryogenesis is sufficient for inducing hepatogenesis. Using this approach, Ishkitiev et al. were the pioneers to demonstrate the hepatogenic differentiation potential of DPSCs. Initially, Ishkitiev et al. developed two staged conditioned media containing a low percentage of fetal bovine serum (FBS) but enriched with essential hepatogenic inducers [21]. Later, they used serum-free conditioned media to generate hepatocyte-like cells from $CD117^+$ DPSC subpopulation [22]. The latter hepatogenesis protocol utilized three developmental stages, i.e., cell specification, differentiation, and maturation, to generate cells with morphological, phenotypical, and functional characteristics like hepatocytes. This approach was further improved and implemented in later studies [11, 23]. Nevertheless, the heterogeneity nature of the DPSCs influences their differentiation capacity and yield; therefore, we focused our efforts to identify and characterize the differentiation potential of a defined subpopulation of DPSCs with pluripotent-like phenotype [24–28].

Dental pulp pluripotent stem cells (DPPSCs) are a unique subpopulation of DPSCs [25], expressing the pluripotency markers Oct4A, NANOG, and SOX2 [24, 29, 30]. DPPSCs exhibit normal human karyotype with no aneuploidy, polyploidy, or any chromosomal abnormality during the metaphase stage even after more than 65 passages [24, 31]. Unlike other adult stem cells, DPPSCs form teratoma-like structures when injected subcutaneously in immunodeficient mice and generate embryonic bodies like in *in vitro* cultures, which are exclusive phenotypes of hESCs and induced pluripotent stem cells (iPSCs) [24, 32–34]. Furthermore, DPPSCs can be differentiated into cells from each of the three embryonic germ layers, including osteocytes and chondrocytes [25, 26], endothelial- and neural-like cells [25, 26], and smooth and skeletal muscles [27].

In this study, we evaluated the adult DPPSC-mediated hepatogenic capacity using a novel serum free-directed stepwise differentiation protocol and collagen scaffolds to induce 3-dimensional (3D) culture conditions. DPPSCs were first differentiated into definitive endoderm (DE), which was progressively directed to the hepatogenic lineage. We observed that treatment of DPPSCs, seeded on scaffolds, with activin A (Act A), Wnt family member 3A (Wnt3A), and knockout serum replacement (KOSR) conditioned media, enhances their commitment capacity toward DE lineage. Subsequently, treatment with fibroblast growth factor 4 (FGF4) and hepatocyte growth factor (HGF) induced gut tube formation, early hepatogenic markers. Finally, functional hepatocyte-like cells were generated in conditional differentiation medium supplemented with HGF, FGF4, dexamethasone (Dex), and oncostatin M (OSM). Preliminary results were previously published in a preprint [35].

2. Materials and Methods

2.1. Ethical Approval and Statement. All the research in the present study was conducted in accordance with the code of ethics of the World Medical Association for experiments involving humans (Helsinki Declaration of 1975) and the *Guidelines for Human Stem Cell Research* issued by the Committee of Bioethics at the Universitat Internacional de Catalunya, Spain.

2.2. DPPSC Culture and Maintenance. DPPSC clones were previously isolated and characterized by our group as previously described [24, 31]. Supplementary Figures 1A and 1C show morphological differences between DPSC and DPPSCs, respectively. In brief, immediately after extraction, the third molars were vigorously washed with 70% ethanol and sterile distilled water. The molar pulp tissues were extracted, and cells were isolated by digesting the pulp tissue with collagenase type I (3 mg/ml, Sigma-Aldrich, Germany) for 60 minutes at 37°C. Then, cells were separated mechanically with an insulin syringe and centrifuged for 10 minutes at 1800 rpm. Primary cell lines were established, the medium was changed every 4 days, and cell density was maintained at a low density of 80-100 cells/cm^2. DPPSCs were cultured in precoated flasks with 100 ng/ml fibronectin (Life Technologies, Waltham, MA, USA) in a medium consisting of 60% DMEM-low glucose (Life Technologies) and 40% MCDB-201 (Sigma-Aldrich), supplemented with 1× SITE Liquid Media Supplement (Sigma-Aldrich), 1× linoleic acid-bovine serum albumin (LA-BSA, Sigma-Aldrich), 10^{-4} M L-ascorbic acid 2-phosphate (Sigma-Aldrich), 1× penicillin-streptomycin (Life Technologies), 2% fetal bovine serum (FBS, Sigma-Aldrich), 10 ng/ml hPDGF-

BB (Abcam, Waltham, MA, USA), 10 ng/ml EGF (Sigma-Aldrich), 1000 U/ml LIF (Millipore, USA), chemically defined lipid concentrate (Life Technologies), 0.8 mg/ml BSA (Sigma-Aldrich), and 55 μM β-mercaptoethanol (Sigma-Aldrich).

2.3. Definitive Endoderm Induction Using Growth Factors. For the DE induction, 5×10^4 cells/cm^2 were seeded on 6-well plates (Cellcoat, UK) and cultured in RPMI medium (Mediatech, Los Altos, CA, USA) containing GlutaMAX (Life Technologies), penicillin/streptomycin, and 0.5% defined fetal bovine serum (FBS, HyClone, Cytiva Europe GmbH, Spain) and supplemented with each one of the following combinations of growth factors: (i) 100 ng/ml Act A (R&D Systems, UK), (ii) 100 ng/ml Act A+50 ng/ml Wnt3A (R&D Systems), (iii) 100 ng/ml Act A+50 ng/ml bone morphogenetic protein-4 (BMP4, R&D Systems), (iv) 100 ng/ml Act A+50 ng/ml Wnt3A+50 ng/ml BMP4, (v) 100 ng/ml Act A+10 ng/ml FGF4 (R&D Systems), or (vi) 100 ng/ml Act A +10 ng/ml basic-FGF (bFGF, Life Technologies). Three days after induction, the medium was changed to the same RPMI-based medium and supplements except for the replacement of FBS with 2% KOSR (Life Technologies) and the incubation was maintained for another 2 days.

2.4. Definitive Endoderm Induction Using Different Biomaterials. Application of biomaterials to cell culture has been shown to enhance cellular programming and differentiation. In this study, we used collagen I or fibronectin, the most abundant components of the extracellular matrix that provide structural networks for the cells microenvironment and were reported to enhance DE differentiation *in vitro* [36, 37]. Using the sample induction media described above, cells were seeded on plates coated with collagen type I, 100 ng/ml fibronectin, or were cocultured with HepG2 cells (20,000 cell/cm^2), in addition to the controls.

2.5. Hepatogenic Differentiation. After setting the optimal conditions for DE induction, we aimed to generate stepwise functional hepatocyte-like cell. The gut tube and hepatocyte specifications were initiated using RPMI medium supplemented with 2% KOSR, 10 ng/ml FGF4, and 10 ng/ml HGF (R&D Systems). Three days later, RPMI was replaced with the enriched minimum essential medium (MEM, Sigma-Aldrich) supplemented with 1% BSA, 10 ng/ml FGF4, and 10 ng/ml HGF. Three days later, hepatocyte maturation was induced using complete hepatocyte culture medium (HCM, SingleQuots, Lonza, USA) with all supplements according to the manufacturer's recommendations, containing 10 ng/ml FGF4, 10 ng/ml HGF, 10 ng/ml OSM, and 10^{-7} M Dex (Sigma-Aldrich). The hepatocyte maturation was proceeded for nine days as previously reported by Ishkitiev et al. [21, 22]. The differentiation protocol was performed for a total of 22 days, and the media were refreshed every 2-3 days.

2.6. Immunofluorescence Microscope Imaging. Immunofluorescence was performed as described previously [38, 39]. Briefly, cells were cultured overnight on glass coverslips coated with collagen I, fixed with 4% paraformaldehyde for 15 min, and permeabilized with 10% Triton X-100 for 30 min. Then, cells were blocked with 5% BSA in PBS for 30 min and incubated for one hour with the primary antibodies: alpha-1 antitrypsin (AAT, Abcam) or albumin (Alb, Abcam) followed by a one-hour incubation with prospective secondary antibodies (Abcam). Between each step, cells were washed with 1% BSA in PBS. Fluorescent images were captured using a fluorescence microscopy Olympus AX70 (Olympus Optical, Tokyo, Japan) as previously described [40, 41].

2.7. Immunocytochemistry. Cells were fixed with ThinPrep CytoLyt solution for 30 min at room temperature and centrifuged at 5,000 rpm for 5 min. Cell's pellet was solubilized in ThinPrep CytoLyt solution and then resuspended in PreservCyt solution (ThinPrep) for 15 min and processed on a ThinPrep 2000 processor. The microscope slides harboring the processed cells were fixed with 96% ethanol, washed twice with distilled water, and blocked in 0.5% hydrogen peroxide/methanol for 10 min. Immunostainings were performed using a Leica Bond-MAX automated IHC and ISH Stainer in accordance with the manufacturer's instructions. Briefly, the slides were washed with bond wash solution (Biosystems, USA) and the antigens retrieval procedure was performed in accordance with bond heat standard protocol (ER1) using citric buffer, pH 6, for 30 min at 95°C. Slides were washed and treated with postprimary solution for 8 min. Next, the slides were incubated in alkaline phosphatase (AP)-Polymer for 8 min and washed. Then, the mixed diaminobenzidine refine solution was applied for 10 min. Samples were counterstained with water hematoxylin for 5 min. Nonimmune immunoglobulins of the same isotype as the primary antibodies were used as a control for each experiment.

2.8. RNA Extraction, cDNA Synthesis, and qRT-PCR Reactions. Total RNA was extracted from cells using the total RNA purification TRIzol Reagent (Life Technologies) in accordance with the manufacturer's protocol. RNA was quantified using a NanoDrop 2000c spectrophotometer (Thermo Fisher Scientific, Waltham, MA, USA), and RNA integrity was evaluated by 2% agarose gel electrophoresis [42]. First-strand cDNA was synthesized from 200 ng RNA by reverse transcription using QuantiTect Reverse Transcription Kit (Qiagen Inc., Germantown, MD, USA). qRT-PCR reactions were performed as previously described [43, 44]. Primer pairs with equivalent efficiencies (Table 1) were selected from PrimerBank [45] or designed using Primer-BLAST tools (http://www.ncbi.nlm.nih.gov/tools/primer-blast/) [46]. qRT-PCR was performed on the ABI7900 system (Applied Biosystems, USA) using SDS software. Relative gene expression was calculated using a comparative Ct method as previously described [47, 48]. Results were normalized to GAPDH CT values, and the relative expressions determined relative to control or day 0 undifferentiated cells. Data show the means ± standard deviation. Total liver RNA (Life Technologies) was used as a positive control.

2.9. Hepatic Biochemical Analysis of Supernatants. Hepatic enzymatic profiles for aspartate transaminase (AST), alanine

Table 1: Oligonucleotide sequences of primers utilized for real-time qRT-PCR.

Gene	Forward primer (5′-3′)	Reverse primer (5′-3′)
GAPDH	TGCACCACCAACTGCTTAGC	GGCATGGACTGTGGTCATGAG
FoxA1	GCCTACTCCTCCGTCCCGGT	CCGGGGTCATGTTGCCGCTC
FoxA2	GCGACCCCAAGACCTACAG	GGTTCTGCCGGTAGAAGGG
Gata4	TCCCTCTTCCCTCCTCAAAT	TTCCCCTAACCAGATTGTCG
AFP	AGGGTGTAGCGCTGCAAACGA	TGTTCCTGGCCTTGGCAGCAT
Oct4A	GACAGGGGGAGGGGAGGAGCTAGG	CTTCCCTCCAACCAGTTGCCCCAAAC
HNF6	CTTAGCAGCATGCAAAAGGA	TGCGTTCATGAAGAAGTTGC
CK19	GAGGAAATCAGTACGCTGAG	GTTTCTGCCAGTGTGTCTTC
HNF4α	ACTACATCAACGACCGCCAGT	ATCTGCTCGATCATCTGCCAG
Alb	CCTTGGTGTTGATTGCCTTTGCTC	CATCACATCAACCTCTGGTCTCACC
G6P	TCAGCTCAGGTGGTCCTCTT	CCTCCTTAGGCAGCCTTCTT
AAT	TCGCTACAGCCTTTGCAATG	TTGAGGGTACGGAGGAGTTCC
CYP7A1	AGGACGGTTCCTACAACATC	CGATCCAAAGGGCATGTAGT

aminotransferase (ALT), alkaline phosphatase (ALP), and gamma-glutamyl transferase (GGT) were analyzed from supernatant extracts of the different samples. The activity was measured by specific colorimetric detection kit (Linear Chemicals, Spain) at 25°C in accordance with the manufacturer's instructions. The specific compounds used for the following kinetics of the reaction were as follows: for AST and ALT, the oxidation of NADH was measured at light absorbance at 340 nm; for ALP, the formation of 4-nitrophenol was measured at light absorbance at 405 nm; for GGT, the catalysis of γ-glutamyl-3-carboxy-4-nitroanilide was measured at light absorbance at 410 nm using spectrophotometer (Thermo Fisher Scientific).

2.10. Cytochrome P450 3A4 Metabolic Activity Assay. Cytochrome P450 3A4 (CYP3A4) enzyme activity assays were assessed by measurement of luciferase activity using P450-Glo CYP3A4 assay kit (Promega, Madison, WI, USA) in accordance with the manufacturer's instructions. Differentiated and undifferentiated control DPPSC cells were treated with 25 μM rifampicin for 48 hrs. Then, treated cells were incubated with a fresh serum-free medium containing 50 μM luciferin PFBE with or without 5 μM erythromycin (an antagonist) for 30 min at 37°C. Then, 50 μl of the medium was transferred into a 96-well plate and mixed with 50 μl luciferin detection reagent to initiate the luminescent reaction. After 20 min incubation at room temperature, the luminescence was measured with a luminometer (BioTek, USA).

2.11. Albumin Assay. Alb secretion was measured by using an Albumin Fluorescence Assay Kit (Fluka, USA) in accordance with the manufacturer's instructions. Briefly, a calibration curve was generated using the kit-supplied standard human Alb concentrations. These calibration samples were mixed with albumin Blue 580 reagent prediluted in buffer solution. The fluorescence was measured in a spectrophotometer (absorbance wavelength peal, λex = 600 nm, and λem = 630 nm). Differentiated and undifferentiated control DPPSCs were mixed with the same reagents, and the fluorescence was measured under the same conditions. Results are extrapolated to the calibration curve. Conditioned medium was collected from equivalent numbers of cells.

2.12. Periodic Acid-Schiff Staining for Glycogen Accumulation. At differentiation day 22, differentiated and undifferentiated control DPPSCs were fixed in 4% formaldehyde for 15 min at room temperature. After two washing steps with PBS, cells were incubated in 1% periodic acid for 5 min and then washed with distilled water. The treated cells were incubated with Schiff's reagent (Sigma-Aldrich) for 15 min. After a 10 min wash in distilled water, hematoxylin counterstain solution was applied for 90 sec and washed with distilled water.

2.13. Statistical Analysis. Results are reported as the mean ± standard deviation (see figure legend for specific details regarding the number of biological replicates, independent experiments, and technical replicates). Statistics were performed using the Statgraphics XVI software. The methods used were two-tailed Student's t-test and ANOVA for multiple factors. Values with $p < 0.05$ were considered statistically significant.

3. Results

3.1. Definitive Endoderm Induction. Using hESCs, iPSCs, and human umbilical cord Wharton's jelly mesenchymal stem cells, studies have shown that Act A is the main DE induction factor [49, 50, 51, 52]. Therefore, we tested this concept on DPPSCs using Act A with or without other signaling factors to delineate the optimal conditional media sufficient to mediate DE differentiation. Quantitative real-time PCR (qRT-PCR) analyses demonstrated a differential induction of the DE genes Forkhead Boxes A1 and A2 (FoxA1 and FoxA2) at day 5. FoxA1 transcripts elevated significantly in conditional media supplemented with Act

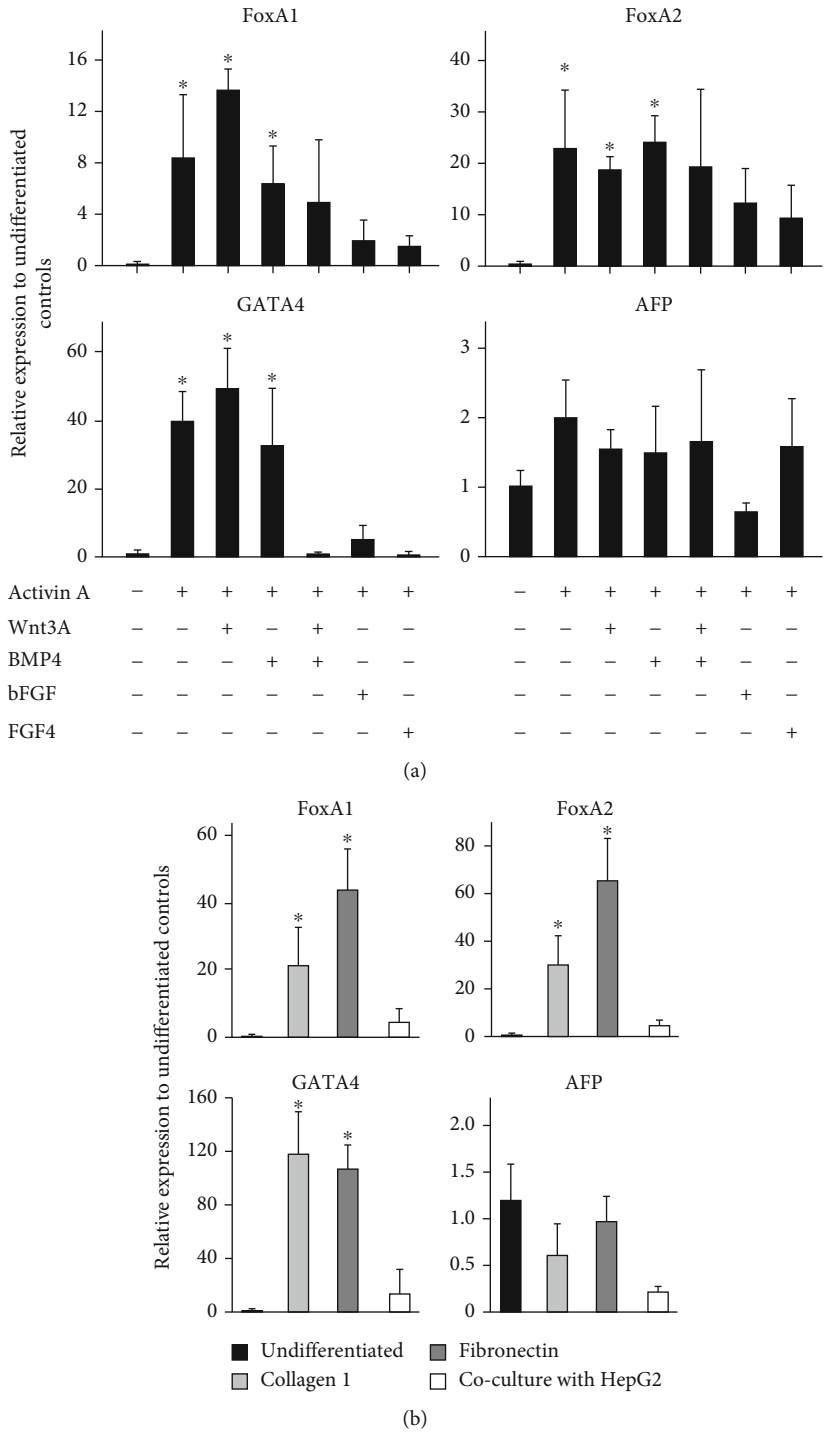

Figure 1: Molecular evaluation of different signaling factors and biomaterials on the generation of definitive endoderm lineage. qRT-PCR was performed for the indicated genes at day 5 of DPPSC differentiation into DE lineage. (a) Cells treated with differentiation conditional media supplemented with indicated signaling factors. (b) Cells were seeded on precoated plates with/without the described scaffolds or cocultured with HepG2 cells. Results were normalized to GAPDH and expressed relative to undifferentiated cells at day. Data are shown as the mean ± SD ($n = 4$). $^{*}p < 0.05$.

A and Wnt3A, 14-fold relative to undifferentiated cells (Figure 1(a)). Similar induction levels were also observed in cells treated with Act A alone or Act A and BMP4, but albeit to a lower degree (6- to 8-fold) and notable variations between different experiments. Alternatively, FoxA2 expression levels were comparable in all tested conditional media, with a statistically significant 20-fold induction in media supplemented with Act A alone, and with Wnt3A or BMP4. Remarkably, conditional media supplemented with Act A and bFGF or FGF4 failed to significantly upregulate

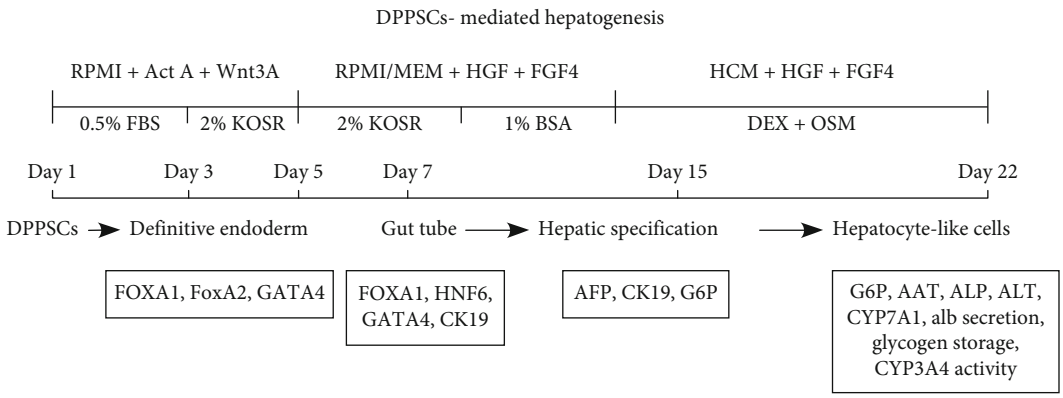

Figure 2: The experimental protocol for DPPSC-mediated hepatocyte-like cell generation. Schematic representation of the differentiation protocol including the key manipulated signaling pathways and the different molecular and functional studies performed.

the studied DE genes. Moreover, qRT-PCR analyses indicated an elevation in the transcript levels of GATA4, with a 40 to 60-fold increase relative to undifferentiated cells, posttreatment with Act A alone or in the presence of Wnt3A or BMP4 (Figure 1(a)). In contrary, no GATA4 transcripts were detected in conditional media containing the three signaling factors together (Figure 1(a)). Noticeably, Act A failed to induce GATA4 in media supplemented with either bFGF or FGF4 (Figure 1(a)).

Worthy to note that at day 5, no significant upregulation of visceral endoderm and the early hepatogenic marker alpha-fetoprotein (AFP) in cells treated with the studied conditional media, suggesting that Act A and other signaling molecules do not support visceral endoderm lineage differentiation and are not sufficient for hepatogenic specification. Taken together, the increase in expression levels of bona-fide DE markers in conditional media supplemented with Act A alone or with Wnt3A suggests that our approaches using chemically defined differentiation conditions have successfully enriched the DE lineage of DPPSCs. Due to the experimental variations in the transcript levels of the DE genes in cells treated with conditional media supplemented with Act A alone, therefore, the following experiments were carried out using Act A and Wnt3A as the main induction cytokines.

It is well documented that biomaterials in cell cultures support viability, differentiation, maturation, and long-term function [36, 53]. To further improve the differentiation protocol and study the influence of biomaterials on DPPSC-mediated DE indication, we perused DE differentiation under three different conditions: cells were cultured on plates precoated with collagen I, fibronectin, or cocultured with HepG2 cells for 5 days.

Interestingly, the DE marker gene expression was significantly elevated in DPPSCs differentiated on the scaffolds (Figure 1(b)) versus on no scaffolds (Figure 1(a)). Relative to DPPSCs differentiated on plain plates (Figure 1(a)), FOXA1 transcript levels in cells differentiated on collagen I or fibronectin were 3- to 4-fold higher, respectively. Similarly, the expression levels of FOXA2 mRNA were elevated by 1.5- to 3-fold when cells were differentiated on the scaffolds (Figure 1(b)). qRT-PCR analyses of GATA4 transcripts were significantly enriched in cells differentiated with collagen I or fibronectin, 120-fold increase relative to undifferentiation cells, at day 5 (Figure 1(b)). No DE marker gene expressions were detected in DPPSCs cocultured with HepG2, suggesting a differentiation suppression effect of hepatic cells (Figure 1(b)). Furthermore, the used biomaterials did not facilitate prospective generation of visceral endoderm cells and did not support early hepatogenic specification, since AFP transcripts were not detected. In summary, biomaterial usage enhanced DPPSC-mediated DE differentiation. Since collagen I is an affordable, inexpensive substrate, and commonly used in stem cell studies, we use it as the scaffold to induce hepatogenic differentiation.

3.2. Hepatic Specification and Maturation. We investigated the developmental progress in the hepatogenic differentiation potential of DPPSCs using a two-step protocol, which is schematically illustrated and presented in Figure 2. At day 5 after DE induction, the conditional media were supplemented with FGF4 and HGF, for 8 days, to enrich for hepatic cell specification, followed by an 8-day culture in HCM supplemented with hepatogenic inducers such as OSM and Dex in addition to the growth factors (Figure 2).

As we have previously reported, DPPSCs grow as a flat monolayer and exhibit a small spindle-shaped fibroblast-like morphology when cultured on polystyrene tissue culture plates or scaffolds (Figure 3(a)) [25]. During the differentiation induction period, DPPSC morphology further changed to a round or epithelioid shape, a characteristic of DE cells (Figure 3(b)) [54]. At day 7, the cells became flat and tightly packed, and by day 22, they adopted a hepatocyte-like morphology (Figures 3(c)–3(e)). In contrast, undifferentiated cells cultured in regular growth medium containing FBS leaned toward an elongated spindle-shaped fibroblastic morphology (Figure 3(f)).

At the molecular level, gene expression studies revealed a distinct early posterior foregut signature at day 7 of DPPSC differentiation. The transcript levels of hepatic nuclear factor 6 (HNF6) and cytokeratin 19 (CK19) were notably elevated at day 7, relative to undifferentiated cells (Figure 4), indicating a significant commitment toward the foregut tube. Although the transcripts of GATA4 were

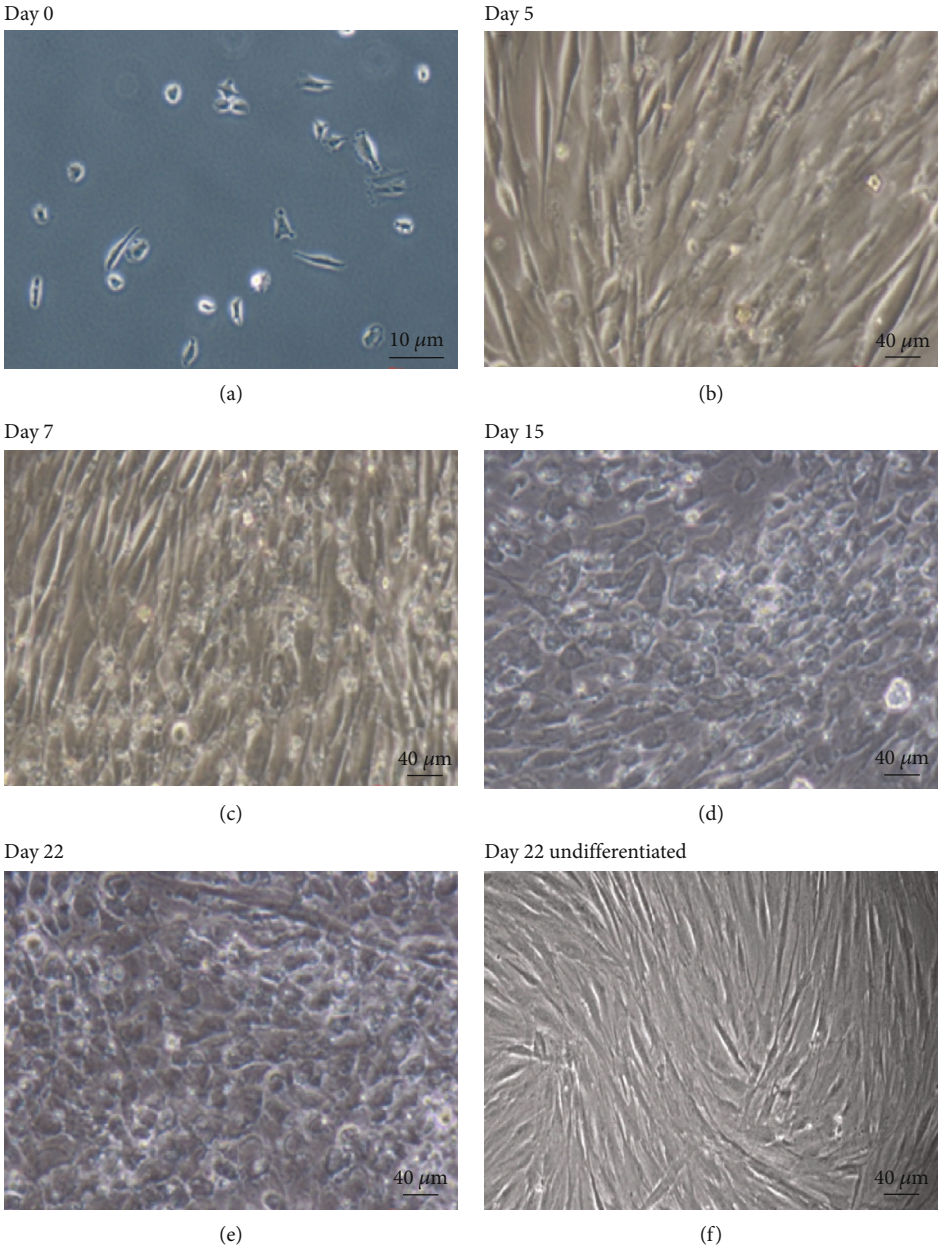

Figure 3: Changes of cellular morphological during the time course of DPPSC-mediated hepatocyte-like cells. Phase-contrast representative images of DPPSCs at different stages of differentiation from day 0 to day 22 and undifferentiated cells at day 22. Scale: (a) 100x magnification and (b–f) 200x magnification.

upregulated at day 5 (Figure 1(b)), simultaneously with the DE markers, its elevated expression levels were maintained until day 7 unlike FoxA1 mRNA levels which were significantly reduced at day 7. This observation is likely due to a possible commitment of a small cell fraction to DE lineage and/or a significant profile of these genes in the early posterior foregut (Figure 4) [52, 55].

Next, the developmental progress of differentiated DPPSCs toward hepatogenic specification was investigated at day 14 of treatment with conditional media. A notable reduction in the expression levels of the foregut tube markers was observed, concomitant with a significant increase in AFP transcripts (Figure 4), which was not observed in earlier stages of differentiation, indicating a progression toward early hepatic specification. In addition, moderate levels of hepatic markers' transcripts were noticed at day 14 (Figure 4), including hepatic nuclear factor 4α (HNF4α), glucose 6-phosphate (G6P), and cholesterol 7 alpha-hydroxylase (CYP7A1). The induction of hepatogenic markers inspired us investigate the differentiation efficiency using flow cytometry. The differentiation protocol resulted in a notable enrichment of prehepatocyte-like cells with

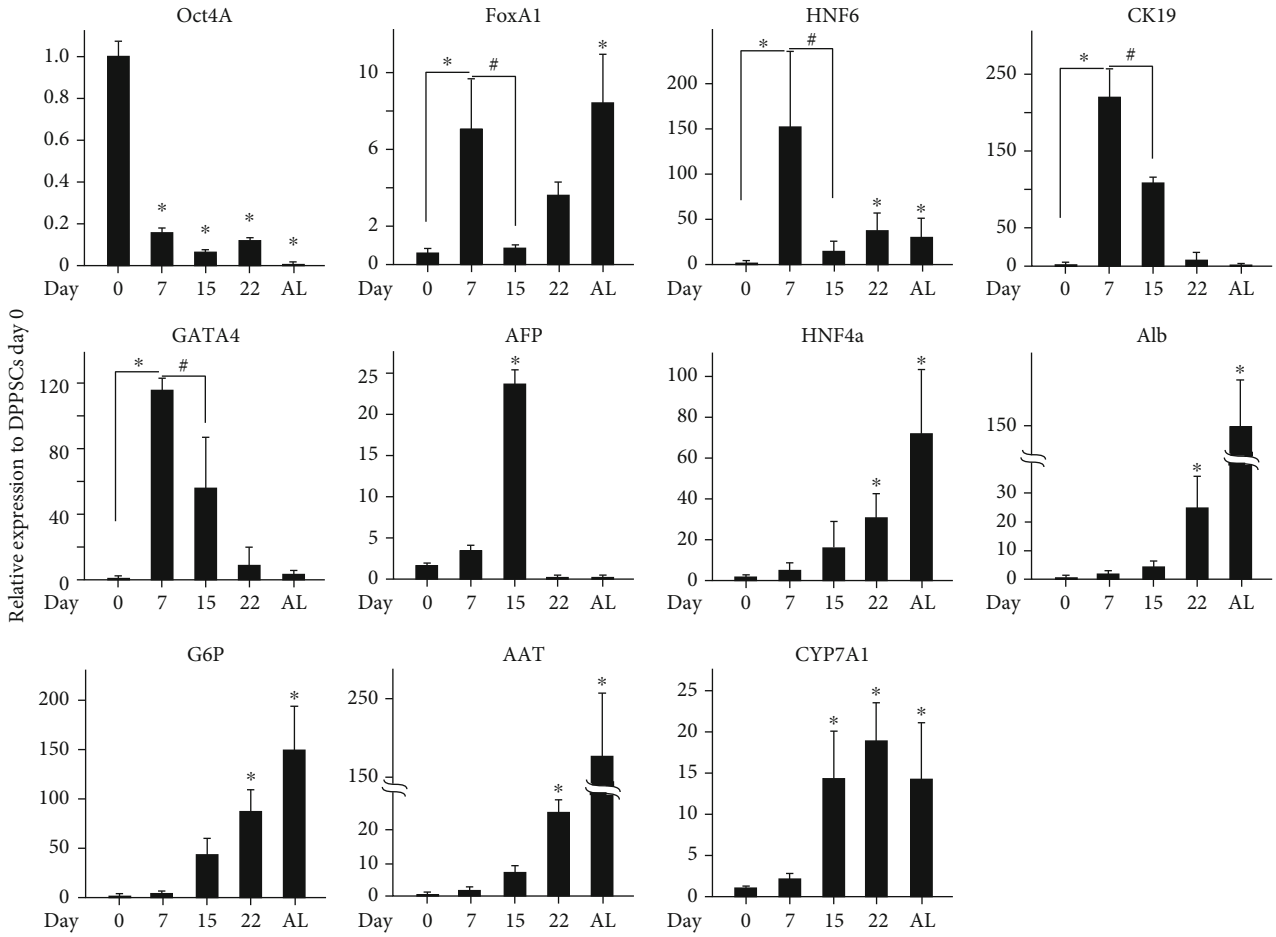

Figure 4: Molecular and cellular evaluation of DPPSC-mediated hepatocyte-like cells. Time course qRT-PCR analysis for lineage-specific gene expression. The differentiation was performed using the previously described experimental protocol. Total RNA was harvested from the cells at the indicated days for gene expression. Results were normalized to GAPDH and expressed relatively to DPPSCs at day 0. $^{*}p < 0.05$ and $^{\#}p < 0.05$ relative to day 7. Data are shown as the mean ± SD ($n = 4$).

44% of the total cell counts which were positive to AFP proteins at differentiation day 14 (Supplementary Figures 1C and 1D).

Simultaneously, an eight-day treatment of these committed DPSSCs with HCM supplemented hepatic induction molecules resulted in a significantly exaggeration in the expression levels of the hepatic markers at differentiation day 22. Relative to undifferentiated DPPSCs, the HNF4α and Alb transcripts were 40-and 15-fold higher, AAT and CYP7A1 transcripts were 20-fold higher, and G6P mRNA levels were 100-fold higher at day 22 (Figure 4). Taken together, we implemented an optimized a 3-stage protocol that directed a stepwise differentiation of DPPSCs to the hepatocyte-like cell populations.

3.3. DPPSC-Derived Hepatocyte-Like Cells Demonstrate Hepatic Function. Next, to corroborate the qRT-PCR analysis and evaluate the differentiation efficiency, we ascertained the protein expression of the hepatogenic markers by immunolocalization and functional analysis. Immunofluorescence with specific antibodies directed against AAT and Alb proteins revealed a significant expression of these hepatic markers at day 22 of DPPSC differentiation (Figures 5(a) and 5(b)).

Mature hepatocytes are characterized by their ability to store glycogen [56]. Interestingly, most of the differentiated DPPSCs showed a significant positive periodic acid-Schiff (PAS) staining in the cytoplasm, albeit to a different degree, at day 22 (Figure 5(c) and Supplementary Figure 2), which is indicative for glycogen storage, and the generation of mature hepatocyte-like cells. Alternatively, no PAS staining was detected in undifferentiated cells (Figure 5(d)).

Then, we investigated the activity of hepatic metabolic enzymes. Time course studies performed on protein extracts from differentiated DPPSCs for GGT, AST, ALP, and ALT activities revealed a time-dependent upregulation of liver metabolic enzymes which beaked at day 18 of differentiation (Figures 6(a)–6(d), respectively). Furthermore, the enzymatic activity of CYP3A4 was significantly induced in differentiated DPPSCs after treatment with rifampicin, 5-fold relative to untreated cells. Cotreatment with erythromycin, a CYP3A4 inhibitor, significantly downregulated the observed enzymatic action against rifampicin (Figure 6(e)).

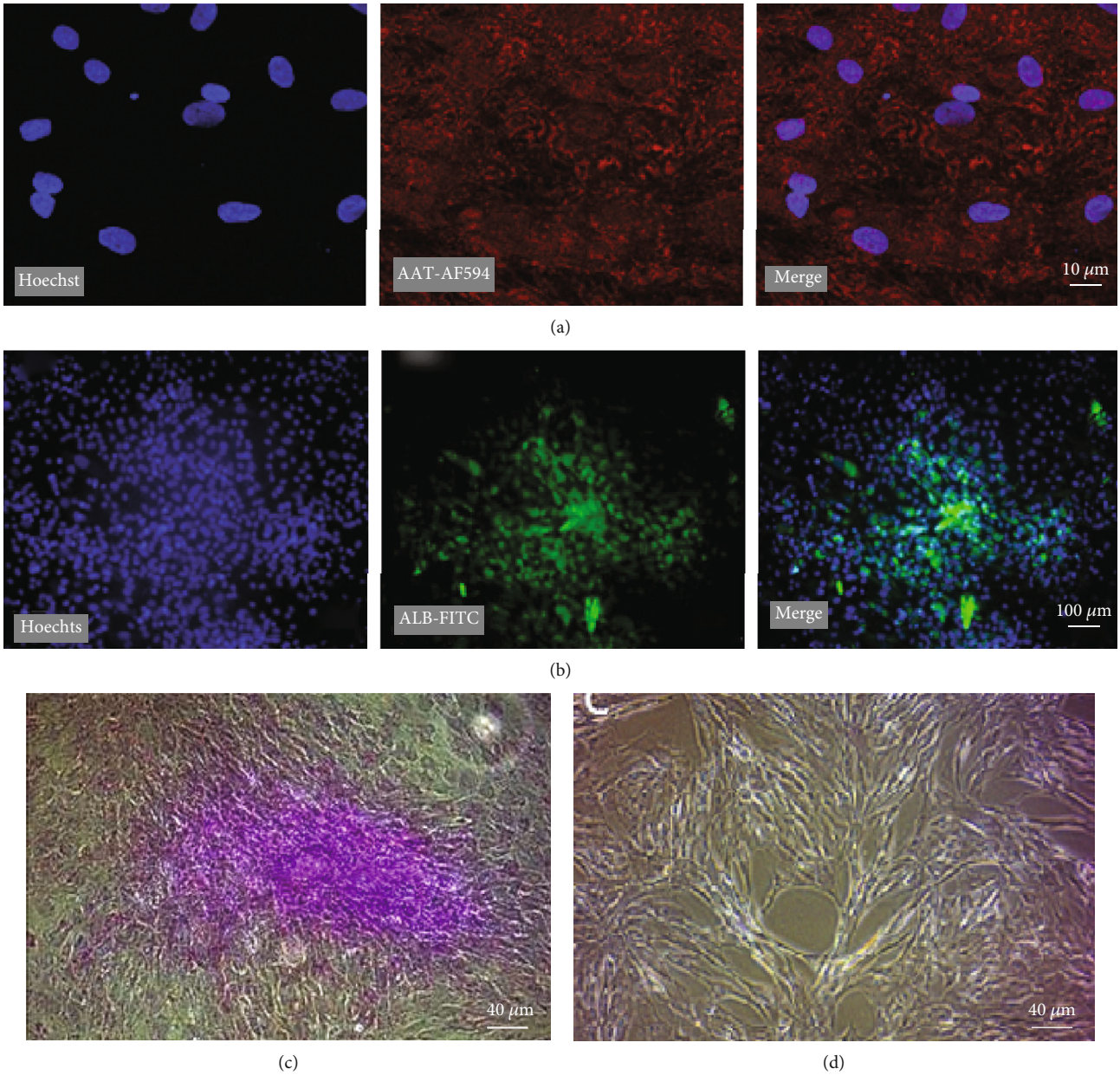

Figure 5: Protein expression and glycogen storage of DPPSC-mediated hepatocyte-like cells. (a, b) Representative fluorescence microscopy images of DPPSC-mediated hepatocyte-like cells at day 22, immunoassayed with antibodies directed against (a) AAT (AF594, red) and (b) ALB (FITC, green) proteins. Hoechst nuclear marker in blue. 200x magnification. (c, d) Representative light microscope images of differentiated and undifferentiated DPPSCs at day 22, respectively, stained with periodic acid-Schiff (PAS) for glycogen storage detection. 100x magnification.

Alb secretion was assayed at the time course of the differentiation process. As shown in Figure 6(f), at earlier stages of hepatogenesis, day 16 of differentiation, a limited amount of secreted Alb was detected in the media. However, at differentiation days 19 and 22, the amount of secreted albumin was triplicated into 3.5 μg/mg protein (Figure 6(f)). Taking these observations together, the described differentiation protocol (Figure 2) efficiently induced the generation of DPPSC-mediated functional hepatocyte-like cells and indicates that DPPSCs are a useful cell model for hepatogenesis.

4. Discussion

The current strategy in stem cell differentiation protocols is to mimic cellular signaling events associated with the embryonic developmental process for the lineage of interest [8, 47, 48]. However, *in vitro* cell differentiation gives a broad range of outcome lineages; thus, the development of a protocol that significantly improves a targeted cell type is of particular interest [49]. Targeted differentiation requires culturing the cells in chemically well-defined media, which regulate cell

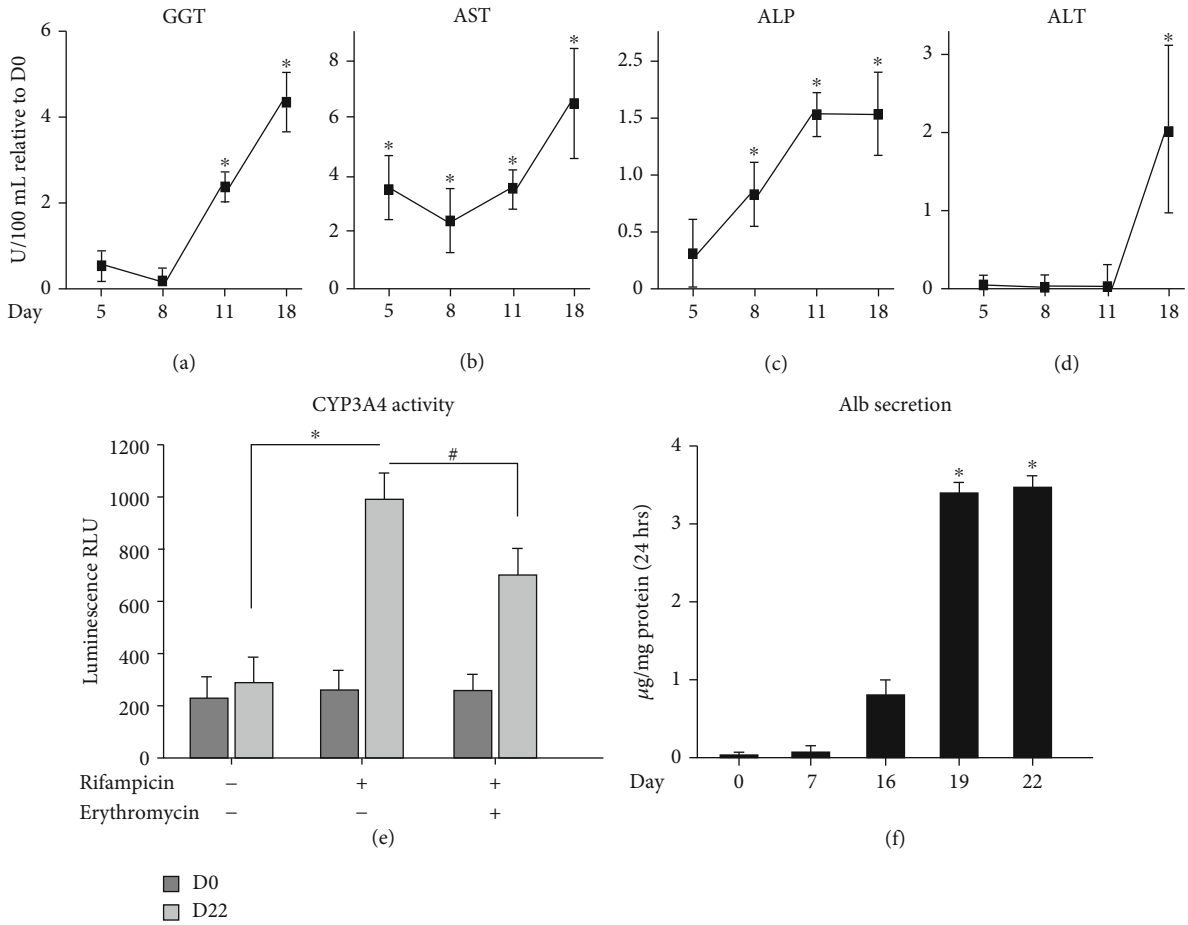

Figure 6: Functional analysis of the generated DPPSC-mediated hepatocyte-like cells. Time course hepatocyte enzymatic activities of (a) GGT, (b) AST, (c) APF, and (d) ALT were performed for the differentiated DPPSCs. A notable induction was observed at day 18. (e) CYP3A4 activity was measured by luminescence in DPPSCs at day 0 and day 22 of differentiation using rifampicin in the presence or absence of the antagonist erythromycin. (f) Alb secretion assay was performed at a time course differentiated DPPSCs; elevated level of secreted Alb was detected at day 19 and later. All measurements are relative to DPPSCs at day 0. $^{*}p < 0.05$ and $^{\#}p < 0.05$ relative to rifampicin treatment alone. Data are shown as the mean ± SD ($n = 4$).

signaling pathways, resulting in the generation of cell type of interest. This approach has been successfully applied to hESCs and iPSCs [51–53], but has yet to be applied to other pluripotent cell types, including adult DPPSCs.

In this study, we applied an optimized 3D and 3-stage protocol directed toward a stepwise differentiation of DPPSCs to hepatocyte-like cells. For efficient differentiation, cells were checked at each developmental stage using lineage-specific markers. Initially, DPPSCs were cultured for 5 days in differentiation media supplemented with Act A, with or without Wnt3a, BMP4, or the growth factors bFGF and FGF4. Interestingly, Act A alone was sufficient to induce DE differentiation. Our results are in accordance with the reported role of Act A inducing DE from pluripotent stem cells [55, 57]. It is well known that nodal signaling is required for endoderm specification during the gastrulation [58]. Furthermore, DE induction depends on the duration of exposure to the stimulation factors. Agarwal et al. reported that 5-day incubations are sufficient to induce DE [49].

Media supplemented with Act A and Wnt3A were superior in inducing DE lineage [57, 59]. Using hESCs, Mathew et al. observed an enhanced DE induction using Act A and Wnt3A supplemented media compared to media contained Act A alone [51]. Like hESCs, in this study, we observed an improved induction of DE markers in DPPSCs cultured with Act A and Wnt3A. Alternatively, the growth factors bFGF or FGF4 suppressed Act A-mediated DE induction [60]. Noteworthy, FGF family members are multifunctional factors. They can maintain hESC pluripotency [61] or DE mediator [62], depending on the associated conditions.

During liver development, the BMP signaling is crucial; however, their functional role during *in vitro* adult stem cell differentiation is not clear. Cultural media supplemented with BMP2 and BMP4 fail to improve hepatogenesis from adipose tissue stem cell [63]. In accordance with the other studies, our results confirmed that the BMP4 signaling has no functional role during DPPSC differentiation into DE reconciled by Act A induction. Otherwise, studies have

shown that a combination of Act A and the BMP4 signaling induces mesoderm formation [64]. Notably, DE induction was further enhanced using three-dimensional (3D) scaffolds. Treatment with either collagen or fibronectin upregulated DE markers indicated that 3D enhances the cellular programming potential, which is in accordance with previously reported observations using hESCs, iPSCs, and other mesenchymal stem cells [36, 37, 65].

The use of minimal amount of FBS in differentiation media has been previously reported to inhibit the PI3K signaling [66], which is necessary to enhance Act A-mediated DE generation. Using 0.5% FBS during the first 5 days of DE induction, D'Amour and her team observed an enhancement in the expression of Sox17 or FoxA2 in hESCs [57]. In our protocol, we used 0.5% FBS media for the first 3 days of differentiation. Then, it was replaced with 2% KOSR for extra 4 days, a serum that has been proven to be effective and suitable with defined components [49]. At differentiation days 7-22, KOSR was removed and hepatogenic lineage induction was carried on with serum-free conditional culture media. As descripted in the schematic Figure 2, the growth factors FGF4 and HGF were used to induce hepatogenesis, followed by the usage of OSM with Dex for the hepatocytes' maturation. The role of FGF4 and HGF in hepatocyte specification has been previously reported for both Wharton's jelly and bone marrow mesenchymal stem cells [67–69]. In accordance, both FGF4 and HGF were required to mediate hepatic specification in DPPSCs. We observed an improved expression of several hepatic markers including immature and mature markers at day 13 of differentiation.

Studies have shown that the interleukin-6 family cytokine (OSM) is required for hepatocyte maturation in combination with glucocorticoids, such as Dex [70, 71]. Additionally, it is well documented that HGF, EGF, and OSM have decisive effects on the maintenance of primary human hepatocytes *in vitro* [72]. The combination of HGF, OSM, and Dex is widely used in protocols to differentiate stem cells into hepatocytes [49, 73]. In our protocol, we applied the maturation factors OSM and Dex at day 13 posting commitment to the hepatic fate. Consequently, we documented hepatocyte-like cell maturation using cellular and molecular techniques. After 15 days of exposure to media containing OSM and Dex, we observed changes in cell morphology with hepatocyte-like structures, which was associated with Alb secretion, and the activation of hepatic-specific enzymes.

After the establishment of the most optimal protocol used for DPPSC, we performed the tests that were available for us to prove the efficacy of the differentiation of DPPSC into hepatocyte-like cells. At the molecular level, differentiated DPPSC expressed AAT, Alb, and G6P transcripts, genes that are markers for mature hepatocytes. Moreover, the protein expression of these markers was also documented in our study. Cellular morphological changes were also detected, and mature cells acquired a polygonal shape typical for hepatocytes [74]. In addition, DPPSC-mediated hepatocyte-like cells were functional. These cells stored glycogen, secreted Alb, and other metabolic enzymes as efficient as other stem cell models used for hepatogenesis including MSCs [39] and hESCs [75, 76]. Furthermore, differentiated DPPSCs have shown an improved Cyp3A4 enzymatic activity, suggesting that the generated hepatocyte-like cells can be used as a model for drug metabolism, which would be useful for the pharmaceutical industry [77].

5. Conclusions

We designed a novel protocol to differentiate the adult DPPSCs into functional hepatocyte-like cells. Our protocol is a directed differentiation protocol mimicking the stepwise process observed during embryonic liver development. Using DPPSCs as pluripotent-like stem cell models suggests their potential usage for liver regenerative medicine and prospective treatments to be developed in the future. However, for clinical applications, there are still many studies that are needed to be improved, yet the generated functional DPPSC-mediated hepatocyte-like cells can be used as a model for drug screening, hepatic metabolism studies, and hepatic disease applications.

Abbreviations

AST: Aspartate aminotransferase
BAL: Bioartificial liver
CGH: Chromosome genomic hybridization
DEX: Dexamethasone
DPMSCs: Dental pulp mesenchymal stem cells
DPPSCs: Dental pulp pluripotent stem cells
EB: Embryoid bodies
ECM: Extracellular matrix
ESDL: End-stage liver disease
GGT: Gamma-glutamyl transferase
HB: Hepatoblasts
HCC: Hepatocellular carcinoma
HT: Hepatocyte transplantation
MSC: Mesenchymal stromal cells
OLT: Orthotopic liver transplantation
OSM: Oncostatin M.

Data Availability

All data are available upon request.

Disclosure

A preprint has previously been published [35].

Conflicts of Interest

The authors declare no conflicts of interest.

Authors' Contributions

C.G.R. is responsible for the collection and assembly of data and first manuscript draft. S.M. and S.A.D. are responsible for the data analysis and interpretation. M.A.A. and C.M. are responsible for the statistical analysis. E.F.P. and E.F.A are responsible for the provision of study patients and cell isolation. M.B., A.A.M., and M.A. are responsible for the

conception and design, collection and assembly of data, data analysis and interpretation, manuscript writing, and final approval of the manuscript.

Acknowledgments

The authors would like to thank Dr. Cámara Vallejo at Oral and Maxillofacial Surgery Department, Hospital Clinico de Barcelona, Barcelona, Spain, for patient's recruitment and molar extractions. This study was funded by the Universitat Internacional de Catalunya (UIC), the Agència de Gestió d'Ajuts Universitaris i de Recerca, Generalitat de Catalunya project number (SGR 1060 for MA), the Kuwait Foundation for the Advancement of Sciences (KFAS), and the Dasman Diabetes Institute under project number (RA-2013-009 for AAM). CGR, EMS, and RNT were funded by the predoctoral grant Junior Faculty award from the Obra Social, "la Caixa" Foundation, and UIC.

Supplementary Materials

Supplementary 1. Supplementary Figure 1: morphological differences between DPSCs and the subpopulation DPPSCs. (A, B) Representative images for DPSC population and isolated DPPSC subpopulation, respectively, showing morphological differences between the two cell populations. (C, D) Representative image for flow cytometry assay showing the expression of GATA4 (green) and AFP (red) markers (yellow color represents cells that overexpress both markers) of DPPSC differentiated to hepatocyte-like cells at day 14. Hoechst nuclear marker in blue.

Supplementary 2. Supplementary Figure 2: DPPSC-mediated hepatocyte-like cells at differentiation day 22 stained. (A) PAS-unstained cells and (B) PAS-stained cells indicate the ability to store glycogen at this differentiation day. The generated hepatocyte-like cells possess a semipolygonal shape.

References

[1] A. M. Zorn, *Liver Development*, StemBook, Cambridge (MA), 2008.

[2] M. Blachier, H. Leleu, M. Peck-Radosavljevic, D. C. Valla, and F. Roudot-Thoraval, "The burden of liver disease in Europe: a review of available epidemiological data," *Journal of Hepatology*, vol. 58, no. 3, pp. 593–608, 2013.

[3] M. F. Dawwas, A. E. Gimson, J. D. Lewsey, L. P. Copley, and J. H. van der Meulen, "Survival after liver transplantation in the United Kingdom and Ireland compared with the United States," *Gut*, vol. 56, no. 11, pp. 1606–1613, 2007.

[4] J. Neuberger, "An update on liver transplantation: a critical review," *Journal of Autoimmunity*, vol. 66, pp. 51–59, 2016.

[5] V. Iansante, R. R. Mitry, C. Filippi, E. Fitzpatrick, and A. Dhawan, "Human hepatocyte transplantation for liver disease: current status and future perspectives," *Pediatric Research*, vol. 83, no. 1-2, pp. 232–240, 2018.

[6] J. A. Wertheim, H. Petrowsky, S. Saab, J. W. Kupiec-Weglinski, and R. W. Busuttil, "Major challenges limiting liver transplantation in the United States," *American Journal of Transplantation : official journal of the American Society of Transplantation and the American Society of Transplant Surgeons*, vol. 11, no. 9, pp. 1773–1784, 2011.

[7] A. Dhawan, R. R. Mitry, and R. D. Hughes, "Hepatocyte transplantation for liver-based metabolic disorders," *Journal of Inherited Metabolic Disease*, vol. 29, no. 2-3, pp. 431–435, 2006.

[8] F. Wang, L. Zhou, X. Ma et al., "Monitoring of intrasplenic hepatocyte transplantation for acute-on-chronic liver failure: a prospective five-year follow-up study," *Transplantation Proceedings*, vol. 46, no. 1, pp. 192–198, 2014.

[9] M. Ott and J. V. Castell, "Hepatocyte transplantation, a step forward?," *Journal of Hepatology*, vol. 70, no. 6, pp. 1049-1050, 2019.

[10] S. Gronthos, M. Mankani, J. Brahim, P. G. Robey, and S. Shi, "Postnatal human dental pulp stem cells (DPSCs) in vitro and in vivo," *Proceedings of the National Academy of Sciences of the United States of America*, vol. 97, no. 25, pp. 13625–13630, 2000.

[11] F. Ferro, R. Spelat, A. P. Beltrami, D. Cesselli, and F. Curcio, "Isolation and characterization of human dental pulp derived stem cells by using media containing low human serum percentage as clinical grade substitutes for bovine serum," *PLoS One*, vol. 7, no. 11, article e48945, 2012.

[12] V. Tirino, F. Paino, A. De Rosa, and G. Papaccio, "Identification, isolation, characterization, and banking of human dental pulp stem cells," *Methods in Molecular Biology*, vol. 879, pp. 443–463, 2012.

[13] W. Zhang, X. F. Walboomers, S. Shi, M. Fan, and J. A. Jansen, "Multilineage differentiation potential of stem cells derived from human dental pulp after cryopreservation," *Tissue Engineering*, vol. 12, no. 10, pp. 2813–2823, 2006.

[14] N. Pilbauerova, T. Soukup, T. Suchankova Kleplova, J. Schmidt, and J. Suchanek, "The effect of cultivation passaging on the relative telomere length and proliferation capacity of dental pulp stem cells," *Biomolecules*, vol. 11, 2021.

[15] L. Rambhatla, C. P. Chiu, P. Kundu, Y. Peng, and M. K. Carpenter, "Generation of hepatocyte-like cells from human embryonic stem cells," *Cell Transplantation*, vol. 12, no. 1, pp. 1–11, 2003.

[16] Y. F. Chen, C. Y. Tseng, H. W. Wang, H. C. Kuo, V. W. Yang, and O. K. Lee, "Rapid generation of mature hepatocyte-like cells from human induced pluripotent stem cells by an efficient three-step protocol," *Hepatology*, vol. 55, no. 4, pp. 1193–1203, 2012.

[17] K. Si-Tayeb, F. K. Noto, M. Nagaoka et al., "Highly efficient generation of human hepatocyte-like cells from induced pluripotent stem cells," *Hepatology*, vol. 51, no. 1, pp. 297–305, 2010.

[18] K. D. Lee, T. K. Kuo, J. Whang-Peng et al., "In vitro hepatic differentiation of human mesenchymal stem cells," *Hepatology*, vol. 40, no. 6, pp. 1275–1284, 2004.

[19] A. Banas, T. Teratani, Y. Yamamoto et al., "Adipose tissue-derived mesenchymal stem cells as a source of human hepatocytes," *Hepatology*, vol. 46, no. 1, pp. 219–228, 2007.

[20] M. J. Seo, S. Y. Suh, Y. C. Bae, and J. S. Jung, "Differentiation of human adipose stromal cells into hepatic lineage in vitro and in vivo," *Biochemical and Biophysical Research Communications*, vol. 328, no. 1, pp. 258–264, 2005.

[21] N. Ishkitiev, K. Yaegaki, B. Calenic et al., "Deciduous and Permanent Dental Pulp Mesenchymal Cells Acquire Hepatic

Morphologic and Functional Features _In Vitro_," *Journal of Endodontia*, vol. 36, no. 3, pp. 469–474, 2010.

[22] N. Ishkitiev, K. Yaegaki, T. Imai et al., "High-purity hepatic lineage differentiated from dental pulp stem cells in serum-free medium," *Journal of Endodontics*, vol. 38, no. 4, pp. 475–480, 2012.

[23] A. Kumar, V. Kumar, V. Rattan, V. Jha, A. Pal, and S. Bhattacharyya, "Molecular spectrum of secretome regulates the relative hepatogenic potential of mesenchymal stem cells from bone marrow and dental tissue," *Scientific Reports*, vol. 7, no. 1, p. 15015, 2017.

[24] M. Atari, C. Gil-Recio, M. Fabregat et al., "Dental pulp of the third molar: a new source of pluripotent-like stem cells," *Journal of Cell Science*, vol. 125, Part 14, pp. 3343–3356, 2012.

[25] M. Atari, M. Barajas, F. Hernandez-Alfaro et al., "Isolation of pluripotent stem cells from human third molar dental pulp," *Histology and Histopathology*, vol. 26, no. 8, pp. 1057–1070, 2011.

[26] M. Atari, J. Caballe-Serrano, C. Gil-Recio et al., "The enhancement of osteogenesis through the use of dental pulp pluripotent stem cells in 3D," *Bone*, vol. 50, no. 4, pp. 930–941, 2012.

[27] E. Martinez-Sarra, S. Montori, C. Gil-Recio et al., "Human dental pulp pluripotent-like stem cells promote wound healing and muscle regeneration," *Stem Cell Research & Therapy*, vol. 8, no. 1, p. 175, 2017.

[28] R. Nunez-Toldra, P. Dosta, S. Montori, V. Ramos, M. Atari, and S. Borros, "Improvement of osteogenesis in dental pulp pluripotent-like stem cells by oligopeptide-modified poly(β-amino ester)s," *Acta Biomaterialia*, vol. 53, pp. 152–164, 2017.

[29] F. Ferro, R. Spelat, F. D'Aurizio et al., "Dental pulp stem cells differentiation reveals new insights in Oct4A dynamics," *PLoS One*, vol. 7, no. 7, article e41774, 2012.

[30] F. N. Faruqu, S. Zhou, N. Sami, F. Gheidari, H. Lu, and K. T. Al-Jamal, "Three-dimensional culture of dental pulp pluripotent-like stem cells (DPPSCs) enhancesNanogexpression and provides a serum-free condition for exosome isolation," *FASEB BioAdvances*, vol. 2, no. 7, pp. 419–433, 2020.

[31] R. Nunez-Toldra, E. Martinez-Sarra, C. Gil-Recio et al., "Dental pulp pluripotent-like stem cells (DPPSC), a new stem cell population with chromosomal stability and osteogenic capacity for biomaterials evaluation," *BMC Cell Biology*, vol. 18, no. 1, p. 21, 2017.

[32] R. V. Nelakanti, N. G. Kooreman, and J. C. Wu, "Teratoma formation: a tool for monitoring pluripotency in stem cell research," *Current Protocols in Stem Cell Biology*, vol. 32, pp. 4A.8.1–4A.8.17, 2015.

[33] H. Hentze, P. L. Soong, S. T. Wang, B. W. Phillips, T. C. Putti, and N. R. Dunn, "Teratoma formation by human embryonic stem cells: evaluation of essential parameters for future safety studies," *Stem Cell Research*, vol. 2, no. 3, pp. 198–210, 2009.

[34] K. Zeevaert, M. H. Elsafi Mabrouk, W. Wagner, and R. Goetzke, "Cell mechanics in embryoid bodies," *Cells*, vol. 9, no. 10, p. 2270, 2020.

[35] C. Gil-Recio, S. Montori, C. Vallejo et al., "Direct differentiation of dental pulp pluripotent-like stem cells differentiation into hepatocyte-like cells," *bioRxiv*, 2020.

[36] S. Nakai, I. Shibata, T. Shitamichi et al., "Collagen vitrigel promotes hepatocytic differentiation of induced pluripotent stem cells into functional hepatocyte-like cells," *Biology open*, vol. 8, 2019.

[37] C. H. Rasmussen, D. R. Petersen, J. B. Moeller, M. Hansson, and M. Dufva, "Collagen type I improves the differentiation of human embryonic stem cells towards definitive endoderm," *PLoS One*, vol. 10, no. 12, article e0145389, 2015.

[38] A. Al Madhoun, S. K. Marafie, D. Haddad et al., "Comparative proteomic analysis identifies EphA2 as a specific cell surface marker for Wharton's jelly-derived mesenchymal stem cells," *International journal of molecular sciences*, vol. 21, no. 17, p. 6437, 2020.

[39] F. Al-Rashed, S. Sindhu, H. Arefanian et al., "Repetitive intermittent hyperglycemia drives the M1 polarization and inflammatory responses in THP-1 macrophages through the mechanism involving the TLR4-IRF5 pathway," *Cell*, vol. 9, no. 8, p. 1892, 2020.

[40] A. Al Madhoun, S. Alkandari, H. Ali et al., "Chemically defined conditions mediate an efficient induction of mesodermal lineage from human umbilical cord- and bone marrow-mesenchymal stem cells and dental pulp pluripotent-like stem cells," *Cellular Reprogramming*, vol. 20, no. 1, pp. 9–16, 2018.

[41] A. Khadir, A. Tiss, J. Abubaker et al., "MAP kinase phosphatase DUSP1 is overexpressed in obese humans and modulated by physical exercise," *American Journal of Physiology. Endocrinology and Metabolism*, vol. 308, no. 1, pp. E71–E83, 2015.

[42] S. Kochumon, A. A. Madhoun, F. Al-Rashed et al., "Adipose tissue gene expression of CXCL10 and CXCL11 modulates inflammatory markers in obesity: implications for metabolic inflammation and insulin resistance," *Therapeutic Advances in Endocrinology and Metabolism*, vol. 11, article 2042018820930902, 2020.

[43] A. Maher, R. Nunez-Toldra, N. Carrio et al., "The effect of commercially available endodontic cements and biomaterials on osteogenic differentiation of dental pulp pluripotent-like stem cells," *Dentistry journal*, vol. 6, no. 4, p. 48, 2018.

[44] S. Kochumon, A. Al Madhoun, F. Al-Rashed et al., "Elevated adipose tissue associated IL-2 expression in obesity correlates with metabolic inflammation and insulin resistance," *Scientific Reports*, vol. 10, no. 1, p. 16364, 2020.

[45] X. W. Wang and B. Seed, "A PCR primer bank for quantitative gene expression analysis," *Nucleic acids research*, vol. 31, no. 24, pp. 154e–1154, 2003.

[46] J. Ye, G. Coulouris, I. Zaretskaya, I. Cutcutache, S. Rozen, and T. L. Madden, "Primer-BLAST: a tool to design target-specific primers for polymerase chain reaction," *BMC Bioinformatics*, vol. 13, no. 1, p. 134, 2012.

[47] A. Voronova, E. Coyne, A. Al Madhoun et al., "Hedgehog Signaling Regulates MyoD Expression and Activity," *Journal of Biological Chemistry*, vol. 288, no. 6, pp. 4389–4404, 2013.

[48] A. Voronova, A. Fischer, T. Ryan, A. Al Madhoun, and I. S. Skerjanc, "Ascl1/Mash1 is a novel target of Gli2 during Gli2-induced neurogenesis in P19 EC cells," *PLoS One*, vol. 6, no. 4, p. e19174, 2011.

[49] S. Agarwal, K. L. Holton, and R. Lanza, "Efficient differentiation of functional hepatocytes from human embryonic stem cells," *Stem Cells*, vol. 26, no. 5, pp. 1117–1127, 2008.

[50] J. Cai, Y. Zhao, Y. Liu et al., "Directed differentiation of human embryonic stem cells into functional hepatic cells," *Hepatology*, vol. 45, no. 5, pp. 1229–1239, 2007.

[51] S. Mathew, M. Jaramillo, X. Zhang, L. A. Zhang, A. Soto-Gutierrez, and I. Banerjee, "Analysis of alternative signaling pathways of endoderm induction of human embryonic stem

cells identifies context specific differences," *BMC Systems Biology*, vol. 6, no. 1, p. 154, 2012.

[52] A. Al Madhoun, H. Ali, S. AlKandari et al., "Defined three-dimensional culture conditions mediate efficient induction of definitive endoderm lineage from human umbilical cord Wharton's jelly mesenchymal stem cells," *Stem Cell Research & Therapy*, vol. 7, no. 1, p. 165, 2016.

[53] T. Takebe, N. Koike, K. Sekine et al., "Engineering of human hepatic tissue with functional vascular networks," *Organogenesis*, vol. 10, no. 2, pp. 260–267, 2014.

[54] E. L. Calderon-Gierszal and G. S. Prins, "Directed differentiation of human embryonic stem cells into prostate organoids in vitro and its perturbation by low-dose bisphenol A exposure," *PLoS One*, vol. 10, article e0133238, 2015.

[55] P. Wang, K. D. McKnight, D. J. Wong et al., "A molecular signature for purified definitive endoderm guides differentiation and isolation of endoderm from mouse and human embryonic stem cells," *Stem Cells and Development*, vol. 21, pp. 2273–2287, 2012.

[56] C. M. Chinnici, F. Timoneri, G. Amico et al., "Characterization of liver-specific functions of human fetal hepatocytes in culture," *Cell Transplantation*, vol. 24, pp. 1139–1153, 2015.

[57] K. A. D'Amour, A. D. Agulnick, S. Eliazer, O. G. Kelly, E. Kroon, and E. E. Baetge, "Efficient differentiation of human embryonic stem cells to definitive endoderm," *Nature Biotechnology*, vol. 23, no. 12, pp. 1534–1541, 2005.

[58] J. G. Robert Lanza, B. Hogan, D. Melton et al., *Essentials of Stem Cell Biology*, 2009.

[59] S. Toivonen, K. Lundin, D. Balboa et al., "Activin A and Wnt-dependent specification of human definitive endoderm cells," *Experimental Cell Research*, vol. 319, pp. 2535–2544, 2013.

[60] R. E. Schwartz, J. L. Linehan, M. S. Painschab, W. S. Hu, C. M. Verfaillie, and D. S. Kaufman, "Defined conditions for development of functional hepatic cells from human embryonic stem cells," *Stem Cells and Development*, vol. 14, pp. 643–655, 2005.

[61] S. Lotz, S. Goderie, N. Tokas et al., "Sustained levels of FGF2 maintain undifferentiated stem cell cultures with biweekly feeding," *PLoS One*, vol. 8, article e56289, 2013.

[62] N. Shiraki, T. Yoshida, K. Araki et al., "Guided differentiation of embryonic stem cells into Pdx1-expressing regional-specific definitive endoderm," *Stem Cells*, vol. 26, pp. 874–885, 2008.

[63] A. Bonora-Centelles, R. Jover, V. Mirabet et al., "Sequential hepatogenic transdifferentiation of adipose tissue-derived stem cells: relevance of different extracellular signaling molecules, transcription factors involved, and expression of new key marker genes," *Cell Transplantation*, vol. 18, pp. 1319–1340, 2009.

[64] M. A. Laflamme, K. Y. Chen, A. V. Naumova et al., "Cardiomyocytes derived from human embryonic stem cells in pro-survival factors enhance function of infarcted rat hearts," *Nature Biotechnology*, vol. 25, no. 9, pp. 1015–1024, 2007.

[65] H. Y. Lin, C. C. Tsai, L. L. Chen, S. H. Chiou, Y. J. Wang, and S. C. Hung, "Fibronectin and laminin promote differentiation of human mesenchymal stem cells into insulin producing cells through activating Akt and ERK," *Journal of Biomedical Science*, vol. 17, p. 56, 2010.

[66] A. B. McLean, K. A. D'Amour, K. L. Jones et al., "Activin A efficiently specifies definitive endoderm from human embryonic stem cells only when phosphatidylinositol 3-kinase signaling is suppressed," *Stem Cells*, vol. 25, pp. 29–38, 2007.

[67] X. Q. Kang, W. J. Zang, L. J. Bao et al., "Fibroblast growth factor-4 and hepatocyte growth factor induce differentiation of human umbilical cord blood-derived mesenchymal stem cells into hepatocytes," *World Journal of Gastroenterology : WJG*, vol. 11, no. 47, pp. 7461–7465, 2005.

[68] R. E. Schwartz, M. Reyes, L. Koodie et al., "Multipotent adult progenitor cells from bone marrow differentiate into functional hepatocyte-like cells," *The Journal of Clinical Investigation*, vol. 109, pp. 1291–1302, 2002.

[69] C. Schmidt, F. Bladt, S. Goedecke et al., "Scatter factor/hepatocyte growth factor is essential for liver development," *Nature*, vol. 373, pp. 699–702, 1995.

[70] A. Kamiya, T. Kinoshita, and A. Miyajima, "Oncostatin M and hepatocyte growth factor induce hepatic maturation via distinct signaling pathways," *FEBS Letters*, vol. 492, pp. 90–94, 2001.

[71] S. Hanada, H. Kayano, J. Jiang et al., "Enhanced in vitro maturation of subcultivated fetal human hepatocytes in three dimensional culture using poly-L-lactic acid scaffolds in the presence of oncostatin M," *The International Journal of Artificial Organs*, vol. 26, pp. 943–951, 2003.

[72] J. Dong, C. F. Mandenius, M. Lubberstedt et al., "Evaluation and optimization of hepatocyte culture media factors by design of experiments (DoE) methodology," *Cytotechnology*, vol. 57, pp. 251–261, 2008.

[73] X. Li, J. Yuan, W. Li et al., "Direct differentiation of homogeneous human adipose stem cells into functional hepatocytes by mimicking liver embryogenesis," *Journal of Cellular Physiology*, vol. 229, pp. 801–812, 2014.

[74] P. Godoy, N. J. Hewitt, U. Albrecht et al., "Recent advances in 2D and 3D in vitro systems using primary hepatocytes, alternative hepatocyte sources and non-parenchymal liver cells and their use in investigating mechanisms of hepatotoxicity, cell signaling and ADME," *Archives of Toxicology*, vol. 87, no. 8, pp. 1315–1530, 2013.

[75] R. Ji, N. Zhang, N. You et al., "The differentiation of MSCs into functional hepatocyte-like cells in a liver biomatrix scaffold and their transplantation into liver-fibrotic mice," *Biomaterials*, vol. 33, pp. 8995–9008, 2012.

[76] K. Subramanian, D. J. Owens, R. Raju et al., "Spheroid culture for enhanced differentiation of human embryonic stem cells to hepatocyte-like cells," *Stem Cells and Development*, vol. 23, pp. 124–131, 2014.

[77] J. Jozefczuk, A. Prigione, L. Chavez, and J. Adjaye, "Comparative analysis of human embryonic stem cell and induced pluripotent stem cell-derived hepatocyte-like cells reveals current drawbacks and possible strategies for improved differentiation," *Stem Cells and Development*, vol. 20, pp. 1259–1275, 2011.

Hindawi
Stem Cells International
Volume 2021, Article ID 7022247, 15 pages
https://doi.org/10.1155/2021/7022247

Research Article

Retinal Lineage Therapeutic Specific Effect of Human Orbital and Abdominal Adipose-Derived Mesenchymal Stem Cells

Bryan Krief,[1,2] Shira Weisthal Algor,[1,2] Itay Nakdimon,[1,2] Ayala Elhikis,[1,2] Moshe Benhamou,[1,2] Anouk Savir Kadmon,[1,2] Shay Keren,[1,2] Oded Ohana,[1,2] Ilan Feldman,[1,2] Ran Ben Cnaan,[1,2] Igal Leibovitch,[1,2] Anat Loewenstein,[1,2] Adiel Barak,[1,2] and Aya Barzelay[1,2]

[1]*Department of Ophthalmology, Tel-Aviv Sourasky Medical Center, Tel-Aviv 6423906, Israel*
[2]*Sackler Faculty of Medicine, Tel-Aviv University, Tel-Aviv 6997801, Israel*

Correspondence should be addressed to Aya Barzelay; aya.barzelay@gmail.com

Received 19 May 2021; Revised 9 August 2021; Accepted 2 September 2021; Published 19 October 2021

Academic Editor: Jun Liu

Retinal degenerative diseases are one of the main causes of complete blindness in aged population. In this study, we compared the therapeutic potential for retinal degeneration of human mesenchymal stem cells derived from abdominal subcutaneous fat (ABASCs) or from orbital fat (OASCs) due to their accessibility and mutual embryonic origin with retinal tissue, respectively. OASCs were found to protect RPE cells from cell death and were demonstrated to increase early RPE precursor markers, while ABASCs showed a raise in retinal precursor marker expression. Subretinal transplantation of OASCs in a mouse model of retinal degeneration led to restoration of the RPE layer while transplantation of ABASCs resulted in a significant restoration of the photoreceptor layer. Taken together, we demonstrated a lineage-specific therapeutic effect for either OASCs or ABASCs in retinal regeneration.

1. Introduction

Blindness and vision impairment affect more than 2 billion people worldwide and will inevitably continue to increase due to population age. Oxidative stress, inflammation, and degeneration of retinal cells are notably implicated in the development of several eye pathologies, in particular, in age-related macular degeneration (AMD) [1, 2].

The retinal pigment epithelium (RPE) is crucial for the retinal function, as it participates in nutrition, protection against photo/light oxidation, secretion of proteins required for retinal homeostasis [3], immune privilege of the eye [4], and phagocytosis of photoreceptor disk membranes [5]. RPE cells and photoreceptors are both specifically sensitive to oxidative damage that leads to their apoptosis [2]. Degeneration of RPE is one of the main pathologic factors of AMD [6]. RPE is not directly involved in the vision process; although, it allows the survival of photoreceptors [7] mainly implicated in the visual phototransduction whose mechanism was described by George Wald (Nobel Price 1967). One of the most extensively studied treatment option for RPE degeneration is RPE transplantation that may prevent photoreceptor cell death. Recently, stem cell therapy has been proposed as a possible option for cell replacement therapy in AMD.

Mesenchymal stem cells (MSCs) are especially attractive population for cell therapy purposes, besides the fact that they can serve as an autologous cell source or even allogenic cell source [8], they are also multipotent, and their paracrine activity promotes cell survival and antioxidative properties [9, 10]. MSCs are able to differentiate into osteocytes, chondrocytes, adipocytes, and to cells of an entirely distinct lineage, including neuron-like cells [10, 11]. The paracrine activation properties of MSCs are known to modulate the microenvironment of the diseased tissues by secretion of cytokines that protect injured cells, promote survival, and activate endogenous repair mechanisms [10, 12] including by an antioxidant effect [13]. MSCs can be isolated from

different tissues as bone marrow and adipose tissue. A special advantage is given to adipose-derived MSCs (ASCs) since the harvesting of adipose tissue may be conducted in a minimal invasive procedure as we have recently shown [14] and could be isolated from many sites [15, 16]. We have recently demonstrated the beneficial effect of MSCs harvested from subcutaneous fat, in protection of RPE from oxidative stress-induced cell death in vitro, as well as their therapeutic effect with the salvage of both RPE and photoreceptor layers in an in vivo model of retinal degeneration after a week of treatment [10]. Most adipose tissues, including subcutaneous, are derived from mesoderm. Interestingly, the orbital fat derives from neural crest origin [17], like most ocular and orbital tissues origin [18], and specifically shares a mutual embryonic origin with RPE [19]. MSCs are known to be responsive to the niche they reside in [20], and it was shown for instance that ASC derived from pericardial fat is more potent in therapy for ischemic cardiomyocytes than ASCs harvested from abdominal or subcutaneous adipose tissue [20]. Hence, orbital fat-derived MSCs are a unique population with great interest when considering a potential for retinal repair. Thus, in this study, we examined whether human orbital adipose-derived mesenchymal stem cells have therapeutic advantage in retinal regeneration, when compared to human abdominal mesenchymal stem cells harvested from subcutaneous fat (ABASCs).

To this end, we studied the phenotypic characterization of OASCs, and we evaluated their protective effect on RPE cell survival when exposed to oxidative stress and their cytokine secretion profile when compared to ABASCs. Next, we studied the ability of OASCs to differentiate toward RPE compared to ABASCs. Finally, we investigated the long-term effect of subretinal transplantation of ABASCs and OASCs in a mouse model of retinal degeneration.

2. Results

2.1. Characterization and Multipotency of OASCs. OASCs positively expressed classic MSC markers (CD29: 93.5 ± 6.9 %; CD73: 93.9 ± 7.6%; CD105: 90.9 ± 5.5%) and were negative for endothelial and hematopoietic markers (CD31: 1.3 ± 1.7%; CD45: 0.1 ± 0.1%), as well as varying levels of CD34, which is expressed in OASCs contrary to ABASCs (an average of 8.3% compared to 0.7% of expression in ABASCs) (Figures 1(a)–1(c)). OASCs showed multipotency ability by their capacity to differentiate adipocytes, as evidenced by high staining Oil Red O and in a lesser extent into osteocytes as shown by Alizarin Red staining (Figures 1(d) and 1(e)).

2.2. OASCs-CM Inhibits RPE Cell Death under Oxidative Stress. We assessed the protective role of OASC–conditioned medium (CM) on RPE cells previously exposed to H_2O_2 as described for ABASCs-CM [10]. RPE cells exposed to CM prior to H_2O_2 treatment exhibited a significant decrease in cell death (32.0 ± 4.1% cell death) compared to non-CM (53.4 ± 4.2% cell death), as evident by FACS analysis for propidium iodide staining (40.0% cell death reduction, $p < 0.01$) (Figures 2(a) and 2(b)). This result highlights the effect of OASC-conditioned medium on oxidation-induced RPE cell death.

2.3. Cytokine Secretion Profile of OASCs and ABASCs. Mesenchymal stem cells exert their effect on their microenvironment by paracrine release [9, 10]. In order to examine the cytokine secretion profile of OASCs and to compare that of ABASCs, we used the RayBio® Human Cytokine Antibody Array G10. The most abundant proteins secreted in all samples by OASCs and ABASCs were angiogenin, HGF, and osteoprotegerin, previously described for their inhibitory effects on oxidative stress [21] and apoptosis [22, 23] (Figure 2(c)). Some cytokines were significantly less released by OASCs (Ck-β8-1, ICAM-1, eotaxin-3) than ABASCs while the neuroprotective growth factor BDNF was significantly more secreted into OASCs-CM (Figure 2(d)). qRT-PCR was performed to further validate these results on mRNA levels of selected cytokines. To summarize, OASCs exhibited a lower expression of the proinflammatory and proangiogenic cytokines ck-β8-1, ICAM-1, and eotaxin-3 than ABASCs (by, respectively, 1.29-, 1.45-, 1.38-fold). Moreover, a higher expression of the neuroprotective factor BDNF was detected in OASCs by 1.57-fold than ABASCs (Figure 2(e)).

2.4. Differentiation of OASCs to RPE

2.4.1. Prestaining for Lineage Marker of OASCs/ABASCs and pRPE. OASCs/ABASCs and pRPE were prelabeled with CFSE and CellTrace Violet, respectively (Figures 3(a) and 4(a)) and were cell sorted by FACS sorter after a week in coculture. Three well-defined homogenous populations were detected: CFSE+ cells (OASCs/ABASCs), violet cell trace+ (pRPE cells), and a rare population of double-positive CFSE+/Violet CellTrace+ (OASCs/ABASC-pRPE-fused cells) (Figures 3(b) and 4(b)). Segregated cells were collected and analyzed for RPE markers by qRT-PCR and immunostaining.

2.4.2. Increase of Early RPE Markers in OASCs and ABASCs following a Differentiation Study. Relative mRNA expression of cocultured OASCs compared to non cocultured OASCs control is presented in Figure 3(c). OASCs upregulated early neural marker OTX2 (929.7 ± 76.2, $p < 0.05$); all three are markers of early eye field differentitaion. OASCs also upregulated RPE65 (30.5 ± 14.8, $p = 0.076$), a late differentitaion marker of RPE (24) PAX6 (57.6 ± 5.6, $p < 0.05$), and SIX3 (338.2 ± 33.0, $p < 0.05$), and all three are markers of early eye field differentiation and late RPE marker RPE65 [24] (30.5 ± 14.8, $p = 0.076$). We noticed downregulation of the pluripotency marker KLF4 which may suggest the decrease in stemness and commitment to a certain lineage [24] (0.68 ± 0.02, $p < 0.05$) (Figure 3(c)). These results may imply to increase of early RPE markers in OASCs, after coculture with primary RPE cells. To further validate the qPCR results at the protein level, we examined by immunocytochemistry the phenotype of coculture cell-sorted OASCs (Figure 3(d)). The immunostaining analysis tend to confirm the capacity of differentiation of OASCs, as shown by the nuclear expression of PAX6 and OTX2 in OASCs (Figure 3(d)(A)–(D)) when compared to noncocultured OASC control (Figure 3(d)(E, F)).

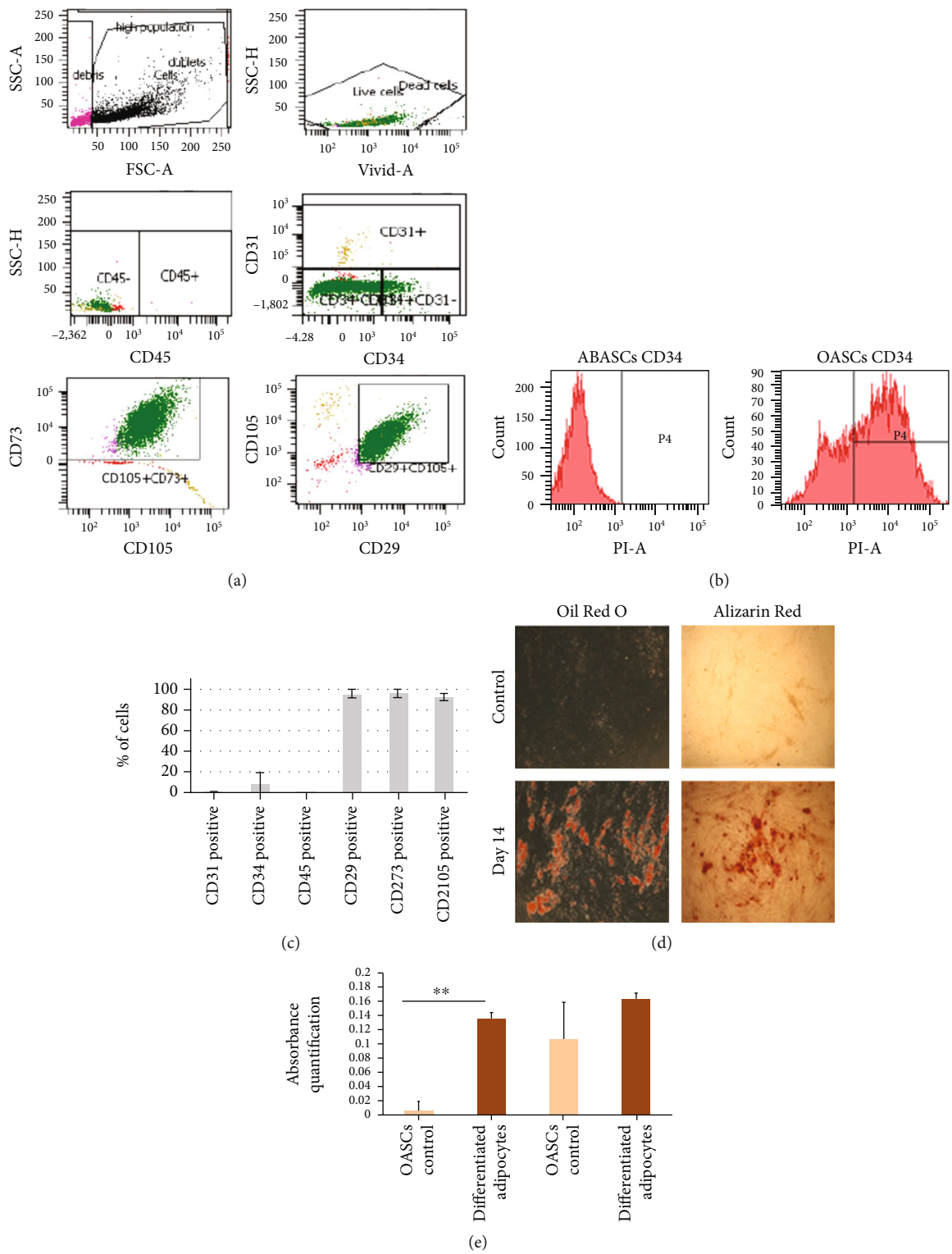

Figure 1: Characterization of OASCs by surface phenotype and differentiation potential. (a)–(c) OASCs were immunostained for CD29, CD31, CD34, CD45, CD73, and CD105 and analyzed by FACS. OASCs exhibited classic MSC phenotype when compared to ABASCs. (b, c) CD34 expression in OASCs was evaluated and compared to that observed in ABASCs. (d, e) Multipotency of OASCs shown by staining for Oil Red O and Alizarin Red and markers for adipocytes and osteocytes. Data are represented as mean ± SD.

To better understand whether or not OASCs have an advantage in differentiation to RPE, we compared the differentiation capacity of ABASCs to that of OASCs under the same differentiation protocol. To this end, ABASCs were cocultured with p-RPE cells as previously described in methods. After their coculture with p-RPE cells, ABASCs

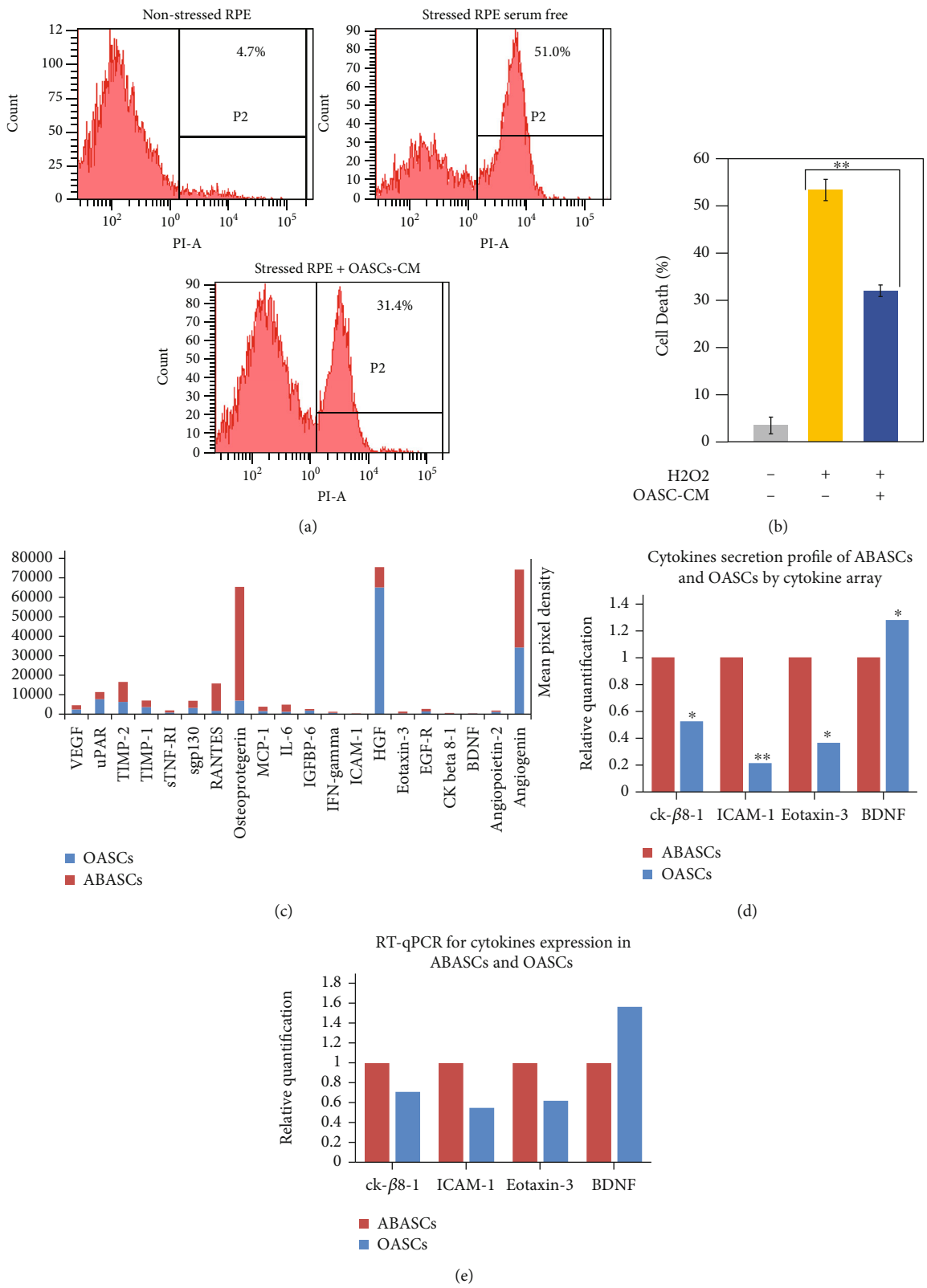

Figure 2: Paracrine activity of OASCs and ABASCs. (a, b) OASCs rescue RPE cells under oxidative stress. RPE cells were incubated with CM or with non-CM for 48 hours, followed by exposure to H2O2 (1 mM, 7 h). Cells were harvested, and cell death rate was analyzed by PI staining followed by flow cytometer analysis. Data are represented as mean ± SD. (c) Medium containing secreted protein of OASCs and ABASCs was examined using RayBio® Human Cytokine Antibody Array G10. Cytokine array membranes used to analyze the secretion of 20 cytokines by OASCs and ABASCs. (d) Summary of significant released proteins elevated in OASCs compared to ABASCs. (e) Gene expression of these proteins in OASCs compared to ABASCs. CM: condition medium.

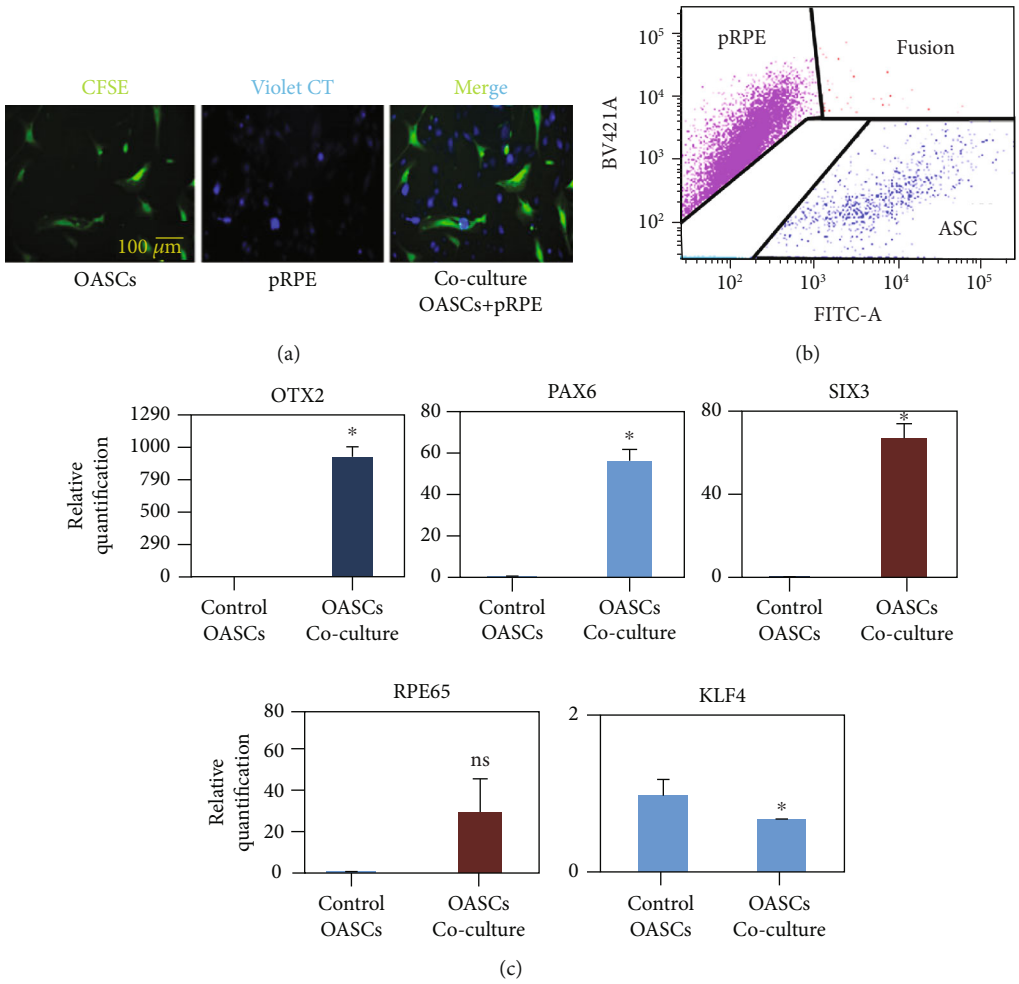

Figure 3: Continued.

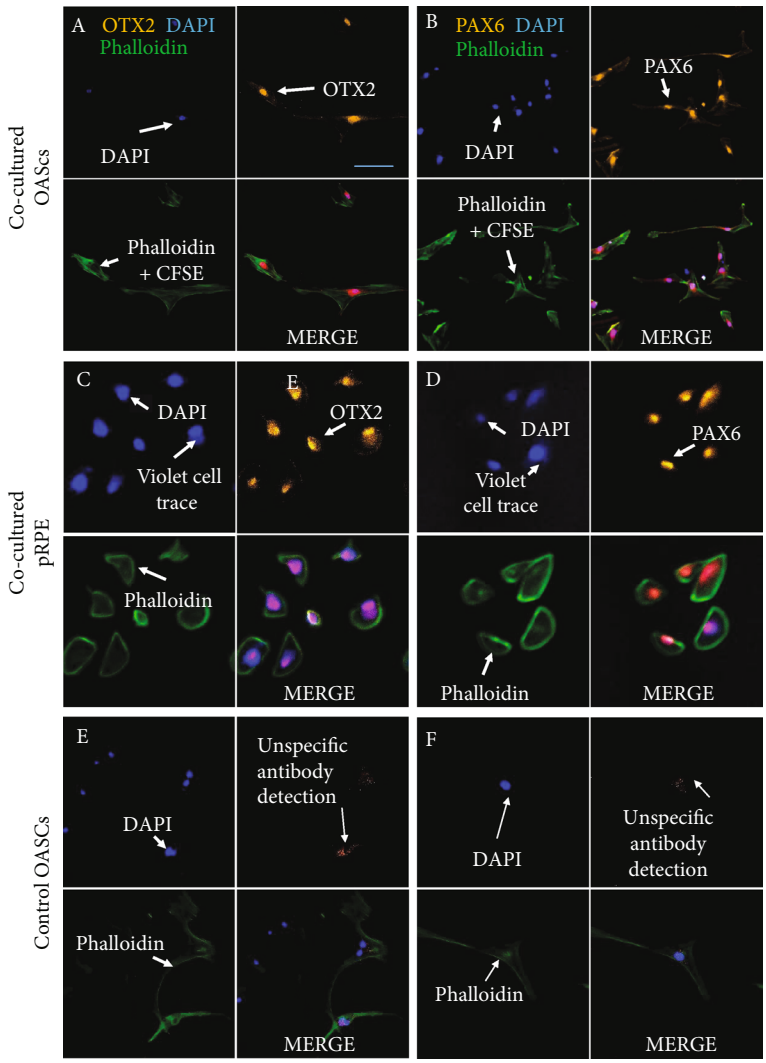

(d)

Figure 3: Differentiation of OASCs to RPE like cells. (a, b) Coculture of p-RPE cells and OASCs. (a) Prestaining of cells: OASCs were marked with CSFE (green color), and RPE mature cells were marked with Violet Cell Trace (blue color). (b) FACS sorter: three distinct populations are defined after coculture: RPE cells, OASCs and OASCs, and RPE cells which were fused together. Autofluorescent cells were excluded according to negative and positive controls of labeled cells. (c) Evidence of differentiation of OASCs to RPE like cells by RT-qPCR. Results are presented as mean increase ± SD relative to sample plot. After coculture with RPE cells, OASCs exhibited an increase in transcription of early and late RPE markers. (d) Evidence of differentiation potential of OASCs by immunofluorescence. (A) Sorted OASCs derived RPE-like cells labeled with CFSE showing nuclear localized OTX2 expression. (B) Sorted OASCs derived RPE-like cells showing nuclear localized PAX6 expression (C) Positive control of sorted RPE cells in Violet Cell Trace showing nuclear localized OTX2 expression. (D) Positive control of sorted RPE cells in Violet Cell Trace showing nuclear localized PAX6 expression. (E, F) Negative control of OASCs that did not show any OTX2 expression or PAX6 expression. CT: cell trace. Scale bar: 100 μm. $n = 3$.

were able to express the eye-field and neural markers PAX6 and OTX2 exhibiting a potential of early differentiation to retinal precursors. It was observed that PAX6 was expressed in sorted ABASCs in the nuclear region (Figure 4(d)(B)) as observed in sorted OASCs (Figure 3(d)(B)); however, the expression of OTX2 was cytoplasmic in ABASCs (Figure 4(d)(A)) unlike nuclear expression in RPE cells [25] (Figure 3(d)(C, D)) and in differentiated OASCs (Figure 3(d)(C)), a fact that may imply on different differentiation capacity of this population of cells [25]. We also noticed the presence of RPE-ABASC fused cells (Figure 4(c)).

2.5. Retinal Lineage Specific Therapeutic Effect of ABASCs and OASCs. To determine the potential of ABASCs and of OASCs in mending retinal injury caused by oxidative stress, we injected those cells to the subretinal space in a sodium iodate mice model, known to describe a retinal degeneration [26].

2.5.1. Cell Location following ASC Transplantation. Transplanted ASCs were detected in the subretinal space at day 0 by hematoxylin and eosin staining (H&E), thus confirming accuracy of transplantation to the desired location (supplementary Figure 1).

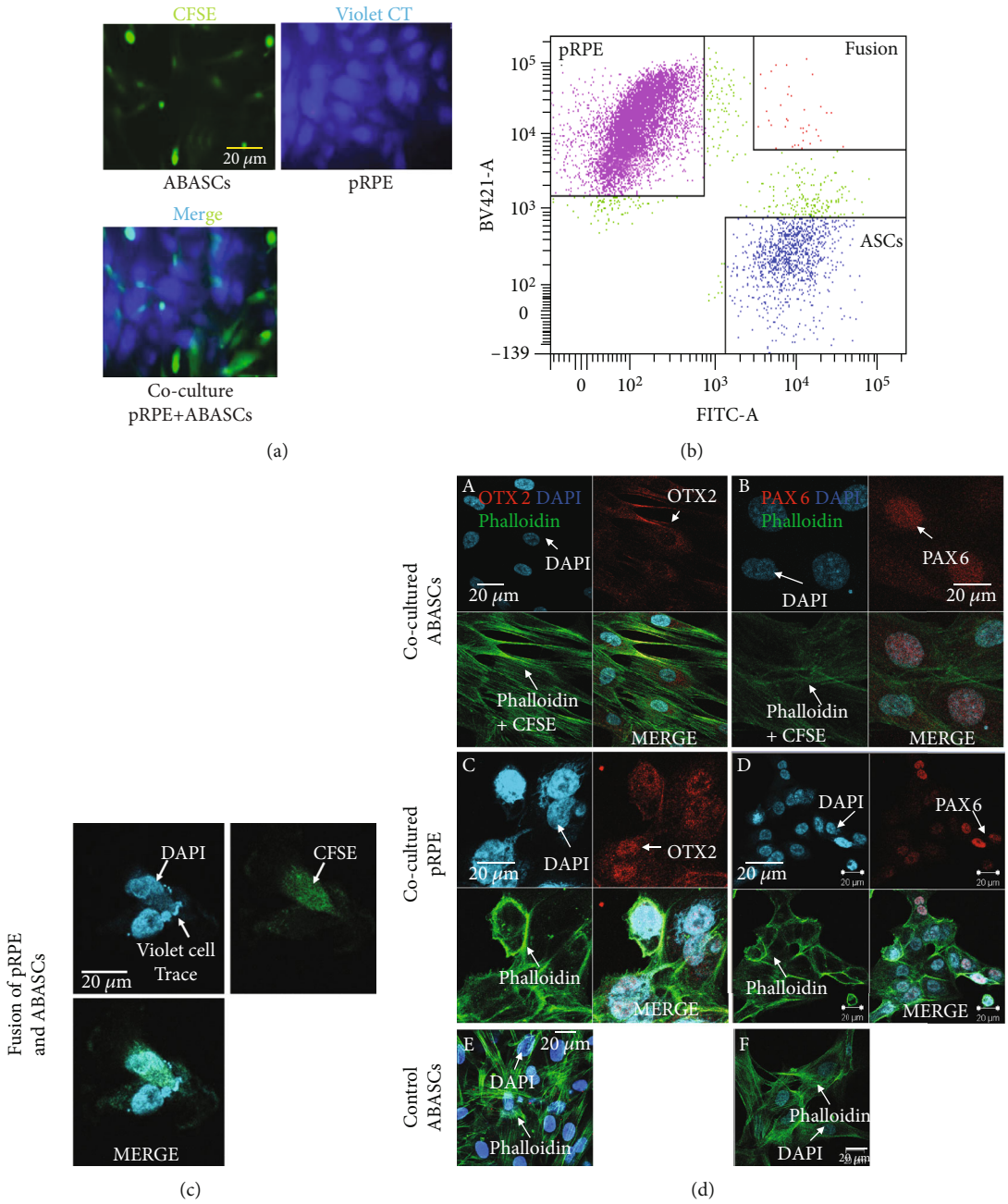

Figure 4: Differentiation potential of ABASCs to retinal precursors cells. (a, b) Coculture of p-RPE and ABASCs. (a) Prestaining of cells: ABASCs were marked with CSFE (green color), and RPE mature cells were marked with Violet Cell Trace (blue color). (b) FACS sorter: three distinct populations are defined after coculture: RPE, ABASCs, RPE and ABASCs which were fused together. (c) Fusion of cells as shown by one cell expressing both Violet Cell Trace (RPE tracer) and CFSE (OASC tracer). (d) Evidence of differentiation potential of ABASCs to retinal precursors cells by immunofluorescence. (A) Sorted ABASCs expressing cytoplasmic OTX2. (B) Sorted ABASCs in CFSE showing nuclear localized PAX6 expression. (C, D) Positive control of sorted RPE cells in Violet Cell Trace showing nuclear localized OTX2 expression and nuclear localized PAX6 expression (E, F) negative controls of undifferentiated ABSCs does not show any OTX2 expression and PAX6 expression. CT: cell trace. $n = 3$.

2.5.2. Effect of ABASC Transplantation on Photoreceptors. ONL thickness and rhodopsin intensity were previously shown to be reduced after a week of 50 mg/kg sodium iodate [10] while INL thickness was reduced after 3 weeks of NaIO3 (sodium iodate) incubation [27] in untreated NaIO3 model.

ONL thickness as well as rhodopsin intensity was significantly higher in ABASC-treated mice, when compared to the PBS-treated group. Also, ONL thickness was higher in ABASC-treated mice, when compared to the OASC-treated group. No significant difference was found with ONL thickness or rhodopsin intensity in OASC-treated

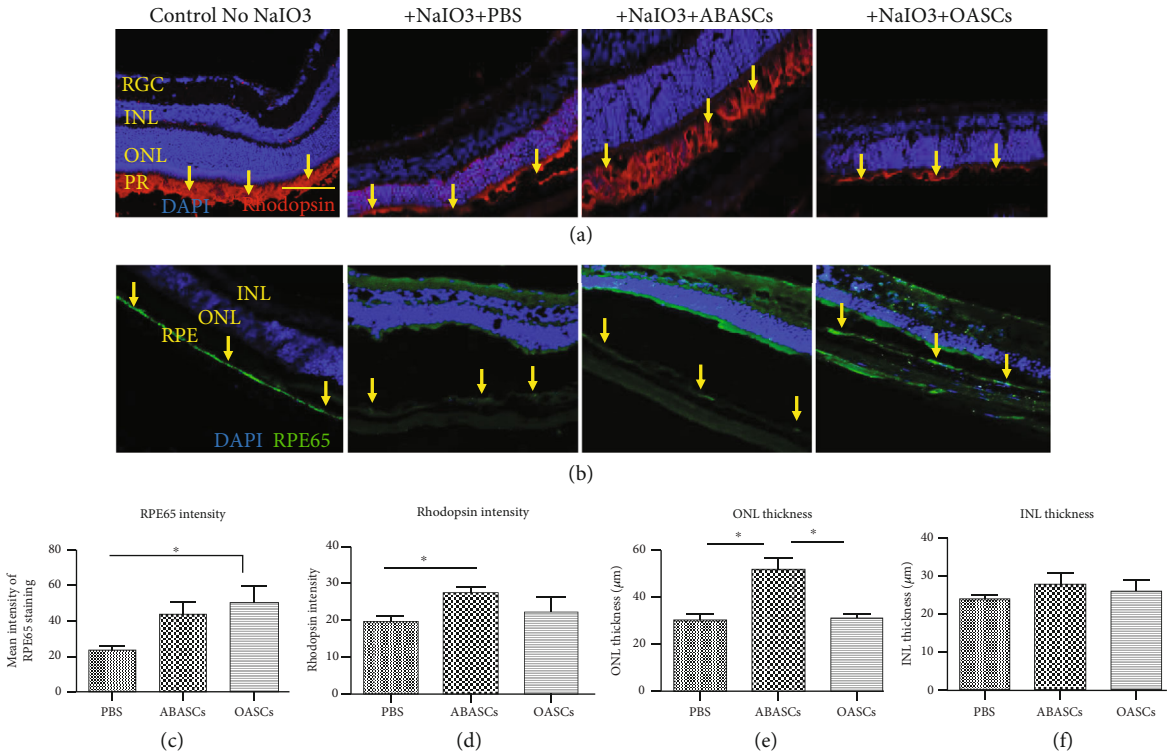

Figure 5: Retinal layers 21 days post transplantation of ABASCs and OASCs in the NaIO3 mice model. (a) Immunohistochemistry pictures of mice retinas for ONL quantification and rhodopsin intensity by DAPI and rhodopsin staining in ABASCs and OASCs transplanted mice versus controls. Yellow arrows indicate the PR layer. (b) Immunohistochemistry pictures of the mice RPE layer after RPE65 and DAPI staining in ABASC and OASC transplanted mice versus controls. Yellow arrows indicate the RPE layer. (c) Graphic summary of RPE65 intensity evident by RPE65. (d) Graphic summary of rhodopsin intensity evident by rhodopsin staining. (e) Graphic summary of ONL thickness evident by DAPI staining. (f) Graphic summary of INL thickness evident by DAPI staining. ONL: outer nuclear layer; INL: inner nuclear layer; RGC: retinal ganglion layer; PR: photoreceptor; RPE: retinal pigment epithelium. Bar = 100 μm. For each group of mice, $n = 5$. Data are represented as mean ± SEM.

mice (Figures 5(a), 5(d), and 5(e)). ABASC and OASC transplantations did not affect the inner nuclear layer (INL) (Figure 5(f)).

2.5.3. Effect of OASC Transplantation on RPE Layer. RPE65 is often used as a marker of RPE functionality [10, 27]. RPE65 was shown to be reduced after a week of 50 mg/kg NaIO3 [10, 28]. Eyes treated with OASCs showed significantly higher levels of RPE65 staining compared to PBS-treated eyes, exhibiting a protective effect of OASCs from NaIO3-induced damage. No significant difference was observed between ABASC-treated mice to OASCs and PBS-treated mice (Figures 5(b) and 5(c)).

2.5.4. ABASC Transplantation Induced Infiltration of Iba1+ Cells. We demonstrated basal CD45+ cell infiltration in NaIO3 mice prior to transplantation of OASCs and ABASCs (Figure 6(a)), as was previously shown [29]. 21 days after transplantation of ABASCs to the subretinal space, we observed an increase of CD45+ cell infiltration (Figures 6(b) and 6(c)) combined with an increase of Iba1+ cells in the retinas of ABASC-treated mice (Figures 6(b) and 6(d)). Iba1+ cells comprised the majority of infiltrating cells in both ABASC- and OASC-treated mice compared to controls (Figures 6(b) and 6(e)). There was no significant difference in infiltration of CD45+ cells and Iba1+ cells in OASC-treated mice compared to PBS-treated mice.

3. Discussion

In this study, we characterized the phenotype of OASCs, we demonstrated the protective effect of OASCs on RPE cell death in the setting of oxidative stress, and defined their cytokine secretion profile compared to that of ABASCs. Next, we showed that OASCs were able to express early RPE markers, while ABASCs expressed less specific retinal markers, after coculture with primary RPE cells. Finally, we demonstrated a lineage specific therapeutic effect of OASC and ABASC transplantation in a mouse model of retinal degeneration.

3.1. Paracrine Activity of OASCs and ABASCs. Treatment of RPE with conditioned medium of OASCs resulted in salvage of RPE from cell death induced by oxidative stress. These data are in line with a previous study conducted by our group that demonstrated a protective effect of ABASCs on RPE cell death [10]. Also, the contribution of cell fusion may supply this protective effect. In our differentiation study, we found that small percentage of OASCs and ABASCs undergo cell fusion with mature RPE. Those hybrid

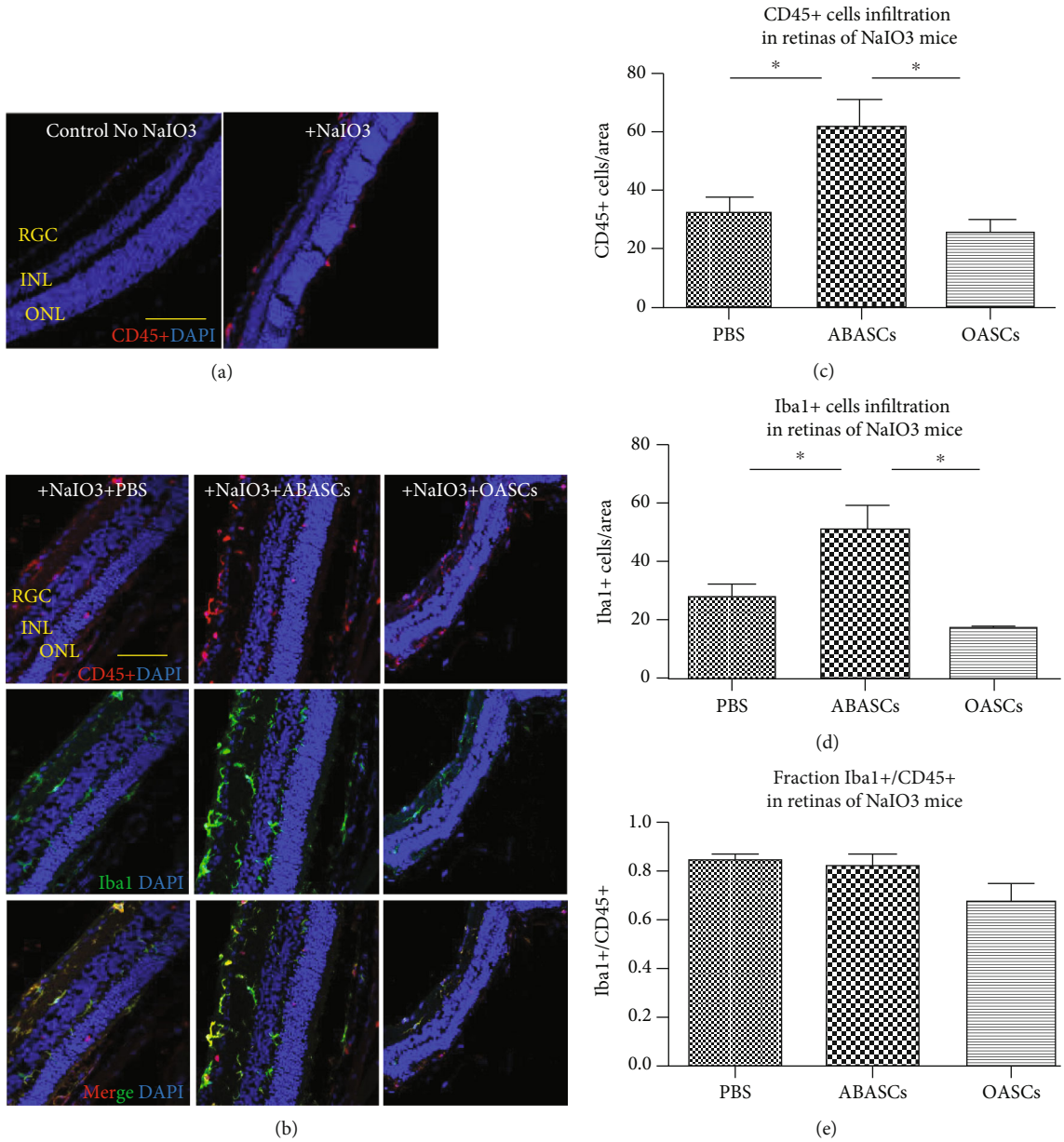

Figure 6: Immune response 21 days post transplantation of ABASCs and OASCs in the NaIO3 mice model. (a) Immunohistochemistry pictures of CD45+ staining in NaIO3-treated mice compared to nontreated mice revealed the infiltration of CD45+ cells in the retinas of NaIO3-treated mice compared to controls. (b) Immunohistochemistry pictures of CD45-Iba1 costaining. (b, c) Quantification of the number of CD45+ cells revealed a higher infiltration of leucocytes in ABASC-treated mice compared to PBS treated mice ($p \leq 0.05$). (b)–(d) Quantification of the number of Iba1+ cells revealed a higher infiltration of Iba1+ cells in ABASC-treated mice compared to OASC-treated mice and to PBS-treated mice ($p \leq 0.05$). (b)–(e) Most of CD45+ cells expressed Iba1 in all treated groups. ONL: outer nuclear layer; INL: inner nuclear layer; RGC: retinal ganglion layer. Bar = 50 μm. For each group of mice, $n = 5$. Data are represented as mean ± SEM.

cells may have an advantage on activating antiapoptotic pathways [30]. OASC and ABASC protective effect might be allowed by high secretion of some cytokines that has been demonstrated in this study. We found in OASCs' and ABASCs' conditioned medium high levels of osteoprotegerin, a cytokine known in the protection from oxidative stress [21]. Also, we showed that OASCs and ABASCs secrete high levels of angiogenin and HGF whose antiapoptotic roles have been elucidated [22, 23]. Moreover, HGF is known for its involvement in tissue regeneration [28] which may explain the beneficial effect seen in vivo in this study.

3.2. Variability in Retinal Marker Expression between OASCs and ABASCs following a Differentiation Study. We demonstrate an increase of the early RPE marker expression in OASCs and a raise in less specific retinal lineage marker expression in ABASCs. Immunocytochemistry studies revealed specific nuclear staining to PAX6 and OTX2 in

OASCs, implying to obvious lineage direction of OASCs towards RPE [31]. Interestingly, we found that ABASCs had a cytoplasmic expression of OTX2 in contrary to the nuclear expression of OTX2 in RPE cells [25] and in sorted OASCs. A cytoplasmic expression of OTX2 was previously correlated with immature rods photoreceptors [25], as well as the expression of SIX3 and PAX6 [32], a fact that may imply to a potential of ABASCs to follow a path towards precursors of photoreceptors lineage.

Moreover, it was previously shown that stem cells could memorize epigenetic marks from their origin [33], and it might improve RPE differentiation tendency of OASCs [34]. The mutual embryonic ectodermal origin of OASCs and RPE compared to mesodermal origin of ABASCs [35] may explain the increase in RPE markers seen in OASCs, exhibited by the nuclear expression of OTX2 when compared to the cytoplasmic expression of OTX2 by ABASCs.

To note, we found a population of cell fusion of RPE with ABASCs and with OASCs. Although cell fusion was a rare phenomenon of less than 0.7% of cases, it may have some implications. First, this may explain why we found increase in RPE65 transcript in the qRT-PCR study only a week after the differentiation study, since RPE65 is known as a mature RPE markers and usually upregulated later during the course of differentiation [24]. Secondly, the phenomenon of cell fusion may be also an opportunity for enhanced regenerative effect, as previous studies have shown that stem cell fusion with mature differentiate cells promotes the increase of plasticity of mesenchymal stem cells leading and promoting their differentiation [36]. Also, it helps the reprogramming of somatic nuclei through epigenetic changes in a matter that form a pluripotent hybrid cell [37], thus providing another regenerative potential by the reprograming of mature cells to activate selective survival pathways [31].

3.3. Long-Term of Subretinal Transplantation of OASCs and ABASCs Leads to Restoration of Different Retinal Layers. As opposed to a recent report by Kuriyan and colleagues, in which transplantation of nonselected mixture of whole adipose tissue cells was injected to the vitreous of AMD patients and caused devastating results, the population of stem cells transplanted in this study was carefully segregated from the whole adipose tissue by a two-step procedure. First, mesenchymal stem cells were isolated from the adipose tissue by collagenase digestion. Second, cells were seeded on tissue culture plate and further purified with specific medium which allowed the selection of purified MSCs. MSC phenotype was then verified by FACS analysis, as mentioned in methods. Moreover, purified MSCs were injected to the subretinal space rather than to the vitreous cavity to reduce the risk of retinal detachment as observed by Kuriyan and colleagues [38].

It is known that NaIO3 injection causes degeneration of ONL and INL [27].We previously reported that subretinal transplantation of ABASCs in NaIO3 mice significantly increased ONL thickness, rhodopsin intensity, and salvaged RPE layer acutely, after one week [10]. In this study, we demonstrate a longer term effect of ABASC transplantation, which showed increase of ONL thickness and rhodopsin intensity after three weeks from NaIO3 administration. However, ABASC transplantation did not result in significant increase of RPE layer after 3 weeks. This may be explained by the destructive effect of NaIO3 on the RPE that is known to be increased with time [39], combined with the fact that ABASCs were shown here to have a more limited ability to increase specific RPE markers than OASCs. Also, OASC transplantation did not affect ONL thickness neither rhodopsin intensity in NaIO3 mice, that might be explained by the differences noticed in immune cell infiltration in retinal layers after ABASC and OASC treatment. ABASC and OASC injections did not result in restoration of the INL layer, whose destruction might be irreversible after a long incubation with high concentration of sodium iodate as shown by Moriguchi et al. [39]. We detected injected ASC at time 0 post transplantation in the subretinal space by H&E staining. However, ASCs were not localized at day 21 post transplantation, neither by H&E staining nor by staining with the human specific markers Ku80 and STEM121 [40]. Nevertheless, the therapeutic effect of each population of transplanted cells was obvious in this study. The explanation to this phenomenon may reside in the strong paracrine effect of ASCs that may have led to a cascade of events resulting in preservation of the RPE layers and photoreceptors layers. Transplanted cells' viability, retention, and engraftment in the tissue have been already described as one of the main issues in stem cell therapy [41] and specifically in retinal transplantation of stem cells [42]. Similar observations of paracrine effect post transplantation were previously described after intra-articular injection of MSCs [43], and many studies are focusing on MSC secretome to improve MSC therapeutic effect in the injured tissue [44, 45]. A completion study to the current investigation will be transplantation of ASCs embedded in a bioscaffold to better improve the survival and retention of the cells in the subretinal space for a longer period of incubation.

3.4. ABASC Transplantation Triggers Immune Cell Infiltration in SI Mice. We observed higher CD45+/Iba1+ cell infiltration in retinal layers after ABASC treatment compared to the PBS group and to OASC group. The implication of microglial cells is correlated with neuroinflammation which triggers the increase of the CD45 expression [46]. Microglial Iba1+ cells have a significant impact on neurons viability and function in either beneficial or detrimental effect, depends on the circumstances [47, 48]. Interestingly, the infiltration of microglial cells is known to be involved in photoreceptor cell death protection [48, 49]. Thus, Iba1 + cell infiltration in photoreceptor layers of ABASC-treated mice might be responsible for the regeneration of photoreceptors layer demonstrated in this study. Interestingly, we showed that ABASCs highly secrete ICAM1, eotaxin 3, and Ckβ-8 that have been previously described to activate microglial infiltration into the brain [50–53]. This secretion may be directly correlated with the higher infiltration of Iba1+ cells in ABASC-treated mice. The absence of Iba1+ cell infiltration increase in mice treated with OASCs may come in line with the absence of photoreceptor protection in this

group. Consequently, it might be interesting to study the effect of ABASCs after Iba1+ cell depletion in the sodium iodate mice model.

We demonstrated preservation of the RPE layer in mice treated with OASCs compared to mice treated with ABASCs or controls of PBS. RPE is one of the contributors to the integrity of the outer blood retinal barrier (oBRB). RPE also exhibits immunosuppressive properties by paracrinely preventing the traffic of cells and proteins from the blood to the retinal region [54]. Therefore, preservation of the RPE layer in mice treated with OASCs may explain the lower Iba1+ cell infiltration exhibited in this group. In summary, OASCs exhibited a specific ability to increase the expression of early RPE markers and a protective effect on RPE in vitro and in vivo. When comparing the therapeutic potential of OASCs versus ABASCs, the criteria of abundance and easy accessibility [14] as seen for ABASCs are considered as a necessity for future development of clinical applications. This, combined with a strong in vivo neuroprotective effect, and the increase in retinal lineage markers by ABASCs demonstrated in this study, implies to a broader therapeutic effect and a possible advantage related to ABASCs as a therapeutic tool. All these data imply for spatial effect of either stem cell lineage, OASCs, or ABASCs, on retinal regeneration, and distinguish the potential of each population in future development of cell therapy for retinal diseases.

4. Materials and Methods

The purpose of the study and the procedures used were presented to all of the subjects, and a signed informed consent was obtained from each. This study was approved by the ethics committee for clinical trials of Tel Aviv Sourasky Medical Center and was conducting according to the Declaration of Helsinki.

4.1. Isolation, Characterization, and Culture of ASCs. Subcutaneous abdominal human adipose tissue was harvested from 4 healthy patients with a mean age of 51 ± 4.2 who had abdominoplasty. Central and medial orbital fat was harvested from 7 patients with a mean age of 72.66 ± 13.57, who underwent routine blepharoplasty. No severe ophthalmopathy, metabolic disease, systemic complications, or recent exposure to chemotherapy or to immunosuppressive agents were reported for these patients. OASCs and ABASCs were isolated according to a protocol previously described [14]. Briefly, the abdominal adipose tissue was extracted by liposuction while orbital fat was extracted during blepheroplasty. The fat tissue was then washed with phosphate-buffered saline (PBS) and digested with collagenase I (0.075% collagenase type I, Sigma-Aldrich, Taufkirchen, Germany) for a 16-hour digestion at 37°C and neutralized with Dulbecco's Modified Eagle Medium (DMEM) containing 10% foetal bovine serum (FBS). Digested fat was centrifuged at 400 g (RCF) for 15 minutes, and the pellet of cells was resuspended in ADSC medium after passage through a 100 μm mesh filter (Cat. no. 542000, EASYstrainer, Greiner Bio-One) to remove all the debris. Cells were then seeded on tissue culture plates. Cell culture medium was replaced twice weekly. All experiments were performed at passage three.

4.2. Characterization of OASCs for MSC Markers by FACS Analysis. Characterization of cultured OASCs was performed at passages 3-4 as follows: after reaching 100% confluence, cells were trypsinized and collected in FACS tubes in aliquots (1×10^5 cells/tube). Cells were stained with fluorescein isothiocyanate (FITC) and phycoerythrin- (PE-) conjugated monoclonal antibodies against human CD34 (Dako), CD45 (Dako), CD90 (Dako), CD105 (eBioscience), and CD73 (BDPharmingen). To exclude dead cells, the samples were stained with ViViD (violet viability dye, Molecular Probes, Invitrogen, Eugene, OR, USA), according to the manufacturers protocols. Cells were then analyzed by FACS Canto II flow cytometer (BD Biosciences). All the fluorochrome-conjugated antibodies were used as isotype controls.

4.3. Multipotency of OASCs by Differentiation to Osteocytes and Adipocytes. OASCs at passage 3 were studied to determine their ability to differentiate into osteocytes and adipocytes. 1×10^4 cells were plated in a 24-well plate and incubated with their respective differentiation media after 100% of confluency (adipocyte: 10% FBS, 1 μM dexamethasone, 0.5 mM 3-isobutyl-1-methylxanthine, 10 μg/mL insulin, and 100 μM indomethacin in high glucose- (HG-)DMEM, osteocyte: Stem pro® osteocyte differentiation basal medium (Gibco)). The media was changed twice a week until osteocyte and adipocyte differentiation, after 2 or 3 weeks, respectively. Differentiation to adipocytes was assessed using an Oil Red O stain as an indicator of intracellular lipid accumulation. The cells were fixed for 20 min at room temperature in 4% paraformaldehyde. Cells were incubated in 0.5% (wt/vol) Oil Red O reagent in 100% isopropanol (Sigma) for 10 min at room temperature. Bone differentiation was followed by Alizarin Red Staining (Sigma) after fixation with 4% paraformaldehyde. Images of stained cells with both Oil Red O and Alizarin red were taken by light microscopy.

4.4. Primary RPE (pRPE) Culture and Preparation of ASC-Conditioned Medium. 5.5×10^5 cells of human pRPE cells (Lonza) were plated in 100 mm culture dishes (Falcon) in retinal epithelial cell growth medium (RtEGM) Bulletkit (Lonza) and incubated at 37°C in a humidified 5% CO_2 atmosphere. The medium was replaced twice weekly, and cells were passaged with 0.25% trypsin/0.05% EDTA (Biological Industries, Israel) upon reaching 90%confluence. Experiments were performed at passage three. OASCs and ABASCs (1.0×10^6 cells) at passage 3 were plated on a 100 mm dish (Falcon) and cultured in ASCs BulletKit™ Medium (Lonza). At 100% confluence, ASCs were washed with PBS and cultured with ASC serum free medium (Lonza) for 48 h before isolation of their respective medium, containing many released growth factors and cytokines. Both OASC-conditioned medium (OASC-CM) and ABASC-conditioned medium (ABASC-CM) were maintained at -80°C for further analysis using protein Array (RayBiotec).

4.5. Rescue Study

4.5.1. RPE Cells Were Preincubated with OASC-CM Followed by Treatment with H2O2. 1×10^4 RPE cells were seeded in a 6-well plate (Falcon), in 1 mL of RtEGM containing 2% FBS (Lonza). The medium was changed to free-FBS RtEGM and renewed every two days until treatments. After reaching approximately 90% confluence, RPE cells were preincubated for 48 hours with either OASCs conditioned medium or with nonconditioned ADSC serum free medium (non-CM) as control. RPE cells were then washed with PBS followed by exposure to 1.5 mM H_2O_2 (Cat. no. 216763, Sigma) or without H_2O_2 exposure as control. After 7 hours, RPE cell death was monitored by propidium iodide (PI) using FACS analysis.

4.5.2. Propidium Iodide Staining and Flow Cytometry Analysis. Following rescue studies as described above, RPE cells at passage three were harvested with 0.25% trypsin/0.05% EDTA (Biological Industries). Cells (3×10^5) were collected by centrifugation at 500 g for 5 min, washed twice with PBS, and resuspended in 400 μl of PBS to which 1 μl of propidium iodide (1 mg/mL, Sigma) was added immediately before flow cytometry measurements. At least 10,000 events were collected and labeled, and fluorescent cells were detected by BD FACS CantoTM II cytometer (BD Pharmingen, USA). Analysis of cell death distribution was conducted by FCS Express 4 software (De Novo Software, Canada).

4.5.3. Human Cytokine Antibody Array. Cytokine secretion of OASCs was studied by cytokine antibody array on collected culture medium and compared to that of ABASCs. Conditioned medium was prepared as described above; briefly, ASCs' medium was changed to serum-free medium, following 48 hours of incubation, and the medium was collected and centrifuged at 4500 rpm for 5 min and supernatants stored at −80°C until they were assayed. Levels of medium released cytokines and growth factors were measured by RayBio® Human Cytokine Antibody Array G10 (Thermo-Fisher) according to manufacturer's protocol.

4.5.4. Differentiation of OASCs to RPE. We evaluated the differentiation potential of OASCs to RPE using a coculture system [55]. First, each cell line was marked with a different fluorescent dye in order to lineage-trace differentiated cells following coculture. OASCs and p-RPE were, respectively, labeled, with green fluorescent dye using carboxyfluorescein succinimidyl ester (CFSE) from CellTrace™ CFSE Cell Proliferation Kit (Invitrogen) and violet fluorescent dye using CellTrace™ Violet Cell Proliferation Kits (Invitrogen) according to the manufacturers' instructions. Then, OASC (1×10^6) cells were cocultured with primary human RPE (1×10^6) cells for one week in a mixture medium composed by 50% of Dulbecco's Modified Eagle Medium (DMEM) containing 10% foetal bovine serum (FBS) and 50% of free-FBS RtEGM and incubated at 37°C in a humidified 5% CO_2 atmosphere. Half of the medium was changed two times a week. All the cells were harvested and analyzed with a BD FACSAria Fusion Cell Sorter instrument (BD Biosciences) according to their respective marker. Results were compared to a negative control-OASCs noncocultured with RPE and a positive control-mature primary RPE cells labeled with CellTrace™ Violet (also called Violet Cell Trace).

4.5.5. Characterization of OASCs and ABASCs Cell Sorted after Coculture. After cell sorting of the cells, we identified OASC-derived RPE cells, and we characterized the level of differentiation by qRT-PCR using primers (Table S1) and immunocytochemistry using, respectively, monoclonal/polyclonal antibodies anti-PAX6/anti-OTX1/2 (1/100, Abcam, Cambridge, England), and a goat anti-rabbit Alexa Fluor 594-conjugated crossadsorbed secondary antibody (1/1000, Invitrogen).

4.5.6. Gene Expression Quantification. The gene expression profile of OTX2, PAX6, SIX3, RPE65, and KLF4 in OASCs after costaining with primary human RPE was quantified using qRT-PCR in order to detect differentiation markers. Results were compared to a negative control-OASCs which were non c-cultured with RPE. We also quantified the expression of Ck-β8, ICAM1, eotaxin-3, and BDNF in OASCs and ABASCs to confirm the cytokine antibody array. Total RNA was extracted from OASC and ABASC cell cultures using High Pure RNA Isolation Kit (Roche) or TRI Reagent (Sigma-Aldrich) according to the manufacturers' instructions. Total RNA concentration was reverse transcribed using qScript cDNA Synthesis Kit (Quantabio) or Verso cDNA synthesis kit (Thermo-Scientific), and the mRNA expression levels of these genes were measured by RT-PCR (StepOnePlus–Applied Biosystems), using SYBR® Green qPCR Mastermix (Qiagen). Results were normalized by using the housekeeping gene GUSB. Results were calculated by the $\Delta\Delta$CT method of relative quantitation. List of primers used is presented in Table S1.

4.5.7. Immunocytochemistry. For detection of retinal precursors markers at the protein level, sorted cells and controls were plated on 13 mm coverslips in a 24 well-plate (Falcon) overnight, respectively, in a mixture medium (50% of DMEM 10% FBS/50% of free-FBS RtEGM) or in DMEM containing 10% of FBS and incubated at 37°C in a humidified atmosphere (respectively, 5 and 8% of CO2). The cells were fixed with 4% paraformaldehyde for 20 minutes, permeabilized with 0.1% Triton™ X-100 for 5 minutes, blocked overnight with PBS diluted 2% BSA, and labeled with rabbit primary antibody anti-OTX1/2 (OTX1 is not expressed in RPE and photoreceptors [56]) or PAX6 for 1 hour at room temperature. Goat anti-Rabbit IgG (H + L) Cross-Adsorbed Secondary Antibody, Alexa Fluor 594 (A-11012), and Alexa Fluor® 488 Phalloidin (Invitrogen) were diluted in phosphate-buffered saline containing 2% BSA for 1 hour at room temperature, for detection of OTX1/2 or PAX6. Nuclei were stained with DAPI in Thermo Scientific™ Shandon™ Immu-Mount™.

4.5.8. Animal Procedure. Wild-type C57BL mice received intraperitoneal (IP) injection of 50 mg/kg of sodium iodate (NaIO3) (Sigma-Aldrich) ($n \geq 4$). The sodium iodate induces oxidative stress and acute injury to RPE that triggers progressive retinal damage [26]. Twenty-four hours after

injection, mice were anesthetized, and a small self-sealing sclerotomy was performed with the tip of a 30-gauge needle. A 36-gauge needle attached to a Hamilton syringe (Hamilton Company, Reno, Nevada, USA) was inserted through sclerotomy into the subretinal space, and an injection of 1.5 μl of PBS containing 4×10^4 cells was performed.

Mice received cyclosporine in drinking water for a week after the transplantation, at a concentration of 210 mg/l. Animal handling and experiments were performed following institutional care guidelines with the approval of the Tel Aviv Sourasky Medical Center Animal Ethics Committee.

4.5.9. Tissue Preparation. Mice were euthanized on day zero and three weeks following subretinal transplantation; the eyes were enucleated and fixed in 4% formaldehyde (Merck, Darmstadt, Germany) overnight. The eyes were washed in PBS and then incubated for cryoprotection with 30% sucrose in PBS overnight at 4°C. Fixed tissue was embedded in OCT Tissue Freezing Medium (Scigen Scientific, Gardena, CA, USA) and frozen on dry ice. Cross-sections (10 μm) were placed on X-tra adhesive slides (Leica Biosystems, Peterborough, UK) and stored at -20°C.

4.5.10. Immunohistochemistry. Frozen slides were stained with hematoxylin and eosin (H&E). For immunofluorescence staining, sections were washed in PBS for 20 minutes and blocked with 5% bovine serum albumin (BSA) (Sigma-Aldrich), 1% normal goat serum (NGS) (Invitrogen, no. 31872), and 0.5% Triton X-100 (Sigma-Aldrich) in PBS for 1 hour at room temperature. The sections were incubated overnight with anti-RPE65 rabbit monoclonal primary antibody (ab231782, 1 : 200), anti-CD45 clone IBL-5/25 Rat monoclonal antibody (EMD Millipore, Merck, Darmstadt, Germany, 1 : 50), Mouse anti-rhodopsin monoclonal antibody (EMD Millipore, Merck, Darmstadt, Germany, 1 : 200), Iba1, and rabbit antibody (Wako, Osaka, Japan, 1 : 1000), in blocking solution at 4°C. The slides were washed three times with PBS-0.5% Triton X-100 (PBST), incubated with Alexa Fluor 488 Goat anti-rabbit, Alexa Fluor 546 Goat-anti-rat, and Alexa Fluor 546 Goat anti-mouse (Invitrogen, 1/200) in PBST for 1 h at room temperature in blocking solution, and washed again three times with PBST. The sections were then incubated with the nuclear dye DAPI (Molecular Probes, Thermo Fisher Scientific) for 10 minutes, washed twice in PBS, and mounted in ImmunoMount (Thermo Scientific, 9990412).

Pictures were carried out with a Zeiss LSM 700 confocal microscope in a blinded manner. Analysis was performed by ImageJ software. RPE65 and rhodopsin intensity and quantification of positive CD45 and Iba1 cells were performed by measuring the fluorescence intensity compared to the image's background. Also, the thickness of ONL and INL was evaluated by measuring length of ONL and INL layers (stained with DAPI) in at least 6 points of the layer. The sections shown were selected at the same distance to the optic disc and in the same retinal quadrant.

4.6. Statistical Analysis. Statistical analyses were performed using GraphPad Prism software (version 9.0, GraphPad Software, San Diego, California). The Mann–Whitney test was used to analyze nonparametric data. For the mice results, a Kruskal-Wallis nonparametric test was used to identify differences between the three groups. Statistical significance was accepted for p value< 0.05.

Data Availability

Will be given upon request.

Ethical Approval

This study was approved by the Tel Aviv Sourasky Medical Center Institutional Review Board (Helsinki Committee, approval number 920120440). All the experimental procedures involving patients in this study were approved by the Tel Aviv Sourasky Medical Center Institutional Review Board (Helsinki Committee, approval number 920120440).

Consent

Written or verbal informed consent was obtained from all patients; the study conforms to the principles outlined in the Declaration of Helsinki.

Disclosure

This study was presented in the Association for Research in Vision and Ophthalmology (ARVO) Annual Meeting Abstract in June 2021.

Conflicts of Interest

The authors declare no competing interests regarding the publication of this paper.

Authors' Contributions

B.K. wrote the paper; B.K., S.W. and I.N. conducted the experiments; A.B. and B.K designed the experiments. Bryan Krief and Shira Weisthal Algor contributed equally to this work.

Acknowledgments

This study was supported by grants from the Moxie Foundation (260375) and from Orion grant (213310).

Supplementary Materials

Table S1: primers used in quantitative RT-PCR experiments. Supplementary Figure 1: detection of cells in the subretinal space on the day of ASC transplantation in the NaIO3 mice model. *(Supplementary Materials)*

References

[1] J. Tan, J. Wang, V. Flood, E. Rochtchina, W. Smith, and P. Mitchell, "Dietary antioxidants and the long-term incidence of age-related macular degeneration. The Blue Mountains Eye Study," *Ophthalmology*, vol. 115, pp. 334–341, 2008.

[2] J. Cai, K. C. Nelson, M. Wu, P. Sternberg Jr., and D. P. Jones, "Oxidative damage and protection of the RPE," *Progress in Retinal and Eye Research*, vol. 19, pp. 205–221, 2000.

[3] S. Lightman and H. M. A. Towler, "Diabetic retinopathy," *Clinical Cornerstone*, vol. 5, no. 2, pp. 12–21, 2003.

[4] S. Grisanti, M. Ishioka, M. Kosiewicz, and L. Q. Jiang, "Immunity and immune privilege elicited by cultured retinal pigment epithelial cell transplants," *Investigative Ophthalmology & Visual Science*, vol. 38, no. 8, pp. 1619–1626, 1997.

[5] R. Simó, M. Villarroel, L. Corraliza, C. Hernández, and M. Garcia-Ramírez, "The Retinal Pigment Epithelium: Something More than a Constituent of the Blood-Retinal Barrier—Implications for the Pathogenesis of Diabetic Retinopathy," *Journal of biomedicine & biotechnology*, vol. 2010, Article ID 190724, 15 pages, 2010.

[6] V. Chichagova, D. Hallam, J. Collin et al., "Cellular regeneration strategies for macular degeneration: past, present and future," *Eye (London, England)*, vol. 32, no. 5, pp. 946–971, 2018.

[7] M. Boulton and P. Dayhaw-Barker, "The role of the retinal pigment epithelium: topographical variation and ageing changes," *Eye (London, England)*, vol. 15, Part 3, pp. 384–389, 2001.

[8] M. M. Lalu, L. McIntyre, C. Pugliese et al., "Safety of cell therapy with mesenchymal stromal cells (SafeCell): a systematic review and meta-analysis of clinical trials," *PLoS One*, vol. 7, no. 10, article e47559, 2012.

[9] H. E. Hong, O. H. Kim, B. J. Kwak et al., "Antioxidant action of hypoxic conditioned media from adipose-derived stem cells in the hepatic injury of expressing higher reactive oxygen species," *Annals of surgical treatment and research*, vol. 97, no. 4, pp. 159–167, 2019.

[10] A. Barzelay, S. Weisthal Algor, A. Niztan et al., "Adipose-derived mesenchymal stem cells migrate and rescue RPE in the setting of oxidative stress," *Stem Cells International*, vol. 2018, Article ID 9682856, 11 pages, 2018.

[11] T. K. Ng, V. R. Fortino, D. Pelaez, and H. S. Cheung, "Progress of mesenchymal stem cell therapy for neural and retinal diseases," *World journal of stem cells*, vol. 6, no. 2, pp. 111–119, 2014.

[12] G. W. Roddy, J. Y. Oh, R. H. Lee et al., "Action at a distance: systemically administered adult stem/progenitor cells (MSCs) reduce inflammatory damage to the cornea without engraftment and primarily by secretion of TNF-α stimulated gene/-protein 6," *Stem cells (Dayton, Ohio)*, vol. 29, no. 10, pp. 1572–1579, 2011.

[13] W. S. Kim, B. S. Park, and J. H. Sung, "The wound-healing and antioxidant effects of adipose-derived stem cells," *Expert Opinion on Biological Therapy*, vol. 9, no. 7, pp. 879–887, 2009.

[14] A. Barzelay, R. Levy, E. Kohn et al., "Power-assisted liposuction versus tissue resection for the isolation of adipose tissue-derived mesenchymal stem cells: phenotype, senescence, and multipotency at advanced passages," *Aesthetic Surgery Journal*, vol. 35, no. 7, pp. NP230–NP240, 2015.

[15] E. Farré-Guasch, C. Martí-Pagè, F. Hernádez-Alfaro, J. Klein-Nulend, and N. Casals, "Buccal fat pad, an oral access source of human adipose stem cells with potential for osteochondral tissue engineering: an in vitro study," *Tissue engineering. Part C, Methods*, vol. 16, no. 5, pp. 1083–1094, 2010.

[16] W. J. Jurgens, M. J. Oedayrajsingh-Varma, M. N. Helder et al., "Effect of tissue-harvesting site on yield of stem cells derived from adipose tissue: implications for cell-based therapies," *Cell and Tissue Research*, vol. 332, no. 3, pp. 415–426, 2008.

[17] N. Billon, P. Iannarelli, M. C. Monteiro et al., "The generation of adipocytes by the neural crest," *Development (Cambridge, England)*, vol. 134, no. 12, pp. 2283–2292, 2007.

[18] T. Langenberg, A. Kahana, J. A. Wszalek, and M. C. Halloran, "The eye organizes neural crest cell migration," *Developmental dynamics : an official publication of the American Association of Anatomists*, vol. 237, no. 6, pp. 1645–1652, 2008.

[19] M. C. Johnston, D. M. Noden, R. D. Hazelton, J. L. Coulombre, and A. J. Coulombre, "Origins of avian ocular and periocular tissues," *Experimental Eye Research*, vol. 29, no. 1, pp. 27–43, 1979.

[20] H. Ni, Y. Zhao, Y. Ji, J. Shen, M. Xiang, and Y. Xie, "Adipose-derived stem cells contribute to cardiovascular remodeling," *Aging*, vol. 11, no. 23, pp. 11756–11769, 2019.

[21] J. Lee, S. Lee, C. Y. Lee et al., "Adipose-derived stem cell-released osteoprotegerin protects cardiomyocytes from reactive oxygen species-induced cell death," *Stem Cell Research & Therapy*, vol. 8, no. 1, p. 195, 2017.

[22] G. H. Xiao, M. Jeffers, A. Bellacosa, Y. Mitsuuchi, G. F. Vande Woude, and J. R. Testa, "Anti-apoptotic signaling by hepatocyte growth factor/met via the phosphatidylinositol 3-kinase/Akt and mitogen-activated protein kinase pathways," *Proceedings of the National Academy of Sciences of the United States of America*, vol. 98, no. 1, pp. 247–252, 2001.

[23] L. I. Shu-Ping and H. U. Guo-Fu, "Mechanism and function of angiogenin in apoptosis regulation," *Zhongguo sheng wu hua xue yu fen zi sheng wu xue bao = Chinese journal of biochemistry and molecular biology*, vol. 31, no. 12, pp. 1258–1260, 2015.

[24] S. R. Mekala, V. Vauhini, U. Nagarajan, S. Maddileti, S. Gaddipati, and I. Mariappan, "Derivation, characterization and retinal differentiation of induced pluripotent stem cells," *Journal of Biosciences*, vol. 38, no. 1, pp. 123–134, 2013.

[25] D. Baas, K. M. Bumsted, J. A. Martinez, F. M. Vaccarino, K. C. Wikler, and C. J. Barnstable, "The subcellular localization of Otx2 is cell-type specific and developmentally regulated in the mouse retina. Brain research," *Molecular Brain Research*, vol. 78, no. 1-2, pp. 26–37, 2000.

[26] B. A. Berkowitz, R. H. Podolsky, J. Lenning et al., "Sodium iodate produces a strain-dependent retinal oxidative stress response measured in vivo using QUEST MRI," *Investigative Ophthalmology & Visual Science*, vol. 58, no. 7, pp. 3286–3293, 2017.

[27] G. Chowers, M. Cohen, D. Marks-Ohana et al., "Course of sodium iodate-induced retinal degeneration in albino and pigmented mice," *Investigative Ophthalmology & Visual Science*, vol. 58, no. 4, pp. 2239–2249, 2017.

[28] Y. Zhang, R. Li, W. Rong et al., "Therapeutic effect of hepatocyte growth factor-overexpressing bone marrow-derived mesenchymal stem cells on CCl4-induced hepatocirrhosis," *Cell Death & Disease*, vol. 9, no. 12, p. 1186, 2018.

[29] W. Ma, Y. Zhang, C. Gao, R. N. Fariss, J. Tam, and W. T. Wong, "Monocyte infiltration and proliferation reestablish myeloid cell homeostasis in the mouse retina following retinal pigment epithelial cell injury," *Scientific Reports*, vol. 7, no. 1, p. 8433, 2017.

[30] A. Acquistapace, T. Bru, P. F. Lesault et al., "Human mesenchymal stem cells reprogram adult cardiomyocytes toward a progenitor-like state through partial cell fusion and

mitochondria transfer," *Stem cells (Dayton, Ohio)*, vol. 29, no. 5, pp. 812–824, 2011.

[31] P. Li, X. Sun, Z. Ma et al., "Transcriptional reactivation of OTX2, RX1 and SIX3 during reprogramming contributes to the generation of RPE cells from human iPSCs," *International Journal of Biological Sciences*, vol. 12, no. 5, pp. 505–517, 2016.

[32] A. O. Barnea-Cramer, W. Wang, S. J. Lu et al., "Function of human pluripotent stem cell-derived photoreceptor progenitors in blind mice," *Scientific Reports*, vol. 6, p. 29784, 2016.

[33] K. Kim, A. Doi, B. Wen et al., "Epigenetic memory in induced pluripotent stem cells," *Nature*, vol. 467, no. 7313, pp. 285–290, 2010.

[34] K. Bharti, S. S. Miller, and H. Arnheiter, "The new paradigm: retinal pigment epithelium cells generated from embryonic or induced pluripotent stem cells," *Pigment Cell & Melanoma Research*, vol. 24, no. 1, pp. 21–34, 2011.

[35] D. C. Berry, D. Stenesen, D. Zeve, and J. M. Graff, "The developmental origins of adipose tissue," *Development (Cambridge, England)*, vol. 140, no. 19, pp. 3939–3949, 2013.

[36] N. Terada, T. Hamazaki, M. Oka et al., "Bone marrow cells adopt the phenotype of other cells by spontaneous cell fusion," *Nature*, vol. 416, no. 6880, pp. 542–545, 2002.

[37] D. J. Ambrosi and T. P. Rasmussen, "Reprogramming mediated by stem cell fusion," *Journal of Cellular and Molecular Medicine*, vol. 9, no. 2, pp. 320–330, 2005.

[38] A. E. Kuriyan, T. A. Albini, J. H. Townsend et al., "Vision loss after intravitreal injection of autologous "stem cells" for AMD," *The New England Journal of Medicine*, vol. 376, no. 11, pp. 1047–1053, 2017.

[39] M. Moriguchi, S. Nakamura, Y. Inoue et al., "Irreversible Photoreceptors and RPE Cells Damage by intravenous sodium iodate in mice is related to macrophage accumulation," *Investigative ophthalmology & visual science*, vol. 59, no. 8, pp. 3476–3487, 2018.

[40] B. T. McLelland, B. Lin, A. Mathur et al., "Transplanted hESC-derived retina organoid sheets differentiate, integrate, and improve visual function in retinal degenerate rats," *Investigative Ophthalmology & Visual Science*, vol. 59, no. 6, pp. 2586–2603, 2018.

[41] J. A. Burdick, R. L. Mauck, and S. Gerecht, "To serve and protect: hydrogels to improve stem cell-based therapies," *Cell Stem Cell*, vol. 18, no. 1, pp. 13–15, 2016.

[42] T. V. Johnson, N. D. Bull, and K. R. Martin, "Identification of barriers to retinal engraftment of transplanted stem cells," *Investigative Ophthalmology & Visual Science*, vol. 51, no. 2, pp. 960–970, 2010.

[43] M. Horie, H. Choi, R. H. Lee et al., "Intra-articular injection of human mesenchymal stem cells (MSCs) promote rat meniscal regeneration by being activated to express Indian hedgehog that enhances expression of type II collagen," *Osteoarthritis and Cartilage*, vol. 20, no. 10, pp. 1197–1207, 2012.

[44] S. R. Baglio, D. M. Pegtel, and N. Baldini, "Mesenchymal stem cell secreted vesicles provide novel opportunities in (stem) cell-free therapy," *Frontiers in Physiology*, vol. 3, p. 359, 2012.

[45] C. Chang, J. Yan, Z. Yao, C. Zhang, X. Li, and H. Q. Mao, "Effects of mesenchymal stem cell-derived paracrine signals and their delivery strategies," *Advanced Healthcare Materials*, vol. 10, no. 7, article e2001689, 2021.

[46] M. Greter, I. Lelios, and A. L. Croxford, "Microglia versus myeloid cell nomenclature during brain inflammation," *Frontiers in Immunology*, vol. 6, p. 249, 2015.

[47] A. Aguzzi, B. A. Barres, and M. L. Bennett, "Microglia: scapegoat, saboteur, or something else?," *Science*, vol. 339, no. 6116, pp. 156–161, 2013.

[48] Y. Okunuki, R. Mukai, E. A. Pearsall et al., "Microglia inhibit photoreceptor cell death and regulate immune cell infiltration in response to retinal detachment," *Proceedings of the National Academy of Sciences of the United States of America*, vol. 115, no. 27, pp. E6264–E6273, 2018.

[49] L. Todd, I. Palazzo, L. Suarez et al., "Reactive microglia and IL1β/IL-1R1-signaling mediate neuroprotection in excitotoxin-damaged mouse retina," *Journal of Neuroinflammation*, vol. 16, no. 1, p. 118, 2019.

[50] N. P. Hailer, I. Bechmann, S. Heizmann, and R. Nitsch, "Adhesion molecule expression on phagocytic microglial cells following anterograde degeneration of perforant path axons," *Hippocampus*, vol. 7, no. 3, pp. 341–349, 1997.

[51] B. J. Evans, A. McDowall, P. C. Taylor, N. Hogg, D. O. Haskard, and R. C. Landis, "Shedding of lymphocyte function-associated antigen-1 (LFA-1) in a human inflammatory response," *Blood*, vol. 107, no. 9, pp. 3593–3599, 2006.

[52] E. Martin and C. Delarasse, "Complex role of chemokine mediators in animal models of Alzheimer's disease," *Biomedical journal*, vol. 41, no. 1, pp. 34–40, 2018.

[53] J. R. Guedes, T. Lao, A. L. Cardoso, and J. El Khoury, "Roles of microglial and monocyte chemokines and their receptors in regulating Alzheimer's disease-associated amyloid-β and tau pathologies," *Frontiers in Neurology*, vol. 9, p. 549, 2018.

[54] P. Zamiri, S. Sugita, and J. W. Streilein, "Immunosuppressive properties of the pigmented epithelial cells and the subretinal space," *Chemical Immunology and Allergy*, vol. 92, pp. 86–93, 2007.

[55] S. Strassburg, S. M. Richardson, A. J. Freemont, and J. A. Hoyland, "Co-culture induces mesenchymal stem cell differentiation and modulation of the degenerate human nucleus pulposus cell phenotype," *Regenerative Medicine*, vol. 5, no. 5, pp. 701–711, 2010.

[56] N. Esumi, S. Kachi, L. Hackler Jr. et al., "BEST1 expression in the retinal pigment epithelium is modulated by OTX family members," *Human Molecular Genetics*, vol. 18, no. 1, pp. 128–141, 2009.

Hindawi
Stem Cells International
Volume 2021, Article ID 7690006, 17 pages
https://doi.org/10.1155/2021/7690006

Research Article

lncRNA-KCNQ1OT1: A Potential Target in Exosomes Derived from Adipose-Derived Stem Cells for the Treatment of Osteoporosis

Shan-zheng Wang,[1] Jun Jia,[2] and Chang-hong Chen[3]

[1]*Department of Orthopaedics, Zhongda Hospital, Medical School of Southeast University, 87 Ding Jia Qiao Road, Nanjing, Jiangsu 210009, China*
[2]*Department of Orthopaedics, The 904th Hospital of Joint Logistic Support Force, PLA, 101 Xingyuan North Road, Wuxi, Jiangsu 214000, China*
[3]*Department of Orthopaedics, Jiangyin Hospital Affiliated to Nanjing University of Chinese Medicine, 130 Renmin Middle Road, Jiangyin, Jiangsu 214400, China*

Correspondence should be addressed to Chang-hong Chen; changhongchen0917@gmail.com

Received 14 August 2021; Revised 21 September 2021; Accepted 29 September 2021; Published 19 October 2021

Academic Editor: Huseyin Sumer

Background. Osteoporosis is a worldwide medical and socioeconomic burden characterized by systemic impairment of bone strength and microstructure. Exosomes derived from adipose-derived stem cells (ADSCs-Exos) have been confirmed to play effective roles in the repair of various tissues and organs. This study was aimed at investigating the role of ADSCs-Exos and a novel long noncoding RNA KCNQ1OT1 played in osteoporosis as well as the underlying mechanism. *Methods*. Primary osteoblasts were treated with different doses of tumor necrosis factor-α (TNF-α) (0, 1, 2.5, 5, and 10 ng/ml) and then cocultured with ADSCs-Exos or exosome-derived from lnc-KCNQ1OT1-modified ADSCs (KCNQ1OT1-Exos). The expression of miRNA-141-5p (miR-141-5p) and lnc-KCNQ1OT1 was evaluated by quantitative real-time polymerase chain reaction (qRT-PCR). The protein expression of cleaved-caspase-3, caspase-3, and Bax was determined by Western blot. Cell viability and apoptosis were assessed by Cell Counting Kit-8 (CCK-8) and flow cytometry analysis, respectively. The binding sites between KCNQ1OT1 and miR-141-5p were validated by dual-luciferase reporter assay. *Results*. TNF-α dose-dependently increased miR-141-5p expression, inhibited viability, and promoted apoptosis of osteoblasts. However, miR-141-5p silencing or cocultured with ADSCs-Exos attenuated these effects. In addition, KCNQ1OT1-Exos could more significantly attenuate the induced cytotoxicity and apoptosis compared to ADSCs-Exos. Moreover, miR-141-5p was confirmed as the target of KCNQ1OT1 by luciferase reporter assay. *Conclusions*. ADSCs-Exos can attenuate cytotoxicity and apoptosis of TNF-α-induced primary osteoblasts. KCNQ1OT1-Exos have a more significant inhibitory effect compared to ADSCs-Exos by the function of sponging miR-141-5p, suggesting that KCNQ1OT1-Exos can be promising agents in osteoporosis treatment.

1. Introduction

Osteoporosis is a common skeletal disease characterized by structural disorders of bone mass caused by increased osteoclast activity and reduced osteoblast generation [1]. Clinical treatment strategies are often based on the promotion of osteoblast proliferation and osteoclast inhibition [2, 3]. In osteoporosis pathogenesis, tumor necrosis factor-α (TNF-α) is a proinflammatory cytokine which has been revealed to contribute to osteoporosis by regulating both osteoblasts and osteoclasts [3, 4]. TNF-α can suppress bone formation and inhibit osteoblast differentiation by inducing cytotoxicity and apoptosis [5, 6]. Therefore, exploring new pathways to arrest TNF-α-induced cytotoxicity and apoptosis in osteoporosis is necessary.

As a subset of mesenchymal stem cells (MSCs), adipose-derived stem cells (ADSCs) can be easily obtained from

adipose tissues and possess the potential of multidifferentiation and self-renewal [7, 8]. ADSCs are found in abundant quantities and can be easily obtained by minimally invasive procedures [9]. Autologous ADSCs can be used to promote bone regeneration under osteoporotic conditions [10]. Thus, the application of ADSCs might be a promising MSC-based strategy for bone formation and structural remodeling in osteoporosis [11, 12].

Exosomes are small, membrane-bound extracellular vesicles that are enriched in selected proteins, lipids, nucleic acids, and glycoconjugates [13]. Exosomes have been proved to play a significant role in the etiology of bone metabolic diseases, especially osteoporosis [14]. Exosomes derived from ADSCs (ADSCs-Exos) contain bioactive substances of ADSCs and might play a similar role to ADSCs [15]. Recent researches have demonstrated that ADSCs-Exos had stimulating effects in the repair of a variety of tissues and organs [10, 16, 17]. Nevertheless, the potential therapeutic effects of ADSCs-Exos on osteoporosis and the underlying mechanism need further investigations.

Exosomes are important mediators between cells by transferring molecules, such as long noncoding RNAs (lncRNA), microRNAs (miRNAs), and cytokines [18–21]. Evidence indicates that exosomes derived from mmu_circ_0000250-modified ADSCs are able to promote wound healing in diabetic mice [22]. Additionally, exosomes derived from miR-188-3p-modified ADSCs can protect Parkinson's disease [23]. Recently, KCNQ1overlapping transcript 1 (lnc-KCNQ1OT1) was found to be able to positively regulate osteogenic differentiation of bone marrow mesenchymal stem cells (BMSCs) by acting as a ceRNA to regulate BMP2 expression through sponging miR-214 [24]. However, few studies have investigated the potential role of KCNQ1OT1 in the treatment of osteoporosis. This study was aimed at investigating the role of ADSCs-Exos and KCNQ1OT1 played in osteoporosis as well as the underlying mechanism.

2. Methods

2.1. Isolation and Culture of ADSCs. The Institutional Animal Care and Use Committee of Southeast University approved the protocol for the use of animals in this study. Adipose tissues were collected from the inguinal fat pad of 2-3-week-old C57BL/6 mice (SLAC, Shanghai, China) and then rinsed in phosphate-buffered saline (PBS) and cut into 1×1 mm pieces. The collected tissues were digested by collagenase type II (Sigma-Aldrich, USA) at 37°C for 1 h. After digestion, tissues were centrifuged at room temperature (1000 rpm, 5 min) and the resultant cell pellet was resuspended in Dulbecco's modified Eagle's medium (DMEM) at the cell density of 5×10^6/ml. Cells were then cultured at 37°C under a 5% CO_2 atmosphere. The culture medium was replaced every 2-3 days, and cells after 3 passages were used in the present study.

2.2. Characterization of Isolated ADSCs. ADSCs were cultured in a 24-well plate at a density of 4×10^4 cells/well with basic culture medium (DMEM-LG) containing 10% FBS, 100 U/ml penicillin, and 100 mg/ml streptomycin. They were subjected to induced differentiation by culturing them in osteogenic (Cyagen Biosciences, Rasmx-90021), adipogenic (Cyagen Biosciences, Rasmx-90031), and chondrogenic (Cyagen Biosciences, Rasmx-90041) medium, respectively. The outcomes were evaluated by Alizarin Red, Oil Red O, and Alcian Blue staining, respectively. In addition, MSC surface markers ($CD90^+$ and CD34-) were detected by flow cytometric analysis. Briefly, adherent cells from passage 4 were resuspended and then incubated in FACS buffer containing 2 μl of Fc receptor-blocking reagent (FcX Blocker, BioLegend, San Diego, CA, USA). Cells were stained with reagent to exclude dead cells (Zombie NIR, Japan). After washing the cells, IC fixation buffer (Affymetrix, Japan) was added. Permeabilization buffer (Affymetrix, Japan) was diluted with purified water for 10 times. After permeabilization, CD90 and CD34 antibodies were used to stain the cells. All antibodies were from BD Biosciences (Tokyo, Japan). Stained cells were sorted by flow cytometry (Accuri C6, BD), and data was analyzed with FlowJo software (Tree Star, Ashland, OR, USA).

2.3. Isolation and Characterization of Primary Osteoblasts. The isolation and characterization of primary osteoblasts were conducted as described before [25]. Briefly, calvarium tissues from C57BL/6 mice were collected and digested in 0.25% trypsin (Thermo Fisher, USA) containing 0.02% EDTA for 25 min at 37°C. Then, the tissues were digested in 5 ml Hanks solution containing 0.1% collagenase I (Thermo Fisher, USA) and 0.05% trypsin for 1 h in a shaking incubator at 37°C with a shaking speed of 200 r/min. The released cells were collected by centrifugation for 10 minutes at 1500 r/min. The cells were suspended in 5 ml of a-MEM (containing 1 g/L D-Glucose and L-Glutamine, BI, USA) containing 10% FBS and then transferred to 25 cm^2 plastic culture flasks (Nest, China). The culture flasks were incubated at 37°C in a 5% CO_2 incubator. The images of cell morphology were taken using a microscope attaching camera (OLYMPUS, IX51). The primary osteoblasts of passage 4 were prepared for further experiments and characterized by alkaline phosphatase staining and Alizarin Red S staining.

2.4. KCNQ1OT1 Transfection. To overexpress lncRNA-KCNQ1OT1, the lncRNA-KCNQ1OT1 mimic was subcloned into pcDNA-3.1 vector (Invitrogen, USA) to generate pcDNA-lnc-KCNQ1OT1 constructs. For stable transduction of pcDNA-lnc-KCNQ1OT1 or pcDNA-3.1 (negative control, NC), pcDNA-lnc-KCNQ1OT1 or NC was transfected into ADSCs using Lipofectamine 2000 (Invitrogen, USA) according to the manufacturer's instructions.

2.5. Isolation and Characterization of Exosomes. At 48 h posttransfection, a Total Exosome Isolation kit (Invitrogen, USA) was applied to isolate the total exosomes from the supernatant of ADSC culture medium and culture medium transfected with pcDNA-lnc-KCNQ1OT1 or NC (ADSCs-Exos, LV-KCNQ1OT1-Exos, or LV-NC-Exos, respectively) according to the manufacturer's protocol [26]. Bicinchoninic acid (BCA) protein assay kit (MACGENE, China) was used

Table 1: Sequences of primers used for qRT-PCR.

Primer name	Primer sequence
lncRNA-KCNQ1OT1-F	5′-TTGGTAGGATTTTGTTGAGG-3′
lncRNA-KCNQ1OT1-R	5′-CAACCTTCCCCTACTACC-3′
GAPDH-F	5-TGGATTTGGACGCATTGGTC-3′
GAPDH-R	5′-TTTGCACTGGTACGTGTTGAT-3′
miR-141-5p-F	5′-GCAGTGTTGGATGGTTGAAGTATG-3′
miR-141-5p-R	5′-GAATTTGCGTGTCATCCTTGC-3′
U6-F	5′-CGCTTCGGCAGCACATATACT-3′
U6-R	5′-GAATTTGCGTGTCATCCTTGC-3′

to measure the concentration of isolated exosomes. Before use, all exosome samples were analyzed for proper size by nanoparticle tracking analysis (NTA; NanoSight, Malvern) and for morphology by transmission electron microscopy (TEM). The protein levels of CD9, CD63, CD81, and Alix (representative markers of exosomes) were then detected.

2.6. Exosome Uptake Assay. ADSCs-Exos were labeled with PKH26 (Sigma Aldrich, USA) according to the manufacturer's protocol. Isolated exosomes were resuspended in diluent C (1 ml). Then, 6 μl PKH26 was added. ADSCs-Exos and PKH26 solutions were mixed for 30 s and then centrifuged (120000 × g, 2 h, 4°C). Exosomes were resuspended in the complete culture medium, and the PKH26-labeled ADSC-Exo solution was added into primary osteoblasts for incubation. After 24 h of culture, osteoblast cells were fixed with 4% formaldehyde for 10 min. DAPI was used to stain the nuclei.

2.7. Cell Viability Assay. The viability of primary osteoblasts was determined by the Cell Counting Kit-8 (CCK-8; Dojindo, Japan) assay. Briefly, cells were seeded into 96-well plates (2×10^4 cell/ml) and incubated for 24 h. Then, 10 μl CCK-8 solution was added into each well for incubation of 1-2 h (37°C, 5% CO_2). Subsequently, the optical density (OD) value was measured at 450 nm using a spectrophotometer (Bio-Rad, USA).

2.8. Cell Apoptosis Assay. The apoptosis of primary osteoblasts was evaluated by Annexin V-FITC/PI Apoptosis Assay Kit (KeyGen Biotech, China). Briefly, primary osteoblasts were collected and washed with PBS. A total of 500 μl binding buffer was added to suspend cells. Firstly, 5 μl Annexin V-FITC was added, and then, 5 μl propidium iodide was added for incubation for 5-15 min in the dark at room temperature. Cell apoptosis was analyzed by flow cytometry (Becton-Dickinson, FACSCalibur, USA).

2.9. Western Blot Analysis. The total protein of primary osteoblasts was extracted using RIPA lysis buffer (Beyotime, China) and quantified by BCA assay (Beyotime, China). Equal amounts of proteins (100 μg) were separated via Beyo-Gel™ Plus PAGE (Beyotime, China) and then transferred to a PVDF membrane (Millipore, USA). After transferring, the membranes were blocked with 5% fat-free milk for 1 h. The membranes were incubated with primary antibodies (Bax, ab32503; Caspase-3, ab32351; and cleaved-Caspase-3, ab32042) purchased from Abcam (USA) and GAPDH, 10494-I-AP purchased from Proteintech (China) at 4°C overnight. The membranes were incubated with second antibodies (goat anti rabbit IgG HRP SE134, goat anti mouse IgG HRP SE131, Solarbio, China) at 37°C for 1 h. The ECL system (CLINX, China) was used for exposing protein bands. The intensity of the bands was analyzed using Image Lab (version 3.0, Bio-Rad, USA).

2.10. Gene Expression Analysis Using Quantitative Real-Time Polymerase Chain Reaction (qRT-PCR). Total RNA was extracted from cells using TRIzol reagent (Invitrogen, USA) according to the manufacturer's protocol. For detecting miR-141-5p expression, MicroRNA cDNA Synthesis Kit (Vazyme, China) was applied for reverse transcription of cDNA, followed by qRT-PCR analysis. U6 was employed as the loading control. The primers of miR-141-5p and U6 were purchased from GeneCopoeia (Guangzhou, China). Meanwhile, the expression of lncRNA-KCNQ1OT1 was evaluated by PrimeScript™ Master Mix (Takara, Japan) and GAPDH was employed as the loading control. The data was calculated using the $2^{-\Delta\Delta Ct}$ method. Primers used in this study are shown in Table 1.

2.11. Dual-Luciferase Reporter Assay. The wild-type (WT) sequence of lncRNA-KCNQ1OT1 containing the miR-141-5p binding sites (KCNQ1OT1-WT) and the mutant sequence (KCNQ1OT1-MUT) were cloned into pMIR vectors (Promega, USA), respectively. Primary osteoblasts and HEK293 cells were cotransfected with miR-141-5p or miR-NC and KCNQ1OT1-WT or KCNQ1OT1-MUT. The luciferase activity was detected using Dual-Luciferase Reporter Assay System (Promega, USA) in the dark.

2.12. Statistical Analysis. Statistical analysis was performed with SPSS 20.0 software (IBM, Armonk, NY, USA). All quantitative data were described as mean ± SD. One-way ANOVA was used to analyze the statistical differences among three or more groups while unpaired Student's *t*-test was applied to analyze the statistical differences

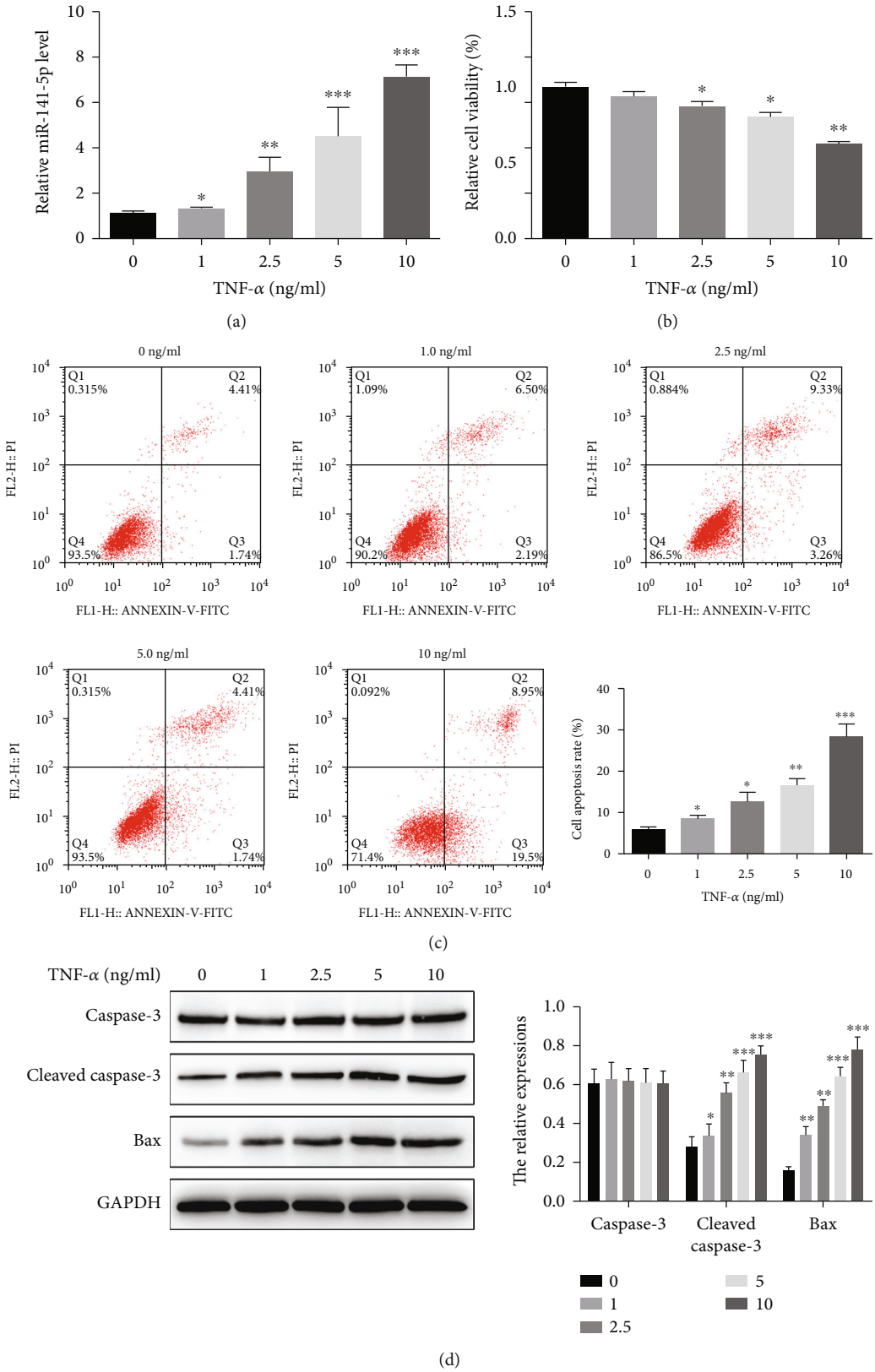

Figure 1: TNF-α increases miR-141-5p expression, suppresses the viability, and promotes the apoptosis of primary osteoblasts in a dose-dependent manner. (a) TNF-α dose-dependently increased miR-141-5p expression as detected by qRT-PCR. (b, c) TNF-α reduced cell viability and increased cell apoptosis in a dose-dependent manner as detected by CCK-8 assay and flow cytometry, respectively. (d) TNF-α increased the protein expression level of Bax and cleaved-Caspase-3 dose-dependently as detected by immunoblotting. $^{*}P < 0.05$, $^{**}P < 0.01$, and $^{***}P < 0.001$.

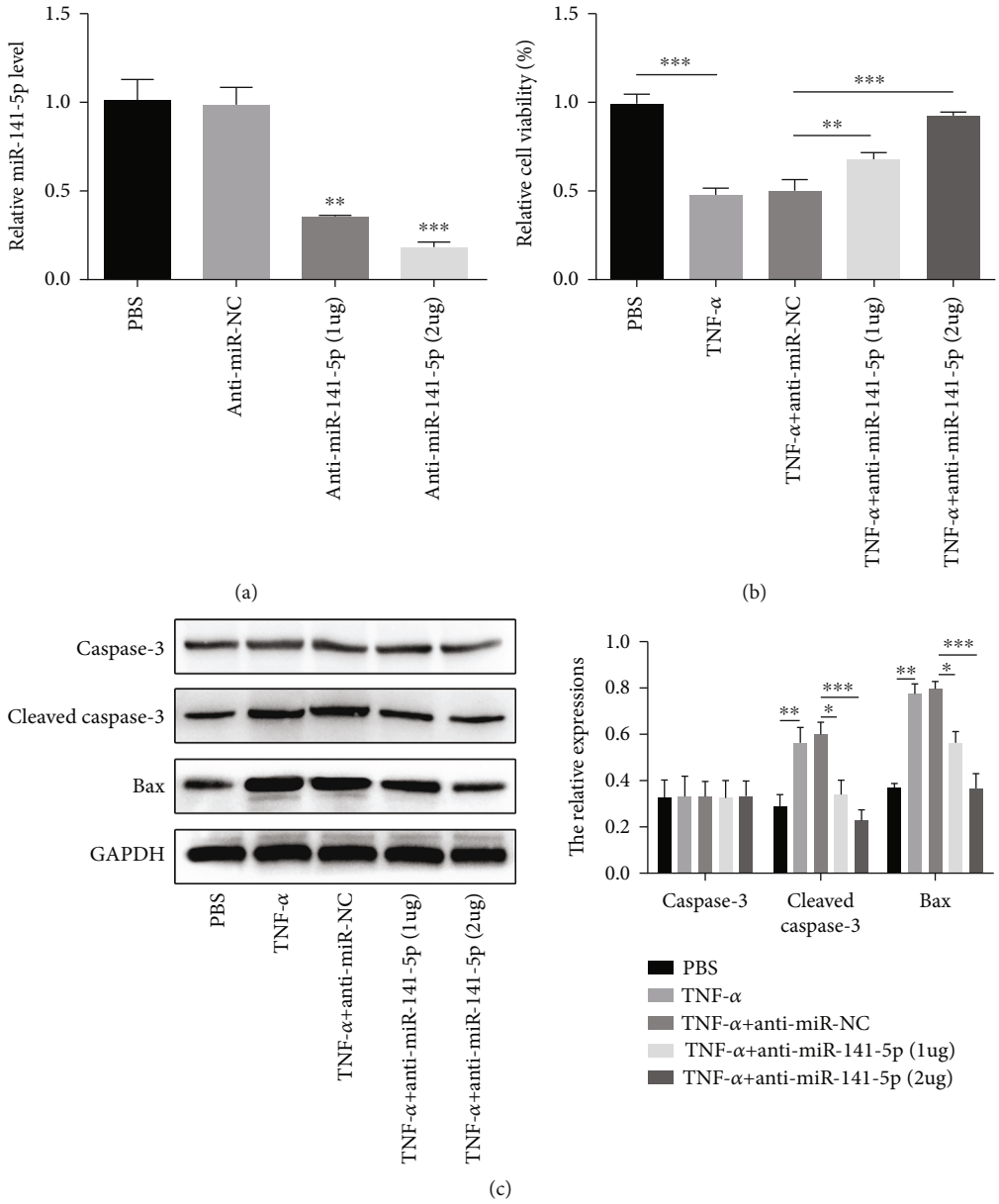

Figure 2: Continued.

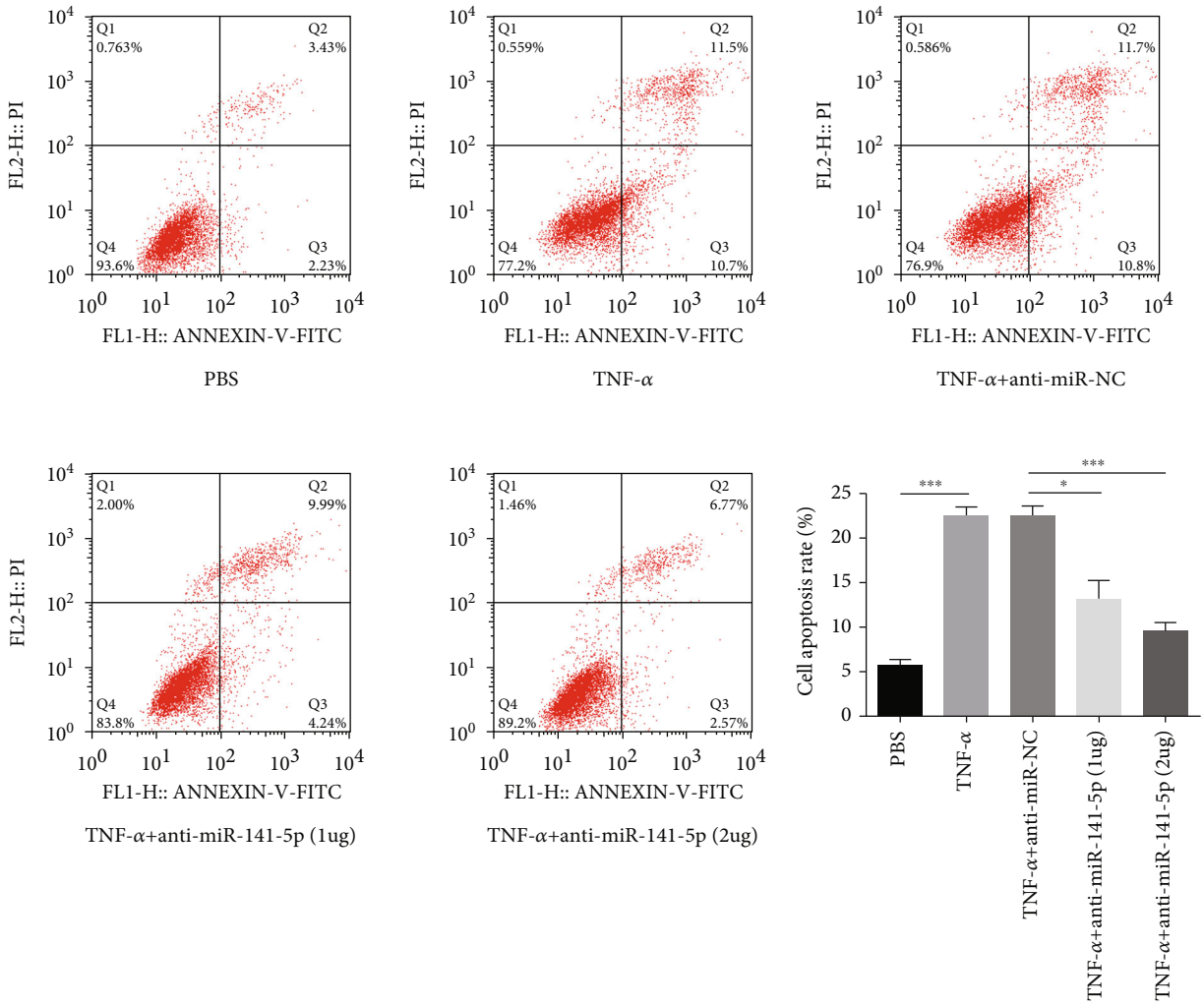

(d)

Figure 2: Knockdown of miR-141-5p reverses the effect of TNF-α on primary osteoblasts. (a) anti-miR-141-5p reduced the expression of miR-141-5p more significantly in primary osteoblasts compared to anti-miR-NC. (b) CCK-8 assays revealed that the knockdown of miR-141-5p partly reversed the inhibition of cell viability induced by TNF-α when cells were treated with PBS, TNF-α, TNF-α+anti-miR-NC, TNF-α+anti-miR-141-5p (1μg), or TNF-α+anti-miR-141-5p (2μg), respectively. (c) The increase of Bax and cleaved-Caspase-3 expression induced by TNF-α was inhibited by downregulating miR-141-5p. (d) Annexin V-FITC/PI revealed that the knockdown of miR-141-5p partly reversed cell apoptosis induced by TNF-α. $^{*}P < 0.05$, $^{**}P < 0.01$, and $^{***}P < 0.001$.

between two groups. $P < 0.05$ was considered statistically significant.

3. Results

3.1. TNF-α Increases miR-141-5p Expression, Suppresses the Viability, and Promotes the Apoptosis of Primary Osteoblasts in a Dose-Dependent Manner. Primary osteoblasts were treated with increased concentrations of TNF-α (0, 1, 2.5, 5, and 10 ng/ml). TNF-α dose-dependently increased miR-141-5p expression (Figure 1(a)). Meanwhile, primary osteoblasts treated with TNF-α showed reduced cell viability and increased apoptosis in a dose-dependent manner (Figures 1(b) and 1(c)). Furthermore, TNF-α increased the protein expression level of Bax and cleaved-Caspase-3 dose-dependently (Figure 1(d)).

3.2. Knockdown of miR-141-5p Reverses the Effect of TNF-α on Primary Osteoblasts. Since miR-141-5p was upregulated in TNF-α-treated primary osteoblasts, we knocked down miR-141-5p expression using anti-miR-141-5p to explore its role in TNF-α-induced cytotoxicity and apoptosis. As expected, anti-miR-141-5p reduced the expression of miR-141-5p more significantly in primary osteoblasts compared to anti-miR-NC (Figure 2(a)). CCK-8 and Annexin V-FITC/PI assays revealed that the knockdown of miR-141-5p partly reversed the inhibition of cell viability and the promotion of cell apoptosis induced by TNF-α when cells were treated with PBS, TNF-α, TNF-α+anti-miR-NC, TNF-α+anti-miR-141-5p (1 μg), or TNF-α+anti-miR-141-5p (2 μg), respectively (Figures 2(b) and 2(d)). In line with this result, the increase of Bax and cleaved-Caspase-3 expression induced by TNF-α was inhibited by downregulating miR-141-5p (Figure 2(c)).

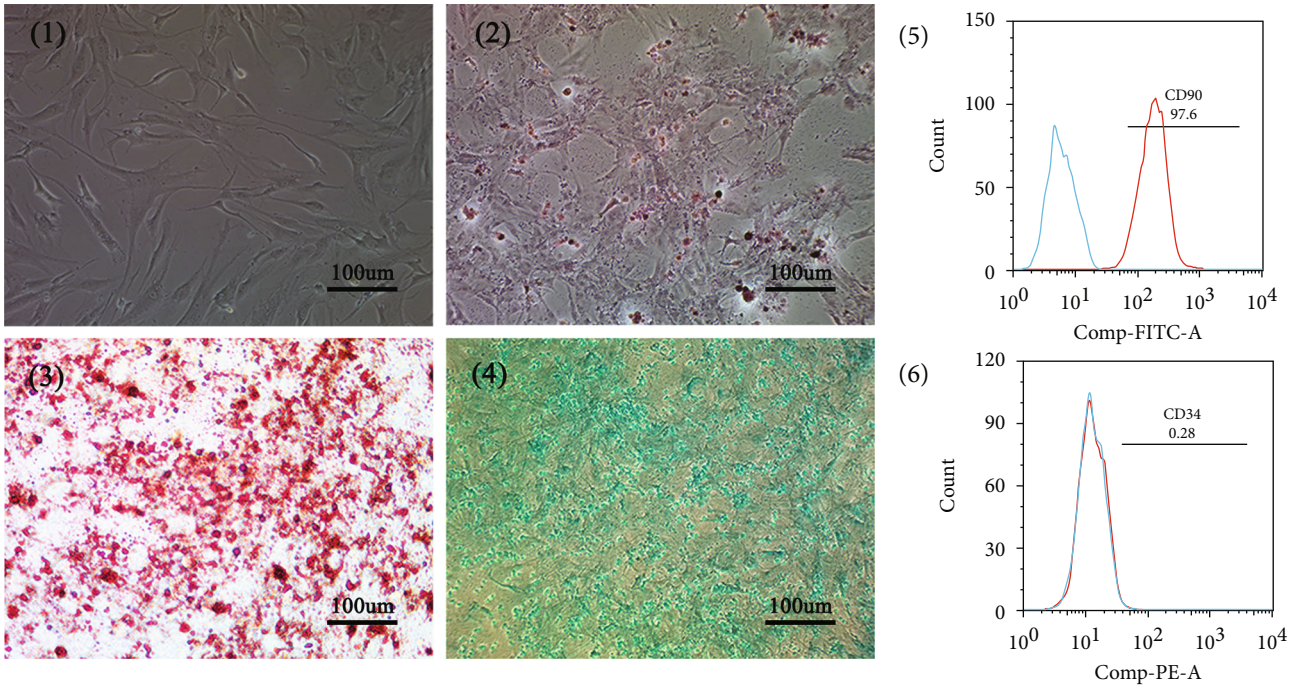

(a)

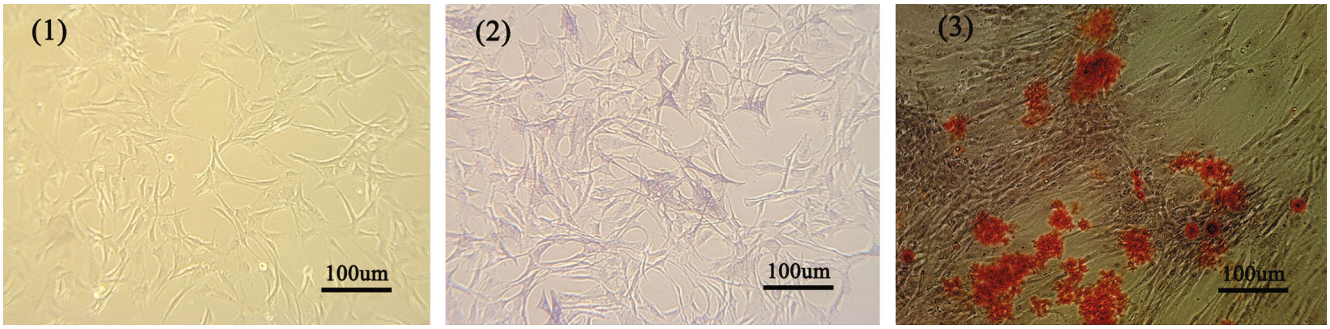

(b)

Figure 3: Continued.

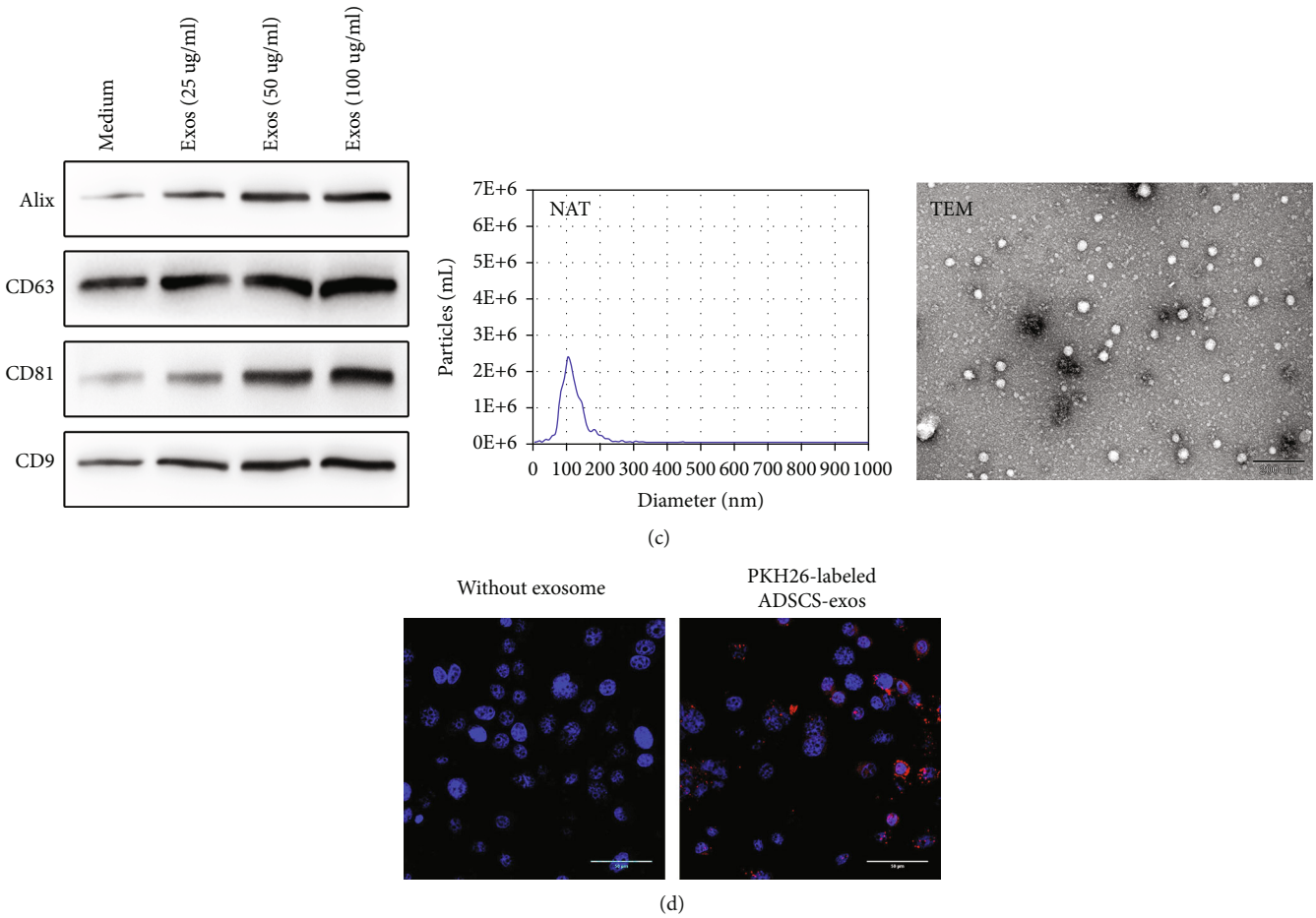

Figure 3: Characteristics of ADSCs, primary osteoblasts, and ADSCs-Exos. (a) (1) ADSCs isolated from C57/BL6 mice had a typical fibroblastic-like morphology. Alizarin Red (2), Oil Red O (3), and Alcian Blue stainings (4) were positive after the induced osteogenic, adipogenic, and chondrogenic differentiations of ADSCs. The isolated ADSCs were positive for CD90 (5) while negative for CD34 (6). (b) (1) Primary osteoblasts isolated from C57/BL6 mice had shuttle, cone, or cube morphology. Alkaline phosphatase staining (2) and Alizarin Red S staining (3) were positive in the isolated osteoblasts. (c) ADSCs-Exos were positive for the exosomes' markers, including CD9, CD81, CD63, and Alix; NAT and TEM results showed that the isolated exosomes were in complete form with the size of 119 + 23.1 nm. (d) Primary osteoblasts could uptake the PKH26-labeled ADSCs-Exos. Red: PKH26-labeled ADSCs-Exos. Blue: nuclei.

3.3. Characteristics of ADSCs, Primary Osteoblasts, and ADSCs-Exos. ADSCs isolated from C57/BL6 mice had a typical fibroblastic-like morphology (Figure 3(a), 1). Alizarin Red (Figure 3(a), 2), Oil Red O (Figure 3(a), 3), and Alcian Blue stainings (Figure 3(a), 4) were positive after the induced osteogenic, adipogenic, and chondrogenic differentiations of ADSCs. The isolated ADSCs were positive for CD90 (Figure 3(a), 5) while negative for CD34 (Figure 3(a), 6). Primary osteoblasts isolated from C57/BL6 mice had shuttle, cone or cube morphology (Figure 3(b), 1). Alkaline phosphatase staining (Figure 3(b), 2) and Alizarin Red S staining (Figure 3(b), 3) were positive in the isolated osteoblasts. The immunoblotting showed that the ADSCs-Exos were positive for the exosomes' markers, including CD9, CD81, CD63, and Alix (Figure 3(c)). NAT and TEM results showed that the isolated exosomes were in complete form with the size of 119 + 23.1 nm (Figure 3(c)). Furthermore, primary osteoblasts were cocultured with PKH26-labeled ADSCs-Exos. The red fluorescence of PKH26 label was observed in primary osteoblasts (Figure 3(d)), indicating primary osteoblasts could uptake ADSCs-Exos.

3.4. ADSCs-Exos Attenuate the Effect of TNF-α on Primary Osteoblasts. To determine the effects of ADSCs-Exos, primary osteoblasts were treated with TNF-α (5 ng/ml) and different doses of ADSCs-Exos (PBS, TNF-α, TNF-α+ADSCs-Exos (25 μg), TNF-α+ADSCs-Exos (50 μg), and TNF-α+ADSCs-Exos (100 μg)). ADSCs-Exos attenuated the upregulation of miR-141-5p induced by TNF-α dose-dependently (Figure 4(a)). Similarly, ADSCs-Exos reversed the inhibition of cell viability caused by TNF-α in a dose-dependent manner (Figure 4(b)). The elevated protein expression of cleaved caspase-3 and Bax induced by TNF-α was suppressed after coculture with ADSCs-Exos (Figure 4(c)). In line with this, the results of flow cytometry

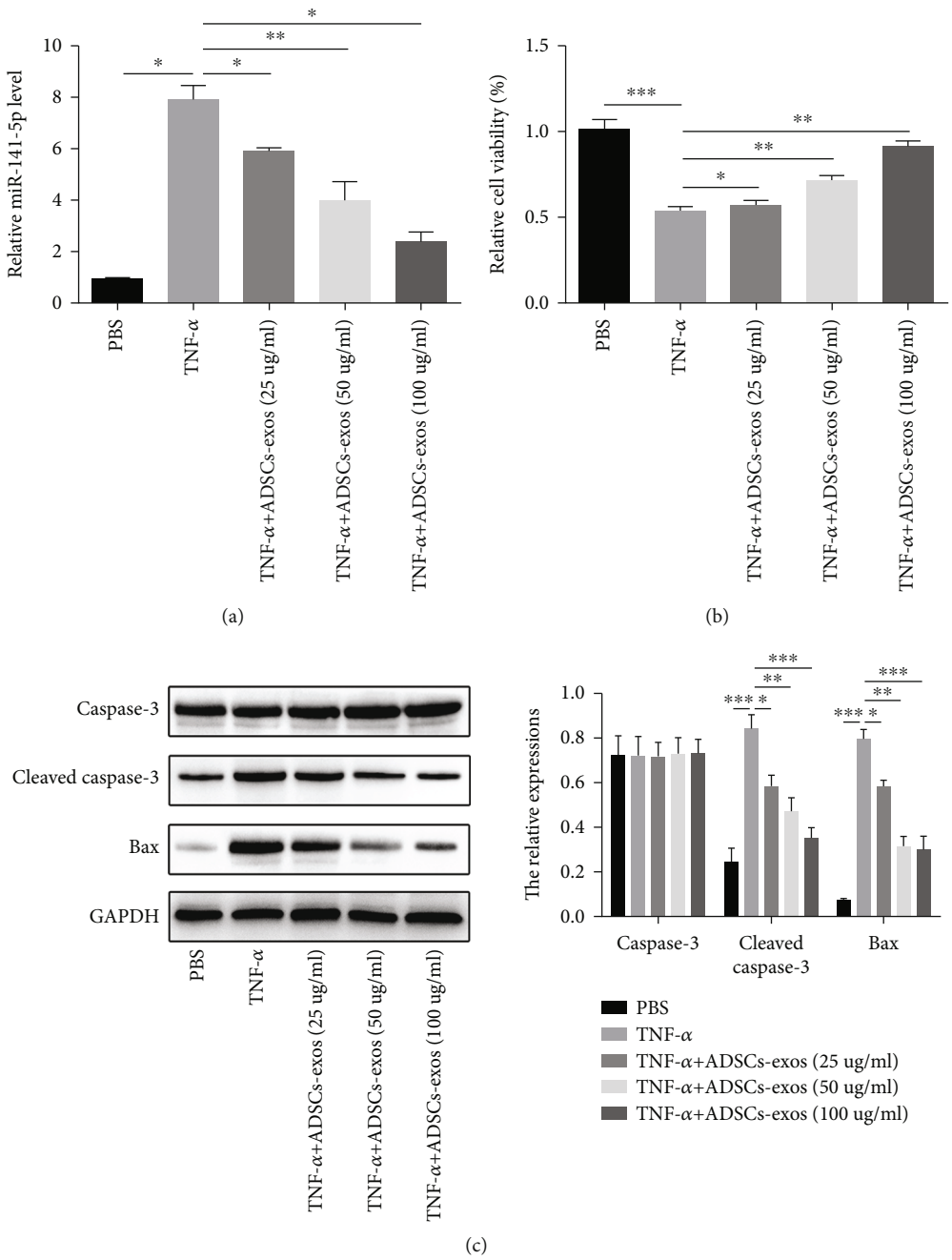

Figure 4: Continued.

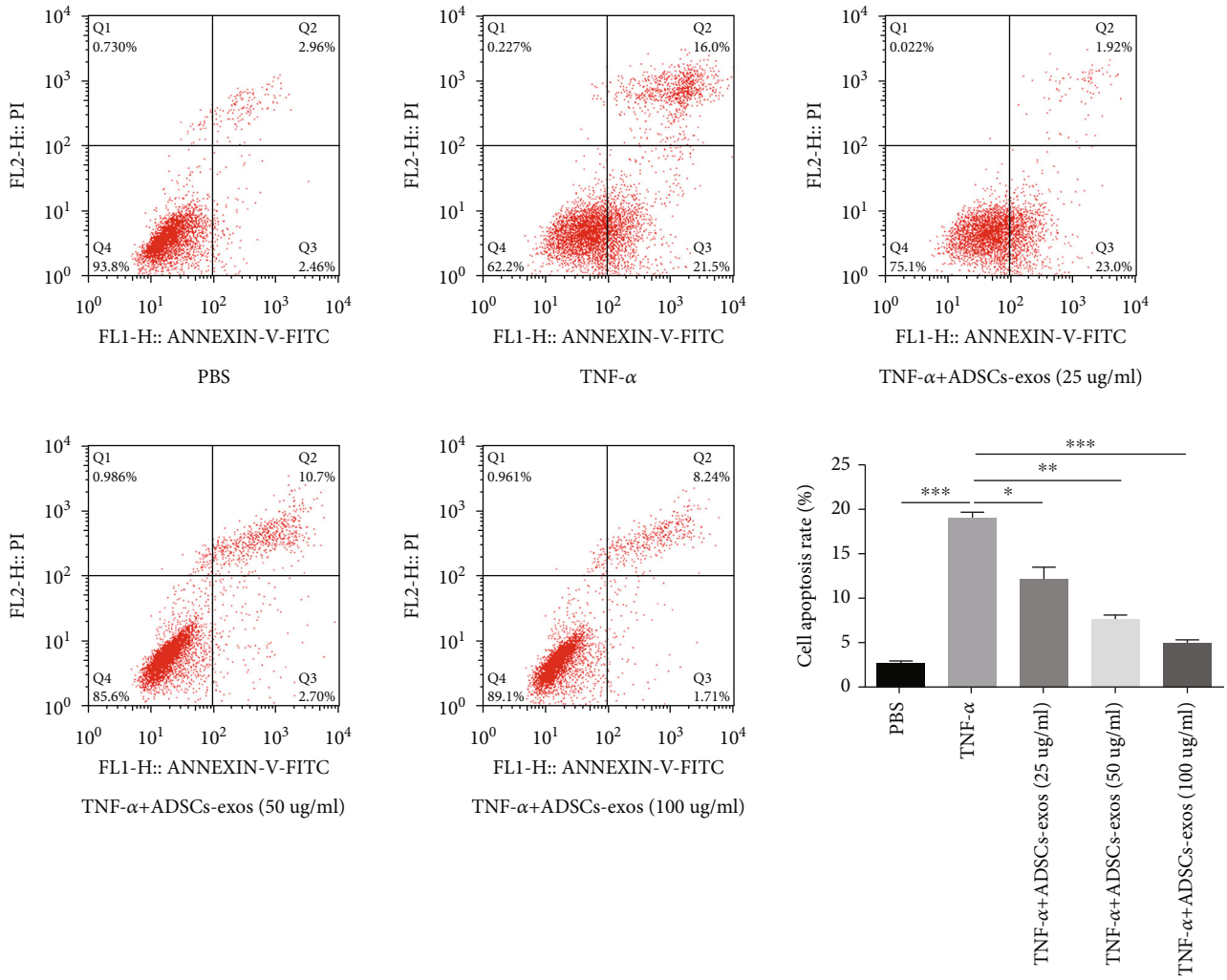

(d)

Figure 4: ADSCs-Exos attenuate the effect of TNF-α on primary osteoblasts. (a) ADSCs-Exos attenuated the upregulation of miR-141-5p induced by TNF-α dose-dependently. (b) ADSCs-Exos mitigated the inhibition of TNF-α on cell viability in a dose-dependent manner. (c) ADSCs-Exos dose-dependently decreased the promotion of TNF-α on cleaved caspase-3 and Bax expression. (d) Flow cytometry analysis showed that ADSCs-Exos dose-dependently reversed TNF-α-induced cell apoptosis. $^{*}P < 0.05$, $^{**}P < 0.01$, and $^{***}P < 0.001$.

indicated ADSCs-Exos dose-dependently blocked cell apoptosis induced by TNF-α (Figure 4(d)).

3.5. KCNQ1OT1-Exos Inhibit TNF-α-Induced Cytotoxicity and Apoptosis of Primary Osteoblasts. ADSCs were transfected with LV-KCNQ1OT1 or LV-NC for the determination of whether ADSCs transfected LV-KCNQ1OT1 into secreted exosomes. At 24 h post-LV-KCNQ1OT1 transfection, the expression of KCNQ1OT1 in ADSCs or exosomes derived from the ADSCs after different transfections was elevated, but the expression of miR-141-5p was downregulated compared with that in LV-NC-treated group (Figures 5(a) and 5(b)). In order to confirm whether ADSCs-Exos carrying LV-KCNQ1OT1 could deliver KCNQ1OT1 into primary osteoblasts, primary osteoblasts were cocultured with LV-NC-Exos or LV-KCNQ1OT1-Exos. KCNQ1OT1 expression was upregulated in primary osteoblasts treated with LV-KCNQ1OT1-Exos (Figure 5(c)). Next, to explore whether KCNQ1OT1-Exos could influence TNF-α-induced cytotoxicity and apoptosis, primary osteoblasts were treated with TNF-α and then cocultured with medium, ADSCs-Exos, LV-NC-Exos, or LV-KCNQ1OT1-Exos. The results of CCK-8 showed the coculture of primary osteoblasts with LV-KCNQ1OT1-Exos mitigated the negative effect of TNF-α on cell viability; ADSCs-Exos exerted a weaker stimulative effect on cell viability compared to LV-KCNQ1OT1-Exos (Figure 5(d)). Flow cytometry analysis indicated that TNF-α-induced cell apoptosis was reversed when primary osteoblasts were cocultured with LV-KCNQ1OT1-Exos; ADSCs-Exos exerted a weaker inhibitory effect on cell apoptosis compared to LV-KCNQ1OT1-Exos (Figure 5(e)). Consistent with that, the expression of Bax and cleaved caspase-3 in primary osteoblasts was blocked after coculture of LV-KCNQ1OT1-Exos (Figure 5(f)).

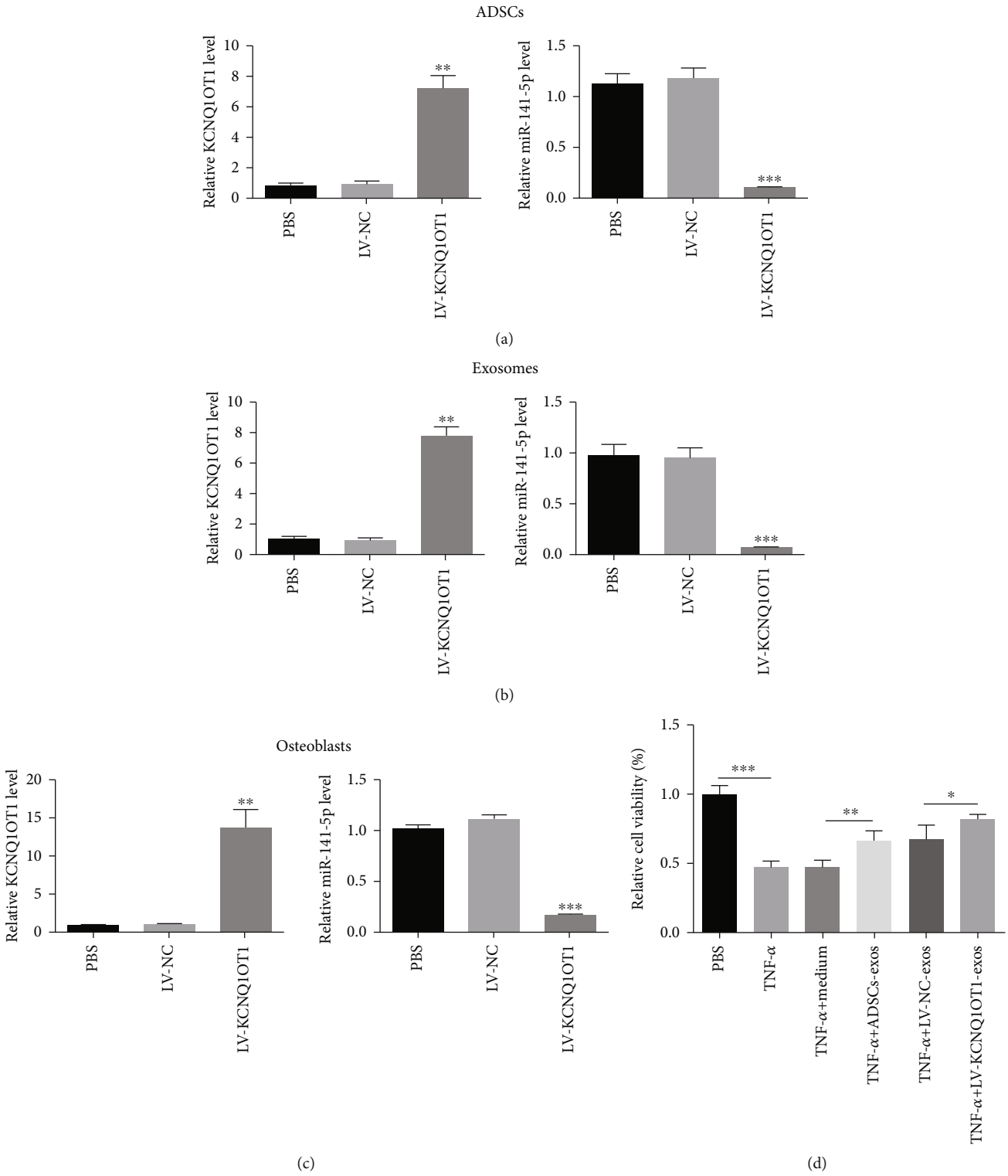

Figure 5: Continued.

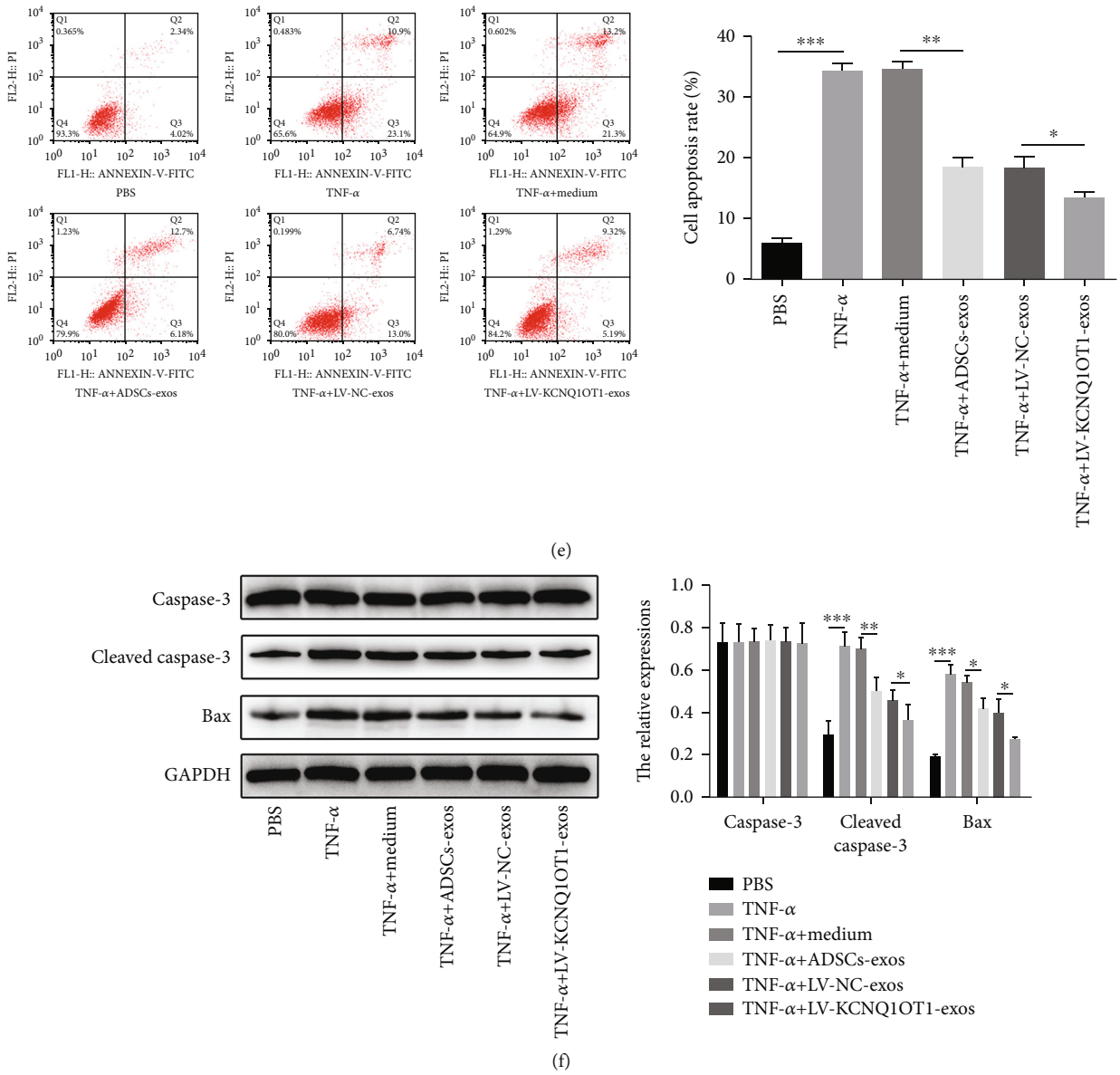

Figure 5: KCNQ1OT1-Exos inhibit TNF-α-induced cytotoxicity and apoptosis of primary osteoblasts. (a, b) The expression of KCNQ1OT1 in ADSCs or exosomes derived from the ADSCs after different transfections was elevated, but the expression of miR-141-5p was downregulated compared with that in LV-NC-treated group after the transfection of LV-KCNQ1OT1. (c) KCNQ1OT1 expression was upregulated in primary osteoblasts treated with LV-KCNQ1OT1-Exos compared to NC-Exos. (d) In primary osteoblasts, LV-KCNQ1OT1-Exos mitigated the negative effect of TNF-α on cell viability, while ADSCs-Exos exerted a weaker stimulative effect on cell viability compared to LV-KCNQ1OT1-Exos. (e) When primary osteoblasts were cocultured with LV-KCNQ1OT1-Exos, the TNF-α-induced cell apoptosis was reversed and ADSCs-Exos exerted a weaker inhibitory effect on cell apoptosis compared to LV-KCNQ1OT1-Exos. (f) The expression of Bax and cleaved caspase-3 in primary osteoblasts was blocked after coculture of LV-KCNQ1OT1-Exos. $^{*}P < 0.05$, $^{**}P < 0.01$, and $^{***}P < 0.001$.

3.6. KCNQ1OT1 Can Sponge miR-141-5p. Given KCNQ1OT1 sequence contains potential binding sites for miR-141-5p, we predicted KCNQ1OT1 could sponge miR-141-5p (Figure 6(a)). The dual-luciferase reporter assay was conducted to confirm the combination between them. As the result showed, overexpressed miR-141-5p weakened the luciferase activity in the KCNQ1OT1-WT group obviously, but the activity of luciferase reporters containing KCNQ1OT1-MUT was not changed significantly in HEK293 and primary osteoblasts (Figures 6(b) and 6(c)). Compared with ADSC-Exos and LV-NC-Exos, LV-KCNQ1OT1-Exos blocked the inhibitory effect of miR-141-5p on the luciferase activity of reporters containing KCNQ1OT1-WT (Figure 6(d)). Overexpressed KCNQ1OT1 decreased the expression of miR-141-5p, yet downregulation of KCNQ1OT1 increased that (Figure 6(e)). Moreover, when primary osteoblasts were cultured with LV-KCNQ1OT1-Exos, the expression of miR-141-5p was inhibited (Figure 6(f)).

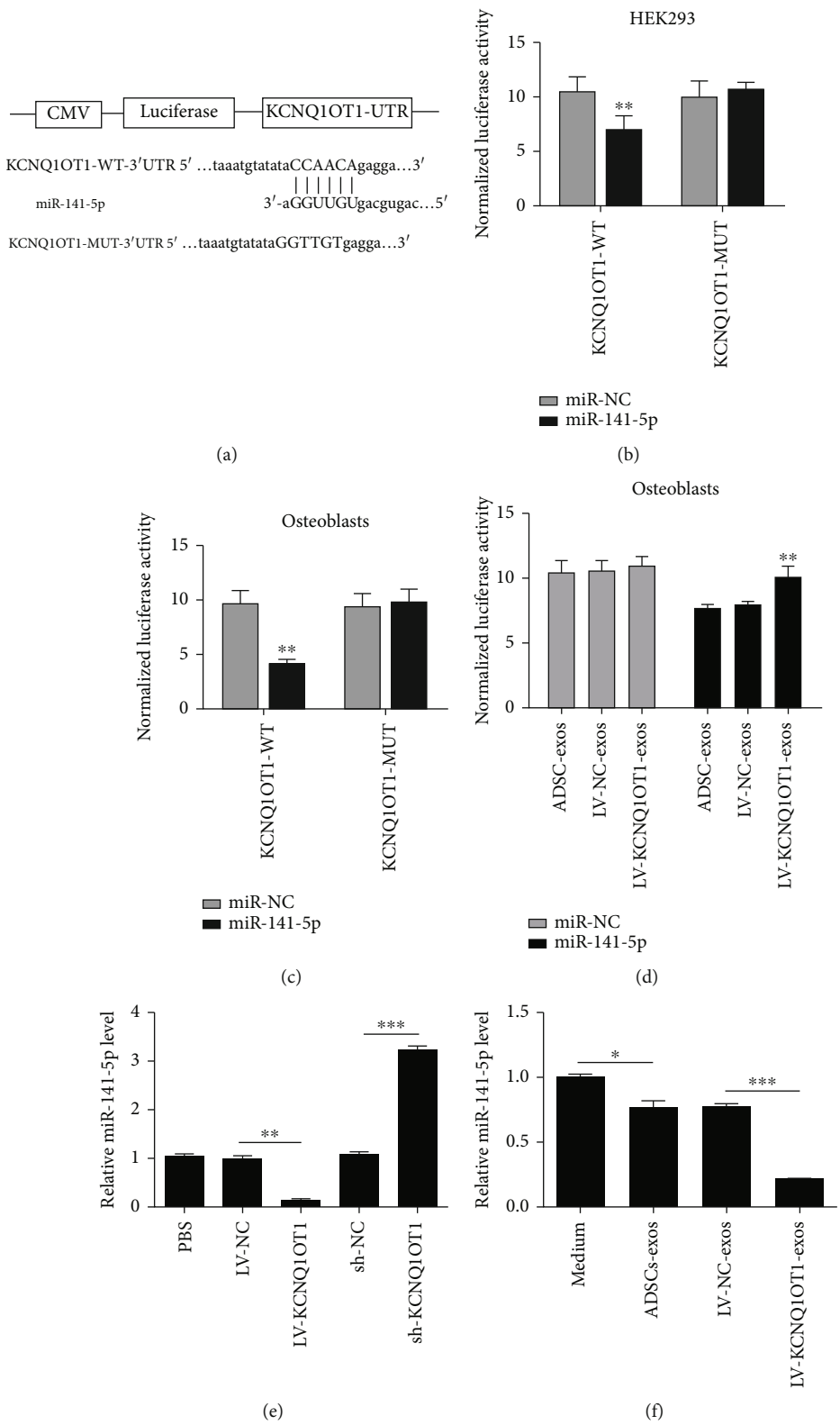

Figure 6: KCNQ1OT1 can sponge miR-141-5p. (a) KCNQ1OT1 and miR-141-5p have potential binding sites. (b, c) As dual-luciferase reporter assay showed, miR-141-5p weakened the luciferase activity in the KCNQ1OT1-WT group obviously, but the activity of luciferase reporters containing KCNQ1OT1-MUT was not changed significantly in both HEK293 and primary osteoblasts. (d) LV-KCNQ1OT1-Exos blocked the inhibitory effect of miR-141-5p on the luciferase activity of reporters containing KCNQ1OT1-WT compared with ADSC-Exos and LV-NC-Exos. (e) KCNQ1OT1 suppressed the expression of miR-141-5p, but the sh-KCNQ1OT1 increased that. (f) The expression of miR-141-5p was downregulated when primary osteoblasts were cocultured with LV-KCNQ1OT1-Exos. $^{*}P < 0.05$, $^{**}P < 0.01$, and $^{***}P < 0.001$.

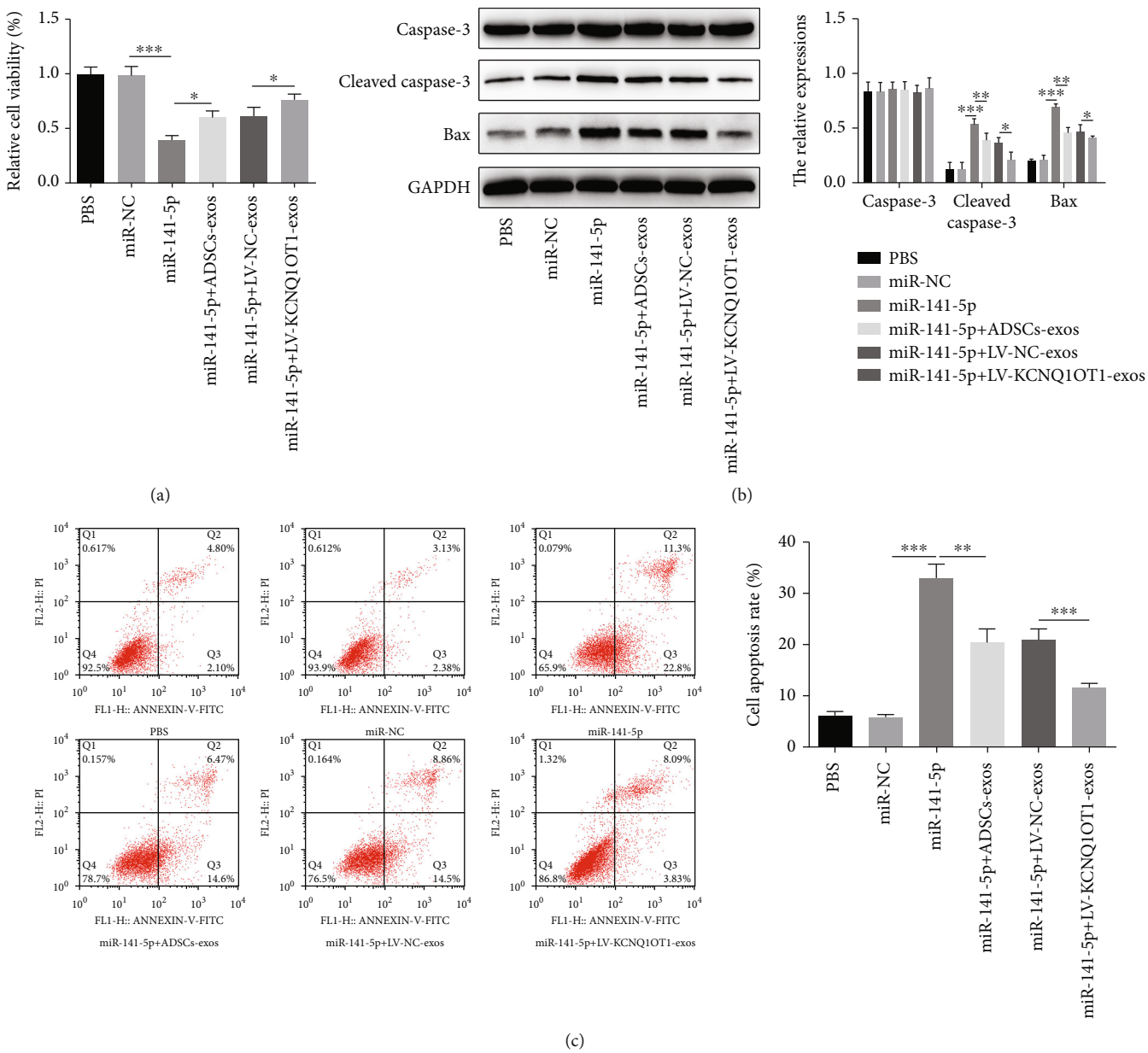

Figure 7: KCNQ1OT1-Exos inhibit the effect of TNF-α in primary osteoblasts by sponging miR-141-5p. (a) Primary osteoblasts were treated with TNF-α and then treated with miR-NC, miR-141-5p, miR-141-5p+ADSCs-Exos, miR-141-5p+LV-NC-Exos, or miR-141-5p+LV-KCNQ1OT1-Exos, respectively. (b) The inhibitory effect of TNF-α on cell viability was blocked by miR-141-5p, and the treatment of ADSCs-Exos or LV-KCNQ1OT1-Exos partly reversed this phenomenon; ADSCs-Exos exerted a weaker stimulative effect on cell viability compared to LV-KCNQ1OT1-Exos; the expression of cleaved caspase-3 and Bax was enhanced by miR-141-5p but was attenuated following coculture with ADSC-Exos or LV-KCNQ1OT1-Exos. (c) As flow cytometry showed, miR-141-5p promoted cell apoptosis while the treatment of ADSC-Exos or LV-KCNQ1OT1-Exos inhibited that; ADSCs-Exos exerted a weaker inhibitory effect on cell apoptosis compared to LV-KCNQ1OT1-Exos. $^{*}P < 0.05$, $^{**}P < 0.01$, and $^{***}P < 0.001$.

3.7. KCNQ1OT1-Exos Inhibit the Effect of TNF-α in Primary Osteoblasts by Sponging miR-141-5p. Primary osteoblasts were transfected with miR-141-5p or miR-NC to confirm whether KCNQ1OT1-Exos attenuate TNF-α-induced cytotoxicity and apoptosis by acting as an miR-146a sponge. After the treatment of TNF-α, primary osteoblasts were transfected with miR-141-5p or miR-NC and cocultured with ADSCs-Exos, LV-NC-Exos, or LV-KCNQ1OT1-Exos. The upregulation of miR-141-5p promoted the inhibitory effect of TNF-α on cell viability, and coculture with ADSCs-Exos or KCNQ1OT1-Exos partly reversed this phenomenon; ADSCs-Exos exerted a weaker stimulative effect on cell viability compared to LV-KCNQ1OT1-Exos (Figure 7(a)). Similarly, the upregulation of miR-141-5p enhanced cleaved caspase-3 and Bax expression. However, these effects were attenuated following coculture with ADSC-Exos or LV-KCNQ1OT1-Exos (Figure 7(b)). In line with this, flow cytometry showed that overexpressed miR-141-5p promoted cell

apoptosis but when cocultured with ADSC-Exos or LV-KCNQ1OT1-Exos, cell apoptosis was inhibited; ADSCs-Exos exerted a weaker inhibitory effect on cell apoptosis compared to LV-KCNQ1OT1-Exos (Figure 7(c)).

4. Discussion

With the deepening understanding of osteobiology, skeletal stem cells and osteoblasts are identified as significant targets in the treatment of osteoporosis by promoting bone formation and remodeling [27]. MSC transplantation provides evidences of enhancing osteogenic differentiation, increasing bone mineral density, and halting the deterioration of osteoporosis [28]. In 2001, Zuk et al. [29] isolated ADSCs from adipose tissues and found they are capable of differentiating into adipogenic, osteogenic, chondrogenic, and myogenic cells. As significant bioactive substances released from ADSCs, ADSCs-Exos have exhibited regenerative potential in many diseases [30–32]. However, few studies have investigated the role of ADSCs-Exos in the treatment of osteoporosis. Thus, whether ADSCs-Exos can effectively protect primary osteoblasts from the TNF-α-induced cytotoxicity and apoptosis is primarily studied in the present study.

Our results indicate that TNF-α can increase miR-141-5p expression and inhibit the cell proliferation in primary osteoblasts. In addition, TNF-α can increase cell apoptosis. Consistent with this, the expression of cleaved caspase-3 and Bax was also elevated. Currently, ADSCs have been widely used in tissue regeneration and bioengineering [7, 33]. However, with the in-depth investigations, the application of ADSCs has the potential risk of iatrogenic infection, malignant transformation, immune rejection, and safety issues [34–37]. Compared to ADSCs, ADSCs-Exos can hardly cause the immune rejection and malignant transformation [38, 39]. To make clear the effects of ADSCs-Exos in osteoporosis, we attempt to culture TNF-α-treated primary osteoblasts with ADSCs-Exos. Interestingly, ADSCs-Exos promote cell viability and decrease cell apoptosis, suggesting that ADSCs-Exos can be promising candidates in the treatment of osteoporosis.

Although we have found ADSCs-Exos can be beneficial in the treatment of osteoporosis, the underlying mechanism has not been revealed. Exosomes derived from MSCs contain multiple lncRNAs, which can be transported and transferred to other cells to regulate biological functions through targeting downstream genes [40, 41]. KCNQ1OT1, a lncRNA which is closely related to cell proliferation, migration, and apoptosis, has been reported to be an oncogene in a variety of tumors [42]. Evidence has showed that KCNQ1OT1 can promote cell proliferation and migration [43]. Therefore, we are curious whether KCNQ1OT1 can play a positive role in the treatment of osteoporosis. In the present study, KCNQ1OT1-Exos were confirmed to exert a more significant inhibitory effect on TNF-α-induced cytotoxicity and apoptosis compared to ADSCs-Exos. Thus, KCNQ1OT1-Exos are expected to be promising candidates in osteoporosis treatment.

lncRNAs can function as miRNA sponges by binding miRNAs [44]. As previously reported, lncRNA-HOTAIR can induce the apoptosis of osteoblasts via modulating the expression of miR-138 [45]. In postmenopausal osteoporosis, lncRNA LOXL1-AS1 regulates osteogenic and adipocytic differentiation of BMSCs via sponging miR-196a-5p [46]. For further mechanistic investigations, we predicted KCNQ1OT1 sequence contained miR-141-5p binding sites *via* bioinformatics analysis. As reported before, miR-141-5p promoted preeclampsia via regulating MAPK1/ERK2 signaling [47]. In chronic myeloid leukemia, microRNA-141-5p acts as a tumor suppressor by downregulating RAB32 [48]. However, the role of miR-141-5p played in osteoporosis has not been reported. In TNF-α-treated primary osteoblasts, we found increased expression of miR-141-5p. Moreover, the knockdown of miR-141-5p promoted cell viability and inhibited cell apoptosis induced by TNF-α. As dual-luciferase reporter assay showed, miR-141-5p was the target gene of KCNQ1OT1. Furthermore, the rescue experiments revealed that when cocultured with KCNQ1OT1-Exos, the effects induced by miR-141-5p on cell viability and apoptosis in TNF-α-treated primary osteoblasts were partly reversed, suggesting that KCNQ1OT1-Exos functioned by sponging miR-141-5p.

5. Conclusions

In the present study, we demonstrate that ADSCs-Exos can attenuate cytotoxicity and apoptosis of TNF-α-induced primary osteoblasts. KCNQ1OT1-Exos have a more significant inhibitory effect compared to ADSCs-Exos by the function of sponging miR-141-5p, suggesting that KCNQ1OT1-Exos can be promising agents in osteoporosis treatment. Further explorations of the pleiotropic effect of KCNQ1OT1 and the crosstalk between KCNQ1OT1 and miR-141-5p will provide new insights for developing new treatments to improve the therapeutic efficacy based on ADSCs-Exos.

Data Availability

The data used to support the findings of this study are available from the corresponding authors upon request.

Disclosure

A preprint related to this study has previously been published and is available at Research Square [49].

Conflicts of Interest

The authors declare that they have no conflicts of interest.

Authors' Contributions

SZW performed the experiments, collected data, and drafted the manuscript. JJ participated in the experimental design and experimentation and helped collect the data. CHC took part in the study design and revised the manuscript. All authors read and approved the final manuscript.

Acknowledgments

This work was supported by Wuxi Health Committee Research Grants for Top Talent Support Program (grant no. 2020) and Nanjing University of Chinese Medicine Research Grant (grant no. XZR2020075).

References

[1] C. B. Johnston and M. Dagar, "Osteoporosis in older adults," *The Medical Clinics of North America*, vol. 104, no. 5, pp. 873–884, 2020.

[2] G. Karsenty, "The complexities of skeletal biology," *Nature*, vol. 423, no. 6937, pp. 316–318, 2003.

[3] T. D. Rachner, S. Khosla, and L. C. Hofbauer, "Osteoporosis: now and the future," *Lancet*, vol. 377, no. 9773, pp. 1276–1287, 2011.

[4] B. Osta, G. Benedetti, and P. Miossec, "Classical and paradoxical effects of TNF-α on bone homeostasis," *Frontiers in Immunology*, vol. 5, p. 48, 2014.

[5] K. J. Armour, K. E. Armour, R. J. van 't Hof et al., "Activation of the inducible nitric oxide synthase pathway contributes to inflammation-induced osteoporosis by suppressing bone formation and causing osteoblast apoptosis," *Arthritis and Rheumatism*, vol. 44, no. 12, pp. 2790–2796, 2001.

[6] L. Gilbert, X. He, P. Farmer et al., "Expression of the osteoblast differentiation factor RUNX2 (Cbfa1/AML3/Pebp2αA) is inhibited by tumor necrosis factor-α," *Journal of Biological Chemistry*, vol. 277, no. 4, pp. 2695–2701, 2002.

[7] M. Sheykhhasan, J. K. L. Wong, and A. M. Seifalian, "Human adipose-derived stem cells with great therapeutic potential," *Current Stem Cell Research & Therapy*, vol. 14, no. 7, pp. 532–548, 2019.

[8] L. Mazini, L. Rochette, M. Amine, and G. Malka, "Regenerative capacity of adipose derived stem cells (ADSCs), comparison with mesenchymal stem cells (MSCs)," *International journal of molecular sciences*, vol. 20, no. 10, p. 2523, 2019.

[9] N. Fahy, M. Alini, and M. J. Stoddart, "Mechanical stimulation of mesenchymal stem cells: Implications for cartilage tissue engineering," *Journal of Orthopaedic Research*, vol. 36, no. 1, pp. 52–63, 2017.

[10] B. S. Cho, J. O. Kim, D. H. Ha, and Y. W. Yi, "Exosomes derived from human adipose tissue-derived mesenchymal stem cells alleviate atopic dermatitis," *Stem Cell Research & Therapy*, vol. 9, no. 1, p. 187, 2018.

[11] G. I. Im, "Bone marrow-derived stem/stromal cells and adipose tissue-derived stem/stromal cells: Their comparative efficacies and synergistic effects," *Journal of Biomedical Materials Research. Part A*, vol. 105, no. 9, pp. 2640–2648, 2017.

[12] Y. An, J. Zhao, F. Nie, Y. Wu, Y. Xia, and D. Li, "Parathyroid hormone (PTH) promotes ADSC osteogenesis by regulating SIK2 and Wnt4," *Biochemical and Biophysical Research Communications*, vol. 516, no. 2, pp. 551–557, 2019.

[13] D. M. Pegtel and S. J. Gould, "Exosomes," *Annual Review of Biochemistry*, vol. 88, no. 1, pp. 487–514, 2019.

[14] C. Murphy, J. Withrow, M. Hunter et al., "Emerging role of extracellular vesicles in musculoskeletal diseases," *Molecular Aspects of Medicine*, vol. 60, pp. 123–128, 2018.

[15] H. Qiu, S. Liu, K. Wu, R. Zhao, L. Cao, and H. Wang, "Prospective application of exosomes derived from adipose-derived stem cells in skin wound healing: a review," *Journal of Cosmetic Dermatology*, vol. 19, no. 3, pp. 574–581, 2020.

[16] M. Lee, J. J. Ban, S. Yang, W. Im, and M. Kim, "The exosome of adipose-derived stem cells reduces β-amyloid pathology and apoptosis of neuronal cells derived from the transgenic mouse model of Alzheimer's disease," *Brain Research*, vol. 1691, pp. 87–93, 2018.

[17] Y. Fang, Y. Zhang, J. Zhou, and K. Cao, "Adipose-derived mesenchymal stem cell exosomes: a novel pathway for tissues repair," *Cell and Tissue Banking*, vol. 20, no. 2, pp. 153–161, 2019.

[18] C. Kilchert, S. Wittmann, and L. Vasiljeva, "The regulation and functions of the nuclear RNA exosome complex," *Nature Reviews. Molecular Cell Biology*, vol. 17, no. 4, pp. 227–239, 2016.

[19] Y. Zhang, J. Bi, J. Huang, Y. Tang, S. du, and P. Li, "Exosome: a review of its classification, isolation techniques, storage, diagnostic and targeted therapy applications," *International Journal of Nanomedicine*, vol. 15, pp. 6917–6934, 2020.

[20] J. P. Sluijter, V. Verhage, J. C. Deddens, F. van den Akker, and P. A. Doevendans, "Microvesicles and exosomes for intracardiac communication," *Cardiovascular Research*, vol. 102, no. 2, pp. 302–311, 2014.

[21] M. Colombo, G. Raposo, and C. Thery, "Biogenesis, secretion, and intercellular interactions of exosomes and other extracellular vesicles," *Annual Review of Cell and Developmental Biology*, vol. 30, no. 1, pp. 255–289, 2014.

[22] R. Shi, Y. Jin, W. Hu et al., "Exosomes derived from mmu_circ_0000250-modified adipose-derived mesenchymal stem cells promote wound healing in diabetic mice by inducing miR-128-3p/SIRT1-mediated autophagy," *American Journal of Physiology. Cell Physiology*, vol. 318, no. 5, pp. C848–C856, 2020.

[23] Q. Li, Z. Wang, H. Xing, Y. Wang, and Y. Guo, "Exosomes derived from miR-188-3p-modified adipose-derived mesenchymal stem cells protect Parkinson's disease," *Mol Ther Nucleic Acids*, vol. 23, pp. 1334–1344, 2021.

[24] C. G. Wang, Z. Liao, H. Xiao et al., "LncRNA KCNQ1OT1 promoted BMP2 expression to regulate osteogenic differentiation by sponging miRNA-214," *Experimental and Molecular Pathology*, vol. 107, pp. 77–84, 2019.

[25] B. Liu, Y. Lu, Y. Wang, L. Ge, N. Zhai, and J. Han, "A protocol for isolation and identification and comparative characterization of primary osteoblasts from mouse and rat calvaria," *Cell and Tissue Banking*, vol. 20, no. 2, pp. 173–182, 2019.

[26] J. C. Santos, N. D. S. Lima, L. O. Sarian, A. Matheu, M. L. Ribeiro, and S. F. M. Derchain, "Exosome-mediated breast cancer chemoresistance via miR-155 transfer," *Scientific Reports*, vol. 8, no. 1, p. 829, 2018.

[27] P. J. Marie and M. Kassem, "Osteoblasts in osteoporosis: past, emerging, and future anabolic targets," *European Journal of Endocrinology*, vol. 165, no. 1, pp. 1–10, 2011.

[28] Y. Jiang, P. Zhang, X. Zhang, L. Lv, and Y. Zhou, "Advances in mesenchymal stem cell transplantation for the treatment of osteoporosis," *Cell Proliferation*, vol. 54, no. 1, article e12956, 2021.

[29] P. A. Zuk, M. Zhu, H. Mizuno et al., "Multilineage cells from human adipose tissue: implications for cell-based therapies," *Tissue Engineering*, vol. 7, no. 2, pp. 211–228, 2001.

[30] Z. Weiliang and G. Lili, "Research advances in the application of adipose-derived stem cells derived exosomes in cutaneous wound healing," *Annals of Dermatology*, vol. 33, no. 4, pp. 309–317, 2021.

[31] J. Tian, X. Cui, J. Sun, and J. Zhang, "Exosomal microRNA-16-5p from adipose mesenchymal stem cells promotes TLR4-mediated M2 macrophage polarization in septic lung injury," *International Immunopharmacology*, vol. 98, article 107835, 2021.

[32] Y. Yang, Y. Cai, Y. Zhang, J. Liu, and Z. Xu, "Exosomes secreted by adipose-derived stem cells contribute to angiogenesis of brain microvascular endothelial cells following oxygen-glucose deprivation in vitro through microRNA-181b/TRPM7 axis," *Journal of Molecular Neuroscience*, vol. 65, no. 1, pp. 74–83, 2018.

[33] S. Gaur and R. Agnihotri, "Application of adipose tissue stem cells in regenerative dentistry: a systematic review," *Journal of International Society of Preventive and Community Dentistry*, vol. 11, no. 3, pp. 266–271, 2021.

[34] A. C. Paula, T. M. M. Martins, A. Zonari et al., "Human adipose tissue-derived stem cells cultured in xeno-free culture condition enhance c-MYC expression increasing proliferation but bypassing spontaneous cell transformation," *Stem Cell Research & Therapy*, vol. 6, no. 1, p. 76, 2015.

[35] J. Tolar and J. P. Neglia, "Transplacental and other routes of cancer transmission between individuals," *Journal of Pediatric Hematology/Oncology*, vol. 25, no. 6, pp. 430–434, 2003.

[36] I. W. Teng, P. C. Hou, K. D. Lee et al., "Targeted methylation of two tumor suppressor genes is sufficient to transform mesenchymal stem cells into cancer stem/initiating cells," *Cancer Research*, vol. 71, no. 13, pp. 4653–4663, 2011.

[37] D. C. Yeh, T. M. Chan, H. J. Harn et al., "Adipose tissue-derived stem cells in neural regenerative medicine," *Cell Transplantation*, vol. 24, no. 3, pp. 487–492, 2015.

[38] E. Manchon, N. Hirt, J. D. Bouaziz, N. Jabrane-Ferrat, and R. al-Daccak, "Stem cells-derived extracellular vesicles: potential therapeutics for wound healing in chronic inflammatory skin diseases," *International journal of molecular sciences*, vol. 22, no. 6, p. 3130, 2021.

[39] J. Jin, Y. Shi, J. Gong et al., "Exosome secreted from adipose-derived stem cells attenuates diabetic nephropathy by promoting autophagy flux and inhibiting apoptosis in podocyte," *Stem Cell Research & Therapy*, vol. 10, no. 1, p. 95, 2019.

[40] Y. Liu, L. Lin, R. Zou, C. Wen, Z. Wang, and F. Lin, "MSC-derived exosomes promote proliferation and inhibit apoptosis of chondrocytes via lncRNA-KLF3-AS1/miR-206/GIT1 axis in osteoarthritis," *Cell Cycle*, vol. 17, no. 21-22, pp. 2411–2422, 2018.

[41] Q. Yang, Y. Yao, D. Zhao et al., "LncRNA H19 secreted by umbilical cord blood mesenchymal stem cells through microRNA-29a-3p/FOS axis for central sensitization of pain in advanced osteoarthritis," *American Journal of Translational Research*, vol. 13, no. 3, pp. 1245–1256, 2021.

[42] X. Liu, Y. Zhang, Y. Wang, C. Bian, and F. Wang, "Long noncoding RNA KCNQ1OT1 up-regulates CTNND1 by sponging miR-329-3p to induce the proliferation, migration, invasion, and inhibit apoptosis of colorectal cancer cells," *Cancer Cell International*, vol. 20, no. 1, p. 340, 2020.

[43] H. Sun, Y. Li, H. Kong, S. Dai, and H. Qian, "Dysregulation of KCNQ1OT1 promotes cholangiocarcinoma progression via miR-140-5p/SOX4 axis," *Archives of Biochemistry and Biophysics*, vol. 658, pp. 7–15, 2018.

[44] J. Venkatesh, M. D. Wasson, J. M. Brown, W. Fernando, and P. Marcato, "LncRNA-miRNA axes in breast cancer: novel points of interaction for strategic attack," *Cancer Letters*, vol. 509, pp. 81–88, 2021.

[45] S. Y. Xu, P. Shi, and R. M. Zhou, "Post-menopausal oestrogen deficiency induces osteoblast apoptosis via regulating HOTAIR/miRNA-138 signalling and suppressing TIMP1 expression," *Journal of Cellular and Molecular Medicine*, vol. 25, no. 10, pp. 4572–4582, 2021.

[46] L. Zhang, H. Xie, and S. Li, "LncRNA LOXL1-AS1 controls osteogenic and adipocytic differentiation of bone marrow mesenchymal stem cells in postmenopausal osteoporosis through regulating the miR-196a-5p/Hmga2 axis," *Journal of Bone and Mineral Metabolism*, vol. 38, no. 6, pp. 794–805, 2020.

[47] Y. Wang, K. Cheng, W. Zhou et al., "miR-141-5p regulate ATF2 via effecting MAPK1/ERK2 signaling to promote preeclampsia," *Biomedicine & Pharmacotherapy*, vol. 115, article 108953, 2019.

[48] J. Bao, X. Li, Y. Li, C. Huang, X. Meng, and J. Li, "MicroRNA-141-5p acts as a tumor suppressor via targeting RAB32 in chronic myeloid leukemia," *Frontiers in Pharmacology*, vol. 10, p. 1545, 2020.

[49] S. Z. Wang, J. Jia, and C. H. Chen, *LncRNA-KCNQ1OT1: a potential target in exosomes derived from ADSCs for the treatment of osteoporosis*, Research Square, 2021.

Hindawi
Stem Cells International
Volume 2021, Article ID 8359582, 7 pages
https://doi.org/10.1155/2021/8359582

Research Article

Wnt/β-Catenin Pathway Balances Scaffold Degradation and Bone Formation in Tissue-Engineered Laminae

Hailong Li,[1] Linli Li,[1] Yiqun He,[1] Wei Mao,[1] Haofei Ni,[1] Aolei Yang,[1] Feizhou Lyu,[1,2] and Youhai Dong[1]

[1]*Department of Orthopedics, Shanghai Fifth People's Hospital, Fudan University, China*
[2]*Department of Orthopedics, Huashan Hospital, Fudan University, China*

Correspondence should be addressed to Feizhou Lyu; lufeizhou@hotmail.com and Youhai Dong; youhaidong1964@163.com

Received 17 July 2021; Accepted 23 August 2021; Published 13 September 2021

Academic Editor: Jun Liu

Tissue engineering provides a promising way for the regeneration of artificial vertebral laminae. Previous studies have confirmed the feasibility of reconstructing vertebral laminae via hydroxyapatite-collagen I scaffolds and mesenchymal stromal cells. However, there were no studies exploring the degradation of hydroxyapatite-collagen I scaffolds and the function of Wnt/β-catenin pathway in the process. In this study, tissue-engineered laminae (TEL) were constructed by nanohydroxyapatite/collagen I scaffolds and umbilical cord Wharton's Jelly mesenchymal stromal cells (WJ-MSCs). Cell attachment was observed by scanning electron microscopy, and cell viability was confirmed by Live/Dead staining. The rat models were randomly divided into control and β-catenin inhibition groups. Vertebral lamina defect rat models were made on the fifth lumbar vertebrate, and TEL was implanted into the defect site. After 14 weeks, the newborn laminae were harvested for microcomputed tomography, histology, or transcriptional profile analysis. We found that, for the control group, the newborn lamina formation matched with the scaffold degradation and complete newborn laminae formed at the 14th week; for the β-catenin inhibition group, the scaffold degradation rate overrated the lamina formation and no complete artificial laminae were formed at the 14th week. In addition, the osteoclastic genes, such as Cathepsin K or RANKL, in the control groups were significantly lower than the β-catenin inhibition group, and the antiosteoclastic gene, OPG, in the control group was significantly higher than the β-catenin inhibition group. In conclusion, inhibition of Wnt/β-catenin pathway led to speedy scaffold degradation and deferred artificial lamina formation. Wnt/β-catenin pathway played a critical role in maintaining the balance between scaffold degradation and bone formation in the process of vertebral lamina reconstruction.

1. Introduction

Laminectomy was a routine surgical protocol for spinal diseases with spinal stenosis [1, 2]. Postoperative epidural scar adhesion can lead to persistent back pain and difficulty for reoperation [3–6]. Tissue engineering techniques have been successfully used to reconstruct the epidural fat or vertebral laminae to avoid epidural scar adhesion in animal studies [7–11].

The common tissue engineering approach involves the use of a biocompatible scaffold, cells, and/or a combination of bioactive molecules such as growth factors and cytokines. Due to the particular structures of the spinal canal, soft biomaterials were favored for the reconstruction of vertebral laminae avoiding compression of the spinal cord after implantation [7]. Nanohydroxyapatite/collagen I scaffolds (nHE/COL) have been well characterized and commercialized for bone defect repair [12, 13]. Its excellent osteoinduction and mechanical properties make it an ideal material for the construction of tissue-engineered laminae (TEL) [14, 15]. Previous studies [7, 16, 17] have successfully constructed TEL with nHE/COL scaffolds and mesenchymal stromal cell (MSC) and reconstructed vertebral laminae. However, the relationship between nHE/COL scaffold degradation and lamina formation remains unclear.

Wnt/β-catenin signaling pathway played a crucial role in bone regeneration [18]. Transcriptional profiling and spatial gene expression analysis have found a series of

Wnt signaling molecules that are involved in the process of fracture healing [19–21]. Besides, Wnts and their antagonists also exhibit a distinct temporal expression pattern by targeting different cell lineages during the bone regeneration process [18]. Specifically, Wnts induce self-renewal and proliferation in skeletal stem/progenitor cells during the early stages of fracture healing, and once osteogenic differentiation has been triggered in these cells, Wnts then activate the differentiation cascade [18]. Moreover, Wnts can induce the expression of OPG on osteoblasts by regulating the differentiation of osteoclasts and affecting the function of osteoclasts, which also ultimately affects the bone resorption process [22]. Thus, Wnt/β-catenin signaling pathway is involved in bone remodeling by regulating both bone resorption and bone formation processes.

In this study, we speculated that Wnt/β-catenin signaling pathway might regulate the balance between scaffold degradation and bone formation and play an important role in the reconstruction of vertebral laminae. Tissue-engineered laminae (TEL) were constructed using rat umbilical cord Wharton's Jelly-derived MSC and nHE/-COL scaffold. The rat models were randomly divided into control and β-catenin inhibition groups. Vertebral lamina defect rat models were made, and TEL was implanted into the defect site. After 14 weeks, the newborn laminae were harvested for microcomputed tomography, histology, or transcriptional profile analysis.

2. Methods

2.1. Ethics Statement. All animal experiments were performed in the Animal Facility of East China Normal University and according to the protocol (Protocol number: 20150482A168) authorized by the Animal Care and Use Committee of Fudan University.

2.2. Cell Culture. Rat mesenchymal stromal cells derived from umbilical cord Wharton's Jelly were purchased from Otwo Biotech (Guangzhou, China). All cells were cultured in Dulbecco's modified Eagle's medium (DMEM; Hyclone, UT, USA) supplemented with 10% fetal bovine serum (FBS; Biological Industries, Beit HaEmek, Israel).

2.3. Construction of Tissue-Engineered Laminae (TEL). The nHE/COL scaffold was bought from the Beijing Allgens Medical Science & Technology Co., Ltd. Under sterile condition, the nHE/COL scaffold was cut to the size of 8 mm × 6 mm. Rat MSC at passage 4-7 was trypsinized and resuspended in media at a concentration of 1×10^6/ml. Then, 100 μl cell suspensions were pipetted on one side of each scaffold, and after 30 min, 100 μl cell suspensions were pipetted on the other side. All constructs were placed in culture medium before implantation.

2.4. Live/Dead Staining. Cell viability of MSC in TEL was measured with a Live/Dead assay kit (Best-Bio, Shanghai, China). Experiments were performed according to the manufacturer's instructions. The representative images were obtained using a ZEISS confocal fluorescence microscope (ZEISS, Jena, Germany).

2.5. Scanning Electron Microscope. The TEL was fixed with electron microscopy fixative solution (Severicebio, Wuhan, China), dehydrated, mounted on an aluminum stub, and sputter-coated with gold-palladium for 30 seconds. The morphology of TEL and MSC adhesion on the scaffolds was then viewed on a scanning electron microscope (Hitachi, Tokyo, Japan).

2.6. Animal Studies. The construction of vertebral lamina defect rat models was performed as previously described [17]. Briefly, spinous processes and interspinous ligaments were removed to expose the vertebral laminae, a bone defect measuring 8 mm × 6 mm was created in the vertebral laminae, and then, the TEL was placed and fixed in the bone defect. For the β-catenin inhibition group, the rats were injected intraperitoneally with XAV-939 (MCE, NJ, USA) according to the standard of 4 mg/kg at the frequency of twice a week for the first two weeks and once a week. For the control group, the rats were injected intraperitoneally with the same dose of saline.

2.7. Micro-CT Examination. The target vertebrates were harvested at the 2nd, 4th, 6th, 10th, and 14th weeks and fixed in 4% (w/v) paraformaldehyde. The specimens were examined using High Resolution in vivo X-ray Microtomograph System (Bruker, Bremen, Germany). The 3D model was reconstructed manually using the NRecon Reconstruction software (1.7.4.2, Bruker) and analyzed using the CTAn software (1.18.8.0, Bruker).

2.8. Histological Staining. After the micro-CT examination, the tissue specimens were decalcified with 10% ethylenediaminetetraacetic acid for 4 weeks. Tissue sections with 6 μm thickness were cut on a microtome and mounted onto glass slides. The sections were processed for routine histological analysis by hematoxylin-eosin (HE), Goldner's trichrome, tartrate-resistant acid phosphatase (TRAP), and immunohistochemistry (IHC) staining.

2.9. IHC Staining. Immunohistochemistry was performed as previously described [17]. The following antibodies were used: anti-RANKL rabbit polyclonal (GB11235, Severicebio), anti-osteoprotegerin rabbit polyclonal (GB11151, Severicebio), anti-OCN rabbit polyclonal (GB11233, Severicebio), and horseradish peroxidase- (HRP-) conjugated secondary antibodies (GB23303, Severicebio). The percentage of positive staining area was analyzed by the plugins of IHC Profiler in the Image J software (Version: 1.8.0_112, NIH, USA).

2.10. Reverse Transcription PCR. Total RNA was isolated from cells or bone tissue using TRIzol Reagent (Invitrogen) according to the manufacturer's instructions. cDNA was synthesized from total RNA (500 ng) using a reverse transcription kit (Takara, Tokyo, Japan). qPCR was performed in triplicate using 1 μL of cDNA in a standard SYBR premix Ex Taq (Takara) on the Applied Biosystems 7500 Real-Time PCR Detection System (Applied Biosystems, CA, USA). GAPDH served as an internal control. The following primers were used: GAPDH, 5′-GGCACAGTCAAGGCTG AGAATG-3′ and 5′-ATGGTGGTGAAGACGCCAGTA-

3′; RANKL, 5′-ATGATGGAAGGTTCGTGG-3′ and 5′-GGACAGACTGACTTTATGGG-3′; OPG, 5′-AGACCG TGAAACAGGAGTG-3′ and 5′-ACCTGAGAAGAACC CATCC-3′; and CTSK, 5′-GAAGAAGACTCACCAGAAG CAG-3′ and 5′-TCCAGGTTATGGGCAGAGATT-3′. The relative gene expression was calculated using the following equation: $\Delta\text{Ct} = \text{Ct (test genes)} - \text{Ct (GAPDH)}$; fold change $= 2^{(-\Delta\text{Ct})}$.

2.11. Statistical Analysis. Statistical analysis was conducted using GraphPad Prism version 6.02 software program for Windows (GraphPad, CA, USA). The Student *t*-test was used for comparison between groups. All tests were two-sided, and *P* values <0.05 were considered to be statistically significant.

3. Results

3.1. TEL Construction. SEM scanning was used to observe the surface morphology of the scaffold. We found that there were enormous micropores and irregular lamellar structures distributed on the surface of nHA/COL scaffolds (Figure 1(a)). MSC formed finger-like filopodia and tightly adhered to the lamellar structure of scaffolds (Figure 1(b)). The Live/Dead staining showed that almost all the MSC survived in the nHA/COL scaffold, and the cells tightly adhered to the lamellar structure of the scaffold (Figure 1(c)). The scaffold has blue autofluorescence (Figure 1(c)).

3.2. Micro-CT Examination. In the control group, the newborn laminae gradually grew from bilateral vertebral pedicles to the middle and formed complete artificial laminae at the 14th week, and the scaffold degradation and trabecular bone formation proceeded orderly and alternately. In the β-catenin inhibition group, the scaffold degradation rate was significantly higher than that of the control group, and bone formation rate was significantly lower than that of the control group. In addition, its scaffold degradation rate was dominant over the bone formation, almost all the scaffold degraded at the 10th week, the newborn laminae grew slowly after the 10th week, and no complete artificial laminae were formed at the 14th week (Figure 2).

3.3. Goldner's Trichrome Staining. New bone formation was evaluated by Goldner's trichrome staining. Bone and bone-like tissues are presented as a substructure visualized in green. In the control group, the new trabecular structure formed and bone mineral deposited at the 10th week, and premature bone structure formed at the 14th week. In the β-catenin inhibition group, the scaffold degraded completely at the 10th week, the artificial laminae stopped growing, and there was still a lamina defect with the size of 400-600 μm at both the 10th and 14th weeks (Figure 3).

3.4. Scaffold Degradation and Bone Formation. The scaffold degradation rate was analyzed by the 3D reconstruction images. The scaffold degradation rate in the control group was significantly lower than that of the β-catenin inhibition group (Figure 4). In the β-catenin inhibition group, almost all the scaffold degraded at the 6th and 10th weeks (Figure 5(a)). The HE staining also showed that the scaffold degraded completely at the 10th week in the β-catenin inhibition group (Figure 5(b)). TRAP staining showed that the osteoblast numbers in the β-catenin inhibition group were significantly higher than that of the control group (Figure 5(c)). The expression levels of OPG in the control group were statistically higher than those in the β-catenin inhibition group at the 10th week, while the RANKL expression showed no statistical difference at the 10th week (Figures 5(c)–5(g)) The mRNA expression levels of *CTSK* in the β-catenin inhibition group were also statistically higher than those in the control group at both the 6th and 10th weeks (Figure 5(h)) The newborn laminae were also confirmed by IHC staining of OCN at the 14th week (Figure 6).

4. Discussion

In this study, we investigated the role of Wnt/β-catenin signaling pathway in the balance of scaffold degradation and bone formation during vertebral lamina reconstruction. We found that, with the inhibition of β-catenin, the newborn laminae increased the expression levels of osteoclastic markers and the number of osteoclasts, thereby promoting the scaffold degradation and deferring the lamina formation.

Previous studies showed that the OPG-RANK-RANKL system plays the principal role in determining the balance between bone resorption and bone formation [22, 23]. Osteoblastic cell lineages can secrete RANKL, which binds to the RANK receptor on the osteoclast or osteoclast progenitor cells and activates the transcription of osteoclastic genes [22, 23]. Osteoblastic cell lineages can also secrete OPG, which can competitively inhibit the binding between RANKL and RANK, thereby inhibiting the formation and differentiation of osteoclasts [22, 23]. β-Catenin can induce the expression of osteoclast inhibitor OPG and regulate osteoclast differentiation, affecting bone resorption ultimately [24]. In this study, we found that the expression levels of OPG in the control group were statistically higher than those in the β-catenin inhibition group at all time points, while the expression levels of *RANKL* in the control group were only statistically lower than those in the β-catenin inhibition group at 6th week. The regulatory function of Wnt/β-catenin signaling pathway in the osteoclast differentiation was mainly played by promoting the expression of OPG.

The coupling balance between scaffold degradation and bone formation is requisite for bone reconstruction [25–27]. The dominance of scaffold degradation inhibits the migration and mineralization of osteoblasts, while the constrained degradation of scaffolds would squeeze the space for osteoblast proliferation [28]. In this study, the scaffold degradation rate in the β-catenin inhibition group was dominant over bone formation rate. Almost all the scaffold degraded at the 6th week, and the bone formation retarded thereafter and could not form complete artificial laminae at the 14th week. In the control group, scaffold degradation and bone formation maintained synchronous balance and realized artificial lamina reconstruction at the

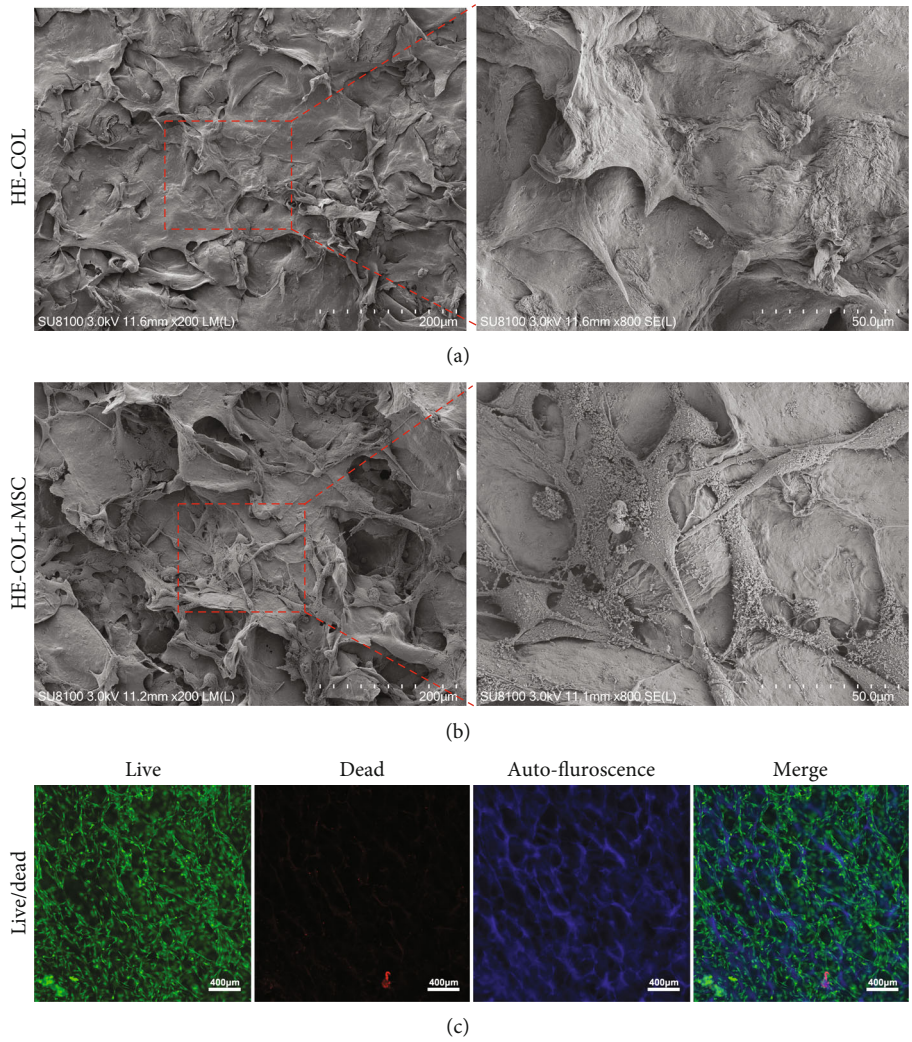

Figure 1: (a) SEM images of nHA/COL scaffolds; (b) SEM images of tissue-engineered laminae (TEL); (c) Live/Dead staining of TEL.

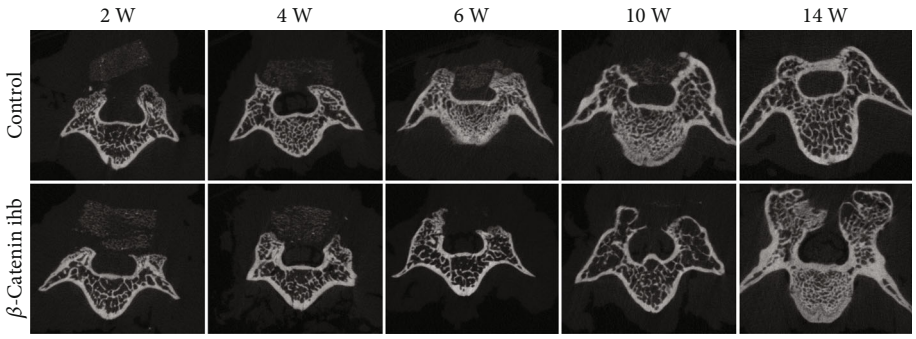

Figure 2: Micro-CT scanning of TEL in the control and β-catenin inhibition groups at the 2nd, 4th, 6th, 10th, and 14th weeks.

14th week. It demonstrated that β-catenin inhibition could expedite the degradation of nHE/COL scaffolds and break down the normal balance between scaffold degradation and bone formation, which was detrimental to the reconstruction of artificial vertebral laminae.

Scaffolding biomaterials, such as natural collagen, synthetic polymers, ceramics, inorganic biomaterials, and their hybrid combinations, have been widely used for bone tissue engineering, due to their outstanding biomechanical, osteoconductive, and biodegradable properties [29]. Bone regeneration is closely associated with Wnt/β-catenin signaling pathway [18]. Many biomaterials, such as titanium with Ti-Nano, laponite-guanidinylated chitosan hydrogels, intrafibrillar mineralized collagen, hydroxyapatite, and

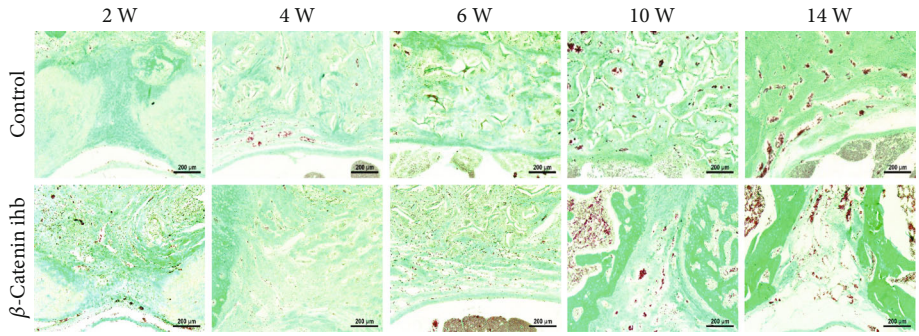

Figure 3: Goldner's trichrome staining of TEL at the 2nd, 4th, 6th, 10th, and 14th weeks.

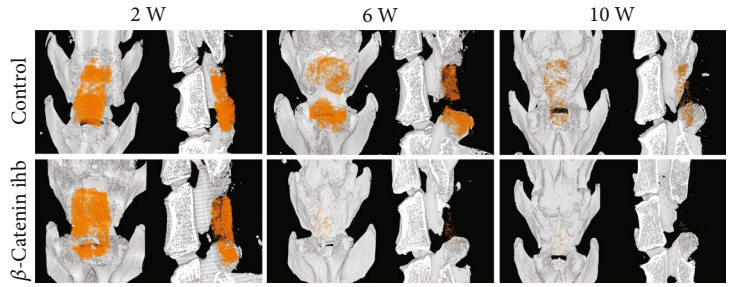

Figure 4: 3D reconstruction images at the 2nd, 6th, and 10th weeks; the pseudo orange color indicates the TEL.

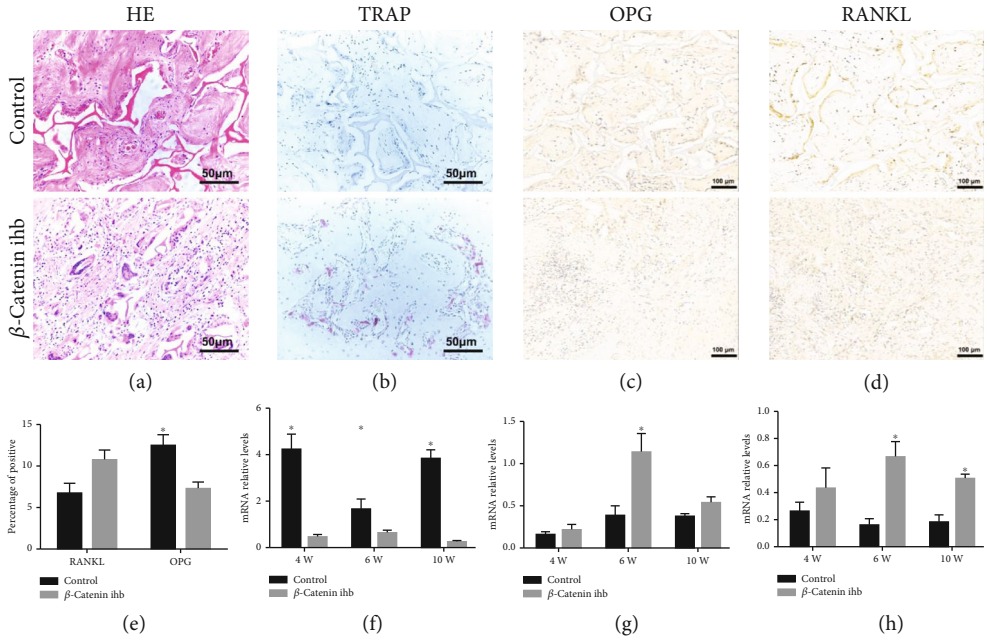

Figure 5: (a) HE staining of the newborn laminae at the 10th week; (b) TRAP staining of the newborn laminae at the 10th week; IHC staining of (c) OPG and (d) RANKL at the 10th week; (e) percentage of positive staining of RANKL and OPG at the 10th week; mRNA expression levels of (f) OPG, (g) RANKL, and (h) CTSK. $^{*}P < 0.05$ (control vs. β-catenin inhibition group at the same time point).

gold nanoparticle-loaded hydroxyapatite composites, possessed great regenerative potential because they can activate Wnt/β-catenin signaling pathway and thereby promoting bone regeneration [30–33]. Bone progenitor stem cells, scaffolding biomaterials, and Wnt/β-catenin signaling pathway must rely on each other to realize successful bone regeneration [19].

Many studies have clearly elucidated the role of Wnt/β-catenin signaling pathway in promoting osteoblast proliferation, migration, and osteogenic differentiation [18, 19].

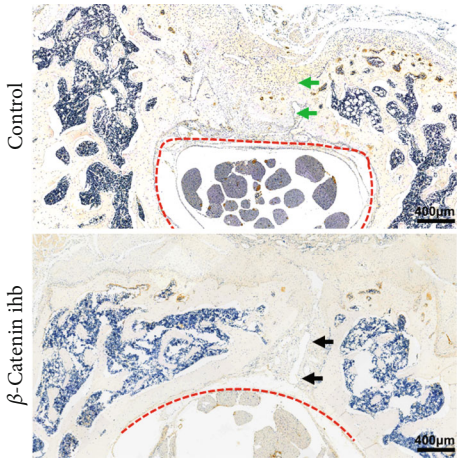

Figure 6: IHC staining of OCN at the 14th week. Green arrow indicates the newborn complete vertebral laminae in the control group, black arrow indicates the lamina defect in the β-catenin inhibition group, and red dish line indicates the vertebral canal.

Previous studies mostly focused on the role of biomaterials in the activation of Wnt/β-catenin signaling pathway, osteogenic differentiation, and inhibition of osteoclastogenesis [20, 22, 24]. In this study, we elucidated the role of Wnt/β-catenin signaling pathway in inhibiting osteoclast genesis and scaffold degradation and thus in maintaining the balance between scaffold degradation and bone formation. It demonstrated that Wnt/β-catenin signaling pathway regulated the reconstruction of tissue-engineered bone in several different ways, which needs more attention in further study.

5. Conclusion

In the process of vertebral lamina reconstruction, Wnt/β-catenin pathway could decrease the degradation rate of nHA/-COL scaffold mainly by decreasing the expression of OPG and promoting osteoclast genesis. Inhibition of β-catenin led to speedy scaffold degradation and deferred artificial lamina formation, disturbing the balance between scaffold degradation and bone formation. This study advances our understanding of the role of Wnt/β-catenin pathway in bone tissue engineering.

Data Availability

The datasets used during the current study are available from the corresponding author on reasonable request.

Conflicts of Interest

The authors declare that there are no conflicts of interest regarding the publication of this paper.

Authors' Contributions

Hailong Li and Linli Li contributed equally to this work.

Acknowledgments

The study was supported by the National Natural Science Foundation of China (File No. 81672179), the Shanghai Leading Medical Talent (File No. 2019LJ08), and the High-level Talent Special Fund of the Minhang District of Shanghai (File No. 5-1).

References

[1] Z. Mo, R. Zhang, M. Chang, and S. Tang, "Exercise therapy versus surgery for lumbar spinal stenosis: a systematic review and meta-analysis," *Pakistan Journal of Medical Sciences*, vol. 34, no. 4, pp. 879–885, 2018.

[2] M. Shah, B. Kolb, E. Yilmaz, D. R. Halalmeh, and M. D. Moisi, "Comparison of lumbar laminectomy alone, lumbar laminectomy and fusion, stand-alone anterior lumbar interbody fusion, and stand-alone lateral lumbar interbody fusion for treatment of lumbar spinal stenosis: a review of the literature," *Cureus*, vol. 11, article e5691, 2019.

[3] J. C. le Huec, S. Seresti, S. Bourret et al., "Revision after spinal stenosis surgery," *European Spine Journal*, vol. 29, no. S1, pp. 22–38, 2020.

[4] A. Sebaaly, M. J. Lahoud, M. Rizkallah, G. Kreichati, and K. Kharrat, "Etiology, evaluation, and treatment of failed Back surgery syndrome," *Asian Spine Journal*, vol. 12, no. 3, pp. 574–585, 2018.

[5] S. Ko and T. Oh, "Comparison of bilateral decompression via unilateral laminotomy and conventional laminectomy for single-level degenerative lumbar spinal stenosis regarding low back pain, functional outcome, and quality of life - a randomized Controlled, Prospective Trial," *Orthopaedic surgery and research*, vol. 14, no. 1, p. 252, 2019.

[6] S. M. Park, J. Park, H. S. Jang et al., "Biportal endoscopic versus microscopic lumbar decompressive laminectomy in patients with spinal stenosis: a randomized controlled trial," *The Spine Journal*, vol. 20, no. 2, pp. 156–165, 2020.

[7] L. Li, X. Chen, Y. He, and Y. Dong, "Biological and mechanical factors promote the osteogenesis of rabbit artificial vertebral laminae: a comparison study," *Tissue Engineering. Part A*, vol. 24, no. 13-14, pp. 1082–1090, 2018.

[8] Y. Dong, X. Chen, and Y. Hong, "Tissue-engineered bone formation in vivo for artificial laminae of the vertebral arch using β-Tricalcium phosphate bioceramics seeded with mesenchymal stem cells," *Spine*, vol. 38, no. 21, pp. E1300–E1306, 2013.

[9] Y. Dong, X. Chen, M. Wang, and Y. Hong, "Construction of artificial laminae of the vertebral arch using bone marrow mesenchymal stem cells transplanted in collagen sponge," *Spine*, vol. 37, no. 8, pp. 648–653, 2012.

[10] C. Li, H. Wang, H. Liu, J. Yin, L. Cui, and Z. Chen, "The prevention effect of poly (L-glutamic acid)/chitosan on spinal epidural fibrosis and peridural adhesion in the post-laminectomy rabbit model," *European Spine Journal*, vol. 23, no. 11, pp. 2423–2431, 2014.

[11] J. Xu, Y. Chen, Y. Yue, J. Sun, and L. Cui, "Reconstruction of epidural fat with engineered adipose tissue from adipose derived stem cells and PLGA in the rabbit dorsal laminectomy model," *Biomaterials*, vol. 33, no. 29, pp. 6965–6973, 2012.

[12] X. Lei, J. Gao, F. Xing, Y. Zhang, Y. Ma, and G. Zhang, "Comparative evaluation of the physicochemical properties of nano-hydroxyapatite/collagen and natural bone ceramic/collagen scaffolds and their osteogenesis-promoting effect on MC3T3-

E1 cells," *Regenerative Biomaterials*, vol. 6, no. 6, pp. 361–371, 2019.

[13] X. Wang, G. Zhang, F. Qi et al., "Enhanced bone regeneration using an insulin-loaded nano-hydroxyapatite/collagen/PLGA composite scaffold," *International Journal of Nanomedicine*, vol. 13, pp. 117–127, 2018.

[14] Y. Xia, S. S. Peng, L. Z. Xie et al., "A novel combination of nano-scaffolds with micro-scaffolds to mimic extracellularmatrices improve osteogenesis," *Journal of Biomaterials Applications*, vol. 29, no. 1, pp. 59–71, 2014.

[15] N. M. Hu, Z. Chen, X. Liu et al., "Mechanical properties and *in vitro* bioactivity of injectable and self- setting calcium sulfate/nano-HA/collagen bone graft substitute," *Journal of the Mechanical Behavior of Biomedical Materials*, vol. 12, pp. 119–128, 2012.

[16] L. Li, Y. He, X. Chen, and Y. Dong, "The role of continuous cerebrospinal fluid pulsation stress in the remodeling of artificial vertebral laminae: a comparison experiment," *Tissue Engineering. Part A*, vol. 25, no. 3-4, pp. 203–213, 2019.

[17] L. Li, Y. He, H. Tang et al., "Cerebrospinal Fluid Pulsation Stress Promotes the Angiogenesis of Tissue- Engineered Laminae," *Stem Cells International*, vol. 2020, Article ID 8026362, 12 pages, 2020.

[18] P. Leucht, S. Lee, and N. Yim, "Wnt signaling and bone regeneration: can't have one without the other," *Biomaterials*, vol. 196, pp. 46–50, 2019.

[19] J. B. Kim, P. Leucht, K. Lam et al., "Bone regeneration is regulated by wnt signaling," *Journal of Bone and Mineral Research*, vol. 22, no. 12, pp. 1913–1923, 2007.

[20] M. Hadjiargyrou, F. Lombardo, S. Zhao et al., "Transcriptional Profiling of Bone Regeneration: insight into the molecular complexity of wound repair," *Journal of Biological Chemistry*, vol. 277, no. 33, pp. 30177–30182, 2002.

[21] N. Zhong, R. P. Gersch, and M. Hadjiargyrou, "Wnt signaling activation during bone regeneration and the role of Dishevelled in chondrocyte proliferation and differentiation," *Bone*, vol. 39, no. 1, pp. 5–16, 2006.

[22] L. Zhou, Y. Huang, J. Zhao, H. Yang, and F. Kuai, "Oridonin promotes osteogenesis through Wnt/β-catenin pathway and inhibits RANKL-induced osteoclastogenesis in vitro," *Life Sciences*, vol. 262, 2020.

[23] B. Kadriu, P. W. Gold, D. A. Luckenbaugh et al., "Acute ketamine administration corrects abnormal inflammatory bone markers in major depressive disorder," *Molecular Psychiatry*, vol. 23, no. 7, pp. 1626–1631, 2018.

[24] I. Kramer, C. Halleux, H. Keller et al., "Osteocyte Wnt/beta-catenin signaling is required for normal bone homeostasis," *Molecular and Cellular Biology*, vol. 30, no. 12, pp. 3071–3085, 2010.

[25] E. Alsberg, H. J. Kong, Y. Hirano, M. K. Smith, A. Albeiruti, and D. J. Mooney, "Regulating bone formation via controlled scaffold degradation," *Journal of Dental Research*, vol. 82, no. 11, pp. 903–908, 2003.

[26] Q. Shi, H. Shui, Q. Chen, and Z. Y. Li, "How does mechanical stimulus affect the coupling process of the scaffold degradation and bone formation: An *in silico* approach," *Computers in Biology and Medicine*, vol. 117, 2020.

[27] Q. Zhao, H. Tang, L. Ren, and J. Wei, "In vitro apatite mineralization, degradability, cytocompatibility and in vivo new bone formation and vascularization of bioactive scaffold of polybutylene succinate/magnesium phosphate/wheat protein ternary composite," *International Journal of Nanomedicine*, vol. 15, pp. 7279–7295, 2020.

[28] X. Huang, H. Xiao, and F. Xue, "Ectopic osteogenesis and scaffold biodegradation of hydroxyapatite-collagen I scaffold in a rabbit mode," *Journal of Biomaterials and Tissue Engineering*, vol. 8, pp. 1315–1319, 2018.

[29] S. Pina, V. P. Ribeiro, C. F. Marques et al., "Scaffolding strategies for tissue engineering and regenerative medicine applications," *Materials*, vol. 12, no. 11, 2019.

[30] R. Abuna, F. S. Oliveira, H. B. Lopes et al., "The Wnt/β-catenin signaling pathway is regulated by titanium with nanotopography to induce osteoblast differentiation," *Colloids and Surfaces. B, Biointerfaces*, vol. 184, 2019.

[31] Z. Zhang, Z. Li, C. Zhang et al., "Biomimetic intrafibrillar mineralized collagen promotes bone regeneration via activation of the Wnt signaling pathway," *International Journal of Nanomedicine*, vol. 13, pp. 7503–7516, 2018.

[32] X. Zhang, J. Fan, C. S. Lee, S. Kim, C. Chen, and M. Lee, "Supramolecular hydrogels based on nanoclay and guanidine-rich chitosan: injectable and moldable osteoinductive carriers," *ACS Applied Materials & Interfaces*, vol. 12, no. 14, pp. 16088–16096, 2020.

[33] H. Liang, X. Xu, X. Feng et al., "Gold nanoparticles-loaded hydroxyapatite composites guide osteogenic differentiation of human mesenchymal stem cells through Wnt/β-catenin signaling pathway," *International Journal of Nanomedicine*, vol. 14, pp. 6151–6163, 2019.

Hindawi
Stem Cells International
Volume 2021, Article ID 7834421, 12 pages
https://doi.org/10.1155/2021/7834421

Review Article

Mesenchymal Stem Cell Therapy for Alzheimer's Disease

A. E. Hernández and E. García

Facultad de Ciencias de la Salud, Universidad Anáhuac México, Mexico

Correspondence should be addressed to E. García; edna.garcia@anahuac.mx

Received 15 June 2021; Accepted 9 August 2021; Published 1 September 2021

Academic Editor: Huseyin Sumer

Alzheimer's disease (AD) is a neurodegenerative disease responsible for 60-70% of the 50 million cases of dementia worldwide. It is characterized by neuronal cell death, shrinkage of brain tissue, and progressive cognitive, motor, and behavioral impairment, which often leads to death. Although current treatment has helped improve the patient's quality of life, it has not been able to alter the underlying disease pathology of AD. Studies have shown that mesenchymal stem cells (MSCs)—a group of multipotent stem cells—have the ability to stimulate neuroregeneration and inhibit disease progression. More recently, extracellular vesicles (EVs) from cytokine-preconditioned MSCs have also shown to induce immunomodulatory and neuroprotective effects in AD models. This review will aim to compile pertinent preclinical AD research on transgenic mice as well as clinical trials on MSC-based therapy from diverse sources.

1. Introduction

According to the World Health Organization, around 50 million individuals worldwide suffer from dementia [1]. This figure is expected to double every 20 years, until 2050 [2]. The most common form of dementia is Alzheimer's disease (AD) and may be responsible for 60-70% of the cases [1]. AD is a neurodegenerative disease characterized by the accumulation of extracellular amyloid plaques primarily composed of amyloid-beta (Aβ) peptides and intracellular neurofibrillary tangles (NFTs) of hyperphosphorylated tau protein [3]. Alois Alzheimer first described the disease in 1906 when he reported a 51-year-old woman with cognitive disturbances, delusions, disorientation, and other behavioral changes. AD is associated with neuronal cell death, shrinkage of brain tissue, and progressive cognitive, motor, and behavioral impairment, which often leads to death. As of today, disease-modifying treatments capable of altering the underlying disease pathology of AD are not available [4].

Mesenchymal stem cells (MSCs) are a group of multipotent stem cells capable of differentiating into nonmesenchymal lineages [5]. MSCs are considered a very promising approach to stimulate neuroregeneration due to their immunomodulatory properties and high biosafety but also because of their ability to synthetize neurotrophic and proangiogenic factors [6]. In AD, stem cell therapies have attempted to replace neurons that have been impaired or lost. MSC-based therapies have shown potential to restore damaged neural tissue as well as slow disease progression. Although the specific therapeutic mechanism effect of stem cell transplantation is not known, MSC therapy has shown to be an alternative therapeutic approach for neurodegenerative diseases such as AD [5].

2. Pathogenesis of AD and Current Treatment

AD is believed to occur when extracellular senile plaques and intracellular NFTs of hyperphosphorylated tau protein accumulate in the brain. These pathological processes cause a series of downstream events that include neurodegeneration with neuronal and synaptic loss leading to macroscopic atrophy [7]. Although the pathophysiology of AD is still subject to debate, the predominant hypothesis known as the amyloid cascade hypothesis predicts that the accumulation and aggregation of Aβ provoke a pathological set of events that ultimately produce what we know as AD [3, 4]. The amyloid precursor protein (APP) is a transmembrane protein that plays an important role in neuronal development, signaling,

and intracellular transport [8]. In the central nervous system (CNS), APP can undergo cleavage either by the nonamyloidogenic or amyloidogenic pathway. In the nonamyloidogenic pathway, APP is first cleaved by α-secretase secreting the extracellular soluble peptide alpha (sAPPα) and an amino acid fragment known C83, which is later cleaved by γ-secretase producing a fragment known as p3. On the other hand, in the amyloidogenic pathway, APP is first cleaved by β-secretase, secreting the extracellular soluble peptide beta (sAPPβ) and an amino acid fragment called C99. γ-Secretase also participates in this pathway by cleaving C99, producing a 37-49 amino acid residue peptide known as Aβ [4]. The two main isoforms of Aβ are Aβ40 and Aβ42. The only difference between them is that Aβ42 has two extra residues at the C-terminus. Most amyloid plaques in AD consist of predominantly Aβ42 [9]. The accumulation of Aβ monomers, as well as the decreased clearance, causes it to self-assemble and aggregate into oligomers and eventually into highly regular amyloid fibrils, generating plaques that lead to neurotoxicity and dementia [4]. Soluble Aβ and amyloid plaques are thought to induce a series of events like inflammation, oxidative stress, excitotoxicity, and hyperphosphorylation of tau. This is a protein known for stabilizing and assembling neuronal microtubules. In AD, the hyperphosphorylation of tau promotes insoluble filamentous aggregates that are part of the intracellular NFTs characteristic of the disease [10]. Although the amyloid cascade hypothesis establishes that the hyperphosphorylation of tau is a downstream event of Aβ accumulation, it is possible that tau and Aβ act in parallel pathways causing AD and intensifying each other's toxic effects [2]. In addition, neuroinflammation has also demonstrated to play a key role in AD pathological process. Specifically, microglia have shown to be one of the main players orchestrating inflammation. In AD, uncontrolled microglia activity aggravates tau pathology, stimulates the secretion of proinflammatory cytokines, and causes neuronal injury [11]. Lastly, mass neuronal and synaptic loss is also involved in the AD pathological process. Neurodegeneration affects the entorhinal cortex first, and then the subiculum and CA1 hippocampal subregion and basal forebrain networks. In the advanced stages of AD, the temporal lobes are also affected, ultimately spreading through most cortical layers [12].

AD is commonly divided into familial AD (fAD) and sporadic AD (sAD). fAD is associated with early symptoms of onset and affects <5% of all AD patients. This type of AD is caused by mutations in APP, presenilin 1 (PS1), and/or presenilin 2 (PS2) [13]. Presenilin 1 along with presenilin 2 is the catalytic components of the γ-secretase enzyme, which as we previously mentioned, cleaves APP into Aβs of varying lengths [14]. Thus, fAd-related mutations in presenilins alter the γ-secretase cleavage site, resulting in the generation of longer and more fibrillogenic Aβ [15]. On the other hand, sAD, which is associated with late onset, represents nearly 95% of patients with AD. sAD is caused by a combination of genetic and environmental risk factors without a documented familial history of AD. The apolipoprotein E4 (APOE4) and the triggering-receptor expressed on myeloid cells 2 (TREM2) have been considered the two major risk factors for sAD [13]. APOE genotypes have a significant impact on the deposition of Aβ to form senile plaques and cerebral amyloid angiopathy (CAA), two main hallmarks of amyloid pathology in AD [16]. Moreover, TREM2 mutations linked to AD generate a loss of TREM2 protein function, which is a receptor primarily expressed by microglia. This mutation affects the behavior of microglial cells, especially their response to Aβ plaques [17].

For both fAD and sAD, the current treatment includes two different types of pharmacological therapy. On one hand, cholinesterase inhibitors (ChEIs) such as donepezil, rivastigmine, and galantamine are prescribed for mild, moderate, or severe AD dementia [18]. ChEIs improve cognitive symptoms by inhibiting the biological activity of acetylcholinesterase and as a result increases acetylcholine levels in the synaptic cleft, a neurotransmitter used by cholinergic neurons which has been shown to improve the function of brain cells [19]. Response rates vary with approximately around one-third of individuals with AD showing no benefit at all and one-fifth having greater benefit. Similarly, about one-third of patients do not tolerate the ChEIs treatment approach because of side effects [20]. Meanwhile, in moderate to severe AD cases, patients are prescribed memantine, which inhibits the N-methyl-D-aspartate (NMDA) receptor and as a consequence may prevent neuron loss, as well as improve symptoms by restoring damaged neurons. In comparison, NMDA receptor antagonists have fewer side effects than ChEIs [18, 20]. Moreover, a nutraceutical, known as Huperzine A, is also used as an alternative treatment; however, it is not regulated by the Food and Drug Administration (FDA). It is important to note that although the current treatment has helped improve the quality of life of patients living with AD when used at the appropriate time, it has not changed the course or rate of decline of the disease [18]. It has a relatively small average overall effect over AD and is not capable of altering the course of the underlying neurodegenerative process [20].

3. MSC as an Alternative Treatment

Stem cells are undifferentiated cells that have the ability to self-renew, proliferate from a single cell, and differentiate into different types of cells and tissues. These cells can be grouped into 4 groups according to their origin: embryonic stem cells (ESCs), induced pluripotent stem cells (iPSCs), and fetal and adult stem cells. MSCs are an example of adult stem cells that can be obtained from various tissues including bone marrow, adipose tissue, bone, Wharton's jelly, umbilical cord blood, and peripheral blood [21]. According to the International Society for Cellular Therapy, MSCs are defined by expressing cluster differentiation (CD), CD90, CD73, CD105, and CD44 while not expressing CD45 and CD31 MSCs normal function in the body includes migrating to injury sites and taking part of a reparative process [22]. In comparison to other stem cells, MSCs differentiation potential is superior as they can differentiate into neuronal cells, osteocytes, chondrocytes, or adipocytes when stimulated with certain growth factors. In addition, MSCs also possess a low risk of differentiating into cancer cells and are infrequently immunogenic [23]. The latter is due to not expressing MHC

class II and costimulatory molecules [24]. Moreover, MSCs also possess the ability to migrate to injury and hypoxia sites, boosting tissue repair, reducing apoptosis, and promoting angiogenesis [25].

In AD models, the reduction of Aβ plaques, β-secretase, and tau hyperphosphorylation as well as the reversal of microglial inflammation, and the stimulation of anti-inflammatory cytokines are among the mechanisms postulated to have a therapeutic effect in MSC therapy. Upregulating neuroprotection and downregulating proinflammatory cytokines have also been shown to have immunomodulatory and anti-inflammatory effects [26]. In addition, MSC excreted neurotrophic factors have been shown to be able to stimulate neurogenesis and synaptogenesis, alter immune cell response through overexpressing neuroprotective cytokines like IL-10, while reducing proinflammatory cytokines such as TNF-α and IL-1β, increase the phagocytic activity of microglial cells, improve neovascularization, overcome cell death induced by Aβ and tau, reduce oxidative stress and apoptosis, alter autophagy pathways, and decrease plaque size [27]. Secreted MSC neurotrophic growth factors include glial cell-derived neurotrophic factor (GDNF), vascular endothelial growth factor (VEGF), brain-derived neurotrophic factor (BDNF), insulin-like growth factor 1(IGF-1), nerve growth factor (NGF), and fibroblast growth factor 2 (FGF2) [22, 27]. MSCs have also demonstrated to set off immune responses through microglia activation, which as a consequence sets off anti-inflammatory response. They have also revealed to change microglia phenotype from classically activated to alternatively activated, causing a drop in proinflammatory cytokines and a rise of anti-inflammatory cytokines [28]. Moreover, MSCs also enhance nerve regeneration because of their ability to differentiate into Schwann cell-like cells, which are known for promoting regeneration. MSCs have also demonstrated to boost nerve regeneration via secretion of neurotrophic factors that induce axonal growth and stem cell differentiation into myelinating cell lines [25].

However, the specific mechanism effect of stem cell transplantation is still not known. Possible theories include direct cell replacement of injured neural cells, activation of endogenous stem cells, and secretion of neurotrophic and neuroprotective factors to increase cell survival [29]. In this regard, studies have suggested that the paracrine activity could be the key therapeutic mechanism due to research that indicated that secreted substances in MSC-derived conditioned media, rather than cell incorporation, were responsible for the considerable therapeutic effect in both *in vitro* and *in vivo* contexts [24].

4. Preclinical Studies

Many animal models of AD have been studied using different species, such as *C. elegans*, *D. melanogaster*, mouse, rat, and nonhuman primates [29]. However, the most used animal models are transgenic mice which overexpress or silence APP, PS1, and PS2 genes associated with fAD. However, these transgenic mice alone have not been able to replicate most of the pathophysiology of AD. With this in mind, a triple transgenic mouse model with modified APP, PS1, and PS2 was generated. However, it is important to highlight that although a triple transgenic mouse is able to produce Aβ plaques and NFTs, the progressive neuronal loss in the hippocampus and other regions of the human AD brain was not found [30, 31]. On the other hand, no animal model is able to nearly resemble the mechanism and progression of the use of sAD, which is a significant restriction given that this type of AD is significantly more frequent than fAD. As a result, many outcomes found in animal models are rarely seen in clinical studies [13]. The latest findings on MSC therapy in transgenic mouse models of AD will be presented in the next section. A summary is provided in Table 1.

The transplantation of Wharton's Jelly mesenchymal stem cells (WJ-MSCs) has been studied in AD mouse models. Lee et al. investigated the stereotactic administration of human WJ-MSCs and their secreted Agouti-related peptide (AgRP) into the hippocampi of 5XFAD mice which improved proteasome activity and reduced the accumulation of ubiquitin-conjugated proteins. The investigators suggest that either WJ-MSCs or AgRP may be used to delay the clinical progression of AD by improving proteasome activity and consequently lowering abnormal protein aggregation [32]. In another study, Xie et al. found that four weeks after transplantation, WJ-MSCs significantly enhanced spatial learning and mitigated memory decline in APP/PS1 mice. In addition, Aβ deposition and soluble Aβ levels were significantly reduced, while anti-inflammatory cytokine IL-10 significantly increased. Proinflammatory microglial activation and proinflammatory cytokines such as IL-1β and TNFα were also significantly reduced [33]. More recently, a group of researchers evaluated the difference between "prime" and "naïve" human WJ-MSCs. Prime human WJ-MSCs were previously exposed to an AD cell line via a coculture system and "naïve" human WJ-MSCs. Although both showed promising results in reducing cell death, ubiquitin conjugate levels, and Aβ levels, "prime" human WJ-MSCs showed greater results. This suggests that exposure of human WJ-MSCs to an AD environment improves its therapeutic effects [34].

The transplantation of umbilical cord blood-derived mesenchymal stem cells (UCB-MSCs) has also showed promising results in AD mouse models. In a 5xFAD mouse AD model, human UCB-MS mitigated spatial learning and memory deterioration and alleviated the hyperphosphorylation of tau by GAL-3 secretion [35]. In the same regard, Kim et al. demonstrated that recurring intrathecal (I.T.) administration of human UCB-MSCs improves adult hippocampal neurogenesis and synaptic activity through growth differentiation factor-15 (GDF-15) secretion in an AD model [36]. Human UCB-MSCs have also demonstrated potential to attenuate Aβ42-induced synaptic dysfunction by regulating thrombospondin-1 (TSP-1) secretion [37]. In a study using Tg2576 mice, Cui et al. discovered that human UCB-MSC transplantation significantly mitigated cognitive deterioration of AD mice without altering Aβ levels in the hippocampus. They suggest that human UCB-MSCs may enhance cognitive deterioration by reducing oxidative stress and promoting hippocampal neurogenesis [38]. Moreover, Wang et al. demonstrated that resveratrol facilitates UCB-MSC

Table 1: Most recent findings of MSCs in AD transgenic mice.

Cell type	Model	Study design	Findings
Human WJ-MSCs	5XFAD	Injection of WJ-MSCs or AgRP directly into the left hippocampus of 5XFAD mice.	Improves proteasome activity by AgRP. Reduces the accumulation of ubiquitin-conjugated proteins [32].
Human WJ-MSCs	APP/PS1	Injection of WJ-MSCs into the tail vein of APP/PS1 mice.	Improves the spatial learning. Mitigates memory decline. Increases IL-10. Reduces Aβ deposition levels. Reduces soluble Aβ levels. Proinflammatory microglial activation. Reduces IL-1β and TNFα levels [33].
Human WJ-MSCs	5XFAD	I.V.T. infusion of WJ-MSCs (exposed to an AD cell line) into 5XFAD mice.	Reduces cell death Reduces ubiquitin conjugate levels Reduces Aβ levels [34].
Human UCB-MSCs	5XFAD	Infusion of recombinant human GAL-3 protein and UCB-MSCs into 5XFAD mice.	Improves the spatial learning. Improves memory impairment. UCB-MSCs mitigate hyperphosphorylation of tau through GAL-3 secretion [35].
Human UCB-MSCs	APP/PS1	Coculture of UCB-MSCs with NSCs to identify paracrine factors. Repeated I.T. injections of UCB-MSCs into APP/PS1 mice.	GDF-15 improves endogenous hippocampal neurogenesis and synaptic activity through CSF [36].
Human UCB-MSCs	5XFAD	Coculture of UCB-MSCs with primary hippocampal neurons under Aβ42 peptide treatment to identify paracrine factors. Transplantation of hUCB-MSCs via I.C.V. route.	Mitigates Aβ42-induced synaptic dysfunction by regulating TSP-1 release [37].
Human UCB-MSCs	Tg2576	UCB-MSCs I.V. transplantation into Tg2576 mice.	Improves cognitive function Attenuates oxidative stress Promotes cell proliferation and newborn cell survival Promotes neurons generating Promotes hippocampal neurogenesis Increases expression of Sirt1, BDNF, and SYN [38].
Human UCB-MSCs	Tg2576	UCB-MSCs I.V. transplantation combined with resveratrol into Tg2576 mice.	Better UCB-MSC engraftment in the hippocampus. Improves learning and memory Enhances neurogenesis Alleviates neural apoptosis in the hippocampus [39].
Human WJ-MSCs and UCB-MSCs	5XFAD	Coculture of MSCs with SVZ-derived NSCs from 5XFAD mice.	Induces neuronal development and neurite outgrowth [40].
Rat BM-MSCs	APP/PS1	I.C.V. injection of BM-MSCs into APP/PS1 mice.	Improves cognitive impairment by ameliorating astrocytic inflammation as well as synaptogenesis by increasing the expression of microRNA-146a in hippocampus [41].
Human BM-MSCs	APP/PS1	Tail I.V. injection of BM-MSCs into APP/PS1 mice.	Reduced levels of IL-1, IL-2, TNF-α, and IFN-γ. Regulates the expression of Aβ-related genes [42].
Mouse BM-MSCs	3xTg-AD	Evaluation of I.V. injected BM-MSCs using serial [18F] florbetaben PET into 3xTg-AD mice.	The reduction of β-amyloid deposits during BMSCs treatment could be confirmed by PET [43].
Mouse BM-MSCs	$3\times$Tg-AD	Infusion of ^{111}In-labeled BM-MSCs via I.V. administration into $3\times$Tg-AD mice.	The number of BM-MSCs reaching the brain is very small [44].
Murine BM-MSCs	APP/PS1	Injection of BM-MSCs into APP/PS1 mice via the tail vein.	Reduces pE3-Aβ plaque size. Reduces gene expression of TNF-α, IL-6, MCP-1, and NGF. Reduces microglial number and microglia size [45].

Table 1: Continued.

Cell type	Model	Study design	Findings
Murine BM-MSCs	APP/PS1	Single I.V. and repeated I.N. administration of secretome collected from MSCS exposed *in vitro* to AD mouse brain homogenates from APP/PS1 mouse.	A single infusion: Transient memory recovery Improves the inflammatory phenotype of astrocytes. Reduces brain amyloidosis and microglial activation. Repeated infusions: Sustains memory recovery Reduces neuroinflammation Decreases brain amyloidosis Increases neuronal density in both cortex and hippocampus Diminishes hippocampal shrinkage [47].
Human MenSCs	APP/PS1	I.C. transplantation of MenSCs into an APP/PS1 mice.	Improves the spatial learning and memory Mitigates amyloid plaques Reduces tau hyperphosphorylation Increases Aβ degrading enzymes Modulates a panel of proinflammatory cytokines associated with an altered microglial phenotype [48].
Rat AD-MSCs	APP/PS1	Transplantation of AD-MSCs into the hippocampi of APP/PS1 mice with an automated infusion pump.	Reduces oxidative stress Alleviates cognitive impairment Promotes neurogenesis in the SGZ of the hippocampus Increases the number of neuroblasts in the SVZ of the hippocampus [49].
AM-MSCs	APP/PS1	Intrahippocampal transplantation of AM-MSCs into APP/PS1 mice.	Reduced amyloid-β peptide (Aβ) deposition and rescued spatial learning and memory Reduced amyloid-β peptide (Aβ) deposition and rescued spatial learning and memory Improves the spatial learning and memory. Reduces Aβ deposition Intensifies release of Aβ degrading enzymes Reduces microglia activation. Increases hippocampal synaptic density and neurogenesis mediated by BDNF [50].
MSC-EVs	3xTg	Administration of EVs derived from cytokine-preconditioned MSCs through the I.N. route into 3xTg mice.	Decrease microglia activation. Increases dendritic spine density [11].
MSC-RVG-Exo	APP/PS1 mice	Use of RVG peptide to target I.V. infused MSC-Exo to the brain of transgenic APP/PS1 mice.	Improves cognitive function better than unmodified exosomes. Decrease plaque deposition and Aβ levels. Reduces the activation of astrocytes. Reduces the expression of proinflammatory mediators such as TNF-α, IL-β, and IL-6. Raises the levels of IL-10, IL-4, and IL-13 [53].

AD-MSCs: adipose tissue-derived mesenchymal stem cells; AgRP: agouti-related peptide; AM-MSCs: amniotic mesenchymal stem cells; Aβ: amyloid-beta; BDNF: brain-derived neurotrophic factor; BM-MSCs: bone marrow-derived mesenchymal stem cells; CSF: cerebrospinal fluid; EVs: extracellular vesicles; GAL-3: galectin-3; I.C.: intracerebral; I.C.V.: intracerebroventricular; I.N.: intranasal; I.T.: intrathecal; I.V.: intravenous; I.V.T.: intraventricular; IFN-γ: interferon-gamma; IL: interleukin; MCP-1: monocyte chemoattractant protein-1; MenSCs: menstrual blood-derived mesenchymal stem cells; MSC-EVs: mesenchymal stem cell-derived extracellular vesicles; MSC-RVG-Exo: RVG-conjugated mesenchymal stem cell-derived; NGF: nerve growth factor; NSCs: neural stem cells; pE3-Aβ: pyroglutamate modified form of amyloid-beta; PET: positron emission tomography; RVG: rabies viral glycoprotein; SGZ: subgranular zone; Sirt1: sirtuin 1; SVZ: subventricular zone; SYN: synaptophysin; TNF-α: tumor necrosis factor alpha; UCB-MSCs: umbilical cord blood-derived mesenchymal stem cells; WJ-MSCs: Wharton's Jelly mesenchymal stem cells.

engraftment in the hippocampus and enhances its therapeutic effect [39]. Similarly, Park et al. studied the coculture of UCB-MSCs, WJ-MSCs, and SVZ-derived neural stem cells (NSCs) in an *in vitro* 5XFAD mouse model. Results demonstrated neuronal development and neurite outgrowth and an increased secretion of activin A. This suggests that both MSCs and activin A may be used to improve neurogenesis for cortical regeneration to treat AD [40].

On the other hand, bone marrow-derived mesenchymal stem cells (BM-MSCs) have also been investigated. Intracerebroventricular (I.C.V.) BM-MSCs have shown potential to improve cognitive deterioration in AD model mice by

mitigating astrocytic inflammation and synaptogenesis. Exosomal transfer of miR-146a—which accumulates in astrocytes—is suggested by Nakano et al. to be involved in the improvement of cognitive deterioration [41]. In another study, IL-1, IL-2, TNF-α, and IFN-γ levels were reduced after human BM-MSC treatment [42]. More recently, a group of researchers investigated the effects of BM-MSCs in 3xTg AD mice using serial [18F] florbetaben positron emission tomography to evaluate the changes in Aβ deposits after MSC therapy. Results showed that a reduction of Aβ deposits in AD mice during BMSC treatment could be confirmed by PET. This opens the possibility that noninvasive PET imaging may be used for the evaluation of MSC response in clinical applications [43]. In the same regard, Park et al. demonstrated that a small number of mouse BM-MSCs are able to reach the brain by intravenous (I.V.) infusion, and a greater distribution of BM-MSCs was found in the $3\times$Tg-AD mice compared to a control group. In addition, the results showed that brain uptake increased in the AD group, while the control group did not change significantly [44]. BM-MSC systemic administration in APP/PS1 mouse has also shown the potential to reduce pyroglutamate-modified amyloid-beta (pE3-Aβ) plaque size, a potential biomarker for Aβ plaque pathology [45, 46]. The systemic administration of secretomes isolated from mouse BM-MSCs exposed to AD mouse brain homogenates has also been studied. Santamaria et al. demonstrated that the secretome derived from AD-conditioned MSCs can fully replicate the neuroreparative effects previously associated with MSC direct transplantation. Repeated intranasal (I.N.) infusions of the secretome of APP/PS1 fully restored mouse memory and improved the neuropathology in advanced stages of the disease. Preconditioning BM-MSCs to an AD environment showed to be crucial to induce the therapeutic activity of the secretome [47].

The therapeutic effects of adipose tissue, menstrual blood, and amniotic fluid mesenchymal stem cells have also been studied. Zhao et al. studied menstrual blood-derived mesenchymal stem cells (MenSCs) that showed that intracerebral (IC) injection of them improved Aβ plaques, reduced tau hyperphosphorylation, and enhanced the spatial learning and memory of APP/PS1 mice. They also demonstrated that MenSCs were able to increment various Aβ degrading enzymes and decrease several proinflammatory cytokines such as IL-1β and TNF-α, which as we previously mentioned are associated with an altered microglial phenotype [48]. On the other hand, adipose tissue-derived mesenchymal stem cells (AD-MSCs) showed to improve endogenous neurogenesis in both the subgranular and subventricular zones, reduce oxidative stress, and mitigate cognitive deterioration in APP/PS1 mice [49]. Similarly, human amniotic mesenchymal stem cell (AM-MSC) intrahippocampal transplantation significantly diminished Aβ deposition and improved the spatial learning and memory deficits in APP/PS1 mice. Zheng et al. suggest that improved cognition may be associated with an increment in hippocampal synaptic density and neurogenesis that is regulated by BDNF [50].

Extracellular vesicles (EVs) from cytokine-preconditioned MSCS are also being investigated as a therapeutic approach for AD due to MSCs reporting paracrine activity. EVs such as exosomes and microvesicles are lipid bilayer vesicles secreted by cells into the extracellular space [11, 51]. Lourdo et al. found that mesenchymal stem cell-derived extracellular vesicles (MCS-EVs) regulate the microglia activation and decreases dendritic spine loss in a triple-transgenic 3xTg mouse [11]. Another study showed that I.V. injected exosomes accumulate mainly in the spleen and liver and not in the brain [52]. Therefore, Cui et al. proposed surface-modified MSC-EVs that target the cortex and hippocampus of AD mice by using a specific rabies viral glycoprotein (RVG) peptide to prevent memory deficits in AD. Results showed that RVG-conjugated mesenchymal stem cell-derived exosomes (MSC-RVG-Exo) improved memory deficits, decreased plaque deposition and Aβ levels, and normalized levels of inflammatory cytokines compared to unmodified exosomes [53].

5. Clinical Studies

Many clinical trials have been conducted to evaluate the role of MSCS derived from various sources in patients with AD. It is important to note that only a few have been officially completed and have published results. A summary of the clinical trials registered on ClinicalTrials.gov evaluating MSCs for AD treatment can be found in Table 2.

5.1. Completed. A phase 1 clinical trial evaluated a single stereotactic brain infusion of human UCB-MSCs in patients with mild-to-moderate AD. 3 subjects received a single low dose infusion (3.0×10^6 cells/60 μL) while 6 subjects received a high dose infusion (6.0×10^6 cells/60 μL). Results showed that a single injection of human UCB-MSCs was safe and well tolerated and did not cause serious adverse effects during the two-year follow-up. However, it failed to produce the same therapeutic effect as seen in animal studies. Kim et al. speculate that the discrepancy between animal and human studies may be related to the Pittsburgh compound B positron emission tomography (PiB-PET), which may not be sensitive enough to detect soluble amyloid or diffuse amyloid plaques in comparison with immunohistochemical staining, enzyme-linked immunosorbent assay, and Western blot used in preclinical studies, which are capable of detecting soluble and insoluble amyloid as well as different types of amyloid plaques. Another reason as to why the human brain did not replicate findings from the animal studies may be due to their AD microenvironment differences. Similarly, preclinical studies rely on xenogeneic transplantation where as human clinical trials rely on allogenic transplantation. Some limitations of this clinical study include the lack of a control group and the small number of participants [54–56].

A phase 1/2a trial evaluated the safety, dose-limiting toxicity, and exploratory efficacy of 3 repeated intraventricular administrations (I.V.T.) of NEUROSTEM® (human UCB-MSCs) versus placebo via an Ommaya reservoir at 4 week intervals in subjects with AD was completed in December 2019. The study was divided into two stages, stage 1 consisted of a dose escalation in which 3 subjects received a low dose (1×10^7 cells/2 mL) and 6 subjects a high dose (3×10^7 cells/2 mL). On the other hand, stage 2, made up

Table 2: Clinical trials of MSCs in humans with AD.

NCT	Stage	Cell type	Study design	Phase	Participants	Route	Intervention	Findings
NCT01297218	Completed	Human UCB-MSCs	Open-label, single-center study	1	9	1 single I.C. infusion	250,000 UCB-MSCs per 5 μL per 1 entry site, 3 million cells per brain. 500,000 UCB-MSCs per 5 μL per 1 entry site, 6 million cells per brain.	The stereotactic injection of UCB-MSCs into the hippocampus and precuneus is feasible, safe, and well tolerated. However, a single injection of UCB-MSCs was not effective in altering the AD pathophysiological process [54, 55].
NCT01696591	Unknown	Human UCB-MSCs	Long-term follow-up study of NCT01297218	Same as NCT01297218 [56]				
NCT02054208	Completed	Human UCB-MSCs	Double-blind, single-center study	1/2a	45	3 I.V.T. infusions	1×10^7 UCB-MSCs/ 2 mL 3×10^7 UCB-MSCs/ 2 mL Placebo	Not yet published results [57].
NCT03172117	Recruiting	Human UCB-MSCs	Long-term follow-up study of NCT02054208	Same as NCT02054208 [61]				
NCT03117738	Completed	Autologous human AD-MSCs	Randomized, double-blind, placebo-controlled, parallel-group comparison study	1/2	21	9 I.V. infusions	2×10^8 AD-MSCs Placebo	Not yet published results [58].
NCT04228666	Withdrawn	Autologous human AD-MSCs	Open-label, nonrandomized study	1/2a	24	4 I.V. infusions	2×10^8 AD-MSCs	N/A [59]
NCT02600130	Active, not recruiting	LMSCs	Randomized, placebo-controlled study	1	33	1 single I.V. infusion	20 million LMSCs 100 million LMSCs Placebo	N/A [60]
NCT04855955	Available	Autologous human AD-MSCs	Single patient emergency expanded access study	N/A	1	N/A	N/A	N/A [62]
NCT02833792	Recruiting	Human MSCs	Multicenter, randomized, single-blind, placebo-controlled, crossover study	2a	40	1 single I.V. infusion	1.5 million MSCs per kilogram body weight Placebo	N/A [63]
NCT04040348	Recruiting	Allogeneic human UCB-MSCs	Prospective open-label study	1	6	4 I.V. infusions	100 million UCB-MSCs	N/A [64]
NCT04388982	Recruiting	Allogenic AD-MSCs-Exos	Single-center, open-label study	1/2	9	24 nasal drip infusions.	5 μg MSCs-Exos/1 mL 10 μg MSCs-Exos/1 mL 20 μg MSCs-Exos/1 mL	N/A [65]
NCT02899091	Recruiting	P-MSCs	Randomized, double-blind, placebo-controlled study	1/2a	24	1 and 2 I.V. infusions.	2.0×10^8 P-MSCs Placebo	N/A [66]

Table 2: Continued.

NCT	Stage	Cell type	Study design	Phase	Participants	Route	Intervention	Findings
NCT04684602	Recruiting	Human UCB-MSCs	Multicenter, prospective, open-label clinical study	1/2	5,000	1 single infusion via condition-specific route of administration.	N/A	N/A [67]
NCT04482413	Not yet recruiting	Autologous AD-MSCs	Randomized, double-blind, active-controlled study	2b	80	4 I.V. infusions	2.0×10^8 AD-MSCs/ 20 mL Placebo	N/A [68]
NCT01547689	Unknown	Human UCB-MSCs	Open-label, single-center, self-control study	1/2	30	8 I.V. infusions	20 million UCB-MSCs (0.5×10^6 UCB-MSCs per kg)	N/A [69]
NCT02672306	Unknown	Human UCB-MSCs	Multicenter, randomized, double-blind, placebo-controlled study	1/2	16	8 I.V. infusions	20 million UCB-MSCs per subject (0.5×10^6 UCMSCs per kg) Placebo	N/A [70]

AD-MSCs: adipose tissue-derived mesenchymal stem cells; AD-MSCs-Exos: adipose tissue-derived mesenchymal stem cells exosomes; AM-MSCs: amniotic mesenchymal stem cells; BM-MSCs: bone marrow-derived mesenchymal stem cells; I.C.: intracerebral; I.C.V.: intracerebroventricular; I.N.: intranasal; I.V.: intravenous; I.V.T.: intraventricular; P-MSCs: placenta-derived mesenchymal stem cells; UCB-MSCs: umbilical cord blood-derived mesenchymal stem cells; WJ-MSCs: Wharton's Jelly mesenchymal stem cells.

by a randomized and multiple-dose cohort parallel design, consisted of 36 individuals, in which 24 subjects received a high dose with the concentration previously mentioned and 12 received placebo. All groups received 3 repeated I.V.T. infusions via an Ommaya Reservoir at 4 week intervals. The study has yet to publish the results [57].

A phase 1/2 randomized, double-blind, placebo-controlled study was completed on 2019. 21 subjects were randomly assigned into the AstroStem (autologous human AD-MSCs) and placebo control groups in a 1 : 1 ratio. Both groups received 9 repeated I.V. infusions at 2 week intervals, however, only 7 subjects completed the AstroStem infusions and 5 the placebo. Results showed 3 serious adverse effects in the AstroStem group including diarrhea, oesophageal, squamous cell carcinoma stage IV, and pulmonary embolism. Other reported adverse effects were open-angle glaucoma, dysphagia, fatigue, infusion site reaction, fall, dehydration, abnormal loss of weight, syncope, and ecchymosis. The changes in ADAS-Cog score from baseline to week 30 in the AstroStem group were 5.9 (6.8) and 3.0 (5.4) in the control group [58].

5.2. Ongoing. A phase 1/2a, open-label, which is currently an ongoing schedule to end in February 2022, was designed to evaluate the safety profile of 4 I.V. infusions of autologous adipose-derived mesenchymal stem cells (HB-adMSCs) in 24 subjects as a possible treatment for AD. 4 I.V. infusions were administered on weeks 0, 2, 6, and 8 at a dose of 2×10^8 total HB-adMSC cells. The main purpose was to evaluate the adverse effects of their treatment as well as the ability of HB-adMSCs to alter AD-related inflammation via measuring the levels of tumor necrosis factor-alpha (TNF-a), interleukin-1 (IL-1), interleukin-6 (IL-6), C-Reactive Protein (CRP), and markers associated with amyloid deposition, Aβ40, and Aβ42. Participants will also be evaluated for cognitive deficits determined by changes in standard values of MMSE, ADCS-ADL, Alzheimer's disease Related Quality of Life (ADRQL), Altoida Neuro Motor Index (NMI) for Digital Biomarkers, and Clinical Dementia Rating Questionnaire (CDR) [59].

A phase 1 placebo-controlled clinical trial designed to evaluate the safety and efficacy of Longeveron Mesenchymal Stem Cells (LMSCs) in individuals with AD is currently ongoing.

A single peripheral I.V. infusion was administered in 25 subjects. Group 1 (10 individuals) received 20 million LMSCs (low-dose), group 2 (10 individuals) received 100 million LMSCs (high-dose), and group 3 (5 individuals) received placebo. To evaluate the safety of the infusion, the incidence of any treatment-emergent serious adverse events was assessed within the first 30 days after treatment administration. Preliminary efficacy was determined by changes in standard values for ADAS-Cog, MMSE, NPI, GDS, University of Pennsylvania Smell Identification Test (UPSIT), ADCS-ADL, Quality of Life-Alzheimer's Disease (QOL-AD), blood inflammatory and AD biomarkers, cerebrospinal fluid inflammatory biomarkers, CSF biomarkers of AD, and brain volumetry calculated using MRI at baseline, 2, 4, 13, 26, 39, and 52 weeks' postinfusion [60].

5.3. Challenges. Despite all favorable findings found in MSC-AD therapy, this treatment has several limitations. To begin, no animal model is able to fully replicate the entire pathophysiology of the disease. Similarly, most transgenic mice utilized in preclinical studies rely on the expression of fAD mutations, the least frequent type of AD, while most clinical trials consist of patients with sAD. This complicates the translation of fundamental research findings into clinical investigations. The lack of an effective model that can replicate the entire pathophysiology of the disease is one of the biggest setbacks in the search for an effective AD treatment [31].

Human UCB-MSCs are the most often employed MSCs in clinical studies. However, further research is required to determine if this source is truly the most effective. Correspondingly, the number of injections and delivery routes must also be optimized [71]. In this regard, of the only three completed clinical trials, they all used a different delivery route including I.V., I.V.T., and I.C. The most effective and noninvasive route must be used as repeated infusions will be needed considering that NCT01297218 showed that a single infusion of MSCs was not enough to alter the AD pathophysiological process [11, 54]. Furthermore, further research and appropriate assessment techniques are required to prove the absence of adverse effects from MSC treatment on a long-term basis.

In regard to the administration of MSC-EVs, although preclinical studies have shown promising potential therapeutic effects, it has yet to be studied in patients with AD. As of May 31, 2021, only one clinical trial which is currently recruiting participants is set to study the safety and efficacy of exosomes for AD treatment. However, as suggested by Salem et al., some limitations including EVs heterogeneity, isolation, and production techniques need to be assessed first [28].

6. Conclusions

Many preclinical trials evaluating MSC treatment in transgenic mouse models of AD have yielded promising therapeutic outcomes. However, this has not been the case with human clinical trials. Although MSC therapy has demonstrated to be safe and tolerable in a single clinical study with published findings, the therapeutic benefit was not replicated. The frequency of unsuccessful clinical trials might be lowered by developing a successful AD model, notably the one for sAD, which accounts for the vast majority of AD patients. This will allow for a more efficient transition from basic research to clinical trials. Nonetheless, we believe that MSC therapy has a promising future and that its paracrine function, in particular, must be harnessed to establish a successful treatment for AD.

Data Availability

No datasets were generated during the current study.

Conflicts of Interest

The authors declare that there is no conflict of interest regarding the publication of this paper.

Acknowledgments

This review was funded by Fondo de Investigación de la Universidad Anáhuac, México.

References

[1] Dementia, "Who.int," 2021, https://www.who.int/news-room/fact-sheets/detail/dementia/.

[2] P. Scheltens, K. Blennow, M. Breteler et al., "Alzheimer's disease," *The Lancet*, vol. 388, no. 10043, pp. 505–517, 2016.

[3] I. Lauritzen, R. Pardossi-Piquard, C. Bauer et al., "The -secretase-derived C-terminal fragment of APP, C99, but not A , is a key contributor to early intraneuronal lesions in triple-transgenic mouse hippocampus," *Journal of Neuroscience*, vol. 32, no. 46, pp. 16243–16255, 2012.

[4] J. Soria Lopez, H. González, and G. Léger, "Alzheimer's disease," in *Handbook of Clinical Neurology*, pp. 231–255, Geriatric Neurology. ST. DeKosky and S. Asthana Editors. Elsevier, 2019.

[5] F. Chakari-Khiavi, S. Dolati, A. Chakari-Khiavi et al., "Prospects for the application of mesenchymal stem cells in Alzheimer's disease treatment," *Life Sciences*, vol. 231, article 116564, 2019.

[6] Y. Mukhamedshina, O. Gracheva, D. Mukhutdinova, Y. Chelyshev, and A. Rizvanov, "Mesenchymal stem cells and the neuronal microenvironment in the area of spinal cord injury," *Neural Regeneration Research*, vol. 14, no. 2, article 244778, pp. 227–237, 2019.

[7] C. Lane, J. Hardy, and J. Schott, "Alzheimer's disease," *European Journal of Neurology*, vol. 25, no. 1, pp. 59–70, 2018.

[8] G. Chen, T. Xu, Y. Yan et al., "Amyloid beta: structure, biology and structure-based therapeutic development," *Acta Pharmacologica Sinica*, vol. 38, no. 9, pp. 1205–1235, 2017.

[9] L. Gu and Z. Guo, "Alzheimer's Aβ42 and Aβ40 peptides form interlaced amyloid fibrils," *Journal of Neurochemistry*, vol. 126, no. 3, pp. 305–311, 2013.

[10] D. Barragán Martínez, M. García Soldevilla, A. Parra Santiago, and J. Tejeiro Martínez, "Alzheimer's disease," *Medicine - Programa de Formación Médica Continuada Acreditado*, vol. 12, no. 74, pp. 4338–4346, 2019.

[11] M. Losurdo, M. Pedrazzoli, C. D'Agostino et al., "Intranasal delivery of mesenchymal stem cell-derived extracellular vesicles exerts immunomodulatory and neuroprotective effects in a 3xTg model of Alzheimer's disease," *STEM CELLS Translational Medicine*, vol. 9, no. 9, pp. 1068–1084, 2020.

[12] T. Duncan and M. Valenzuela, "Alzheimer's disease, dementia, and stem cell therapy," *Stem Cell Research & Therapy*, vol. 8, no. 1, p. 111, 2017.

[13] L. Zhang, C. Chen, M. Mak et al., "Advance of sporadic Alzheimer's disease animal models," *Medicinal Research Reviews*, vol. 40, no. 1, pp. 431–458, 2020.

[14] B. De Strooper, "Loss-of-function presenilin mutations in Alzheimer disease," *EMBO reports*, vol. 8, no. 2, pp. 141–146, 2007.

[15] M. Kabir, M. Uddin, J. Setu, G. Ashraf, M. Bin-Jumah, and M. Abdel-Daim, "Exploring the role of *PSEN* mutations in the pathogenesis of Alzheimer's disease," *Neurotoxicity Research*, vol. 38, no. 4, pp. 833–849, 2020.

[16] C. Liu, C. C. Liu, T. Kanekiyo, H. Xu, and G. Bu, "Apolipoprotein E and Alzheimer disease: risk, mechanisms and therapy," *Nature Reviews Neurology*, vol. 9, no. 2, pp. 106–118, 2013.

[17] S. Carmona, K. Zahs, E. Wu, K. Dakin, J. Bras, and R. Guerreiro, "The role of *TREM2* in Alzheimer's disease and other neurodegenerative disorders," *The Lancet Neurology*, vol. 17, no. 8, pp. 721–730, 2018.

[18] J. Weller and A. Budson, "Current understanding of Alzheimer's disease diagnosis and treatment," *F1000Research*, vol. 7, article 1161, 2018.

[19] K. Sharma, "Cholinesterase inhibitors as Alzheimer's therapeutics (Review)," *Molecular Medicine Reports*, vol. 20, no. 2, pp. 1479–1487, 2019.

[20] R. Briggs, S. Kennelly, and D. O'Neill, "Drug treatments in Alzheimer's disease," *Clinical Medicine*, vol. 16, no. 3, pp. 247–253, 2016.

[21] G. Kolios and Y. Moodley, "Introduction to stem cells and regenerative medicine," *Respiration*, vol. 85, no. 1, pp. 3–10, 2013.

[22] N. P. Staff, D. Jones, and W. Singer, "Mesenchymal stromal cell therapies for neurodegenerative diseases," *Mayo Clinic Proceedings*, vol. 94, no. 5, pp. 892–905, 2019.

[23] J. Kim, Y. Lee, S. Lee, K. Kim, M. Song, and J. Lee, "Mesenchymal stem cell therapy and Alzheimer's disease: current status and future perspectives," *Journal of Alzheimer's Disease*, vol. 77, no. 1, pp. 1–14, 2020.

[24] L. Liew, T. Katsuda, L. Gailhouste, H. Nakagama, and T. Ochiya, "Mesenchymal stem cell-derived extracellular vesicles: a glimmer of hope in treating Alzheimer's disease," *International Immunology*, vol. 29, no. 1, pp. 11–19, 2017.

[25] D. Cooney, E. Wimmers, Z. Ibrahim et al., "Mesenchymal stem cells enhance nerve regeneration in a rat sciatic nerve repair and hindlimb transplant model," *Scientific Reports*, vol. 6, no. 1, 2016.

[26] X. Liu, L. Yang, and L. Zhao, "Stem cell therapy for Alzheimer's disease," *World Journal of Stem Cells*, vol. 12, no. 8, pp. 787–802, 2020.

[27] M. Alipour, S. Nabavi, L. Arab et al., "Stem cell therapy in Alzheimer's disease: possible benefits and limiting drawbacks," *Molecular Biology Reports*, vol. 46, no. 1, pp. 1425–1446, 2019.

[28] H. Salem, G. Colpo, and A. Teixeira, "Stem cells in Alzheimer's disease: current standing and future challenges," *Advances in Experimental Medicine and Biology*, vol. 1079, pp. 93–102, 2018.

[29] F. Han, J. Bi, L. Qiao, and O. Arancio, "Stem cell therapy for Alzheimer's disease," *Advances in Experimental Medicine and Biology*, vol. 1266, pp. 39–55, 2020.

[30] F. Han, W. Wang, and C. Chen, "Research progress in animal models and stem cell therapy for Alzheimer’s disease," *Journal of Neurorestoratology*, vol. 2015, no. 3, pp. 11–22, 2014.

[31] E. Drummond and T. Wisniewski, "Alzheimer's disease: experimental models and reality," *Acta Neuropathologica*, vol. 133, no. 2, article 1662, pp. 155–175, 2017.

[32] N. Lee, S. Park, S. Kwon et al., "Agouti Related Peptide Secreted Via Human Mesenchymal Stem Cells Upregulates Proteasome Activity in an Alzheimer's Disease Model," *Scientific Reports*, vol. 7, no. 1, 2017.

[33] Z. Xie, Z. Liu, X. Zhang et al., "Wharton's Jelly-derived mesenchymal stem cells alleviate memory deficits and reduce amyloid-β deposition in an APP/PS1 transgenic mouse model," *Clinical and Experimental Medicine*, vol. 16, no. 1, pp. 89–98, 2016.

[34] S. Park, H. Kim, S. Kwon et al., "Exposure of mesenchymal stem cells to an Alzheimer's disease environment enhances

therapeutic effects," *Stem Cells International*, vol. 2021, Article ID 6660186, 14 pages, 2021.

[35] H. Lim, D. Lee, W. Choi, S. Choi, W. Oh, and D. Kim, "Galectin-3 secreted by human umbilical cord blood-derived mesenchymal stem cells reduces aberrant tau phosphorylation in an Alzheimer disease model," *Stem Cells International*, vol. 2020, Article ID 8878412, 14 pages, 2020.

[36] D. Kim, D. Lee, E. Chang et al., "GDF-15 secreted from human umbilical cord blood mesenchymal stem cells delivered through the cerebrospinal fluid promotes hippocampal neurogenesis and synaptic activity in an Alzheimer's disease model," *Stem Cells and Development*, vol. 24, no. 20, pp. 2378–2390, 2015.

[37] D. Kim, H. Lim, D. Lee et al., "Thrombospondin-1 secreted by human umbilical cord blood-derived mesenchymal stem cells rescues neurons from synaptic dysfunction in Alzheimer's disease model," *Scientific Reports*, vol. 8, no. 1, article 18542, p. 354, 2018.

[38] Y. Cui, S. Ma, C. Zhang et al., "Human umbilical cord mesenchymal stem cells transplantation improves cognitive function in Alzheimer's disease mice by decreasing oxidative stress and promoting hippocampal neurogenesis," *Behavioural Brain Research*, vol. 320, pp. 291–301, 2017.

[39] X. Wang, S. Ma, B. Yang et al., "Resveratrol promotes hUC-MSCs engraftment and neural repair in a mouse model of Alzheimer's disease," *Behavioural Brain Research*, vol. 339, pp. 297–304, 2018.

[40] S. Park, J. Lee, E. Chang et al., "Activin A secreted by human mesenchymal stem cells induces neuronal development and neurite outgrowth in an in vitro model of Alzheimer's disease: neurogenesis induced by MSCs via activin A," *Archives of Pharmacal Research*, vol. 39, no. 8, pp. 1171–1179, 2016.

[41] M. Nakano, K. Kubota, E. Kobayashi et al., "Bone marrow-derived mesenchymal stem cells improve cognitive impairment in an Alzheimer's disease model by increasing the expression of microRNA-146a in hippocampus," *Scientific Reports*, vol. 10, no. 1, article 10772, 2020.

[42] Y. Wei, Z. Xie, J. Bi, and Z. Zhu, "Anti-inflammatory effects of bone marrow mesenchymal stem cells on mice with Alzheimer's disease," *Experimental and Therapeutic Medicine*, vol. 16, no. 6, pp. 5015–5020, 2018.

[43] B. Park, J. Kim, T. Lim et al., "Therapeutic effect of mesenchymal stem cells in an animal model of Alzheimer's disease evaluated by β-amyloid positron emission tomography imaging," *Australian & New Zealand Journal of Psychiatry*, vol. 54, no. 9, pp. 883–891, 2020.

[44] B. Park, T. Lim, J. Yoon, and Y. An, "In vivo tracking of intravenously injected mesenchymal stem cells in an Alzheimer's animal model," *Cell Transplantation*, vol. 27, no. 8, pp. 1203–1209, 2018.

[45] Y. Naaldijk, C. Jäger, C. Fabian et al., "Effect of systemic transplantation of bone marrow-derived mesenchymal stem cells on neuropathology markers in APP/PS1 Alzheimer mice," *Neuropathology and Applied Neurobiology*, vol. 43, no. 4, pp. 299–314, 2017.

[46] P. Wang, K. Lin, H. Liu et al., "Plasma pyroglutamate-modified amyloid beta differentiates amyloid pathology," *Alzheimer's & Dementia: Diagnosis, Assessment & Disease Monitoring*, vol. 12, no. 1, article e12029, 2020.

[47] G. Santamaria, E. Brandi, P. Vitola et al., "Intranasal delivery of mesenchymal stem cell secretome repairs the brain of Alzheimer's mice," *Cell Death & Differentiation*, vol. 28, no. 1, pp. 203–218, 2021.

[48] Y. Zhao, X. Chen, Y. Wu, Y. Wang, Y. Li, and C. Xiang, "Transplantation of human menstrual blood-derived mesenchymal stem cells alleviates Alzheimer's disease-like pathology in APP/PS1 transgenic mice," *Frontiers in Molecular Neuroscience*, vol. 11, 2018.

[49] Y. Gong, Y. Yan, T. Ma, K. Gong, Q. Ao, and X. Zhang, "Adipose-derived mesenchymal stem cell transplantation promotes adult neurogenesis in the brains of Alzheimer's disease mice," *Neural Regeneration Research*, vol. 9, no. 8, article 131596, pp. 798–805, 2014.

[50] X. Zheng, Q. Wan, C. Zheng et al., "Amniotic mesenchymal stem cells decrease Aβ deposition and improve memory in APP/PS1 transgenic mice," *Neurochemical Research*, vol. 42, no. 8, pp. 2191–2207, 2017.

[51] L. Doyle and M. Wang, "Overview of extracellular vesicles, their origin, composition, purpose, and methods for exosome isolation and analysis," *Cell*, vol. 8, no. 7, p. 727, 2019.

[52] C. Lai, O. Mardini, M. Ericsson et al., "Dynamic biodistribution of extracellular vesicles *in vivo* using a multimodal imaging reporter," *ACS Nano*, vol. 8, no. 1, pp. 483–494, 2014.

[53] G. Cui, H. Guo, H. Li et al., "RVG-modified exosomes derived from mesenchymal stem cells rescue memory deficits by regulating inflammatory responses in a mouse model of Alzheimer's disease," *Immunity & Ageing*, vol. 16, no. 1, 2019.

[54] H. Kim, S. Seo, J. Chang et al., "Stereotactic brain injection of human umbilical cord blood mesenchymal stem cells in patients with Alzheimer's disease dementia: a phase 1 clinical trial," *Alzheimer's & Dementia: Translational Research & Clinical Interventions*, vol. 1, no. 2, pp. 95–102, 2015.

[55] "The safety and the efficacy evaluation of NEUROSTEM®-AD in patients with Alzheimer's disease," 2021, https://clinicaltrials.gov/ct2/show/NCT01297218.

[56] "The long-term safety and efficacy follow-up study of subjects who completed the Phase I Clinical Trial of Neurostem®-AD," 2021, https://clinicaltrials.gov/ct2/show/NCT01696591.

[57] "Safety and exploratory efficacy study of NEUROSTEM® versus placebo in patients with Alzheimer's disease," 2021, https://clinicaltrials.gov/ct2/show/NCT02054208.

[58] "A study to evaluate the safety and efficacy of AstroStem in treatment of Alzheimer's disease," 2021, https://clinicaltrials.gov/ct2/show/NCT03117738.

[59] "A clinical trial to determine the safety and efficacy of hope biosciences autologous mesenchymal stem cell therapy (HB-adMSCs) for the treatment of Alzheimer's disease," 2021, https://clinicaltrials.gov/ct2/show/NCT04228666.

[60] "Allogeneic human mesenchymal stem cell infusion versus placebo in patients with Alzheimer's disease," 2021, https://clinicaltrials.gov/ct2/show/NCT02600130.

[61] "Follow-up study of safety and efficacy in subjects who completed NEUROSTEM® Phase-I/IIa Clinical Trial," 2021, https://clinicaltrials.gov/ct2/show/NCT03172117.

[62] "Autologous human adipose-derived mesenchymal stem cells in Alzheimer's disease," 2021, https://clinicaltrials.gov/ct2/show/NCT04855955?term=Mesenchymal+stem+cell&cond=Alzheimer+Disease&draw=3&rank=3.

[63] "Allogeneic human mesenchymal stem cells for Alzheimer's disease," 2021, https://clinicaltrials.gov/ct2/show/NCT02833792.

[64] "Alzheimer's disease stem cells multiple infusions," 2021, https://clinicaltrials.gov/ct2/show/NCT04040348.

[65] "The safety and the efficacy evaluation of allogenic adipose MSC-Exos in patients with Alzheimer's disease," 2021, https://clinicaltrials.gov/ct2/show/NCT04388982.

[66] "Evaluation of the safety and potential therapeutic effects after intravenous transplantation of CB-AC-02 in patients with Alzheimer's disease," 2021, https://clinicaltrials.gov/ct2/show/NCT02899091.

[67] "Mesenchymal stem cells for the treatment of various chronic and acute conditions," 2021, https://clinicaltrials.gov/ct2/show/NCT04684602.

[68] "Study to evaluate the safety and efficacy of AstroStem in treatment of Alzheimer's disease," 2021, https://clinicaltrials.gov/ct2/show/NCT04482413.

[69] "Safety and efficiency of umbilical cord-derived mesenchymal stem cells(UC-MSC) in patients with Alzheimer's disease (SEMAD)," 2021, https://clinicaltrials.gov/ct2/show/NCT01547689.

[70] "Safety and exploratory efficacy study of UCMSCs in patients with Alzheimer's disease (SEESUPAD)," 2021, https://clinicaltrials.gov/ct2/show/NCT02672306.

[71] S. Wang, C. Lee, and H. Lim, "Stem cell therapies for Alzheimer's disease," *Current Opinion in Psychiatry*, vol. 32, no. 2, pp. 105–116, 2019.

Hindawi
Stem Cells International
Volume 2021, Article ID 1439563, 18 pages
https://doi.org/10.1155/2021/1439563

Review Article

Evaluation of the Efficacy of Stem Cell Therapy in Ovariectomized Osteoporotic Rats Based on Micro-CT and Dual-Energy X-Ray Absorptiometry: A Systematic Review and Meta-Analysis

Zhencheng Xiong,[1,2] **Ping Yi**,[3] **Jialiang Lin**,[4] **Shengfeng Qiu**,[5] **Li Shu**,[6] **and Chi Zhang**[1,6,7]

[1]*Institute of Medical Technology, Peking University Health Science Center, Beijing 100191, China*
[2]*Peking University Third Hospital, Beijing 100191, China*
[3]*Department of Spine Surgery, China-Japan Friendship Hospital, Beijing 100029, China*
[4]*Department of Orthopedics, Peking University Third Hospital, Beijing 100191, China*
[5]*Department of Obstetrics and Gynecology, Xingguo County People's Hospital, Ganzhou, Jiangxi 342400, China*
[6]*Department of Orthopedics, Peking University International Hospital, Beijing 102206, China*
[7]*Biomedical Engineering Department, Peking University, Beijing 100191, China*

Correspondence should be addressed to Chi Zhang; chi.zhang@case.edu

Received 4 May 2021; Accepted 26 July 2021; Published 15 August 2021

Academic Editor: Sangho Roh

Objective. Osteoporosis is an abnormal bone metabolism disease characterized by microstructural degeneration of bone tissue and reduction in bone mass, resulting in increased brittleness of bone tissue and susceptibility to fracture. Due to the tissue regenerative potential of stem cell transplantation, it is now used in the treatment of various disease models such as osteoporosis. The purpose of this work is to carry out a systematic review and meta-analysis of the efficacy of stem cell therapy in ovariectomized (OVX) osteoporotic rats. *Methods*. PubMed, Cochrane Library, ScienceDirect, Embase, CNKI, and Wanfang Databases were used to search for articles that met the inclusion criteria. Two researchers independently screened the articles that met the inclusion criteria. RevMan 5.3 and STATA 16.0 were used for data analysis. This meta-analysis was registered at INPLASY with reference number ID: INPLASY202150017. *Results*. Thirteen eligible studies were selected, including 405 rats. The sources of stem cells are divided into four main categories: bone marrow mesenchymal stem cells (BMSCs), adipose-derived stem cells (ADSCs), amniotic membrane mesenchymal stem cells (AM-MSCs), and human umbilical cord blood-derived mesenchymal stem cells (hUCB-MSCs). Compared with the OVX group, both stem cell transplantation groups had higher bone mineral density (BMD) (BMSCs: SMD = 2.01, 95% CI: [1.38, 2.63], $P < 0.001$, $I^2 = 76.6\%$; ADSCs: SMD = 2.24, 95% CI: [0.79, 3.69], $P = 0.003$, $I^2 = 86.7\%$) and bone volume/total volume (BV/TV) (hUCB-MSCs: SMD = 1.71, 95% CI: [0.97, 2.44], $P < 0.001$, $I^2 = 0\%$; ADSCs: SMD = 2.16, 95% CI: [0.27, 4.04], $P = 0.025$, $I^2 = 82.6\%$). In the BMSC treatment groups, the trabecular numbers (Tb.N) (SMD = 4.28, 95% CI: [0.91, 7.64], $P = 0.013$, $I^2 = 94.9\%$) were significantly higher, whereas the results for trabecular thickness (Tb.Th) (SMD = 2.7, 95% CI: [-0.34, 5.73], $P = 0.081$, $I^2 = 95.4\%$) and trabecular spacing (Tb.Sp) (SMD = −3.08, 95% CI: [-6.55, 0.38], $P = 0.081$, $I^2 = 96.3\%$) were not statistically significant compared to those of the OVX group. The stem cell transplantation group had a low BMD, BV/TV, and Tb.N compared to the sham operation group. *Conclusion*. Stem cell therapy may increase bone strength, bone volume, and the number of trabeculae in OVX osteoporotic rats. The results of this meta-analysis showed the potential therapeutic effect of stem cell transplantation in OVX osteoporotic rats, bringing new therapeutic ideas and directions to the clinical treatment of osteoporosis. Due to the limited number and quality of studies related to some outcomes, more high-quality RCTs are still needed in the future to complement the existing findings.

1. Introduction

Osteoporosis is a metabolic bone disease characterized by low bone mass and destruction of bone tissue microarchitecture, leading to increased bone fragility and fracture risk in patients [1]. Osteoporosis is more common in the elderly, especially in postmenopausal women [2]. As the average life expectancy increases, more and more countries are entering an aging society, and the social burden caused by the increase in the incidence of osteoporosis is becoming more and more serious [3]. Deficiency of estrogen after menopause usually leads to the development of osteoporosis. The ovariectomized (OVX) rat model provides us with a suitable model to examine the mechanism of osteoporosis [4]. Because osteoporosis is usually an imbalance of bone resorption and bone formation caused by estrogen deficiency or aging, certain pharmacological agents, such as those that promote bone formation (parathyroid hormone) and those that inhibit osteoclast resorption (bisphosphonates), are widely used in the treatment of osteoporosis [4]. However, with the widespread clinical use of these drugs, adverse side effects have also been observed, such as drug-related osteonecrosis of the jaw [5]. Therefore, the search for new osteoporosis treatment strategies is of great clinical importance.

In recent years, tissue engineering technology has been rapidly developed in the fields of bone and cartilage tissue construction, tendon ligaments, blood vessels, nerves, skin, and oral tissues [6]. Stem cells, an important component of tissue engineering technology, have received a lot of attention due to their potential capabilities [7]. Stem cells, a class of undifferentiated or partially differentiated cells with unlimited self-proliferative and multidirectional differentiation capabilities, have been shown to be closely associated with the progression of osteoporosis [7]. Stem cell transplantation is proposed as a potential treatment strategy for patients with osteoporosis [8]. Some experimental studies have been conducted in animal models of osteoporosis to evaluate the therapeutic effect of stem cell transplantation [8–21]. Stem cells used in animal models of osteoporosis include bone marrow mesenchymal stem cells (BMSCs) [21], adipose-derived stem cells (ADSCs) [16], amniotic membrane mesenchymal stem cells (AM-MSCs) [12], and human umbilical cord blood-derived mesenchymal stem cells (hUCB-MSCs) [20]. Among them, BMSCs are able to differentiate into multiple cell types, including osteoblasts, chondrocytes, and adipocytes, under appropriate culture conditions and are the most commonly used MSC for osteoporosis due to their easy accessibility and strong osteogenic differentiation [4, 19]. Some of the current experimental studies evaluated the potential therapeutic effects of stem cell transplantation in OVX osteoporotic rats by using micro-CT and dual-energy X-ray absorptiometry [9–21]. In order to investigate the potential efficacy of stem cell transplantation in OVX osteoporotic rats and thus provide some support for the possibility of stem cell transplantation in the treatment of osteoporosis, we constructed this meta-analysis by pooling the relevant studies mentioned above.

2. Materials and Methods

2.1. Search Method. After identifying the topics for this meta-analysis, in order to obtain all relevant studies, two researchers from our research team each independently searched multiple databases according to the Cochrane Collaboration guidelines, including PubMed (1966 to April 1, 2021), Cochrane Library (1966 to April 1, 2021), ScienceDirect (1980 to April 1, 2021), Embase (1980 to April 1, 2021), CNKI (1980 to April 1, 2021), and Wanfang Databases (1980 to April 1, 2021). Literature search is achieved by concatenating MeSH terms and corresponding keywords using Boolean operators (AND or OR), including "stem cell," "mesenchymal stem cell or MSC," "bone marrow-derived mesenchymal stem cell or BMSC," "adipose-derived stem cell or ADSC," "osteoporosis," "ovariectomized or OVX," and "rat." Two researchers independently screened all the retrieved articles, first one by one, based on title and abstract, and then later on for full-text detailed reading. Finally, additional screening of relevant studies is performed based on the references of the identified included studies. The two lists of literature obtained above will be discussed in our team to integrate and resolve differences. The Preferred Reporting Items for Systematic Reviews and Meta-Analyses (PRISMA) statement is an indispensable reference for the current meta-analysis [22].

2.2. Study Screening. All retrieved articles were screened by our research team according to the inclusion and exclusion criteria developed by the subject of this meta-analysis. Inclusion criteria included the following: (1) all studies involved comparing the effects of stem cell therapy to OVX control group or sham-operated group, (2) all included studies could be of either randomized controlled trial (RCT) or non-RCT, (3) the animal model was rat and osteoporosis model establishment was achieved by ovariectomy, (4) the source of stem cells was not limited, (5) the data of outcome measurements were obtained by micro-CT or dual-energy X-ray absorptiometry, and (6) the data related to the outcome measurements could be successfully extracted.

Exclusion criteria included the following: (1) the study lacked a control group that met the inclusion criteria; (2) the animal model was a mouse, rabbit, or other experimental animals; (3) the osteoporosis model was not established by ovariectomy; (4) the data related to outcome measurements could not be extracted; (5) the study type was a review, conference abstract, commentary, case report, or letter; and (6) all studies that did not meet the inclusion criteria.

2.3. Required Data Extraction. The extraction of the required data was done independently by two researchers, and then, another researcher aggregated the data and resolved the divergent data after discussion within the research team. The main data extracted for this meta-analysis were the results of micro-CT and dual-energy X-ray absorptiometry, where bone mineral density (BMD) was the primary outcome measurement, and bone volume/total volume (BV/TV), trabecular number (Tb.N), trabecular thickness (Tb.Th), and trabecular spacing (Tb.Sp) were the secondary

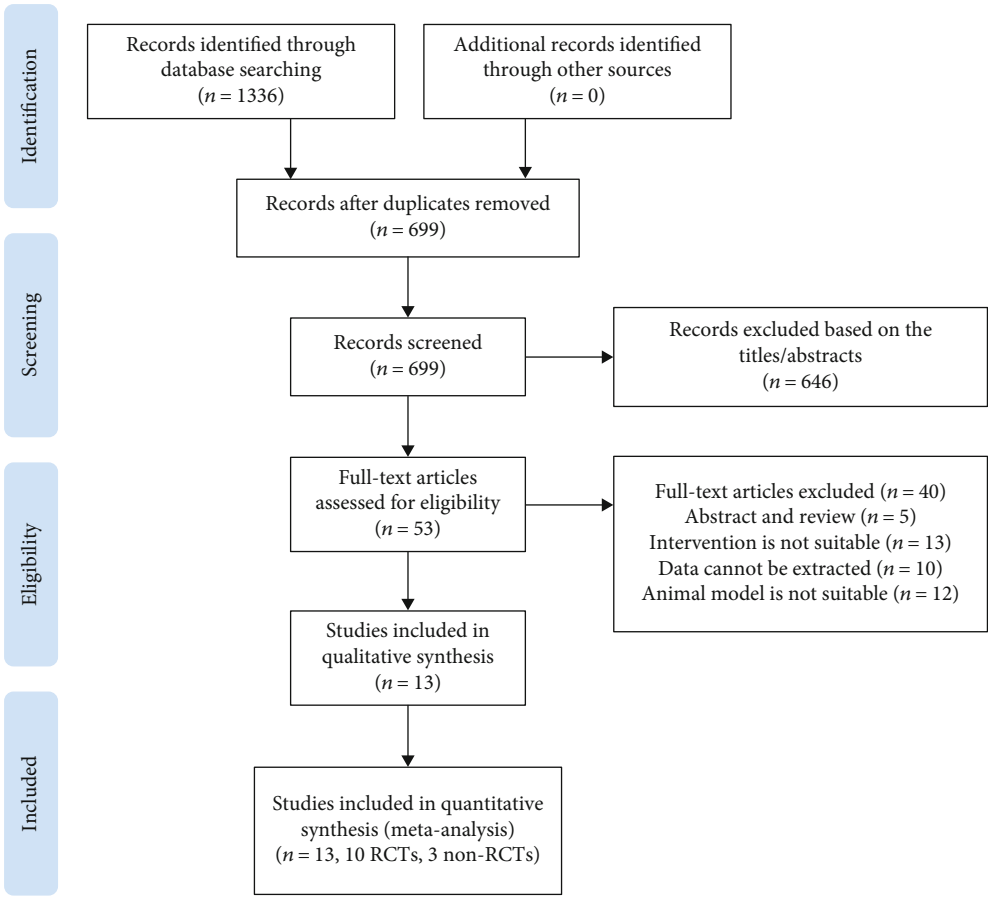

Figure 1: Flow chart of literature search and screening for meta-analysis.

outcome measurement. We also extracted the following data: first author, year of publication, country/region, study type, number of rats (experimental group : control group), rat type, rat month age, sex, surgical method, and intervention (experimental group : control group).

2.4. Quality Assessment of Included Studies. The quality of RCTs in meta-analyses was usually assessed according to the Cochrane Handbook for Systematic Reviews [23]. Two researchers independently used RevMan software to create a "risk of bias" table with seven main elements to assess the quality of each included RCT. Each element could be judged as one of high risk of bias, low risk of bias, or unclear risk of bias based on the actual content of the study.

The Newcastle-Ottawa Scale (NOS) containing three main items (selection, comparability, and outcome) can be used to assess the quality of the included non-RCTs [24]. This scale is also subdivided into eight detailed quality items (selection: 4 quality items; comparability: 1 quality item; outcome: 3 quality items). In "selection" and "outcome," each item can be awarded up to one star; in "comparability", a maximum of two stars can be given to a unique item. The more stars a study receives, the higher the quality assessment. Low quality (0-3), medium quality (4-6), and high quality (7-9) studies each have a range of scores.

2.5. Statistical Analysis. Outcome measurements were analyzed in subgroups according to stem cell source or bone trabecula assessment methods. Because the included outcome measurements were continuous data, as well as unit differences, we used standard mean difference (SMD) and 95% confidence interval (CI) for the analysis. Heterogeneity of the included studies was assessed by I^2, which was considered as low, moderate, and high heterogeneity when the value of I^2 was 25%, 50%, and 75%, respectively [25]. The choice of the random effect model and fixed effect model is determined by I^2, and the former is executed when $I^2 > 50\%$ and $P < 0.1$. Otherwise, the latter is executed. Statistical analysis of all data was performed by using STATA software version 16.0 and RevMan 5.3 for Windows. In this meta-analysis, the results were considered statistically significant when $P < 0.05$.

3. Results

3.1. Search Results from Literature. Based on the search strategy and inclusion and exclusion criteria, a total of 1,336 potentially relevant articles were generated, including from PubMed ($n = 494$), Cochrane Library ($n = 17$), ScienceDirect ($n = 468$), Embase ($n = 88$), CNKI ($n = 207$), and Wanfang Databases ($n = 62$). After two researchers carefully screened the titles and abstracts independently, and briefly reviewed

Table 1: Characteristics of all studies included in the meta-analysis.

Study	Country	Study type	Animal models	Age and weight	No. of rats	Osteoporosis model	Experimental group	Injection dose	Control group	Detection time*	Detection sites	Outcome measures
Uejima et al. (2008)	Japan	Non-RCT	SD, female, rats	12 w	10/10	OVX	BMSCs	1×10^5 1×10^5 2×10^5	Sham-operation +saline	8 w 24 w 24 w	Femur	(1)
Yang et al. (2013)	China	RCT	SD, female, rats	230 ± 10 g	10/10/10	OVX	BMSCs	3×10^6	OVX control, sham-operation	12 w	Femur, lumbar vertebrae	(1)
Shuai et al. (2014)	China	RCT	SD, female, rats	140-150 g	4/4/4	OVX	BMSCs	1.5×10^7 0.375×10^7	OVX control, sham-operation+PBS	10 w 10 w	Femur	(1), (3)
Lei et al. (2016)	China	RCT	Wistar, female, rats	210-255 g	15/15/45	OVX	AM-MSCs +zoledronic acid	NP	OVX control, sham-operation	13 w	Femur	(1)
Li et al. (2016)	China	RCT	SD, female, rats	7 w, 180-220 g	10/10/10	OVX	ADSCs	2×10^6	OVX control, sham-operation+PBS	6 w	Femur	(1), (2)
Chen et al. (2017)	China	RCT	SD, female, rats	7 w, 180-220 g	10/10/10	OVX	BMSCs	3.5×10^9	OVX control, sham-operation+PBS	2 w	Femur, lumbar vertebrae	(1), (2), (3)
Duan et al. (2017)	China	RCT	SD, female, rats	10 w, 110 ± 8.73 g	18/10	OVX	BMSCs	2×10^5	OVX control, sham-operation	8 w	Tibia	(2), (3)
Hong et al. (2018)	South Korea	RCT	SD, female, rats	12 w	10/10/10	OVX	hUCB-MSCs	1×10^7 1×10^7	OVX control, sham-operation	4 w 8 w	Femur	(3)
Tang et al. (2018)	China	RCT	SD, female, rats	3 m, 250 ± 20 g	10/10/10	OVX	ADSCs+icariin	NP	OVX control, sham-operation	12 w	Femur, lumbar vertebrae	(1)
Uri et al. (2018)	Israel	RCT	SD, female, rats	5 m, 260 – 320 g	15/15	OVX	ADSCs	NP	OVX control	NP	Femur	(3)
Xue et al. (2019)	China	RCT	SD, female, rats	205 ± 11 g	30/10/10	OVX	BMSCs	2×10^6 4×10^6 6×10^6	OVX control, sham-operation	4 w, 8 w 4 w, 8 w 4 w, 8 w	Tibia	(1)
Sadat-Ali et al. (2019)	Saudi Arabia	Non-RCT	SD, female, rats	NP	10/10	OVX	BMSCs	2×10^6	OVX control+saline	8 w	Femur	(2), (3)
Aglan et al. (2020)	Egypt	Non-RCT	Wistar, female, rats	130-150 g	30/10/10	OVX	BMSCs+nano-HA BMSCs+Pt-NPs BMSCs+Pt-HA-nanocomposite	3×10^6	OVX control, sham-operation	2 m	Femur	(1)

RCT: randomized controlled trial; SD: Sprague Dawley; OVX: ovariectomized; BMSCs: bone marrow mesenchymal stem cells; ADSCs: adipose-derived stem cells; AM-MSCs: amniotic membrane mesenchymal stem cells; hUCB-MSCs: human umbilical cord blood-derived mesenchymal stem cells; PBS: phosphate-buffered saline; NP: not provided. Outcome measures: (1): BMD; (2): BV/TV; (3): Tb.N, Tb.Th, and Tb.Sp. * Detection time: from after stem cell injection.

the full text, a total of 646 articles were excluded. Then, according to the inclusion and exclusion criteria, a detailed evaluation was carried out for the full text of the remaining 53 articles. Finally, the meta-analysis included 10 RCTs and 3 non-RCTs (Figure 1) [9–21].

3.2. Characteristics of the Included Studies. A total of 10 RCTs and 3 non-RCTs involving 405 rats were included in this meta-analysis, all published from 2008 to 2020 [9–21]. All included studies explored the efficacy of stem cell transplantation in OVX osteoporotic rats. There are 4 sources of stem cells in the included studies, of which 8 studies are BMSCs [9, 10, 13, 14, 17–19, 21], 3 studies are ADSCs [11, 15, 16], one study is AM-MSCs [12], and the remaining 1 study is hUCB-MSCs [20]. Female rats were used in all 13 included studies, 11 of which were Sprague Dawley (SD) rats [9–11, 13–18, 20, 21] and 2 of which were Wistar rats [12, 19]. The establishment of osteoporosis models was all achieved by ovariectomy. Of the 13 studies, 10 included an OVX blank control group and a sham-operated group [9–15, 18–20], 2 studies included only an OVX control group [16, 17], and one study remained that included only a sham-operated group [21]. In the OVX blank control group, only ovariectomy was performed, and no stem cell transplantation was performed; in the sham-operated group, no ovariectomy or stem cell transplantation was performed, and only the skin was cut and sutured. The method of stem cell transplantation also varies, with most studies involving the injection of stem cells via the tail vein and others involving direct injection into the femur or tibia. The site of tissue sampling varied, with eight studies sampling only the femur [10–12, 16, 17, 19–21], two studies sampling only the tibia [13, 18], and three studies sampling the femur and the lumbar vertebrae [9, 14, 15]. One study was a combination of AM-MSCs and zoledronic acid [12], another study was a combination of ADSCs and icariin [15], and finally, another study was BMSCs cocultured with nano-HA, Pt-NPs, or Pt-HA-nanocomposite [19]. The 13 included studies were also not entirely consistent in the injection doses of stem cells and the timing of specimens taken after injection. Table 1 lists the characteristics of all included studies.

3.3. Assessment of the Risk of Bias in the Included Studies. The risk of bias assessment for the 10 included RCTs is displayed in Figure 2. The included studies were all animal studies, none of the 10 studies explicitly mentioned blinding and allocation concealment, but all stated random assignment [9–16, 18, 20]. No selective reporting or incomplete outcome data were found. Other biases could not be accurately determined.

The risk of bias assessment for these 3 non-RCTs is displayed in Table 2. Item-by-item scoring of the 3 studies according to the NOS showed that 2 studies [17, 21] received a score of 6 and the remaining one [19] a score of 7, indicating that the quality of the included studies was acceptable.

3.4. Results of the Meta-Analysis

3.4.1. BMD. Among the 13 included studies, there are a total of 9 studies with BMD as the primary outcome measurement

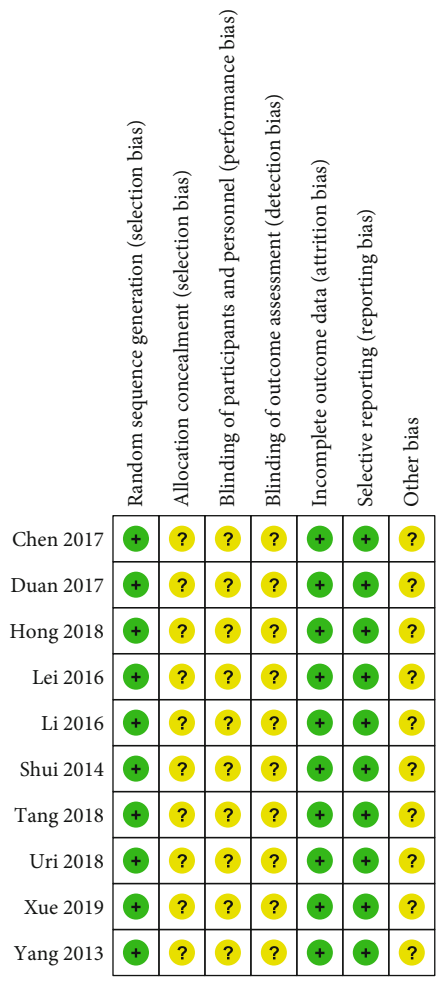

Figure 2: Risk of bias summary. +: low risk of bias; −: high risk of bias; ?: bias unclear.

[9–12, 14, 15, 18, 19, 21]. According to the difference of the control group, we conducted a comparative analysis of the stem cell treatment group and the OVX control group, as well as the stem cell treatment group and the sham operation group. The forest plot in Figure 3 shows the effect of the stem cell treatment group on BMD compared to the OVX control group, with a total of eight studies included [9–12, 14, 15, 18, 19]. BMD was divided into 3 subgroups based on different stem cell sources. A total of five studies (128 rats) provided BMD data after BMSC transplantation [9, 10, 14, 18, 19], two studies (40 rats) provided BMD data after ADSC transplantation [11, 15], and one study (30 rats) provided BMD data after AM-MSC transplantation [12]. In view of the significant heterogeneity ($I^2 > 50\%$, $P < 0.1$), we used a random effect model. There was a statistically significant difference on BMD between the BMSC transplantation group and the OVX control group based on the results of the pooled analysis (SMD = 2.01, 95% CI: [1.38, 2.63], $P < 0.001$, $I^2 = 76.6\%$), and there was a statistically significant difference between the ADSC transplantation and the OVX control group (SMD = 2.24, 95% CI: [0.79, 3.69], $P = 0.003$, $I^2 = 86.7\%$). There is only one study on AM-MSC transplantation, and the results

Table 2: The Newcastle-Ottawa Scale (NOS) for assessing the quality of non-RCTs.

Study	Selection	Comparability	Outcomes	Total scores (maximum 9)
Uejima et al. [21]	3	1	2	6
Sadat-Ali et al. [17]	3	1	2	6
Aglan et al. [19]	3	2	2	7

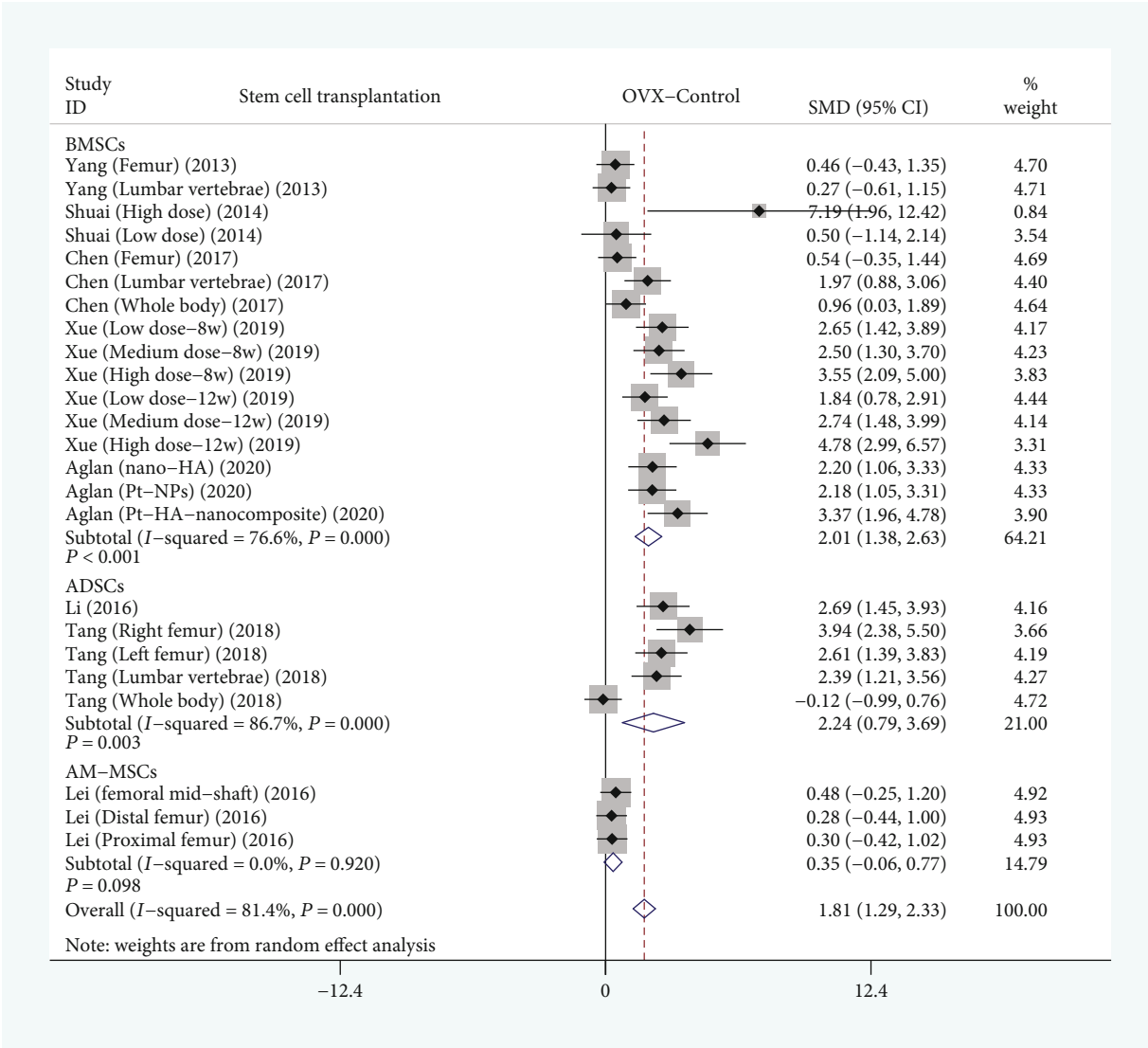

Figure 3: Forest plot showing the effect of stem cell treatment group compared with OVX control group on BMD. OVX: ovariectomized; BMD: bone mineral density; BMSCs: bone marrow mesenchymal stem cells; ADSCs: adipose-derived stem cells; AM-MSCs: amniotic membrane mesenchymal stem cells; SMD: standard mean difference.

showed no statistically significant differences (SMD = 0.35, 95% CI: [-0.06, 0.77], $P = 0.098$, $I^2 = 0\%$).

The forest plot in Figure 4 shows the effect of the stem cell treatment group on BMD compared to the sham operation group, with a total of nine studies included [9–12, 14, 15, 18, 19, 21]. BMD was divided into 3 subgroups based on different stem cell sources. A total of six studies (148 rats) provided BMD data after BMSC transplantation [9, 10, 14, 18, 19, 21], two studies (40 rats) provided BMD data after ADSC transplantation [11, 15], and one study (30 rats) provided BMD data after AM-MSC transplantation [12]. In view of the significant heterogeneity ($I^2 > 50\%$, $P < 0.1$), we used a random effect model. There was a statistically significant difference on BMD between the BMSC transplantation group and the sham operation group based on the results of the pooled analysis (SMD = −1.78, 95% CI: [-2.72, -0.85], $P < 0.001$, $I^2 = 89.7\%$), and there was a statistically significant difference between the ADSC transplantation and the sham operation group (SMD = −0.65, 95% CI: [-1.24, -0.05], $P = 0.032$, $I^2 = 51.9\%$), and there was a statistically significant

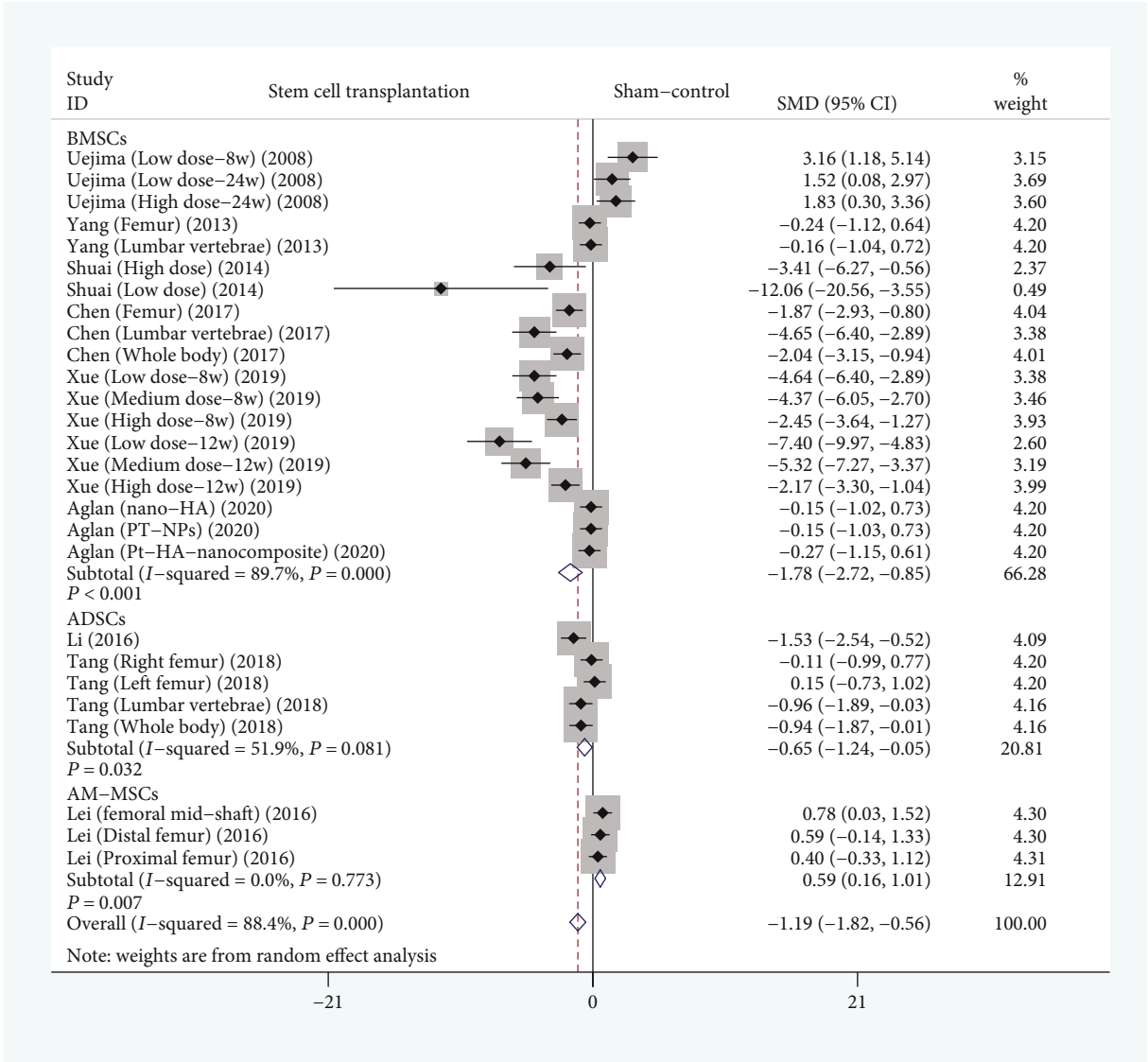

Figure 4: Forest plot showing the effect of stem cell treatment group compared with sham operation group on BMD. BMD: bone mineral density; BMSCs: bone marrow mesenchymal stem cells; ADSCs: adipose-derived stem cells; AM-MSCs: amniotic membrane mesenchymal stem cells.

difference between the AM-MSC transplantation and the sham operation group (SMD = 0.59, 95% CI: [0.16, 1.01], $P = 0.007$, $I^2 = 0\%$).

3.4.2. BV/TV. Among the 13 included studies, there are a total of 6 studies with BV/TV as the secondary outcome measurement [11, 13, 14, 16, 17, 20]. The forest plot in Figure 5 shows the effect of the stem cell treatment group on BV/TV compared to the OVX control group, with a total of six studies included. BV/TV was divided into 3 subgroups based on different stem cell sources. A total of three studies (58 rats) provided BV/TV data after BMSC transplantation [13, 14, 17], two studies (50 rats) provided BV/TV data after ADSC transplantation [11, 16], and one study (20 patients) provided BV/TV data after hUCB-MSC transplantation [20]. In view of the significant heterogeneity ($I^2 > 50\%$, $P < 0.1$), we used a random effect model. There was a statistically significant difference on BV/TV between the ADSC transplantation group and the OVX control group based on the results of the pooled analysis (SMD = 2.16, 95% CI: [0.27, 4.04], $P = 0.025$, $I^2 = 82.6\%$), and there was a statistically significant difference between the hUCB-MSC transplantation and the OVX control group (SMD = 1.71, 95% CI: [0.97, 2.44], $P < 0.001$, $I^2 = 0\%$). However, there were no statistically significant differences between the BMSC transplantation group and the OVX control group (SMD = 4.22, 95% CI: [-0.78, 9.23], $P = 0.098$, $I^2 = 97\%$).

The forest plot in Figure 6 shows the effect of the stem cell treatment group on BV/TV compared to the sham operation group, with a total of four studies included [11, 13, 14, 20]. BV/TV was divided into 3 subgroups based on different stem cell sources. A total of two studies (48 rats) provided BV/TV data after BMSC transplantation [13, 14], one study (20 rats) provided BV/TV data after ADSC transplantation [11], and

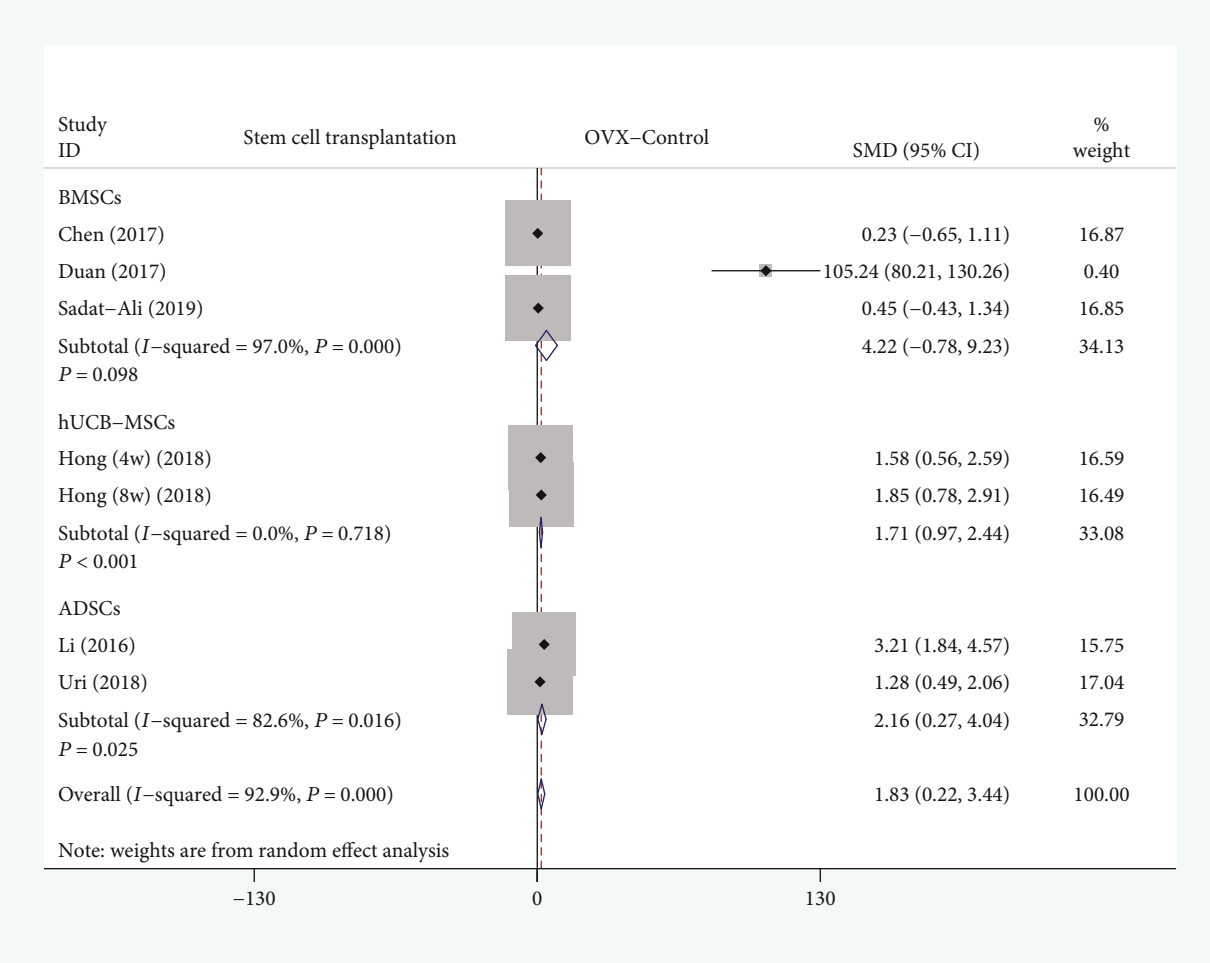

Figure 5: Forest plot showing the effect of stem cell treatment group compared with OVX control group on BV/TV. BV/TV: bone volume/total volume; BMSCs: bone marrow mesenchymal stem cells; hUCB-MSCs: human umbilical cord blood-derived mesenchymal stem cells; ADSCs: adipose-derived stem cells.

one study (20 patients) provided BV/TV data after hUCB-MSC transplantation [20]. In view of the significant heterogeneity ($I^2 > 50\%$, $P < 0.1$), we used a random effect model. There was a statistically significant difference between the hUCB-MSC transplantation and the sham operation group (SMD = −0.69, 95% CI: [-1.33, -0.05], $P = 0.035$, $I^2 = 0\%$). However, there were no statistically significant differences between the BMSC transplantation group and the sham operation group (SMD = −8.47, 95% CI: [-24.94, 8.01], $P = 0.314$, $I^2 = 97.9\%$). Because there is only one set of data that provides data on BV/TV between the ADSC transplantation group and the sham operation group, no conclusion can be drawn.

3.4.3. Tb.N, Tb.Th, and Tb.Sp. Among the 13 included studies, there are a total of 4 studies with Tb.N, Tb.Th, and Tb.Sp as the secondary outcome measurement [10, 13, 14, 17]. The forest plot in Figure 7 shows the effect of the BMSC transplantation group on Tb.N, Tb.Th, and Tb.Sp compared to the OVX control group, with a total of four studies included. A total of four studies (67 rats) provided Tb.N data [10, 13, 14, 17], and three studies (58 rats) provided Tb.Th and Tb.Sp data [13, 14, 17]. In view of the significant heterogeneity ($I^2 > 50\%$, $P < 0.1$), we used a random effect model. There was a statistically significant difference on Tb.N between the BMSC transplantation group and the OVX control group based on the results of the pooled analysis (SMD = 4.28, 95% CI: [0.91, 7.64], $P = 0.013$, $I^2 = 94.9\%$). However, there were no statistically significant differences on Tb.Th and Tb.Sp between the BMSC transplantation group and the OVX control group (Tb.Th: SMD = 2.7, 95% CI: [-0.34, 5.73], $P = 0.081$, $I^2 = 95.4\%$; Tb.Sp: SMD = −3.08, 95% CI: [-6.55, 0.38], $P = 0.081$, $I^2 = 96.3\%$).

The forest plot in Figure 8 shows the effect of the BMSC transplantation group on Tb.N, Tb.Th, and Tb.Sp compared to the sham operation group, with a total of three studies included [10, 13, 14]. A total of three studies (57 rats) provided Tb.N data [10, 13, 14], and two studies (48 rats) provided Tb.Th and Tb.Sp data [13, 14]. In view of the significant heterogeneity ($I^2 > 50\%$, $P < 0.1$), we used a random effect model. There was a statistically significant difference on Tb.N between the BMSC transplantation group and the sham operation group based on the results of the pooled analysis (SMD = −6.84, 95% CI: [-12.37, -1.32], $P =$

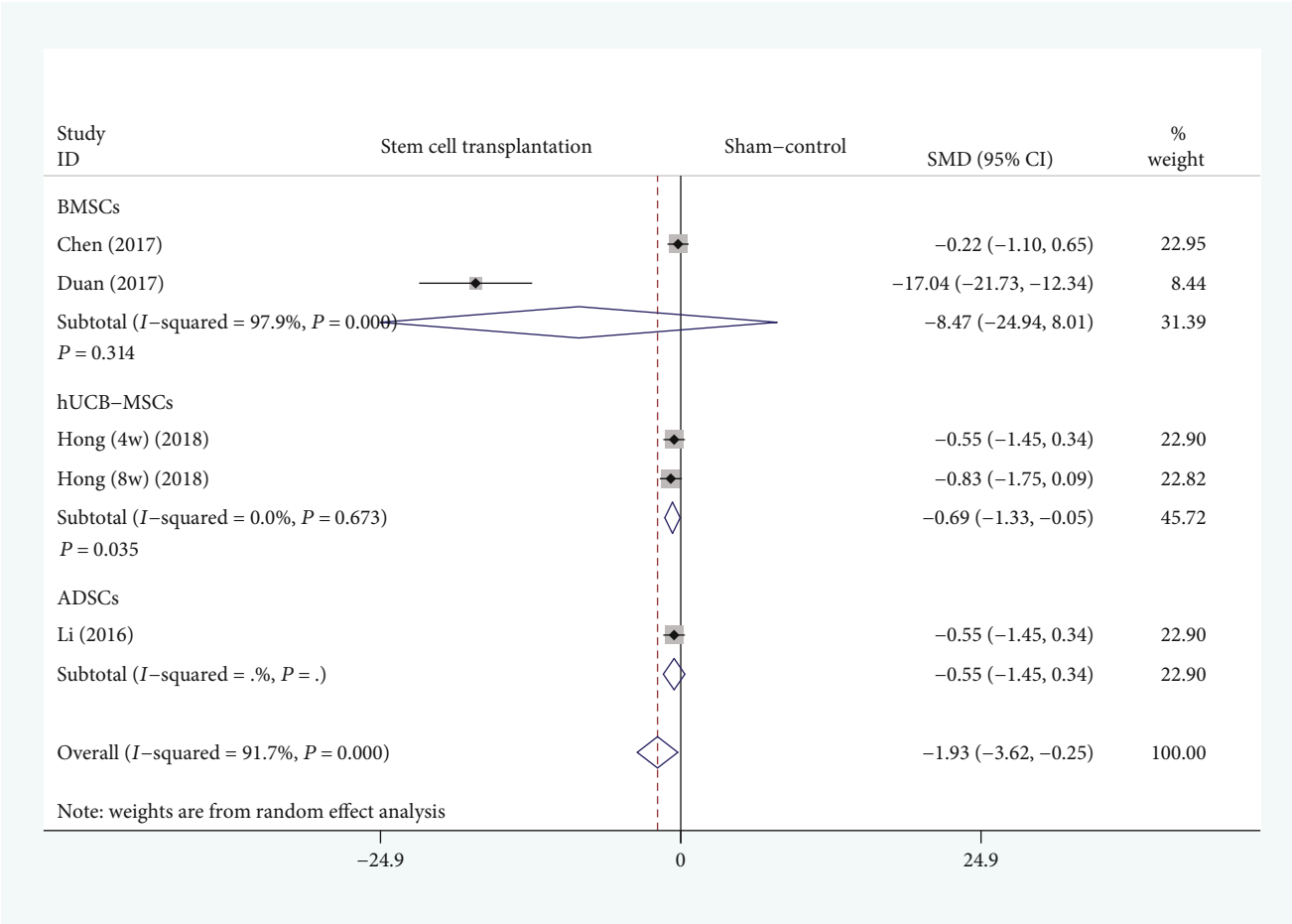

Figure 6: Forest plot showing the effect of stem cell treatment group compared with sham operation group on BV/TV. BV/TV: bone volume/total volume; BMSCs: bone marrow mesenchymal stem cells; hUCB-MSCs: human umbilical cord blood-derived mesenchymal stem cells; ADSCs: adipose-derived stem cells.

0.015, $I^2 = 93.5\%$). However, there were no statistically significant differences on Tb.Th and Tb.Sp between the BMSC transplantation group and the sham operation group (Tb.Th: SMD = −2.95, 95% CI: [-8.1, 2.2], $P = 0.261$, $I^2 = 96.5\%$; Tb.Sp: SMD = 5.59, 95% CI: [-5.22, 16.41], $P = 0.311$, $I^2 = 97.7\%$).

3.5. Publication Bias. Publication bias is now commonly assessed in meta-analysis using Begg's funnel plot and Egger's test and is usually performed in at least 10 studies [24]. Because of the high heterogeneity in the results of the above pooled analysis, we performed an assessment of publication bias. Since $P < 0.05$ for Begg's test and Egger's test results, this suggests a possible publication bias for the included studies of BMD (stem cell treatment group vs. OVX control group: Begg's test: $P < 0.001$, Egger's test: $P < 0.001$; stem cell treatment group vs. sham operation group: Begg's test: $P < 0.001$, Egger's test: $P = 0.001$) and BV/TV (stem cell treatment group vs. OVX control group: Begg's test: $P = 0.016$, Egger's test: $P = 0.001$; stem cell treatment group vs. sham operation group: Begg's test: $P = 0.027$, Egger's test: $P < 0.001$). There was no publication bias in the studies included in the Tb.N, Tb.Th, and Tb.Sp because $P > 0.05$ for the results of Begg's test and Egger's test (BMSC transplantation group vs. OVX control group: Begg's test: $P = 0.213$, Egger's test: $P = 0.289$; BMSC transplantation group vs. sham operation group: Begg's test: $P = 0.174$, Egger's test: $P = 0.44$). We discussed the following reasons for the above conclusions: BMD and BV/TV are subgroup analyses based on different stem cell types, and the conditions of interventions are significantly different. Each stem cell type was explored with different characteristics, so the results of BMD and BV/TV showed a possible publication bias. In contrast, the analyses of Tb.N, Tb.Th, and Tb.Sp all belonged to one stem cell type, BMSCs, but were evaluated in different ways, so no publication bias was found. Figure 9 shows the results of Begg's test and Egger's test assessing the publication bias of related studies that include Tb.N, Tb.Th, and Tb.Sp.

3.6. Sensitivity Analysis. Sensitivity analysis is also usually performed in a meta-analysis to assess the stability of the results of the pooled literature analysis [24]. We used a sensitivity analysis by removing all the included literature for all outcome measurements one by one and also used STATA software to plot the sensitivity analysis figures (Figure 10). Sensitivity analysis could not be effectively performed due

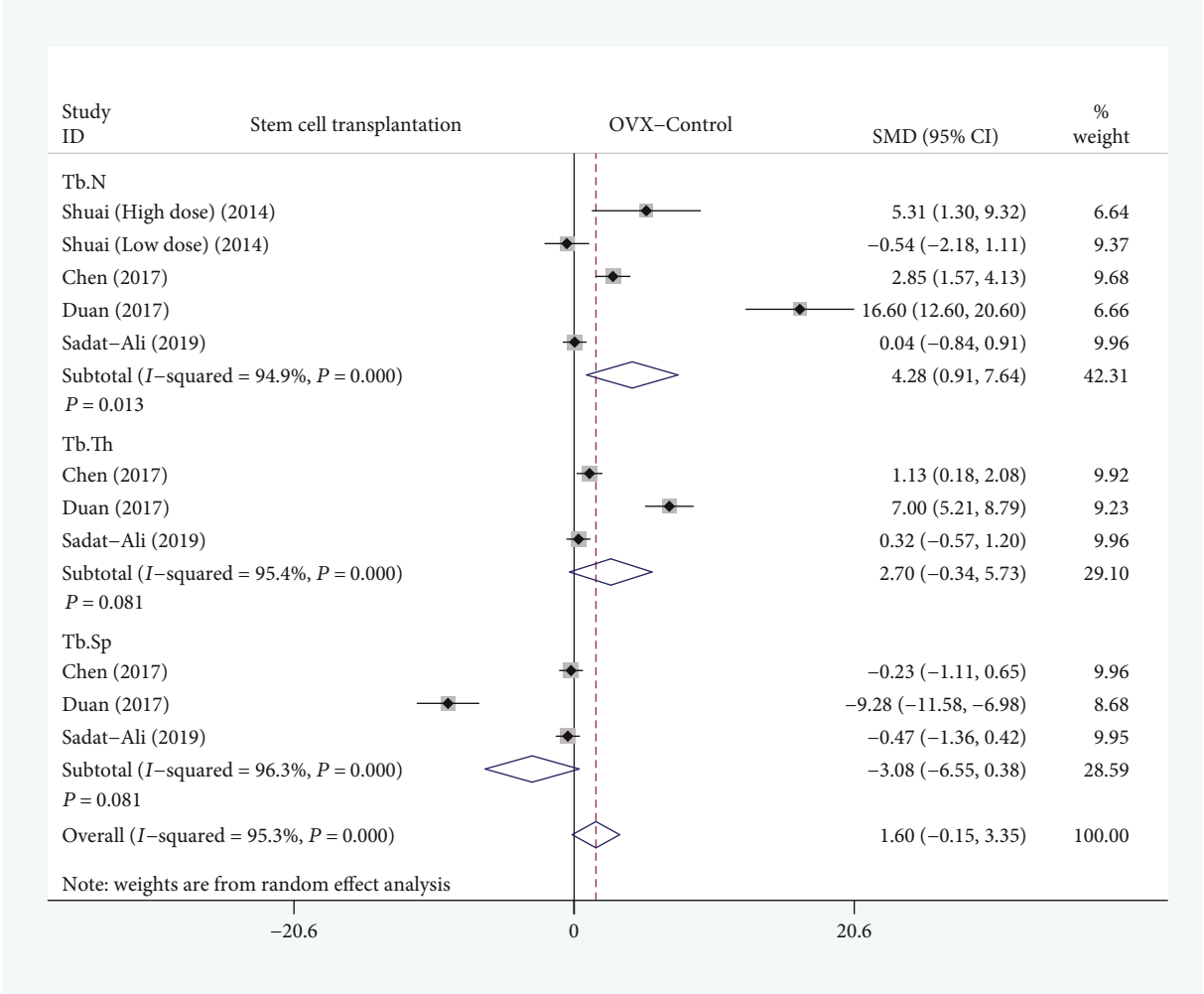

Figure 7: Forest plot showing the effect of the BMSC transplantation group compared with the OVX control group on Tb.N, Tb.Th, and Tb.Sp. Tb.N: trabecular number; Tb.Th: trabecular thickness; Tb.Sp: trabecular spacing.

to the limited number of relevant literature or less than 2 articles for some of the outcome indicators. We analyzed the outcome measurements for which the number of literature was sufficient, and no significant changes were found in their results, thus confirming the robustness and reliability of the results. Sources of the high heterogeneity in outcome measurements that emerged in this meta-analysis may be as follows: (1) different dosing regimens and timing of interventions in the included studies in each stem cell type, (2) limited number of studies included for the outcome measurements, (3) sample sizes and timing of collection of the outcome measurements were not identical in the included studies, and (4) inherent differences between studies.

4. Discussion

This meta-analysis explored the efficacy of stem cells in the treatment of osteoporosis. Osteoporosis is defined as a systemic bone disease characterized by decreased bone mass and deterioration of bone microstructure, resulting in increased bone fragility and prone to fractures [7]. As a type of cell with unlimited proliferation and differentiation potential, stem cells have been used in the treatment and prevention of a variety of complex diseases [17]. Currently, stem cell transplantation is mostly used in animal models of osteoporosis, including rats, mice, rabbits, experimental monkeys, and pigs. The establishment of animal models of osteoporosis is mostly achieved by ovariectomy. The commonly used stem cells include BMSCs, ADSCs, AM-MSCs, and hUCB-MSCs [9–21]. Uejima et al. [21] demonstrated that direct BMSC injection may improve bone strength. Uri et al. [16] found that the implantation of autologous ADSCs into the proximal femur of OVX osteoporotic rats could promote bone regeneration and enhance bone strength during short-term follow-up. Lei et al. [12] demonstrated that the synergistic application of AM-MSCs and zoledronic acid could improve the symptoms of OVX osteoporosis rats. Hong et al. [20] found that hUCB-MSCs could enhance bone regeneration in a rat model of osteoporosis. Elseweidy et al. [26] demonstrated that the combination of MSC and the antioxidant resveratrol was more effective in increasing bone mass and improving osteoporosis than treatment alone. Some studies had shown that the combination of platelet-rich fibrin releasates (PRFr) and BMSCs [27] or ADSCs

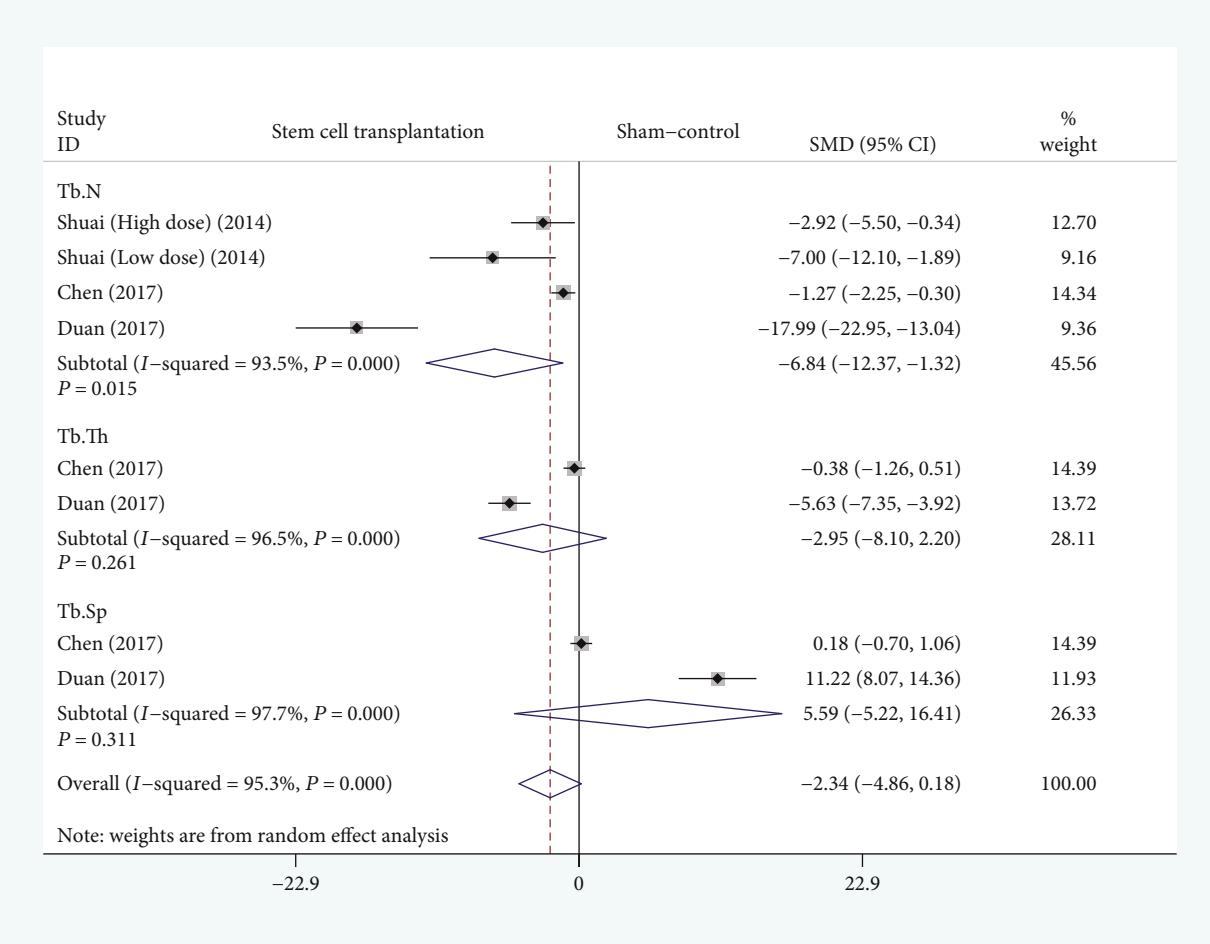

Figure 8: Forest plot showing the effect of the BMSC transplantation group compared with the sham operation group on Tb.N, Tb.Th, and Tb.Sp. Tb.N: trabecular number; Tb.Th: trabecular thickness; Tb.Sp: trabecular spacing.

[28] could reduce bone loss in OVX osteoporotic mice. Based on the above findings, we can find that stem cell transplantation holds promise as a potential treatment for osteoporosis.

Thirteen articles that met the inclusion criteria were included in this meta-analysis, seven of which were written in English [13, 15–17, 19–21] and the remaining six were written in Chinese [9–12, 14, 18]. The 13 studies included four different sources of stem cells, and the osteoporosis models were all constructed by ovariectomy [9–21]. The control group included two types, one for the osteoporosis model constructed successfully but without stem cell transplantation (OVX control) and the other for the osteoporosis model not constructed but with skin incision (sham operation). Outcome measurement obtained based on micro-CT and dual-energy X-ray absorptiometry included BMD, BV/TV, Tb.N, Tb.Th, and Tb.Sp [9–21]. BMD, an important indicator of bone strength; BV/TV, a histomorphometric parameter used to measure bone strength; and Tb.Th, Tb.Sp, and Tb.N, standard parameters used to investigate structural changes in bone trabeculae, are common analytical indicators to evaluate the effectiveness of osteoporosis treatment [29]. Therefore, because of the differences in the control groups, a pooled analysis was performed for both scenarios for these outcome measurements.

For BMD, the primary outcome measurement, BMD, was higher in the BMSC and ADSC transplantation groups when compared to the OVX control group, with no significant difference in the AM-MSC transplantation group; BMD was lower in the BMSC, ADSC, and AM-MSC transplantation groups when compared to the sham-operated group. The higher the BMD, the higher the strength of the bone [6]. Therefore, based on the results after this pooled analysis, we hypothesized that stem cell transplantation could increase bone strength in OVX osteoporotic rats, and the increased strength was lower than that in normal rats (sham-operated group). For BV/TV, a secondary outcome measurement, BV/TV, was higher in the hUCB-MSC and ADSC transplant groups when compared with OVX controls; when compared with the sham-operated group, BV/TV was lower in the hUCB-MSC transplant group and not significantly different in the BMSC transplant group, and ADSC could not be compared due to the limited number of studies. A higher BV/TV represents a relatively higher bone volume in the tissue [6]. Therefore, based on the results after this pooled analysis, we hypothesized that stem cell transplantation might increase bone volume in OVX osteoporotic rats, and the increased bone volume was lower than that in normal rats (sham-operated group). For Tb.N, Tb.Th, and

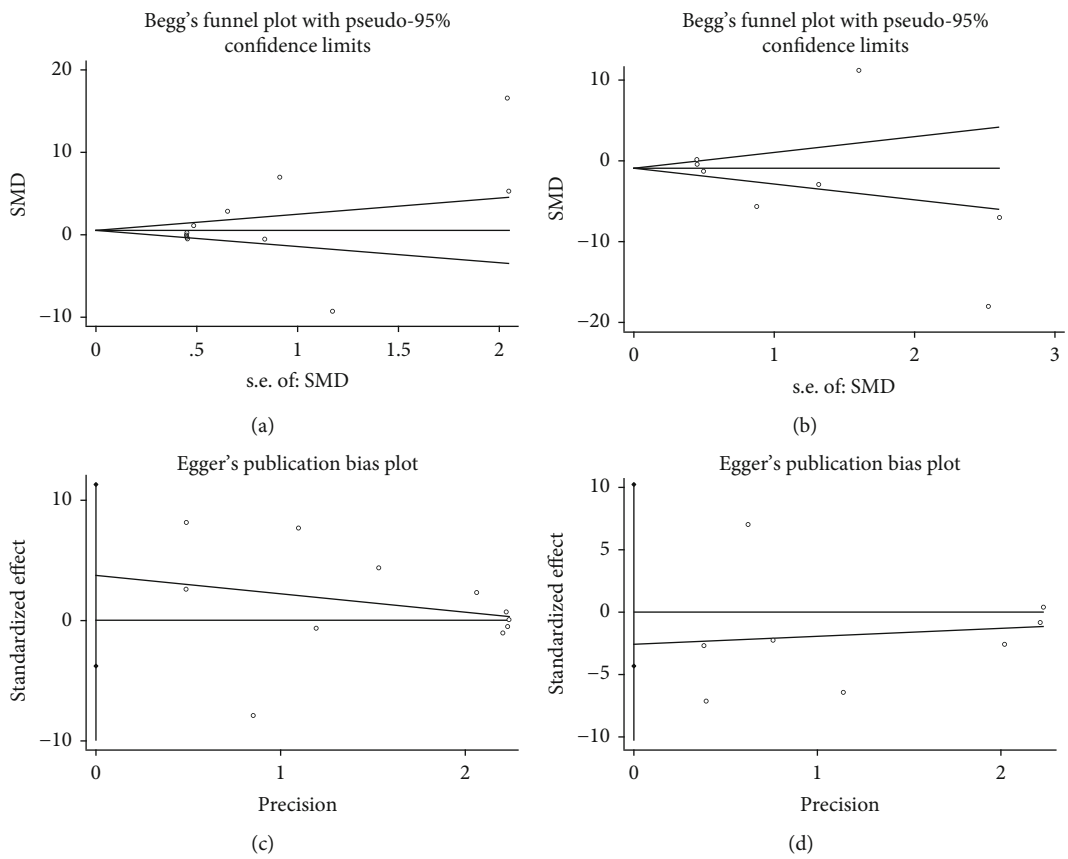

Figure 9: Assessment of publication bias in relevant studies that include Tb.N, Tb.Th, and Tb.Sp. Begg's test: (a) BMSCs vs. OVX control and (b) BMSCs vs. sham control; Egger's test: (c) BMSCs vs. OVX control and (d) BMSCs vs. sham control.

Tb.Sp, a secondary outcome measurement, Tb.N, was higher in the BMSC transplantation group when compared with the OVX control group, while Tb.Th and Tb.Sp were not significantly different; Tb.N was lower in the BMSC transplantation group when compared with the sham-operated group, while Tb.Th and Tb.Sp were not significantly different. A higher Tb.N represents a relatively higher number of bone trabeculae in the tissue [6]. Therefore, based on the results after this pooled analysis, we hypothesized that stem cell transplantation could increase the number of bone trabeculae in OVX osteoporotic rats, and the increased number of bone trabeculae was lower than that in normal rats (sham-operated group). Moreover, the results of Tb.Th and Tb.Sp were not significant due to the relatively limited number of studies. The results of the pooled analysis suggest that increasing bone strength and bone mass, as well as the number of trabeculae, may make stem cell transplantation a potential treatment modality for osteoporosis. However, because the therapeutic effect varies with different sources of stem cells, there is still a need to explore more deeply the effect of different stem cells for the treatment of osteoporosis in the future. The details explored include which stem cells are the best choice, as well as the dose, timing, and manner of use.

We summarized the original results of the included studies and presented the results of the group comparisons between the BMSC group and the OVX control group and sham control group on BMD in a table (Table 3). As can be seen from the raw results above, data for the same outcome measurements from different studies were pooled, meta-analysis was performed, and the results obtained were generally consistent with the raw results. It also shows the credibility of the results of the meta-analysis. However, for subgroup analyses containing only one study, the results still need to be supplemented by additional studies in the future. The results of this meta-analysis were analyzed by pooling data from several related studies, expanding the sample size, and yielding results that are generally consistent with individual data, providing direction for the next step in conducting related studies. Therefore, this article is necessary and the results are relatively reliable.

It is well known that cancer cells and stem cells share a remarkable commonality of continuous self-replication, and the molecular mechanisms remain a hot topic of research for scientists worldwide [30]. Therefore, there is also a risk of developing cancer cells after stem cell transplantation. Along with the possibility of recurrence of the original cancer after treatment with stem cell transplantation, there is also the possibility of a second cancer developing after transplantation [31]. Studies have shown that people who have received allogeneic hematopoietic stem cell transplantation are at higher risk of developing a second cancer [32]. Other types of stem cells are also at risk of developing into cancer cells, influenced by the tumor microenvironment in which

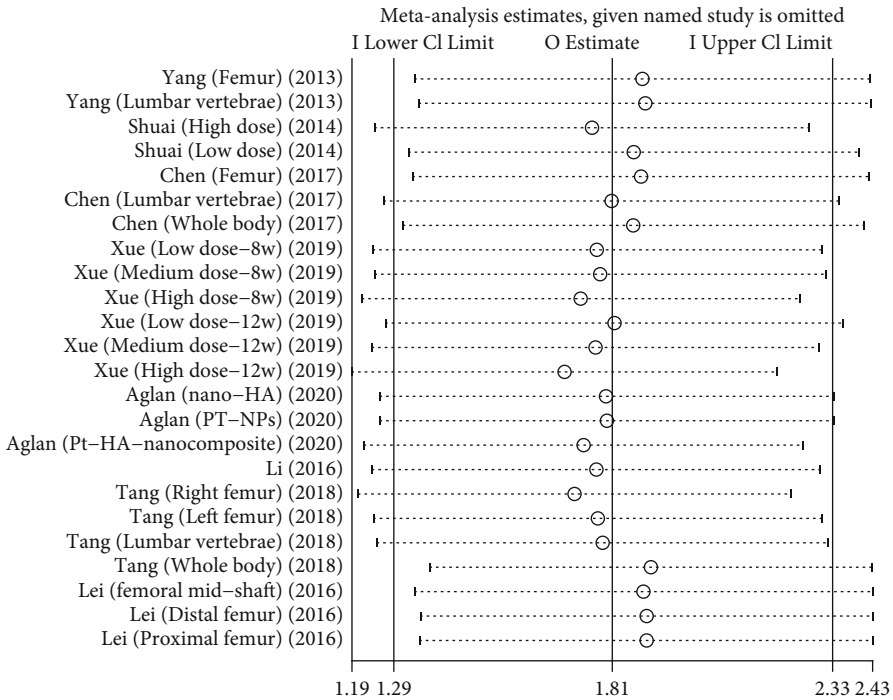

(a)

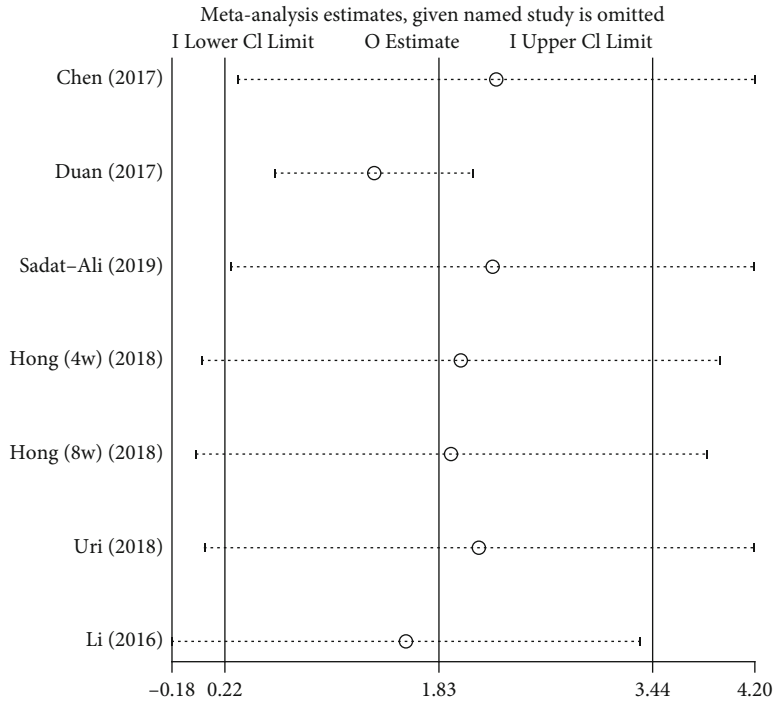

(b)

Figure 10: Continued.

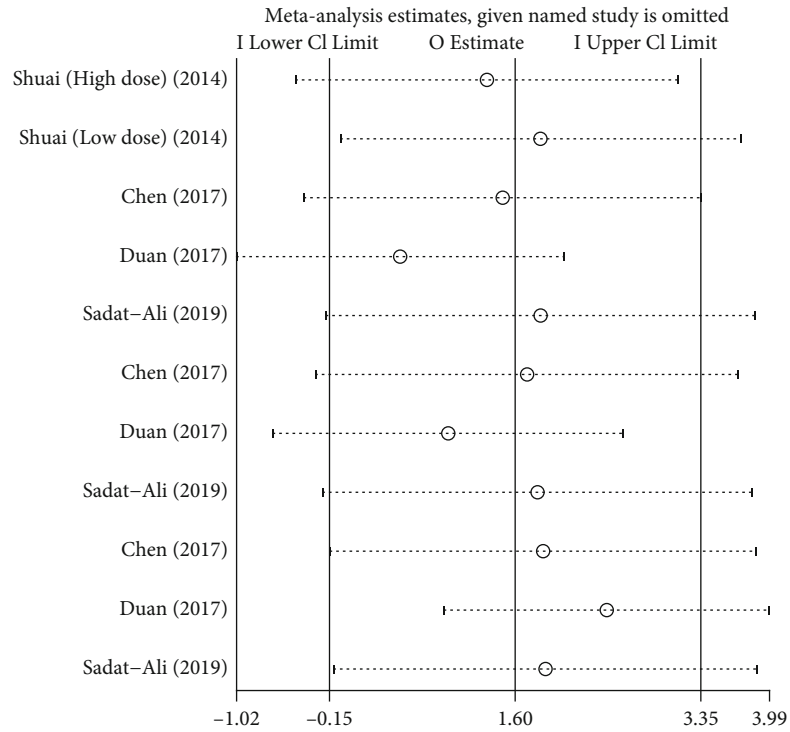

(c)

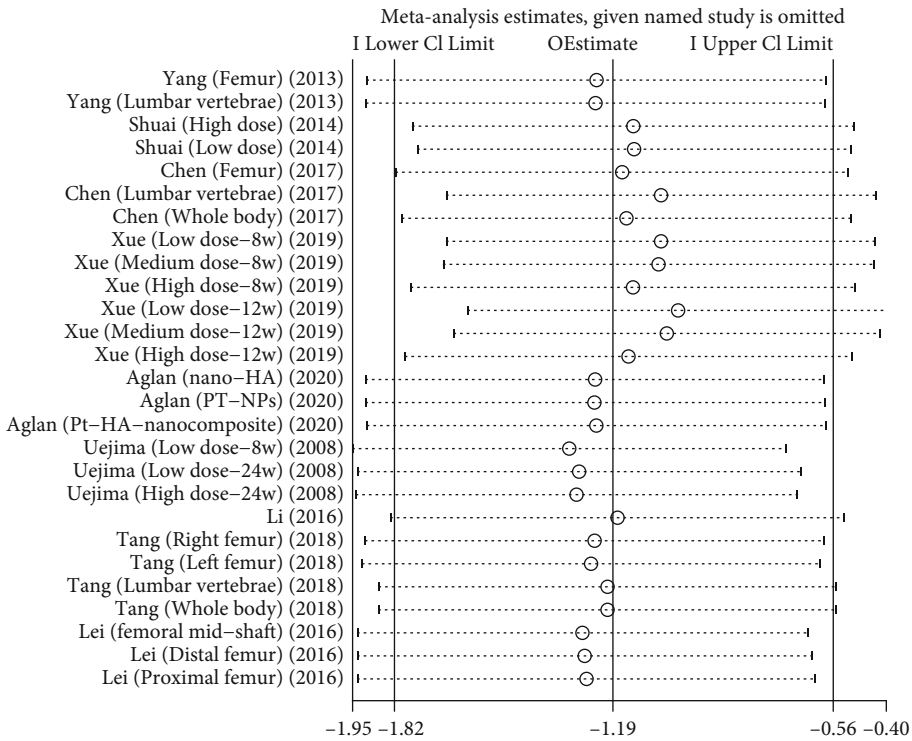

(d)

Figure 10: Continued.

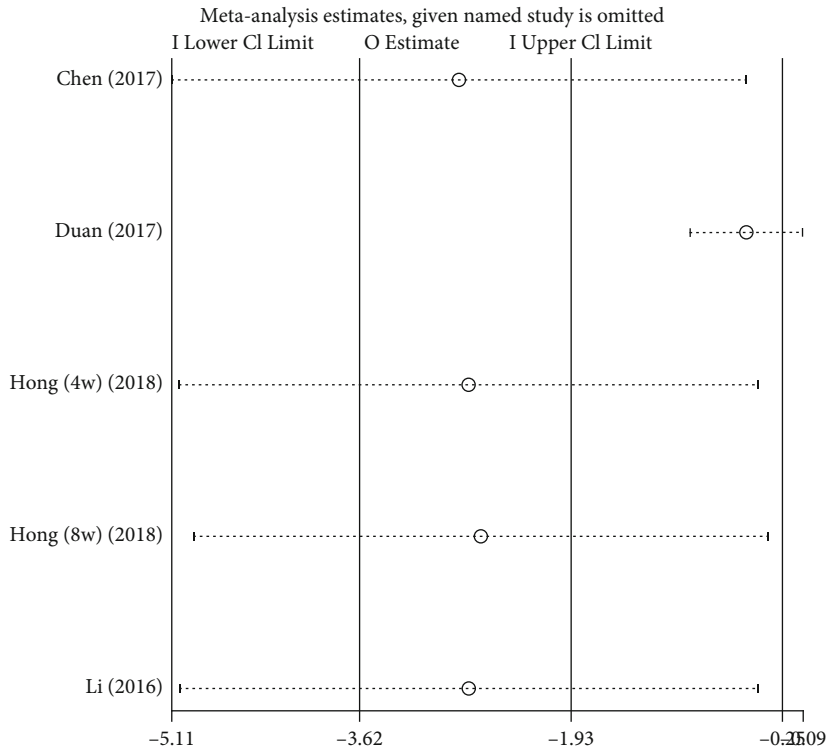

(e)

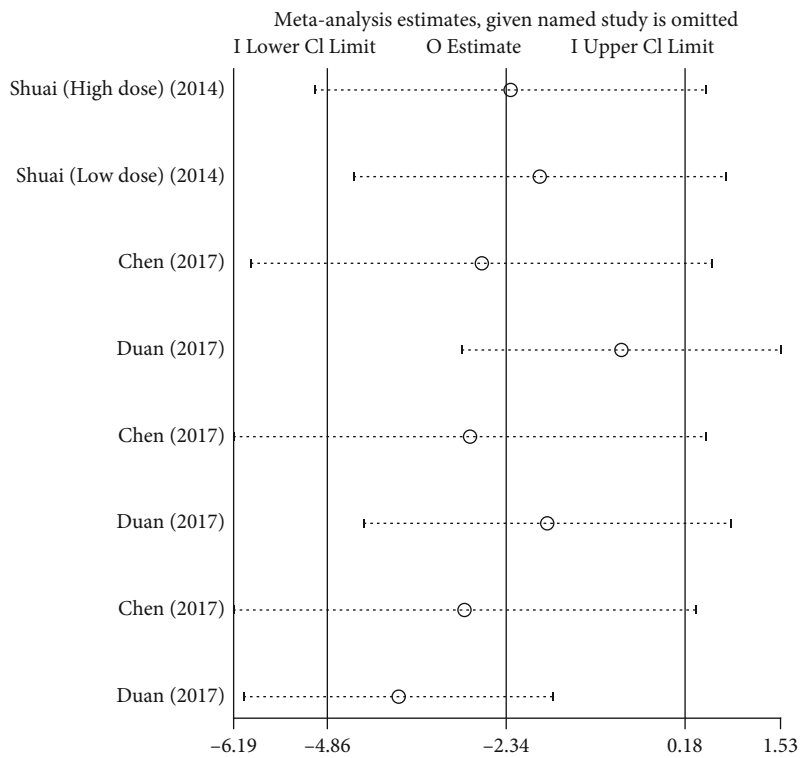

(f)

Figure 10: Sensitivity analysis of this meta-analysis. BMSCs vs. OVX control: (a) BMD, (b) BV/TV, and (c) Tb.N, Tb.Th, and Tb.Sp; BMSCs vs. sham control: (d) BMD, (e) BV/TV, (f) Tb.N, Tb.Th, and Tb.Sp.

Table 3: Basic information about the included studies containing BMD.

Study	Stem cell transplantation	OVX control	Sham control	Unit of measurement	Stem cell type	Subgroup
Yang et al. [9]	$0.1797 \pm 0.0292^{*\#}$	0.1539 ± 0.0745	0.189 ± 0.0461	g/cm^2	BMCs	Femur
Yang et al. [9]	$0.1607 \pm 0.0893^{*\#}$	0.1396 ± 0.0631	0.1742 ± 0.0796	g/cm^2	BMCs	Lumbar vertebrae
Xue et al. [18]	$0.173 \pm 0.0027^{*\#}$	0.165 ± 0.0033	0.187 ± 0.0033	g/cm^2	BMCs	Low dose-8 w
Xue et al. [18]	$0.173 \pm 0.0031^{*\#}$	0.165 ± 0.0033	0.187 ± 0.0033	g/cm^2	BMCs	Medium dose-8 w
Xue et al. [18]	$0.178 \pm 0.004^{*\#}$	0.165 ± 0.0033	0.187 ± 0.0033	g/cm^2	BMCs	High dose-8 w
Xue et al. [18]	$0.165 \pm 0.0026^{*\#}$	0.158 ± 0.0047	0.185 ± 0.0028	g/cm^2	BMCs	Low dose-12 w
Xue et al. [18]	$0.169 \pm 0.0032^{*\#}$	0.158 ± 0.0047	0.185 ± 0.0028	g/cm^2	BMCs	Medium dose-12 w
Xue et al. [18]	$0.178 \pm 0.0036^{*\#}$	0.158 ± 0.0047	0.185 ± 0.0028	g/cm^2	BMCs	High dose-12 w
Shuai et al. [10]	$361 \pm 21^{*\#}$	250 ± 6	431 ± 20	mg/cm^3	BMCs	High dose
Shuai et al. [10]	$253 \pm 6^{\#}$	250 ± 6	431 ± 20	mg/cm^3	BMCs	Low dose
Chen et al. [14]	$206.29 \pm 19.55^{*\#}$	193.98 ± 25.38	243.31 ± 20.11	mg/cm^2	BMCs	Femur
Chen et al. [14]	$126.11 \pm 12.69^{*\#}$	102.21 ± 11.56	180.32 ± 10.55	mg/cm^2	BMCs	Lumbar vertebrae
Chen et al. [14]	$110.33 \pm 10.21^{*\#}$	101.21 ± 8.75	130.21 ± 9.21	mg/cm^2	BMCs	Whole body
Aglan et al. [19]	$191.6 \pm 26.9^{*}$	147.7 ± 8.7	194.9 ± 16.9	mg/cm^2	BMCs	Nano-HA
Aglan et al. [19]	$191.5 \pm 27^{*}$	147.7 ± 8.7	194.9 ± 16.9	mg/cm^2	BMCs	Pt-NPs
Aglan et al. [19]	$190.5 \pm 15.7^{*}$	147.7 ± 8.7	194.9 ± 16.9	mg/cm^2	BMCs	Pt-HA-nanocomposite
Uejima et al. [21]	$139.35 \pm 4.63^{\#}$	NP	124.32 ± 4.88	mg/cm^2	BMCs	Low dose-8 w
Uejima et al. [21]	$154.65 \pm 5.1^{\#}$	NP	147.42 ± 4.36	mg/cm^2	BMCs	Low dose-24 w
Uejima et al. [21]	$149.89 \pm 10.37^{\#}$	NP	133.42 ± 7.37	mg/cm^2	BMCs	High dose-24 w

OVX: ovariectomized; BMSCs: bone marrow mesenchymal stem cells; NP: not provided. *Significant change at $P < 0.05$ in comparison with the OVX control group. #Significant change at $P < 0.05$ in comparison with the sham control group.

they are embedded [33]. Therefore, stem cell transplantation also has two sides to it, and it is important to recognize the beneficial effects it has in treating diseases, but also not to ignore the potential side effects, such as the risk of cancer.

4.1. Limitations. Due to the number and quality of included studies, this meta-analysis has certain limitations. First, the number of RCTs included is relatively limited, and some studies are of relatively low quality. Secondly, in different studies, the dosage, time, and method of using the same type of stem cells are different. Third, the heterogeneity of some results is high. Fourth, the type of rats, the age of the month, the average weight, and the construction time of the osteoporosis model are not completely consistent. Finally, the number of studies on some outcome measurements is limited, and effective results cannot be obtained.

5. Conclusion

This is a meta-analysis based on the results of micro-CT and dual-energy X-ray absorptiometry to evaluate the effect of stem cell transplantation on OVX osteoporotic rats. The results of the above analysis suggest that stem cell transplantation is a potential therapeutic direction for osteoporosis by possibly increasing bone strength, bone volume, and the number of trabeculae in OVX osteoporotic rats. However, the levels of these outcome measurements after the increase were lower than those of normal rats (sham-operated group). Due to the limited number and quality of studies related to this, more high-quality RCTs are still needed in the future to complement the existing findings.

Data Availability

The data supporting this meta-analysis is from previously reported studies and datasets, which have been cited.

Conflicts of Interest

The authors declare that there are no conflicts of interest regarding the publication of this article.

Authors' Contributions

Zhencheng Xiong and Ping Yi are joint first authors.

Acknowledgments

This study was supported by the Beijing Municipal Science & Technology Commission (grant no. Z181100001818006).

References

[1] J. A. Kanis, "Diagnosis of osteoporosis and assessment of fracture risk," *The Lancet*, vol. 359, no. 9321, pp. 1929–1936, 2002.

[2] T. D. Rachner, S. Khosla, and L. C. Hofbauer, "Osteoporosis: now and the future," *The Lancet*, vol. 377, no. 9773, pp. 1276–1287, 2011.

[3] J. Compston, A. Cooper, C. Cooper et al., "UK clinical Guideline for the prevention and treatment of osteoporosis," *Archives of osteoporosis.*, vol. 12, no. 1, p. 43, 2017.

[4] R. Xu, Z. Fu, X. Liu et al., "Transplantation of osteoporotic bone marrow stromal cells rejuvenated by the overexpression of SATB2 prevents alveolar bone loss in ovariectomized rats," *Experimental Gerontology*, vol. 84, pp. 71–79, 2016.

[5] Z. Xiong, C. Zheng, Y. Chang, K. Liu, L. Shu, and C. Zhang, "Exploring the pharmacological mechanism of Duhuo Jisheng decoction in treating osteoporosis based on network pharmacology," *Evidence-based Complementary and Alternative Medicine*, vol. 2021, Article ID 5510290, 21 pages, 2021.

[6] Z. Jin, J. Chen, B. Shu, Y. Xiao, and D. Tang, "Bone mesenchymal stem cell therapy for ovariectomized osteoporotic rats: a systematic review and meta-analysis," *BMC Musculoskeletal Disorders*, vol. 20, no. 1, p. 556, 2019.

[7] Y. Jiang, P. Zhang, X. Zhang, L. Lv, and Y. Zhou, "Advances in mesenchymal stem cell transplantation for the treatment of osteoporosis," *Cell Proliferation*, vol. 54, no. 1, article e12956, 2021.

[8] F. Li, C. Zhou, L. Xu, S. Tao, J. Zhao, and Q. Gu, "Effect of stem cell therapy on bone mineral density: a meta-analysis of preclinical studies in animal models of osteoporosis," *PLoS One*, vol. 11, no. 2, 2016.

[9] T. Yang, Y. Ma, L. Wang, Z. Luo, and Y. Liu, "Effect of transplantation of bone marrow mesenchymal stem cells on bone mass in ovariectomized osteoporotic rats," *Chinese Journal of Osteoporosis*, vol. 19, no. 2, p. e0149400, 2013.

[10] Y. Shuai, Y. Yu, B. Shao et al., "Exogenous BMMSCs ameliorate osteoporosis of ovariectomized rat via improving osteogenesis of endogenous BMMSCs," *Basic & Clinical Medicine*, vol. 34, no. 5, p. 610, 2014.

[11] G. Li, Z. Jiang, and Z. Liu, "Adipose-derived stem cell transplantation for osteoporosis rats: evaluation by bone mineral density and histomorphometry measurement," *Chinese Journal of Tissue Engineering Research*, vol. 20, no. 32, p. 4825, 2016.

[12] M. Lei, X. Liu, C. Liu et al., "Synergistic effect of zoledronic acid on human amniotic mesenchymal stem cell transplantation for treatment osteoporosis in ovariectomized rats," *Chinese Journal of Osteoporosis*, vol. 22, no. 9, p. 1143, 2016.

[13] Y. Duan, W. Ma, D. Li, T. Wang, and B. Liu, "Enhanced osseointegration of titanium implants in a rat model of osteoporosis using multilayer bone mesenchymal stem cell sheets," *Experimental and Therapeutic Medicine*, vol. 14, no. 6, pp. 5717–5726, 2017.

[14] G. Chen, G. Huang, H. Lin, H. Wu, and H. Chen, "Bone marrow mesenchymal stem cell transplantation increases bone mineral density of an ovariectomized rat model of osteoporosis," *Chinese Journal of Tissue Engineering Research*, vol. 21, no. 1, p. 49, 2017.

[15] D. Tang, C. Ju, Y. Liu, F. Xu, Z. Wang, and D. Wang, "Therapeutic effect of icariin combined with stem cells on postmenopausal osteoporosis in rats," *Journal of Bone and Mineral Metabolism*, vol. 36, no. 2, pp. 180–188, 2018.

[16] O. Uri, E. Behrbalk, and Y. Folman, "Local implantation of autologous adipose-derived stem cells increases femoral strength and bone density in osteoporotic rats: a randomized controlled animal study," *Journal of orthopaedic surgery*, vol. 26, no. 3, p. 230949901879953, 2018.

[17] M. Sadat-Ali, D. Al-Dakheel, S. AlMousa et al., "Stem-cell therapy for ovariectomy-induced osteoporosis in rats: a comparison of three treatment modalities," *Stem cells and cloning : advances and applications*, vol. 12, p. 17, 2019.

[18] Y. Xue, Y. Wang, D. Ke, S. Zhao, Q. Lin, and J. Hou, "Effects of transplantation with different amount of bone marrow mesenchymal stem cells on osteoporosis in ovariectomized rats," *Chinese Journal of Geriatrics*, vol. 38, no. 3, p. 322, 2019.

[19] H. Aglan, H. Ahmed, N. Mahmoud, R. Aly, N. Ali, and A. Abd-Rabou, "Nanotechnological applications hold a pivotal position in boosting stem cells osteogenic activity: in vitro and in vivo studies," *Applied Biochemistry and Biotechnology*, vol. 190, no. 2, pp. 551–573, 2020.

[20] B. Hong, S. Lee, N. Shin et al., "Bone regeneration with umbilical cord blood mesenchymal stem cells in femoral defects of ovariectomized rats," *Osteoporosis and sarcopenia*, vol. 4, no. 3, pp. 95–101, 2018.

[21] S. Uejima, K. Okada, H. Kagami, A. Taguchi, and M. Ueda, "Bone marrow stromal cell therapy improves femoral bone mineral density and mechanical strength in ovariectomized rats," *Cytotherapy*, vol. 10, no. 5, pp. 479–489, 2008.

[22] D. Moher, A. Liberati, J. Tetzlaff, D. G. Altman, and for the PRISMA Group, "Preferred reporting items for systematic reviews and meta-analyses: the PRISMA statement," *BMJ*, vol. 339, no. jul21 1, p. b2535, 2009.

[23] J. P. Higgins, D. G. Altman, P. C. Gotzsche et al., "The Cochrane Collaboration's tool for assessing risk of bias in randomised trials," *BMJ*, vol. 343, no. oct18 2, p. d5928, 2011.

[24] Z. Xiong, K. Wu, J. Zhang et al., "Different dose regimens of intravenous tranexamic acid in adolescent spinal deformity surgery: a systematic review and meta-analysis," *BioMed Research International*, vol. 2020, Article ID 3101358, 16 pages, 2020.

[25] J. P. Higgins, S. G. Thompson, J. J. Deeks, and D. G. Altman, "Measuring inconsistency in meta-analyses," *BMJ*, vol. 327, no. 7414, pp. 557–560, 2003.

[26] M. Elseweidy, S. E. el-Swefy, M. Shaheen, N. Baraka, and S. Hammad, "Effect of resveratrol and mesenchymal stem cell monotherapy and combined treatment in management of osteoporosis in ovariectomized rats: role of SIRT1/FOXO3a and Wnt/β-catenin pathways," *Archives of Biochemistry and Biophysics*, vol. 703, p. 108856, 2021.

[27] C. Wong, J. Liao, S. Sheu, P. Lin, C. Chen, and T. Kuo, "Novel transplant of combined platelet-rich fibrin releasate and bone marrow stem cells prevent bone loss in ovariectomized osteoporotic mice," *BMC Musculoskeletal Disorders*, vol. 21, no. 1, p. 527, 2020.

[28] S. Sheu, Y. Hsu, M. Chuang et al., "Enhanced bone formation in osteoporotic mice by a novel transplant combined with adipose-derived stem cells and platelet-rich fibrin releasates," *Cell Transplantation*, vol. 29, p. 963689720927398, 2020.

[29] N. L. FAZZALARI and I. H. PARKINSON, "Fractal dimension and architecture of trabecular bone," *The Journal of Pathology*, vol. 178, no. 1, pp. 100–105, 1996.

[30] R. Tsai and R. McKay, "A nucleolar mechanism controlling cell proliferation in stem cells and cancer cells," *Genes & Development*, vol. 16, no. 23, pp. 2991–3003, 2002.

[31] C. Vajdic, E. Mayson, A. Dodds et al., "Second cancer risk and late mortality in adult Australians receiving allogeneic

hematopoietic stem cell transplantation: a population-based cohort study," *Biology of blood and marrow transplantation : journal of the American Society for Blood and Marrow Transplantation*, vol. 22, no. 5, pp. 949–956, 2016.

[32] on behalf of the CAST study investigators, A. S. Nelson, L. J. Ashton et al., "Second cancers and late mortality in Australian children treated by allogeneic HSCT for haematological malignancy," *Leukemia*, vol. 29, no. 2, pp. 441–447, 2015.

[33] L. Chen, T. Kasai, Y. Li et al., "A model of cancer stem cells derived from mouse induced pluripotent stem cells," *PLoS One*, vol. 7, no. 4, article e33544, 2012.

Hindawi
Stem Cells International
Volume 2021, Article ID 6546780, 17 pages
https://doi.org/10.1155/2021/6546780

Review Article

Applications of Mesenchymal Stem Cells in Liver Fibrosis: Novel Strategies, Mechanisms, and Clinical Practice

Mengmei Zhu,[1] **Tianzhen Hua**,[1] **Tao Ouyang**,[1] **Huofu Qian**,[2] **and Bing Yu**[1]

[1]*Department of Cell Biology, Center for Stem Cell and Medicine, Naval Medical University (Second Military Medical University), Shanghai 200433, China*
[2]*Department of Gastroenterology, The Second People's Hospital of Taizhou, China*

Correspondence should be addressed to Huofu Qian; 47844240@qq.com and Bing Yu; smmucellyu@163.com

Received 28 April 2021; Revised 7 June 2021; Accepted 14 July 2021; Published 15 August 2021

Academic Editor: Huseyin Sumer

Liver fibrosis is a common result of most chronic liver diseases, and advanced fibrosis often leads to cirrhosis. Currently, there is no effective treatment for liver cirrhosis except liver transplantation. Therefore, it is important to carry out antifibrosis treatment to reverse liver damage in the early stage of liver fibrosis. Mesenchymal stem cells (MSCs) are the most widely used stem cells in the field of regenerative medicine. The preclinical and clinical research results of MSCs in the treatment of liver fibrosis and cirrhosis show that MSC administration is a promising treatment for liver fibrosis and cirrhosis. MSCs reverse liver fibrosis and increase liver function mainly through differentiation into hepatocytes, immune regulation, secretion of cytokines and other nutritional factors, reduction of hepatocyte apoptosis, and promotion of hepatocyte regeneration. Recently, many studies provided a variety of new methods and strategies to improve the effect of MSCs in the treatment of liver fibrosis. In this review, we summarized the current effective methods and strategies and their potential mechanisms of MSCs in the treatment of liver fibrosis, as well as the current research progress in clinical practice. We expect to achieve complete reversal of liver injury with MSC-based therapy in the future.

1. Introduction

Liver fibrosis is a fibrotic and inflammatory process caused by chronic liver injury. During liver fibrosis, the continued accumulation of extracellular matrix (ECM), which is rich in collagen I and III, leads to scar deposition [1]. The most common pathogeneses are viral hepatitis infections (hepatitis B and C viral infections (HCV/HBV)), alcoholism, nonalcoholic fatty liver disease (NAFLD)/nonalcoholic steatohepatitis (NASH), and autoimmune hepatitis [2–6]. Although their pathogenesis is different, their common endpoint is the development of liver cirrhosis. Due to the lack of effective treatment, reversible liver fibrosis may develop into cirrhosis [7]. Liver cirrhosis has steadily increased morbidity and mortality in high-income countries and has become a major health problem worldwide. Although liver transplantation offers hope to patients with end-stage liver disease, it is still an expensive and complex procedure with significant side effects [8].

Mesenchymal stem cells (MSCs) are pluripotent stem cells that have received a broad focus in differentiation, transplantation, and immune response in various diseases [9, 10]. MSCs can be isolated from a variety of tissues and are suitable for experimental and possible clinical applications [11]. Many studies have shown that MSCs can provide effective treatments for animal models of liver fibrosis and cirrhosis, and a number of clinical trials have been conducted. In this review, we discuss the therapeutic potential of MSCs in liver fibrosis and new strategies to improve their antifibrotic capacity. We summarize the current effective methods and potential mechanisms of MSCs treatment of liver fibrosis and discuss the current clinical trial process.

2. Source of MSCs

MSCs are the most widely used stem cells that have the unique ability to self-renew and differentiate into many different cell types. For the existing sources of mesenchymal

stem cells, the two main issues regarding cell therapy are the cell donor and the location from which the cells are isolated.

2.1. MSCs are Isolated from Different Locations. MSCs are stromal cells that can be easily isolated from a variety of tissue sources, including bone marrow, placenta, umbilical cord, amniotic fluid, adipose tissue, dental pulp, breast milk, and synovium [12]. MSCs can be culture-expanded and will not be rejected after transplantation. At present, many studies have demonstrated that bone marrow- [13, 14], umbilical cord- [15, 16], and fat- [17, 18] derived mesenchymal stem cells can inhibit liver fibrosis in preclinical animal models, suggesting their potential application in the treatment of liver fibrosis. Furthermore, Park et al. firstly demonstrated that tonsil-derived mesenchymal stem cells (T-MSCs) can differentiate into hepatocyte-like cells and ameliorate liver fibrosis via autophagy activation and downregulation of TGF-β [19]. The transplantation of human amnion-derived mesenchymal stem cells (hAMSCs) may provide significant improvement in rat liver fibrosis models by inhibiting the activation of Kupffer cells and hepatic stellate cells [20, 21]. Moreover, a preclinical study shows that the infusion of human amniotic stem cells effectively decreases portal pressure by ameliorating liver microcirculation [22]. These findings suggest that MSCs may serve as new potential approaches to treat liver fibrosis and can be used as a new source of stem cell therapy for liver disease.

2.2. Advantages of Allogeneic MSCs for Therapeutic Applications. The cell donor can be the same as the cell recipient (autologous) or different from the cell recipient (allogeneic). In recent clinical trials of liver fibrosis and cirrhosis, the trend of MSC therapy seems to have shifted from the administration of autologous cells to allogeneic cells. The choice of autologous therapy is ideal because they ensure major histocompatibility and are unlikely to cause immunological rejection. However, autologous therapy still has some potential limitations, and it may be difficult to obtain a sufficient number of healthy active MSCs from patients [23]. The advantages of using allogeneic compared to autologous MSCs have been fully demonstrated, of which the most notable thing is to obtain cells from healthy donors and proliferate to required number in vitro. Another commonly touted advantage of allogeneic MSCs is their low immunogenicity. Due to their immunomodulatory properties and low immunogenicity, they have become a promising approach to treat graft-versus-host disease (GVHD) and autoimmune disease [24]. Lohan et al. introduced the causes of the immunosuppressive properties and low immunogenicity of allogeneic MSCs through changes in the expression of immunogenic markers on the cell surface and changes in the secretion of immunosuppressive molecules [25]. Although there may be some reasons compared with other allogeneic cell types, some results show that allogeneic MSCs can indeed induce a strong immune response in the body, which may lead to serious consequences [26]. Although various studies have reached inconsistent results on the treatment of allogeneic mesenchymal stem cells, allogeneic mesenchymal stem cells are still promising choices in immunosuppression and tissue repair therapy.

3. The Applications of MSCs in the Treatment of Liver Fibrosis

Cell-based therapy using MSCs has been proven to be beneficial to alleviate liver fibrosis in some basic and clinical studies. To further strengthen the therapeutic effect of MSCs in liver fibrosis, many MSC-based treatment methods for liver fibrosis have been explored and tested. Here, we summarized the proposed possible strategies to improve the antifibrotic ability of MSCs. The sources of MSCs and novel strategies for the applications of MSCs in liver fibrosis were summarized in Figure 1.

3.1. Pretreatments Enhance the Therapeutic Effects of MSCs in Liver Fibrosis. When cultured in vitro, the proliferative ability and activity of MSCs were often affected by culture media and additives (such as glucose level, growth factors, trace elements, lipids, and vitamins) as well as culture conditions and processes, including the oxygen concentration in the incubator, cell dissociating agent, and the density of the inoculated cells [27]. In addition, the regenerative capacity of MSCs was significantly decreased by the harsh microenvironment of injured organ, anoikis, and inflammation after transplantation in vivo, while pretreatment with growth factors, cytokines, chemical agents, hypoxia, inflammatory microenvironment, and gene modification can not only protect MSCs against injury but also improve the hepatogenic differentiation, homing capacity, survival, and paracrine effects of MSCs in vitro and in vivo, thus increasing the ability to attenuate liver injury [28].

In vitro data showed that MSCs pretreated with cytokines have better antifibrosis potential. The pretreatment of MSCs with melatonin (MT) has shown encouraging results in animal models of myocardial infarction, renal ischemia, and cerebral ischemia. Mortezaee et al. used this strategy for the treatment of CCl4-induced liver fibrosis [29]. The results showed that MT pretreatment was at play in improving the homing potential of BMMSCs and can better maintain the balance between matrix degradation and accumulation factors. Fiore et al. showed that insulin-like growth factor-I- (IGF-I-) pretreated MSCs are able to induce hepatic macrophages (hMø) to transform from profibrotic to a resolutive phenotype, as a key early event driving liver fibrosis amelioration [30]. The combination of granulocyte colony-stimulating factor (G-CSF) and MSCs will greatly improve the prognosis of patients with advanced liver disease treated with stem cells [31]. Pretreatment of adipose tissue-derived stromal cells (ADSCs) with basic fibroblast growth factor (bFGF) promoted the transdifferentiation of ADSCs into liver lineage cells in vitro, thereby reducing liver fibrosis in mice [32].

3.2. Gene Modification Enhances the Therapeutic Effects of MSCs in Liver Fibrosis. A series of genes and microRNAs with clear biological functions have been introduced into MSCs through viral or nonviral vectors to improve their differentiation, immune regulation, homing ability, and other repair-related abilities. Hepatocyte growth factor (HGF) is a potent mitogen for mature hepatocytes, which has been shown to play critical roles in liver regeneration and has been applied in gene therapy in cirrhosis and achieved a better

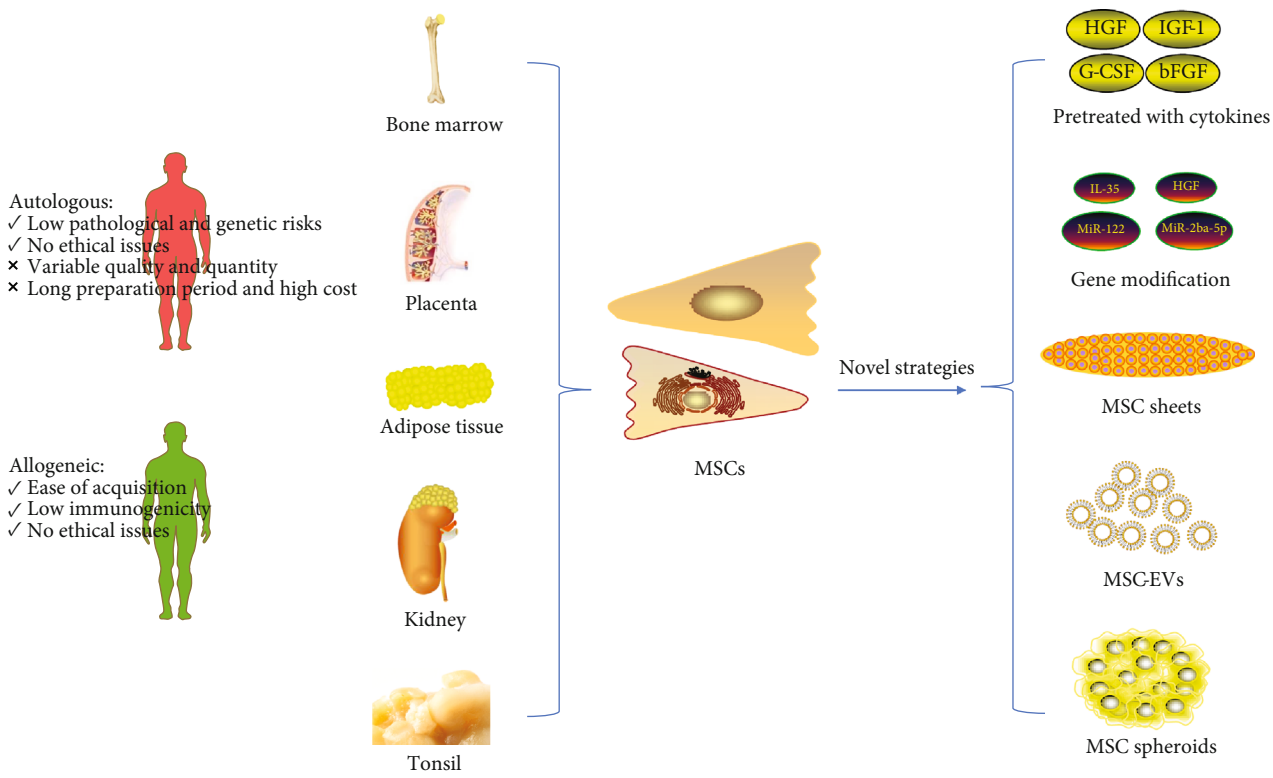

Figure 1: Sources of mesenchymal stem cells and novel strategies for the applications of MSCs in liver fibrosis. MSCs can be obtained from various sources, including bone marrow, placenta, adipose tissue, kidney, and the tonsil. Autologous and allogeneic MSCs have different therapeutic characteristics.

therapeutic effect [33]. Hence, HGF were broadly used to modify MSCs to improve the therapeutic effects on liver fibrosis [34–36]. Kim et al. showed that cell therapy with genetically engineered human bone marrow MSCs, which were overexpressed HGF mediated by adenovirus, significantly promotes liver function and attenuates liver fibrosis than treatment with MSCs alone [34]. Seo et al. also showed that transplantation of human HGF-overexpressing human umbilical cord blood-derived MSCs (hHGF-HUCB-MSCs) in CCL4-induced rat liver fibrosis model has higher liver function improvement and lower collagen fiber deposition than treatment with unmodified HUCB-MSCs [35]. Moreover, the other genes, such as erythropoietin (EPO) [37], forkhead box A2 (Fox A2) [38, 39], FGF4 [40], FGF21 [41], IGF-1 [42]and IL-10 [43], modified MSCs also showed better therapeutic effect in the treatment of liver fibrosis.

MiR-122 is abundant in the adult liver and is a core player in liver biology and disease [44]. Lou et al. showed that miR-122 modified adipose tissue-derived MSCs (AMSC-122), which were constructed through lentivirus-mediated transfer of pre-miR-122, more effectively inhibited the proliferation of hepatic stellate cells (HSCs) and the maturation of collagen [45]. In the latest study, the secreted proteome released from AMSC-122 has higher antifibrotic and anti-inflammatory properties than the pure secreted proteome [46]. The research by Chen et al. reported that inhibition of miR-26a-5p can further improve the therapeutic effect of MSCs on liver cirrhosis through increasing the expression of HGF protein in MSCs [47].

In addition, gene-modified MSCs can also enhance the immunomodulation of MSCs, thus increasing the therapeutic effect of MSCs. For example, MSCs overexpressing IL-35 have higher immunosuppressive capabilities. IL-35-MSCs induce CD4 + T cells to produce IL-10, but have no effect on IFN-γ [48, 49]. Therefore, modifying some specific genes is a potential new strategy for treating liver fibrosis.

3.3. MSC Sheets Have Great Therapeutic Potential. Tissue engineering and/or regenerative medicine is the field of life science that uses engineering and biological principles to create new tissues and organs and promote the regeneration of damaged or diseased tissues and organs [50]. "Cell sheet engineering" is a unique scaffold-free tissue technology, which does not require trypsin digestion. Compared with tissue suspension injection or tissue engineering, the number of cells in the membrane is larger. In addition, transplanted cells can be efficiently delivered to the damaged site and fully maintain their viability at the targeted site [51, 52]. MSC sheets have been successfully applied to the repair of various tissues and organs including Achilles tendon [53], bone tendon [54], blood vessels [55], kidney [56], and heart [57]. In the study of antifibrosis, MSC sheets also have great potential. Itaba et al. combined cell sheet technology with a single small-molecule compound, IC-2, and the results showed that orthotopic transplantation of IC-2 engineered MSC sheets can significantly ameliorate liver fibrosis caused by long-term administration of CCl4 [58]. However, Fernández-Colino et al. analyzed cases of tissue engineering and

regenerative medicine (TERM) interventions with adverse outcomes, suggesting that they may also trigger fibrosis [59]. How to improve the therapeutic potential of MSC sheets has become a question for many people. Chemical disruption (e.g., trypsin or collagenase enzyme treatment) deconstructs the extracellular matrix and intercellular proteins (via cell–cell and cell–ECM junctions). Nakao et al. used temperature responsive cell culture dishes (TRCD) cell sheet technology to harvest human umbilical cord mesenchymal stem cell (HUC-MSC) sheets which retain the typical structure of natural tissue-like interconnected cells, including ECM components and cell connections [60]. The results show that these proteins are kept intact in MSC cultures using cell sheet technology to enhance stem cell survival and its function in stem cell-based therapies. Chuah et al. believed that different combinations of matrix properties (including stiffness, roughness, and wettability) can affect MSC behaviors, such as adhesion, diffusion, and proliferation during cell sheet development [61]. In addition, Rahmi G and others proposed that attention should be paid to the fate of implanted cells in vivo, and multimodal imaging was used to track cell sheets and noninvasively follow-up of their regenerative characteristics [62].

3.4. The Application of MSC-Derived Extracellular Vesicles (MSC-EVs) in Liver Fibrosis. Extracellular vesicles (EVs) can be secreted by almost any type of cells and are found to be high levels in biological fluids. According to the size of the vesicles and the method of cell release, extracellular vesicles can be roughly divided into three subtypes: exosomes (30–130 nm), microvesicles (100–1000 nm), and apoptotic bodies (50–4000 nm) [63, 64]. Multiple studies have consistently demonstrated that extracellular vesicles transfer proteins, lipids, and RNA between various cell types, participate in important biological functions, and serve as a means of communication between cells [65, 66]. MSCs are considered to be the strongest cells that produce EVs. MSC-EVs play an important role in repairing bone damage, skin damage, and nerve damage, but the mechanism of action is not clear. A number of recent studies have investigated the therapeutic effect of MSC-EVs in animal models of liver disease.

Sabry et al. found that bone marrow-derived MSC (BM-MSC) microvesicles can promote the regression of rat liver fibrosis induced by CCL4 by reducing serum alanine aminotransferase (ALT), collagen-1α and IL-1β, *increasing* serum albumin levels and inactivating the TGF-β/Smad signaling pathway [67]. Another study investigated the role of hUCMSC-EVs in liver repair in *S. japonicum*-infected mice. They pointed out that by reducing type I/III collagen, the activation of hepatic stellate cells induced by TGF-β1 is suppressed, and liver damage of schistosomiasis is improved. At the same time, the levels of TNF-α and IL-1β decreased significantly, indicating that hUCMSC-EVs inhibited the inflammatory response [68]. Similarly, Jiang et al. found that hUCMSC-EVs have the potential of antioxidant and hepatoprotective and can reduce CCl4-induced liver damage by reducing apoptosis and oxidative stress [69]. Studies by Mardpour et al. showed that ES-MSC EVs increased the secretion of anti-inflammatory cytokines (examples: TGF-β and IL-10) and reduced IFN-γ level in TAA-induced chronic rat liver injury, showing immunoregulatory activity to ameliorate liver fibrosis [70]. In addition, Qiu et al. summarized the mechanism and role of miRNA transfer in mediating MSC-EVs in human disease models [63]. For example, in a mouse model of CCl4-induced liver fibrosis, MSC-EVs with miRNA-181-5p overexpression ameliorated liver fibrosis by autophagy activation [71]. Moreover, the identification of particular miRNAs at a given concentration within EVs circulating in the bloodstream would be used as molecular biomarkers for disease diagnosis and prognosis monitoring [72].

Therefore, for liver fibrosis and other liver injuries, MSC-EVs may be a promising alternative to MSC treatment. It should be noted that although the experimental results strongly suggest the therapeutic potential of MSC-EVs, there is still a lot of experimental work to be done before putting MSC-EVs into clinical application. However, MSC-EVs will not fully realize its potential in new cell-free therapy until the key questions such as the separation and purification of MSC-EVs, long-term storage, donor, and tissue source are solved.

3.5. The Application of MSC Spheroids in Liver Fibrosis. Three-dimensional (3D) cell culture technology is a new method of MSC culture in vitro. There are a variety of methods for 3D culture of MSCs, including microsphere culture, biopolymer scaffold culture, and 3D culture of hydrogel [73]. There are significant differences in cell phenotypes and biological activities between 3D cell culture and 2D monolayer cell culture. MSC microsphere culture is considered to be an optimal way to improve MSC cell therapy [74]. MSC microspheres have been shown to improve the stemness of MSCs, enhance anti-inflammatory effects, enhance angiogenesis, and promote tissue regeneration and repair [75].

MSC spheroids robustly enhance the therapeutic potential of MSCs in following ways. First, the 3D-cultured MSCs are evenly distributed in organs like the liver, heart, and kidney, enhancing the internal microcirculation of MSCs [76]. Second, pluripotent gene expression of MSC spheroids, such as OCT4, Nanog, SOX-2, and REX-1 is increased. The senescence of MSCs cultured in vitro is delayed, while multipotent differentiation and stemness of MSC spheroids are also enhanced [77]. Third, MSC spheroids play an anti-inflammatory role by secreting anti-inflammatory factors and regulating immune cells, such as inhibiting the activation of macrophages [78]. Last, MSCs cultured in 3D spheres had high expression of cytokines related to angiogenesis and tissue repair to enhance angiogenesis and tissue regeneration [79].

Specifically speaking, MSCs with various sources have confirmed their effects in managing liver fibrosis. Study showed that hUC-MSC spheroids could migrate to the injured liver more effectively compared with the hUC-MSCs in 2D culture. The hUC-MSCs could promote liver regeneration and repair in mice with liver injury [80]. Yoshiaki et al. utilized stem cells from human exfoliated deciduous teeth (SHED) to develop microhepatic tissues. SHED-converted hepatocyte-like cells (SHED-HLCs) form human 3D-spheriacal microhepatic tissues and exert the therapeutic effect by secreting bioactive products like hALB in mice, thus providing a new method in treating chronic

liver fibrosis [81]. Another research indicates that 3D cultured human adipose-derived MSCs (AD-MSCs) were endowed with higher expression of antifibrotic factors like IGF-1, IL-6, and HGF and also better capability of protecting hepatocyte injury and apoptosis. Transplanted AD-MSCs are expected to reverse hepatic fibrosis and improve hepatic function [82].

The utilization of MSC spheroids was not all booming. Restrictions still occur in several aspects. Firstly, the transport of nutrients and oxygen as well as the waste in the 3D sphere are restricted by the size of sphere, causing relatively high mortality of cells in the center. Secondly, the culture system composed of MSCs and 3D scaffold biomaterials is transplanted concurrently; the immunogenicity and histocompatibility of the biomaterials should be fully considered. Finally, differences still occur between the constructed 3D culture system and the environment in vivo, and the interaction mechanism between cells and ECM remains to be elucidated [83–85].

Despite these restrictions, MSC spheroids show great application prospects in the field of regeneration. MCS multicellular spheres may replace single-liver cells as the cellular component of current artificial liver, providing novel strategies to obtain artificial liver with low immunogenicity and solving the problem of donor shortage in liver transplantation.

4. Mechanisms of MSC-Based Therapy in Liver Fibrosis

MSC administration is a promising therapeutic approach that can promote liver regeneration and repair liver fibrosis through the migration of cells into liver, hepatogenic differentiation, paracrine mechanisms, autophagy, and immunoregulation. Many articles have introduced the potential mechanisms of MSCs in treating liver fibrosis. Here, we supplement the latest research progress. The potential mechanisms of MSC-based therapy in liver fibrosis were shown in Figure 2.

4.1. MSCs Had the Potential for Differentiating into Hepatocyte-Like Cells. MSCs have plasticity and multidirectional differentiation potential. Adipose tissue-derived mesenchymal stem cells (AT-MSCs) and BM-MSCs have liver differentiation potential in vivo and in vitro to acquire hepatocyte-like cell morphology and hepatocyte-specific markers (including albumin and alpha-fetoprotein) [86, 87]. Therefore, MSCs have the ability to differentiate into hepatocyte-like cells and are a promising source of liver regeneration [88, 89]. However, hepatic differentiation of MSCs is still insufficient for clinical application. They cannot effectively differentiate into liver cells but can be transformed into myofibroblasts, limiting their applications. Further research is needed to improve the efficacy and consistency of differentiation from MSCs to liver cells. After incubation with some specific growth factors, including hepatocyte growth factor (HGF) and basic fibroblast growth factor (bFGF), MSCs show high liver differentiation capacity [90]. Compared with undifferentiated cells, predifferentiation of AT-MSCs into hepatocytes in vitro contributes to a long-term liver function integration in vivo [91]. Compared with BM-MSCs cultured on uncoated plates, the viability and hepatocyte differentiation of BM-MSCs cultured on Matrigel and ECM coatings were significantly enhanced [92]. Engineered multicellular aggregates constructed from E-cadherin-modified microparticles have constructed a bionic microenvironment to promote endoderm differentiation and subsequent liver differentiation in human MSCs [93]. At the posttranscriptional level, microRNA is a key factor in cell differentiation and proliferation. Zhou et al. screened the best miRNA candidates for hepatocyte differentiation. MiR-30a and miR-1290 are essential for liver differentiation. The remaining five miRNAs (miR-122, miR-148a, miR-424, miR-542-5p, and miR-1246) are also crucial for this process [94]. Therefore, we can improve MSC hepatocyte-like cell differentiation ability by adding cytokines and growth factors, adjusting the microenvironment, modifying genes, and so on.

4.2. Paracrine Effect of Mesenchymal Stem Cells. Although MSCs have the ability to differentiate into hepatocyte-like cells, many studies have shown that other effects of MSCs in treating liver fibrosis can be attributed to paracrine effects [95, 96]. This secretion is due to the release of EVs and other soluble molecules by MSCs. Conditioned medium (CM) obtained from cultured MSCs contains a combination of EVs and soluble proteins. Both MSCs and MSC-CM can play a role in the pathogenesis of chronic fibrosis by acting on various key cells [97]. The therapeutic potential and mechanism of MSC-EVs have been described in detail above, and soluble molecules secreted by MSCs also have important roles. These paracrine factors, such as cytokines, growth factors, and chemokines, have effects including apoptosis, anti-inflammatory property, angiogenesis promotion, and repair [98].

Activation of HSCs has been recognized as the main driver of experimental liver fibrosis [99]. Transforming growth factor beta subtype 3 (TGF-β3) and hepatocyte growth factor (HGF) can induce G (0)/G (1) block in HSCs, thereby ameliorating liver fibrosis [100]. With the participation of the transcription factors nuclear factor κB (NF-Kappa B) and B-cell leukemia-XL (Bcl-XL), NGF can enhance the apoptosis of HSCs [101]. Tumor necrosis factor-inducible gene 6 protein (TSG-6), a cytokine released from MSCs, influences MSC stemness and the biological effect of HSCs. Human primary HSCs treated with TSG-6 show significant downregulation of HSC activation markers and upregulation of senescence markers [102]. MFGE8 is an antifibrotic protein in the MSC secretome, which strongly inhibits TGF-β signaling and reduces extracellular matrix deposition and liver fibrosis in mice [103].

MSCs can show anti-inflammatory effects through increasing anti-inflammatory cytokines (interleukin (IL)-10, tumor necrosis factor-α (TNF-α)) and reducing proinflammatory cytokines (IL-1a, IL-6, IL-17, IFN- g, GCSF, GMCSF, MIP-2a, and MCP-1) [104, 105]. MSCs can secrete vascular endothelial growth factor (VEGF) and Ang1/Ang2 to promote angiogenesis. VEGF can also cooperate with HGF to stabilize the barrier function of endothelial cells [106]. Hepatocyte growth factor, fibroblast growth factor, insulin-like

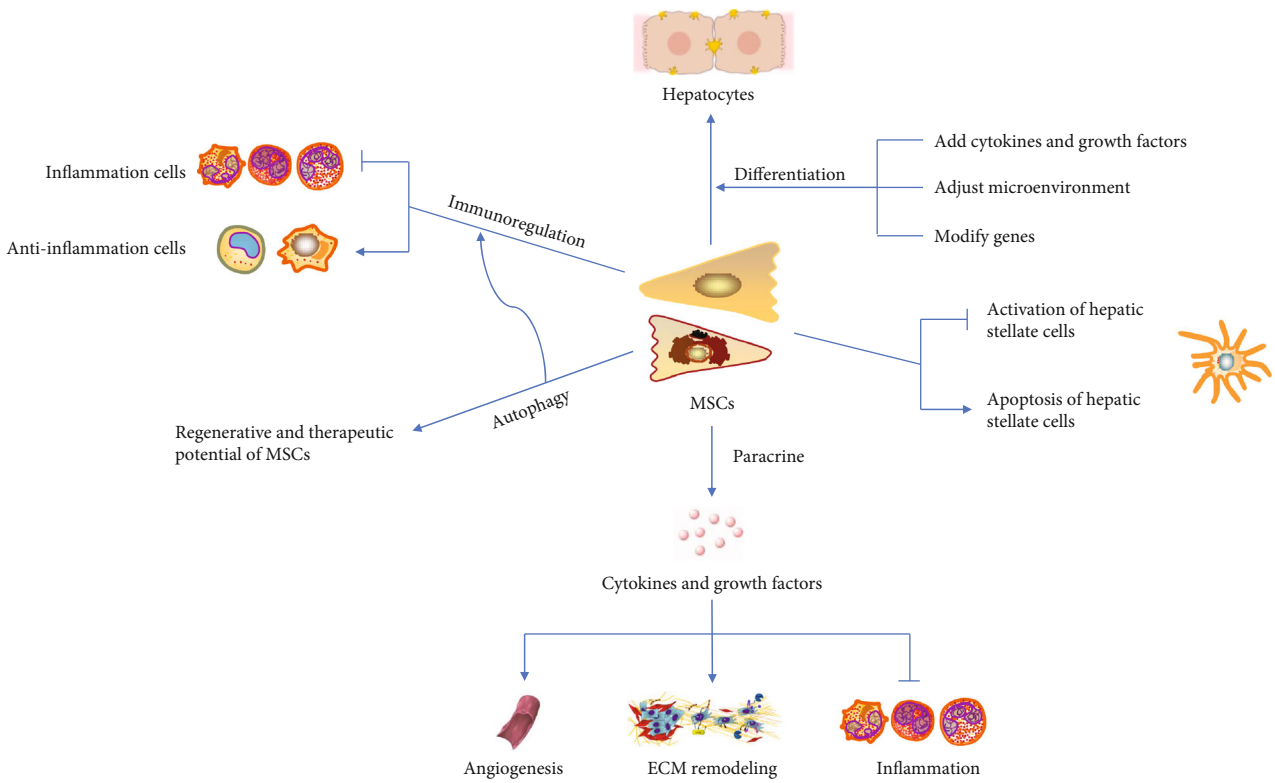

Figure 2: The potential mechanisms of MSC-based therapy in liver fibrosis. MSCs have various effects including the differentiation of hepatocytes and the regulation of inflammation response. Additionally, MSCs affect the regenerative process through autophagy and paracrine effects.

growth factor 1, and thymosin b4 (TB4) produced by MSCs have cytoprotective effects. In addition, VEGF-α, IGF-1, EGF, angiopoietin-1, matrix-derived factor-1, macrophage inflammatory protein-1 α and β, and erythropoietin are important molecules in normal wound healing [107].

Based on the important role of mesenchymal stem cells (MSCs) in the treatment of diseases, how to improve the efficacy of paracrine has attracted more and more attention. Previous studies have shown that MSC paracrine activity may vary with its microenvironment [108]. Recent experimental research results show that compared with conventional two-dimensional (2D) culture systems, three-dimensional (3D) culture systems (such as scaffolds, hydrogels, or spheres) enhance MSC paracrine secretion activity, promote the differentiation of MSCs, and maximize MSC potential for regeneration [82, 109, 110]. In addition, compared to MSCs with a single-gene modification and controlled MSCs, dually genetically modified MSCs have enhanced paracrine effects [111].

4.3. Immunoregulation of Mesenchymal Stem Cells. MSCs exert a wide range of immunosuppressive potentials and can regulate the activity of innate and adaptive immune system cells through cell-to-cell contact or secreted factors. However, the underlying mechanisms of MSC-mediated immune regulation have not been fully elucidated so far. Preliminary observations indicate that the immunomodulatory properties of MSCs derived from different sources are slightly different. For example, BM-MSCs and AT-MSCs have similar immunomodulatory capabilities [112, 113], but the difference in cytokine secretion leads to a stronger immunomodulatory effect in AT-MSCs than BM-MSCs. Adipose tissue-derived MSCs (AD-MSCs) express higher levels of IL-6 and transforming growth factor-β (TGFβ) than bone marrow-derived MSCs (BM-MSCs). This is related to the higher metabolic activity of AD-MSCs [114]. However, it is unclear why MSCs from different tissues differ in their tissue-protective and immunomodulatory properties.

There is growing evidence that paracrine factors derived from MSCs can regulate the immune system by interacting with various immune cells, including macrophages, neutrophils, myeloid-derived suppressor cells, dendritic cells, natural killer (NK) cells, Kupffer cells, T lymphocytes, and B lymphocytes. Indoleamine-2,3-dioxygenase (IDO), and prostaglandin E2 (PGE2) secreted by MSCs are important paracrine factors for MSCs to exert immunosuppressive [115]. Specifically, IDO and PGE2 are key mediators of MSC-induced NK cell inhibition [116]. This inhibitory effect is associated with a sharp downregulation of the surface expression of activated NK receptors NKp30, NKp44, and NKG2D. IDO and PGE2 also inhibit the differentiation of Th1 cells, promote the differentiation of Tregs, and increase the migration of CD4 + T cells [117, 118]. IDO promotes the expansion of CD4 + FoxP3 + IL-10 + T regulatory cells and inhibits the proliferation of Th17 cells [119]. PGE2 is a soluble factor that mediates most of the immunosuppressive of Ad-MSCs and BM-MSCs on p-DC maturation and activates T lymphocyte proliferation [120]. Bone marrow

dendritic cells (DCs) are also susceptible to this immunosuppressive [121]. The interaction between MSCs and Kupffer cells (KCs) has received little attention, but studies have shown that overexpression of PGE2 in MSCs increases the effect of MSCs on KC reprogramming [122]. In addition, UC-MSCs can increase IL-4 in vitro and in vivo and promote the mobilization of KCs, thereby reducing DMN-induced liver fibrosis [15].

Macrophages are one of the key cells connecting the innate and adaptive immune system. PGE2 secreted by MSCs plays a key role in manipulating the macrophage metabolic state and plasticity [123]. MSCs can cause macrophages to differentiate into immunosuppressive phenotypes and that these macrophages can inhibit T lymphocyte subsets at least as effectively as MSCs [124]. However, studies have shown that inhibition of M1 polarization during inflammation and inhibition of M2 polarization under anti-inflammatory conditions strongly depend on functional IL-6 signaling in macrophages. MSC-mediated macrophage polarization is strongly dependent on IL-6, while PGE2 has a smaller effect [125]. In MSC coculture and MSC-EV, due to the significant upregulation of PGE2 levels, the production of IL-23 and IL-22 is downregulated, thereby enhancing the anti-inflammatory phenotype of mature human regulatory macrophages (Mreg) [126].

In addition to interacting with various immune cells, PGE2 is able to induce MSC migration, which may be through the activation of EP2 receptors and FAK/ERK pathways to accelerate MSC homing efficiency [127]. The secretion of PGE2 can enhance the clearance of apoptotic cells (AC) by MSCs. Mechanistically, ACs stimulate MSCs to express COX2, thereby producing more PGE2 that suppresses T-cell responses. NF-κB signaling pathway mediates COX2/PGE2 activation in MSCs [128].

MSCs are also capable of generating an immunoregulatory environment for Treg amplification through a variety of mechanisms [129]. MSCs induce the transformation of fully differentiated Th17 cells into functional Treg cells, thereby regulating the balance of Treg/Th17 cells in the CD4 + T cell population, which is partly attributed to HGF secreted by MSCs [130]. However, the number of MSCs and other cytokines also affect the Treg/Th17 ratio [131]. MSCs can inhibit the activation and differentiation of effector T cells by promoting the association of programmed death 1 (PD-1) with its ligands PD-L1 and PD-L2 [132, 133]. It is well established that nitric oxide (NO) production catalysed by iNOS leads to cell cycle arrest in T cells by affecting Janus kinase (JAK)—signal transduction and transcription activation (STAT) signaling pathways [134]. The lack of iNOS in MSCs also abolishes the therapeutic effects of MSCs in liver fibrosis models [135]. MSCs can also directly affect T cells by producing other immunosuppressive molecules, such as heme oxygenase 1 (HO1) [136], TGFβ [137], and galectin [138, 139]. Compared with the extensive researches on the effect of MSCs on T cells, the effect of MSCs on B cell activation, proliferation, and B cell function has received less attention [140, 141].

4.4. Autophagy of Mesenchymal Stem Cells in Liver Fibrosis. Autophagy is a cell degradation pathway that uses lysosomes to degrade its damaged organelles and macromolecules. The amino acids and small molecules produced by it are reused to achieve intracellular material circulation and internal environment balance [142]. According to substrate degradation and substrate transport methods, autophagy can be categorized as macroautophagy, microautophagy, and molecular chaperone-mediated autophagy [143]. Generally, macroautophagy refers to autophagy, which is the most widely and clearly studied type [144]. In addition to its essential homeostasis, autophagy is involved in the development of many diseases, including cancer [145], inflammatory diseases [146], metabolic diseases [147], neurodegenerative diseases [148], and cardiovascular diseases [149]. Many studies have discussed the role of autophagy in these diseases and potential strategies for therapeutic regulation [150, 151]. In mesenchymal stem cells, autophagy also plays an important role in reducing inflammation, apoptosis, and oxidative stress in cells related to disease pathology and ultimately helps MSCs play a therapeutic role [152].

Autophagy affects the nature of MSCs and may have an impact on their regeneration and therapeutic potential. First, autophagy is closely related to aging [153]. Studies by Squillaro et al. have shown that MSCs in lysosomal storage disorders (LDS) are prone to apoptosis and aging due to impaired autophagy and DNA repair capabilities [154]. Zhang et al. observed that autophagy plays a protective role in D-gal-induced MSC aging, and ROS/JNK/p38 signaling plays an important mediating role in autophagy delaying MSC senescence [155]. In addition, reducing autophagy reduces hypoxia tolerance in aging MSCs [156].

Autophagy can regulate MSC-mediated immune regulatory functions, reduce inflammation, and promote anti-inflammatory effects. Cen et al. pretreated MSCs with 3-methyladenine (3-MA) and rapamycin to regulate autophagy and then cocultured them with CD4 + T cells [157]. The results showed that 3-MA inhibited autophagy in MSCs, while rapamycin was able to activate autophagy. Rapamycin increased the migration of CD4 + T cells, while 3-MA reduced their migration. They demonstrated that MSC autophagy increases the migration of CD4 + T cells through CXCL8 and promotes Treg cell differentiation, while suppressing Th1 cell differentiation by secreting TGF-β1. Similarly, Gao et al. believed that autophagy levels regulate the immune suppression of CD4 + T cells by MSCs by affecting the secretion of TGF-β1 [158]. The homeostasis of CD4 + T cells is considered to be the key in the process of hepatitis and liver fibrosis [159, 160].

Previous studies have shown that autophagy inhibition results in enhanced antifibrotic effect of MSCs. Wang et al. found that autophagy inhibition via Becn1 downregulation improves the mesenchymal stem cells antifibrotic potential in CCl4-induced mouse liver fibrosis model, which may be partially regulated by elevated PTGS2/PGE2 in the paracrine pathway [161]. Dang et al. found that autophagy promotes the apoptosis of MSCs induced by TNF-α and IFN-γ, and this effect may be related to the inhibition of autophagy in MSCs that upregulates PGE2 secretion [162]. Therefore, manipulation of autophagy in MSCs may be a new strategy to improve its antifibrotic ability.

Table 1: Summary of clinical trials using mesenchymal stem cells for the treatment of liver fibrosis.

ClinicalTrials.gov identifier	Country	Conditions	Phase	Estimated enrollment	Allocation/masking	Intervention model	Biological	Auto/Allo	Cell number	Cell injection times	Cell injection route
NCT02705742	Turkey	HCV-related liver cirrhosis	I/II	5 participants	N/A/open label	Single group assignment	AT-MSC	Auto	1×10^6/kg	N/A	Hepatic artery and peripheral vein
NCT02652351	China	Liver cirrhosis	I	20 participants	N/A/open label	Single group assignment	UC-MSC	Allo	A single dose of 2×10^7	4	Intravenous or hepatic artery
NCT02786017	China	Decompensated cirrhosis	I/II	40 participants	Randomized/double (participant, outcome assessor)	Parallel assignment	Injectable Collagen scaffold + HUC-MSCs	Allo	The total amount was 5 $\times 10^8$	N/A	peripheral vein
NCT03209986	China	HBV/HCV-related liver cirrhosis	N/A	200 participants	Randomized/single (outcomes assessor)	Parallel assignment	MSC	N/A	1×10^6/kg	3	Peripheral vein
NCT03668145	China	Primary biliary cirrhosis	N/A	140 participants	Randomized/quadruple (participant, care provider, investigator, outcome assessor)	Parallel assignment	MSC	N/A	$0.1 - 1 \times 10^6$/kg	3	Peripheral vein
NCT03529136	China	Decompensated cirrhosis	II	252 participants	Nonrandomized/open label	Parallel assignment	UC-MSC	Allo	1.5×10^6/kg	2~4	Peripheral vein
NCT03626090	Singapore	Liver cirrhosis	I/II	20 participants	N/A/open label	Single-group assignment	BM-MSC	Auto	$0.5 - 1 \times 10^6$/kg	N/A	Peripheral vein
NCT03826433	China	Decompensated hepatitis b cirrhosis	I	20 participants	Nonrandomized/open label	Parallel assignment	UC-MSC	Allo	6×10^7/30 ml	N/A	Peripheral vein
NCT03945487	China	Decompensated cirrhosis	II	200 participants	Randomized/open label	Parallel assignment	UC-MSC	Allo	1.0×10^6/kg	3	Intravenous
NCT03838250	United States	Alcoholic liver cirrhosis	I	10 participants	N/A/open label	Single-group assignment	Cellgram™ (BM-MSC)	Auto	5×10^7/10 ml	N/A	Hepatic artery
NCT04243681	India	Decompensated cirrhosis	IV	5 participants	Nonrandomized/open label	Parallel assignment	CD 34 and MSC	Auto	N/A	N/A	Hepatic artery
NCT03460795	China	Decompensated cirrhosis	I/II	30 participants	N/A/open label	Single-group assignment	MSCs and Tregs	N/A	N/A	N/A	N/A
NCT01454336	Iran	Liver fibrosis/decompensated cirrhosis	I	3 participants	N/A/open label	Single-group assignment	MSC	Auto	N/A	N/A	N/A
NCT01220492	China	Liver fibrosis	I/II	266 participants	Randomized/open label	Parallel assignment	UC-MSC	N/A	N/A	N/A	N/A
NCT01342250	China		I/II		Randomized/open label		UC-MSC	N/A	N/A	N/A	N/A

Table 1: Continued.

ClinicalTrials.gov identifier	Country	Conditions	Phase	Estimated enrollment	Allocation/masking	Intervention model	Biological	Auto/Allo	Cell number	Cell injection times	Cell injection route
		Decompensated cirrhosis		20 participants		Parallel assignment					
NCT01499459	Turkey	Liver cirrhosis	N/A	25 participants	N/A/open label	Single-group assignment	MSC	Auto	N/A	N/A	N/A
NCT01233102	China	Liver cirrhosis	I/II	200 participants	Randomized/single (single (participant))	Parallel assignment	MSC	N/A	N/A	N/A	Hepatic artery or vein
NCT01741090	Republic of Korea	Alcoholic liver cirrhosis	II	12 participants	N/A/open label	Single-group assignment	MSC	N/A	N/A	N/A	N/A
NCT00976287	China	Liver cirrhosis	II	50 participants	Randomized/single (single (participant))	Parallel assignment	BM-MSC	Auto	N/A	N/A	Hepatic artery
NCT00993941	China	Liver cirrhosis	II	60 participants	Nonrandomized/open label	Parallel assignment	BM-MSC	N/A	N/A	N/A	N/A
NCT01728727	China	HBV-related liver cirrhosis	I/II	240 participants	Randomized/open label	Parallel assignment	UC-MSC	N/A	N/A	N/A	N/A
NCT01483248	China	Liver fibrosis/liver cirrhosis	I/II	50 participants	Randomized/open label	Single-group assignment	hMB-MSC	N/A	N/A	N/A	N/A
NCT03254758	Japan	Decompensated cirrhosis	I/II	15 participants	N/A/open label	Single-group assignment	MSC	N/A	N/A	N/A	N/A
NCT04357600	Indonesia	Liver cirrhosis	I/II	12 participants	N/A/open label	Single-group assignment	UC-MSC	N/A	N/A	N/A	N/A
NCT01573923	China	Liver cirrhosis	I/II	320 participants	Nonrandomized/open label	Parallel assignment	UC-MSC	N/A	N/A	N/A	N/A
NCT01224327	China	Liver cirrhosis	I/II	50 participants	Randomized/open label	Parallel assignment	UC-MSC	N/A	N/A	N/A	Hepatic artery
NCT04522869	Vietnam	Primary Biliary cirrhosis	I/II	34 participants	Nonrandomized/open label	Parallel assignment	UC-MSC	N/A	N/A	N/A	N/A
NCT01662973	China	Primary biliary cirrhosis	I/II	100 participants	Randomized/open label	Parallel assignment	UC-MSC	N/A	N/A	N/A	N/A
NCT02943889	Egypt	Liver cirrhosis	I/II	40 participants	Nonrandomized/open label	Parallel assignment	MSC	N/A	N/A	N/A	N/A
NCT00476060	Iran	Decompensated cirrhosis	II	36 participants	Randomized/double (participant, outcome assessor)	Parallel assignment	MSC	Auto	N/A	N/A	N/A
NCT01440309	China	Primary biliary cirrhosis	I	20 participants	Randomized/open label	Parallel assignment	MSC	Allo	N/A	N/A	N/A

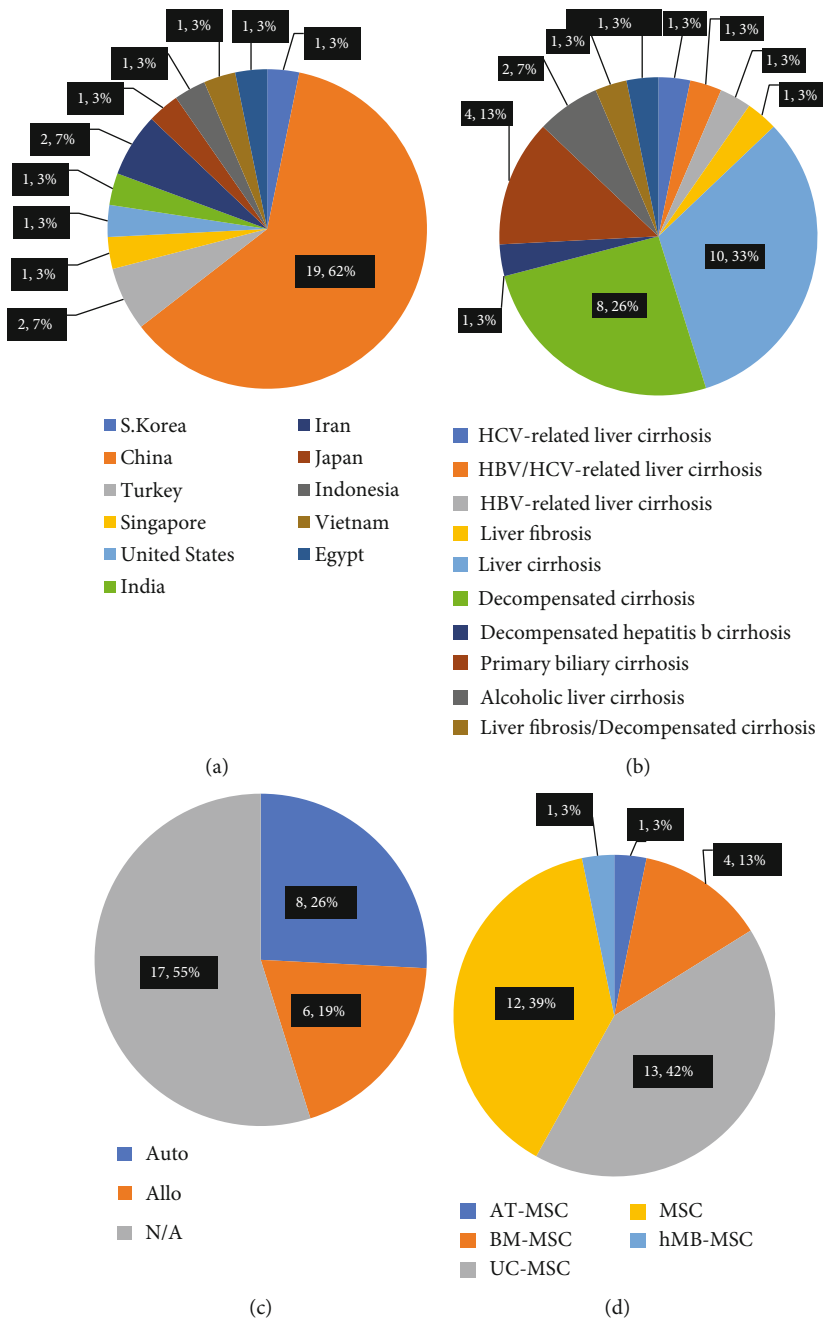

Figure 3: Recent trends in clinical trials using MSCs. Proportion of country (a), disease conditions (b), autologous or allogeneic (c), and sources of MSCs (d) in recent clinical trials.

5. Clinical Practice

5.1. Recently Started or Planned Clinical Trials. A number of clinical trials have begun to evaluate the safety of MSCs in the treatment of patients with liver cirrhosis, observe the efficacy of MSCs treatment, and explore the optimal MSC infusion protocol. According to ClinicalTrials.gov, we evaluated clinical studies which began after 1 January, 2007. The results show that 31 clinical trials are registered. As shown in Table 1, 19 of the 31 cases (61.3%) are from China, 2 cases (6.5%) from Turkey, and 1 case (3.2%) occurs in S. Korea, Iran, Japan, Indonesia, Egypt, Vietnam, Singapore, the United States, and India (Figure 3(a)). The etiology of liver cirrhosis is slightly different in each of the 31 cases. 10 cases (32.3%) are liver cirrhosis, and 8 cases (25.8%) are decompensated cirrhosis. The third liver cirrhosis is primary biliary cirrhosis, which has 4 cases (12.9%). Alcoholic liver cirrhosis has 2 cases (6.5%), while HCV-related liver cirrhosis, HBV-related liver cirrhosis, liver fibrosis, and decompensated hepatitis b cirrhosis each has 1 case (3.2%). Liver fibrosis and decompensated cirrhosis result in 1 case (3.2%) while liver fibrosis and liver cirrhosis result in another. The etiology of liver cirrhosis manifests the

morbidity of different diseases, and it may provide potential methods for corresponding intervention (Figure 3(b)). The source of MSCs also differs in 31 cases, 6 of the 31 cases (19.4%) were treated with allogeneic MSCs, and 8 of the 31 (25.8%) cases were treated with autologous MSCs (Figure 3(c)). Of the 31 cases, 17 cases (54.8%) were unclear whether allogeneic or autologous cells were used. However, the results still indicate an increase in the frequency of treatment with allogeneic MSCs compared to previously reported frequencies. In terms of cell origin, MSCs can be derived from umbilical cord tissue (13 cases, 41.9%), bone marrow (4 cases; 12.9%), adipose tissue (1 case; 3.2%), menstrual blood (1 case; 3.2%), and unknown (12 cases, 38.7%) (Figure 3(d)). The number of cells used in the experiment was slightly different, approximately 2-4 injections at a dose of $0.1 - 1.5 \times 10^6$ cells/kg. Of the 31 cases, 9 (29.0%) were administered via the peripheral vein, 6 (19.4%) were administered via the hepatic artery, 1 (3.2%) were administered via the peripheral vein and hepatic artery simultaneously, and 15 were unknown (48.4%). Peripheral vein and hepatic arterial injections have become the main methods of cell administration. In addition, 2 of the 31 cases are more special. One is the safety study of the combined use of autologous CD34-selected cells and MSCs; the other is the safety study of the combined use of MSCs and Tregs, suggesting that combined cell therapy may become an effective treatment. Most of the 31 clinical trials are still in phase I or/and II, and one of them is in phase IV clinical trials.

5.2. Published Reports on the Results of Clinical Trials Conducted by MSCs. The above shows 31 completed or ongoing clinical trials of MSC therapy or MSC combined cell therapy for liver cirrhosis (LC). At the same time, many reports have been published describing the results of clinical trials using MSCs. Sang et al. published a meta-analysis to evaluate the efficacy and safety of UMSCs combined with traditional supportive therapy (TST) in the treatment of LC patients [163]. They evaluated a total of 14 trials including 717 LC patients who met their selection criteria. The results of their meta-analysis indicated that the combination of UMSCs and TST had more satisfied therapeutic effects for LC patients than TST alone (improved liver function is shown by reduced total bilirubin, alanine aminotransferase, prothrombin time, increased serum albumin, cholinesterase, and prothrombin activity).

Jang et al. reported a phase II study whose purpose was to elucidate the antifibrotic effect of BM-MSCs in patients with alcoholic cirrhosis [164]. Twelve baseline patients with alcoholic liver cirrhosis confirmed by alcohol biopsy were recruited, BM-MSCs were isolated from each patient's bone marrow and expanded for 1 month. Then, 5×10^7 cells were injected twice through the hepatic artery at 4 and 8 weeks. Finally, laboratory examination and biopsy results 12 weeks after the second injection showed that histological improvement was observed in 6 (54.5%) of the 11 patients (one patient withdrew because of drinking). Ten patients' Child-Pugh scores (90.9%) had been improved. In addition, Suk et al. subsequently reported a multicenter, randomized, open-label, phase 2 trial to evaluate the effectiveness and safety of autologous BM-MSC transplantation in the treatment of alcoholic cirrhosis [165]. The results showed that fibrotic areas were reduced, and liver function was significantly improved. Other studies have shown that MSC is a potential choice for the treatment of liver cirrhosis caused by autoimmune diseases [166], and it also plays a therapeutic role in decompensated cirrhosis [167].

6. Conclusion

Liver fibrosis is a pathophysiological process caused by various pathogenic factors and abnormal hyperplasia of connective tissue in liver. If the pathogenic factors cannot be eliminated in time, the process of fibrosis will continue for a long time and develop into cirrhosis. At present, there is no effective treatment for liver cirrhosis. In recent years, many experimental studies and clinical trials have shown that MSCs have a good therapeutic effect in the treatment of liver fibrosis and cirrhosis. Especially, many new therapies, such as MSC sheets, MSCs-EV, gene-modified MSCs, and MSC spheroids, have significantly improved the effect of MSCs in the treatment of liver fibrosis. Although some products of MSCs are approved to be listed in some countries, their safety and effectiveness have not been officially recognized. At present, there is no standardized treatment strategies for MSCs, including the source of MSCs, treatment indications, optimal dosage, administration time, and delivery route. Therefore, it is difficult to apply MSC-based liver fibrosis therapy to clinical practice in the short term. Nevertheless, we believed that cell-free therapy based on MSCs, gene-modified or pretreated MSCs, and MSC spheroids may be the research hotspot and development trend in the future. In conclusion, MSC-based therapies have great potential for the alleviation or treatment of liver fibrosis. However, the challenges associated with this therapy must be addressed before it can be widely used in clinical practice. Therefore, MSC-based therapy still needs to be further studied before widely clinical application.

Data Availability

The references used to support the findings of this study are included within the article.

Conflicts of Interest

The authors declare that they have no conflict of interest.

Authors' Contributions

MMZ, TZH, and BY conceptualized this study. MMZ, TOY, and HFQ performed the literature research and drafted the manuscript. All authors participated in revising the paper and finalizing the paper. All authors read and approved the final manuscript. MMZ and TZH contributed equally to this work. Mengmei Zhu and Tianzhen Hua contributed equally to this work.

Acknowledgments

This study was supported by the National Key R&D Program of China (2018YFA0107500), National Natural Science

Foundation of China (31771511), Foundation Strengthening Program in Technical Field of China (2019-JCJQ-JJ-068), and Innovation Fund for College Students of Naval Medical University (FH2019012 and FH2019013).

References

[1] W. Fan, T. Liu, W. Chen et al., "ECM1 prevents activation of transforming growth factor β, hepatic stellate cells, and fibrogenesis in mice," *Gastroenterology*, vol. 157, no. 5, pp. 1352–1367.e13, 2019.

[2] F. About, L. Abel, and A. Cobat, "HCV-associated liver fibrosis and *HSD17B13*," *The New England Journal of Medicine*, vol. 379, no. 19, pp. 1875-1876, 2018.

[3] W. K. Seto, Y. R. Lo, J. M. Pawlotsky, and M. F. Yuen, "Chronic hepatitis B virus infection," *Lancet*, vol. 392, no. 10161, pp. 2313–2324, 2018.

[4] C. D. Byrne and G. Targher, "NAFLD: a multisystem disease," *Journal of Hepatology*, vol. 62, no. 1, pp. S47–S64, 2015.

[5] D. Schuppan, R. Surabattula, and X. Y. Wang, "Determinants of fibrosis progression and regression in NASH," *Journal of Hepatology*, vol. 68, no. 2, pp. 238–250, 2018.

[6] C. L. Mack, D. Adams, D. N. Assis et al., "Diagnosis and management of autoimmune hepatitis in adults and children: 2019 practice guidance and guidelines from the American Association for the study of liver diseases," *Hepatology*, vol. 72, no. 2, pp. 671–722, 2020.

[7] R. C. Benyon and J. P. Iredale, "Is liver fibrosis reversible?," *Gut*, vol. 46, no. 4, pp. 443–446, 2000.

[8] R. Barnett, "Liver cirrhosis," *Lancet*, vol. 392, no. 10144, p. 275, 2018.

[9] D. C. Ding, W. C. Shyu, and S. Z. Lin, "Mesenchymal stem cells," *Cell Transplantation*, vol. 20, no. 1, pp. 5–14, 2011.

[10] Y. Shi, Y. Wang, Q. Li et al., "Immunoregulatory mechanisms of mesenchymal stem and stromal cells in inflammatory diseases," *Nature Reviews. Nephrology*, vol. 14, no. 8, pp. 493–507, 2018.

[11] J. Galipeau and L. Sensébé, "Mesenchymal stromal cells: clinical challenges and therapeutic opportunities," *Cell Stem Cell*, vol. 22, no. 6, pp. 824–833, 2018.

[12] D. Macrin, J. P. Joseph, A. A. Pillai, and A. Devi, "Eminent sources of adult mesenchymal stem cells and their therapeutic imminence," *Stem Cell Reviews and Reports*, vol. 13, no. 6, pp. 741–756, 2017.

[13] X. Y. Luo, X. J. Meng, D. C. Cao et al., "Transplantation of bone marrow mesenchymal stromal cells attenuates liver fibrosis in mice by regulating macrophage subtypes," *Stem Cell Research & Therapy*, vol. 10, no. 1, p. 16, 2019.

[14] Z. G. Ma, X. D. Lv, L. L. Zhan et al., "Human urokinase-type plasminogen activator gene-modified bone marrow-derived mesenchymal stem cells attenuate liver fibrosis in rats by down-regulating the Wnt signaling pathway," *World Journal of Gastroenterology*, vol. 22, no. 6, pp. 2092–2103, 2016.

[15] N. L. Chai, X. B. Zhang, S. W. Chen, K. X. Fan, and E. Q. Linghu, "Umbilical cord-derived mesenchymal stem cells alleviate liver fibrosis in rats," *World Journal of Gastroenterology*, vol. 22, no. 26, pp. 6036–6048, 2016.

[16] G. Xue, X. Han, X. Ma et al., "Effect of microenvironment on differentiation of human umbilical cord mesenchymal stem cells into hepatocytes in vitro and in vivo," *BioMed Research International*, vol. 2016, Article ID 8916534, 13 pages, 2016.

[17] Y. Wang, F. Lian, J. Li et al., "Adipose derived mesenchymal stem cells transplantation via portal vein improves microcirculation and ameliorates liver fibrosis induced by CCl4 in rats," *Journal of Translational Medicine*, vol. 10, no. 1, p. 133, 2012.

[18] F. Yu, S. Ji, L. Su et al., "Adipose-derived mesenchymal stem cells inhibit activation of hepatic stellate cells *in vitro* and ameliorate rat liver fibrosis *in vivo*," *Journal of the Formosan Medical Association*, vol. 114, no. 2, pp. 130–138, 2015.

[19] M. Park, Y. H. Kim, S. Y. Woo et al., "Tonsil-derived mesenchymal stem cells ameliorate CCl_4-induced liver fibrosis in mice via autophagy activation," *Scientific Reports*, vol. 5, no. 1, p. 8616, 2015.

[20] K. Kubo, S. Ohnishi, H. Hosono et al., "Human amnion-derived mesenchymal stem cell transplantation ameliorates liver fibrosis in rats," *Transplantation direct*, vol. 1, no. 4, article e16, pp. 1–9, 2015.

[21] M. Ohara, S. Ohnishi, H. Hosono et al., "Extracellular vesicles from amnion-derived mesenchymal stem cells ameliorate hepatic inflammation and fibrosis in rats," *Stem Cells International*, vol. 2018, Article ID 3212643, 15 pages, 2018.

[22] G. Pietrosi, A. Fernández-Iglesias, M. Pampalone et al., "Human amniotic stem cells improve hepatic microvascular dysfunction and portal hypertension in cirrhotic rats," *Liver International*, vol. 40, no. 10, pp. 2500–2514, 2020.

[23] B. Lukomska, L. Stanaszek, E. Zuba-Surma, P. Legosz, S. Sarzynska, and K. Drela, "Challenges and controversies in human mesenchymal stem cell therapy," *Stem Cells International*, vol. 2019, Article ID 9628536, 10 pages, 2019.

[24] V. Pistoia and L. Raffaghello, "Mesenchymal stromal cells and autoimmunity," *International Immunology*, vol. 29, no. 2, pp. 49–58, 2017.

[25] P. Lohan, C. M. Coleman, J. Murphy, M. D. Griffin, T. Ritter, and A. E. Ryan, "Changes in immunological profile of allogeneic mesenchymal stem cells after differentiation: should we be concerned?," *Stem Cell Research & Therapy*, vol. 5, no. 4, p. 99, 2014.

[26] N. Eliopoulos, J. Stagg, L. Lejeune, S. Pommey, and J. Galipeau, "Allogeneic marrow stromal cells are immune rejected by MHC class I- and class II-mismatched recipient mice," *Blood*, vol. 106, no. 13, pp. 4057–4065, 2005.

[27] I. Nikolits, S. Nebel, D. Egger, S. Kreß, and C. Kasper, "Towards physiologic culture approaches to improve standard cultivation of mesenchymal stem cells," *Cells*, vol. 10, no. 4, p. 886, 2021.

[28] C. Hu, Z. Wu, and L. Li, "Pre-treatments enhance the therapeutic effects of mesenchymal stem cells in liver diseases," *Journal of Cellular and Molecular Medicine*, vol. 24, no. 1, pp. 40–49, 2020.

[29] K. Mortezaee, N. Khanlarkhani, F. Sabbaghziarani et al., "Preconditioning with melatonin improves therapeutic outcomes of bone marrow-derived mesenchymal stem cells in targeting liver fibrosis induced by CCl4," *Cell and Tissue Research*, vol. 369, no. 2, pp. 303–312, 2017.

[30] E. Fiore, M. Malvicini, J. Bayo et al., "Involvement of hepatic macrophages in the antifibrotic effect of IGF-I-overexpressing mesenchymal stromal cells," *Stem Cell Research & Therapy*, vol. 7, no. 1, p. 172, 2016.

[31] H. Salama, A. R. N. Zekri, E. Medhat et al., "Peripheral vein infusion of autologous mesenchymal stem cells in Egyptian

HCV-positive patients with end-stage liver disease," *Stem Cell Research & Therapy*, vol. 5, no. 3, p. 70, 2014.

[32] Y. Kamada, Y. Yoshida, Y. Saji et al., "Transplantation of basic fibroblast growth factor-pretreated adipose tissue-derived stromal cells enhances regression of liver fibrosis in mice," *American Journal of Physiology. Gastrointestinal and Liver Physiology*, vol. 296, no. 2, pp. G157–G167, 2009.

[33] H. Atta, M. el-Rehany, O. Hammam et al., "Mutant MMP-9 and HGF gene transfer enhance resolution of CCl4-induced liver fibrosis in rats: role of ASH1 and EZH2 methyltransferases repression," *PLoS One*, vol. 9, no. 11, article e112384, 2014.

[34] M. D. Kim, S. S. Kim, H. Y. Cha et al., "Therapeutic effect of hepatocyte growth factor-secreting mesenchymal stem cells in a rat model of liver fibrosis," *Experimental & Molecular Medicine*, vol. 46, no. 8, article e110, 2014.

[35] K. W. Seo, S. Y. Sohn, D. H. Bhang, M. J. Nam, H. W. Lee, and H. Y. Youn, "Therapeutic effects of hepatocyte growth factor-overexpressing human umbilical cord blood-derived mesenchymal stem cells on liver fibrosis in rats," *Cell Biology International*, vol. 38, no. 1, pp. 106–116, 2014.

[36] Y. Zhang, R. Li, W. Rong et al., "Therapeutic effect of hepatocyte growth factor-overexpressing bone marrow- derived mesenchymal stem cells on CCl_4-induced hepatocirrhosis.," *Cell Death & Disease*, vol. 9, no. 12, p. 1186, 2018.

[37] X. Wang, H. Wang, J. Lu et al., "Erythropoietin-modified mesenchymal stem cells enhance anti-fibrosis efficacy in mouse liver fibrosis model," *Tissue Eng Regen Med.*, vol. 17, no. 5, pp. 683–693, 2020.

[38] Y. J. Chae, D. W. Jun, J. S. Lee et al., "The use of Foxa2-overexpressing adipose tissue-derived stem cells in a scaffold system attenuates acute liver injury," *Gut Liver.*, vol. 13, no. 4, pp. 450–460, 2019.

[39] J. W. Cho, C. Y. Lee, and Y. Ko, "Therapeutic potential of mesenchymal stem cells overexpressing human forkhead box A2 gene in the regeneration of damaged liver tissues," *Journal of Gastroenterology and Hepatology*, vol. 27, no. 8, pp. 1362–1370, 2012.

[40] J. Wang, L. Xu, Q. Chen, Y. Zhang, Y. Hu, and L. Yan, "Bone mesenchymal stem cells overexpressing FGF4 contribute to liver regeneration in an animal model of liver cirrhosis," *International Journal of Clinical and Experimental Medicine*, vol. 8, no. 8, pp. 12774–12782, 2015.

[41] H. Kang, E. Seo, J. M. Park, N. Y. Han, H. Lee, and H. S. Jun, "Effects of FGF21-secreting adipose-derived stem cells in thioacetamide-induced hepatic fibrosis," *Journal of Cellular and Molecular Medicine*, vol. 22, no. 10, pp. 5165–5169, 2018.

[42] E. J. Fiore, J. M. Bayo, M. G. Garcia et al., "Mesenchymal stromal cells engineered to produce IGF-I by recombinant adenovirus ameliorate liver fibrosis in mice," *Stem Cells and Development*, vol. 24, no. 6, pp. 791–801, 2015.

[43] J. S. Choi, I. S. Jeong, J. H. Han, S. H. Cheon, and S. W. Kim, "IL-10-secreting human MSCs generated by TALEN gene editing ameliorate liver fibrosis through enhanced anti-fibrotic activity," *Biomaterials Science*, vol. 7, no. 3, pp. 1078–1087, 2019.

[44] S. Bandiera, S. Pfeffer, T. F. Baumert, and M. B. Zeisel, "miR-122 - A key factor and therapeutic target in liver disease," *Journal of Hepatology*, vol. 62, no. 2, pp. 448–457, 2015.

[45] G. Lou, Y. Yang, F. Liu et al., "MiR-122 modification enhances the therapeutic efficacy of adipose tissue-derived mesenchymal stem cells against liver fibrosis," *Journal of Cellular and Molecular Medicine*, vol. 21, no. 11, pp. 2963–2973, 2017.

[46] K. H. Kim, J. I. Lee, O. H. Kim et al., "Ameliorating liver fibrosis in an animal model using the secretome released from miR-122-transfected adipose-derived stem cells," *World Journal of Stem Cells*, vol. 11, no. 11, pp. 990–1004, 2019.

[47] L. Chen, W. Zeng, B. Yang et al., "Expression of antisense of microRNA-26a-5p in mesenchymal stem cells increases their therapeutic effects against cirrhosis," *American Journal of Translational Research*, vol. 9, no. 3, pp. 1500–1508, 2017.

[48] N. Zhao, H. Li, Y. Yan, R. Jiang, and X. He, "Mesenchymal stem cells overexpressing IL-35 effectively inhibit $CD4^+$ T cell function," *Cellular Immunology*, vol. 312, pp. 61–66, 2017.

[49] H. Guo, B. Li, W. Wang, N. Zhao, and H. Gao, "Mesenchymal stem cells overexpressing IL-35: a novel immunosuppressive strategy and therapeutic target for inducing transplant tolerance," *Stem Cell Research & Therapy*, vol. 9, no. 1, p. 254, 2018.

[50] K. Dzobo, N. E. Thomford, D. A. Senthebane et al., "Advances in regenerative medicine and tissue engineering: innovation and transformation of medicine," *Stem Cells International*, vol. 2018, Article ID 2495848, 24 pages, 2018.

[51] M. LI, J. Ma, Y. Gao, and L. Yang, "Cell sheet technology: a promising strategy in regenerative medicine," *Cytotherapy*, vol. 21, no. 1, pp. 3–16, 2019.

[52] A. Alghuwainem, A. T. Alshareeda, and B. Alsowayan, "Scaffold-free 3-D cell sheet technique bridges the gap between 2-D cell culture and animal models," *International Journal of Molecular Sciences*, vol. 20, no. 19, p. 4926, 2019.

[53] M. Maruyama, L. Wei, T. Thio, H. W. Storaci, Y. Ueda, and J. Yao, "The effect of mesenchymal stem cell sheets on early healing of the Achilles tendon in rats," *Tissue Engineering Part A*, vol. 26, no. 3-4, pp. 206–213, 2020.

[54] Y. Tang, C. Chen, F. Liu et al., "Structure and ingredient-based biomimetic scaffolds combining with autologous bone marrow-derived mesenchymal stem cell sheets for bone-tendon healing," *Biomaterials*, vol. 241, p. 119837, 2020.

[55] J. Homma, H. Sekine, K. Matsuura, E. Kobayashi, and T. Shimizu, "Mesenchymal stem cell sheets exert antistenotic effects in a rat arterial injury model," *Tissue Engineering. Part A*, vol. 24, no. 19-20, pp. 1545–1553, 2018.

[56] S. Takemura, T. Shimizu, M. Oka, S. Sekiya, and T. Babazono, "Transplantation of adipose-derived mesenchymal stem cell sheets directly into the kidney suppresses the progression of renal injury in a diabetic nephropathy rat model," *Journal of Diabetes Investigation*, vol. 11, no. 3, pp. 545–553, 2020.

[57] K. Kim, S. Bou-Ghannam, S. Kameishi, M. Oka, D. W. Grainger, and T. Okano, "Allogeneic mesenchymal stem cell sheet therapy: a new frontier in drug delivery systems," *Journal of Controlled Release*, vol. 330, pp. 696–704, 2021.

[58] N. Itaba, Y. Kono, K. Watanabe et al., "Reversal of established liver fibrosis by IC-2-engineered mesenchymal stem cell sheets," *Scientific Reports*, vol. 9, no. 1, p. 6841, 2019.

[59] A. Fernández-Colino, L. Iop, M. S. Ventura Ferreira, and P. Mela, "Fibrosis in tissue engineering and regenerative medicine: treat or trigger?," *Advanced Drug Delivery Reviews*, vol. 146, pp. 17–36, 2019.

[60] M. Nakao, K. Kim, K. Nagase, D. W. Grainger, H. Kanazawa, and T. Okano, "Phenotypic traits of mesenchymal stem cell

sheets fabricated by temperature-responsive cell culture plate: structural characteristics of MSC sheets," *Stem Cell Research & Therapy*, vol. 10, no. 1, p. 353, 2019.

[61] Y. J. Chuah, Y. Zhang, Y. Wu et al., "Combinatorial effect of substratum properties on mesenchymal stem cell sheet engineering and subsequent multi-lineage differentiation," *Acta Biomaterialia*, vol. 23, pp. 52–62, 2015.

[62] G. Rahmi, L. Pidial, A. K. A. Silva et al., "Designing 3D mesenchymal stem cell sheets merging magnetic and fluorescent features: when cell sheet technology meets image-guided cell therapy," *Theranostics*, vol. 6, no. 5, pp. 739–751, 2016.

[63] G. Qiu, G. Zheng, M. Ge et al., "Mesenchymal stem cell-derived extracellular vesicles affect disease outcomes via transfer of microRNAs," *Stem Cell Research & Therapy*, vol. 9, no. 1, p. 320, 2018.

[64] H. Kalra, G. Drummen, and S. Mathivanan, "Focus on extracellular vesicles: introducing the next small big thing," *International Journal of Molecular Sciences*, vol. 17, no. 2, p. 170, 2016.

[65] M. Mathieu, L. Martin-Jaular, G. Lavieu, and C. Théry, "Specificities of secretion and uptake of exosomes and other extracellular vesicles for cell-to-cell communication," *Nature Cell Biology*, vol. 21, no. 1, pp. 9–17, 2019.

[66] A. G. Zhao, K. Shah, B. Cromer, and H. Sumer, "Mesenchymal stem cell-derived extracellular vesicles and their therapeutic potential," *Stem Cells International*, vol. 2020, Article ID 8825771, 10 pages, 2020.

[67] D. Sabry, A. Mohamed, M. Monir, and H. A. Ibrahim, "The effect of mesenchymal stem cells derived microvesicles on the treatment of experimental CCL4 induced liver fibrosis in rats," *International Journal of Stem Cells*, vol. 12, no. 3, pp. 400–409, 2019.

[68] L. Dong, Y. Pu, X. Chen et al., "hUCMSC-extracellular vesicles downregulated hepatic stellate cell activation and reduced liver injury in S. japonicum-infected mice," *Stem Cell Research & Therapy*, vol. 11, no. 1, p. 21, 2020.

[69] W. Jiang, Y. Tan, M. Cai et al., "Human umbilical cord MSC-derived exosomes suppress the development of CCl4-induced liver injury through antioxidant effect," *Stem Cells International*, vol. 2018, Article ID 6079642, 11 pages, 2018.

[70] S. Mardpour, S. N. Hassani, S. Mardpour et al., "Extracellular vesicles derived from human embryonic stem cell-MSCs ameliorate cirrhosis in thioacetamide-induced chronic liver injury," *Journal of Cellular Physiology*, vol. 233, no. 12, pp. 9330–9344, 2018.

[71] Y. Qu, Q. Zhang, X. Cai et al., "Exosomes derived from miR-181-5p-modified adipose-derived mesenchymal stem cells prevent liver fibrosis via autophagy activation," *Journal of Cellular and Molecular Medicine*, vol. 21, no. 10, pp. 2491–2502, 2017.

[72] S. Eleuteri and A. Fierabracci, "Insights into the secretome of mesenchymal stem cells and its potential applications," *International Journal of Molecular Sciences*, vol. 20, no. 18, p. 4597, 2019.

[73] L. Li, X. Liu, B. Gaihre, Y. Li, and L. Lu, "Mesenchymal stem cell spheroids incorporated with collagen and black phosphorus promote osteogenesis of biodegradable hydrogels," *Materials Science & Engineering. C, Materials for Biological Applications*, vol. 121, p. 111812, 2021.

[74] S. Ezquerra, A. Zuleta, R. Arancibia, J. Estay, F. Aulestia, and F. Carrion, "Functional properties of human-derived mesenchymal stem cell spheroids: a meta-analysis and systematic review," *Stem Cells International*, vol. 2021, Article ID 8825332, 12 pages, 2021.

[75] S. Zhang, P. Liu, L. Chen, Y. Wang, Z. Wang, and B. Zhang, "The effects of spheroid formation of adipose-derived stem cells in a microgravity bioreactor on stemness properties and therapeutic potential," *Biomaterials*, vol. 41, pp. 15–25, 2015.

[76] S. Tietze, M. Kräter, A. Jacobi et al., "Spheroid culture of mesenchymal stromal cells results in morphorheological properties appropriate for improved microcirculation," *Advanced Science*, vol. 6, no. 8, p. 1802104, 2019.

[77] S. Lee, H. S. Kim, B. H. Min et al., "Enhancement of anti-inflammatory and immunomodulatory effects of adipose-derived human mesenchymal stem cells by making uniform spheroid on the new nano-patterned plates," *Biochemical and Biophysical Research Communications*, vol. 552, pp. 164–169, 2021.

[78] D. Kouroupis and D. Correa, "Increased mesenchymal stem cell functionalization in three-dimensional manufacturing settings for enhanced therapeutic applications," *Frontiers in Bioengineering and Biotechnology*, vol. 9, p. 621748, 2021.

[79] M. A. Nilforoushzadeh, M. Khodadadi Yazdi, S. Baradaran Ghavami et al., "Mesenchymal stem cell spheroids embedded in an injectable thermosensitive hydrogel: an in situ drug formation platform for accelerated wound healing," *ACS Biomaterials Science & Engineering*, vol. 6, no. 9, pp. 5096–5109, 2020.

[80] Y. Sun, Y. Wang, L. Zhou et al., "Spheroid-cultured human umbilical cord-derived mesenchymal stem cells attenuate hepatic ischemia-reperfusion injury in rats," *Scientific Reports*, vol. 8, no. 1, p. 2518, 2018.

[81] Y. Takahashi, R. Yuniartha, T. Yamaza et al., "Therapeutic potential of spheroids of stem cells from human exfoliated deciduous teeth for chronic liver fibrosis and hemophilia A," *Pediatric Surgery International*, vol. 35, no. 12, pp. 1379–1388, 2019.

[82] X. Zhang, M. G. Hu, K. Pan, C. H. Li, and R. Liu, "3D spheroid culture enhances the expression of antifibrotic factors in human adipose-derived MSCs and improves their therapeutic effects on hepatic fibrosis," *Stem Cells International*, vol. 2016, Article ID 4626073, 8 pages, 2016.

[83] J. Whitehead, J. Zhang, J. N. Harvestine, A. Kothambawala, G. Y. Liu, and J. K. Leach, "Tunneling nanotubes mediate the expression of senescence markers in mesenchymal stem/-stromal cell spheroids," *Stem Cells*, vol. 38, no. 1, pp. 80–89, 2020.

[84] L. de Moor, S. Fernandez, C. Vercruysse et al., "Hybrid bioprinting of chondrogenically induced human mesenchymal stem cell spheroids," *Frontiers in Bioengineering and Biotechnology*, vol. 8, p. 484, 2020.

[85] N. Komatsu, M. Kajiya, S. Morimoto et al., "Cox2-mediated PGE2 production via p38/JNK-c-fos signaling inhibits cell apoptosis in 3D floating culture clumps of mesenchymal stem cell/extracellular matrix complexes," *Biochemical and Biophysical Research Communications*, vol. 530, no. 2, pp. 448–454, 2020.

[86] L. Yin, Y. Zhu, J. Yang et al., "Adipose tissue-derived mesenchymal stem cells differentiated into hepatocyte-like cells in vivo and in vitro," *Molecular Medicine Reports*, vol. 11, no. 3, pp. 1722–1732, 2015.

[87] Y. Sato, H. Araki, J. Kato et al., "Human mesenchymal stem cells xenografted directly to rat liver are differentiated into human hepatocytes without fusion," *Blood*, vol. 106, no. 2, pp. 756–763, 2005.

[88] A. Banas, T. Teratani, Y. Yamamoto et al., "Adipose tissue-derived mesenchymal stem cells as a source of human hepatocytes," *Hepatology*, vol. 46, no. 1, pp. 219–228, 2007.

[89] L. Deng, G. Liu, X. Wu et al., "Adipose derived mesenchymal stem cells efficiently rescue carbon tetrachloride-induced acute liver failure in mouse," *ScientificWorldJournal*, vol. 2014, article 103643, 8 pages, 2014.

[90] Q. Zhao, H. Ren, X. Li et al., "Differentiation of human umbilical cord mesenchymal stromal cells into low immunogenic hepatocyte-like cells," *Cytotherapy*, vol. 11, no. 4, pp. 414–426, 2009.

[91] H. Aurich, M. Sgodda, P. Kaltwasser et al., "Hepatocyte differentiation of mesenchymal stem cells from human adipose tissue in vitro promotes hepatic integration in vivo," *Gut*, vol. 58, no. 4, pp. 570–581, 2009.

[92] B. Wang, W. Li, D. Dean, M. K. Mishra, and K. S. Wekesa, "Enhanced hepatogenic differentiation of bone marrow derived mesenchymal stem cells on liver ECM hydrogel," *Journal of Biomedical Materials Research Part A*, vol. 106, no. 3, pp. 829–838, 2018.

[93] L. Cao, Y. Zhang, M. Qian et al., "Construction of multicellular aggregate by E-cadherin coated microparticles enhancing the hepatic specific differentiation of mesenchymal stem cells," *Acta Biomaterialia*, vol. 95, pp. 382–394, 2019.

[94] X. Zhou, L. Cui, X. Zhou et al., "Induction of hepatocyte-like cells from human umbilical cord-derived mesenchymal stem cells by defined microRNAs," *Journal of Cellular and Molecular Medicine*, vol. 21, no. 5, pp. 881–893, 2017.

[95] J. Driscoll and T. Patel, "The mesenchymal stem cell secretome as an acellular regenerative therapy for liver disease," *Journal of Gastroenterology*, vol. 54, no. 9, pp. 763–773, 2019.

[96] X. Liang, Y. Ding, Y. Zhang, H. F. Tse, and Q. Lian, "Paracrine mechanisms of mesenchymal stem cell-based therapy: current status and perspectives," *Cell Transplantation*, vol. 23, no. 9, pp. 1045–1059, 2014.

[97] B. Huang, X. Cheng, H. Wang et al., "Mesenchymal stem cells and their secreted molecules predominantly ameliorate fulminant hepatic failure and chronic liver fibrosis in mice respectively," *Journal of Translational Medicine*, vol. 14, no. 1, p. 45, 2016.

[98] H. Kupcova Skalnikova, "Proteomic techniques for characterisation of mesenchymal stem cell secretome," *Biochimie*, vol. 95, no. 12, pp. 2196–2211, 2013.

[99] T. Tsuchida and S. L. Friedman, "Mechanisms of hepatic stellate cell activation," *Nature Reviews Gastroenterology & Hepatology*, vol. 14, no. 7, pp. 397–411, 2017.

[100] J. Wang, C. Bian, L. Liao et al., "Inhibition of hepatic stellate cells proliferation by mesenchymal stem cells and the possible mechanisms," *Hepatology Research*, vol. 39, no. 12, pp. 1219–1228, 2009.

[101] N. Lin, K. Hu, S. Chen et al., "Nerve growth factor-mediated paracrine regulation of hepatic stellate cells by multipotent mesenchymal stromal cells," *Life Sciences*, vol. 85, no. 7-8, pp. 291–295, 2009.

[102] S. Wang, J. Kim, C. Lee et al., "Tumor necrosis factor-inducible gene 6 reprograms hepatic stellate cells into stem-like cells, which ameliorates liver damage in mouse," *Biomaterials*, vol. 219, p. 119375, 2019.

[103] S. Y. An, Y. J. Jang, H. J. Lim et al., "Milk fat globule-EGF factor 8, secreted by mesenchymal stem cells, protects against liver fibrosis in mice," *Gastroenterology*, vol. 152, no. 5, pp. 1174–1186, 2017.

[104] M. S. Khubutiya, A. V. Vagabov, A. A. Temnov, and A. N. Sklifas, "Paracrine mechanisms of proliferative, anti-apoptotic and anti-inflammatory effects of mesenchymal stromal cells in models of acute organ injury," *Cytotherapy*, vol. 16, no. 5, pp. 579–585, 2014.

[105] S. P. Lam, J. M. Luk, K. Man et al., "Activation of interleukin-6-induced glycoprotein 130/signal transducer and activator of transcription 3 pathway in mesenchymal stem cells enhances hepatic differentiation, proliferation, and liver regeneration," *Liver Transplantation*, vol. 16, no. 10, pp. 1195–1206, 2010.

[106] Y. Yang, Q. H. Chen, A. R. Liu, X. P. Xu, J. B. Han, and H. B. Qiu, "Synergism of MSC-secreted HGF and VEGF in stabilising endothelial barrier function upon lipopolysaccharide stimulation via the Rac1 pathway," *Stem Cell Research & Therapy*, vol. 6, no. 1, p. 250, 2015.

[107] L. Chen, E. E. Tredget, P. Y. G. Wu, and Y. Wu, "Paracrine factors of mesenchymal stem cells recruit macrophages and endothelial lineage cells and enhance wound healing," *PLoS One*, vol. 3, no. 4, article e1886, 2008.

[108] G. D. Kusuma, J. Carthew, R. Lim, and J. E. Frith, "Effect of the microenvironment on mesenchymal stem cell paracrine signaling: opportunities to engineer the therapeutic effect," *Stem Cells and Development*, vol. 26, no. 9, pp. 617–631, 2017.

[109] T. H. Qazi, D. J. Mooney, G. N. Duda, and S. Geissler, "Niche-mimicking interactions in peptide-functionalized 3D hydrogels amplify mesenchymal stromal cell paracrine effects," *Biomaterials*, vol. 230, p. 119639, 2020.

[110] B. Follin, M. Juhl, S. Cohen, A. E. Pedersen, J. Kastrup, and A. Ekblond, "Increased paracrine immunomodulatory potential of mesenchymal stromal cells in three-dimensional culture," *Tissue Engineering Part B: Reviews*, vol. 22, no. 4, pp. 322–329, 2016.

[111] X. Ni, C. Ou, J. Guo et al., "Lentiviral vector-mediated co-overexpression of VEGF and Bcl-2 improves mesenchymal stem cell survival and enhances paracrine effects in vitro," *International Journal of Molecular Medicine*, vol. 40, no. 2, pp. 418–426, 2017.

[112] C. H. Mun, M. I. Kang, Y. D. Shin, Y. Kim, and Y. B. Park, "The expression of immunomodulation-related cytokines and genes of adipose- and bone marrow-derived human mesenchymal stromal cells from early to late passages," *Tissue Engineering and Regenerative Medicine*, vol. 15, no. 6, pp. 771–779, 2018.

[113] J. Valencia, B. Blanco, R. Yáñez et al., "Comparative analysis of the immunomodulatory capacities of human bone marrow- and adipose tissue-derived mesenchymal stromal cells from the same donor," *Cytotherapy*, vol. 18, no. 10, pp. 1297–1311, 2016.

[114] S. M. Melief, J. J. Zwaginga, W. E. Fibbe, and H. Roelofs, "Adipose tissue-derived multipotent stromal cells have a higher immunomodulatory capacity than their bone marrow-derived counterparts," *Stem Cells Translational Medicine*, vol. 2, no. 6, pp. 455–463, 2013.

[115] C. D. Hu, Y. Kosaka, P. Marcus, I. Rashedi, and A. Keating, "Differential immunomodulatory effects of human bone

marrow-derived mesenchymal stromal cells on natural killer cells," *Stem Cells and Development*, vol. 28, no. 14, pp. 933–943, 2019.

[116] G. M. Spaggiari, A. Capobianco, H. Abdelrazik, F. Becchetti, M. C. Mingari, and L. Moretta, "Mesenchymal stem cells inhibit natural killer-cell proliferation, cytotoxicity, and cytokine production: role of indoleamine 2,3-dioxygenase and prostaglandin E2," *Blood*, vol. 111, no. 3, pp. 1327–1333, 2008.

[117] Y. Yu, S. M. Yoo, H. H. Park et al., "Preconditioning with interleukin-1 beta and interferon-gamma enhances the efficacy of human umbilical cord blood-derived mesenchymal stem cells-based therapy via enhancing prostaglandin E2 secretion and indoleamine 2,3-dioxygenase activity in dextran sulfate sodium-induced colitis," *Journal of Tissue Engineering and Regenerative Medicine*, vol. 13, no. 10, pp. 1792–1804, 2019.

[118] A. Rozenberg, A. Rezk, M. N. Boivin et al., "Human mesenchymal stem cells impact Th17 and Th1 responses through a prostaglandin E2 and myeloid-dependent mechanism," *Stem Cells Translational Medicine*, vol. 5, no. 11, pp. 1506–1514, 2016.

[119] N. Milosavljevic, M. Gazdic, B. Simovic Markovic et al., "Mesenchymal stem cells attenuate liver fibrosis by suppressing Th17 cells - an experimental study," *Transplant International*, vol. 31, no. 1, pp. 102–115, 2018.

[120] R. Yañez, A. Oviedo, M. Aldea, J. A. Bueren, and M. L. Lamana, "Prostaglandin E2 plays a key role in the immunosuppressive properties of adipose and bone marrow tissue-derived mesenchymal stromal cells," *Experimental Cell Research*, vol. 316, no. 19, pp. 3109–3123, 2010.

[121] G. M. Spaggiari, H. Abdelrazik, F. Becchetti, and L. Moretta, "MSCs inhibit monocyte-derived DC maturation and function by selectively interfering with the generation of immature DCs: central role of MSC-derived prostaglandin E2," *Blood*, vol. 113, no. 26, pp. 6576–6583, 2009.

[122] Y. You, J. Zhang, J. Gong et al., "Mesenchymal stromal cell-dependent reprogramming of Kupffer cells is mediated by TNF-α and PGE2 and is crucial for liver transplant tolerance," *Immunologic Research*, vol. 62, no. 3, pp. 292–305, 2015.

[123] A. B. Vasandan, S. Jahnavi, C. Shashank, P. Prasad, A. Kumar, and S. J. Prasanna, "Human Mesenchymal stem cells program macrophage plasticity by altering their metabolic status *via* a PGE_2-dependent mechanism," *Scientific Reports*, vol. 6, no. 1, p. 38308, 2016.

[124] R. B. Ö. Özdemir, A. T. Özdemir, A. E. Sarıboyacı, O. Uysal, M. İ. Tuğlu, and C. Kırmaz, "The investigation of immunomodulatory effects of adipose tissue mesenchymal stem cell educated macrophages on the CD4 T cells," *Immunobiology*, vol. 224, no. 4, pp. 585–594, 2019.

[125] D. Philipp, L. Suhr, T. Wahlers, Y. H. Choi, and A. Paunel-Görgülü, "Preconditioning of bone marrow-derived mesenchymal stem cells highly strengthens their potential to promote IL-6-dependent M2b polarization," *Stem Cell Research & Therapy*, vol. 9, no. 1, p. 286, 2018.

[126] K. Hyvärinen, M. Holopainen, V. Skirdenko et al., "Mesenchymal stromal cells and their extracellular vesicles enhance the anti-inflammatory phenotype of regulatory macrophages by downregulating the production of interleukin (IL)-23 and IL-22," *Frontiers in Immunology*, vol. 9, p. 771, 2018.

[127] X. Lu, J. Han, X. Xu et al., "PGE2 promotes the migration of mesenchymal stem cells through the activation of FAK and ERK1/2 pathway," *Stem Cells International*, vol. 2017, Article ID 8178643, 11 pages, 2017.

[128] Z. Zhang, S. Huang, S. Wu et al., "Clearance of apoptotic cells by mesenchymal stem cells contributes to immunosuppression *via* PGE2," *eBioMedicine*, vol. 45, pp. 341–350, 2019.

[129] N. Negi and M. D. Griffin, "Effects of mesenchymal stromal cells on regulatory T cells: current understanding and clinical relevance," *Stem Cells*, vol. 38, no. 5, pp. 596–605, 2020.

[130] Q. H. Chen, F. Wu, L. Liu et al., "Mesenchymal stem cells regulate the Th17/Treg cell balance partly through hepatocyte growth factor in vitro," *Stem Cell Research & Therapy*, vol. 11, no. 1, p. 91, 2020.

[131] K. Wang, Y. J. Shi, Z. L. Song et al., "Regulatory effect of rat bone marrow mesenchymal stem cells on Treg/Th17 immune balance in vitro," *Molecular Medicine Reports*, vol. 21, no. 5, pp. 2123–2130, 2020.

[132] L. C. Davies, N. Heldring, N. Kadri, and K. le Blanc, "Mesenchymal stromal cell secretion of programmed death-1 ligands regulates T cell mediated immunosuppression," *Stem Cells*, vol. 35, no. 3, pp. 766–776, 2017.

[133] Y. Ma, Z. Wang, A. Zhang et al., "Human placenta-derived mesenchymal stem cells ameliorate GVHD by modulating Th17/Tr1 balance via expression of PD-L2," *Life Sciences*, vol. 214, pp. 98–105, 2018.

[134] K. Sato, K. Ozaki, I. Oh et al., "Nitric oxide plays a critical role in suppression of T-cell proliferation by mesenchymal stem cells," *Blood*, vol. 109, no. 1, pp. 228–234, 2007.

[135] X. Chen, Y. Gan, W. Li et al., "The interaction between mesenchymal stem cells and steroids during inflammation," *Cell Death & Disease*, vol. 5, no. 1, article e1009, 2014.

[136] D. Chabannes, M. Hill, E. Merieau et al., "A role for heme oxygenase-1 in the immunosuppressive effect of adult rat and human mesenchymal stem cells," *Blood*, vol. 110, no. 10, pp. 3691–3694, 2007.

[137] J. Niu, W. Yue, Z. le-le, L. Bin, and X. Hu, "Mesenchymal stem cells inhibit T cell activation by releasing TGF-β1 from TGF-β1/GARP complex," *Oncotarget*, vol. 8, no. 59, pp. 99784–99800, 2017.

[138] J. Fan, X. Tang, Q. Wang et al., "Mesenchymal stem cells alleviate experimental autoimmune cholangitis through immunosuppression and cytoprotective function mediated by galectin-9," *Stem Cell Research & Therapy*, vol. 9, no. 1, p. 237, 2018.

[139] M. Sioud, A. Mobergslien, A. Boudabous, and Y. Fløisand, "Evidence for the involvement of galectin-3 in mesenchymal stem cell suppression of allogeneic T-cell proliferation," *Scandinavian Journal of Immunology*, vol. 71, no. 4, pp. 267–274, 2010.

[140] V. Palomares Cabeza, M. J. Hoogduijn, R. Kraaijeveld et al., "Pediatric mesenchymal stem cells exhibit immunomodulatory properties toward allogeneic T and B cells under inflammatory conditions," *Frontiers in Bioengineering and Biotechnology*, vol. 7, p. 142, 2019.

[141] D. Khare, R. Or, I. Resnick, C. Barkatz, O. Almogi-Hazan, and B. Avni, "Mesenchymal stromal cell-derived exosomes affect mRNA expression and function of B-lymphocytes," *Frontiers in Immunology*, vol. 9, p. 3053, 2018.

[142] A. L. Anding and E. H. Baehrecke, "Cleaning house: selective autophagy of organelles," *Developmental Cell*, vol. 41, no. 1, pp. 10–22, 2017.

[143] K. R. Parzych and D. J. Klionsky, "An overview of autophagy: morphology, mechanism, and regulation," *Antioxidants & Redox Signaling*, vol. 20, no. 3, pp. 460–473, 2014.

[144] L. Galluzzi and D. R. Green, "Autophagy-independent functions of the autophagy machinery," *Cell*, vol. 177, no. 7, pp. 1682–1699, 2019.

[145] C. M. Dower, C. A. Wills, S. M. Frisch, and H. G. Wang, "Mechanisms and context underlying the role of autophagy in cancer metastasis," *Autophagy*, vol. 14, no. 7, pp. 1110–1128, 2018.

[146] Y. Matsuzawa-Ishimoto, S. Hwang, and K. Cadwell, "Autophagy and inflammation," *Annual Review of Immunology*, vol. 36, no. 1, pp. 73–101, 2018.

[147] K. H. Kim and M. S. Lee, "Autophagy–a key player in cellular and body metabolism," *Nature Reviews Endocrinology*, vol. 10, no. 6, pp. 322–337, 2014.

[148] F. M. Menzies, A. Fleming, and D. C. Rubinsztein, "Compromised autophagy and neurodegenerative diseases," *Nature Reviews Neuroscience*, vol. 16, no. 6, pp. 345–357, 2015.

[149] J. M. Bravo-San Pedro, G. Kroemer, and L. Galluzzi, "Autophagy and mitophagy in cardiovascular disease," *Circulation Research*, vol. 120, no. 11, pp. 1812–1824, 2017.

[150] D. C. Rubinsztein, P. Codogno, and B. Levine, "Autophagy modulation as a potential therapeutic target for diverse diseases," *Nature Reviews Drug Discovery*, vol. 11, no. 9, pp. 709–730, 2012.

[151] P. Chen, M. Cescon, and P. Bonaldo, "Autophagy-mediated regulation of macrophages and its applications for cancer," *Autophagy*, vol. 10, no. 2, pp. 192–200, 2014.

[152] S. Ceccariglia, A. Cargnoni, A. R. Silini, and O. Parolini, "Autophagy: a potential key contributor to the therapeutic action of mesenchymal stem cells," *Autophagy*, vol. 16, no. 1, pp. 28–37, 2020.

[153] D. C. Rubinsztein, G. Mariño, and G. Kroemer, "Autophagy and aging," *Cell*, vol. 146, no. 5, pp. 682–695, 2011.

[154] T. Squillaro, I. Antonucci, N. Alessio et al., "Impact of lysosomal storage disorders on biology of mesenchymal stem cells: evidences from in vitro silencing of glucocerebrosidase (GBA) and alpha-galactosidase A (GLA) enzymes," *Journal of Cellular Physiology*, vol. 232, no. 12, pp. 3454–3467, 2017.

[155] D. Zhang, Y. Chen, X. Xu et al., "Autophagy inhibits the mesenchymal stem cell aging induced by D-galactose through ROS/JNK/p38 signalling," *Clinical and Experimental Pharmacology & Physiology*, vol. 47, no. 3, pp. 466–477, 2020.

[156] M. Yang, T. Wen, H. Chen, J. Deng, C. Yang, and Z. Zhang, "Knockdown of insulin-like growth factor 1 exerts a protective effect on hypoxic injury of aged BM-MSCs: role of autophagy," *Stem Cell Research & Therapy*, vol. 9, no. 1, p. 284, 2018.

[157] S. Cen, P. Wang, Z. Xie et al., "Autophagy enhances mesenchymal stem cell-mediated $CD4^+$ T cell migration and differentiation through CXCL8 and TGF-β1," *Stem Cell Research & Therapy*, vol. 10, no. 1, p. 265, 2019.

[158] L. Gao, S. Cen, P. Wang et al., "Autophagy improves the immunosuppression of $CD4^+$ T cells by mesenchymal stem cells through transforming growth factor-β1," *Stem Cells Translational Medicine*, vol. 5, no. 11, pp. 1496–1505, 2016.

[159] L. S. Cheng, Y. Liu, and W. Jiang, "Restoring homeostasis of $CD4^+$ T cells in hepatitis-B-virus-related liver fibrosis," *World Journal of Gastroenterology*, vol. 21, no. 38, pp. 10721–10731, 2015.

[160] B. Binder and R. Thimme, "$CD4^+$ T cell responses in human viral infection: lessons from hepatitis C," *The Journal of Clinical Investigation*, vol. 130, no. 2, pp. 595–597, 2020.

[161] H. Y. Wang, C. Li, W. H. Liu et al., "Autophagy inhibition via Becn1 downregulation improves the mesenchymal stem cells antifibrotic potential in experimental liver fibrosis," *Journal of Cellular Physiology*, vol. 235, no. 3, pp. 2722–2737, 2020.

[162] S. Dang, Z. M. Yu, C. Y. Zhang et al., "Autophagy promotes apoptosis of mesenchymal stem cells under inflammatory microenvironment," *Stem Cell Research & Therapy*, vol. 6, no. 1, p. 247, 2015.

[163] W. Sang, B. Lv, K. Li, and Y. Lu, "Therapeutic efficacy and safety of umbilical cord mesenchymal stem cell transplantation for liver cirrhosis in Chinese population: a meta-analysis," *Clinics and Research in Hepatology and Gastroenterology*, vol. 42, no. 3, pp. 193–204, 2018.

[164] Y. O. Jang, Y. J. Kim, S. K. Baik et al., "Histological improvement following administration of autologous bone marrow-derived mesenchymal stem cells for alcoholic cirrhosis: a pilot study," *Liver International*, vol. 34, no. 1, pp. 33–41, 2014.

[165] K. T. Suk, J. H. Yoon, M. Y. Kim et al., "Transplantation with autologous bone marrow-derived mesenchymal stem cells for alcoholic cirrhosis: Phase 2 trial," *Hepatology*, vol. 64, no. 6, pp. 2185–2197, 2016.

[166] J. Liang, H. Zhang, C. Zhao et al., "Effects of allogeneic mesenchymal stem cell transplantation in the treatment of liver cirrhosis caused by autoimmune diseases," *International Journal of Rheumatic Diseases*, vol. 20, no. 9, pp. 1219–1226, 2017.

[167] Q. Zhou, T. Gu, Y. Zhang et al., "Human umbilical cord mesenchymal stem cells ameliorate hepatic stellate cell activation and liver fibrosis by upregulating microRNA-455-3p through suppression of p21-activated kinase-2," *BioMed Research International*, vol. 2021, Article ID 6685605, 13 pages, 2021.